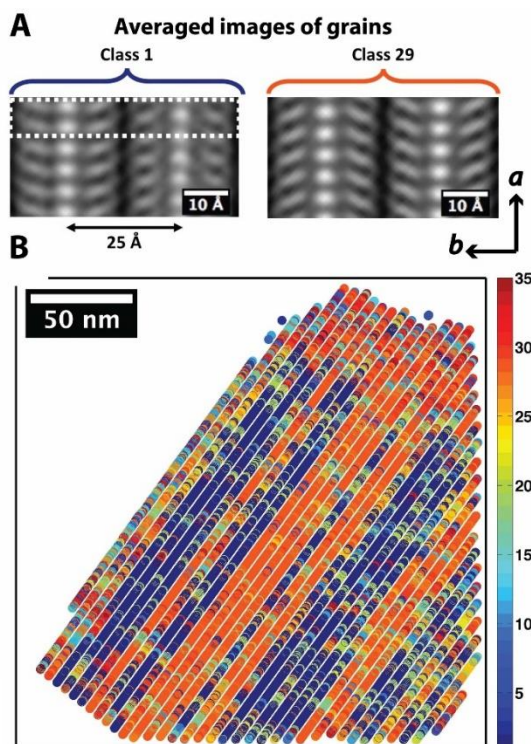
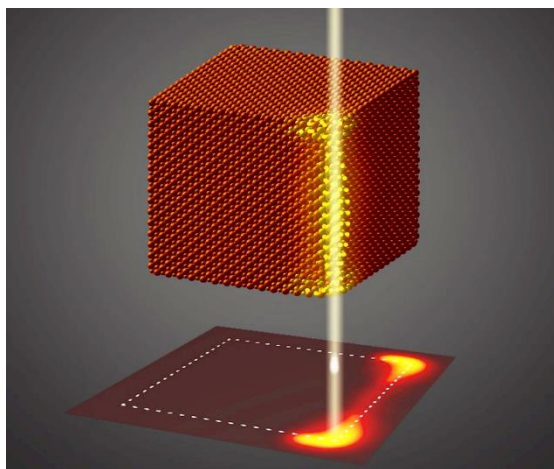
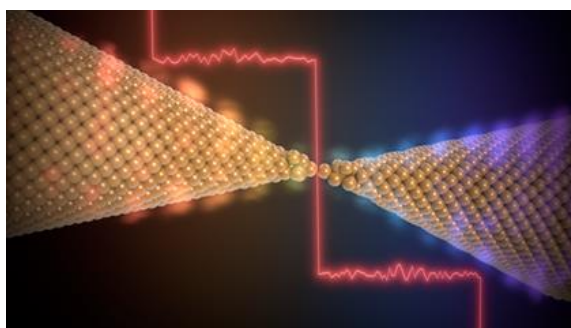


Electron and Scanning Probe Microscopies

2018 Principal Investigators' Meeting



Marriott Washingtonian
Gaithersburg, Maryland
November 14-16, 2018



U.S. DEPARTMENT OF
ENERGY

Office of
Science

Office of Basic Energy Sciences
Materials Sciences and Engineering Division

On the Cover

- Left Top: *Discovering the Ultimate Limit of Heat Transport: Measurements across a Single-Atom Junction.* As gold is stretched into a strand one atom thick (center of artist's sketch), an expressway for heat transport is formed. Designated as a "quantum of thermal conductance," this phenomena was observed for the first time and reveals that the heat flow rate in single-atom metallic junctions has an upper limit that is set by the laws of quantum mechanics (as illustrated by the red conductance trace through the junction). Work published in *Science* **355**, 1192 (2017).
Courtesy: Pramod Reddy, University of Michigan
- Left Bottom: *Bright Vibrations: Mapping Phonons at the Nanoscale.* Mapping the interaction of a 60 keV electron with a surface vibrational mode at the edge of a 100 nm sized MgO cube, using 10 meV resolution electron energy-loss spectroscopy (EELS). Work published in *Nature* **543**, 529 (2017).
Courtesy: Philip E. Batson, Rutgers University
- Right: *Imaging Synthetic Soft Matter on Atomic-Length-Scales using Cryogenic Electron Microscopy.* A Images obtained by sorting unit cells in the micrograph into classes; B Distribution of crystalline motifs in a contiguous film. Work published in *Macromolecules* **51** (19), 7794 (2018).
Courtesy: Lawrence Berkeley National Laboratory

This document was produced under contract number DE-SC0014664 between the U.S. Department of Energy and Oak Ridge Associated Universities.

The research grants and contracts described in this document are supported by the U.S. DOE Office of Science, Office of Basic Energy Sciences, Materials Sciences and Engineering Division.

Foreword

This volume comprises the scientific content of the 2018 Electron and Scanning Probe Microscopies Principal Investigators' Meeting sponsored by the Materials Sciences and Engineering Division (MSED) in the Office of Basic Energy Sciences (BES) of the U. S. Department of Energy (DOE). The meeting, held on November 14–16, 2018, in Gaithersburg, Maryland, is the seventh biennial meeting in the Electron and Scanning Probe Microscopies area organized by BES. The purpose of the meeting is to bring together researchers funded in this core research area to facilitate the exchange of new results and research highlights, to foster new ideas and collaborations among the participants, and to discuss how to advance electron and scanning probe microscopy and spectroscopy, as well as the associated theoretical tools, in order to address forefront scientific challenges. The meeting also affords BES program managers an opportunity to assess the state of the entire program collectively on a periodic basis, in order to chart future directions and identify new programmatic needs.

To address the materials science grand challenges, the Electron and Scanning Probe Microscopies Core Research Activity supports basic research using advanced electron and scanning probe microscopy and spectroscopy techniques to understand the atomic, electronic, and magnetic structures and properties of materials. This activity also supports the development of new instrumentation and techniques to advance basic science and materials characterizations for energy applications. Topical areas highlighted in this year's meeting include: quantum materials, van der Waals materials, topological states and defects, 4D STEM, new microscopy and spectroscopy methods, and ultrafast dynamics in materials. Special at this year's meeting are two panel discussions on topical areas of current interest to the PIs in the program: (i) quantum science and (ii) machine learning.

I thank all of the meeting attendees, for their active participation and for sharing their ideas and new research results. The dedicated efforts and invaluable assistance of the Meeting Chairs, Paul Voyles and Amir Yacoby, in organizing this meeting are greatly appreciated. My sincere thanks also go to Teresa Crockett in MSED and Linda Severs and her colleagues at the Oak Ridge Institute for Science and Education for their excellent work providing all the logistic support for the meeting.

Jane G. Zhu
Program Manager, Electron and Scanning Probe Microscopies
Division of Materials Sciences and Engineering, Basic Energy Sciences
Office of Science
U. S. Department of Energy

Table of Contents

Agenda	ix
Poster Sessions List	xv
Laboratory Projects	
<i>The Ferroionic State in Layered Ferroelectrics</i> Nina Balke, Petro Maksymovych, Rama Vasudevan, and Albina Borisevich	3
<i>Atomic Resolution Electron Microscopy of Soft Matter</i> Nitash Balsara, Kenneth Downing, Andrew Minor, Ronald Zuckermann, and David Prendergast	11
<i>Spectroscopic Imaging STM and Complex Electronic Matter</i> Kazuhiro Fujita and J.C. Séamus Davis	15
<i>Spin Physics and Nanoscale Probes of Quantum Materials</i> David Goldhaber-Gordon, Marc Kastner, Hari C. Manoharan, Joseph Orenstein, and Shoucheng Zhang	23
<i>Charge and Spin Behavior in Ferroics</i> Myung-Geun Han, Joe Garlow, and Yimei Zhu	27
<i>Atomic and Mesoscopic Phenomena in Quantum Systems with Broken Translational Symmetry</i> S.V. Kalinin, M.F. Chisholm, A.R. Lupini, C.T. Nelson, and M.P. Oxley	31
<i>Diffraction Imaging of Soft Matter with 4DSTEM</i> Andrew Minor, Kenneth Downing, Ronald Zuckermann, David Prendergast, and Nitash Balsara	35
<i>Atomic and Mesoscopic Phenomena in Quantum Systems with Broken Translational Symmetry</i> M. P. Oxley, A. R. Lupini, C. T. Nelson, M. F. Chisholm, and S. V. Kalinin	40
<i>Emergent Behavior in Nanoscale Functional Heterostructures</i> Amanda K. Petford-Long, Saidur Bakaul, and Charudatta Phatak	44
<i>Tracing Non-equilibrium Phenomena in Quantum Materials by Using MeV Ultrafast Electron Probes</i> Jing Tao, Junjie Li, and Jun Li	50

<i>Liquid Cell Electron Microscopy: Heterogeneity and Fluctuations at Solid-Liquid Interfaces</i> Haimei Zheng, Peter Ercius, Emory Chan, and Lin-Wang Wang	55
<i>Revealing Transient States and Electron, Spin and Lattice Correlations in Quantum Materials</i> Yimei Zhu, Lijun Wu, Xuewen Fu, Junjie Li, Jing Tao, and Tatiana Konstantinova	60
University Grant Projects	
<i>Quantitative Interpretation of Phonon EELS Mapping in Nanoscale Structures</i> P. E. Batson and M. J. Lagos	71
<i>Nanoscale Imaging of Optical-Frequency Plasmonic Energy Transfer in Individual Nanoparticles and their Assemblies</i> Jon P. Camden and David J. Masiello	76
<i>Superconductivity, Magnetism and Spin-Orbit Interactions in SrTiO₃ Based Heterostructures</i> Venkat Chandrasekhar	81
<i>Predicting and Understanding New Polar States Guided by Phase-Field Simulations</i> Long-Qing Chen	86
<i>Combined Microscopy and Transport Studies of Two-Dimensional Semiconductors and Topological Semimetals</i> David H. Cobden	93
<i>Novel Developments in Spectroscopy and In Situ Imaging of Photocatalytic Nanoparticles for Solar Fuel Generation</i> Peter A. Crozier	98
<i>Controlling Interfacial Spin Polarization due to Chemisorption</i> Daniel B. Dougherty	103
<i>Real-Time Measurements of Complex Transition Metal Oxide Nanostructure Growth</i> Michael A. Filler and Frances M. Ross	106
<i>Localized Spatiotemporal Behaviors of Coherent Structural Dynamics Revealed with Ultrafast Electron Microscopy</i> David J. Flannigan	110
<i>Growth, Characterization, and Nanoscale Transport of Chiral Magnetic Materials</i> Gregory D. Fuchs	115

<i>Understanding Dynamic Processes in Hybrid Perovskite Semiconductors</i> David S. Ginger	120
<i>Collaborative Research: Atomistic Studies of Individual Impurities and Impurity Complexes in III–V Semiconductors</i> Jay A. Gupta and Michael Flatté	126
<i>Understanding and Control of Spin Currents at Magnetic Interfaces</i> P. Chris Hammel	130
<i>Probing Emergent Phenomena in Ferroelectric/MoS₂ Composite Structures</i> Xia Hong	135
<i>Superconductor/Ferromagnet Heterostructures</i> Maria Iavarone	140
<i>Atomic Scale Imaging of Spin and Magnetism in Two-Dimensional Materials and Devices</i> Roland K. Kawakami and Jay A. Gupta	144
<i>Mesoscopic Conductivity Imaging of Novel Field-Effect Transistors</i> Keji Lai	148
<i>Interfacial Superconductivity in Epitaxial Single Layer FeSeTe on SrTiO₃(001)</i> Lian Li	152
<i>STM Studies of Unconventional Superconductors</i> Vidya Madhavan	156
<i>Oxides Surfaces: Unexpected Flexoelectricity and New Phenomena</i> Laurence D. Marks	160
<i>Advancing In situ Analytical Electron Microscopy for Probing Dynamic Nano-Scale Solid State Electrochemistry</i> Ying Shirley Meng	165
<i>Capturing the Structure and Dynamics of Materials at 4D Atomic Resolution</i> Jianwei (John) Miao	169
<i>Imaging of Topological Textures and Their Order Parameters Enabled by a New Generation of High-Dynamic-Range, Momentum-Resolved STEM Detectors</i> David A. Muller, Craig J. Fennie, and Darrell G. Schlom	174
<i>Magnetic Imaging of Spatially Modulated Superconductivity in Focus Ion Beam Defined Microstructures</i> Katja Nowack	180

<i>Structure and Dynamics of Domains in Ferroelectric Nanostructures – In Situ TEM Studies</i> Xiaoqing Pan	184
<i>Physics of Complex Materials Systems through Theory and Microscopy/EELS</i> Sokrates T. Pantelides	189
<i>Emerging Functionality in Transition-Metal Compounds Driven by Spatial Confinement</i> Ward Plummer	193
<i>Nano-Optical Imaging, Spectroscopy, and Control of Quantum Materials</i> Markus B. Raschke	202
<i>Scanning Thermal Microscopy for Studying Nanoscale Thermal Radiation</i> Pramod Reddy and Edgar Meyhofer	206
<i>Symmetry-Breaking Mechanism and Metastable States in Charge-Ordered Systems Probed using Femtosecond Electron Diffraction and Spectroscopy</i> Chong-Yu Ruan	210
<i>Atomic-Scale Surface Studies of Bulk Metallic Glasses</i> Udo Schwarz	214
<i>Electronic Properties of Organic Photovoltaic Systems under Mechanical Stress</i> Santiago D. Solares and Hanning Chen	219
<i>Probing Correlated Phenomena in Oxide Structures with Quantitative STEM</i> Susanne Stemmer	223
<i>Atomically Thin Energy Materials: In Situ Microscopy of Synthesis and Local Light-Matter Interactions</i> Peter Sutter and Eli Sutter	227
<i>Dielectrics under Extreme Electric Fields: In Situ Studies on Nanoscale Mechanisms</i> Xiaoli Tan and Geoff Brennecke	232
<i>Probing Majorana States in Topological-Superconductor Proximity Systems</i> Stuart Tessmer, Dale Van Harlingen, and Alex Levchenko	236
<i>Imaging Point Defects with 4D STEM</i> Paul M. Voyles and Dane Morgan	241
<i>Visualizing Emergent Phenomena in Topological and Quantum Materials</i> Weida Wu	245

<i>Transport and Imaging of Mesoscopic Phenomena in Novel Low-Dimensional Materials</i> Amir Yacoby and Pablo Jarillo-Herrero	249
<i>Probing Correlated Superconductors and Their Phase Transitions on the Nanometer Scale</i> Ali Yazdani	254
<i>Dislocation Avalanche Mechanism in High Entropy Alloys</i> Jian-Min Zuo	259
Author Index	265
Participant List	269

AGENDA

**2018 Electron and Scanning Probe Microscopies
Principal Investigators' Meeting
Materials Sciences and Engineering Division, Office of Basic Energy Sciences
U. S. Department of Energy**

WEDNESDAY, NOVEMBER 14, 2018

- 7:00 – 8:20 am *****Breakfast*****
- 8:20 – 8:50 am *BES/DMSE Update and Outlook*
Linda Horton, DMSE Director
- 8:50 – 9:00 am *Welcome and Introductory Remarks*
Jane Zhu, ESPM Program Manager
- Meeting Chairs: Paul Voyles and Amir Yacoby
University of Wisconsin/ Harvard University
- Session I Quantum Materials**
Chair: Amir Yacoby, Harvard University
- 9:00 – 9:25 am Séamus Davis, Brookhaven National Laboratory/Cornell University
Spectroscopic Imaging STM and Complex Electronic Matter
- 9:25 – 9:50 am Ali Yazdani, Princeton University
Probing Correlated Superconductors and Their Phase Transitions on the Nanometer Scale
- 9:50 – 10:15 am Stuart Tessmer, Michigan State University
Probing Majorana States in Topological-Superconductor Proximity Systems
- 10:15 – 10:40 am David Goldhaber-Gordon, SLAC/Stanford University
Spin Physics and Nanoscale Probes of Quantum Materials
- 10:40 – 11:00 am *****Break*****
- Session II 4D STEM**
Chair: Paul Voyles, University of Wisconsin
- 11:00 – 11:25 am David Muller, Cornell University
Imaging of Topological Textures and Their Order Parameters Enabled by a New Generation of High-Dynamic-Range, Momentum-Resolved STEM Detectors

11:25 – 11:50 am M. P. Oxley, Oak Ridge National Laboratory
Atomic and Mesoscopic Phenomena in Quantum Systems with Broken Translational Symmetry

11:50 – 12:15 pm Andrew Minor, Lawrence Berkeley National Laboratory
Diffraction Imaging of Soft Matter with 4DSTEM

12:15 pm *****Working Lunch*****

Session III **van der Waals Materials**
Chair: Jay Gupta, Ohio State University

1:20 – 1:45 pm Xia Hong, University of Nebraska
Probing Emergent Phenomena in Ferroelectric/MoS₂ Composite Structures

1:45 – 2:10 pm Vidya Madhavan, University of Illinois
STM Studies of Unconventional Superconductors

2:10 – 2:35 pm Roland Kawakami, Ohio State University
Atomic Scale Imaging of Spin and Magnetism in Two-Dimensional Materials and Devices

2:35 – 3:00 pm Keji Lai, University of Texas
Mesoscopic Conductivity Imaging of Novel Field-Effect Transistors

3:00 – 5:00 pm ******* Poster Session I (and refreshments/coffee break) *******

Session IV **Topological States and Defects**
Chair: Maria Iavarone, Temple University

5:00 – 5:25 pm Gregory Fuchs, Cornell University
Growth, Characterization, and Nanoscale Transport of Chiral Magnetic Materials

5:25 – 5:50 pm Weida Wu, Rutgers University
Visualizing Emergent Phenomena in Topological and Quantum Materials

5:50 – 6:15 pm David Cobden, University of Washington
Combined Microscopy and Transport Studies of Two-Dimensional Semiconductors and Topological Semimetals

6:20 pm *****Working Dinner*****

THURSDAY, NOVEMBER 15, 2018

- 7:00 – 8:30 am *****Breakfast*****
- Session V** **New Methods (I)**
Chair: Susanne Stemmer, University of California Santa Barbara
- 8:30 – 8:55 am David Ginger, University of Washington
Understanding Dynamic Processes in Hybrid Perovskite Semiconductors
- 8:55 – 9:20 am Chris Hammel, Ohio State University
Understanding and Control of Spin Currents at Magnetic Interfaces
- 9:20 – 9:45 am John Miao, University of California, Los Angeles
Capturing the Structure and Dynamics of Materials at 4D Atomic Resolution
- 9:45 – 10:10 am Amanda Petford-Long, Argonne National Laboratory
Emergent Behavior in Nanoscale Functional Heterostructures
- 10:10 – 10:30 am *****Break*****
- Session VI** **New Methods (II)**
Chair: Nitash Balsara, Lawrence Berkeley National Laboratory
- 10:30 – 10:55 am Markus Raschke, University of Colorado
Nano-optical Imaging, Spectroscopy, and Control of Quantum Materials
- 10:55 – 11:20 am Pramod Reddy, University of Michigan
Scanning Thermal Microscopy for Studying Nanoscale Thermal Radiation
- 11:20 – 11:45 am Haimei Zheng, Lawrence Berkeley National Laboratory
Liquid Cell Electron Microscopy: Heterogeneity and Fluctuations at Solid-Liquid Interfaces
- 11:45 – 12:10 pm Shirley Meng, University of California San Diego
Advancing In Situ Analytical Electron Microscopy for Probing Dynamic Nano-Scale Solid State Electrochemistry
- 12:15 pm *****Working Lunch*****

Session VII**Ferroic Materials**

Chair: Sergei Kalinin, Oak Ridge National Laboratory

1:20 – 1:45 pm

Nina Balke, Oak Ridge National Laboratory
The Ferroionic State in Layered Ferroelectrics

1:45 – 2:10 pm

Myung-Geun Han, Brookhaven National Laboratory
Charge and Spin Behavior in Ferroics

2:10 – 2:35 pm

Long-Qing Chen, Pennsylvania State University
*Predicting and Understanding New Polar States Guided by Phase-Field Simulations***Panel Discussion I****Quantum Science**

2:35 – 3:35 pm

Chair: Amir Yacoby
Panel Members: M. Kasevich, G. Fuchs, S. Jesse

3:40 – 5:40 pm

***** **Poster Session II (and refreshments/coffee break)** *****

6:00 pm

*****Working Dinner*******FRIDAY, NOVEMBER 16, 2018**

7:00 – 8:30 am

*****Breakfast*******Panel Discussion II****Machine Learning**

8:30 – 9:30 am

Chair: Paul Voyles
Panel Members: S. Kalinin, S. Davis, J. Zuo**Session VIII****Phonons and Ultrafast Dynamics**

Chair: Yimei Zhu, Brookhaven National Laboratory

9:30 – 9:55 am

Phil Batson, Rutgers
Quantitative Interpretation of Phonon EELS Mapping in Nanoscale Structures

9:55 – 10:20 am

Peter Crozier, Arizona State University
Novel Developments in Spectroscopy of Photocatalytic Nanoparticles for Solar Fuel Generation

10:20 – 10:40 am

*****Break*****

- 10:40 – 11:05 am David Flannigan, University of Minnesota
Localized Spatiotemporal Behaviors of Coherent Structural Dynamics Revealed with Ultrafast Electron Microscopy
- 11:05 – 11:30 am Chong-Yu Ruan, Michigan State University
Femtosecond Imaging of Dynamical Texture (Re)formation in Charge-Density Wave Systems with Coherent Electron Beams
- 11:30 – 11:55 am Jing Tao, Brookhaven National Laboratory
Tracing Nonequilibrium Phenomena in Quantum Materials by using MeV Ultrafast Electron Probes
- 11:55 – 12:30 pm ***Discussions and Concluding Comments***
Paul Voyles and Amir Yacoby, Meeting Chairs
Jane Zhu, Program Manager, ESPM/BES

ESPM PI Meeting

Poster Session I

Wednesday, November 14, 3:00 – 5:00 PM

- I.1 **Nitash Balsara, Downing, Minor, Zuckermann, Prendergast**, Lawrence Berkeley National Laboratory
Atomic Resolution Microscopy of Soft Matter
- I.2 **Venkat Chandrasekhar**, Northwestern University
Superconductivity, Magnetism, and Spin-Orbit Interactions in SrTiO₃ Based Heterostructures
- I.3 **Dan Dougherty**, North Carolina State University
Controlling Interfacial Spin Polarization due to Chemisorption
- I.4 **Sergei Kalinin, Chisholm, Lupini, Nelson, Oxley**, Oak Ridge National Laboratory
Atomic and Mesoscopic Phenomena in Quantum Systems with Broken Translational Symmetry
- I.5 **Lian Li**, West Virginia University
Interfacial Superconductivity in Epitaxial Single Layer FeSeTe on SrTiO₃(001)
- I.6 **Maria Iavarone**, Temple University
Superconductor/Ferromagnet Heterostructures
- I.7 **Xiaoli Tan**, Iowa State University
Dielectrics under Extreme Electric Fields: In Situ Studies on Nanoscale Mechanisms
- I.8 **Jay A. Gupta and Michael Flatté**, Ohio State University and University of Iowa
Atomistic Studies of Individual Impurities and Impurity Complexes in III-V Semiconductors
- I.9 **Xiaoqing Pan**, University of California, Irvine
Structure and Dynamics of Domains in Ferroelectric Nanostructures – In-situ TEM Studies
- I.10 **Santiago D. Solares**, The George Washington University
Electronic Properties of Organic Photovoltaic Systems under Mechanical Stress
- I.11 **Amir Yacoby**, Harvard University
Transport and Imaging of Mesoscopic Phenomena in Novel Low-Dimensional Materials

- I.12 **Peter Crozier**, Arizona State University
Connecting Structure to Functionality in Photocatalysts through In Situ and Aberration Corrected TEM

Poster Session II

Thursday, November 15, 3:40 – 5:40 PM

- II.1 **Jon P. Camden and David J. Masiello**, University of Notre Dame/ University of Washington
Nanoscale Imaging of Optical-Frequency Plasmonic Energy Transfer in Individual Nanoparticles and Their Assemblies
- II.2 **Susanne Stemmer**, University of California, Santa Barbara
Probing Correlated Phenomena in Oxide Structures with Quantitative STEM
- II.3 **Sokrates T. Pantelides**, Vanderbilt University
Physics of Complex Materials Systems through Theory and Microscopy/EELS
- II.4 **Udo Schwarz**, Yale University
Atomic-Scale Surface Studies of Bulk Metallic Glasses
- II.5 **Jian-Min Zuo**, University of Illinois
Dislocation Avalanche Mechanism in High Entropy Alloys
- II.6 **Peter Sutter**, University of Nebraska-Lincoln
Atomically Thin Energy Materials: In-Situ Microscopy of Synthesis and Local Light-Matter Interactions
- II.7 **Laurence D. Marks**, Northwestern University
Oxides Surfaces: Unexpected Flexoelectricity and New Phenomena
- II.8 **Ward Plummer**, Louisiana State University
Emerging Functionality in Transition-Metal Compounds Driven by Spatial Confinement
- II.9 **Michael Filler and Frances Ross**, Georgia Institute of Technology/MIT
Real-Time Measurements of Complex Transition Metal Oxide Nanostructure Growth

- II.10 **Yimei Zhu, Wu, Fu, Li, Tao**, Brookhaven National Laboratory
Revealing Transient States and Electron, Spin and Lattice Correlations in Quantum Materials
- II.11 **Katja Nowack**, Cornell University
Magnetic Imaging of Spatially Modulated Superconductivity in Focus Ion Beam Defined Microstructures
- II.12 **Paul Voyles**, University of Wisconsin
Imaging Point Defects with 4D STEM
- II.13 **Mark Kasevich**, Stanford University
Multi-pass Electron Microscopy

***LABORATORY
PROJECTS***

The Ferroionic State in Layered Ferroelectrics

Nina Balke, Petro Maksymovych, Rama Vasudevan, Albina Borisevich

Oak Ridge National Laboratory

Research Scope

For materials with structural, electronic and magnetic order parameters, the presence of microscopic disorder is critical in determining their physical properties and qualitatively altering the macroscopic behavior. One of the primary reasons is the finite length-scale over which the dipolar, magnetic or electronic lattice can efficiently screen the disorder. However, the coupling to the chemical degrees of freedom is often neglected and the role of chemical disorder on the atomic scale is unknown. The overarching goal of this project is to control ferroic material properties through chemical tuning and chemical disorder on multiple length scales. To achieve this goal, we will pursue three Specific Aims: (1) Develop an atomistic-level understanding of the coupling between chemical and ferroic order parameters at surfaces and interfaces, (2) Manipulate ferroic properties on the mesoscopic scale through chemical tuning, and (3) Achieve atomic-scale control over chemical disorder. These three Specific Aims will be addressed through local functional imaging with scanning probe microscopy and atomically resolved imaging and spectroscopy with scanning transmission electron microscopy. The unique enabling capability is the synergy between imaging tools and data science, which will nucleate fundamental physical insights and build a foundation toward tailoring material properties via chemical disorder. These approaches will enable the design of non-equilibrium states of matter which can result in the discovery of new physics and materials with enhanced functional properties for energy applications.

Recent Progress

In the concurrence period, the research was focused on exploring the coupling between ferroic behavior and chemical degrees of freedom, called the ferroionic state. One of the most challenging aspects of studying the role of chemistry and chemical disorder in ferroic material systems is the simultaneous probing of different processes and their subsequent quantification. This is especially true if the goal is insight into *local* origins of this coupling. This can be achieved by using atomic force microscopy and carefully chosen model materials and phenomena. An ideal model system exhibit ferroic properties and ionic conductivity in an accessible temperature range and is free of surface dead layers. To this end, we have studied layered van-der-Waals thiophosphates (such as CuInP_2S_6) which is a promising model system for ferroionic states as well as prospective 2D material heterostructures for catalytic or electronic applications. In this abstract, we demonstrate the quantification and physical interpretation of the ferroelectric properties in CuInP_2S_6 , the characteristics of ionic motion, and show pathways to modify local chemistry driving control over ferroic material properties.

Understanding the ferroelectric properties in layered materials

Copper indium thiophosphate CuInP_2S_6 (CIPS) is a van-der-Waals layered crystal with ferroelectric ordering below 310K.^{1,2} We have for the first time revealed giant negative electrostriction in this material – a rare property so far exhibited by only one polymer composition. Subsequently, we have shown by density functional theory (DFT) calculations that the ferroelectric displacement of Cu ions is dramatically modified by the van der Waals interactions. Instead of the commonly anticipated double-well potential for Cu displacement within a single layer, the interactions across the van-der-Waals gap effectively produce a quadruple-well. The multi-well structure explains the negative longitudinal piezoelectric effect and enables multi-level ferroelectric states defined by atomic configurations within and across the van-der-Waals gap. The overall picture predicted by DFT calculations was verified by combining piezoresponse force microscopy (PFM), elastic property mapping, and cantilever dynamic quantification (Fig. 1).

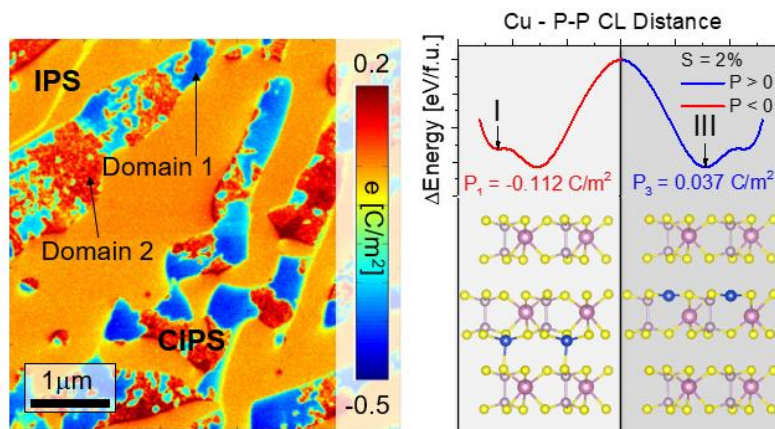


Figure 1: Measured piezoelectric constant e for a dual phase material containing ferroelectric CIPS featuring two different domains. By comparing with calculated values, we were able to identify two out of four possible polarization states and a material strain of 2%.

Ionic conductivity on the nanoscale

It is known, from macroscopic measurements, that CuInP_2S_6 attains significant copper ionic conductivity.³ The ionic conduction on the nanoscale was tracked through local redox reactions in the field of the scanning probe providing a current-free probing technique allowing for local studies.⁴ The local redox process manifested with an almost complete reversibility of a reaction involving millions of atoms locally deposited and redissolved in the material. (Fig. 2). The remarkable resilience of CuInP_2S_6 to large scale ionic displacement and Cu-vacancies is, in part enabled by metastability of Cu-deficient phases.

Furthermore, electrodeposition of copper on the surface of CuInP_2S_6 injects copper vacancies into the bulk, enabling nanoscale tuning of electromechanical response and ferroelectric properties (Fig. 3). The

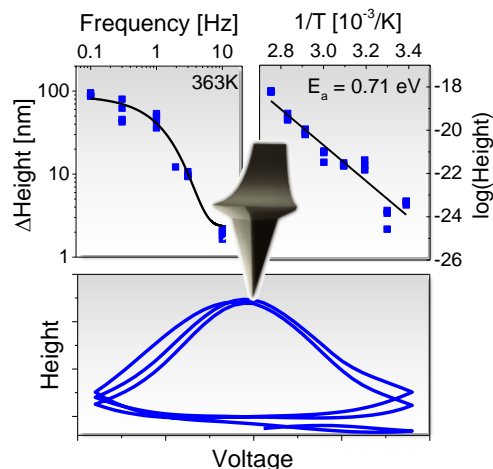


Figure 2: A biased AFM tip is used to induce and detect reversible copper transport in CIPS on a local scale

electrochemical modification of thiophosphate surfaces open new possibilities for nanostructuring of materials toward local modification of their properties as well as interfaces with other electronic materials. and provided a prototype of nanoscale material design via reversible lattice manipulation.

New approaches to modify surface chemistry

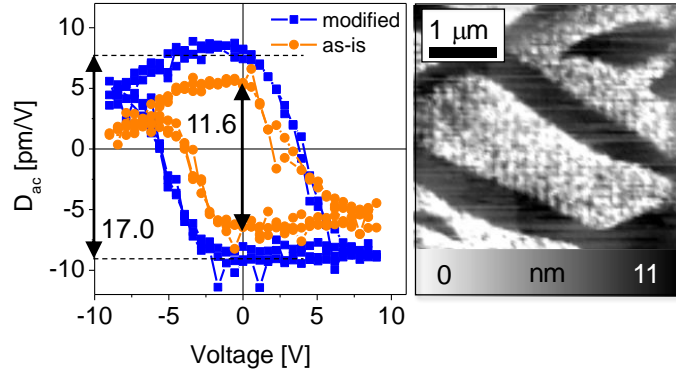
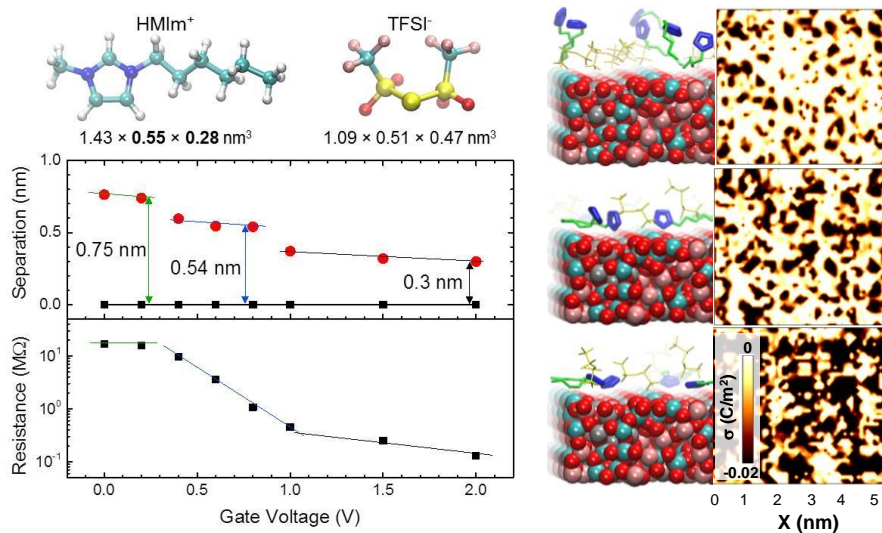


Figure 3: Locally induced redox processes form copper on the surface and chemically modified bulk material boosting the ferroelectric response.

Having demonstrated local control over chemistry in layered thiophosphates we explored the feasibility of ionic liquid gating to exert electrochemical control on the macroscopic scale. This was first explored on an oxide material with known gating properties. Despite much research activity little is known about the correlation of the structure of the liquids in contact with the transition metal oxide surface, its evolution with the applied electric potential, and its correlation with the measured electronic properties of the oxide. We investigate the structure of an ionic liquid at a semiconducting oxide interface during the operation of a thin film transistor using force distance curves and compared the results with molecular dynamic modeling.⁵ We found that the transition between the high and low resistivity states of amorphous indium gallium zinc oxide is accompanied by a densification and preferential spatial orientation of counter-ions at the oxide channel surface. This process occurs in three distinct steps, corresponding to ion orientations and consequently regimes of different electrical conductivity. The reason for this can be found in the surface charge densities on the oxide surface when different ion arrangements are present (Fig. 4).

Figure 4: Ionic liquid structure at the solid-liquid interface is measured as function of gate voltage and correlated with resistance and charge density through molecular dynamics simulations.



Future Plans

For the specific material system CIPS and related layered ferroelectrics we are aiming at exploring the quadrupole well as potential for a new class of ferroelectrics with true multi-state functionality. This includes the accessibility of polarization states with voltage and time and exploring switching dynamics and stability using local AFM techniques. In parallel, we will explore the strain state using localized structural characterization techniques to understand the polarization-strain relationship. This understanding will be used to explore ways to modify the strain state on global and local length scales to take advantage of the four possible polarization states. To better quantify the ion conductivity in CIPS we are aiming at extracting quantitative numbers for conductivity by exploring the frequency-dependent response which can be analyzed based on our previous work.⁶ Combined with chemical imaging we aim to answer questions about the chemical modification volume and the exact reason for the modified ferroelectric response after chemical modification which will be done by AFM as well as ionic liquid gating. The next milestone in the understanding of these materials is atomically resolved surface imaging, so as to gain insight into the coupling between chemical and ferroic order parameters on the atomic scale needed to understand polarization screening towards ultrathin heterostructures between CIPS and other traditional 2D materials as well as the atomistic underpinning of frustrated dipolar states.

References

1. Simon, A.; Ravez, J.; Maisonneuve, V.; Payen, C.; Cajipe, V. B., Paraelectric ferroelectric transition in the lamellar thiophosphate CuInP2S6. *Chem. Mater.* **1994**, *6*, 1575-1580.
2. Belianinov, A.; He, Q.; Dziaugys, A.; Maksymovych, P.; Eliseev, E.; Borisevich, A.; Morozovska, A.; Banys, J.; Vysochanskii, Y.; Kalinin, S. V., CuInP2S6 Room Temperature Layered Ferroelectric. *Nano Lett.* **2015**, *15* (6), 3808-3814.
3. Banys, J.; Macutkevicius, J.; Samulionis, V.; Brilingas, A.; Vysochanskii, Y., Dielectric and ultrasonic investigation of phase transition in CuInP2S6 crystals. *Phase Transitions* **2004**, *77* (4), 345-358.
4. Balke, N.; Neumayer, S. M.; Brehm, J. A.; Susner, M. A.; Rodriguez, B. J.; Jesse, S.; Kalinin, S. V.; Pantelides, S. T.; McGuire, M. A.; Maksymovych, P., Locally Controlled Cu-Ion Transport in Layered Ferroelectric CuInP2S6. *ACS Appl. Mater. Interfaces* **2018**, *10* (32), 27188-27194.
5. Black, J. M.; Come, J.; Bi, S.; Zhu, M. Y.; Zhao, W.; Wong, A. T.; Noh, J. H.; Pudasaini, P. R.; Zhang, P. F.; Okatan, M. B.; Dai, S.; Kalinin, S. V.; Rack, P. D.; Ward, T. Z.; Feng, G.; Balke, N., Role of Electrical Double Layer Structure in Ionic Liquid Gated Devices. *ACS Applied Materials & Interfaces* **2017**, *9* (46), 40949-40958.
6. Morozovska, A. N.; Eliseev, E. A.; Kalinin, S. V., Electromechanical probing of ionic currents in energy storage materials. *Appl. Phys. Lett.* **2010**, *96* (22).

Publications

1. Cao, Y.; Kalinin, S. V., Phase-field modeling of chemical control of polarization stability and switching dynamics in ferroelectric thin films. *Phys. Rev. B* 2016, 94 (23).
2. Cao, Y.; Yang, S. Z.; Jesse, S.; Kravchenko, I.; Yu, P.; Chen, L. Q.; Kalinin, S. V.; Balke, N.; Li, Q., Exploring Polarization Rotation Instabilities in Super-Tetragonal BiFeO₃ Epitaxial Thin Films and Their Technological Implications. *Advanced Electronic Materials* 2016, 2 (12).
3. Ziatdinov, M.; Fujii, S.; Kiguchi, M.; Enoki, T.; Jesse, S.; Kalinin, S. V., Data mining graphene: correlative analysis of structure and electronic degrees of freedom in graphenic monolayers with defects. *Nanotechnology* 2016, 27 (49).
4. Ziatdinov, M.; Banerjee, A.; Maksov, A.; Berlijn, T.; Zhou, W.; Cao, H. B.; Yan, J. Q.; Bridges, C. A.; Mandrus, D. G.; Nagler, S. E.; Baddorf, A. P.; Kalinin, S. V., Atomic-scale observation of structural and electronic orders in the layered compound alpha-RuCl₃. *Nat. Commun.* 2016, 7.
5. Vasudevan, R. K.; Ziatdinov, M.; Chen, C.; Kalinin, S. V., Analysis of citation networks as a new tool for scientific research. *MRS Bull.* 2016, 41 (12), 1009.
6. Somnath, S.; Belianinov, A.; Kalinin, S. V.; Jesse, S., Rapid mapping of polarization switching through complete information acquisition. *Nat. Commun.* 2016, 7.
7. Ziatdinov, M.; Maksov, A.; Li, L.; Sefat, A. S.; Maksymovych, P.; Kalinin, S. V., Deep data mining in a real space: separation of intertwined electronic responses in a lightly doped BaFe₂As₂. *Nanotechnology* 2016, 27 (47).
8. Ponath, P.; O'Hara, A.; Cao, H. X.; Posadas, A. B.; Vasudevan, R.; Okatan, M. B.; Jesse, S.; Berg, M.; Li, Z. Y.; Zhang, D. S.; Kellock, A. J.; de Lozanne, A.; Zhou, J. S.; Kalinin, S.; Smith, D. J.; Demkov, A. A., Contradictory nature of Co doping in ferroelectric BaTiO₃. *Phys. Rev. B* 2016, 94 (20).
9. Meyer, T. L.; Herklotz, A.; Lauter, V.; Freeland, J. W.; Nichols, J.; Guo, E. J.; Lee, S.; Ward, T. Z.; Balke, N.; Kalinin, S. V.; Fitzsimmons, M. R.; Lee, H. N., Enhancing interfacial magnetization with a ferroelectric. *Phys. Rev. B* 2016, 94 (17).
10. Morozovska, A. N.; Eliseev, E. A.; Genenko, Y. A.; Vorotiahin, I. S.; Silibin, M. V.; Cao, Y.; Kim, Y.; Glinchuk, M. D.; Kalinin, S. V., Flexocoupling impact on size effects of piezoresponse and conductance in mixed-type ferroelectric semiconductors under applied pressure. *Phys. Rev. B* 2016, 94 (17).
11. Ievlev, A. V.; Maksymovych, P.; Trassin, M.; Seidel, J.; Ramesh, R.; Kalinin, S. V.; Ovchinnikova, O. S., Chemical State Evolution in Ferroelectric Films during Tip-Induced Polarization and Electroresistive Switching. *Acs Applied Materials & Interfaces* 2016, 8 (43), 29588.
12. Li, L. L.; Cao, Y.; Somnath, S.; Yang, Y. D.; Jesse, S.; Ehara, Y.; Funakubo, H.; Chen, L. Q.; Kalinin, S. V.; Vasudevan, R. K., Direct Imaging of the Relaxation of Individual Ferroelectric Interfaces in a Tensile-Strained Film. *Advanced Electronic Materials* 2017, 3 (4).

13. Ziatdinov, M.; Maksov, A.; Kalinin, S. V., Learning surface molecular structures via machine vision. *Npj Computational Materials* 2017, 3.
14. Guo, E. J.; Petrie, J. R.; Roldan, M. A.; Li, Q.; Desautels, R. D.; Charlton, T.; Herklotz, A.; Nichols, J.; van Lierop, J.; Freeland, J. W.; Kalinin, S. V.; Lee, H. N.; Fitzsimmons, M. R., Spatially Resolved Large Magnetization in Ultrathin BiFeO₃. *Adv. Mater.* 2017, 29 (32).
15. Yang, S. M.; Morozovska, A. N.; Kumar, R.; Eliseev, E. A.; Cao, Y.; Mazet, L.; Balke, N.; Jesse, S.; Vasudevan, R. K.; Dubourdieu, C.; Kalinin, S. V., Mixed electrochemical-ferroelectric states in nanoscale ferroelectrics. *Nat. Phys.* 2017, 13 (8), 812.
16. Kurchak, A. I.; Eliseev, E. A.; Kalinin, S. V.; Strikha, M. V.; Morozovska, A. N., p-n Junction Dynamics Induced in a Graphene Channel by Ferroelectric-Domain Motion in the Substrate. *Physical Review Applied* 2017, 8 (2).
17. Morozovska, A. N.; Eliseev, E. A.; Kurchak, A. I.; Morozovsky, N. V.; Vasudevan, R. K.; Strikha, M. V.; Kalinin, S. V., Effect of surface ionic screening on the polarization reversal scenario in ferroelectric thin films: Crossover from ferroionic to antiferroionic states. *Phys. Rev. B* 2017, 96 (24).
18. Jang, J. H.; Kim, Y. M.; He, Q.; Mishra, R.; Qiao, L.; Biegalski, M. D.; Lupini, A. R.; Pantelides, S. T.; Pennycook, S. J.; Kalinin, S. V.; Borisevich, A. Y., In Situ Observation of Oxygen Vacancy Dynamics and Ordering in the Epitaxial LaCoO₃ System. *ACS Nano* 2017, 11 (7), 6942.
19. Eliseev, E. A.; Morozovska, A. N.; Glinchuk, M. D.; Kalinin, S. V., Lost surface waves in nonpiezoelectric solids. *Phys. Rev. B* 2017, 96 (4).
20. Vasudevan, R. K.; Balke, N.; Maksymovych, P.; Jesse, S.; Kalinin, S. V., Ferroelectric or non-ferroelectric: Why so many materials exhibit "ferroelectricity" on the nanoscale. *Applied Physics Reviews* 2017, 4 (2).
21. Cao, Y.; Chen, L. Q.; Kalinin, S. V., Role of flexoelectric coupling in polarization rotations at the a-c domain walls in ferroelectric perovskites. *Appl. Phys. Lett.* 2017, 110 (20).
22. Morozovska, A. N.; Eliseev, E. A.; Morozovsky, N. V.; Kalinin, S. V., Ferroionic states in ferroelectric thin films. *Phys. Rev. B* 2017, 95 (19).
23. Morozovska, A. N.; Eliseev, E. A.; Morozovsky, N. V.; Kalinin, S. V., Piezoresponse of ferroelectric films in ferroionic states: Time and voltage dynamics. *Appl. Phys. Lett.* 2017, 110 (18).
24. Cao, Y.; Morozovska, A.; Kalinin, S. V., Pressure-induced switching in ferroelectrics: Phase-field modeling, electrochemistry, flexoelectric effect, and bulk vacancy dynamics. *Phys. Rev. B* 2017, 96 (18).
25. Vasudevan, R. K.; Cao, Y.; Laanait, N.; Ievlev, A.; Li, L. L.; Yang, J. C.; Chu, Y. H.; Chen, L. Q.; Kalinin, S. V.; Maksymovych, P., Field enhancement of electronic conductance at ferroelectric domain walls. *Nat. Commun.* 2017, 8.
26. Vlcek, L.; Vasudevan, R. K.; Jesse, S.; Kalinin, S. V., Consistent Integration of Experimental and Ab Initio Data into Effective Physical Models. *Journal of Chemical Theory and Computation* 2017, 13 (11), 5179.

27. Black, J. M.; Come, J.; Bi, S.; Zhu, M. Y.; Zhao, W.; Wong, A. T.; Noh, J. H.; Pudasaini, P. R.; Zhang, P. F.; Okatan, M. B.; Dai, S.; Kalinin, S. V.; Rack, P. D.; Ward, T. Z.; Feng, G.; Balke, N., Role of Electrical Double Layer Structure in Ionic Liquid Gated Devices. *ACS Applied Materials & Interfaces* 2017, 9 (46), 40949.
28. Damodaran, A. R.; Pandya, S.; Agar, J. C.; Cao, Y.; Vasudevan, R. K.; Xu, R. J.; Saremi, S.; Li, Q.; Kim, J.; McCarter, M. R.; Dedon, L. R.; Angsten, T.; Balke, N.; Jesse, S.; Asta, M.; Kalinin, S. V.; Martin, L. W., Three-State Ferroelastic Switching and Large Electromechanical Responses in PbTiO₃ Thin Films. *Adv. Mater.* 2017, 29 (37).
29. Vlcek, L.; Maksov, A.; Pan, M. H.; Vasudevan, R. K.; Kahnin, S. V., Knowledge Extraction from Atomically Resolved Images. *ACS Nano* 2017, 11 (10), 10313.
30. Vorotiahin, I. S.; Eliseev, E. A.; Li, Q.; Kalinin, S. V.; Genenko, Y. A.; Morozovska, A. N., Tuning the polar states of ferroelectric films via surface charges and flexoelectricity. *Acta Mater.* 2017, 137, 85.
31. Das, S.; Wang, B.; Cao, Y.; Cho, M. R.; Shin, Y. J.; Yang, S. M.; Wang, L. F.; Kim, M.; Kalinin, S. V.; Chen, L. Q.; Noh, T. W., Controlled manipulation of oxygen vacancies using nanoscale flexoelectricity. *Nat. Commun.* 2017, 8.
32. Pradhan, D. K.; Kumari, S.; Strelcov, E.; Pradhan, D. K.; Katiyar, R. S.; Kalinin, S. V.; Laanait, N.; Vasudevan, R. K., Reconstructing phase diagrams from local measurements via Gaussian processes: mapping the temperature-composition space to confidence. *Npj Computational Materials* 2018, 4.
33. Kannan, R.; Ievlev, A. V.; Laanait, N.; Ziatdinov, M. A.; Vasudevan, R. K.; Jesse, S.; Kalinin, S. V., Deep data analysis via physically constrained linear unmixing: universal framework, domain examples, and a community-wide platform. *Advanced Structural and Chemical Imaging* 2018, 4.
34. Somnath, S.; Law, K. J. H.; Morozovska, A. N.; Maksymovych, P.; Kim, Y.; Lu, X.; Alexe, M.; Archibald, R.; Kalinin, S. V.; Jesse, S.; Vasudevan, R. K., Ultrafast current imaging by Bayesian inversion. *Nat. Commun.* 2018, 9.
35. Fabrikant, I.; Karapetian, E.; Kalinin, S. V., Interaction between a punch and an arbitrary crack or inclusion in a transversely isotropic half-space. *Zeitschrift Fur Angewandte Mathematik Und Physik* 2018, 69 (1).
36. Li, L.; Zheng, Q.; Zou, Q.; Rajput, S.; Ijaduola, A. O.; Wu, Z.; Wang, X. P.; Cao, H. B.; Somnath, S.; Jesse, S.; Chi, M.; Gai, Z.; Parker, D.; Sefat, A. S., Improving superconductivity in BaFe₂As₂-based crystals by cobalt clustering and electronic uniformity (vol 7, 949, 2017). *Sci. Rep.* 2018, 8.
37. Vasudevan, R. K.; Laanait, N.; Ferragut, E. M.; Wang, K.; Geohegan, D. B.; Xiao, K.; Ziatdinov, M.; Jesse, S.; Dyck, O.; Kalinin, S. V., Mapping mesoscopic phase evolution during E-beam induced transformations via deep learning of atomically resolved images. *Npj Computational Materials* 2018, 4.

38. Li, L. L.; Yang, Y. D.; Zhang, D. W.; Ye, Z. G.; Jesse, S.; Kalinin, S. V.; Vasudevan, R. K., Machine learning-enabled identification of material phase transitions based on experimental data: Exploring collective dynamics in ferroelectric relaxors. *Science Advances* 2018, 4 (3).
39. Young, S. R.; Maksov, A.; Ziatdinov, M.; Cao, Y.; Burch, M.; Balachandran, J.; Li, L. L.; Somnath, S.; Patton, R. M.; Kalinin, S. V.; Vasudevan, R. K., Data mining for better material synthesis: The case of pulsed laser deposition of complex oxides. *J. Appl. Phys.* 2018, 123 (11).

Atomic Resolution Electron Microscopy of Soft Matter

Nitash Balsara, Kenneth Downing, Andrew Minor, Ronald Zuckermann, David Prendergast

Materials Sciences Division, Lawrence Berkeley National Laboratory, Berkeley, CA 94709

Research Scope

The goal of our program is to produce images of soft materials with atomic resolution using electron microscopy. The proposed work is inherently challenging because soft materials are unstable under the electron beam. Our work encompasses both cryogenic scanning transmission electron microscopy (cryo-STEM) and cryogenic transmission electron microscopy (cryo-EM). This abstract focuses on atomic resolution cryo-EM. Our experiments were conducted on crystalline nanostructures formed by self-assembly of amphiphilic peptoid molecules in water. The sequences of the peptoids were specifically designed to enable high resolution electron microscopy. Molecular dynamics simulations are used to characterize thermal fluctuations and disorder, and this information is convoluted with the contrast transfer function of the microscope used in experiments to obtain theoretical images. We demonstrate the application of our technique to imaging amorphous vesicles on Angstrom length-scales. The methodology that we have developed will be extended to a wide variety of soft materials.

Recent Progress

Crystalline polymers comprise lamellar domains with numerous defects and trapped amorphous domains between and possibly within lamellae. In landmark studies dating back to 1957, electron diffraction was used to study thin, single crystal lamellae grown from solution [1]. While considerable knowledge on polymer crystals has been obtained in the intervening sixty years, the challenge of imaging polymer crystals in position space remains unaddressed; all images of atoms in the literature on synthetic polymers are drawn either by hand or by computer programs. Here we present the first electron micrographs of synthetic polymer crystals and defects that can be interpreted in terms of atomic models.

Electron microscopy is routinely used to image two classes of materials with angstrom level resolution: hard crystalline materials such as metals and biological macromolecules such as proteins. Many metals are stable to electron beam exposure, which makes it possible to obtain images under high dose conditions in which individual atoms are resolved. Proteins, on the other hand, are unstable to electron beam exposure, and determining high resolution structures requires the application of sophisticated data analysis algorithms on numerous images that each have low signal-to-noise ratio because they are obtained under low dose conditions. The algorithms exploit the fact that in a given sample, the protein molecules have the same atomic structure (or a limited

set of structures), even though the images represent unknown rotations of that structure. Crystals of synthetic polymers are also unstable to electron beam exposure [2]. Since the degree of homogeneity at the atomic level in synthetic polymer crystals is generally quite limited, the atomic scale resolution of radiation sensitive soft materials is desired, it is of great importance to minimize the damage from the electron beam. In order to preserve the high spatial frequency signal, the accumulated dose that can be used for imaging has to be carefully controlled by using a low-dose imaging technique. In addition, the effects of radiation damage are minimized when the specimen is cooled to cryogenic temperatures. The resolution of structures obtained from radiation-sensitive biological macromolecules using cryo-EM has been significantly improved with the introduction of direct electron detectors and novel image processing algorithms. The high detective quantum efficiency (DQE) of these detectors and their ability to acquire images rapidly enable dose-fractionated movie recording and beam-induced motion correction, thereby providing substantial enhancement of resolution for low-dose imaging. In the present study, we have leveraged these advances along with algorithms developed in the structural biology community to obtain images of vitrified, hydrated synthetic polymer crystals using cryo-EM at a resolution sufficient to enable direct comparisons with atomic models.

A nearly monodisperse diblock polypeptoid comprising a hydrophobic poly-N-decylglycine (pNdc) block and a hydrophilic poly-N-2-(2-(2-methoxyethoxy) ethylglycine) (pNte) block was synthesized for this project. The self-assembly of this material in water results in the formation of molecularly thin sheets of the crystalline hydrophobic pNdc chains stabilized by dissolved pNte chains [3,4]. The sheets were divided into $87 \times 87 \text{ \AA}$ boxes and analyzed using the Relion software package [5,6]. We detected the presence of 35 different classes. In this abstract, we focus on two classes: 1 and 29 that are mirror images of one another. In order to interpret the images, it is instructive to start with a simulation of a molecularly thin sheet of peptoid crystal, shown in Fig. 1A. Also shown in Fig. 1A are the in-plane and through-plane views of simulations of a single pNdc9 chain in the crystal. Fig. 1B shows simulations of two crystalline unit cells that are mirror images of each other with a concomitant grain boundary. The backbones stayed roughly parallel to each other and the pNdc sidechains maintain the ordered V-shaped motifs that exclude water, while the pNte sidechains extend into solution and are disordered (not shown for simplicity). Figure 1C shows the experimentally obtained micrographs for classes 1 and 29. The correspondence between these micrographs and the through-plane views of our model is clear. The average distances between adjacent backbones and sidechains are 25 \AA and 4.7 \AA in the model, in agreement with the spacings in the images. Grain boundaries are frequently observed in our samples. Averaging unit cells along such grain boundaries results in the image shown in Fig. 1D. Here we obtain two adjacent V-shaped motifs that are parallel to each other in the middle of the micrograph, representing a grain boundary. This is in sharp contrast to the interior of grains that exhibit chains with two anti-parallel sets V-shaped motifs.

The present study is the first to demonstrate the possibility of atomic-scale imaging of synthetic polymer crystals and concomitant defects. The approach developed is robust and can be applied

to other synthetic polymer crystals provided the samples contain sufficient numbers of crystalline motifs to allow the hybrid analysis using crystallographic and single particle methods.

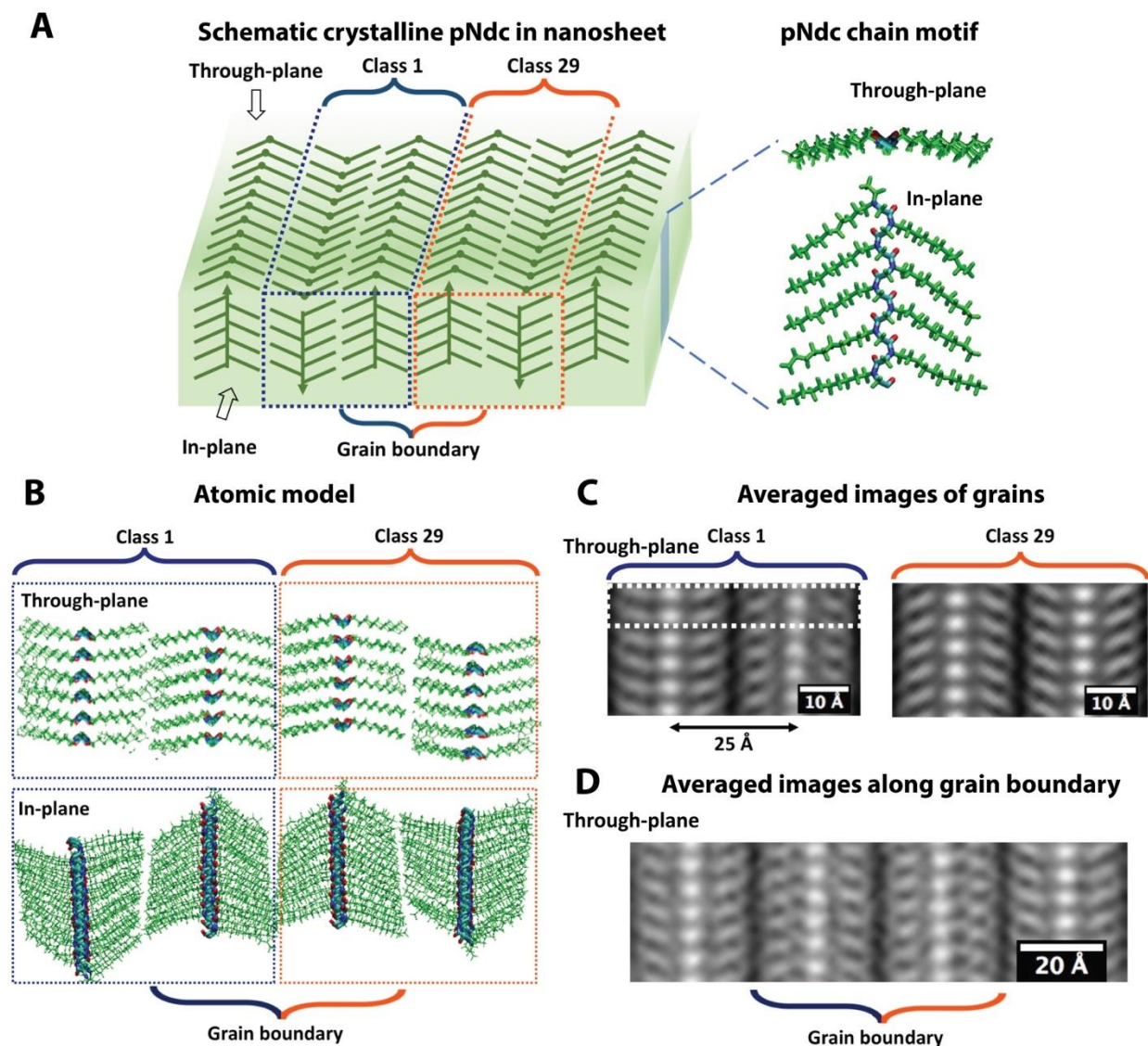


Figure 1. Model and imaging of individual crystals and grain boundaries. **A**, Cartoon shows overall arrangement of crystallized pNdc block in nanosheet (left) with through plane (“top”) and in plane (“front”) views indicated, and enlarged single pNdc block, which has side chains arranged in a V shape along the *cis* backbone. Nitrogen atoms are blue, oxygen red, carbon cyan in backbones. **B**, Region extracted from relaxed atomic model of crystal that includes a grain boundary, with regions marked corresponding to images in class averages 1 and 29. **C**, Averaged TEM images. **D**, An image obtained by averaging boxes along the domain boundaries.

Future Plans

We are synthesizing and imaging peptoids wherein all of the crystals are identical. Preliminary results show the peptoid structure can be resolved at 1.5 Å. This has the potential to open the door to resolving individual atoms without the resorting to a model. Atomic scale imaging of crystalline tubes has proven to be challenging due to issues related to the registry of

the front and back halves of the tubes. We are working on algorithms to average over such collections of images with fidelity.

References

1. Keller, A. A Note on Single Crystals in Polymers - Evidence for a Folded Chain Configuration. *Philos Mag* 1957, 2 (21), 1171.
2. Glaeser, R. M.; Taylor, K. A. Radiation damage relative to transmission electron microscopy of biological specimens at low temperature: a review. *Journal of microscopy* 1978, 112 (1), 127-38.
3. Sun, J.; Jiang, X.; Lund, R.; Downing, K. H.; Balsara, N. P.; Zuckermann, R. N. Self-assembly of crystalline nanotubes from monodisperse amphiphilic diblock copolypeptoid tiles. *P Natl Acad Sci USA* 2016, 113 (15), 3954-3959.
4. Greer, D. R.; Stolberg, M. A.; Kundu, J.; Spencer, R. K.; Pascal, T.; Prendergast, D.; Balsara, N. P.; Zuckermann, R. N. Universal Relationship between Molecular Structure and Crystal Structure in Peptoid Polymers and Prevalence of the cis Backbone Conformation. *J Am Chem Soc* 2018, 140 (2), 827-833.
5. Li, X. M.; Mooney, P.; Zheng, S.; Booth, C. R.; Braunfeld, M. B.; Gubbens, S.; Agard, D. A.; Cheng, Y. F. Electron counting and beam-induced motion correction enable near-atomic-resolution single-particle cryo-EM. *Nat Methods* 2013, 10 (6), 584.
6. Scheres, S. H. RELION: implementation of a Bayesian approach to cryo-EM structure determination. *Journal of structural biology* 2012, 180 (3), 519-30.

Publications

1. "Swelling of Individual Nanodomains in Hydrated Block Copolymer Electrolyte Membranes", X.C. Chen, X. Jiang, N.P. Balsara, *Journal of Chemical Physics*, vol. 149, pg. 163325, 2018.
2. "Universal Relationship between Molecular Structure and Crystal Structure in Peptoid Polymers and Prevalence of the cis Backbone Conformation", D.R. Greer, M.A. Stolberg, J. Kundu, R.K. Spencer, T. Pascal, D. Prendergast, N.P. Balsara, R.N. Zuckermann, *Journal of the American Chemical Society*, vol. 140(2). pg. 827-833, 2018.
3. "Effect of Pore Penetration on Transport through Supported Membranes studied by Electron Microscopy and Pervaporation", C. Shin, X. Jiang, W. Ko, N.P. Balsara, *Journal of Membrane Science*, vol. 542, pg. 18-23, 2017.
4. J.B. Kortright, J. Sun, R.K. Spencer, X. Jiang, R.N. Zuckermann, "Oxygen K Edge Scattering from Bulk Comb Diblock Copolymer Reveals Extended, Ordered Backbones above Lamellar Order-Disorder Transition", *The Journal of Physical Chemistry B*, vol. 121 , pg. 298-305, 2017.
5. "Reentrant phase behavior and coexistence in asymmetric block copolymer electrolytes", W.S. Loo, X. Jiang, J.A. Maslyn, H.J. Oh, C. Zhu, K.H. Downing, N.P. Balsara, *Soft Matter*, vol. 14 (15), pg. 2789-2795, 2018.
6. "Anomalous Self-Assembly and Ion Transport in Nanostructured Organic-Inorganic Solid Electrolytes", G.K. Sethi, X. Jiang, R. Chakraborty, W.S. Loo, I. Villaluenga, N.P. Balsara, vol. 7, pg. 1056-1061, *ACS Macro Letters*, 2018.
7. "Liquid Sulfur Impregnation of Microporous Carbon Accelerated by Nanoscale Interfacial Effects", T.A. Pascal, I. Villaluenga, K. Wujcik, D. Devaux, X. Jiang, D.R. Wang, N. Balsara, D. Prendergast, *Nano Letters*, vol. 17(4), pg. 2517-2523, 2017.

Spectroscopic Imaging STM and Complex Electronic Matter

Kazuhiro Fujita

CMP&MS Department, Brookhaven National Laboratory, Upton, NY 11973, USA
Office: 631-344-3933 / Mobile: 607-351-5800 / Email: kfujita@bnl.gov

J.C. Séamus Davis

CMP&MS Department, Brookhaven National Laboratory, Upton, NY 11973, USA
LASSP, Physics Department, Cornell University, Ithaca, NY 14853, USA.
Mobile: 607-220-8685 / +353 83 039 2937 / Email: jcseamusdavis@gmail.com

Research Scope:

We study electronic quantum matter with a focus on the quantum many-body phenomena driven by strong correlations in high temperature superconductors, gapped topological electron phases, quantum spin and monopole liquids, and electronic liquid crystal broken-symmetry states. The primary technique is direct atomic scale visualization with a suite of specialized SI-STM systems.

Recent Research Progress:

Discovery of the Pair Density Wave State in Cuprate HTS

The quantum condensate of Cooper-pairs forming a superconductor was originally conceived to be translationally invariant. In theory, however, pairs can exist with finite momentum Q and thereby generate states with spatially modulating Cooper-pair density^{1,2}. For some time, it has been widely hypothesized that the cuprate pseudogap phase³ contains such a ‘pair density wave’ (PDW) state⁴⁻²⁰. We introduced nanometer resolution scanned Josephson tunneling microscopy (SJTM) to image Cooper-pair tunneling from a d-wave superconducting STM tip to the condensate of underdoped $\text{Bi}_2\text{Sr}_2\text{CaCu}_2\text{O}_{8+x}$. Condensate visualization capabilities are demonstrated directly using the Cooper-pair density variations known from μSR to occur surrounding Zn impurity atoms^{21,22}. Fourier analysis of Josephson current images reveals the direct signature of a Cooper-pair density wave at wavevectors $Q_p \approx (0.25,0)2\pi/a_0; (0,0.25)2\pi/a_0$ in $\text{Bi}_2\text{Sr}_2\text{CaCu}_2\text{O}_8$. This is the first observation of a PDW in any material. ([*Nature* 532, 343 \(2016\)](#)).

Universality of Cuprate Commensurate $4a_0$ -period Charge Density Modulations

Strong Coulomb interactions between electrons on adjacent Cu sites result in complete charge localization in the cuprate Mott insulator (MI) state. When holes are introduced, theories based upon the same strong real space (r -space) interactions have long predicted a state of unidirectional modulation of spin and charge frequently with four-unit-cell ($4a_0$) periodicity. However, with increasing hole density p , the wavevector Q of the CDM is

reported to increase or diminish continuously as if driven primarily by Fermi surface effects. Distinguishing between the r -space and Fermi-surface-based theoretical perspectives is critical to identifying fundamental theories for the phase diagram and Cooper pairing mechanism in underdoped cuprates. We introduced a new technique based upon phase-resolved electronic structure visualization and demonstrate directly that the CDM of $\text{Bi}_2\text{Sr}_2\text{CaCu}_2\text{O}_8$ exhibits a doping-independent commensurate wavevector $Q_0=2\pi/4a_0$ throughout the entire pseudogap region. This doping-independent, commensurate $Q_0=2\pi/4a_0$ phenomenology indicates that strong-interactions in r -space drive the microscopic mechanism of the cuprate CDM state. ([*PNAS* **113**, 12661 \(2016\)](#))

Theory of Orbital Selective Superconductivity in Fe-based HTS

We studied the influence on spin-fluctuation mediated Cooper pairing theory, of orbital selective strong correlations in Fe-based superconductors - particularly the Fe chalcogenide systems. We hypothesized that a key ingredient for itinerant Cooper pairing theory in these materials is orbital selectivity, i.e., reduced coherence of quasiparticles whose spectral weight is contributed by specific orbital states. We showed that this modifies the usual spin-fluctuation theory via suppression of pair scattering processes involving those less coherent states, and predicts orbital selective Cooper pairing of electrons in the remaining coherent states. This predicts highly anisotropic gap structures for FeSe, as well as LiFeAs, indicating that orbital selective Cooper pairing plays a key role strongly correlated Fe-based superconductors ([*Phys. Rev.* **B95**, 1745054 \(2017\)](#)).

Discovery of Orbital Selective Superconductivity in Fe-based HTS

The superconductor FeSe has been of intense interest thanks to its unusual non-magnetic nematic state and potential for high temperature superconductivity. We used Bogoliubov quasiparticle interference imaging to determine the Fermi surface geometry of FeSe, and to measure the corresponding superconducting energy gaps. We showed that both gaps are extremely anisotropic but nodeless, and exhibit gap maxima oriented orthogonally in momentum space. Moreover, by implementing a novel technique we demonstrated that these gaps have opposite sign with respect to each other. This complex and highly unusual gap configuration revealed the existence of orbital-selective Cooper pairing which, in FeSe, is based preferentially on electrons from the d_{yz} orbitals of the iron atoms. This is the first observation of orbital-selective Cooper pairing in any material. ([*Science* **357**, 75 \(2017\)](#))

Theory of Pair Density Waves in superconducting Vortex Halos

We analyzed the interplay between a d-wave uniform superconducting and a pair-density wave (PDW) order parameter about a superconducting vortex. We developed and solve a phenomenological nonlinear sigma model, for the order parameter configuration and computed the resulting local density of states within the vortex halo. The intertwining

of the two superconducting orders is predicted to lead to a charge density modulation with the same periodicity as the PDW, which is twice the period of the charge-density-wave at the second-harmonic of the PDW itself. (*Phys. Rev. B 97, 174510 (2018)*)

Theory of Quantum Oscillations in a Biaxial Pair Density Wave State

Numerous predictions indicate that a pair density wave (PDW) state may be a key component of the phenomenology of the pseudogap phase in cuprates. Recently, we found direct evidence for such a state within halos around the cuprate vortex cores. By extrapolation, these vortex halos would overlap at a magnetic field scale where the mysterious quantum oscillations have long been observed in cuprates. In this study, we showed theoretically that a biaxial pair density wave state gives a unique but highly consistent description of the cuprate quantum oscillation data. Thus, our model supports the hypothesis that the cuprate pseudogap phase is a PDW. (*PNAS 115, 5389 (2018)*)

Visualizing orbital-selective quasiparticle interference in the FeSe Hund's Metal

The undoped phase proximate to superconductivity in Cu-based HTS materials is a strong Mott insulator^{23,24}, while that proximate to iron-based superconductivity is generally metallic^{25,26}. This has motivated a perception that the mechanisms of HTS must be quite different in these two canonical materials classes and, moreover, that strong electronic correlations are not indispensable to HTS. Importantly, however, the electronic structure of the Fe-based materials can still be governed by intense electronic correlations if an orbital-selective Hund's Metal state exists²⁷⁻³⁴. In this novel metallic state, alignment of the Fe spins is predicted to suppress inter-orbital fluctuations producing orbitally selective (but hidden) strong correlations. The spectral weights Z_m of quasiparticles associated with different Fe orbitals m should then become radically different. To test his prediction, we used QPI resolved by orbital content in the canonical Fe-based HTS, FeSe. Signatures of strong, orbitally selective differences of quasiparticle Z_m are observed on all detectable bands over a wide energy range. Further, the quasiparticle interference amplitudes reveal that $Z_{xy} < Z_{xz} \ll Z_{yz}$. Thus, we reveal that orbital-selective strong correlations dominate the parent state of iron-based HTS in FeSe. (*Nature Materials 17, Sept 3 (2018)*)

Discovery of Magnetic-field induced Pair Density Wave in the Cuprate Vortex Halo

When very high magnetic fields suppress the superconductivity in underdoped cuprates, an exceptional new electronic phase appears. It supports remarkable quantum oscillations and exhibits an unidentified density wave (DW) state. Although generally referred to as a 'charge' density wave (CDW) because of the observed charge density modulations, theory indicates that this could actually be the far more elusive electron-pair density wave state (PDW). To search for evidence of a field-induced PDW in cuprates, we visualize the modulations in the density of electronic states $N(r)$ within the halo surrounding $\text{Bi}_2\text{Sr}_2\text{CaCu}_2\text{O}_8$ vortex cores. This yielded multiple signatures of a PDW,

including two sets of $N(r)$ modulations occurring at wavevectors Q_P and $2Q_P$, both being energetically particle-hole symmetric, both having predominantly s -symmetry form factors, and the amplitude of the $2Q_P$ modulations decaying twice as rapidly from the vortex center as that of Q_P . Such a microscopic phenomenology is in detailed agreement with theories for a field-induced primary PDW that generates secondary CDWs within the vortex halo. [***arXiv:1802.04673***](#) (2018)

Using Machine Learning for Scientific Discovery in Electronic Quantum Matter

Automated instrumentation and large-scale data acquisition have revolutionized empirical science by generating data sets of such volume and complexity as to defy human analysis. To achieve scientific discovery using these enormous empirical data sets requires revolutionary new approaches^{35,36}. This is particularly true of modern visualization studies of electronic quantum matter (EQM) which yield dense arrays of electronic structure images that are often astonishingly complex at the atomic-scale³⁷. Given the spectacular recent advances in machine learning (ML) studies of synthetically generated EQM states³⁸⁻⁴⁹, the outstanding challenge now is to engage ML with experimentally generated EQM data. An important milestone would be a demonstration of scientific discovery using ML working with data sets from advanced EQM visualization experiments. In this regard, we reported development and training of an array of artificial neural networks (ANN) designed to recognize different types of hypothesized order hidden in EQM image-arrays. The ANNs are used to analyze a large, experimentally-derived EQM image archive, spanning a wide range of electron densities and energies, in carrier-doped cuprate Mott isolators. This ML system repeatedly and reliably identifies, throughout all these instrumentally noisy and intrinsically chaotic data, the features of a very specific ordered state of EQM: lattice-commensurate, precisely four-unit-cell periodic, unidirectional, translational-symmetry-breaking state, consistent with those long predicted within particle-like strong-coupling theories of electronic liquid crystals⁵⁰. This marks a rapid advance in the capability of ML to achieve physics discovery. [***arXiv:1808.00479***](#) (2018)

OASIS

The OASIS combined oxide MBE, ARPES and SISTM system at BNL is now operational. Initial test experiments at OASIS have already yielded interesting results including: *In-situ angle-resolved photoemission spectroscopy of copper-oxide thin films synthesized by molecular beam epitaxy* Chung Koo Kim, Ilya K. Drozdov, Kazuhiro Fujita, J. C. Séamus Davis, Ivan Bozovic, Tonica Valla. [***arXiv:1805.04811***](#) (2018). In future we plan to study the hole-doped Cu-based HTS materials $\text{YBa}_2\text{Cu}_3\text{O}_7$ and $\text{La}_{2-x}\text{Sr}_x\text{CuO}_4$, which are among the most important cuprate materials but are virtually never examined by ARPES or SISTM because they are not charge-neutral cleavable. We will pursue the k -space structure of the superconducting energy gap in $\text{DyBa}_2\text{Cu}_3\text{O}_7$ and $\text{La}_{2-x}\text{Sr}_x\text{CuO}_4$ synthesized at OASIS, measurements of the ‘Fermi arc’ for this $\text{DyBa}_2\text{Cu}_3\text{O}_7$ and $\text{La}_{2-x}\text{Sr}_x\text{CuO}_4$ versus carrier

density; and plan atomic-scale visualizations of the DW state of $\text{DyBa}_2\text{Cu}_3\text{O}_7$ and $\text{La}_{2-x}\text{Sr}_x\text{CuO}_4$. Similarly, by using $\text{Nd}_{2-x}\text{Ce}_x\text{CuO}_4$ films synthesized at OASIS, we will pursue measurements of energy gap structure in an electron doped cuprate $\text{Nd}_{2-x}\text{Ce}_x\text{CuO}_4$, search for evidence of a 'Fermi arc' in k -space, and attempt to visualize of a DW state of an electron doped compound.

Publications

Detection of a Cooper Pair Density Wave in $\text{Bi}_2\text{Sr}_2\text{CaCu}_2\text{O}_{8+x}$, M. H. Hamidian, S. D. Edkins, Sang Hyun Joo, A. Kostin, H. Eisaki, S. Uchida, M. J. Lawler, E. -A. Kim, A. P. Mackenzie, K. Fujita, Jinho Lee, J. C. Séamus Davis, *Nature* **532**, 343 (2016)

Commensurate $4a_0$ -period charge density modulations throughout the $\text{Bi}_2\text{Sr}_2\text{CaCu}_2\text{O}_{8+x}$ pseudogap regime, Andrej Mesaros, Kazuhiro Fujita, Stephen D. Edkins, Mohammad H. Hamidian, Hiroshi Eisaki, Shin-ichi Uchida, J. C. Séamus Davis, Michael J. Lawler, and Eun-Ah Kim *Proc. Nat'l Acad. Sci.* **113**, 12661 (2016)

Orbital selective pairing and gap structures of iron-based superconductors, Andreas Kreisel, Brian M. Andersen, P. O. Sprau, A. Kostin, J. C. Séamus Davis and P. J. Hirschfeld *Phys. Rev. B* **95**, 174504 (2017)

Discovery of orbital-selective Cooper pairing in FeSe, P.O. Sprau, A. Kostin, A. Kreisel, A. E. Böhrer, V. Taufour, P.C. Canfield, S. Mukherjee, P.J. Hirschfeld, B.M. Andersen, J. C. Séamus Davis *Science* **357**, 75 (2017)

Pair density waves in superconducting vortex halos Y. Wang, S. D. Edkins, M. H. Hamidian, J. C. Séamus Davis, E. Fradkin, S. A. Kivelson *Phys. Rev. B* **97**, 174510 (2018)

Quantum oscillations in a biaxial pair density wave state M. R. Norman, J. C. Séamus Davis *Proc. Nat'l Acad. Sci.* **115**, 5389 (2018)

Visualizing orbital-selective quasiparticle interference in the Hund's metal state of FeSe Andrey Kostin, Peter O. Sprau, A. Kreisel, Yi Xue Chong, Anna E. Böhrer, Paul C. Canfield, Peter J. Hirschfeld, Brian M. Andersen, J.C. Séamus Davis *Nature Materials*, Sept. 3 (2018)

Magnetic-field induced pair density wave state in the cuprate vortex halo, Stephen D. Edkins, Andrey Kostin, Kazuhiro Fujita, Andrew P. Mackenzie, Hiroshi Eisaki, Shin-Ichi Uchida Subir Sachdev, Michael J. Lawler, Eun-Ah Kim, J. C. Seamus Davis, Mohammad H. Hamidian. *arXiv:1802.04673* (2018)

In-situ angle-resolved photoemission spectroscopy of copper-oxide thin films synthesized by molecular beam epitaxy, Chung Koo Kim, Ilya K. Drozdov, Kazuhiro Fujita, J. C. Séamus Davis, Ivan Bozovic, Tonica Valla *arXiv:1805.04811* (2018)

Using machine learning for scientific discovery in electronic quantum matter visualization experiments, Yi Zhang, A. Mesaros, K. Fujita, S. D. Edkins, M. H. Hamidian, K. Ch'ng, H. Eisaki, S. Uchida, J. C. Séamus Davis, E. Khatami, Eun-Ah Kim *arXiv:1808.00479* (2018).

References

- 1 Fulde, P & Ferrell, R. A. *Phys. Rev.* **135**, A550 (1964).
- 2 Larkin, A. I. & Ovchinniko, Yu. N.. *Sov. Phys. JETP* **20**, 762 (1965).
- 3 Norman, M. R. & Pépin, C. *Rep. Prog. Phys.* **66**, 1547 (2003).
- 4 Fradkin, E., Kivelson, S. A., & Tranquada, J. *Rev. Mod Phys.* **87**, 457 (2015).
- 5 Himeda, A., Kato, T. & Ogata, M. *Phys. Rev. Lett.* **88**, 117001 (2002).
- 6 Raczkowski, M. *et al*, *Phys. Rev. B* **76**, 140505 (2007).
- 7 Yang, K.-Y., Chen, W. Q., Rice, T. M., Sigrist, M. & Zhang F.-C. *New J. Phys.* **11**, 055053 (2009).
- 8 Loder, F., Graser, S., Kampf, A. P. & Kopp, T. *Phys. Rev. Lett.* **107**, 187001 (2011).
- 9 Corboz, P., Rice, T. M. & Troyer, M. *Phys. Rev. Lett.* **113**, 046402 (2014)
- 10 Berg, E. *et al*. *Phys. Rev. Lett.* **99**, 127003 (2007).
- 11 Seo, K., Chen, H.-D. & Hu, J. *Phys. Rev. B.* **78**, 94510 (2008).
- 12 Berg, E., Fradkin, E. & Kivelson, S.A. *Nature Phys.* **5**, 830 (2009).
- 13 Agterberg, D. F., & Tsunetsugu, H. *Nature Phys.* **4**, 639 (2008).
- 14 Zelli, M., Kallin, K., & Berlinsky, J. *Phys. Rev. B* **86** 104507 (2012).
- 15 Lee, P. A. *Amperean Phys. Rev. X* **4**, 31017 (2014).
- 16 Chen, H. -D., Vafek, O., Yazdani, A., & Zhang, S.-C. *Phys. Rev. Lett.* **93**, 187002 (2004).
- 17 Pépin, C., de Carvalho, V. S., Kloss, T. & Montiel, X. *Phys. Rev. B* **90**, 195207 (2014).
- 18 Freire, H., de Carvalho, V. S. & Pépin, C.. *Phys. Rev. B* **92**, 045132 (2015).
- 19 Wang, Y. & Chubukov, A. *Phys. Rev. B* **90**, 035149 (2014).
- 20 Wang, Y., Agterberg, D. F. & Chubukov, A. *Phys. Rev. Lett.* **114**, 197001 (2015).
- 21 Bernhard, C. *et al*. *Phys. Rev. Lett.* **77**, 2304 (1996).
- 22 Nachumi, B. *et al*. Muon spin relaxation studies of Zn-substitution effects in cuprate high-Tc superconductors. *Phys. Rev. Lett.* **77**, 5421 (1996).
- 23 Dagotto, E. *Rev. Mod. Phys.* **66**, 763 (1994).
- 24 Georges, A., Kotliar, G., Krauth, W. & Rozenberg, M. J. *Rev. Mod. Phys.* **68**, 13 (1996).
- 25 Paglione, J. & Greene, R. L. *Nat. Phys.* **6**, 645–658 (2010).
- 26 Wang, F. & Lee, D. H. *Science* **332**, 200-204 (2011).
- 27 Haule, K. & Kotliar, G. *New J. Phys.* **11** 025021 (2009).
- 28 Yin, Z. P., Haule, K., & Kotliar, G. *Kinetic Nat. Mater.* **10**, 932-935 (2011).
- 29 de'Medici, L., Mravlje, J., & Georges, *Phys. Rev. Lett.*, **107**, 256401 (2011).
- 30 Lanata, N. *et al*. *Phys. Rev. B*, **87**(4), 045122 (2013).
- 31 Georges, A., de'Medici, L., & Mravlje, J. *Annu. Rev. Condens. Matter Phys.* **4**, 137-178 (2013).
- 32 de' Medici, L., Giovannetti, G. & Capone, M. *Phys. Rev. Lett.* **112**, 177001 (2014).
- 33 L. Fanfarillo and E. Bascones, *Phys. Rev. B* **92**, 075136 (2015).
- 34 de' Medici, L. & Capone, M. *The Iron Pnictide Superconductors*. Springer Series in Solid-State Sciences, vol. **186**, Springer, Cham (2017).
- 35 Amplifying Scientific Discovery with Machine Learning, *Science* **346**, 171 (2014)

-
- 36 How Machine Learning is Changing How We Do Science, doi:10.1126/science.aan7049 (2017)
 - 37 K. Fujita *et al*, *Spectroscopic Imaging STM: Strongly Correlated Systems - Experimental Techniques* pp 73-100. Springer (2014)
 - 38 G. Carleo and M. Troyer, *Science* 355, 602 (2017).
 - 39 J. Carrasquilla and R. G. Melko, *Nature Physics* 13, 431(2017).
 - 40 E. P. L. van Nieuwenburg, Y.-H. Liu, and S. D. Huber, *Nature Physics* 13, 435439 (2017).
 - 41 P. Broecker, J. Carrasquilla, R. G. Melko, and S. Trebst, *Scientific Reports* 7, 8823 (2017).
 - 42 E.M. Stoudenmire and D.J. Schwab, *Advances in Neural Information Processing (NIPS)* 29, 4799 (2016).
 - 43 Giacomo Torlai and Roger G. Melko, *Phys. Rev. Lett.* 119, 030501 (2017).
 - 44 Lei Wang, *Phys. Rev. B*, 94, 195105 (2016).
 - 45 Yi Zhang and E.-A. Kim, *Phys. Rev. Lett.* 118, 216401 (2017).
 - 46 D.-L. Deng, X. Li, and S. Das Sarma, *Phys. Rev. X* 7,021021 (2017).
 - 47 K. Ch'ng, J. Carrasquilla, R. G. Melko, and E. Khatami, *Phys. Rev. X* 7, 031038 (2017).
 - 48 G. Torlai, G. Mazzola, J. Carrasquilla, M. Troyer, R. Melko, G. Carleo, *Nature Physics* 14, 447 (2018).
 - 49 F. Schindler, N. Regnault, and T. Neupert, *Phys. Rev.*B95, 245134 (2017).
 - 50 S. A. Kivelson, E. Fradkin, V. J. Emery, *Nature* **393**, 550 (1998).

Spin Physics and Nanoscale Probes of Quantum Materials

David Goldhaber-Gordon¹, Marc Kastner², Hari C. Manoharan¹, Joseph Orenstein³, Shoucheng Zhang¹

¹ *Stanford Institute for Materials and Energy Sciences, SLAC National Accelerator Laboratory & Department of Physics, Stanford University;* ³ *Science Philanthropy Alliance, Palo Alto, CA;* ² *Lawrence Berkeley National Laboratory & Department of Physics, University of California, Berkeley*

Program Scope

The Spin Physics and Nanoscale Probes of Quantum Matter FWP, co-located at SIMES/SLAC and LBNL, has the vision of assembling a world-class collaboration to fabricate and characterize material systems, in which electron spin plays an essential role in giving rise to emergent phenomena, such as topological order and exotic quasiparticles. In particular, the FWP focuses on the discovery of new states of quantum matter and novel physical effects associated with spin, isospin, and electronic degrees of freedom. The overarching goal of the research team is to observe and manipulate these quantum states at microscopic to mesoscopic scales, and to use the resulting insights to design and identify transformative quantum materials with tailored functionality.

Recent Progress

Spin liquids. The transition metal trihalide, α - RuCl_3 , is under intense scrutiny as a potential realization of a Kitaev spin liquid (KSL) under application of a large in-plane magnetic field. Orenstein has made the first measurements of α - RuCl_3 's low-energy magnetic fluctuation spectrum by time-domain THz spectroscopy [1]. The THz spectra showed that the spectral weight of any magnetic continuum – expected for a spin liquid – is significantly smaller than the $Q=0$ spin wave, which remains a well-defined mode even approaching the loss of magnetic order at 7 tesla. These results implied that the transition at 7 tesla could not be interpreted simply as a transition from zig-zag order to KSL: a more complex picture, in which the transition proceeds through other ordered phases, and eventually to a topologically ordered spin liquid, remain as exciting possibilities. In further work (Fig. 1), Orenstein and Goldhaber-Gordon showed that linear spin wave theory can be used to understand the detailed structure of the THz spectra below the Neel temperature, leading to significant revision of the widely-accepted spin Hamiltonian parameters and revealing details of the magnetic field dependence of zig-zag magnetic order [2].

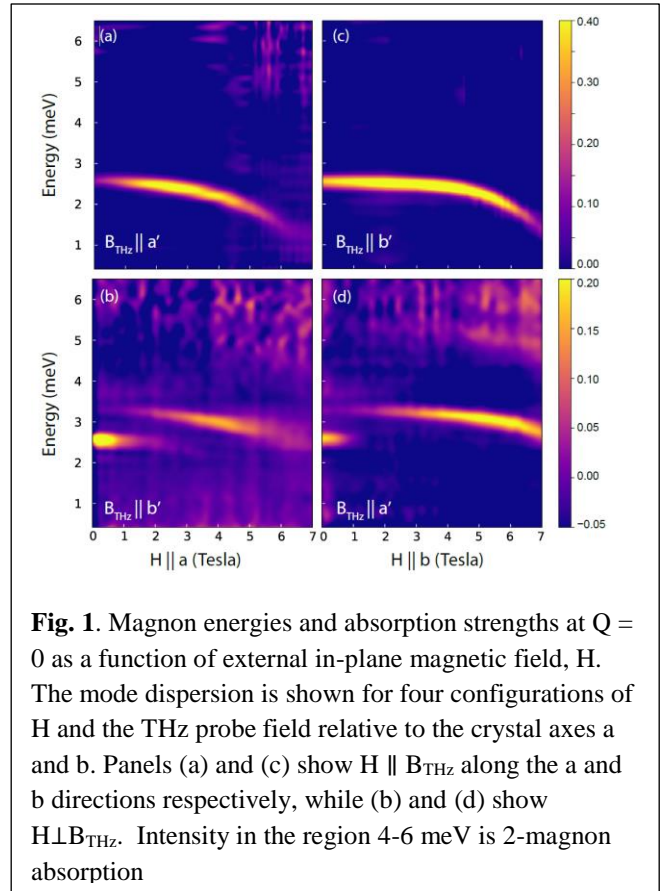


Fig. 1. Magnon energies and absorption strengths at $Q = 0$ as a function of external in-plane magnetic field, H . The mode dispersion is shown for four configurations of H and the THz probe field relative to the crystal axes a and b . Panels (a) and (c) show $H \parallel B_{\text{THz}}$ along the a and b directions respectively, while (b) and (d) show $H \perp B_{\text{THz}}$. Intensity in the region 4-6 meV is 2-magnon absorption

Magnetic topological insulators. When the Fermi level lies in the surface state gap of a thin-film magnetic topological insulator, the absence of available states for backscattering should lead to chiral, dissipationless conduction characterized by Hall resistance quantized to h/e^2 and vanishing longitudinal resistivity, with possible technological applications from low-energy-dissipation electronics to metrology. Goldhaber-Gordon collaborated with researchers at NIST to observe the Hall resistance to be quantized to h/e^2 within 2 parts in 10^7 , with zero external magnetic field [3], showing potential for practical resistance standards if dissipation can be made even less sensitive to temperature; we have made progress in identifying the source of dissipation, offering hope for reducing it. Goldhaber-Gordon also demonstrated that the chiral edge states need not run only along the edge of the film but rather can flow along induced magnetic domain boundaries. Using the Meissner screening of a superconducting Nb pellet placed above an MTI device, we applied a spatially varying magnetic field to create a non-uniform magnetization in the MTI film (Fig. 2). We confirmed the prediction that domain walls host a pair of co-propagating 1D chiral conduction channels [4].

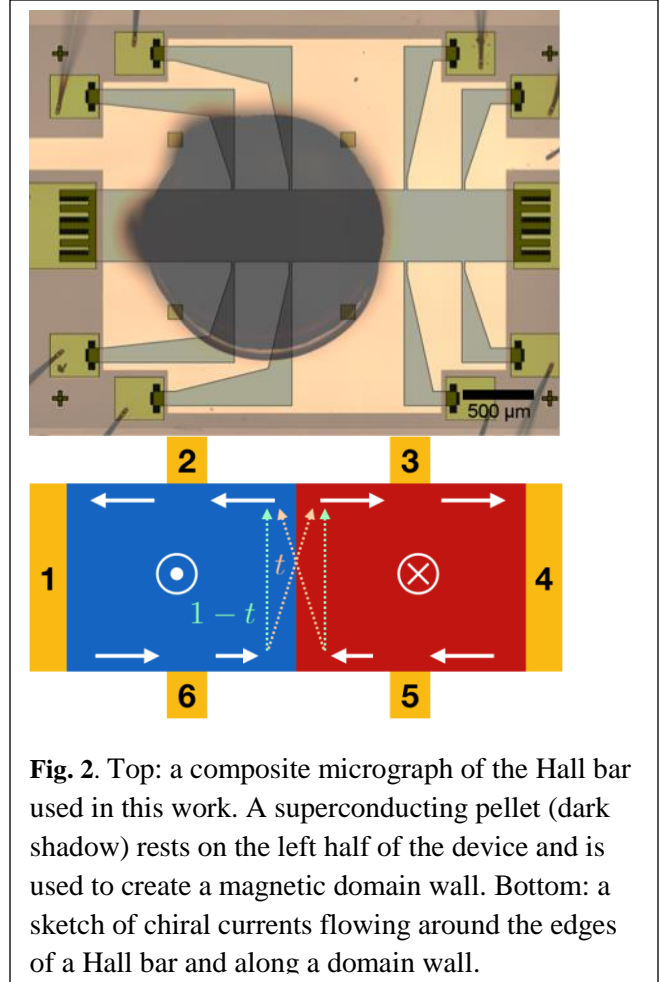


Fig. 2. Top: a composite micrograph of the Hall bar used in this work. A superconducting pellet (dark shadow) rests on the left half of the device and is used to create a magnetic domain wall. Bottom: a sketch of chiral currents flowing around the edges of a Hall bar and along a domain wall.

Researchers in Kang Wang’s group at UCLA in collaboration with Zhang recently observed a signature half-integer resistance plateau in a strip of magnetic topological insulator with a central region covered by a superconductor to make a topological superconductor, a possible experimental realization of a chiral Majorana mode [5].

Following this work, Zhang investigated the possibility of using chiral Majoranas for topological quantum computation. Though other proposals for topological quantum computation have focused on the braiding of localized Majorana zero modes, Zhang showed the same unitary transformations could be implemented with propagating Majoranas, and proposed a specific structure for experimental tests.

Future Plans

Magnetic interactions are central to many phases of quantum matter, yet are largely unprobed at the single-spin level. We will study 2D materials and surface states, examining the correlation between strain, atomic defects, and electronic and magnetic structure. Orenstein will perform THz spectroscopy and time-resolved Kerr effect measurements on the same samples Manoharan probes by scanning tunneling spectroscopy, including 2D magnetic transition metal dichalcogenide semiconductors. We will also study arrays of local spins with and without

coupling to reservoirs. Manoharan will implement these with atomic manipulation while Goldhaber-Gordon will do so using semiconductor quantum dots, and the two will work with each other and with Kastner on experiments and analysis.

We will spatially pattern phases of magnetic topological insulators, notably the quantum anomalous Hall phase and the recently discovered phase dubbed the “axion insulator,” and infer current flow patterns by mapping where potential drops in these heterogeneous systems. Goldhaber-Gordon will pattern samples and measure transport. Manoharan and Goldhaber-Gordon will perform novel scanning probe microscopy on these same samples. Orenstein will perform Kerr microscopy to map magnetization patterns and correlate them with potential drops measured with those other techniques. Kastner will work with the other investigators to plan, guide, and interpret experiments.

We will aim to detect exotic and robust quasiparticles at the interface between a superconductor and a topologically ordered state. Manoharan will use a tip to locally induce superconductivity into topological ground states, deducing the nature and strength of the coupling from tunneling spectroscopy; he will apply this both to unpatterned topological films and crystals, and near edges of films patterned by Goldhaber-Gordon. Goldhaber-Gordon will also nanopattern electrodes to locally induce superconductivity; Manoharan will perform scanning tunneling spectroscopy on these hybrid structures, at varied distances from the interface.

Goldhaber-Gordon, Kastner and Orenstein will measure photoconductivity in α - RuCl_3 , and Goldhaber-Gordon and Kastner will aim to induce metallic conduction by gating and will study resulting chemical modifications of the material in operando using NEXAFS at SSRL. Manoharan will use AFM to explore atomic-scale defects. Goldhaber-Gordon and Manoharan will measure inelastic tunneling through atomically-thin exfoliated layers. Goldhaber-Gordon and Kastner will aim to study magnetism in insulators arising from twisted bilayer graphene, which also connects to topological magnetic phases.

References

1. A. Little, Liang Wu, P. Lampen-Kelley, A. Banerjee, S. Patankar, D. Rees, C. A. Bridges, J.-Q. Yan, D. Mandrus, S. E. Nagler, and J. Orenstein, *Antiferromagnetic Resonance and Terahertz Continuum in α - RuCl_3* , Phys. Rev. Lett. **119**, 227201 (2017).
2. L. Wu, A. Little, E. E. Aldape, D. Rees, E. Thewalt, P. Lampen-Kelley, A. Banerjee, C. A. Bridges, J. Yan, S. Patankar, D. Goldhaber-Gordon, D. Mandrus, S. E. Nagler, E. Altman, J. Orenstein, *Field evolution of magnons in α - RuCl_3 by high-resolution polarized terahertz spectroscopy*, arXiv:1806.00855 (2018).
3. I. T. Rosen, E. J. Fox, X. Kou, L. Pan, K. L. Wang, D. Goldhaber-Gordon, *Chiral transport along magnetic domain walls in the quantum anomalous Hall effect*, NPJ Quantum Mater. **2**, 69 (2017).
4. E. J. Fox, I. T. Rosen, Yanfei Yang, George R. Jones, Randolph E. Elmquist, Xufeng Kou, Lei Pan, Kang L. Wang, D. Goldhaber-Gordon, *Part-per-million quantization and current-induced breakdown of the quantum anomalous Hall effect*, Phys. Rev. B **98**, 075145 (2018).
5. Q.L. He, L. Pan, A.L. Stern, E. Burks, X. Che, G. Yin, J. Wang, B. Lian, Q. Zhou, E.S. Choi, K. Murata, X. Kou, T. Nie, Q. Shao, Y. Fan, S.-C. Zhang, K. Liu, J. Xia, K.L. Wang, *Chiral Majorana fermion modes in a quantum anomalous Hall insulator-superconductor structure*, Science **357**, 294 (2017).

Publications

1. A. Little, Liang Wu, P. Lampen-Kelley, A. Banerjee, S. Patankar, D. Rees, C. A. Bridges, J.-Q. Yan, D. Mandrus, S. E. Nagler, and J. Orenstein, *Antiferromagnetic Resonance and Terahertz Continuum in α - RuCl_3* , Phys. Rev. Lett. **119**, 227201 (2017).
2. A. C. Mahoney, J. Colless, L. Peeters, S. J. Pauka, E. J. Fox, X. Kou, Lei Pan, K. L. Wang, D. Goldhaber-Gordon, D. J. Reilly, *Zero-field edge plasmons in a magnetic topological insulator*, Nat. Commun. **8**, 1836 (2017).
3. M. R. Calvo, F. de Juan, R. Ijan, E. J. Fox, A. J. Bestwick, M. Muehlbauer, J. Wang, C. Ames, P. Leubner, C. Bruene, S.C. Zhang, H. Buhmann, L. W. Molenkamp, D. Goldhaber-Gordon, *Interplay of Chiral and Helical States in a Quantum Spin Hall Insulator Lateral Junction*, Phys. Rev. Lett. **119**, 226401 (2017).
4. I. T. Rosen, E. J. Fox, X. Kou, L. Pan, K. L. Wang, D. Goldhaber-Gordon, *Chiral transport along magnetic domain walls in the quantum anomalous Hall effect*, NPJ Quantum Mater. **2**, 69 (2017).
5. E. J. Fox, I. T. Rosen, Yanfei Yang, George R. Jones, Randolph E. Elmquist, Xufeng Kou, Lei Pan, Kang L. Wang, D. Goldhaber-Gordon, *Part-per-million quantization and current-induced breakdown of the quantum anomalous Hall effect*, Phys. Rev. B **98**, 075145 (2018).
6. C. Parra, T.H.R. da Cunha, A.W. Contryman, D. Kong, F. Montero-Silva, P.H.R. Gonçalves, D.D. Dos Reis, P. Giraldo-Gallo, R. Segura, F. Olivare, F. Niestemski, Y. Cui, R. Magalhaes-Paniago, H.C. Manoharan, *Phase Separation of Dirac Electrons in Topological Insulators at the Spatial Limit*, Nano Lett., **17**, 97-103 (2017).
7. P. Tang, Q. Zhou, G. Xu, S.-C. Zhang, *Dirac Fermions in an Antiferromagnetic Semimetal*, Nat. Phys. **12**, 1100 (2016).
8. C.-X. Liu, S.-C. Zhang and X.-L. Qi, *The Quantum Anomalous Hall Effect: Theory and Experiment*, Annu. Rev. Condens. Matter Phys. **7**, 301-321 (2016).
9. M. Guo, Z. Wang, Y. Xu, H. Huang, Y. Zang, C. Liu, W. Duan, Z. Gan, S.-C. Zhang, K. He, *Tuning thermo-electricity in a Bi_2Se_3 topological insulator via varied film thickness*, New J. Phys. **18**, 015008 (2016).
10. J. Wang, B. Lian, S.-C. Zhang, *Dynamical axion field in a magnetic topological insulator superlattice*, Phys. Rev. B **93**, 045115 (2016).

Charge and spin behavior in ferroics

Myung-Geun Han, Joe Garlow, and Yimei Zhu
Department of Condensed Matter Physics and Materials Science
Brookhaven National Laboratory, Upton, NY 11973

Research Scope

The focus of this research task under the FWP Number MA-015-MACA is to study charge-spin-lattice interactions at relevant time and length scales in advanced multiferroics under external stimuli to unveil the underlying physical principles that control emergent macroscopic functionalities. The research areas include (i) intriguing electronic or magnetic phenomena at domain walls and interfaces, and (ii) understanding topological natures and switching of ferroelectric and ferromagnetic textures under external stimuli. We combine *in situ* electron microscopy with synchrotron X-ray scattering to study dynamics of topological defects across phase transitions, induced by electric/magnetic fields and cooling/heating.

Recent Progress

In the last two years, we have mainly focused on topological defects and their roles in ferroelectric materials and polarization-lattice interactions at ferroelectric/correlated oxide interfaces and their field effects using novel *in situ* TEM methods.

Linear alignment of topological vortex domains in hexagonal manganites

Nanoscale topological defects, such as vortices and skyrmions in ferroic systems, have been intensively investigated due to their intriguing properties and behaviors [1-2]. In addition to harnessing and tuning their functionalities, spatial manipulation and control of topological defects as functional elements are important for quantum information science. We report linear alignment behavior of single-chiral vortices observed in thin multiferroic hexagonal manganites during *in situ* heating experiment [3]. In order to avoid chemical degradation during high-temperature heating in vacuum, we have utilized a rapid heating and quenching by novel *in situ* electric arcing. Using atomic resolution electron microscopy and phase-field simulation, we found that vortices and antivortices formed near the phase transition temperature are pulled out in the opposite directions by mechanical

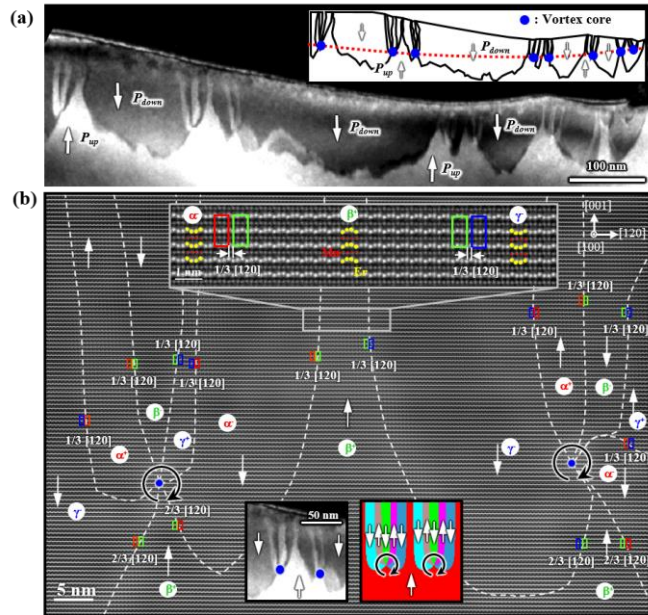


Fig. 1. (a) Dark-field TEM image showing vortices lined up after *in situ* electric arc heating. (b) STEM images showing two neighboring vortices with the same chirality, determined by the separation of unit cells across each domain wall (see the top inset). Bottom insets compare experiment (left) and simulation (right).

strain to leave single-chiral vortices linearly aligned along an isothermal line formed during quenching (Fig. 1). Our study provides new insight into spatial manipulation of the topological defects in oxide multiferroics by interrogating far-equilibrium dynamics of symmetry breaking continuous phase transitions.

Tuning correlated electrons using ferroelectric polarization

Rich correlated-electron physics in nickelates, including metal-insulator transition, charge and magnetic ordering, is due to intimate competition among electronic bandwidth, on-site Coulomb repulsion, charge transfer energy, and a wide range of structural variants [4]. Recently successful growth of ultrathin films of RENiO_3 (RE = La, Pr, Nd, etc.) on various substrates with atomic precision provides additional tuning parameters via strain engineering [5]. Pursuing an understanding and controlling of the interplay between structural distortions and electronic correlations in nickelates, in collaboration with C. Ahn at Yale University, we investigated ferroelectric $\text{PbZr}_{0.2}\text{Ti}_{0.8}\text{O}_3$ (PZT)/ LaNiO_3 (LNO,

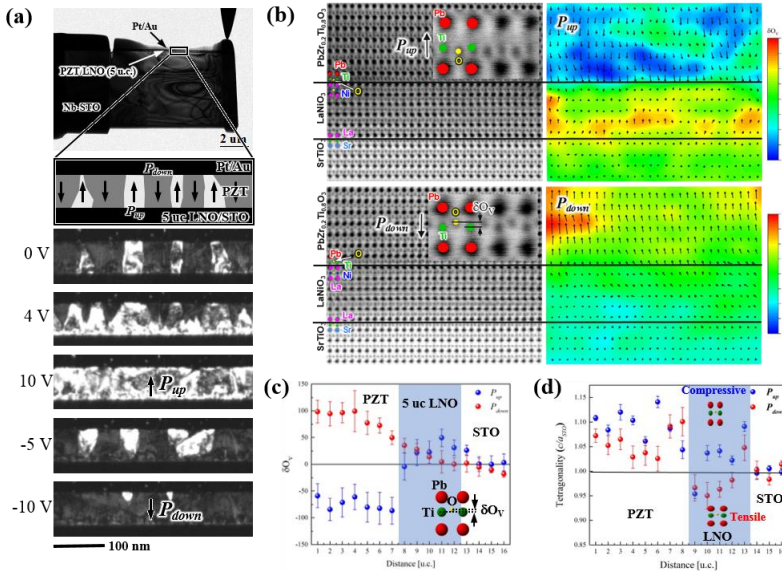


Fig. 2. *In situ* domain switching and interfacial atomic structures at PZT/LNO interface. (a) TEM and dark-field TEM images showing in situ domain switching in PZT thin films. (b) Annular bright-field STEM images from the areas with downwards (P_{down}) and upwards (P_{up}) polarizations and oxygen displacements maps. (c) Profiles of oxygen displacements and (d) tetragonalities across the interface.

domain growth for P_{down} is controlled by slow motion of neutral domain walls in contrast to P_{up} growth mainly controlled by head-to-head domain wall motion. Atomic resolution images taken from areas with P_{up} and P_{down} at the interface show distinctive atomic structures in ultrathin LNO (oxygen displacements and strains), as shown in Fig. 2(b-d), providing an important insight into the question on how structural distortions related to polarization across interfaces under various strain conditions affect the overall electronic and magnetic properties of the ultrathin nickelates.

Future Plan

Expanding our study on charge-spin-lattice interactions to quantum regimes, we will study topological charge and spin textures and their emergent phenomena under magnetic

5 unit cell) heterostructures grown on (001) plane of SrTiO_3 substrate using *in situ* electrical biasing and atomic resolution imaging and spectroscopy [6]. Two distinct polarization states at PZT/LNO interface were induced by *in situ* electric biasing, as shown in Fig. 2(a). The presence of metallic LNO layer ensures uniform bidirectional bias fields within the PZT film, enabling complete domain switching from upwards (P_{up}) to downwards (P_{down}) polarization and vice versa. We found that due to NiO_2 termination the

and/or electric fields at low temperatures. To elucidate spin-charge-lattice interplays, we combine TEM and X-ray scattering with development of instruments and methods.

Skyrmion dynamics and their electric field control in multiferroic Cu_2OSeO_3

Skyrmions are nanoscale magnetic quasiparticles that offer tremendous potential in spintronic-based applications. However, controlled skyrmion manipulation including its creation and annihilation remains an important challenge towards not only practical applications, but also for the full exploitation of their functional properties. We will systematically study skyrmion dynamics in insulating Cu_2OSeO_3 and their collective control by external electric fields by combining momentum- (X-ray scattering) and real-space (Lorentz TEM and off-axis electron holography) observations. With the

development of time-resolved *in situ* electrical biasing capability, electric field control of skyrmions will be correlatively studied to shed new light on the skyrmion dynamics and their manipulation. In our preliminary study in collaboration with Jan Seidel (UNSW, Australia), using liquid-helium cooling holder we have observed helical-skyrmion phase transitions as function of temperature, magnetic field, Te-doping, and TEM sample thickness (Fig. 3). In collaboration with Claudio Mazzoli and Valentina Bisogni (NLS II, BNL), X-ray photon correlation spectroscopy (XPCS) in transmission geometry will be performed on the same TEM samples used for Lorentz TEM for direct comparison. With sufficient elastic signals of skyrmion lattice,

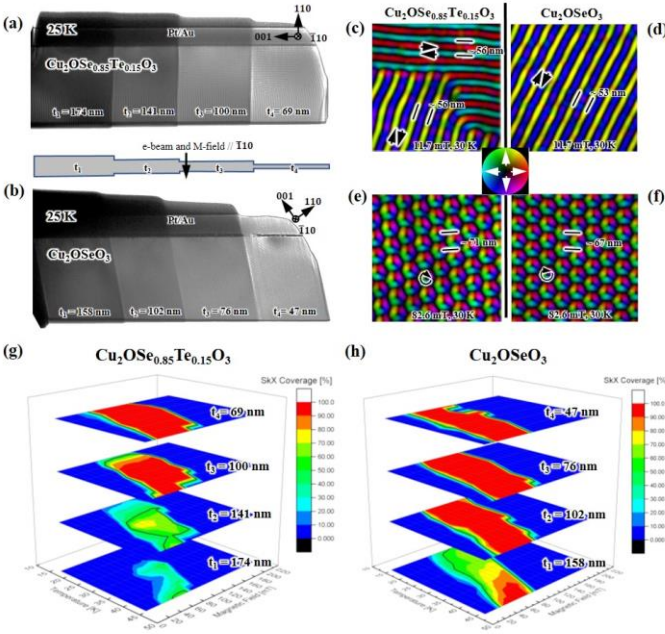


Fig. 3. Cryo-Lorentz imaging of undoped and Te-doped Cu_2OSeO_3 with four-thickness sections prepared by focused-ion-beam. Magnetization maps reconstructed by the transport-intensity-equation method for Te-doped (c and e) and undoped (d and f) samples. Magnetic field (H) vs. temperature (T) phase diagrams of skyrmions (g and h). The black solid lines represent 50 % of skyrmion coverage.

~ 10 msec of temporal resolution can be achieved in XPCS and Lorentz TEM. Ultimately, we aim to perform external electric field control of skyrmion lattices using both TEM and X-ray scattering. We have developed a custom-made TEM sample cartridge that allows electrical connections to FIB-prepared TEM samples at liquid-helium cooling temperature. This TEM sample cartridge with attached macroscale electrodes can be also used for XPCS for electric field control experiments. The outcome from this correlative study will provide detailed understanding of skyrmion dynamics towards collective skyrmion control in future skyrmionics for quantum information science.

References

[1] Huang, F.-T. and Cheong, S.-W., Nat. Rev. Mater. 2, 17004 (2017).

- [2] Nagaosa, N. and Tokura, Y., *Nat. Nanotech.* 8, 899-911 (2013).
- [3] Han, M.-G., *et al.*, *Phys. Rev. Mater.* 2, 064004 (2018).
- [4] Catalano, S., *et al.*, *Rep. Prog. Phys.* 81, 046501 (2018).
- [5] King, P.D.C., *et al.*, *Nat. Nanotech.* 9, 443-447 (2014).
- [6] Han, M.-G., *et al.*, in preparation (2018).

Publications

1. Dong, Z., Zhao, H., DiMarzio, D., Han, M.-G., Zhang, L., Tice, J., Wang, H., and Guo, J. “Atomically thin CBRAM enabled by 2D materials: Scaling behaviors and performance limits”, *IEEE Transactions on Electron Devices*, 99, 1-7 (2018).
2. Han, M.-G., Li, J., Xue, F., Wang, X., Meng, Q.-P., Tao, J., Chen, L.-Q., Cheong, S.-W., and Zhu, Y., “Linearly aligned single-chiral vortices in hexagonal manganites by *in situ* electric arc heating”, *Physical Review Materials* 2, 064004 (2018).
3. Cheng, S., Xu, C., Deng, S., Han, M.-G., Bao, S., Ma, J., Nan, C., Duan, W., Bellaiche, L., Zhu, Y., and Zhu, J., “Interface reconstruction with emerging charge ordering in hexagonal manganite”, *Science Advances* 4, eaar4298 (2018).
4. Kim, J.*, Han, M.-G.*, Lien, M.-B.*, Magonov, S., Zhu, Y., Ferguson, H. J., Norris, T., and Kotov, N. A., “Hidden electrostatic asymmetry of gold nanorods” *Science Advances*, 4, e1700682 (2018). *equally contributing authors
5. Bae, I.-T., Ichinose, T., Han, M.-G., Zhu, Y., Yasui, S., and Naganuma, H., “Tensile stress effect on epitaxial BiFeO₃ thin film grown on KTaO₃” *Scientific Reports*, 8, 893 (2018).
6. Zhao, H., Dong, Z., Tian, H., Dimarzio, D., Han, M.-G., Zhang, L., Yang, X., Liu, F., Shen, L., Han, S.-J., Cronin, S., Wu, W., Tice, J., Guo, J., and Wang, H., “Atomically thin femtojoule memristive device”, *Advanced Materials* 1703232, 29 (2017).
7. Lien, M.-B., Kim, J., Han, M.-G., Chang, Y.-C., Chang, Y.-C., Ferguson, H. J., Zhu, Y., Schotland, J. C., Kotov, N. A., and Norris, T. B., “Optical asymmetry and nonlinear light scattering from gold nanorods”, *ACS Nano* 11, 5925-5932 (2017).
8. McBean, C. L., Lewis, C. S., Tiano, A. L., Simonson, J. W., Han, M.-G., Gannon, W., Yue, S., Patete, J. M., Corrao, A., Santulli, A. C., Wu, L., Aronson, M. C., Zhu, Y., and Wong, S. S., “A Generalizable multi-gram synthesis and mechanistic investigation of YMnO₃ nanoplates”, *Industrial & Engineering Chemistry Research*, 56, 5573-5585 (2017).
9. Cheng, S., Li, J., Han, M.G., Deng, S., Tan, G., Zhang, X., Zhu, J., and Zhu, Y., “Topologically allowed non-six-fold vortices in a six-fold multiferroic material: Observation and classification”, *Physical Review Letters* 118, 145501 (2017).
10. Han, M.-G., Garlow, J. A., Marshall, M. S. J., Tiano, A. L., Wong, S. S., Cheong, S.-W., Walker, F. J., Ahn, C. H., and Zhu, Y., “Electron-beam-induced-current and active secondary-electron voltage contrast with aberration-corrected electron probes”, *Ultramicroscopy* 177, 14-19 (2017).
11. Kornblum, L., Fenning, D. P., Faucher, J., Hwang, J., Boni, A., Han, M. G., Morales-Acosta, M. D., Zhu, Y., Altman, E. I., Lee, M. L., Ahn, C. H., Walker, F. J., and Shao-Horn, Y., “Solar Hydrogen Production Using Epitaxial SrTiO₃ on a GaAs Photovoltaic”, *Energy & Environmental Science* 10, 377 (2017).

Atomic and Mesoscopic Phenomena in Quantum Systems with Broken Translational Symmetry

S.V. Kalinin, M.F. Chisholm, A.R. Lupini, C.T. Nelson, and M.P. Oxley

Oak Ridge National Laboratory, Oak Ridge, TN 37831

Research Scope

Quantum phenomena emerge from the interplay between the discrete atomic lattice and the continuous character of electronic wavefunctions, often giving rise to complex electronic phenomena that span atomic to mesoscopic scales. Understanding and ultimately designing quantum materials necessitates the detailed knowledge of local atomic structures and chemical states of individual atoms, as well as their effect on local- and mesoscale electronic functionalities. The overarching goal of this proposal is to build a comprehensive picture of the physics and chemistry of quantum materials on the level of individual atomic and structural units, through harnessing recent advances in Scanning Transmission Electron Microscopy (STEM) and associated spectroscopic techniques, and to link it to the mesoscopic quantum functionalities. This goal will be achieved through three specific aims: (1) exploring the static and dynamic structure-property relationships and quantum phenomena on the atomic level, (2) establishing the link between atomistic and mesoscale mechanisms in quantum systems and (3) developing novel probes of local electronic and quantum behaviors. These three goals are synergistically combined to maximize the immediate physics impact from extant STEM instrumentation and to guide the development of imaging tools towards acute physics problems. We will aim to enable full information capture in STEM, develop correlative libraries of structure property relationships on the atomic level, and use these for physics-based models. This effort will be complemented by modelling workflows that establish the potential signatures and enable quantification of quantum phenomena from STEM data. This will enable predictive modelling and development of quantum materials and devices.

Recent Progress

In the previous funding period (FY15-18) the project was led by M. Chisholm, and focused on the exploration of structure-property relationships in materials using high-resolution Scanning Transmission Electron Microscopy (STEM) and Electron Energy Loss Spectroscopy (EELS). In the current period (FY19-21), the project will be led by Sergei V. Kalinin. In this abstract, we discuss the work on applications of big data, machine learning, and artificial intelligence techniques for exploring physics and chemistry of 2D materials and ferroics obtained under different DOE support but that led to the present proposal, including (a) probing

flexoelectric interactions via computer vision analysis of vortex domains in ferroics, (b) analysis of interaction parameters of solid solutions from atomically resolved images of compositional fluctuations, and (c) probing solid state chemistry transformation pathways in 2D solids on the level of individual point defects and defect clusters. These results are derived via the synergy of STEM imaging and deep learning applications, both at the stage of the feature extraction/image analysis, but more importantly as a universal tool to reveal the presence of physically-significant low dimensional latent variables, and establish the connection between generative models (Ising Hamiltonian, phase field model for known GLD free energy) and experimental data with multiple spatially-distributed degrees of freedom. The results obtained under this FWP, including development of theory of STEM-EELS and 4D STEM theory are reported in second abstract.

Flexoelectricity from atomically-resolved images:

Flexoelectricity is one of the most fascinating properties of ferroic systems, describing directly coupling between the strain gradients and electric polarization. On microscopic level, flexoelectric coupling strongly affects the structure and properties of topological defects such as domains walls, and can lead to the emergence of modulated phases. We demonstrated a computer vision-based approach that allowed us to systematically explore the shape of the ferroelectric vortices in multilayers, and develop theory matching algorithm that allowed direct matching to the phase field theory and extraction of the coefficient of flexoelectric tensor.ⁱ This approach is universally applicable for analysis of the mesoscopic physics of ferroic systems if the form of the corresponding GLD expansion is known or postulated and sufficiently rich topological defect populations are observed.

Interaction parameters from atomically-

resolved images of fluctuations: We pose that by studying the characteristic structural and chemical fluctuations that exist within a single chemical composition, we can infer the relevant interactions and produce a generative model that can predict properties over a range of scales in a finite region of the chemical and temperature space. We use the compositional and structural fluctuations in the quenched (static) system to build a generative model encoding the effective interactions in the system.ⁱⁱ Using the principles of statistical inference, we develop a framework for incorporating structural fluctuations into statistical mechanical models and use it to derive effective inter-atomic interactions driving segregation in a $\text{La}_{5/8}\text{Ca}_{3/8}\text{MnO}_3$. Variational

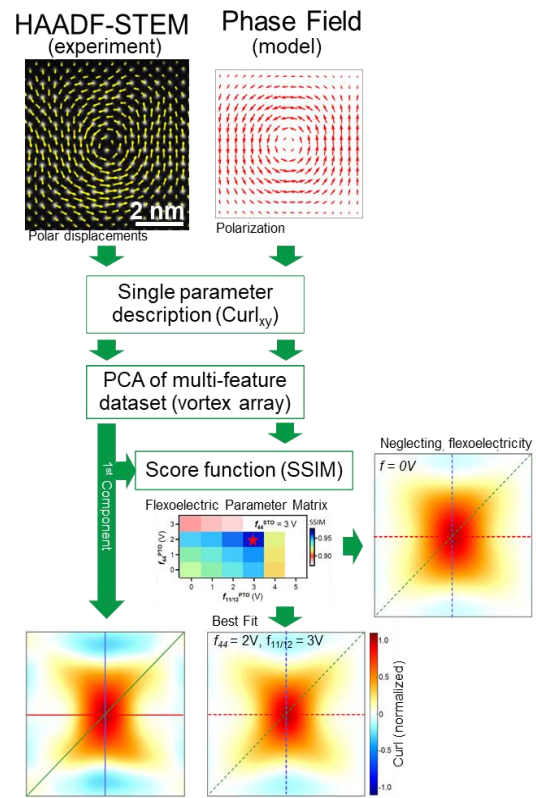


FIGURE 1. Machine learning of flexoelectric tensor from STEM data on ferroelectric vortices

autoencoder further allows to detect anomalous behaviors in the composition phase diagram. This study provides a framework for creating generative models from diverse data, including compositional fluctuation, structural distortions corresponding to frustrated and non-frustrated interactions, and their interactions.

Mapping solid state transformations pathways on a single-defect level: Functionalities of solids is underpinned by the point defect, their clusters, and extended defects, linked through the networks of solid state reactions. Here we utilize the fact that STEM of 2D materials allows visualization of (almost) all atomic species in real space, and that electron beam can be used to induce complex atomic transformations in these materials, open pathway to metastable defects states and allowing exploration of reaction mechanisms. We developed a deep learning approach that allows fully automated identification of individual atoms in STEM images, using theoretical or labeled images as a training set. We use this approach to construct reaction pathways for point defects in 2D materials, trace the structural evolution of atomic species during the electron beam manipulation, and create the library of defect configurations in Si- and vacancy doped graphene. In particular, we show that the diffusion coefficient of S vacancy and transformation of the $\text{Mo}_w - \text{S}_{\text{vac}}$ complex can be explored quantitatively and mapped on the Markov model, giving rise to the transition probabilities on single defect level.

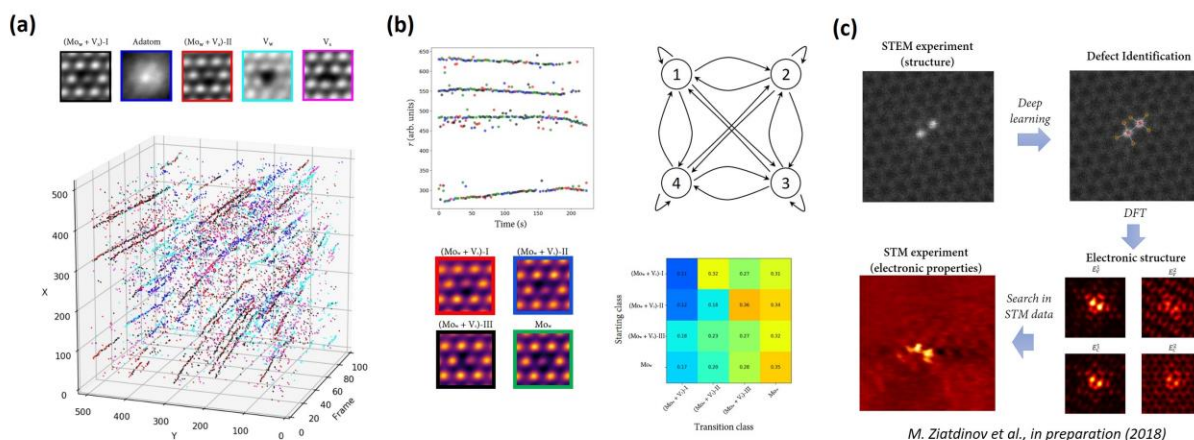


FIGURE 2. (a) Trajectories of single atomic defects in WS_2 material. (b) Markov analysis of transition probabilities for selected trajectories. (c) Construction of single defect libraries that allow to link together different atomically-resolved measurements.

Future plans: We aim to explore the emergent physics and chemistry in 2D materials and 3D materials with ferroic properties via combination of the STEM structural and spectral data augmented by big data and machine learning strategies to learn physically relevant information. Both for 2D and 3D systems, we aim to establish the nature of major building blocks and structural point and extended defects, creating the large-scale structure of the material. We will further build upon this picture to establish the nature of symmetry breaking distortions constituting the order parameter fields and their interaction with defects, surfaces, and interfaces,

revealing the nature of underlying pairwise interactions and collective phenomena driving materials functionality.

For 2D materials, we aim to create the comprehensive picture of the defect chemistry of 2D chalcogenides with the doping on the metal and chalcogen sublattice, explore the collective interactions between the dopants including cationic and anionic segregation, formation of defect pairs and nucleation of the extended defects. A similar approach will be used for layered MHal₃ systems, demonstrating complex Kitaev and spin liquid physicsⁱⁱⁱ The availability of EELS and high-resolution EELS on MAC STEM will further allow to tie this information with the local phonon behaviors.

For 3D ferroic oxides, one of the long-standing puzzles of systems with broken translational periodicity is the emergence of mesoscopic spatially inhomogeneous states, often spanning multiple length scales. We aim to understand these system, using the top-down approach based on the functional fit of mesoscopic solution for Ginzburg-Landau model for chosen materials symmetry onto STEM data, and bottom up approaches based on the use of variation autoencoder networks to establish latent variables underpinning the observations, and directly link them to order parameters.

Dynamic effects in ferroics. We aim to combine the structural analysis and modeling approaches above with direct property measurements using in-situ excitations. Specifically, applied electric fields induce highly non-linear electrical polarizations, phase-changes across morphotropic boundaries, and rearrangement of ferroelectric polarization topologies. These outcomes are accessible to STEM characterization, allowing coupling coefficients thereof to be determined, often quantitatively. We will also study the dynamic and steady-state response of complex ferroelectric topologies such as vortices and bubbles in thin film multilayers, where the extent of topological protection, chirality, and field coupling dynamics remains unknown.

DOE-sponsored publications 2015-2018 [117 refereed journal publications, including 15 in the *Nature* family; 2 in *Science*; 1 in *PRL*.; 10 in *ACS Nano*; 7 in *Nano Lett.*; and 5 in *Adv. Mat.*]

References

ⁱ Q. Li, C.T. Nelson, S.L. Hsu, A.R. Damodaran, L.L. Li, A.K. Yadav, M. McCarter, L.W. Martin, R. Ramesh, and S.V. Kalinin, *Quantification of flexoelectricity in PbTiO₃/SrTiO₃ superlattice polar vortices using machine learning and phase-field modeling*, Nat. Comm. **8**, 1468 (2017).

ⁱⁱ L. VLCEK, A. Maksov, M. Pan, R. VASUDEVAN, and S.V. KALININ, *Knowledge Extraction from Atomically Resolved Images*, ACS Nano, in print

ⁱⁱⁱ M. ZIATDINOV, A. BANERJEE, A. MAKSOV, T. BERLIJN, W. ZHOU, H.B. CAO, J.Q. YAN, C.A. BRIDGES, D.G. MANDRUS, S.E. NAGLER, A.P. BADDORF, and S.V. KALININ, *Atomic-scale observation of structural and electronic orders in the layered compound α -RuCl₃*, Nat. Comm. **7**, 13774 (2016).

Diffraction Imaging of Soft Matter with 4DSTEM

Andrew Minor, Kenneth Downing, Ronald Zuckermann, David Prendergast, Nitash Balsara
Materials Sciences Division, Lawrence Berkeley National Laboratory, Berkeley, CA 94720.

Research Scope

The goal of our program is to produce images of soft materials with atomic resolution using electron microscopy. The proposed work is inherently challenging because soft materials are unstable under the electron beam. Our work encompasses both cryogenic scanning transmission electron microscopy (cryo-STEM) and cryogenic transmission electron microscopy (cryo-EM). This abstract focuses on atomic resolution cryo-EM. This abstract focuses on diffraction imaging using scanning nanobeam electron diffraction, also known as 4DSTEM. We have used this technique to visualize and quantify the local nanostructure in systems such as semicrystalline polymers, organic molecular thin films and protein nanocrystals. The 4DSTEM method uses a scanning electron beam to raster across the sample and acquires a diffraction image at each probe position. This method can produce orientation maps that can quantify the size and distribution of nanoscale crystalline regions as well as reveal previously unknown structural features such as grains overlapping through the thickness of the thin film. More dramatically, it allows us to visualize the molecular chains and understand the continuity of the structure at high spatial resolution. Our recent results demonstrate the power of scanning electron nanobeam diffraction to provide insight into the structure of functional organic solids and show how structure-property relationships can be visualized in organic systems using techniques previously only available for hard materials such as metals and ceramics.

Recent Progress

The structure and morphology of any functional material can be directly correlated with its properties, including organic solids such as polymers and metal organic frameworks [1-3]. However, direct imaging using conventional electron microscopy methods to study structural ordering at the level of individual defects and nanoscale domains is not routine for organic solids or other soft materials in the same manner as it is for inorganic or hard materials such as metals and ceramics. This difficulty is typically due to the complex (and often hierarchical) internal structure in thin-films and the inherent sensitivity to electron beam induced damage in soft materials. Thus, new and more robust methods for systematically investigating structure are necessary. Towards this end, we have investigated the use of the 4D Scanning Electron Transmission Microscopy (4DSTEM) technique for the controlled, systematic, and facile investigation of nano-scale order in a hierarchal, organized soft matter systems.

Typical structural characterization techniques for soft materials provide data that is averaged and cannot provide a local map of the dispersion and relative orientation of molecules or crystallites within a local area. There are intrinsic and practical limitations to scanning probe microscopy and traditional TEM for providing quantitative information about the structure of polymer and small molecule systems on the nanometer scale such as the morphology, size, and mutual arrangement of the crystalline domains. The 4DSTEM technique can provide visualization and quantification of local structure on the order of a few nanometers [4], and our efforts here are focused on applying this technique to soft matter using a cryostage, high speed direct electron detector and custom algorithms to analyze the fleeting diffraction patterns from beam sensitive samples.

As one example, we have characterized the nanostructure and defects of a small molecule 7,7'- (4,4 - bis(2 - ethylhexyl) - 4*H* - silolo[3,2-*b*:4, 5-*b'*] dithiophene - 2,6 - diyl) bis(6 - fluoro - 4 - (5' - hexyl[2,2'-bithiophen] - 5 - yl)benzo[*c*][1,2,5] - thiadiazole), abbreviated as T1[5], under two different processing conditions using 4DSTEM. When the samples are processed using a small concentration of the co-solvent 1,8-diiodooctane (DIO), the morphology and functional properties are significantly changed. Two samples of the T1 molecule, one with DIO treatment (T1+DIO) and one without, were blade-coated and imaged using the 4DSTEM technique. The fragile nature of the samples' crystallinity under the electron beam presents a significant challenge, as do the relatively weak diffraction from the ordered domains. In order to reduce beam damage, the samples were cooled with liquid nitrogen and the acquisition parameters were empirically tuned to obtain the best diffraction signal possible; a step size of 10 nm was found to be the limit below which the beam started damaging the crystallinity of regions it had yet to sample, providing the spatial resolution limit for any image resulting from the data.

Figure 1 shows how the 4DSTEM method can extract previously unseen structural information about the small molecule thin film. The traditional high angle annular dark field (HAADF) images acquired during a standard capture (square images in Figures 1a and b) provide effectively no information about the film's structure. Likewise, virtual dark field reconstructions measuring the brightness of the amorphous halo (rectangular images in Figures 1a and b) do not provide any information that can be directly related to the properties of the material. In contrast, the 4DSTEM technique can reveal the underlying structure of the small molecule films by assigning every pixel of a raster scan to a specific in-plane crystal orientation or distribution of crystal orientations. Mapping the angle of orientation of the brightest diffraction spot pair for each probe location reveals the impact of DIO on the morphology of the polymer, as seen by comparing the grain morphology from Figures 1 c and d).

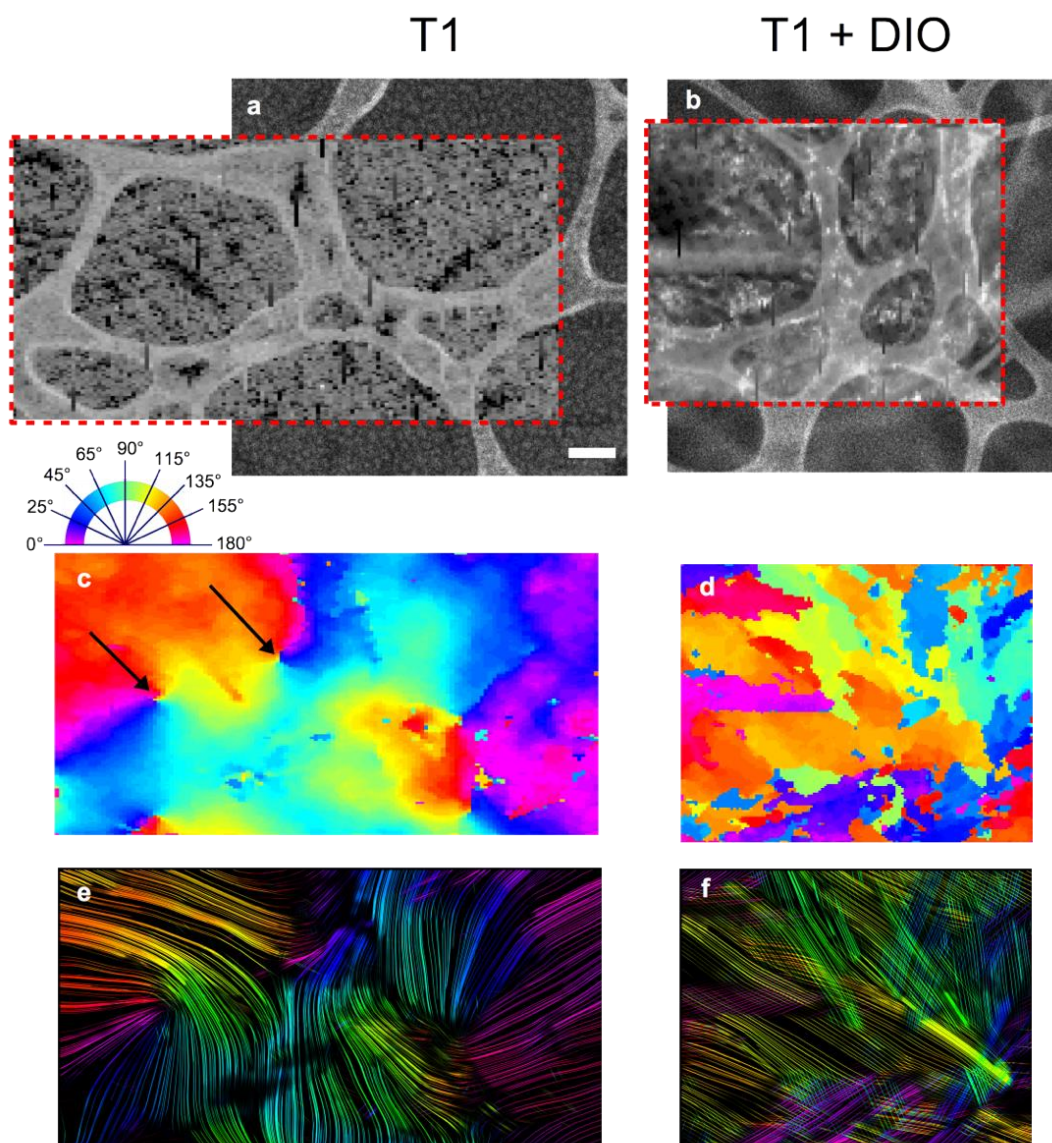


Figure 1. Comparison of grain morphology between samples drop cast with DIO (a, c, e) and without DIO (b, d, f). (a,b) The background HAADF images show few, if any, of the molecular film details; the web-like features are components of the supporting lacy carbon grid. Dotted lines represent the area over which the 4D-STEM scan was performed. Within the scan areas, a virtual dark field of the scattered amorphous signal reconstructed from the DPs is overlaid onto the HAADF. Vertical lines of dark pixels in the HAADF image are defects in the acquisition due to the fast scanning. The angle maps (c, d) show the orientation of the brightest reflection found on the DP at that location. Black arrows in c) indicate disclination discontinuities. Most noise within the maps is due to the bright scattered signal from the relatively thick carbon supports overwhelming the diffraction spots. Flow maps (e, f) show the continuity of lattice orientations in space, with the T1 sample demonstrating gradual lattice rotations while the T1+DIO sample shows rigid crystalline domains with significant overlap. Scale bar is 200 nm.

The DPs for the T1+DIO sample also exhibit several distinct lattice reflections at certain probe locations that persist over dozens of real space positions, providing demonstrative evidence that distinct crystalline domains overlap through the film thickness of this sample on the sample size of the probe. While it is not possible to determine the order of the grains along the beam direction (through the thickness of the film), the line plots presented in Figure 1e and f, visualized using flow line methods (often seen in fluid dynamics measurements), allows us to visualize the molecular chains and understand the continuity of the structure, as each lattice reflection found at (x, y) is represented by a line colored and oriented according to its lattice orientation angle θ . The lines in these drawings are oriented perpendicular to their reciprocal space reflections and align with what is believed to be the molecular long axis in real space. While the density of the lines is not indicative of the lattice spacing, their orientation and extent are a direct illustration of the local orientation of the lattice planes, also called the director field. These results demonstrate the ability to characterize the structure of soft materials with nanometer resolution using electron microscopy, and show how the arrangement of nanoscale domains and their coupling from nano-scale to mesoscale can be directly visualized for these types of materials systems.

Future Plans

The 4DSTEM method is straightforward in that the only criteria for the method to work is if the local structure of the sample represented by the diffraction patterns can be detected and analyzed. We intend to investigate the full parameter space of the technique to find the optimal conditions for soft matter, including systems with less crystallinity than those we have investigated so far. The challenge is to obtain sufficient signal/noise in the diffraction patterns such that a computer algorithm can find and identify the location of the spots with few errors. Fast direct electron detectors improve signal/noise by capturing the diffracted image before the damage adds noise. Therefore, as new and faster detectors are developed, including a planned 100kHz direct electron detector at LBNL, we believe this method has dramatically more potential to visualize and quantify the microstructure of soft matter at the nanoscale and below.

References

1. Van Krevelen, D. W. & Te Nijenhuis, K. *Properties of polymers: their correlation with chemical structure; their numerical estimation and prediction from additive group contributions*. (Elsevier, 2009).
2. Wilmer, C. E. *et al.* Large-scale screening of hypothetical metal–organic frameworks. *Nature Chemistry* **4**, 83 (2012).
3. Fratini, S., Ciuchi, S., Mayou, D., de Laissardière, G. T. & Troisi, A. “A map of high-mobility molecular semiconductors”. *Nature materials* **16**, 998 (2017).
4. C. Gammer, V. B. Ozdol, C.H. Liebscher, and A.M. Minor, “Diffraction Contrast Imaging Using Virtual Apertures”, *Ultramicroscopy*, **155**, p. 1-10 (2015)
5. Zhang, L. *et al.* Poly(3-butylthiophene) Inducing Crystallization of Small Molecule Donor for Enhanced Photovoltaic Performance. *The Journal of Physical Chemistry C* **119**, 23310-23318, doi:10.1021/acs.jpcc.5b04850 (2015).

Publications

1. Ouliana Panova, X. Chelsea Chen, Karen C. Bustillo, Colin Ophus, Mahesh P. Bhatt, Nitash Balsara, Andrew M. Minor, “Orientation mapping of semicrystalline polymers using scanning electron nanobeam diffraction”, *Micron*, 88, 30-36 (2016)
2. Lu Yan, Karen C Bustillo, Ouliana Panova, Andrew M Minor, Karen Winey, “Solution-Grown Crystals of Precise Acid- and Ion-Containing Polyethylenes”, *Polymer*, 135, 111-119 (2018)
3. Ouliana Panova, Christopher J. Takacs, Karen C. Bustillo, Colin Ophus, Nitash Balsara, and Andrew M. Minor, “Diffraction imaging of nanocrystalline structure in an organic semiconductor molecular thin film”, submitted

Atomic and Mesoscopic Phenomena in Quantum Systems with Broken Translational Symmetry

Principle Investigators: M. P. Oxley, A. R. Lupini, C. T. Nelson, M. F. Chisholm, S. V. Kalinin*

Materials Science & Technology Division, Oak Ridge National Laboratory, TN 37831

***Center for Nanophase Materials Sciences, Oak Ridge National Laboratory, TN 37831**

Research Scope

To directly image new quantum materials at high spatial resolution will require novel imaging and spectroscopic techniques. The overarching goal of this work is to harness recent advances in Scanning Transmission Electron Microscopy (STEM) and associated spectroscopic techniques to build a comprehensive picture of quantum materials on the level of individual atomic units, and link it to the mesoscopic functionalities.

4D STEM: Simulation and Quantification

Recent advances in camera technology have allowed the routine acquisition of convergent beam electron diffraction (CBED) patterns as a function of probe position. While traditional methods of utilizing such data sets, such as ptychography (a form of exit surface wave function reconstruction) and differential phase contrast (DPC), provide valuable insights into material structures, they largely fail to take advantage of the rich features contained within these data sets. Machine learning offers a potential path to routine analysis of these large, complex data sets. To achieve meaningful result in this way requires suitable large-scale training sets as input to these algorithms, and it is the role of simulation to provide this data. It is important that these simulations accurately reflect real world specimens and experimental parameters. Unlike STEM images, which can include modelling of spatial incoherence by applying a suitable source size blur after the calculation, CBEDs must be calculated on a suitably fine real space grid to allow correct incoherent addition of individual CBED patterns. Temporal incoherence also requires the summation over varying defocus values. In addition, since aberrations strongly affect the Ronchigram, the correct inclusion of residual aberrations is also necessary¹. Perhaps more important, the structure of the features within the CBED patterns are also sensitive to the scattering potential used by the simulation. We aim to construct scattering potentials based on electron densities obtained from density functional theory (DFT), and preliminary work has begun on this approach.

Recent Progress

4D STEM data results in large data sets which, while feature rich, are often difficult to interpret directly. This can be especially the case for data sets from two-dimensional materials such as graphene where the SNR and contrast are low. We have applied data-driven manifold

learning approaches to 4D data sets acquired from specimens of graphene with silicon impurities¹. These methods have clearly identified the main lattice as well as separating the two mirrored sub-lattices. More importantly, the presence of a four-fold bonded silicon impurity results in a “vacancy” in the resulting cluster maps, since it has a structure different to all other positions in the lattice.

An alternative approach is to use simulated data to train a deep learning (DL) algorithm and then use it to identify features in a data set. As part of a recent ORNL Lab Directed Research and Development artificial intelligence initiative, we have used DL to characterize a model interface between STO and LAO². Imaging based on annular dark field (ADF) or electron energy loss spectroscopy (EELS) are often used to infer if an interface is sharp or diffuse. Such an approach however has difficulty in determining the difference between a buried step at the interface or simple diffusion. We have used a modified version of the μ STEM package³, ported to run on ORNL’s supercomputers Titan and Summit. Using hundreds of simulations describing both cases, we are able to differentiate between these two possibilities. This work is currently being prepared for submission.

For simulation to become a useful tool for training DL algorithms, it needs to reflect the model structures as closely as possible. Most simulations are carried out using scattering potentials based on scattering factors from isolated, neutral atoms. Scattering potentials based on electron densities calculated from DFT provide a more realistic description of the local electric fields within the specimen. They can be obtained with little extra effort from DFT calculations of structures, which should be used to provide the basic structural input for image simulations. While traditionally calculated from all electron codes such as Wien2k, suitable electron densities can also be obtained from VASP, a pseudopotential code. Some early results of scattering potentials calculated from VASP electron densities are shown in figure 1.

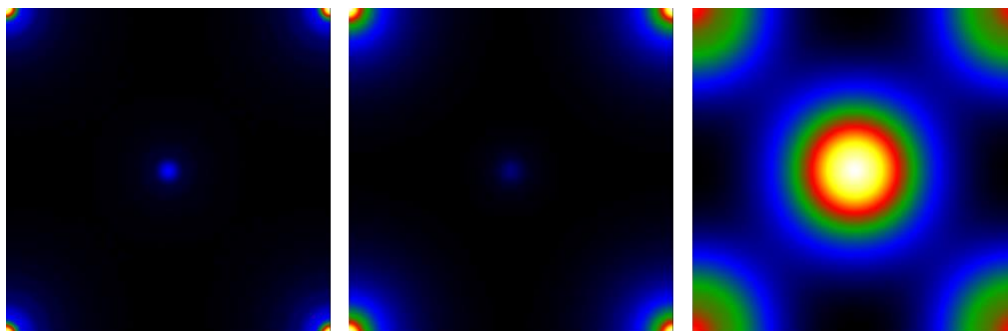


Figure 1: Elastic scattering potentials for 100 kV electrons incident on STO. The highly peaked potential for scattering from the nuclei is shown on the left. The scattering potentials for the core and valence electrons are shown in center and right panels respectively. Note that the color schemes of the electron potentials are inverted for clarity.

The scattering potentials due to the nuclei and core electrons are highly localized about the atomic positions. For a quantum excitation of phonons/frozen phonon calculation these potentials will be randomly moved. The more delocalized valence electron potential will be

blurred to account for average atomic motion, but otherwise held fixed. Due to convergence issues with real space calculations of the highly localized core electrons, it is proposed to calculate core electron densities using Dirac-Hartree-Fock calculations and parameterize the resulting scattering factors, similar to conventional methods.

Electron Energy Loss and Gain Spectroscopy: Nanoscale Temperature Measurement

Most methods to measure relevant physical parameters will depend on prior knowledge and previous calibrations of materials properties, which can be a problem in working with new or unknown materials. Recent demonstration of the ability to measure temperature at the nanoscale by looking at the plasmon response has prompted renewed interest in other methods to determine the local temperature. In collaboration with Dr. J.C. Idrobo of the ORNL user facility at CNMS we were able to use ORNL's newly installed monochromated aberration-corrected STEM (MAC-STEM) to measure the local temperature in hexagonal boron nitride flakes⁵. This work was based on the suggestion that it might be possible to measure the local temperature by looking at the ratio of energy loss to energy gain phonons, which was also published in *Physical Review Letters*, some 50 years before our experimental demonstration that the same principle applies for nanoscale materials in the electron microscope. The other benefit of this method is that it is essentially parameter-free, and does not rely on previously known calibrations, making more applicable to novel materials. What this work also shows is that the new generation of monochromated aberration-corrected machines is able to obtain extremely high-spatial resolution after monochromation and to use these abilities to directly probe quantum phenomena at the nanoscale⁶.

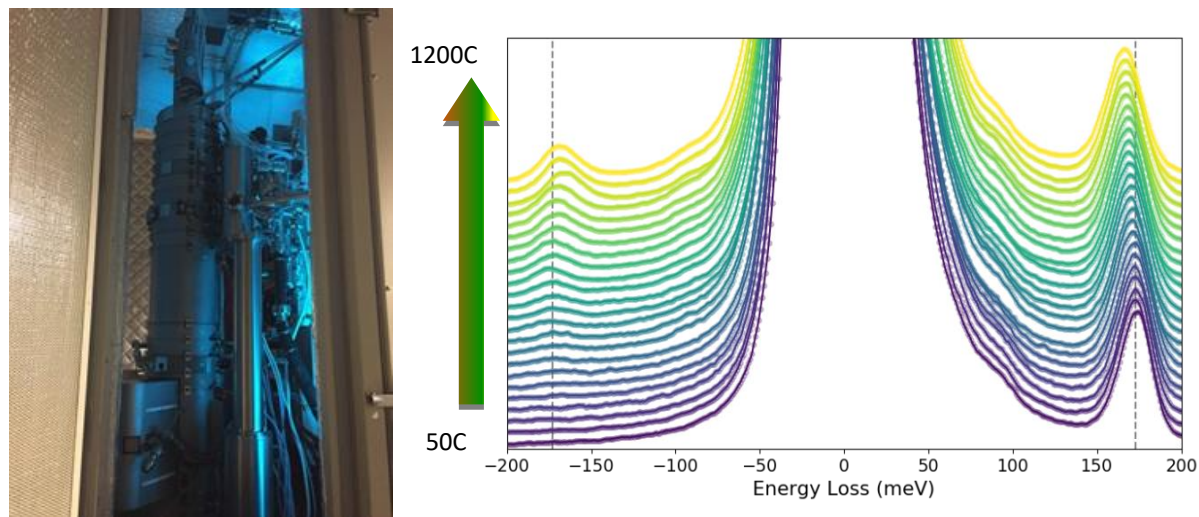


Figure 2: The recently installed MACSTEM at ORNL, and example spectra demonstrating energy loss (right) and energy gain (left) phonon peaks from hexagonal BN as a function of temperature. Adapted from Idrobo et al.⁵

Future Plans

While several authors have used DFT to calculate scattering potentials in the past, this has usually been as one-off publications to illustrate a particular point. In order to generate the large data sets required for training DL algorithms we intend to create an automated workflow to go directly from DFT calculations to CBED simulations. This workflow is outlined in figure 3.

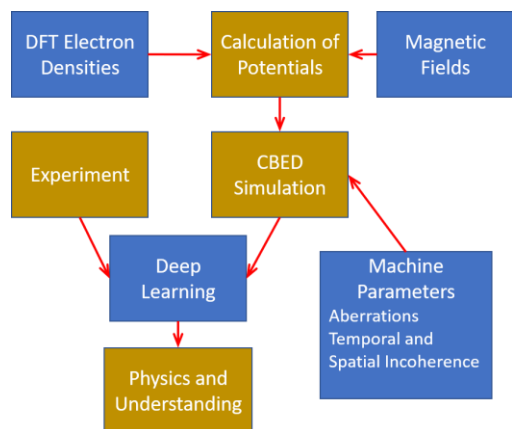


Figure 3: Automated workflow for high performance simulation and analysis of multidimensional datasets.

DFT calculations of model structures provide the primary input into the calculation of scattering potentials. In addition to electron densities they also provide relaxed atomic locations. Magnetic fields may also be added to the potential. This, along with appropriate machine parameters provides the primary input into the CBED simulations. Multiple simulations for different machine parameters and DFT models can be carried out simultaneously on ORNL’s Summit supercomputer. The results of these calculations will form the basis of the training sets used by the deep learning algorithm.

The inclusion of meaningful machine parameters is essential for providing realistic simulations. Perhaps the most overlooked requirement for accurate CBED simulations is temporal and spatial incoherence. Correctly including spatial incoherence requires CBED patterns to be calculated for many more probe positions than usually required, so that patterns can be added incoherently. Temporal incoherence can be accounted for by incoherently summing over multiple defocus values. The generation of multiple large datasets makes the use of automation essential for this task.

References

- [1] Xin Li *et al.*, “Manifold Learning of Four-dimensional Scanning Transmission Electron Microscopy”, *submitted*.
- [2] M. P. Oxley *et al.*, *in preparation*.
- [3] Allen, L. J., D’Alfonso, A. J. & Findlay, S. D. “Modelling the inelastic scattering of fast electrons. *Ultramicroscopy*” 151, 11–22 (2015).
- [4] A. Lupini, M. Chi, S. Jesse. (2016) Rapid aberration measurement with pixelated detectors, *JOURNAL OF MICROSCOPY* 263(1), pages 43-50.
- [5] J-C Idrobo, A.R. Lupini, et al. Temperature Measurement by a Nanoscale Electron Probe Using Energy Gain and Loss Spectroscopy *Phys. Rev. Lett.* 120, 095901 (2018)
- [6] J.A. Hachtel, A.R. Lupini, & J.C. Idrobo (2018) Exploring the capabilities of monochromated electron energy loss spectroscopy in the infrared regime, *SCIENTIFIC REPORTS* 8, 5637

Emergent Behavior in Nanoscale Functional Heterostructures

Amanda K. Petford-Long, Saidur Bakaul, Charudatta Phatak

Materials Science Division, Argonne National Laboratory, 9700 S Cass Avenue, Argonne, IL 60439

petford.long@anl.gov, sbakaul@anl.gov, cd@anl.gov

Research Scope

The functional behavior of ferroic and oxide materials at the nanoscale is governed by their complex energy landscape, which must be understood if emergent behavior is to be controlled. We focus on heterostructure nanosystems whose building blocks show ferromagnetic and resistance switching properties. A particular strength of our program is the use of 2D and 3D aberration-corrected Lorentz transmission electron microscopy and advanced scanning probe microscopy, combined with theory and simulation, to determine the quantitative parameters that control domain and transport behavior in nanostructures. We aim to obtain a fundamental understanding of the novel spin and charge distributions that are created in these nanostructures through control of the parameters that contribute to their energy landscape, such as interlayer coupling, geometric effects, and interactions between adjacent nanostructures. We further aim to understand the way in which these spin and charge distributions can be controlled through modification of their energy landscape via external stimuli such as electric and magnetic fields, temperature and/or time. Specific scientific challenges that we are addressing include elucidating the competing effects of curvature on chiral spin textures in ferromagnetic nanostructures, and understanding the energy terms that control spin and charge transport and memristive behavior in geometrically-confined nanostructures.

Recent Progress

Quasicrystalline artificial spin ices We have been exploring the role that magnetic frustration plays in controlling the behavior of aperiodic quasicrystalline artificial spin ices (QC-ASIs). Figure 1 shows a map of the in-plane magnetic induction of a QC-ASI patterned on a P2 Penrose tiling. The induction map was reconstructed from experimental Lorentz TEM (LTEM) images using the transport-of-intensity formalism. We mapped the local energy landscape across the lattice for different states by comparing experimental LTEM images with micromagnetic simulations and showed that we could get closer to the ground state via demagnetizing in a rotating magnetic field than through thermal

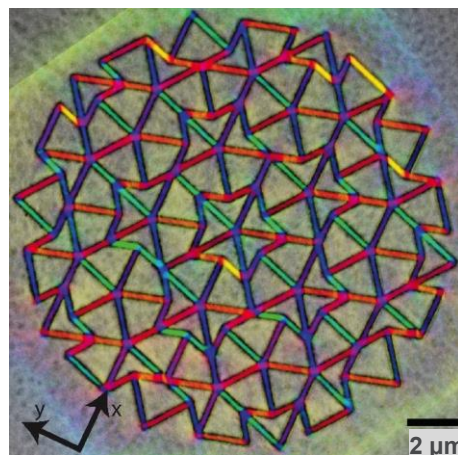


Figure 1 In-plane magnetic induction map of as-fabricated QC-ASI, reconstructed from LTEM data. Brajuskovic et al., Sci. Rep. 6, 34384 (2016). Licence: CC 4.0.

treatment. We ascribe this to the rotational, rather than translational, symmetry of the underlying QC lattice. We also showed that the magnetization reversal of such lattices occurs via branching 2D avalanches, distinct from that seen in ASIs patterned on periodic lattices. We further explored transient behavior in these systems in response to temperature and applied magnetic field. The configurational magnetic frustration across the lattice leads to the formation of high energy vortex domain walls within bar as a result of two adjacent vertices (at which the magnetic bars meet) both trying to reach their ground state energy.

In order to compare the behavior of QC-ASIs patterned on different lattices, we have developed a statistical graph-theory approach that offers new insight by considering the way in which the magnetic bars form connected communities in the QC-ASIs. We showed that the P2 Penrose tiling leads to enhanced topological frustration as compared to the P3 tiling, and we elucidate the emergence of local anti-aligned magnetic order as well as disordered spin liquid states in the QC-ASIs. During magnetization reversal, communities of magnetic bars nucleate and then aggregate as the ASI reaches the coercive field. As reversal proceeds to saturation, the communities shrink and finally disappear. The communities have low net magnetization and offer a different way to view the reversal process. Figure 2 shows a large community in a P3 Penrose-tiled QC-ASI near coercivity, together with the spin structure factor map, in which closely spaced peaks corresponding to long-range anti-aligned magnetic order within the community.

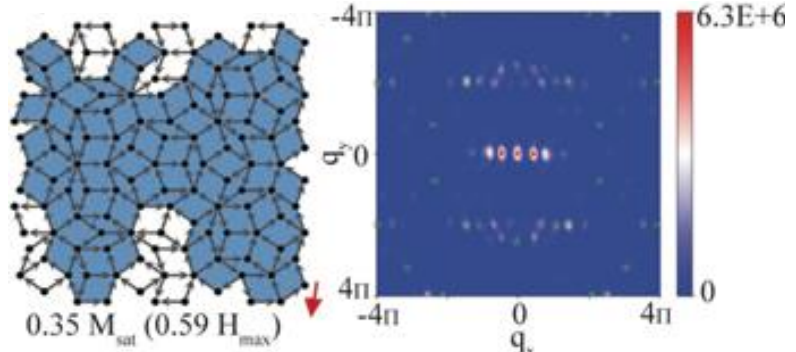


Figure 2 Community map of P3 Penrose-tiled QC-ASI with corresponding spin structure factor map.

spin structure factor map, in which closely spaced peaks corresponding to long-range anti-aligned magnetic order within the community.

Structured quantum waves We have used the inherent quantum mechanical properties of magnetic monopole excitations in square ASIs to modify the local topology of propagating coherent electrons in a controlled manner. We have shown, using LTEM, that magnetic monopole excitations at the nodes in a square artificial spin ice lattice can impart local orbital angular momentum (OAM) to a propagating electron wave, resulting in the formation of localized electron vortex states. We have shown that the magnitude and sign of the topological charge of the vortex states are directly correlated with the magnitude and sign of the magnetic charge of the monopole excitation.

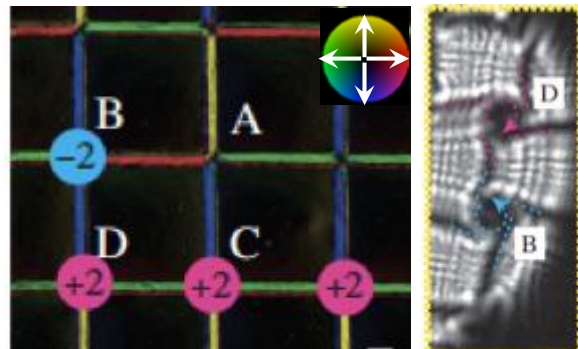


Figure 3 Magnetic induction map of region of square ASI together with defocused electron pattern of vertices B and D showing the transfer of OAM to the electron beam with sign corresponding to that of the magnetic charge at each node. Phatak, Petford-Long, *Nano Lett.* (Oct 2018) © Amer Chem Soc 2018.

Figure 3 shows a magnetic induction map of a region of a square ASI, together with inset color wheel indicating direction of magnetization in each island (island length = 2 μm). The numbers at each node indicate the magnetic charge. To the right is shown a highly defocused electron diffraction pattern of vertices B and D. The sense of rotation of the electron vortex state induced by vertices B and D is opposite, in agreement with the opposite signs of the magnetic charge and phase maps show that the magnitude of the induced OAM matches the magnitude of the magnetic charge.

2D RSO networks We have used self-assembled PS-PMMA block-copolymers and sequential infiltration synthesis [1] into alumina to create nanoscale honeycombs that we use as masks to transfer the pattern into an underlying resistive-switching oxide (RSO) layer such as TiO_2 or HfO_2 . Figure 4 shows an RSO network patterned into a thin TiO_2 film using this technique. Simple modifications in the block-copolymer deposition provide us with slightly different pattern, providing us a new means to control the geometry of our resistive switching films. To facilitate electronic transport, two lateral Pt electrodes with a 100 nm gap have been fabricated on top of the TiO_2 network. In a similarly configured control sample with an unetched TiO_2 film we have observed a voltage-dependent hysteretic change in current, which suggests resistive switching in the lateral devices.

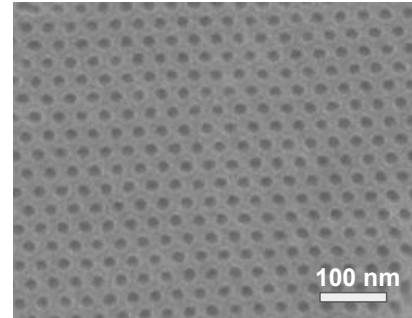


Figure 4 Nanoscale oxide network patterned into a thin TiO_2 film.

Future Plans

Magnetism in curved structures It has been shown that a curvilinear geometry leads to two additional exchange-driven interactions that affect magnetic spins at equilibrium, namely an effective anisotropy and an antisymmetric vector exchange, which is a DM-like interaction. These novel effects are dependent on the curvature and the curvature-gradient of the nanostructure, and result in magnetochiral and topologically-induced spin textures that have led to theoretical predictions of unlimited domain wall velocities and spin chirality symmetry breaking.

We have recently shown we can use focused electron beam deposition (FEBID) to create free-standing sculpted cobalt 3D magnetic nanostructures such as spirals and helices, as shown for example in Figure 5. LTEM shows that these nanostructures are ferromagnetic as-deposited, enabling us to create designer structures by direct deposition without further processing. We will now use these nanostructures to explore the additional contributions to the energy landscape that geometric curvature induces, by carefully controlling the curvature of the structures and comparing our experimental LTEM data with micromagnetic simulations.

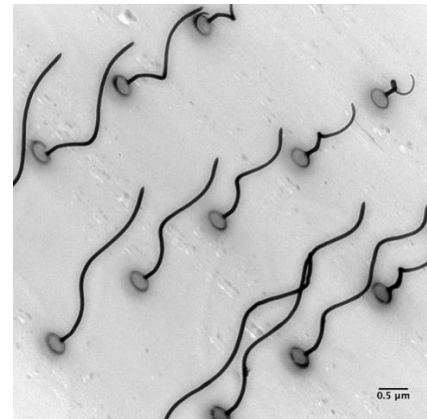


Figure 5 Co nanospirals directly deposited by FEBID

Creation of artificial topologically non-trivial spin textures We are interested in understanding and controlling how geometric confinement of ferromagnetic heterostructures modifies the energy landscape of magnetic spin textures. Based on our previous work, we can create stable chiral spin structures, such as skyrmions at room temperature through geometric confinement. We will then work to understand the effect that the presence of artificially imprinted skyrmions has on the magnetotransport and in-situ domain behavior of spin textures that are generated by spin currents and spin torque effects, and which interact with the implanted skyrmions. Our aberration-corrected LTEM instrument will allow us to explore this behavior in situ in the TEM so that we can simultaneously record transport data and image the magnetic domain behavior. A recent addition to our instrument has been a new CCD camera that will allow us to record up to 300 frames per second so that we can capture faster events than we were previously able to do.

Transport of magnetic excitations in ASIs As a continuation of our exploration of the behavior of artificial spin ices, we will explore the magneto-transport and stochastic behavior of domain walls in connected aperiodic ASIs. Our interest is in determining how the frustration in the QC-ASI influence this behavior, and in particular how different vertex motifs across the spin ice lattices are more or less influential in controlling behavior. We already have some preliminary data that show the feasibility of the studies that we intend to carry out, and we will make full use of our previously-developed graph theory approaches to enable comparisons to be made between ASIs patterned on different quasicrystalline lattices.

Resistive-switching oxide networks We have developed all of the nanofabrication capabilities associated with creating nanoscale RSO networks across which we can apply currents. We will now use both our recently acquire probe station, and in-situ TEM bias experiments, to explore the electroforming and resistive-switching behavior of our networks as a function of different parameters such as material, geometry and electromagnetic excitation. By modifying the patterned film we will explore the energy parameters and microstructure controlling the formation of conducting filaments.

References

[1] T Segal-Peretz, J Winterstein, M Doxastakis, A Ramirez-Hernández, M Biswas, J Ren, HS Suh, SB Darling, JA Liddle, JW Elam, JJ De Pablo, NJ Zaluzec, PF Nealey, *ACS Nano* **9**(5) (2015) 5333–5347.

Publications (FY17 and FY18)

V. Brajuskovic, F. Barrows, C. Phatak, and A. K. Petford-Long, “Real-space observation of magnetic excitations and avalanche behavior in artificial quasicrystal lattices”, *Sci. Rep.* **6**, 34384 (2016).

- C. Phatak, V. Brajuskovic, F. Barrows, and A. Petford-Long, “Modified Transport-of-Intensity Approach for Mapping In-situ Magnetic Induction,” *Microsc. Microanal.* **23(S1)**, 930–931 (2017).
- F. Barrows, P. Nealey, T. Segal-Peretz, L. Stan, J. Elam, A. Mane, E. Porath, C. Phatak, and A. Petford-Long, “Honeycomb Networks of Metal Oxides from Self-Assembling PS-PMMA Block Copolymers,” *Microsc. Microanal.* **23(S1)**, 16534–1655 (2017).
- Y. Sharma, R. Agarwal, C. Phatak, B. Kim, S. Jeon, R. S. Katiyar, and S. Hong, “Long-range Stripe Nanodomains in Epitaxial (110) BiFeO₃ Thin Films on (100) NdGaO₃ Substrate,” *Sci. Rep.* **7(1)**, 4857 (2017).
- K. C. Prabhat, K. Aditya Mohan, C. Phatak, C. Bouman, and M. De Graef, “3D reconstruction of the magnetic vector potential using model based iterative reconstruction,” *Ultramicrosc.* **182**, 131–144 (2017)
- P. N. Lapa, J. Ding, C. Phatak, J. E. Pearson, J. S. Jiang, A. Hoffmann, and V. Novosad, “Magnetic vortex nucleation/annihilation in artificial-ferrimagnet microdisks,” *J. Appl. Phys.* **122**, 83903 (2017).
- M. Owczarek, K.A. Hujsak, D.P. Ferris, A. Prokofjevs, I. Majerz, P. Szklarz, H. Zhang, A.A. Sarjeant, C.L. Stern, R. Jakubas, S. Hong, V.P. Dravid, J.F. Stoddart, “Flexible ferroelectric organic crystals”, *Nat. Comm.* **7**, 13108 (2016).
- T. Varga, T. C. Droubay, L. Kovarik, M. I. Nandasiri, V. Shutthanandan, D. Hu, B. Kim, S. Jeon, S. Hong, Y. Li, and S. A. Chambers, “Coupled Lattice Polarization and Ferromagnetism in Multiferroic NiTiO₃ Thin Films”, *ACS Appl. Mater. Interfaces* **9**, 21879–21890 (2017)
- H. Kim, S. Lee, S. Kim, C. Oh, J. Ryu, J. Kim, E. Park, S. Hong, K. No, “Membrane crystallinity and fuel crossover in direct ethanol fuel cells with Nafion composite membranes containing phosphotungstic acid”, *J. Mater. Sci.* **52(5)**, 2400–2412 (2017).
- F. Hellman, A. Hoffmann, Y. Tserkovnyak, G. S. D. Beach, E. E. Fullerton, C. Leighton, A. H. MacDonald, D. C. Ralph, D. A. Arena, H. A. Dürr, P. Fischer, J. Grollier, J. P. Heremans, T. Jungwirth, A. V. Kimel, B. Koopmans, I. N. Krivorotov, S. J. May, A. K. Petford-Long, J. M. Rondinelli, N. Samarth, I. K. Schuller, A. N. Slavin, M. D. Stiles, O. Tchernyshov, and A. Thiaville, “Interface-induced phenomena in magnetism”, *Rev. Mod. Phys.* **89**, 025006 (2017).
- T. Roy Kim, C. Phatak, A. K. Petford-Long, Y. Liu, C. Taylor, B. Zhang, S. Myers, A. Greene, T. Seki, M. Alex, G. A. Bertero, and R. Sinclair, “Correlative magnetic imaging of heat-assisted magnetic recording (HAMR) media in cross-section using Lorentz TEM and MFM”, *IEEE Trans. Mag.* **54(1)**, 6500105 (2018). DOI: [10.1109/TMAG.2017.2753170](https://doi.org/10.1109/TMAG.2017.2753170)
- B. Kim, F.P. Barrows, Y. Sharma, R.S. Katiyar, C. Phatak, A.K. Petford-Long, S. Jeon, S. Hong, “Ferroelectric domain studies of patterned (001) BiFeO₃ by angle-resolved piezoresponse force microscopy”, *Sci.Rep.* **8:203** (2018). DOI: [10.1038/s41598-017-18482-9](https://doi.org/10.1038/s41598-017-18482-9)
- K. Aditya Mohan, K.C. Prabhat, C. Phatak, M. De Graef, C. A. Bouman, “Model-Based Iterative Reconstruction of Magnetization using Vector Field Electron Tomography”, *IEEE Trans. on Comp. Imag.* (2018). DOI: [10.1109/TCI.2018.2838454](https://doi.org/10.1109/TCI.2018.2838454)
- A. Hierro-Rodriguez, D. Gursoy, C. Phatak, C. Quiros, A. Sorrentino, L. Alvarez-Prado, M. Velez, J. Ignacio Martin, J. M. Alameda, E. Pereiro, and S. Ferrer, “3D reconstruction of magnetization from dichroic soft X-ray transmission tomography,” *J. Synchrotron Radiat.*, **25**, 1–9 (2018).

- C. Phatak, F. Barrows, V. Brajuskovic, S. Bakaul, O. Heinonen, M. De Graef, W. Jiang, S. G.E. te Velthuis, A. Hoffmann, A. Petford-Long, “Imaging magnetic domains in functional nanoscale heterostructures using Lorentz microscopy”, *Microsc. Microanal.* **24(S1)**, 910–911 (2018).
- Frank Barrows, Amanda Petford-Long and Charudatta Phatak, “Topological defects and interaction of electron waves and localized magnetic charge”, *Microsc. Microanal.* **24(S1)**, 940–941 (2018).
- X. Xu., S. Haile, C. Phatak, “In-situ Electron Holography Study of Grain Boundaries in Cerium Oxide”, *Microsc. Microanal.* **24(S1)**, 1466–1467 (2018). doi:10.1017/S143192761800781X
- C. Phatak, A.K. Petford-Long, “Direct evidence of topological defects in electron waves due to localized magnetic charge”, submitted to *Nano Lett.* (2018).
- V. Brajuskovic, A. Addi, C. Phatak, A. K. Petford-Long, “Observation of transient states during magnetization reversal in a quasicrystal artificial spin ice”, submitted to *Phys. Rev. B* (2018).
- F. Barrows, V. Brajuskovic, C. Phatak, A.K. Petford-Long, “Emergent magnetic ordering and topological frustration in quasicrystal artificial spin ices”, submitted to *PNAS* (2018).

Tracing non-equilibrium phenomena in quantum materials by using MeV ultrafast electron probes

Jing Tao (PI), Junjie Li and Jun Li
Condensed Matter Physics and Materials Science Division,
Brookhaven National Laboratory, Upton, NY 11973

Research Scope

This Early Career Award project aims to establish a better understanding of the role competing degrees of freedom play in correlated materials and quantum materials by tracing structural dynamics of non-equilibrium states using MeV ultrafast electron diffraction (UED). We have focused on the transient states through structural phase transitions in several quantum materials, including Cu_2S and 1T-TaSeTe, with charge-density-wave (CDW), to study the entanglement between the electronic degrees of freedom and the lattice. For Cu_2S , we distinguished the temporal characteristics of crystal symmetry breaking and lattice expansion, the two order parameters that have been long considered as “simultaneous” change during a structural phase transition. Our observations redefine the pathway of structural transitions in a crystal and indicate the electronic-phonon coupling to be the transition mechanism in Cu_2S . For an ongoing project exploring CDW and related structure dynamics in 1T-TaSeTe material, preliminary analysis from MeV UED measurements show a momentum-dependent variation in the structural dynamics of both the Bragg and the CDW reflections. We find that the UED results are essential to the understanding of the physical origin of a number of phenomena including the photon-induced atomic displacements and the dynamic dephasing between electronic structures and the lattice.

Recent Progress

Cu_2S has recently attracted increasing attention due to its intriguing properties. This material is known as a superionic conductor with liquid-like behavior of copper ions above the critical temperature, giving rise to applications in electrochemical, thermoelectric and battery devices [1-3]. The structural phase transition occurring at the critical temperature close to ambient has been studied intensively in Cu_2S [4-6]. The structural phase transition involves a symmetry breaking of the crystalline lattice and a volume expansion, *i.e.*, Cu_2S is monoclinic (hereafter called the “L-phase”) at room temperature whereas is hexagonal (hereafter called the “H-phase”) at temperatures above 375 K. However, research efforts have mainly concentrated on the study of the motion of ions through the structural phase transition with little attention being paid to the electronic structure of this material. This has led to the lack of a consensus on the role of the electronic structure in the structural phase transition of Cu_2S and the transition mechanism remains elusive.

To address the above issue, we performed structural characterizations of Cu_2S nanoplates with *in situ* observations using TEM and UED facilities. In TEM observations, we demonstrate that electron-induced changes in the electronic structure can lead to a macroscopic reconstruction of the crystal structure. In UED measurements, we reveal the transition pathway in a crystal-symmetry *vs.* lattice-expansion parameter-space and argue that the mechanism of the structural phase transition in Cu_2S is dominated by the electron-phonon coupling.

Manipulating the structure of Cu_2S by electronic perturbation using TEM

We conduct the concurrent pump and probe experiments of Cu_2S nanoplates (synthesized by Prof. J-Y. Chen's group at University of Arkansas) using an electron beam to directly manipulate the transition between the L- and H- phases with distinct crystal symmetries and charge carrier concentrations, and show that the transition is the result of charge generation for one phase and charge depletion for the other. We demonstrate that this manipulation is fully reversible and non-thermal in nature. Our study sheds light on the hotly debated question of whether a change in electronic structure can facilitate a change of crystal symmetry, or whether vice versa is always the case. We illustrate that a minimal perturbation to the electronic degrees of freedom can drive the structural phase transition in Cu_2S , hence resolving this dilemma in this case [7].

Probing the transition pathway and illuminating the transition mechanism using UED

In a wide range of materials associated with structural phase transition, crystal symmetry breaking and the "simultaneous" lattice expansion are identified to be the primary and secondary order parameters, respectively. The focus on both order parameters brings forth a basic question: what are temporal scales governing the two order parameters during the onset of a structural transition? A simplified case illustrating this issue using a 1D assembly of atoms is demonstrated in Fig. 1a, which shows that a material can take multiple pathways on transforming from one phase to another in parameter space. In Cu_2S , we obtained UED patterns (shown in Fig. 1b) in pump-probe experiments and measured the characteristics of reflection rings in the UED patterns including the peak width and the peak center positions of the reflection rings. Based on the understanding of the crystal structures established by our previous TEM study, we correlate the peak-width measurements to the crystal symmetry change and the peak-center-position to the lattice expansion. Hence we are able to follow the transient states along the transition pathway and observe the dynamics of both the primary and secondary order parameters (the measurements from the (120) ring are shown in Fig. 2c). Based on these observations, we argue that the mechanism of the structural phase transition in Cu_2S is dominated by the electron-phonon coupling [8].

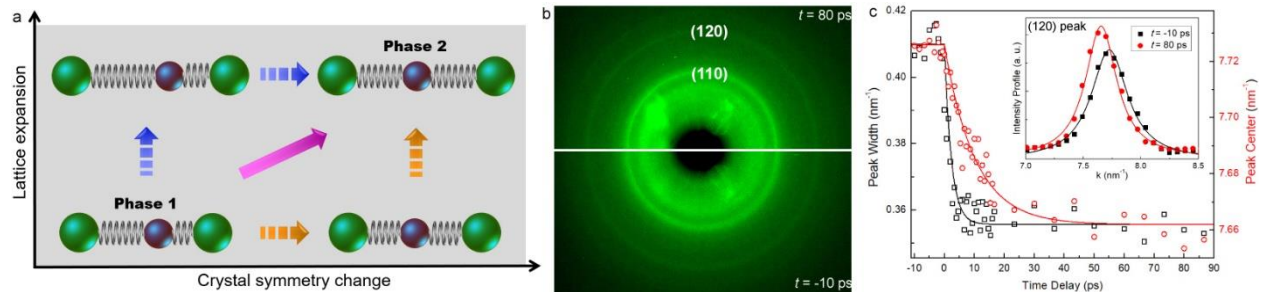


Figure 1. **a**, Schematic of a structural phase transition that involves both the crystal symmetry breaking and the lattice expansion in a 1D assembly of atoms. Phase 1 has two types of atoms that have unequal spacing. Phase 2 has the same group of atoms with altered lattice symmetry and spacing. Arrows in orange, purple and blue indicate possible transition pathways in the ultrafast time domain. **b**, A comparison of UED patterns taken before (bottom) and after (top) laser pump. (110) and (120) reflection rings are indexed using the notation of the hexagonal structure. **c**, Peak width (plotted by black squares) and peak center position (plotted by red circles) in reciprocal space are given as a function of time delay for the (120) reflection ring in **b**. The time constant of peak width change is $\sim 2.3 \pm 0.2$ ps, whereas the time constant of the shift in the peak center position is $\sim 10.2 \pm 0.3$ ps, indicating the transition pathway similar to the orange route in **a**. Black and red lines are guide for eyes. Peak width was measured using the full width of half maximum of the peak intensity profiles, which are shown as the insets of the plots with a Lorentzian curve fitting.

Future Plans

The CDW electronic structure is of great interest to the research community of correlated electron materials/quantum materials not only due to its mysterious and intimate relationship with superconductivity but also due to its elusive origin arising from the charge and lattice coupling. Indeed, CDW in many transition metal dichalcogenides lack characterizations that are essential to delve into the fundamental physics. Particularly, periodic lattice distortions (PLDs) are often associated with electronic modulations in the CDW structures. Among the difficulties that hinder further exploration, the crystal symmetry (or supersymmetry) of those PLDs and the dynamic coupling between the electronic modulation and the PLD are at the center of the study.

Electron diffraction techniques are sensitive to both the valence charge distribution (at small scattering angles) and ionic displacements (at large scattering angles). With the additional resolution in the ultrafast time-domain, UED patterns hence empower us to possibly separate the dynamics of the electronic structure and the lattice during a non-equilibrium process and further explore the charge-lattice interaction in the material. We have collected a comprehensive set of UED measurements from 1T-TaSeTe single-crystals (synthesized by Prof. R. J. Cava's group at Princeton University) under various temperatures and pump fluences. To obtain high quality UED patterns (one example shown in Fig. 2a), each UED pattern at a specific time delay is an accumulation from 1200 pulses at the same time delay. We repeated at least 5 times of the pump-probe experiments at each temperature and each pump fluence to increase the signal-noise ratio of the data. We have developed computer codes to align all the UED patterns with 2D curve fitting of the intensity profiles of *all the reflections*. Preliminary measurements from the UED patterns during the pump-probe process are shown in Fig. 2b for the CDW reflections and in Fig. 2c for the Bragg peaks. In the future, we plan to complete the data measurements and analysis in this material, and correlate the UED results with the theoretical modeling and density functional theory (DFT) calculations to advance our understanding on the CDW mechanisms.

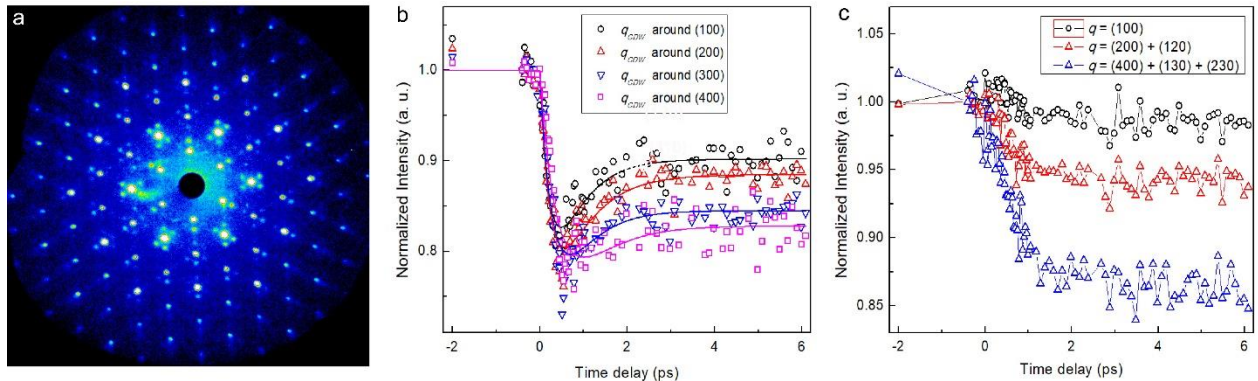


Figure 2. a, An UED pattern obtained from 1T-TaSeTe sample at [001] zone axis at $T = 28$ K. Note that 96 Bragg peaks and 84 CDW reflections can be identified with measurable intensities in one pattern. **b**, Using pump-probe technique with the optical pump fluence of 3.5 mJ/cm^2 , the intensity of the CDW reflections has a quick drop in ~ 400 fs and recovers at a longer time scale. Measurements of intensity vs. time delay are from four sets of the first-order CDW reflections around different Bragg peaks ($\{100\}$, $\{200\}$, $\{300\}$, and $\{400\}$), plotted with circles, triangles and squares in black, red, blue and magenta, respectively. Solid lines in black, red, blue and magenta are guide for eyes. **c**, Intensities of selective Bragg reflections are plotted as a function of time delay. To increase the signal-noise ratio, measurements from the Bragg reflections at nearby q values are added and plotted together, e.g., intensities from $\{200\}$ and $\{210\}$ were added together, and intensities from $\{400\}$, $\{130\}$ and $\{230\}$ were added together.

References

1. Okamoto, K. & Kawai, S., “Electrical conduction and phase transition of copper sulfides”, *J. Phys. Soc. Japan* **12**, 1130 (1973).
2. Liu, H. *et al.*, “Copper ion liquid-like thermoelectrics”, *Nature Materials* **11**, 422 (2012)
3. Miller, T. A., Wittenberg, J. S., Wen, H., Connor, S., Cui, Y. & Lindenberg, A. M., “The mechanism of ultrafast structural switching in superionic copper (I) sulphide nanocrystals”, *Nat. Commun.* **4**, 1369 (2013).
4. Evans, H. T., “Crystal structure of Low Chalcocite”. *Nature* **232**, 69, (1971).
5. Cava, R. J., Reidinger, F. & Wuensch, B. J., “Mobile ion distribution and anharmonic thermal motion in fast ion conducting Cu_2S ”, *Solid State Ionics* **5**, 501 (1981).
6. Wang, L. W., “High Chalcocite Cu_2S : A Solid-Liquid Hybrid Phase”, *Phys. Rev. Lett.* **108**, 085703 (2012).
7. Tao, J. *et al.*, “Reversible structure manipulation by tuning carrier concentration in metastable Cu_2S ”, *Proc. Natl. Acad. Sci. USA* **114**, 9832 (2017).
8. Li, J. J. *et al.*, “Probing pathway of an ultrafast structural phase transition to illuminate the transition mechanism in Cu_2S ”, *Appl. Phys. Lett.* **113**, 041904 (2018).

Publications

1. Li, J. J., ... Cava, R. J., Zhu, Y., & Tao, J., “Probing pathway of an ultrafast structural phase transition to illuminate the transition mechanism in Cu_2S ”, *Appl. Phys. Lett.* **113**, 041904 (2018).
2. Han, M.-G., Li, J., Xue, F., Wang, X., Meng, Q.-P., Tao, J., Chen, L.-Q., Cheong, S.-W., & Zhu, Y., “Linearly aligned single-chiral vortices in hexagonal manganites by in situ electric arc heating”, *Phys. Rev. Materials* **2**, 64004 (2018).
3. Li, J., Cheng, S., Wu, L., Tao, J., & Zhu, Y., “The Effect of Scanning Jitter on Geometric Phase Analysis in STEM Images”, *Ultramicroscopy* **194**, 167-174 (2018).
4. Mathurin, L. E., Tao, J., Xin, H., Li, J., Zhu, Y., & Chen, J., “Dendritic Core-Frame and Frame Multimetallic Rhombic Dodecahedra: A Comparison Study of Composition and Structure Effects on Electrocatalysis of Methanol Oxidation”, *Chem. Nano. Mat.* **4**, 76–87 (2018).
5. Oey, Y. M., Park, J. E., Tao, J., Carnicom, E. M., Kong, T., Sanders, M. B. & Cava, R. J., “Stabilizing the Tb-based 214 cuprate by partial Pd substitution”, *J. Mater. Res.* **33**, 1690 (2018).
6. Zhang, W., Yan, D. H., Li, J., Wu, Q. Y., Cen, J., & Zhang, L., Orlov, A., Xin, H., Tao, J., & Liu, M., “Anomalous Conductivity Tailored by Domain-Boundary Transport in Crystalline Bismuth Vanadate Photoanodes”, *Chem. Mater.* **30**, 1677 (2018).
7. Tao, J., Chen, J., Li, J., Mathurin, L., Zheng, J. C., Li, Y., Lu, D., Cao, Y., Wu, L., Cava, R. J. & Zhu, Y., “Reversible structure manipulation by tuning carrier concentration in metastable Cu_2S ”, *Proc. Natl. Acad. Sci. USA* **114**, 9832 (2017).

8. Cameron, C. C., Wang, F., Li, J., Tao, J., Zhu, Y., & Chen, J., “Synthesis of Copper-Silica Core-Shell Nanostructures with Sharp and Stable Localized Surface Plasmon Resonance”, *J. Phys. Chem. C* **121**, 5684-5692 (2017).
9. Tao, J., Sun, K., Tranquada, J. M. & Zhu, Y., “Anomalous nanoclusters, anisotropy and electronic nematicity in doped manganite $\text{La}_{1/3}\text{Ca}_{2/3}\text{MnO}_3$ ”, *Phys. Rev. B* **95**, 235113 (2017).
10. Luo, H., Strychalska-Nowak, J., Li, J., Tao, J., Klimczu, T., & Cava, R. J., “S-Shaped Suppression of the Superconducting Transition Temperature in Cu-Intercalated NbSe_2 ”, *Chem. Mater.* **29**, 3704 (2017).

Liquid Cell Electron Microscopy: Heterogeneity and Fluctuations at Solid-Liquid Interfaces

Principal Investigators: Haimei Zheng*, Peter Ercius, Emory Chan, Lin-Wang Wang

*Materials Sciences Division, Lawrence Berkeley National Laboratory, Berkeley, CA 94709.

email:

Email: hmzheng@lbl.gov

Research Scope

The overarching goal of this program is to develop and utilize the advanced in-situ liquid cell transmission electron microscopy (TEM) to elucidate how atomic level heterogeneity and fluctuations at solid-liquid interfaces control the physical and chemical processes of materials, currently with a focus on nucleation, growth and structural transformations of materials. With the development of liquid cell TEM, we investigate the transient nucleation events in an oversaturated solution, growth and transformation dynamics of materials in liquids, and precipitation and dissolution at solid-liquid interfaces under an external stimulus, such as a chemical or electrochemical potential. Special attention has been made on the correlation of concentration fluctuations to structural ordering; characteristics of prenucleation clusters or intermediates; and how surface inhomogeneity or defects impact the dynamic phenomena at solid-liquid interfaces. The development of advanced instrumentation allowing for imaging and chemical identification through liquids with high spatial and temporal resolution may provide transformative opportunities for investigating the dynamic phenomena at solid-liquid interfaces in this program and it also provides opportunities to elucidate many other materials processes at the frontiers of basic energy sciences.

Recent Progress

1. Nucleation, growth and materials transformations

In situ liquid cell TEM enables visualization of materials dynamics in liquids. With development and growth of the liquid cell TEM, a variety of materials dynamic phenomena have been observed¹⁻⁵, many of which are not available through any other means. For the future growth of liquid cell TEM, it is critical to develop capabilities allowing the study of controllable reactions, enabling/implementing multimodal characterizations and fostering quantitative measurements and understanding.

Our recent study of nanoscale dendrite growth represents a milestone of liquid cell TEM moving from qualitative observations towards more

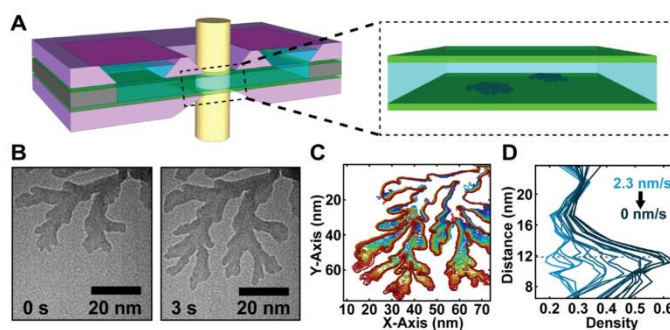


Figure 1. In situ liquid cell TEM imaging, tracking and data analysis of iron oxide nanodendrite growth. (A) Liquid cell schematic. (B) Video frames showing nanodendrite growth. (C) Outlines of the iron oxide nanostructures from each frame and overlaid on each other. Color shows time sequence with blue as the initial time and red as the later time. (D) Quantification of the effect of neighboring branches competing for precursor on the tip growth.

quantitative characterizations⁶. As we know, formation mechanisms of dendrite structures have been extensively explored theoretically and many theoretical predictions have been validated for micro- or macroscale dendrites. However, it is challenging to determine whether classical dendrite growth theories are applicable at the nanoscale due to the lack of detailed information on the nanodendrite growth dynamics. We have studied iron oxide nanodendrite formation using liquid cell TEM (**Figure 1**). We have been able to observe “seaweed”-like iron oxide nanodendrites growing predominantly in two dimensions on the membrane of a liquid cell. By tracking the trajectories of their morphology development with high spatial and temporal resolution, it is possible to explore the relationship between the tip curvature and growth rate, tip splitting mechanisms, and the effects of precursor diffusion and depletion on the morphology evolution. We found that the growth of iron oxide nanodendrites is remarkably consistent with the existing

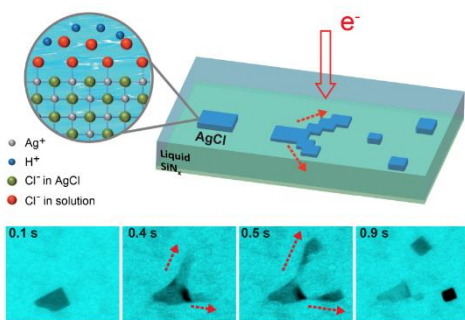


Figure 2. Rich dynamics of spontaneous reshaping and splitting of AgCl nanocrystals through liquid cell TEM. AgCl nanocrystals maintain single crystalline while simultaneously exhibits liquid-like behavior. Charging related Rayleigh instability accounts for the dynamics.

theoretical predictions on dendritic morphology evolution during growth, despite occurring at the nanoscale. This is the first time that one can verify the applicability of classical dendrite growth theories at the nanoscale, which opens many opportunities to the future design of complex nanoscale materials.

It is a common issue as well as a great challenge in liquid cell TEM that electron beam can introduce unwanted chemical reactions. It is critical to understand and control electron beam effects. In many studies, low dose imaging has been employed to limit the energy input from the electron beam. Nevertheless, an understanding of the electron beam-matter interactions is key to exploration of the potential as well as limits of liquid cell TEM techniques. A series of studies on electron beam-matter interactions in liquids have been performed.

For example, AgCl is photosensitive thus often used as micromotors. However, the dynamics of individual AgCl nanoparticle motion in liquids upon illumination remains elusive and their potential applications as nanoactuators has not been explored. With liquid cell TEM, we found that AgCl nanocrystals can reshape and split spontaneously in an aqueous solution under electron beam illumination⁷ (**Figure 2**). The AgCl nanocrystals can be negatively charged in the aqueous solution, and the charges induce a repulsive Coulomb force that may stretch and reshape the nanocrystals. The splitting of AgCl nanocrystals is analogous to the electrified liquid droplets or other reported Coulomb fission phenomena.

As another example, we have captured the reversible nanocrystal transformations between Pb nanocrystals and Pb-organic gel-like phase⁸ (**Figure 3**). By revealing of the reaction pathways and energetic states during transformations, we found metastable

For example, AgCl is photosensitive thus often used as micromotors. However, the dynamics of individual AgCl nanoparticle motion in liquids upon illumination remains elusive and their potential applications as nanoactuators has not been explored. With liquid cell TEM, we found that AgCl nanocrystals can reshape and split spontaneously in an aqueous solution under electron beam illumination⁷ (**Figure 2**). The AgCl nanocrystals can be negatively charged in the aqueous solution, and the charges induce a repulsive Coulomb force that may stretch and reshape the nanocrystals. The splitting of AgCl nanocrystals is analogous to the electrified liquid droplets or other reported Coulomb fission phenomena.

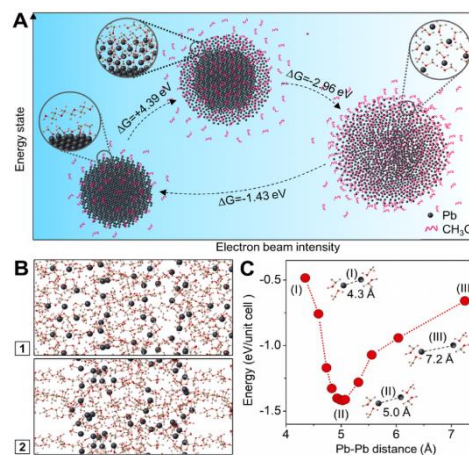


Figure 3. Nanocrystal transformations between a solid and a gel-like phase. (A-C) reaction pathways and energetic states during transformations.

structures may exist in broad nanocrystal transformations in liquids which may be significant for various applications.

2. Precipitation and dissolution at solid-liquid interfaces with external stimuli

With the liquid cell platform, we study precipitation and dissolution at electrode-electrolyte interfaces under an electric bias. Nanoscale features have been introduced to the electrode surface by E-beam lithography. The characteristics of precipitation/dissolution on the electrode are modified by the changes of local electric field. The initial precipitation sites and structure of the deposits correlated with the local ion distribution has been achieved, which provide critical information for the understanding of the impact of heterogeneity at solid-liquid interfaces on device properties⁹ (**Figure 4**). The results are highly relevant to research in areas of batteries, fuel cells, and materials degradation or corrosion protection.

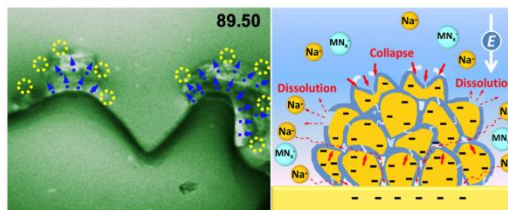


Figure 4. Electrodeposition of Na on patterned electrode. Various dynamic phenomena are observed including dissolution accompanied with deposition from the “base” (left). The “grain growth” characteristics of deposition is highlighted (right).

Future Plans

We plan to develop a new generation of liquid cells that will enable unprecedented control over the location, volume, and timing of chemical reactions accelerating image acquisition and providing new insights into the reaction of colloidal nanoparticles. Using our expertise in nanofabrication of liquid cells with silicon nitride membranes, graphene cells, and multiphase microfluidic devices, effort has been made towards fabricating liquid cells that leverage the deterministic mass and fluid transport that is inherent to fluids in confined geometries. A step towards this direction has been made by producing controllable vesicle nanoreactors (**Figure 5**). Robust nanoreactors with uniform size distribution have been achieved. Dynamic processes such as nanobubble formation and reactions inside the “reactors” have been captured. Additionally, as the systems of study undergo structural and chemical transformations with fast dynamics and they are often electron beam sensitive, it is increasingly important to develop/employ advanced image detection and image processing techniques. Through collaboration and participation in the cutting-edge development, our program engages the growing technologies on fast image detection and image processing with “machine learning” capabilities.

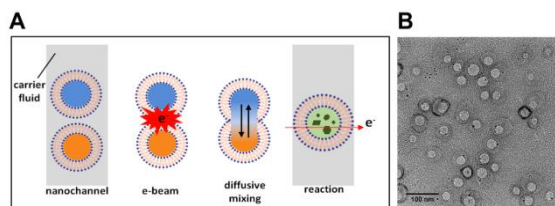


Figure 5. Controlled reactions through vesicle “nanoreactors”. (A). Schematic showing reactions between two types of solutions. (B). TEM image of the highly reproducible vesicle nanoreactors. Dynamics within the “reactor” has been captured.

In summary, the on-going effort and future plans in our program offer great potential for achieving break-throughs in the atomic level imaging through liquids allowing for revealing dynamic phenomena at solid-liquid interfaces and elucidating the role of solid-liquid interfaces in controlling the physical and chemical properties of materials significant to basic energy sciences.

References

1. H. G. Liao, L. Cui, S. Whitlam, H. Zheng, "Real time imaging Pt₃Fe nanorod growth in solution." *Science* 336, 1011 (2012).
2. H. G. Liao, D. Zherebetsky, H. Xin, C. Czarnik, P. Ercius, H. Elmlund, M. Pan, L. W. Wang, H. Zheng, "Facet development during platinum nanocube growth." *Science* 345, 916 (2014).
3. Z. Zeng, W. Liang, H. G. Liao, H. L. Xin, Y. H. Chu, H. Zheng, "Visualization of electrode-electrolyte interfaces in LiPF₆/EC/DEC electrolyte for lithium ion batteries via in situ TEM." *Nano Lett.* 14, 1745 (2014).
4. K. Y. Niu, T. Frolov, H. L. Xin, J. Wang, M. Asta, H. Zheng*, "Bubble nucleation and migration in a lead-iron hydroxide core-shell nanoparticle." *PNAS* 112, 12928 (2015).
5. C. Zhu, S. Liang, E. Song, Y. Zhou, W. Wang, F. shan, Y. Shi, C. Hao, K. Yin, T. Zhang, J. Liu, H. Zheng, L. Sun "In situ liquid cell transmission electron microscopy investigation on oriented attachment of gold nanoparticles" *Nature Communications* 9, 421(2018).
6. M. R. Hauwiller, X. Zhang, W. Liang, C. Chiu, Q. Zhang, W. Zheng, C. Ophus, E. Chan, C. Czarnik, M. Pan, F. M. Ross, W. Wu, Y. Chu, M. Asta, P. W. Voorhees, A. P. Alivisatos, H. Zheng, "Dynamics of nanoscale dendrite formation in solution growth revealed through in situ liquid cell electron microscopy" *Nano Lett. asap* (2018).
7. X. Tian, U. Anand, U. M. Mirsaidov, H. Zheng, "Spontaneous reshaping and splitting of AgCl nanocrystals under electron beam illumination" *Small accepted* (2018).
8. K. Niu, W. Zheng, J. Kang, C. Ophus, H. L. Xin, Y. Han, X. Du, J. Wu, E. M. Chan, P. Ercius, L. W. Wang, H. Zheng "Reversible nanocrystal transformations between a solid and a gel-like phase" *submitted* (2018).
9. Z. Zeng, J. Yang, X. Zhang, W. Zheng, Y. Liu, K. Bustillo, P. Ercius, J. Guo, Y. Cui, H. Zheng, "Role of solid electrolyte interphase in sodium electrodeposition revealed through liquid phase transmission electron microscopy" *submitted* (2018).

Publications

1. Z. Zeng, J. Yang, X. Zhang, W. Zheng, Y. Liu, K. Bustillo, P. Ercius, J. Guo, Y. Cui, H. Zheng, "Role of solid electrolyte interphase in sodium electrodeposition revealed through liquid phase transmission electron microscopy" *submitted* (2018).
2. K. Niu, W. Zheng, J. Kang, C. Ophus, H. L. Xin, Y. Han, X. Du, J. Wu, E. M. Chan, P. Ercius, L. W. Wang, H. Zheng "Reversible nanocrystal transformations between a solid and a gel-like phase" *submitted* (2018).
3. M. R. Hauwiller, X. Zhang, W. Liang, C. Chiu, Q. Zhang, W. Zheng, C. Ophus, E. Chan, C. Czarnik, M. Pan, F. M. Ross, W. Wu, Y. Chu, M. Asta, P. W. Voorhees, A. P. Alivisatos, H. Zheng, "Dynamics of nanoscale dendrite formation in solution growth revealed through in situ liquid cell electron microscopy" *Nano Lett. asap* (2018).
4. X. Tian, U. Anand, U. M. Mirsaidov, H. Zheng, "Spontaneous reshaping and splitting of AgCl nanocrystals under electron beam illumination" *Small accepted* (2018).

5. J. Yang, S. B. Alam, L. Yu, E. Chan, H. Zheng, “Dynamic behavior of nanoscale bubble formation in aqueous liquid on graphene surface revealed by liquid phase transmission electron microscopy” *Micron* 10.1016/j.micron.2018.09.009 (2018).
6. Q. Zhang, Z. Shi, K. Yin, H. Dong, F. Xu, X. Peng, K. Yu, H. Zhang, C. Chen, I. Valov, H. Zheng, L. Sun, “Spring-like pseudoelectroelasticity of monocrystalline Cu₂S nanowire”, *Nano Lett.* **18**, 5070 (2018).
7. Y. Zhou, A. S. Powers, X. Zhang, T. Xu, K. Bustillo, L. Sun, H. Zheng, “Growth and assembly of cobalt oxide nanoparticle rings at liquid nanodroplets with solid junction” *Nanoscale* **9**, 13915-13921 (2017).
8. J. Tan, M. Scott, W. Hao, T. Baikie, C. T. Nelson, S. Pedireddy, R. Tao, X. Ling, S. Magdassi, T. White, S. Li, A. M. Minor, H. Zheng, L. H. Wong, “Revealing cation exchange induced phase transformations in multi-elemental chalcogenide nanoparticles” *Chemistry of Materials* **29**, 9192 (2017).
9. Z. Zeng, W. Zheng, H. Zheng, “Visualization of colloidal nanocrystal formation and electrode-electrolyte interfaces in liquids using TEM” *Accounts of Chemical Research* **50** (8) 1808–1817 (2017).
10. Y. A. Wu, M. Farmand, Y. S. Yu, D. A. Shapiro, H.G. Liao, W. Liang, Y. Chu, H. Zheng, “*In situ* multimodal imaging and spectroscopy of Mg electrodeposition at electrode-electrolyte Interfaces”. *Scientific Reports* **7**, 42527 (2017).
11. H. Zheng, Y. Zhu, “Perspectives on in-situ electron microscopy” *Ultramicroscopy* **180**, 188 (2017).
12. X. Tian, H. Zheng, U. Mirsaidov, “Aggregation dynamics of nanoparticles at solid-liquid interface” *Nanoscale* DOI: 10.1039/C7NR01985H (2017).
13. Q. Zhang, K. Yin, H. Dong, Y. Zhou, X. Tan, K. Yu, X. Hu, T. Xu, C. Zhu, W. Xia, F. Xu, H. Zheng, L. Sun, “Electrically driven cation exchange for in-situ fabrication of individual nanostructures” *Nature Communications* **8** 14889 (2017).

Revealing Transient States and Electron, Spin and Lattice Correlations in Quantum Materials

Yimei Zhu, Lijun Wu, Xuwen Fu, Junjie Li, Jing Tao and Tatiana Konstantinova

Condensed Matter Physics and Materials Science Division

Brookhaven National Laboratory, Upton, NY 11973

Research Scope

The ability to visualize atomic and electronic structure that controls material functionalities at unprecedented spatial and temporal resolution creates enormous opportunities for modern science and technologies [1]. The goal of this FWP (No. MA-015-MACA) is to advance such abilities by developing electron-microscopy based methods and instrumentation to study strongly correlated electron systems and quantum materials. Our main focus is on revealing transient or “hidden” states and understanding the competing order of electron, spin, orbital and lattice and the role of defects, interfaces and electronic inhomogeneity in condensed matter. Three classes of materials are studied: correlated electron systems, multiferroics and energy materials. The study of multiferroics is a subtask of this FWP, which is covered by a separate abstract.

Recent Progress

To understand materials’ structural behavior at quantum and atomic level we try to address the following questions: What is the origin of inhomogeneity and disorder that controls the overall material properties? What is the role of charge and chemical doping and strain in interfacial phenomena, including superconductivity? How can we improve our ability in dynamically visualizing the competing orders of electrons and phonons and “hidden” states by developing novel instrumentation? Over the past two years we have unraveled several long-standing puzzles regarding electron-lattice correlation, in particular, the unique structural behavior in quantum materials (see the publication list).

Direct imaging of interfacial electron transfer and its influence on superconducting pairing One distinct characteristic of strongly correlated quantum materials is that their electronic states are often spatially

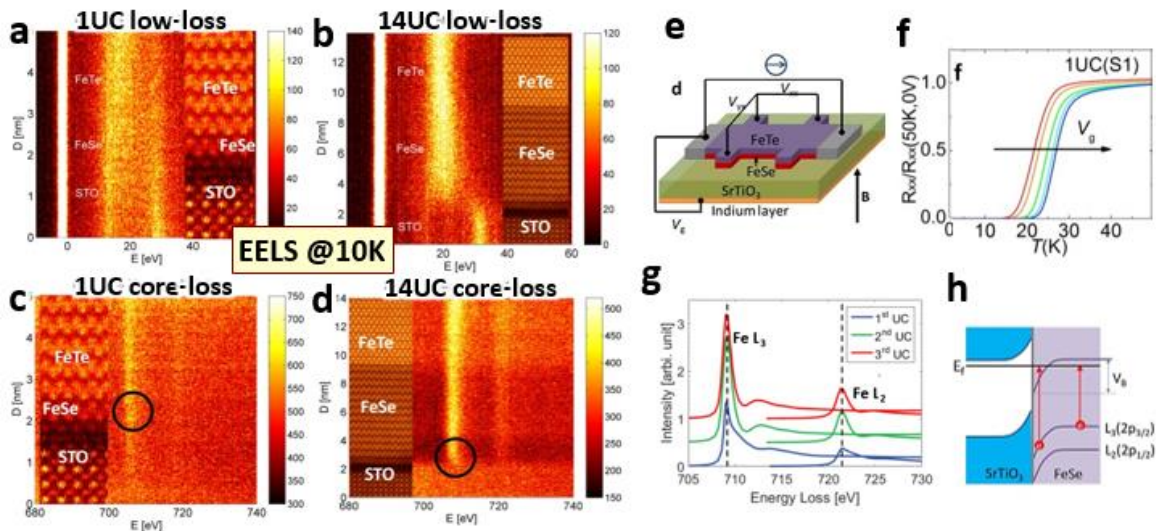


Fig. 1. Interfacial superconductivity of FeSe films on STO substrates. (a-d) atomically resolved low-loss and core-loss EELS mapping at 10K across the FeSe of 1UC and 14UC thickness. (e-f) Normalized resistivity vs. temperature measurements showing backgating voltage V_g can enhance interfacial superconductivity. (g-h) Origin of the blue-shift of Fe L₂₃ peaks in FeSe films observed in core-loss EELS (circled areas in c-d) is attributed to the interfacial band bending (h) rather than chemical environment (g) or interfacial strain (not shown) [2].

inhomogeneous and is very well suited for spatially resolved electron probes. A good example is the tenfold increase in the superconducting transition temperature (T_c) in 1UC (unit-cell) FeSe on SrTiO₃ (STO) over the bulk FeSe. Despite intensive studies the exact mechanism responsible for the enhancement remained elusive. For instance, angle-resolved photoemission spectroscopy and scanning tunneling microscopy show no superconducting gap in the 2UC system, in sharp contrast to the transport measurement where superconductivity is clearly seen. Demystifying the role of the interface on superconductivity requires characterizations below T_c with sufficient energy and spatial resolution. Facing the challenge, we for the first time conducted atomic resolution low-temperature (10K) electron energy-loss spectroscopy (EELS) (Fig.1 a-d) along with Hall transport measurements (Fig.1 e) on various FeSe/STO samples in collaboration with researchers at MIT and Penn State University. We successfully mapped fine structure of EELS across the FeSe/STO interfaces with 1UC, 2UC, 8UC, and 14UC thick FeSe films. The low-loss data, allowing measurements of local plasmonic excitation and hence carrier density, were taken simultaneously with the core-loss data. At 10K, a temperature below T_c , we clearly observe an energy shift of Fe core-loss localized within 2UC proximal FeSe layer (black circles in Fig.1c-d). This provides direct evidence of electrons transfer from STO into FeSe. Spectroscopy simulation with the FEFF codes on the blue shift mechanism of the Fe-L_{2,3} edge excludes the local chemical environment and strain as the cause (Fig.1g). Our backgated transport measurements further confirm the contribution of electronic band-bending effect on superconductivity by pulling electrons through gate voltage toward the FeSe/STO interface, which could be used to tune T_c of the films (Fig.1f). The observations suggest the STO substrate can play a dual role in enhancing the superconducting transition, namely by increasing the electron density close to the interface and by providing the high Debye temperature phonon bath that condenses these interfacial electrons. Our approach demonstrates that atomically resolved cryo-EELS can be a powerful tool to study the interfacial electronic structure and superconducting phenomena [2].

Electron-lattice interaction dynamics in cuprate superconductors In the area of ultrafast science we systematically studied Bi₂Sr₂CaCu₂O_{8+δ} single crystal superconductors to understand the interplay between the electronic and lattice degrees of freedom in nonequilibrium states. The nonequilibrium approach allows us not only to separate fundamental interactions in time domain, but also to study dynamics of collective states (i.e. melting of Cooper pairs' condensate) and to get insight about processes that are involved in creation and relaxation of photoinduced transient states, not accessible through static ambient conditions. We carried out the first combined experiments of ultrafast electron diffraction (UED) and time- and angle-resolved photoemission spectroscopy (trARPES). The two techniques are complementary, the former provides direct measurement of lattice movements but lacks information about the spectral content of the electronic degrees of freedom. In contrast, the latter probes electron dynamics but cannot unambiguously determine the nature of the bosons involved. The techniques provide momentum-resolved information about electron and phonon population – an advantage over momentum-averaged techniques such as all-optical pump-probe experiments.

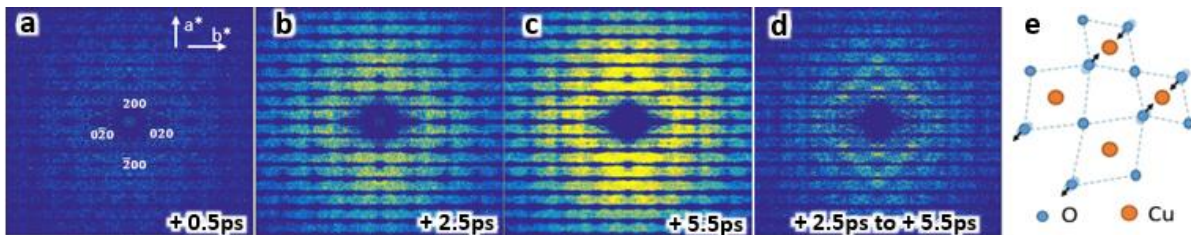


Fig. 2. Analysis of the thermal diffuse scattering (TDS) dynamics at 30K using ultrafast electron diffraction in Bi₂Sr₂CaCu₂O_{8+δ} superconductors. (a-d) TDS images obtained by subtracting intensities before photoexcitation at certain delays after the laser pulse arrival. (a) high-energy mode, (b) mostly optical phonons, (c) optical and acoustic phonons, (d) mostly acoustic phonons with correlated atomic motions along the $\langle 110 \rangle$ directions. Dark horizontal lines along the $\langle 110 \rangle$ directions are depleted intensity of Bragg and superlattice peaks after subtraction. (e) Schematic motion of atoms for the half-breathing phonon mode [3].

In our UED study quantitative analysis of the intensity changes of Bragg and superlattice reflections as well as thermal diffuse scattering (TDS) at various time delays after photoexcitation reveals how the energy is transferred from electrons to phonons and from one phonon branch to others along with the time scales related to the path of energy thermalization within the lattice. Bloch wave simulations show that the energy absorbed by electrons is transferred to Cu-O breathing phonons only (Fig. 2e). Thus, the electron-phonon coupling on the sub-picosecond time scale is anisotropic and is limited to the ab-plane. The lowest energy acoustic branches with correlated atomic motions along the $\langle 110 \rangle$ directions forms on 10 ps scale, the characteristic time is much slower than dynamics of the electronic states. Detailed analysis of the lattice and electron subsystems' dynamics provides a unified picture of nonequilibrium electron-phonon interactions in the cuprates beyond the N-temperature model. The work provides new insights on the specific phonon branches involved in the nonequilibrium heat dissipation from the high-energy Cu-O bond stretching "hot" phonons to the lowest-energy acoustic phonons. It reveals a highly nonthermal phonon population during the first several picoseconds after the photoexcitation. The approach, taking advantage of the distinct nature of electrons and photons as probes, is applicable for studying energy relaxation in other strongly correlated electron systems [3].

Future Plans

Retrieving loss-function from VEELS to study band structure and charge transfer We recently developed an algorithm and a procedure to retrieve the energy-loss function and real part of inverse complex dielectric function from raw data of valence electron energy-loss spectroscopy (VEELS) [4]. The development allows us to separate bulk-, surface-losses from Cherenkov radiation, which is a longstanding problem in studying valence electron plasmon response using VEELS even in simple semiconductors and insulators. With the progress we made we plan to study band structure, charge transfer, optical properties, and phonon behavior in strongly correlated quantum materials, including their interfaces and defects. The results will be compared with Fourier transform infrared spectroscopy and DFT calculations.

Explore "hidden" states and spin-lattice and charge-lattice dynamics Magnetic quasi-particles such as Majorana fermions, Skyrmions and topological vortices are promising candidates for quantum information science and technology. In vortices, various spin states associated with chirality and/or polarity can be manipulated by controlling their relaxation dynamics upon excitation. Comparing to the vortex switching through the core gyrotropic motion driven by external magnetic fields, spin-polarized currents, or spin waves, the optical excitation has advantages due to the absence of gyrotropic motion. Here we plan to study transient spin phenomena using in-situ ultrafast optical quenching in spin vortex systems. Figure 3 shows our recent work on femtosecond (fs)-laser-pulse induced spin states and switching behavior confined in Permalloy (Py) disks. Under the $>10^{12}$ K/s quenching rate induced by the fs-laser, a plenitude of new symmetric and complex "hidden states" with different occurrence frequencies were observed. These "hidden states" consist of a number of unexpected topological defects, vortex and antivortex, that strictly conserve the topological winding number, indicating the direct impact of the topological invariant on the magnetization dynamics in these Py disks. Furthermore, the unique spin configurations show high mirror- or rotation-symmetry because of their geometrical confinement [5].

We will take advantage of the extraordinary high quenching rate in TEM to directly visualize the dynamical process of micro/nanoscale spin structures under fs-laser stimuli. Besides the Py disks we will focus on Skyrmions and the related non-trivial chiral spin textures in multi-layer films with strong Dzyaloshinskii-Moriya interactions. Systematic micromagnetic simulations will be carried out to assist experimental observations and to uncover the underlying magnetization dynamics and the origin of these "hidden states" and their formation-growth energetics and pinning mechanism. Similar studies on charge-lattice dynamics in ferroelectric vortices in hexagonal manganites and charge- and orbital-ordered systems will also be carried out. Further direction in studying nonequilibrium behavior using UED is targeting specific collective excitations through application of the pump in 5–100 meV range. This approach allows to study the effect of specific phonon modes on collective electronic states as well as phonon-phonon interactions.

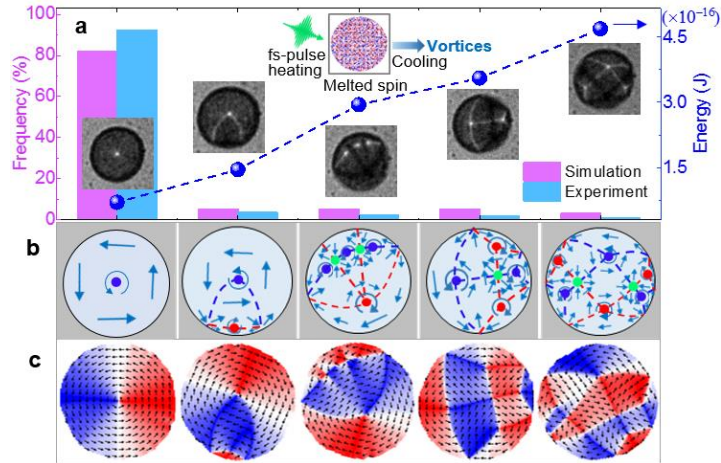


Fig.3 Optical manipulation of spin vortex visualized by in-situ 4D microscopy. Selected magnetic structures in Py circular disks after the fs-laser pulse excitation (fluence of 12 mJ/cm^2) and quenching at a cooling rate up to 10^{12} K/s . (a-c) Statistic occurrence frequency distribution and energy evolution of experimentally observed magnetic structures (a-b) along with the micromagnetic simulations (c) of vortex and antivortex pairs, revealing the “hidden states” that have not been seen in traditional field- and current-induced spin switching processes. Red and blue colors correspond to opposite spin directions. [5]

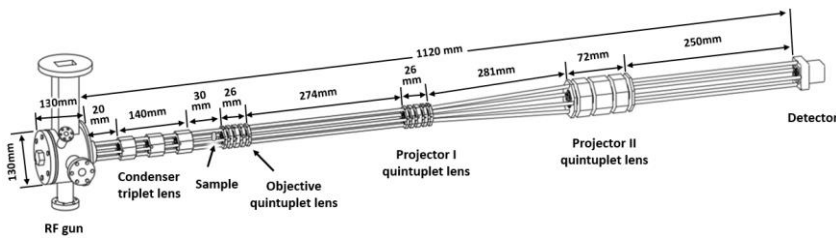


Fig. 4. Design of a compact 3 MeV ultrafast electron microscope based on the compound condenser, objective, projector quadrupole multiplets imaging system with a RF-gun [6].

Development of a compact MeV ultrafast electron microscope Recently we have successfully calculated and designed a compact 3MeV ultrafast electron microscope based on compact quadrupole lenses [6]. The entire system is only a little over 1 meter long (Fig.4). Quadrupole lenses are known to have very strong focusing power, especially for high-energy electrons compared to traditional round lenses. However, they are notorious for their property of focusing in one direction and defocusing in the other. As a result, it is very challenging to adopt them for electron microscopy. We overcome the problem by designing quadrupole-based multiplets, including triplet, quadruplet and quintuplet to achieve optical performance similar to round-lens systems. Our calculations involving up to the 5th order spherical and chromatic aberrations show the instrument can achieve 0.4 nm spatial resolution. With a bright electron source picosecond temporal resolution is possible for single-shot imaging [6]. We plan to build these quadrupole lenses and test their performance step by step. Our final goal is to assemble a MeV microscope that can fit into a small-sized laboratory for ultrafast observations and measurements. This development is in part supported by the SBIR and BNL-LDRD grants.

References

- [1] “Quantum Materials for Energy Relevant Technology”, DOE Basic Research Needs Workshop Report. <http://science.energy.gov/bes/news-and-resources/reports/> (2016).
- [2] Zhao, et al., ”Direct imaging of electron transfer and its influence on superconducting pairing at FeSe/SrTiO₃ interface”, *Sci. Adv.* 4, eaao2682 (2018).
- [3] Konstantinova, et al., “Non-equilibrium electron and lattice dynamics of strongly correlated Bi₂Sr₂CaCu₂O_{8+δ} single crystals”, *Sci. Adv.* 4, eaap7427 (2018).
- [4] Meng, et al., “Retrieving the energy-loss function from valence electron energy-loss spectrum: separation of bulk-, surface-losses and Cherenkov radiation”, *Ultramicroscopy* 194, 175-181 (2018).
- [5] Fu, X., Pollard, S.D., Chen, B., Yoo, B.K., and Zhu, Y., “Optical manipulation of magnetic vortex visualized in situ by 4D electron microscopy”, *Sci. Adv.* 4, aat3077 (2018).
- [6] Wan, W., Chen, F-R., and Zhu, Y., “Design of compact ultrafast microscopes for single- and multi-shot imaging with MeV electrons”, *Ultramicroscopy*, 194 143-153 (2018).

Selected Publications (Total 84)

2018

1. Bae, I-T., Ichinose, T., Han, M.-G., Zhu, Y., Yasui, S., and Naganuma, H., “Tensile stress effect on epitaxial BiFeO₃ thin film grown on KTaO₃”, *Sci. Rep.* 8:893 (2018).
2. Baldini, E., Kubacka, T., Mallett, B.P.P., Ma, C., Koohpayeh, S.M., Zhu, Y., Bernhard, C., Johnson, S.L., and Carbone, F., “Lattice-mediated magnetic order melting in TbMnO₃”, *Phys. Rev. B* 97, 125149 (2018).
3. Cao, Y., Wang, Z., Park, S.Y., Yuan, Y., Liu, X., Nikitin, S., Akamatsu, H., Kareev, M., Middey, S., Meyers, D., Thompson, P., Ryan, P., Shafer, P., N'Diaye, A., Arenholz, E., Gopalan, V., Zhu, Y., Rabe, K., and Chakhalian, J., “Artificial two-dimensional polar metal at room temperature”, *Nat. Commun.* 9, 1547 (2018).
4. Cheng, S., Xu, C., Deng, S., Han, M.-G., Bao, S., Ma, J., Nan, C., Duan, W., Bellaiche, L., Zhu, Y., Zhu, J., “Interface reconstruction with emerging charge ordering in hexagonal manganite”, *Sci. Adv.* 4, aar4298 (2018).
5. Cheng, S., Zhang, D., Deng, S., Li, X., Li, J., Tan, G., Zhu, Y., and Zhu, J., “Domain configurations in dislocations embedded hexagonal manganite systems: From the view of graph theory”, *Appl. Phys. Lett.* 112, 162905 (2018).
6. Fu, X., Pollard, S.D., Chen, B., Yoo, B.K., and Zhu, Y., “Optical Manipulation of Magnetic Vortex Visualized in situ by 4D Electron Microscopy”, *Sci. Adv.* 4, aat3077 (2018).
7. Guo, R., Zhou, Y., Wu, L., Wang, Z., Lim, Z., Yan, X., Lin, W., Wang, H., Yoong, Y., Chen, S., Venkatesan, T., Wang, J., Chow, G.M., Gruverman, A., Miao, X., Zhu, Y., and Chen, J., “Control of synaptic plasticity learning of ferroelectric tunnel memristor by nanoscale interface engineering”, *ACS Appl. Mater. Interfaces* 10, 12862–12869 (2018).
8. Han, M-G., Li, J., Xue, F., Wang, X., Meng, Q.-P., Tao, J., Chen, L.-Q., Cheong, S.-W., and Zhu, Y., “Linearly aligned single-chiral vortices in hexagonal manganites by *in situ* electric arc heating”, *Phys. Rev. Mater.* 2, 64004 (2018).
9. Hu, X., Huang, J., Wu, L., Kaltak, M., Fernandez-Serra, M., Meng, Q., Wang, L., Marschilok, A.C., Takeuchi, E.S., Takeuchi, K.J., Hybertsen, M.S., and Zhu, Y., “Revealing effect of oxygen vacancy and surface disorder on ionic transport in one-dimensional tunneled structure”, *Chemistry of Materials*, DOI: 10.1021/acs.chemmater.8b02575 (2018).
10. Hu, X., Kitchaev, D.A., Wu, L., Zhang, B., Meng, Q., Poyraz, A.S., Marschilok, A.C., Takeuchi, E.S., Takeuchi, K.J., Ceder, G., and Zhu, Y., “Revealing and rationalizing the rich polytypism of todorokite MnO₂”, Cover article, *J. Am. Chem. Soc.*, 140, 6961-6968 (2018).
11. Kim, J.-Y., Han, M.-G., Lien, M.-B., Magonov, S., Zhu, Y., George, H., Norris, T. B., and Kotov, N. A., “Dipole-like electrostatic asymmetry of gold nanorods”, *Sci. Adv.* 4, e1700682 (2018).
12. Konstantinova, T., Rameau, J.D., Reid, A.H., Abdurazakov, O., Wu, L., Li, R.K., Shen, X., Gu, G., Huang, Y., Rettig, L., Avigo, I., Ligges, M., Freericks, J., Kemper, A. F., Dürr, H.A., Bovensiepen, U., Johnson, P.D., Wang, X., and Zhu, Y., “Non-equilibrium electron and lattice dynamics of strongly correlated Bi₂Sr₂CaCu₂O_{8+δ} single crystals”, *Sci. Adv.* 4, eaap7427 (2018).
13. Kwon, J.-H., Meng, Y., Wu, L., Zhu, Y., Zhang, Y., Selvamanickam, V., Welp, U., Kwok, W.-K., and Zuo, J.-M., “Extended electronic structure inhomogeneity created by double chain layer defects surrounding columnar tracks in heavy ion irradiated YBa₂Cu₃O_{7-δ}”, *Supercon. Sci. Technol.* 1361-6668, aad842 (2018).
14. Li, J., Cheng, S., Wu, L., Tao, J., and Zhu, Y., “The effect of scanning jitter on geometric phase analysis in STEM images”, *Ultramicroscopy* 194 167-174 (2018).
15. Li, J., Sun, K., Li, J., Meng, Q.-P., Fu, X., Yin, W.-G., Lu, D., Li, Y., Babzien, M., Fedurin, M., Swinson, C., Malone, R., Palmer, M., Mathurin, L., Manso, R., Chen, J., Konik, R. M., Cava, R.J., Zhu, Y., and Tao, J., “Probing pathway of an ultrafast structural phase transition to illuminate the transition mechanism in Cu₂S”, *Appl. Phys. Lett.* 113, 041904 (2018).

16. Li, M., Tsurimaki, Y., Meng, Q.-P., Andrejevic, N., Zhu, Y., Mahan, G.D., and Chen, G., “Theory of electron–phonon–dislon interacting system—toward a quantized theory of dislocations”, *New J. Phys.* 20, 023010 (2018).
17. Lu, C., Jiang, T., Liu, S., Wang, R., Zhao, L., Zhu, P., Liu, Y., Xu, J., Yu, D., Wan, W., Zhu, Y., Xiang, D., and Zhang, J., “Imaging nanoscale spatial modulation of a relativistic electron beam with a MeV ultrafast electron microscope”, *Appl. Phys. Lett.* 112, 113102 (2018).
18. Meng, Q., Wu, L., Welch, D.O., Tang, Meng., and Zhu, Y., “Non-uniform stress-free strains in a spherically symmetrical nanosized particle and its applications to lithium-ion batteries”, *Sci. Rep.* 8, 4936 (2018).
19. Meng, Q.-P., Wu, L., Xin, H.L., and Zhu, Y., “Retrieving the energy-loss function from valence electron energy-loss spectrum: separation of bulk-, surface-losses and Cherenkov radiation”, *Ultramicroscopy* 194, 175-181 (2018).
20. Peng, L., Fang, Z., Li, J., Wang, L., Bruck, A. M., Zhu, Y., Zhang, Y., Takeuchi, K. J., Marschilok, A. C., and Stach, E. A., “Two-dimensional holey nanoarchitectures created by confined self-assembly of nanoparticles via block copolymers: From synthesis to energy storage property”, *ACS Nano* 12, 820–828 (2018).
21. Precner, M., Polaković, T., Qiao, Q., Trainer, DJ., Putilov, AV., Di Giorgio, C., Cone, I., Zhu, Y., Xi, X., Iavarone, M., and Karapetrov, G., "Evolution of metastable defects and its effect on the electronic properties of MoS₂ films", *Sci. Rep.* 8, 6724 (2018).
22. Reid, A. H., Shen, X., Maldonado, P., Chase, T., Jal, E., Granitzka, P.W., Carva, K., Li, R.K., Li, J., Wu, L., Vecchione, T., Liu, T., Chen, Z., Higley, D.J., Hartmann, N., Coffee, R., Wu, J., Dakowski, G.L., Schlotter, W., Ohldag, H., Takahashi, Y.K., Mehta, V., Hellwig, O., Fry, A., Zhu, Y., Cao, J., Fullerton, E.E., Stöhr, J., Oppeneer, P.M., Wang, X.J., and Dürr, H.A., “Beyond a phenomenological description of magnetostriction”, *Nat. Commun.* 9, 388 (2018).
23. Wan, W., Chen, F.-R., and Zhu, Y., “Design of compact ultrafast microscopes for single- and multi-shot imaging with MeV electrons”, *Ultramicroscopy*, 194 143-153 (2018).
24. Wang, P.P., Qiao, Q., Zhu, Y., and Ouyang, M., “Colloidal binary supracrystals with tunable structural lattices”, *J. Am. Chem. Soc.* 140, 9095-9098 (2018).
25. Wang, Z., Guo, H., Shao, S., Saghayezhian, M., Li, J., Fittipaldi, R., Vecchione, A., Siwakoti, P., Zhu, Y., Zhang, J., and Plummer, E.W., “Designing antiphase boundaries by atomic control of heterointerfaces”, *Proc. of Natl. Acad. Sci.*, (2018); doi/10.1073/pnas.1808812115.
26. Xia, W., Yang, Y., Meng, Q.-P., Deng, Z., Gong, M., Wang, J., Wang, D., Zhu, Y., Sun, L., Xu, F., Li, J., and Xin, H. L., “Bimetallic nanoparticle oxidation in three dimensions by chemically sensitive electron tomography and in situ transmission electron microscopy”, *ACS Nano*, (2018), DOI: 10.1021/acsnano.8b02170
27. Zhang, B., Wu, L., Zheng, J., Yang, P., Yu, X., Ding, J., Heald, S. M., Rosenberg, R. A., Venkatesan, T., Chen, J., Sun, C.-J., Zhu, Y., and Chow, G. M., “Control of magnetic anisotropy by orbital hybridization with charge transfer in (La_{0.67}Sr_{0.33}MnO₃)_n/(SrTiO₃)_n superlattice”, *NPG Asia Materials*, accepted (2018).
28. Zhang, W., Yu, H.-C., Wu, L., Liu, H., Abdellahi, Z., Qiu, B., Bai, J., Orvananos, B., Strobridge, F.C., Zhou, X., Liu, Z., Ceder, G., Zhu, Y., Thornton, K., Grey, C.P., and Wang, F., “Localized concentration reversal of lithium during intercalation into nanoparticles”, *Sci. Adv.* 4, eaao2608 (2018).
29. Zhao, W., Li, M., Chang, C.-Z., Jiang, J., Wu, L., Liu, C., Moodera, J.S., Zhu, Y.*, and Chan, M.H.W., ”Direct imaging of electron transfer and its influence on superconducting pairing at FeSe/SrTiO₃ interface”, *Sci. Adv.* 4, eaao2682 (2018).

2017

30. Cheng, S., Li, J., Han, M.-G., Deng, S., Tan, G., Zhang, X., Zhu, J., and Zhu, Y., “Topologically allowed non-six-fold vortices in a six-fold multiferroic material: Observation and classification”, *Phys. Rev. Lett.* 118, 145501 (2017).
31. Dai, Y., Fang, Y., Cai, S., Wu, L., Yang, W., Yan, H., Xie, J., Zheng, J.-C., Takeuchi, E., and Zhu, Y., “Surface modified pinecone shaped hierarchical structure fluorinated mesocarbon microbeads for ultrafast discharge and improved electrochemical performances”, *J. Electrochem. Soc.* 164, A1-A7 (2017).
32. Guo, H. W., Wang, Z., Dong, S., Saghayezhian, M., Chen, L., Weng, Y. K., Jin, R. Y., Zhu, Y., Zhang, J. D., and Plummer, E. W., “Role of spin-lattice coupling in ultrathin magnetoelectric oxide superlattices”, *Pro. Nat. Acad. Sci.*, 114, 26 (2017)
33. Han, M.-G., Garlow, J.A., Marshall, M.S.J., Tiano, A.L., Wong, S.S., Cheong, S.-W., Walker, F.J., Ahn, C.H., and Zhu, Y., “Electron-beam-induced-current and active secondary-electron voltage-contrast with aberration-corrected electron probes”, *Ultramicroscopy* 177, 14-19 (2017).
34. Hwang, S., Meng, Q., Chen, P-F., Kisslinger, K., Cen, J., Orlov, A., Zhu, Y., Stach, E.A., Chu, Y-H., and Su, D., “Strain coupling of conversion-type Fe₃O₄ thin films for lithium ion batteries”, *Angew. Chem. Int. Ed.* 56 7813-7816 (2017).
35. Kornblum, L., Fenning, D. P., Faucher, J., Hwang, J., Boni, A., Han, M. G., Morales-Acosta, M. D., Zhu, Y., Altman, E. I., Lee, M. L., Ahn, C. H., Walker, F. J., and Shao-Horn, Y., “Solar hydrogen production using epitaxial SrTiO₃ on a GaAs photovoltaic”, *Energy Environ. Sci.* 10, 377 (2017).
36. Lee, S. -Y., Wu, L., Poyraz, A. S., Marschilok A.C., Takeuchi, K. J., Takeuchi, E. S., Kim, M., and Zhu, Y., “Lithiation mechanism of tunnel-structured MnO₂ nanowire investigated by in situ transmission electron microscopy”, *Adv. Mater.* 29 (43), 1703186 (2017).
37. Lei, Q., Golalikhani, M., Davidson, B., Liu, G., Schlom, D., Qiao, Q., Zhu, Y., Chandrasena, R., Yang, W., Gray, A., Arenholz, E., Farrar, A., Tenne, D., Hu, M., Guo, J., Singh R., and Xi, X.X., “Constructing oxide interfaces and heterostructures by atomic layer-by-layer laser molecular beam epitaxy”, *npj Quantum Mater.* 2, 10 (2017).
38. Li, L., Deng, X., Wang, Z., Liu, Y., Abeykoon, M., Dooryhee, E., Tomic, A., Huang, Y., Warren, J., Bozin, E., Billinge, S., Sun, Y., Zhu, Y., Kotliar, G., and Petrovic, C., "Superconducting order from disorder in 2H-TaSe_{2-x}S_x", *npj Quantum Mater.* 2, 11 (2017).
39. Li, M., Ding, Z., Meng, Q., Zhou, J., Zhu, Y., Liu, H., Dresselhaus, M.S., and Chen, G., "Nonperturbative quantum nature of the dislocation-phonon interaction", *Nano Lett.* 17, 1587-1594 (2017).
40. Li, M., Song, Q., Zhao, W., Garlow, J.A., Liu, T.H., Wu, L., Zhu, Y., Moodera, J.S., Chan, M.H.W., Chen, G., and Chang, C.-Z., “Dirac-electron-mediated magnetic proximity effect in topological insulator/magnetic insulator heterostructures”, *Phys. Rev. B*, 96, 201301(R) (2017).
41. Li, M., Tsurimaki, Y., Meng, Q.-P., Andrejevic, N., Zhu, Y., Mahan, G., and Chen, G., “Theory of electron-phonon-dislon interacting system – Toward a quantized theory of dislocations”, *New J. Phys.* 107595.R1 (2017).
42. Lien, M.-B., Kim, J-Y., Han, M.-G., Chang, Y.-C., Chang, Y.-C., Ferguson, H.J., Zhu, Y., Herzing, A. A., Schotland, J.C., Kotov, N.A., and Norris, T. B. "Optical asymmetry and nonlinear light scattering from colloidal gold nanorods", *ACS Nano* 11, 5925-5932 (2017).
43. Pollard, S.D., Garlow, J.A., Yu, J., Wang, Z., Zhu, Y.*, and Yang, H., “Observation of stable Néel skyrmions in Co/Pd multilayers with lorentz TEM”, *Nat. Commun.* 8, 14761 (2017). *corresponding author.
44. Poyraz, A.S., Huang, J.P., Pelliccione, C.J., Tong, X., Cheng, S.B., Wu, L., Zhu, Y., Marschilok, A.C., Takeuchi, K.J., and Takeuchi, E.S. "Synthesis of cryptomelane type a-MnO₂ (K_xMn₈O₁₆) cathode

- materials with tunable K^+ content: The role of tunnel cation concentration on electrochemistry", *J. Mater. Chem. A* 5, 16914-16928 (2017).
45. Qiao, Q., Zhou, S., Tao, J., Zheng, J.-C., Wu, L., Ciocys, S.T., Iavarone, M., Srolovitz, D.J., Karapetrov, G., and Zhu, Y., "Anisotropic charge density wave in layered 1T-TiSe₂", *Phys. Rev. Mater.* 1, 054002 (2017).
 46. Saghayezhian, M., Wang, Z., Guo, H. W., Zhu, Y., Plummer, E. W., and Zhang, J. D., "Control of polar discontinuity at the interface complex oxides: LaNiO₃/SrTiO₃(111)", *Phys. Rev. B*, 95, 165434 (2017).
 47. Tao, J., Chen, J., Li, J., Mathurin, L., Zheng, J.C., Li, Y., Lu, D., Cao, Y., Wu, L., Cava, R. J., and Zhu, Y., "Reversible structure manipulation by tuning carrier concentration in metastable Cu₂S", *Proc. Natl. Acad. Sci.*, 114, 9832 (2017).
 48. Tao, J., Sun, K., Tranquada, J. M., and Zhu, Y., "Anomalous nanoclusters, anisotropy and electronic nematicity in doped manganite La_{1/3}Ca_{2/3}MnO₃", *Phys. Rev. B*, 95, 235113 (2017).
 49. Wu, D., Wu, L., He, D., Zhao, L.-D., Li, W., Wu, M., Jin, M., Xu, J., Jiang, J., Huang, L., Zhu, Y., Kanatzidis, M.G., and He, J.Q., "Direct observation of vast off-stoichiometric defects in single crystalline SnSe", *Nano Energy* 35, 321 (2017).
 50. Xu, F., Wu, L., Meng, Q., Kaltak, M., Huang, J., Durham, J.L., Fernandez-Serra, M., Sun, L., Marschilok, A.C., Takeuchi, E.S., Takeuchi, K.J., Hybertsen, M.S., and Zhu, Y., "Visualization of lithium-ion transport and phase evolution within and between manganese oxide nanorods", *Nat. Commun.* 8, 15400 (2017).
 51. Zhang, W., Topsakal, M., Cama, C., Pelliccione, C. J., Zhao, H., Ehrlich, S., Wu, L., Zhu, Y., Frenkel, A. I., Takeuchi, K. J., Takeuchi, E. S., Marschilok, A. C., Lu, D., and Wang, F., "Multi-stage structural transformations in zero-strain lithium titanate unveiled by in-situ X-ray absorption fingerprints", *J. Am. Chem. Soc.* 139, 16591–16603 (2017).
 52. Zhou, H., Wu, L., Wang, H.-Q., Zhang, L., Kisslinger, K., Zheng, J.-C., Li, Y., Wang, Z., Cheng, H., Ke, S., Li, Y., Kang, J., and Zhu, Y., "Interfaces between hexagonal and cubic oxides and their structure alternatives", *Nat. Commun.* 8, 1474 (2017).
 53. Zhou, L., Huang, S., Tatsumi, Y., Wu, L., Guo, H., Bie, Y.-Q., Ueno, K., Yang, T., Zhu, Y., Kong, J., Saito, R., and Dresselhaus, M., "Sensitive phonon-based probe for structure identification of 1T' MoTe₂", *J. Am. Chem. Soc.* 139 8396–8399 (2017).

***UNIVERSITY GRANT
PROJECTS***

Quantitative Interpretation of Phonon EELS Mapping in Nanoscale Structures

P.E. Batson and M.J. Lagos

Departments of Physics, and Materials Science
Rutgers, the State University of New Jersey
607 Taylor Road, Piscataway, NJ 08854-8019
batson@physics.rutgers.edu

Research Scope

This project seeks to develop spatially resolved EELS to better understand the *spatial* and *time* dependent behavior of charge density excitations in nanoscale structures on time scales that range from atto-seconds through pico-seconds. A theoretical goal of the work is to explore how the specimen time evolution might be derived from EELS spectral data, and to reveal general rules for using that information to better understand the nanoscale specimen dielectric response. In Fig. 1, we show a graphic depiction of a keV electron passing the edge of a nanoscale MgO cube. Atomic level displacements in response to the field imposed by the passing electron produce scattering that is mapped at a screen below. A goal of this project is to extract details of the excited state from the mapped aloof and bulk scattering of the electron beam. The graphic also suggests that the atomic displacements are pinned at the cube edges, by the nano-scale cube surfaces, and that they respond to the applied field of the swift electron, averaged over the whole path of the electron as visualized by Ritchie in 1957.[1]

On the other hand, a time resolved measurement of the electron position might result in a well defined location, such as the one in Fig. 1, about half way between the cube and the imaging screen in this graphic. For meV energy phonons, the specimen excitation and the electron position cannot be displayed realistically within the same graphic. For high energy excitations, however, a realistic view of a “wake” in the pattern of lateral forces on a 2 nm Au nanoparticle, and the instantaneous position of the passing electron -- at 9 atto-seconds after a close approach – can be shown in the same illustration, as in Fig. 2. [2]

We hope to reveal both short and long time behavior in a unified way for aloof electron paths, as depicted in these Figures, but also for the more typical paths that link the bulk material.

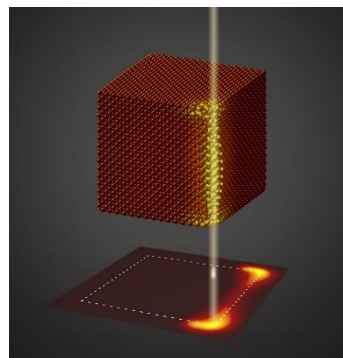


Fig. 1. A keV electron passing the edge of an MgO cube creates a phonon polariton mode pinned to the edge. An energy loss map is displayed below.

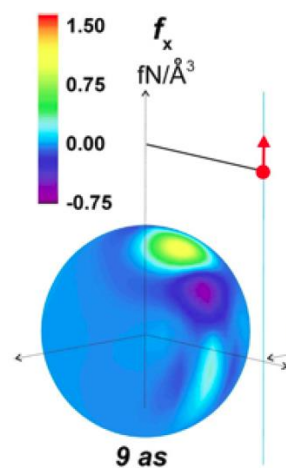


Fig. 2. A snapshot of the surface forces and electron position, 9 atto-sec after a close approach to a 2nm Au sphere. [2]

Recent Progress:

Acoustic Phonon Scattering Physics

In our first attempts to understand phonon mapping in MgO, we found that the polaritonic, *aloof* scattering was easy to understand using electrostatic field continuity conditions at the MgO surfaces, for the bulk Longitudinal Optical (LO) phonon mode. However, the Transverse Optical (TO) mode, prominent in IR absorption, is not obvious in EELS, while Acoustic modes, absent in the IR, are very strong in EELS spectra. In Fig. 3, we show four symmetry averaged EELS maps (left, from bottom to top) for the bulk LO, face, corner, and bulk Acoustic modes. On the right, we show a molecular dynamics calculation that strongly captures both dipole and non-dipole interactions. This method successfully describes dipole coupling in aloof locations; short ranged, high resolution atomic column interactions within the bulk; and even “Begrenzen”, or limiting, behavior of the LO modes near surfaces. These results are similar to Bloch wave calculations that also include very short wavelength modes. [4]

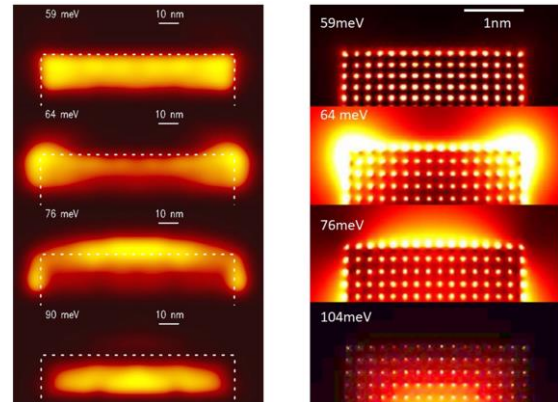


Fig. 3. Comparison of experiment with molecular dynamics calculations for the MgO case. Notice the aloof and bulk information are unified – resulting from the same microscopic physics. Note difference in size on the right. [3]

Spatially Resolved Phonon Thermometry

With the new equipment, energies down to 10 meV are accessible for the first time. As shown in Fig. 4, at finite temperatures we easily obtain both energy loss and energy gain. We also notice very strong intensity enhancement below room temperature (~ 25 meV). We know from microscopic reversibility that a *Principle of Detailed Balance* should apply. [5] This principle requires that at thermal equilibrium, each scattering process is accompanied by a reverse process,

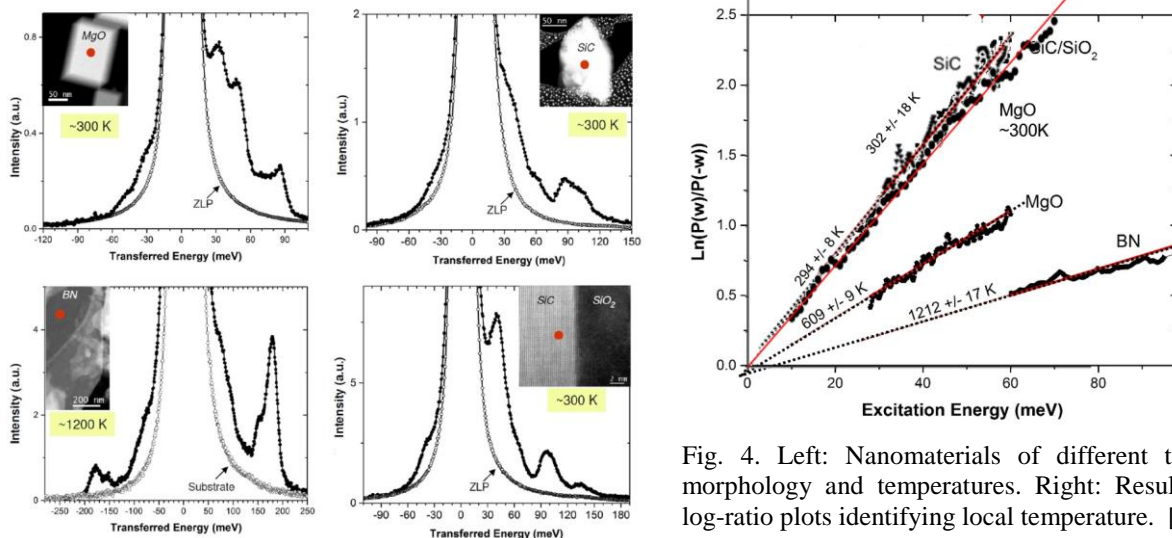


Fig. 4. Left: Nanomaterials of different type, morphology and temperatures. Right: Resulting log-ratio plots identifying local temperature. [6]

which occurs at a rate controlled by the Boltzmann distribution, $S(\mathbf{q}, \omega) = e^{\beta\omega} S(\mathbf{q}, -\omega)$, where $S(\mathbf{q}, \omega)$ is the Dynamical Form Factor which describes the electron scattering, and $\beta = 1/kT$, with k being the Boltzmann factor. This process is enabled by the temperature driven occupation of excited states which are then available to participate in the transfer of energy to the incident electron as an energy gain. So, in principle, the logarithm of a simple ratio of the energy loss intensity, to the energy gain intensity, should yield a straight line whose slope is $1/kT$. We illustrate this also in Fig. 4, for five different materials at various temperatures. Remarkably, we found in this and other examples, that the results do follow the simple form above, depending only on the local temperature, and not at all on the specimen morphology, or microscope collection conditions. This work has been published this year in ACS NanoLett.[6] Work from others finds similar results.[7]

Obtaining an Experimental Acoustic Phonon Density of States

The measurement of acoustic phonon intensities using an Angstrom sized electron probe is new to science. In the past, these excitations have been accessible only to inelastic neutron and x-ray scattering, both also governed by the dynamical form factor $S(\mathbf{q}, \omega)$ with differing pre-factors. In EELS the pre-factor is derived from the Coulomb potential and the geometry of the electron path with respect to the specimen. In addition, in the meV energy range at finite temperatures, we also expect a distortion of the EELS scattering driven by the non-zero occupation of available excitation states which obey Boson statistics for the phonons. Both the Coulomb prefactor and the occupation statistics produce multiplicative distortions of the EELS scattering in the very low energy range. Therefore, in order to derive an experimental ground state projected Phonon Density of States, or PDOS, we need to correct for distortions caused by these factors. Fig. 5 shows preliminary results

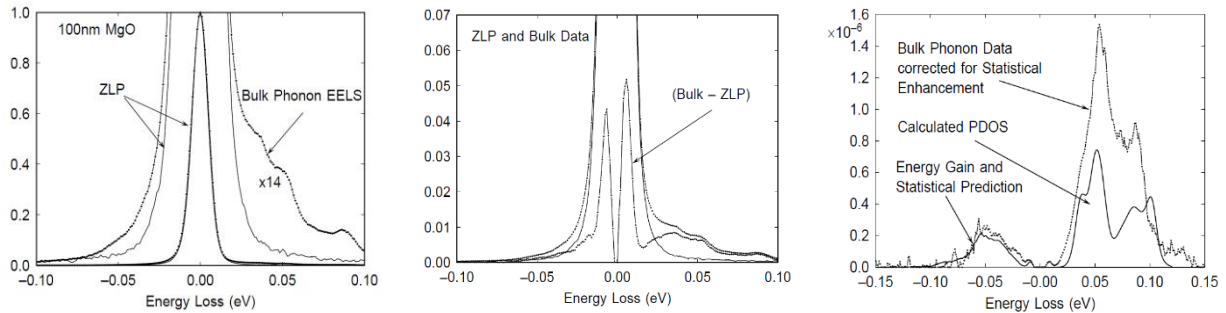


Fig. 5. Left: The vacuum Zero Loss Peak is compared with the Bulk Phonon EELS. Middle: After normalization of the ZLP with the EELS, the ZLP is subtracted to obtain energy loss and gain intensity. The strong peaks at very low energy are verified to be real inelastic scattering. Right: After correction for the strong energy dependent multiplicative factors, the experimental PDOS is compared with a calculated PDOS.[3] The energy gain comparison is derived from the experimental PDOS through the Principle of Detailed Balance.[6]

after removal of Bose-Einstein occupation and Coulomb pre-factors to display a *spatially resolved* ground state PDOS that in principle might be used as a basis for constructing a time resolved map of phonon excitations. This PDOS includes both Acoustic and LO Phonon modes, and non-zero momentum transfer, integrated over the probe forming optics, but it remains to be determined whether TO modes are included as well.

The work discussed above as Recent Progress has been published in Nature (Highly Cited), PRB, Ultramicroscopy, Microscopy and NanoLetters, and in M&M extended abstracts during 2017-2018. We also gave thirteen invited presentations during 2017-2018, with seven at international conferences, with acknowledgment of DOE BES support.

Future Plans

The result in Fig. 5 (right) might be the first ground state bulk PDOS obtained by EELS. It is similar to results obtained with inelastic x-ray scattering, [9] as it should be since each are proportional to $S(\mathbf{q}, \omega)$ when the pre-factors are removed. A **Goal** for the future now is to use it with valence and core losses to create a view of an excited state measurement in the time domain.

A second **Goal** for this project is to use these ideas at higher spatial resolution to experimentally reproduce the atomic resolution behavior predicted by the theoretical modeling described above.

Finally, we point out that standard mathematical methods for calculating electromagnetic behavior in heterogeneous nanostructures are cumbersome, particularly when mixed with relativistic electrons. These require elaborate modeling of heterogeneous boundaries, and strong assumptions about behavior. An example of this is the assumption that magnetic fields which accompany a relativistic electron are too weak to influence the electron scattering behavior. This turns out not to be true for very close approaches of the swift electron to a nanoparticle, where the magnetic interaction can actually dominate the lateral forces exerted by the electron on a metallic nanostructure.[2] Therefore, a third **Goal** for future work is to explore more complete mathematical methods for describing electromagnetic interactions between nanostructures and relativistic electrons. We think that the four-vector “Clifford” algebra [10] might help with this and we will spend some effort to explore how to use this geometric algebra for “unification” of bulk and aloof scattering within and nearby nanoscale structures.

References

- [1] R. H. Ritchie, Phys. Rev., **106** 874-881 (1957).
- [2] M. J. Lagos, A. Reyes-Coronado, A. Konečná, P. M. Echenique, J. Aizpurua, and P. E. Batson, Phys. Rev. B, **93** 205440 (2016).
- [3] U. Hohenester, A. Trügler, P.E. Batson and M.J. Lagos, Phys. Rev. B, **97** 165418 (2018).
- [4] B. D. Forbes and L. J. Allen, Phys. Rev. B, **94** (2016) 014110.
- [5] D. Pines and P. Nozières, The theory of quantum liquids (W. A. Benjamin, NY, 1966), p.132.
- [6] M.J. Lagos and P.E. Batson, NanoLett, **18** 4556 – 4563 (2018).
- [7] J. C. Idrobo, A. R. Lupini, T. Feng, R. R. Unocic, F. S. Walden, D. S. Gardiner, T. C. Lovejoy, N. Dellby, S. T. Pantelides, and O. L. Krivanek, Phys. Rev. Lett., **120** 095901 (2018).
- [8] P.E. Batson and M.J. Lagos, Microscopy and Microanalysis, in press (2018).
- [9] A.Q.R. Baron, arXiv:1504.01098v4 [cond-mat.mtrl-sci], (2015).
- [10] J. Dressel, K.Y. Bliokh, and F. Nori, Physics Reports, **589** 1-71 (2015).

Publications

Journal Articles:

- [1] M.J. Lagos, A. Trügler, U. Hohenester and P.E. Batson, Mapping Vibrational Surface and Bulk Modes in a Single Nanocube, *Nature*, 543 529 – 532 (2017) doi:10.1038/nature21699.
- [2] P.E. Batson and M.J. Lagos, Characterization of Misfit Dislocations in Si Quantum Well Structures Enabled by STEM Based Aberration Correction, *Ultramicroscopy*, 180 34-40 (2017) doi:10.1016/j.ultramic.2017.03.002.
- [3] M.J. Lagos, A. Trügler, V. Amarasinghe, L.C. Feldman, C. Leonard, U. Hohenester and P.E. Batson, Excitation of long-wavelength surface optical vibrational modes in films, cubes and film/cube composite system using an atom-sized electron beam, *Microscopy*, 67 i3-i13 (2018) doi:10.1093/jmicro/dfx130.
- [4] U. Hohenester, A. Trügler, P.E. Batson and M.J. Lagos, Inelastic vibrational bulk and surface losses of swift electrons in ionic nanostructures, *Phys. Rev. B*, 97 165418 (2018) doi:10.1103/PhysRevB.97.165418.
- [5] M.J. Lagos and P.E. Batson, Nanoscale thermometry with angstrom-resolution in the electron microscope, *NanoLett*, 18 4556 – 4563 (2018) doi:10.1021/acs.nanolett.8b01791.

Extended Abstracts:

- [1] M.J. Lagos and P.E. Batson, Electron Energy-Gain Processes in Nanostructures in induced by Fast Electrons, *Microscopy and Microanalysis*, Post Deadline Poster-44 (2017).
- [2] P.E. Batson and M.J. Lagos, Interpretation of meV Resolution Phonon EELS Data, *Microscopy and Microanalysis*, in press (2018).
- [3] M.J. Lagos and P.E. Batson, Nanoscale Temperature Measurements Using Phonon Scattering, *Microscopy and Microanalysis*, in press (2018).

Nanoscale Imaging of Optical-Frequency Plasmonic Energy Transfer in Individual Nanoparticles and their Assemblies

Jon P. Camden¹ and David J. Masiello²

¹Department of Chemistry and Biochemistry, University of Notre Dame, Notre Dame, IN 46556, ²Department of Chemistry, University of Washington, Seattle, WA 98195

Research Scope: Energy transfer induced by the decay of a localized surface plasmon (LSP) has attracted significant interest recently due to its importance in the design of next-generation energy harvesting devices. Understanding energy transfer pathways in different nanoparticle/environment interfaces are therefore essential in controlling and potentially improving energy transfer efficiency. In general, LSPs may enhance the efficiency of energy harvesting through one or more of the following mechanisms (Figure 1): (1) photon-plasmon scattering, increasing the likelihood of absorption by a nearby semiconductor or molecule;¹ (2) plasmonic resonance energy transfer (PRET), which occurs between an excited plasmon and the electronic transition dipole moment of a nearby semiconductor or molecule;² and (3) hot carrier transfer (HCT) from the nanoparticle to a nearby semiconductor or molecule, in which an LSP decays, through Landau damping,³ into hot carriers that may then scatter into the neighboring material if they have sufficient energy.^{4, 5} Importantly, energy transfer is a process strongly dependent on many factors such as the nanostructure's electronic properties, size, geometry, hybridization with other nearby nanoparticles, and its interface/contact to neighboring materials. For instance, theoretical calculations have shown that small (<20nm) nanoparticles generate hot electrons with higher energy benefiting hot electron injection,⁶ and structures supporting LSP modes with highly enhanced electric fields produce more energetic hot carriers and yield higher transfer efficiency.⁷ Understanding the underlying physics of these effects are critical for rational design of working nanosystems. However due to the high spatial localization of LSPs, studying the differing and competing energy transfer pathways is still a challenge for most optical spectroscopies due to the diffraction limit. To this end, electron energy loss spectroscopy (EELS) performed in a scanning transmission electron microscope (STEM) has proved sub-nanometer resolving power with the capability to interact with

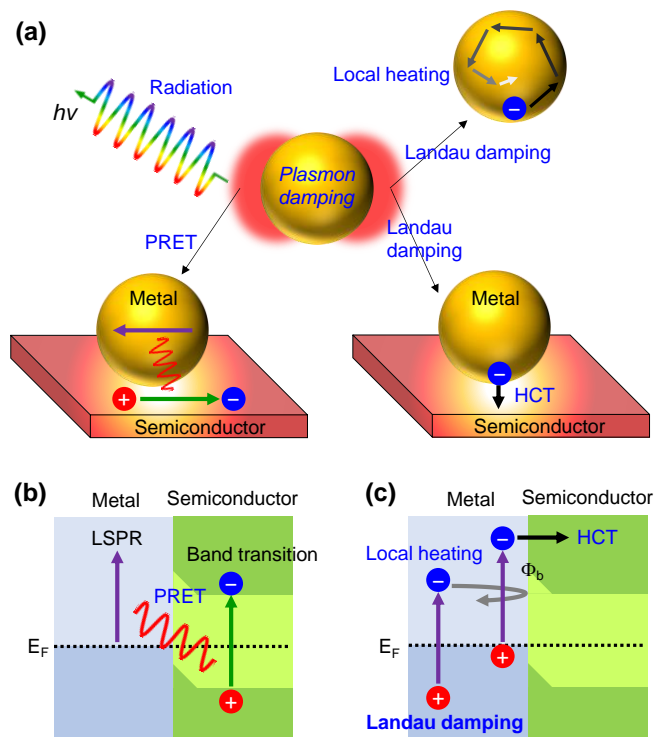


Figure 1. (a) A localized surface plasmon (LSP) can decay either radiatively via emitting photons to the far-field or non-radiatively via near-field dipole-dipole interaction with a neighboring semiconductor (PRET) or Landau damping. The hot carriers generated via Landau damping will either remain inside the metal and cause local heating, or overcome the Schottky barrier and enter the neighboring semiconductor (HCT). (b, c) Band diagrams illustrating PRET and HCT.

the full spectral range of LSP modes supported by the nanoparticle, and therefore has become the leading technique in plasmon characterization. Our goal is to utilize STEM/EELS techniques (Camden) to directly measure and even control energy transfer in hybrid plasmon-semiconductor systems and leverage detailed theoretical models combined with simulation (Masiello) to understand the essential underlying physics.

Recent Progress: *Completed and published an invited review describing STEM/EELS in plasmon characterization in Chemical Reviews.* This review provides a comprehensive description of EELS characterization of plasmonic nanoparticles, and we expect it will benefit both general and specialist readers interested in this field. *Chemical Reviews* is a high-impact publication (Impact Factor = 52.6). [Y. Wu, G. Li, and J. P. Camden, “Probing Nanoparticle Plasmons with Electron Energy Loss Spectroscopy”, *Chem. Rev.* 118, 6, 2994-3031.]

2. *STEM/EELS characterization of electron-driven Fano interferences in plasmonic nanostructures:* Fano antiresonances can result from the coupling between a spectrally broad (near-continuum) plasmon mode and a narrow (near-discrete) mode, giving rise to an asymmetric spectral lineshape. In a Fano antiresonance, the emission to the far field is significantly reduced compared to excitation of a bright resonant mode, and the field intensity near the nanostructure surface is greatly enhanced. These features may specifically benefit hot electron generation. In the past few years we have theoretically explored the formation and observation of Fano antiresonances using EELS.⁸ Following these studies, we have recently demonstrated the first ever experimental observation of plasmonic Fano antiresonances in STEM-EELS.

To do this, we synthesized Au disk-rod dimer nanostructures that were predicted to support antiresonances and collected EEL spectra showing a transition from strong coupling to weak coupling. In clusters of metal nanoparticles, the qualitative nature of the coupling between optically bright and dark LSPs of each particle with those on neighboring particles can vary depending upon their relative interaction strength and dissipation rates. Weak coupling occurs when energy is lost via dissipation faster than it is transferred between modes, while strong coupling occurs whenever the dissipation rate is slow enough to allow energy to coherently flow back and forth many times before being lost. The latter regime is characterized by plasmon hybridization into super and subradiant collective plasmons that are spectrally split from those resonances of the free-space monomer modes. The spectral behavior in the former regime, however, is distinctly different. Depending upon the relative linewidths of the weakly coupled bright (spectrally broad) and dark (spectrally narrow) modes,

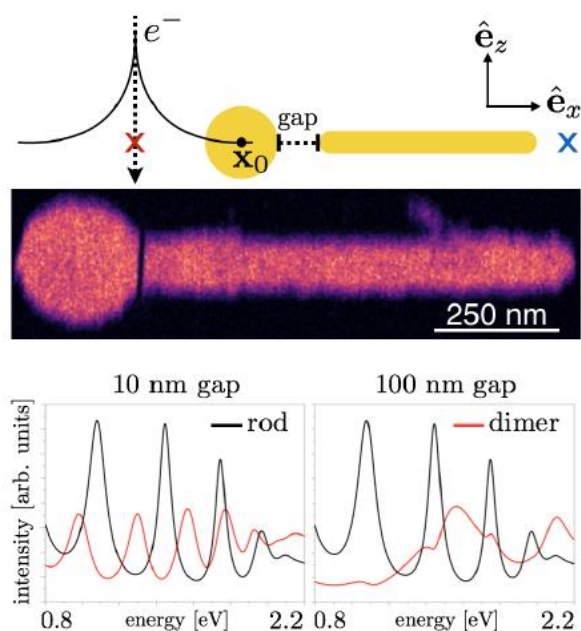


Figure 2. (upper) Illustration of the coupled Fano dimer system. (middle) TEM image of the Au disk-rod dimer. (bottom) EEL spectra in the strong coupling (left) and weak coupling (right) regims.

Fano antiresonances can emerge in the spectrum at those frequencies where energy is lost in its incoherent exchange between plasmon resonances, appearing as sharp asymmetric spectral dips. Fano antiresonances have not been experimentally observed in the STEM-EEL spectrum of plasmonic nanoparticle clusters due to limitations in spectral resolution of ≥ 150 meV. Our study utilizes the ~ 10 meV energy resolution EELS of a Nion Hermes MAC STEM at Oak Ridge National Laboratory, to spectrally resolve the crossover from weak to strong coupling in individual gold heterodimers. We have successfully captured the signature of Fano antiresonances in the weak-coupling limit as shown in Figure 2.

3. STEM/EELS characterization of surface plasmon damping in gold nanorods: a full plasmon mode study from the mid-IR to visible regime: One of the key signatures of plasmon-enhanced energy transfer is its contribution to plasmon damping, which can be probed by analyzing the linewidth of EELS peak profiles. The fantastic (10-15 meV) energy resolution of the Nion MAC STEM makes it possible to resolve and capture a small changes in LSP linewidth induced by energy transfer process. Interestingly, the effects of plasmon damping on a dielectric substrate without energy exchange at interfaces has not been studied and is essential for further understanding of energy transfer contributions. We have recently performed a comprehensive study of plasmon damping in individual Au nanorods on SiO₂ substrates, revealing interesting linewidth broadening as a function of plasmon energy spanning from mid-IR to the visible region. The mid-IR is reached as the tail of the zero loss peak is significantly reduced with the increase of energy resolution. Nanorods have been an intriguing plasmonic nanostructure supporting resonant modes that can be easily tuned by its aspect ratio. Calculation⁹ shows that nanorods have electron injection efficiencies that are several orders of magnitude higher than their spherical or pallet-shaped counterparts, making them suitable candidates for hot-electron based applications. Our preliminary results are displayed in Figure 3. Au nanorods of 70 nm width and six different lengths (350 nm, 520 nm, 675 nm, 837 nm, 1010 nm, and 1320 nm) are synthesized directly on a 20 nm SiO₂ membrane. EEL spectra collected at the rod end with an impact parameter of ~ 5 nm are plotted in Figure 3a, and plasmon dephasing times extracted from the linewidth of each mode are presented in Figure 3b. Interestingly, due to the longer propagation length of Au plasmons in the infrared, the resultant linewidth of the Fabry-Pérot (F-P) plasmon resonances in gold nanorods increases with plasmon energy. This indicates a longer plasmon lifetime in the IR compared to the visible. While the linewidth contribution from Landau damping and radiation will also be analyzed

(in progress), the long lived plasmons in the IR have exciting opportunities in coupling to many molecular resonances and driving correlated chemical reactions (PRET as categorized in Figure 1). Based on this idea, the same Au nanorods and substrates will be coated with low-density polyethylene (LDPE) or poly(methyl methacrylate) (PMMA), as they support strong vibrational resonances associated with the C-H stretching modes around 0.38 eV. Resultant LSPR linewidth broadening due to PRET will be extracted from EEL spectra.

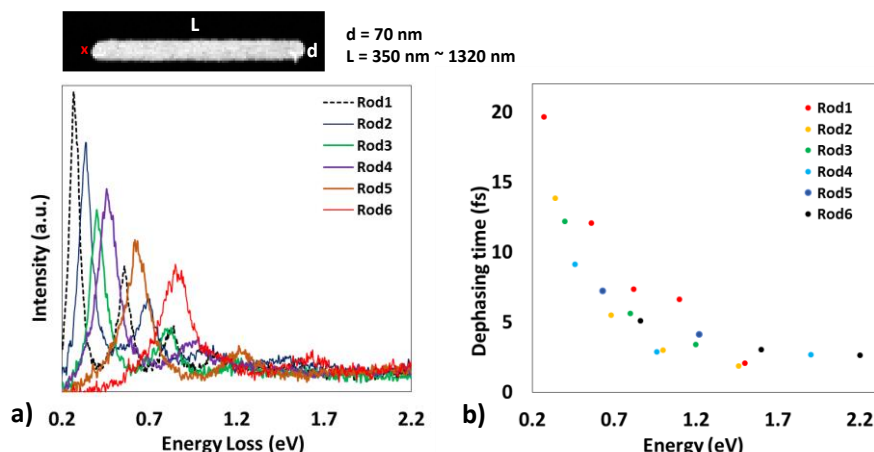


Figure 3. (a) EEL spectra of individual gold nanorods on an SiO₂ substrate. (b) Plasmon dephasing times extracted from linewidths of the rod modes shown in a. Length of gold nanorods 1 to 6 shown in a and b: L₁ = 350 nm; L₂ = 520 nm, L₃ = 675 nm; L₄ = 837 nm, L₅ = 1010 nm, L₆ = 1320 nm

Future Plans

Future experiments will involve (1) replacing the insulating substrate with resonant semiconducting substrates for more insight into the effect of energy transfer on the plasmon modes supported in gold nanorods. We will study how the electron injection rate is affected by aspect ratio of nanorods, bandgap of semiconductors, contact area between rod and semiconductor, and contact roughness at metal/semiconductor interfaces that can change the direction of momentum of incident electrons; (2) Following our rod study, we will further explore other geometry effects on plasmon energy transfer. Simultaneously selected alloy systems such as AuAg and AuAl will be included as nanostructure materials and examined in STEM/EELS, aiming to optimize LSP-interband overlap to enhance hot-carrier generation and injection.

References

1. Atwater, H. A.; Polman, A. *Nat. Mater.* **2010**, 9, (3), 205-213.
2. Li, J.; Cushing, S. K.; Meng, F.; Senty, T. R.; Bristow, A. D.; Wu, N. *Nat. Photon.* **2015**, 9, 601-607.
3. Thakkar, N.; Montoni, N. P.; Cherqui, C.; Masiello, D. J. "Plasmonic Landau damping in active environments," *Phys. Rev. B - Rapid Communication* 97, 2018, 121403(R).
4. Brongersma, M. L.; Halas, N. J.; Nordlander, P. *Nat. Nanotechnol.* **2015**, 10, (1), 25-34.
5. Clavero, C. *Nat. Photonics* **2014**, 8, (2), 95-103.
6. Govorov, A. O.; Zhang, H.; Gun'ko, Y. K., *J Phys. Chem. C* **2013**, 117, 16616–16631
7. Zhang, H.; Govorov, A. O., *J. Phys. Chem. C*, **2014**, 118, 7606–7614
8. Bigelow, N. W.; Vaschillo, A.; Camden, J. P.; Masiello, D. J. *ACS Nano* **2013**, 7, (5), 4511-4519.
9. Kumarasinghe, C. S.; Premaratne, M.; Bao, Q.; Agrawal, G. P., *Sci. Rep.* **2015**, 5, 12140.

Publications from BES support (2016-2018)

- 1) Wu, Y.; Li, G.; Camden, P. D., “Probing Nanoparticle Plasmons with Electron Energy Loss Spectroscopy”, *Chem. Rev.* **2018**, 118, 6, 2994-3031.
- 2) Thakkar, N.; Montoni, N. P.; Cherqui, C.; Masiello, D. J. “Plasmonic Landau damping in active environments,” *Phys. Rev. B - Rapid Communication* 97, **2018**, 121403(R).
- 3) Cherqui, C.; Li, G.; Busche, J. A.; Quillin, S. C.; Camden, J. P.; Masiello, D. J., “Multipolar Nanocube Plasmon Mode-Mixing in Finite Substrates” *J. Phys. Chem. Lett.* **2018**, 9, 504-512.
- 4) J. C. Idrobo, Y. Wu, J. Busche, P.D. Rack, J. P. Camden, D. J. Masiello “Spanning the Gap From Hybridization to Fano in Au Nanodimers”, in prepration.
- 5) R. Collette, Y. Wu, A. A. Olafsson, J. P. Camden, and P. D. Rack, “Combinatorial Thin Film Sputtering AuxAl_{1-x} alloys: Correlating Composition and Structure With Optical Properties”, *ACS Combinatorial Science*, submitted.
- 6) Wu, Y.; Li, G.; Cherqui, C.; Bigelow, N. W.; Thakkar, N.; Masiello, D. J.; Camden, J. P.; Rack, P. D. “Electron Energy Loss Spectroscopy Study of the Full Plasmonic Spectrum of Self-Assembled Au-Ag Alloy Nanoparticles: Unraveling Size, Composition, and Substrate Effects” *ACS Photonics* **2016**, 3, (1), 130-138.
- 7) Cherqui, C.; Thakkar, N.; Li, G.; Camden, J. P.; Masiello, D. J. “Characterizing Localized Surface Plasmons Using Electron Energy-Loss Spectroscopy” *Annu. Rev. Phys. Chem.* **2016**, 67, (1), 331-357.
- 8) Quillin, S. C.; Cherqui, C.; Montoni, N. P.; Li, G.; Camden, J. P.; Masiello, D. J., “Imaging Plasmon Hybridization in Metal Nanoparticle Aggregates with Electron Energy-Loss Spectroscopy” *J. Phys. Chem. C* **2016**, 120, 37, 20852-20859.
- 9) Griffin, S, Montoni, N., Li, G., Straney, P., Millstone, J., Masiello, D. J., Camden, J.P., “Imaging Energy Transfer in Pt-Decorated Au Nanoprisms via Electron Energy-Loss Spectroscopy”, *J. Phys. Chem. Lett.*, **2016**, 7, 3825–3832.
- 10) Cherqui, C., Wu, Y., Li, G., Quillin, S. C., Busche, J. A., Montoni, N.P., Thakkar, N., West, C. A., Rack, P.D., Camden, J. P.; Masiello, D. J. “STEM/EELS Imaging of Magnetic Hybridization in Symmetric and Symmetry-Broken Plasmon Oligomer Dimers and All-Magnetic Fano Interference” *Nano Lett.* **2016**, 16, 6668.

Superconductivity, magnetism and spin-orbit interactions in SrTiO₃ based heterostructures

Venkat Chandrasekhar, Department of Physics, Northwestern University

Research Scope

The primary current focus of this project is the investigation of correlated electron physics in the two-dimensional carrier gas (2DCG) that forms at interfaces in SrTiO₃ (STO) based heterostructures. Two specific types of heterostructures are being studied: LaAlO₃/SrTiO₃ (LAO/STO) and La_{0.3}Sr_{0.7}Al_{0.65}Ta_{0.35}/SrTiO₃ (LSAT/STO). While LAO/STO heterostructure devices have been investigated extensively in the (001) crystal orientation, our focus is on devices in the (111) orientation, where many new effects have been observed.

Recent Progress

(111) Oriented LAO/STO

In the past two years, we have extensively investigated the electrical transport properties of LAO/STO interfaces grown along the (111) crystal plane. In this plane, the bands arising from the Ti t_{2g} orbitals have hexagonal symmetry, and hence it has been proposed that they might have topological character.¹ In particular, it has been proposed that superconductivity in (111) LAO/STO, if it existed, might be time reversal symmetry breaking.² Thus, the properties of (111) STO surface structures are of great interest.

We have measured tens of (111) LAO/STO devices down to millikelvin temperatures. The most surprising result is that all the measured transport properties of the devices are anisotropic with respect to surface crystal direction, in that properties of Hall bars aligned along the $[1\bar{1}0]$ and $[\bar{1}\bar{1}2]$ are different, particularly at very low temperatures and when the carrier density in the 2DCG is low.^{6,7,9-11} The properties include the electrical resistance, the Hall effect, the capacitance, superconductivity and magnetism. The anisotropy can be tuned by modulating the oxygen vacancy concentration by annealing in different gaseous environments: typically, more oxygen vacancies lead to a smaller anisotropy.⁶

While anisotropies in the electrical resistance have also been observed in (001) LAO/STO samples, these anisotropies are relatively small (typically a factor of 2), and associated either with step edges in the surface structure, or tetragonal crystal domains arising from a well-known cubic-to-tetragonal structural transition that occurs in STO at ~ 105 K. As such, the anisotropies in (001) LAO/STO change with sample or on thermal cycling. In contrast, the anisotropy in the (111) LAO/STO samples is always in the same direction across multiple samples and multiple cooldowns. In addition, we do not observe systematic anisotropies around the STO structural

transition at 105 K or even at 77 K. In order to determine the temperature at which the anisotropy onsets, we recently measured the temperature dependence of the resistance and the Hall effect in (111) LAO/STO devices.¹⁰ These data are shown in Fig. 1, which shows the temperature dependence of the resistance along two orthogonal surface crystal over a range of back-gate voltages V_g . Figure 1(b) shows that the resistance at low temperatures along both directions shows an activated behavior, with activation temperatures on the order of a few Kelvin. Similar behavior is also seen in the capacitance.¹⁰ At all gate voltages, the anisotropy onsets at ~ 22 K, far from any known structural or other transition in the system. This indicates that the anisotropy is a signature of an electronic nematic transition in the system, which is completely unexpected from previous studies in LAO/STO heterostructures.

(111) Oriented LSAT/STO

Recently, we have also begun to investigate LSAT/STO heterostructures, which have not been previously studied in detail by other groups. The rationale for studying LSAT/STO is that the lattice mismatch between LSAT and STO is only $\sim 1\%$, in comparison to $\sim 3\%$ for LAO and STO, so that the intrinsic disorder at the interface should be much less. This has been confirmed by initial measurements by our collaborators at the National University of Singapore,³ who grow the films: they found that the residual resistance ratio of LSAT/STO films was much higher than those of LAO/STO films grown under similar conditions. This was also confirmed by our own magnetoresistance (MR) measurements on these films,^{12,13} where we have found a number of experimental signatures indicating that the interfaces have less disorder: a) a classical MR that onsets at relatively low magnetic fields; b) Shubnikov-de Haas oscillations in both the longitudinal and transverse magnetoresistance; c) and electron-phase coherence lengths (L_ϕ) of the order of $\sim 1 \mu\text{m}$ at the lowest temperatures, which is relatively long for such oxide interfaces.¹³

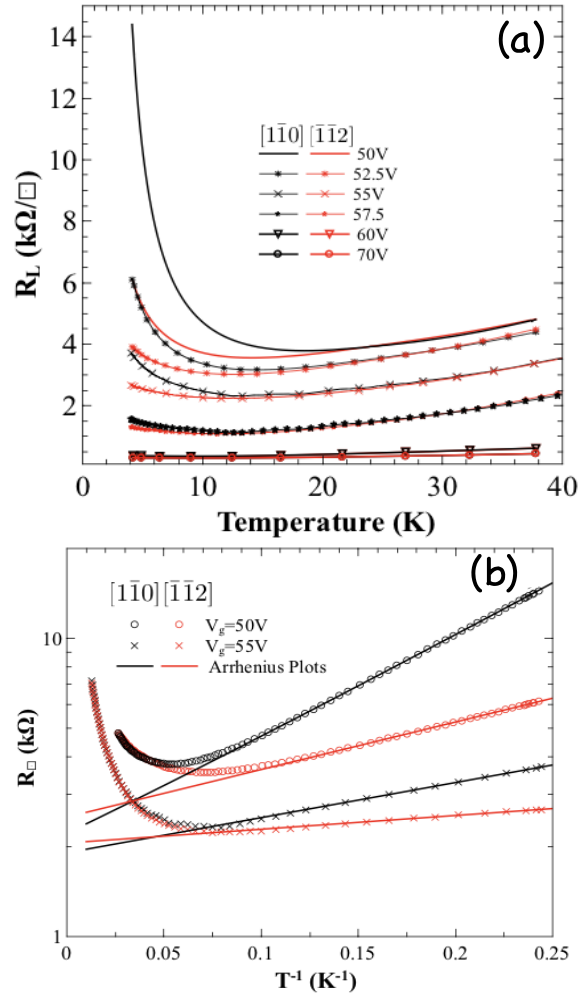


Figure 1. (a) Resistance as a function of temperature of a (111) LAO/STO device along two different surface crystal directions, at different gate voltages. (b) Data for two gate voltages from (a), showing activated dependence of the resistance at low temperatures.

Figure 2(a) shows the longitudinal resistance of a LSAT/STO sample at liquid helium temperatures, with the inset showing the weak localization/anti-localization contribution at low magnetic fields. Figure 2(b) shows the nonlinear Hall effect for the same sample.

Analysis of the low field weak localization/anti-localization MR can give estimates of both L_ϕ and the spin-orbit scattering length L_{so} . As we have noted above, L_ϕ is relatively long in LSAT/STO devices, and shows the expected dependence with temperature and gate voltage. The dependence of L_{so} on V_g in these (111) oriented samples is opposite to what is observed in (001) oriented LAO/STO

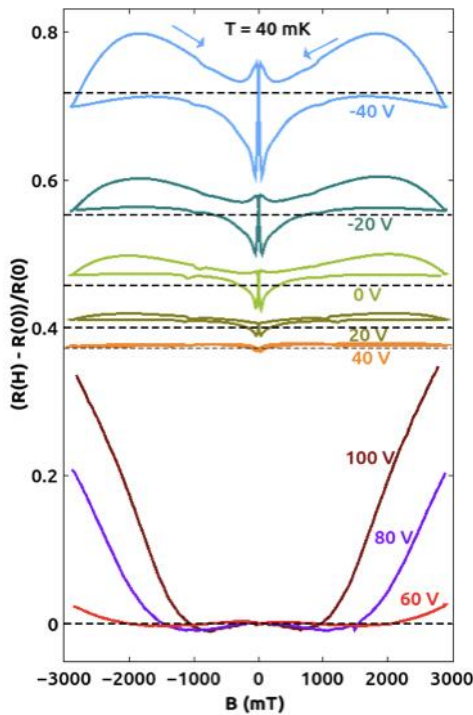


Figure 3. MR of the same sample as in Fig. 2, at 40 mK, showing the onset of a hysteresis below $V_g \sim 40$ V.

samples:⁴ the spin-orbit interaction increases with decreasing V_g ,^{12,13} consistent with calculations that take into account the symmetry of the (111) interface.⁵ Even without any detailed analysis, the low field MR shown in the inset to Fig. 2(a) shows a strong turn-on of spin orbit interactions in this sample when the gate voltage is reduced below $V_g \sim 40$ V, as evidenced by a transition from weak localization to weak anti-localization at this gate voltage. This transition correlates with a Lifshitz transition corresponding to a depopulation of a higher energy, higher-mobility band, signatures of which are seen in the Hall coefficient as a function of V_g .¹²

More surprisingly, the onset of strong spin-orbit

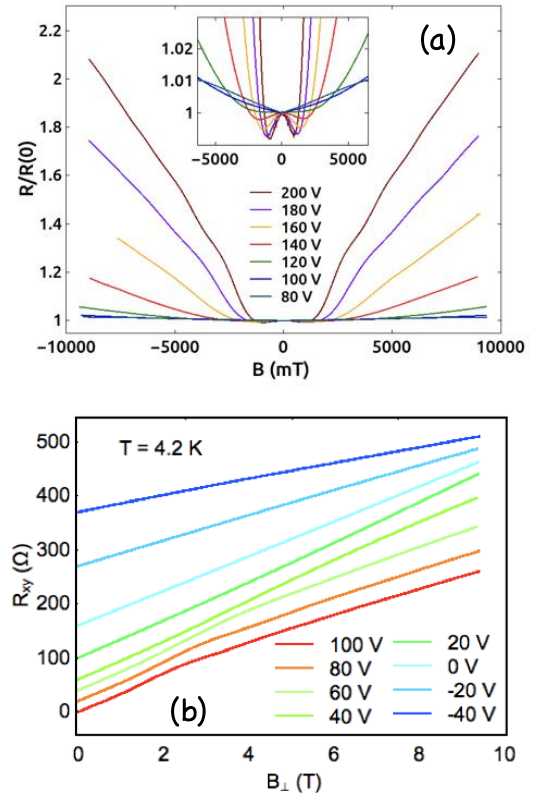


Figure 2. (a) MR of a LSAT/STO Hall bar at 4.4 K at different gate voltages. Inset shows the low field MR. (b) Hall resistance as a function of magnetic field at different gate voltages.

account the symmetry of the (111) interface.⁵

Even without any detailed analysis, the low field MR shown in the inset to Fig. 2(a) shows a strong turn-on of spin orbit interactions in this sample when the gate voltage is reduced below $V_g \sim 40$ V, as evidenced by a transition from weak localization to weak anti-localization at this gate voltage. This transition correlates with a Lifshitz transition corresponding to a depopulation of a higher energy, higher-mobility band, signatures of which are seen in the Hall coefficient as a function of V_g .¹²

More surprisingly, the onset of strong spin-orbit

hysteresis: The first is increasing glassiness in the sample, whose origin is not known, but results in hysteretic “wings” at large magnetic fields. The second is magnetism, which contributes sharp hysteretic dips in the MR at low fields. These low-field hysteretic features can be suppressed by applying a parallel magnetic field, showing their magnetic origin.¹² The correlation between increased spin-orbit interactions and the onset of magnetism is surprising, as the spin-orbit interactions are time-reversal invariant, while magnetism is time reversal symmetry breaking. These are some of the first detailed measurements on the LSAT/STO system, and we plan to explore the system in more detail in the near future.

Future Plans

One potential explanation for the anisotropic behavior that we have observed in (111) LAO/STO structures is that they may be due to edge states that have different character along different directions. Investigating edge states in the large Hall bars that we have studied so far is difficult, so we are currently in the process of fabricating mesoscopic devices using e-beam lithography and etching. By appropriately designing these devices, we should be able to determine if edge states play a role in the transport.

We are also in the process of modifying our tuning fork SPM to do microwave impedance microscopy (MIM). This has been used to image edge states in devices, and we hope to be able to do the same with the LAO/STO devices.

Finally, one of the interesting predictions regarding (111) LAO/STO is the possibility of exotic superconductivity. By making mesoscopic interferometers, we hope to be able to detect signatures of unconventional superconducting order parameters, if present.

As noted above, we have made some of the first detailed measurements on the LSAT/STO system, and much remains to be done. We are particularly interested in seeing if we can observe superconductivity in (111) LSAT/STO; so far, we have not, but by appropriately annealing the samples as we have done for LAO/STO, we might be able to induce superconductivity.

References

1. D. Doenning, W.E. Pickett and R. Pentcheva, *Phys. Rev. Lett.* **111**, 126804 (2013).
2. M.S. Scheurer, D.F. Agterberg and J. Schmalian, *npj Quantum Materials* **2**, Article No. 9 (2017).
3. Z. Huang *et al.*, *Nano Letters* **16**, 2307 (2016).
4. A.D. Caviglia *et al.*, *Phys. Rev. Lett.* **104**, 126803 (2010).
5. D. Xiao *et al.*, *Nature Communications* **2**, 596 (2011).

Publications

6. S. Davis, V. Chandrasekhar, Z. Huang, K. Han, Ariando and T. Venkatesan, “Electrical transport anisotropy controlled by oxygen vacancy concentration in (111) $\text{LaAlO}_3/\text{SrTiO}_3$ interface structures,” *Advanced Materials* **4**, 1600830 (2016).
7. S. Davis, V. Chandrasekhar, Z. Huang, K. Han, Ariando and T. Venkatesan, “Anisotropic multicarrier transport at the (111) $\text{LaAlO}_3/\text{SrTiO}_3$ interface, *Phys. Rev. B.* **95**, 035127 (2017).
8. V.V. Bal, Z. Huang, K. Han, Ariando, T. Venkatesan and V. Chandrasekhar, “Electrostatic tuning of magnetism at the conducting (111) $(\text{La}_{0.3}\text{Sr}_{0.7})(\text{Al}_{0.65}\text{Ta}_{0.35})/\text{SrTiO}_3$ interface,” *Appl. Phys. Lett.* **111**, 081604 (2017).
9. S. Davis, Z. Huang, K. Han, Ariando T. Venkatesan and V. Chandrasekhar, “Magnetoresistance in the superconducting state at the (111) $\text{LaAlO}_3/\text{SrTiO}_3$ interface,” *Phys. Rev. B* **96**, 134502 (2017).
10. S. Davis, Z. Huang, K. Han, Ariando T. Venkatesan and V. Chandrasekhar, “Signatures of electronic nematicity in the (111) $\text{LaAlO}_3/\text{SrTiO}_3$ interfaces,” *Phys. Rev. B* **97**, 041408(R) (2018).
11. S. Davis, Z. Huang, K. Han, Ariando T. Venkatesan and V. Chandrasekhar, “Anisotropic superconductivity and frozen electronic states at the (111) $\text{LaAlO}_3/\text{SrTiO}_3$ interface,” *Phys. Rev. B* **98**, 024504 (2018).
12. V.V. Bal, Z. Huang, K. Han, Ariando, T. Venkatesan and V. Chandrasekhar, “Strong spin-orbit coupling and magnetism in (111) $(\text{La}_{0.3}\text{Sr}_{0.7})(\text{Al}_{0.65}\text{Ta}_{0.35})/\text{SrTiO}_3$,” *Phys. Rev. B* **98**, 085416 (2018).
13. V.V. Bal, Z. Huang, K. Han, Ariando, T. Venkatesan and V. Chandrasekhar, “Low temperature magnetoresistance of (111) $(\text{La}_{0.3}\text{Sr}_{0.7})(\text{Al}_{0.65}\text{Ta}_{0.35})/\text{SrTiO}_3$,” under review at *Phys. Rev. B* (<https://arxiv.org/abs/1803.00553>).

Predicting and Understanding New Polar States Guided by Phase-field Simulations

Long-Qing Chen, The Pennsylvania State University

Research Scope

Domain pattern formation is one of the most common phenomena in nature and is a topic of immense interest in many fields ranging from materials science, physics, chemistry, to biology. The primary objective of this research program is to explore the basic science concerning the thermodynamic stability of mesoscale polar domain patterns and their temporal evolution mechanisms during formation and subsequent switching in ferroelectric nanostructures and heterostructures. We employ the phase-field method in combination with microelasticity and electrostatic theories. Specifically, the research is focused on the fundamental understanding of (1) the spatial length scales and electromechanical conditions leading to the emergence of both transient and stable novel polarization states containing vortex lattices in ferroelectric superlattices; (2) the switching and relaxation mechanisms of these polarization vortex lattices under electrical and mechanical excitations; and (3) defect-induced novel polar/vortex states. We also explore designing ultrahigh dielectric and piezoelectric performances of ferroelectrics by manipulating local polar structures guided by phase-field simulations. All our computational research is being carried out in close collaboration with experimental groups who use High Resolution Transmission Electron Microscopy (HRTEM), *in situ* TEM with Scanning Probe Microscopy (SPM), or Piezoresponse Force Microscopy (PFM). Fundamental understandings of these exotic polar states will not only advance the basic science on the stability of mesoscale polar states and pattern evolution but also improve our ability to control and engineer polar structures for potential applications in nanoscale devices.

Recent Progress

Predicting stability of polar vortex states in ferroelectric superlattices

There is increasing evidence that ferroelectric states at the nanoscale can exhibit fascinating topological structures including polar vortices and skyrmions, akin to those observed in the ferromagnetic systems. Using phase-field simulations, we determined the thermodynamic conditions and geometric length scales that are critical for the observation of the polar vortices [1]. We show that the stability of these vortex lattices involves an intimate competition between long-range electrostatic, long-range elastic, and short-range polarization gradient-related interactions leading to both an upper and a lower bound to the length scale at which these states can be observed. Our key finding is that the critical length scale for the formation of vortices is directly related to the intrinsic bulk domain wall width. We further constructed SrTiO₃-thickness-dependent phase diagrams, which shows remarkably good agreements with experimental observations

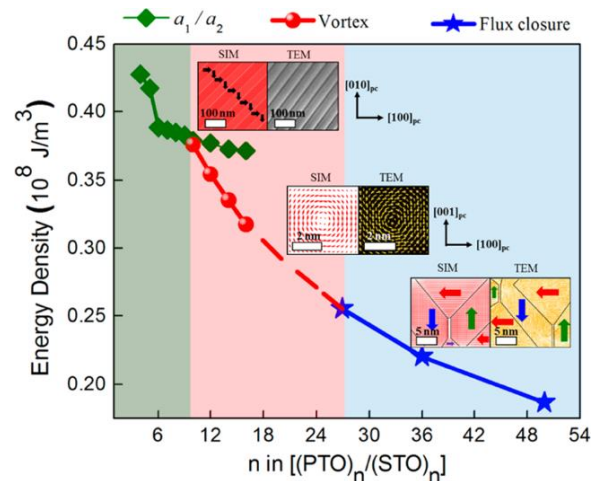


Figure 1. Phase diagram for (PTO)_n/(STO)_n superlattices on DSO substrate from by phase-field simulations and verified experimentally. Insets: The top shows the simulation and planar TEM result of in-plane view of a₁a₂ twin-domain structure for n = 6. The middle is the vortex structure for n = 10. The bottom insets are the cross sections of flux-closure structure for n = 50. “SIM” and “TEM” stand for simulation and transmission electron microscopy data.

(Figure 1).

By exploring superlattice period-, temperature- and field-dependent evolution of these polar structures, we demonstrate it is possible to engineer phase coexistence mediated by a first-order phase transition between an emergent, low-temperature vortex phase with electric toroidal order and a high-temperature ferroelectric a_1/a_2 phase [2]. At room temperature, the coexisting vortex and ferroelectric phases form a mesoscale, fiber-textured hierarchical superstructure. The vortex phase possesses an axial polarization, set by the net polarization of the surrounding ferroelectric domains.

We predicted a field-induced topological phase transition from polar vortices to polar skyrmions, reminiscent of the Plateau-Rayleigh instability in fluid mechanics [3]. We further calculated the topological charge Q at a different applied field, showing a topological phase transition between $Q=0$ and $Q=\pm 1$ states. The electric-field phase diagram is also constructed, which could serve as a roadmap for the experimental observation of the polar skyrmions.

We also predicted a new type of polar topological structure—ordered array of nanoscale spirals in the $\text{PbTiO}_3/\text{BiFeO}_3/\text{SrTiO}_3$ tricolor ferroelectric superlattice system via phase-field simulation [4]. This polar spiral structure is composed of fine ordered semi-vortex arrays with vortex cores forming a wavy distribution. It is demonstrated that this tricolor system has an ultrahigh Curie temperature of ~ 1000 K and a temperature of ~ 650 K for the phase transformation from spiral structure to in-plane orthorhombic domain structure, showing a greatly enhanced thermal stability than the recently discovered polar vortex lattices in the $\text{PbTiO}_3/\text{SrTiO}_3$ superlattice system. Moreover, the spiral structure has a net in-plane polarization that could be switched by an experimentally-feasible irrotational in-plane field. The switching process involves a metastable vortex state, and is fully reversible. This discovery could open up a new routine to design novel polar topological structures with enhanced stability and tunability towards future applications in next-generation nanoscale electronics.

Another major accomplishment is the prediction of room temperature skyrmion bubbles in ferroelectric oxide superlattices (i.e., $\text{PbTiO}_3/\text{SrTiO}_3$ superlattice on a SrTiO_3 substrate), which has been validated by the experimental observations through polar displacement mapping by Transmission Electron Microscopy by our collaborators at UC Berkeley (Figure 2). It is proved that the skyrmion is a topological protected state with a topological charge of $+1$. It is also shown by the Phase-field simulations that the volume ratio of skyrmion increases with increasing superlattice thickness, in good agreement with the experimental observations, suggesting a Raleigh-Plateau like phase transition from vortex lines to skyrmion bubbles.

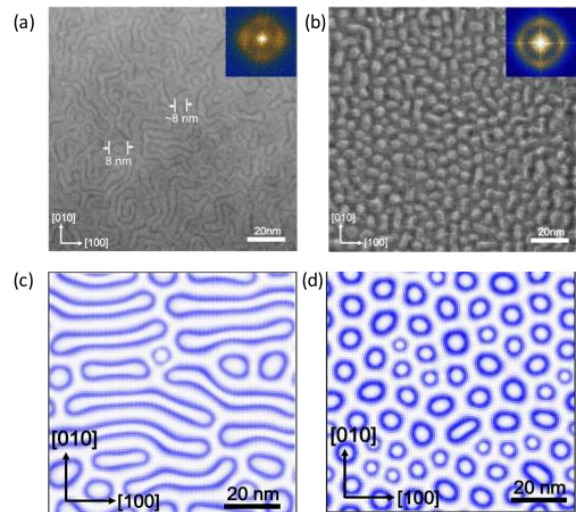


Figure 2. Observation of skyrmion bubbles. TEM Planar view of the polar structure in (a) $\text{SrTiO}_3/\text{PbTiO}_3/\text{SrTiO}_3$ trilayer on a SrTiO_3 substrate (b) $(\text{SrTiO}_3/\text{PbTiO}_3)_8$ superlattice on a SrTiO_3 substrate. Phase-field predictions for (c) $\text{SrTiO}_3/\text{PbTiO}_3/\text{SrTiO}_3$ trilayer on SrTiO_3 and (d) $(\text{SrTiO}_3/\text{PbTiO}_3)_8$ superlattice on a SrTiO_3 substrate.

Interactions between defects and polar structures

One of the approaches to manipulate the polar domain structures is to deliberately introduce defects [5,6]. As an example, Professor Xiaoqing Pan's group showed that complex electrical polarization structures in the prototypical multiferroic BiFeO_3 can be achieved under the influence of nanoscale charged defects, such as nonstoichiometric nanoregions (NSNRs) [5]. Atomic-scale scanning transmission electron microscopy (STEM) imaging reveals exotic polarization rotation patterns around these NSNRs, that resembles hedgehog, vortex topologies or even mixed-phase structures similar to the morphotropic phase boundary with high piezoelectricity.

To understand the effect of such complicated charge defects on the local polar configurations, we performed phase-field simulations assuming a charged defect of similar geometry to those observed in STEM. Starting from an initial random distribution, the simulation almost perfectly reproduced the polarization pattern obtained from experiment, indicating that the local polarization distribution is dominated by the shape and the local charge distribution at the defect (Figure 3). The simple mechanism of charged defect steering local polarization opens a door for controllable nanodomain design, which makes it possible to push the limit of device density, as it overcomes the scaling law that relates the domain size to film thickness.

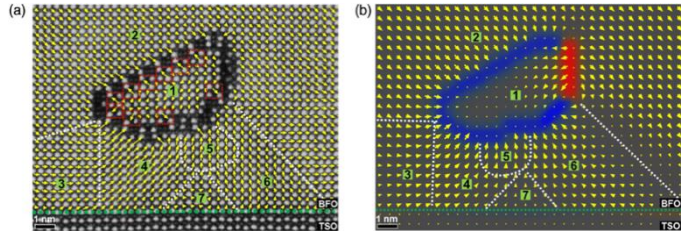


Figure 3. Comparison of phase-field simulation with STEM results. (a). HAADF STEM images of charge defect. (b) phase-field simulation results. Phase-field simulations confirm the existence of a positive charged segment on the right of the defect loop. White dashed lines indicate domain wall locations, and each domain is labelled with a number.

Theory-guided design of ultrahigh piezoelectricity by judiciously manipulating nanoscale local polar heterogeneity

Guided by phenomenological theories and phase-field simulations, we designed a strategy to manipulate the thermodynamics of a heterogeneous system to produce ultrahigh piezoelectricity in polycrystalline relaxor-ferroelectrics by enhancing the polar disorder at the nanoscale. This is an alternative design strategy to the commonly used morphotropic phase boundaries that further flatten the energy landscape by judiciously introducing local structural and polar heterogeneity to manipulate interfacial energies, i.e. extra interaction energies, such as electrostatic and elastic energies associated with the interfaces. To validate this, our experimental collaborators synthesized rare-earth doped $\text{Pb}(\text{Mg}_{1/3}\text{Nb}_{2/3})\text{O}_3\text{-PbTiO}_3$ (PMN-PT), as rare-earth dopants tend to change the local polar structure of Pb-based perovskite ferroelectrics. We achieved ultrahigh piezoelectric coefficients d_{33} up to 1500 pC N^{-1} and dielectric permittivity ϵ_{33}/ϵ_0 above 13,000 in a Sm-doped PMN-PT ceramic [7]. The record-high dielectric and piezoelectric properties of the newly designed ceramics are associated with the polar

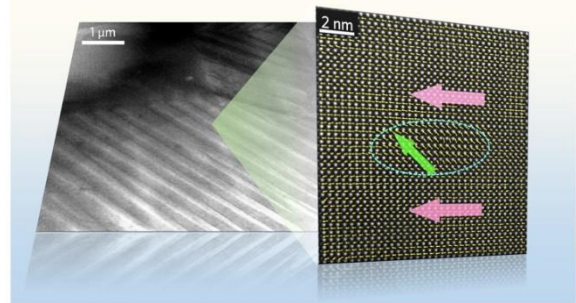


Figure 4. This high-resolution transmission electron microscope image shows a long-range ferroelectric domain with nanoscale structural heterogeneity (4–8 nm).

nanoregions (Figure 4) and of practical importance for high-performance electromechanical applications such as medical ultrasound. Our research provides a new paradigm for designing material properties through engineering local structural and polar heterogeneity, which is expected to be applicable to a wide range of functional materials.

Future Plans

Our existing DOE efforts have been mainly focused on 1) understanding and predicting novel topological polar vortex lattices, 2) studying the role of electrostatic interactions between structural defect and local polarization distribution in the overall polarization patterns, 3) optimizing the piezoelectric and dielectric properties by manipulating local polar structures guided by phase-field simulations. For the next two years, we propose to focus our research efforts on the following tasks:

1. *To integrate electronic defects, e.g., electrons and holes into the phase-field model of ferroelectric domain structures and investigate the interactions among electronic and ionic defects and local polar structures.*
2. *To investigate the electromechanical interactions between structurally inhomogeneous sites, such as dislocations and complex interfacial geometry, and polarization.*
3. *To study the role of interfaces in polar structures and explore the possibility of other novel polar structures in ferroelectric superlattices.*
4. *To model the switching mechanisms of polarization vortices under mechanical stimuli and understand the impact of flexoelectric effects.*

References

1. Z.J. Hong, A.R. Damodaran, F. Xue, S.L. Hsu, J. Britson, A.K. Yadav, C.T. Nelson, J.J. Wang, J.F. Scott, L.W. Martin, R. Ramesh, L.Q. Chen, Stability of Polar Vortex Lattice in Ferroelectric Superlattices, *Nano Letters* 17(4) (2017) 2246-2252.
2. A.R. Damodaran, J.D. Clarkson, Z. Hong, H. Liu, A.K. Yadav, C.T. Nelson, S.L. Hsu, M.R. McCarter, K.D. Park, V. Kravtsov, A. Farhan, Y. Dong, Z. Cai, H. Zhou, P. Aguado-Puente, P. Garcia-Fernandez, J. Iniguez, J. Junquera, A. Scholl, M.B. Raschke, L.Q. Chen, D.D. Fong, R. Ramesh, L.W. Martin, Phase coexistence and electric-field control of toroidal order in oxide superlattices, *Nature Materials* 16(10) (2017) 1003-+.
3. Z.J. Hong, L.Q. Chen, Blowing polar skyrmion bubbles in oxide superlattices, *Acta Materialia* 152 (2018) 155-161.
4. Z. Hong, L.Q. Chen, Switchable polar spirals in tricolor oxide superlattices, *Acta Materialia* Submitted (2018).
5. L. Li, X. Cheng, J.R. Jokisaari, P. Gao, J. Britson, C. Adamo, C. Heikes, D.G. Schlom, L.-Q. Chen, X. Pan, Defect-Induced Hedgehog Polarization States in Multiferroics, *Physical Review Letters* 120(13) (2018).
6. L. Li, J.R. Jokisaari, Y. Zhang, X. Cheng, X.H. Yan, Colin, Q. Lin, C. Gadre, D.G. Schlom, L.Q. Chen, X. Pan, Control of Domain Structures in Multiferroic Thin Films through Defect Engineering, *Advanced Materials* Published (2018).
7. F. Li, D.B. Lin, Z.B. Chen, Z.X. Cheng, J.L. Wang, C.C. Li, Z. Xu, Q.W. Huang, X.Z. Liao, L.Q. Chen, T.R. Shrout, S.J. Zhang, Ultrahigh piezoelectricity in ferroelectric ceramics by design, *Nature Materials* 17(4) (2018) 349-+.

Publications

1. Z.L. Bai, X.X. Cheng, D.F. Chen, D.W. Zhang, L.-Q. Chen, J.F. Scott, C.S. Hwang, A.Q. Jiang, Hierarchical Domain Structure and Extremely Large Wall Current in Epitaxial BiFeO₃ Thin Films, *Adv Funct Mater* 28(31) (2018).
2. L. Li, X. Cheng, J.R. Jokisaari, P. Gao, J. Britson, C. Adamo, C. Heikes, D.G. Schlom, L.-Q. Chen, X. Pan, Defect-Induced Hedgehog Polarization States in Multiferroics, *Physical Review Letters* 120(13) (2018).
3. M.G. Han, J. Li, F. Xue, X.Y. Wang, Q.P. Meng, J. Tao, L.Q. Chen, S.W. Cheong, Y.M. Zhu, Linearly aligned single-chiral vortices in hexagonal manganites by in situ electric arc heating, *Physical Review Materials* 2(6) (2018).
4. Z.J. Hong, L.Q. Chen, Blowing polar skyrmion bubbles in oxide superlattices, *Acta Materialia* 152 (2018) 155-161.
5. M.Q. Li, X.X. Cheng, N. Li, H.J. Liu, Y.L. Huang, K.H. Liu, Y.H. Chu, D.P. Yu, L.Q. Chen, Y. Ikuhara, P. Gao, Atomic-scale mechanism of internal structural relaxation screening at polar interfaces, *Physical Review B* 97(18) (2018).
6. F. Li, D.B. Lin, Z.B. Chen, Z.X. Cheng, J.L. Wang, C.C. Li, Z. Xu, Q.W. Huang, X.Z. Liao, L.Q. Chen, T.R. Shrout, S.J. Zhang, Ultrahigh piezoelectricity in ferroelectric ceramics by design, *Nature Materials* 17(4) (2018) 349-+.
7. H. Liu, J. Chen, H.B. Huang, L.L. Fan, Y. Ren, Z. Pan, J.X. Deng, L.Q. Chen, X.R. Xing, Role of Reversible Phase Transformation for Strong Piezoelectric Performance at the Morphotropic Phase Boundary, *Physical Review Letters* 120(5) (2018).
8. K.E. Kim, S. Jeong, K. Chu, J.H. Lee, G.Y. Kim, F. Xue, T.Y. Koo, L.Q. Chen, S.Y. Choi, R. Ramesh, C.H. Yang, Configurable topological textures in strain graded ferroelectric nanoplates, *Nature Communications* 9 (2018).
9. F. Xue, N. Wang, X.Y. Wang, Y.Z. Ji, S.W. Cheong, L.Q. Chen, Topological dynamics of vortex-line networks in hexagonal manganites, *Physical Review B* 97(2) (2018).
10. Y. Zhang, H. Lu, L. Xie, X. Yan, T.R. Paudel, J. Kim, X. Cheng, H. Wang, C. Heikes, L. Li, M. Xu, D.G. Schlom, L. Chen, R. Wu, E.Y. Tsybal, A. Gruverman, X. Pan, Direct observation of strongly anisotropic polarization-induced conduction at the ferroelectric/insulator interface, *Nature Nanotechnology* Accepted (2018).
11. L. Li, J.R. Jokisaari, Y. Zhang, X. Cheng, X.H. Yan, Colin, Q. Lin, C. Gadre, D.G. Schlom, L.Q. Chen, X. Pan, Control of Domain Structures in Multiferroic Thin Films through Defect Engineering, *Advanced Materials* Published (2018).
12. Z.B. Chen, L. Hong, F.F. Wang, X.H. An, X.L. Wang, S. Ringer, L.Q. Chen, H.S. Luo, X.Z. Liao, Kinetics of Domain Switching by Mechanical and Electrical Stimulation in Relaxor-Based Ferroelectrics, *Physical Review Applied* 8(6) (2017).
13. R.K. Vasudevan, Y. Cao, N. Laanait, A. Ievlev, L.L. Li, J.C. Yang, Y.H. Chu, L.Q. Chen, S.V. Kalinin, P. Maksymovych, Field enhancement of electronic conductance at ferroelectric domain walls, *Nature Communications* 8 (2017).

14. A.R. Damodaran, J.D. Clarkson, Z. Hong, H. Liu, A.K. Yadav, C.T. Nelson, S.L. Hsu, M.R. McCarter, K.D. Park, V. Kravtsov, A. Farhan, Y. Dong, Z. Cai, H. Zhou, P. Aguado-Puente, P. Garcia-Fernandez, J. Iniguez, J. Junquera, A. Scholl, M.B. Raschke, L.Q. Chen, D.D. Fong, R. Ramesh, L.W. Martin, Phase coexistence and electric-field control of toroidal order in oxide superlattices, *Nature Materials* 16(10) (2017) 1003-+.
15. J.M. Hu, B. Wang, Y.Z. Ji, T.N. Yang, X.X. Cheng, Y. Wang, L.Q. Chen, Phase-Field Based Multiscale Modeling of Heterogeneous Solid Electrolytes: Applications to Nanoporous Li_3PS_4 , *Acs Applied Materials & Interfaces* 9(38) (2017) 33341-33350.
16. F. Xue, X.Y. Wang, Y. Shi, S.W. Cheong, L.Q. Chen, Strain-induced incommensurate phases in hexagonal manganites, *Physical Review B* 96(10) (2017).
17. L. Xie, L.Z. Li, C.A. Heikes, Y. Zhang, Z.J. Hong, P. Gao, C.T. Nelson, F. Xue, E. Kioupakis, L.Q. Chen, D.G. Schlom, P. Wang, X.Q. Pan, Giant Ferroelectric Polarization in Ultrathin Ferroelectrics via Boundary-Condition Engineering, *Advanced Materials* 29(30) (2017).
18. J. Wang, H.B. Huang, W.Q. He, Q.H. Zhang, D.N. Yang, Y.L. Zhang, R.R. Liang, C.S. Wang, X.Q. Ma, L. Gu, L.Q. Chen, C.W. Nan, J.X. Zhang, Nanoscale Bandgap Tuning across an Inhomogeneous Ferroelectric Interface, *Acs Applied Materials & Interfaces* 9(29) (2017) 24704-24710.
19. Q.H. Zhang, X. He, J.N. Shi, N.P. Lu, H.B. Li, Q. Yu, Z. Zhang, L.Q. Chen, B. Morris, Q. Xu, P. Yu, L. Gu, K.J. Jin, C.W. Nan, Atomic-resolution imaging of electrically induced oxygen vacancy migration and phase transformation in $\text{SrCoO}_{2.5}$ -sigma, *Nature Communications* 8 (2017).
20. F. Xue, Y.Z. Ji, L.Q. Chen, Theory of strain phase separation and strain spinodal: Applications to ferroelastic and ferroelectric systems, *Acta Materialia* 133 (2017) 147-159.
21. Z.Y. Liao, F. Xue, W. Sun, D.S. Song, Q.Q. Zhang, J.F. Li, L.Q. Chen, J. Zhu, Reversible phase transition induced large piezoelectric response in Sm-doped BiFeO_3 with a composition near the morphotropic phase boundary, *Physical Review B* 95(21) (2017).
22. D.V. Karpinsky, E.A. Eliseev, F. Xue, M.V. Silibin, A. Franz, M.D. Glinchuk, I.O. Troyanchuk, S.A. Gavrilov, V. Gopalan, L.Q. Chen, A.N. Morozovska, Thermodynamic potential and phase diagram for multiferroic bismuth ferrite (BiFeO_3), *Npj Computational Materials* 3 (2017).
23. Y. Cao, L.Q. Chen, S.V. Kalinin, Role of flexoelectric coupling in polarization rotations at the a-c domain walls in ferroelectric perovskites, *Applied Physics Letters* 110(20) (2017).
24. F. Li, S.J. Zhang, Z. Xu, L.Q. Chen, The Contributions of Polar Nanoregions to the Dielectric and Piezoelectric Responses in Domain-Engineered Relaxor- PbTiO_3 Crystals, *Adv Funct Mater* 27(18) (2017).
25. L.L. Li, Y. Cao, S. Somnath, Y.D. Yang, S. Jesse, Y. Ehara, H. Funakubo, L.Q. Chen, S.V. Kalinin, R.K. Vasudevan, Direct Imaging of the Relaxation of Individual Ferroelectric Interfaces in a Tensile-Strained Film, *Advanced Electronic Materials* 3(4) (2017).

26. Z.J. Hong, A.R. Damodaran, F. Xue, S.L. Hsu, J. Britson, A.K. Yadav, C.T. Nelson, J.J. Wang, J.F. Scott, L.W. Martin, R. Ramesh, L.Q. Chen, Stability of Polar Vortex Lattice in Ferroelectric Superlattices, *Nano Letters* 17(4) (2017) 2246-2252.
27. Y.L. Tang, Y.L. Zhu, Z.J. Hong, E.A. Eliseev, A.N. Morozovska, Y.J. Wang, Y. Liu, Y.B. Xu, B. Wu, L.Q. Chen, S.J. Pennycook, X.L. Ma, 3D polarization texture of a symmetric 4-fold flux closure domain in strained ferroelectric PbTiO₃ films, *Journal of Materials Research* 32(5) (2017) 957-967.
28. Z.B. Chen, L. Hong, F.F. Wang, S.P. Ringer, L.Q. Chen, H.S. Luo, X.Z. Liao, Facilitation of Ferroelectric Switching via Mechanical Manipulation of Hierarchical Nanoscale Domain Structures, *Physical Review Letters* 118(1) (2017).
29. F. Li, S.J. Zhang, T.N. Yang, Z. Xu, N. Zhang, G. Liu, J.J. Wang, J.L. Wang, Z.X. Cheng, Z.G. Ye, J. Luo, T.R. Shrout, L.Q. Chen, The origin of ultrahigh piezoelectricity in relaxor-ferroelectric solid solution crystals, *Nature Communications* 7 (2016).
30. F. Xue, Y.J. Li, Y.J. Gu, J.X. Zhang, L.Q. Chen, Strain phase separation: Formation of ferroelastic domain structures, *Physical Review B* 94(22) (2016).
31. Y. Cao, S.Z. Yang, S. Jesse, I. Kravchenko, P. Yu, L.Q. Chen, S.V. Kalinin, N. Balke, Q. Li, Exploring Polarization Rotation Instabilities in Super-Tetragonal BiFeO₃ Epitaxial Thin Films and Their Technological Implications, *Advanced Electronic Materials* 2(12) (2016).
32. H.H. Huang, Z.J. Hong, H.L.L. Xin, D. Su, L.Q. Chen, G.Z. Huang, P.R. Munroe, N. Valanoor, Nanoscale Origins of Ferroelastic Domain Wall Mobility in Ferroelectric Multilayers, *Acs Nano* 10(11) (2016) 10126-10134.
33. F. Xue, L.Z. Li, J. Britson, Z.J. Hong, C.A. Heikes, C. Adamo, D.G. Schlom, X.Q. Pan, L.Q. Chen, Switching the curl of polarization vectors by an irrotational electric field, *Physical Review B* 94(10) (2016).
34. G.Q. Liu, Q. Zhang, H.H. Huang, P. Munroe, V. Nagarajan, H. Simons, Z.J. Hong, L.Q. Chen, Reversible Polarization Rotation in Epitaxial Ferroelectric Bilayers, *Advanced Materials Interfaces* 3(18) (2016).
35. L.Z. Li, J. Britson, J.R. Jokisaari, Y. Zhang, C. Adamo, A. Melville, D.G. Schlom, L.Q. Chen, X.Q. Pan, Giant Resistive Switching via Control of Ferroelectric Charged Domain Walls, *Advanced Materials* 28(31) (2016) 6574-+.

Combined microscopy and transport studies of two-dimensional semiconductors and topological semimetals

David H. Cobden - Department of Physics, University of Washington, Seattle, WA 98195

Research Scope

The broad aim of this project is to determine and understand the electronic properties of electronic materials which are only available as micron-scale samples or which contain microscopic inhomogeneity. They exhibit phenomena such as charge-density waves, superconductivity, magnetism, topological protection, metal-insulator transitions, excitonic insulation, and structural transitions at lower temperatures. Examples of interest are VO₂, with its still mysterious metal-insulator and structural phase transitions; WTe_{2-x}S_x, combining superconductivity and nontrivial topology; W_{1-x}Re_xTe₂, a doped topological/Weyl semimetal; NbSe₂, in which density waves compete with superconductivity; and FeSe_{1-x}Te_x, which hosts superconductivity, antiferromagnetism and nematicity. We employ control of temperature, magnetic field, mechanical strain, and electrical transport, allied to multiple submicron scanning microscopies including photocurrent microscopy (SPCM), scanning tunneling electron microscopy (STEM), atomic force microscopy (AFM), scanning microwave impedance microscopy (MIM) and micron-scale angle-resolved photoemission spectroscopy (μ -ARPES).

Recent Progress

During the past two years we succeeded in producing well behaved heterostructures incorporating air-sensitive 2D materials, including WTe₂ as well as several magnets. It was predicted¹ in 2014 that WTe₂, which is a semimetal in 3D, could become a 2D topological insulator in monolayer form, depending on whether it has a band gap. We found that the monolayer indeed exhibits the characteristics of a topological insulator (Publication #7). At low temperatures there is a ~ 50 meV gap for conductivity in the 2D bulk, while the edges remain conducting, consistent with topologically protected boundary modes². The edge conductivity is suppressed by an in-plane magnetic field, consistent with increased backscattering in helical edge modes when time reversal symmetry is broken. Similar results were obtained later by researchers at MIT³.

Figure 1 shows characteristics of 3-, 2- and 1-layer exfoliated WTe₂ encapsulated in hBN with graphite gates above and below; the gate voltage V_g is applied to both. Only the monolayer shows a plateau of edge conduction at low V_g . The bilayer was expected to be topologically trivial and thus not have boundary modes, as we confirmed. For 3+ layers the material is just metallic. The conductance of the plateau is less than e^2/h in all devices, implying that some backscattering occurs and/or contacts are imperfect, for reasons still being explored. Proof of edge conduction came from a combination of transport measurements, such as those in Fig. 2a, and from MIM measurements (Fig. 2b) performed in collaboration with Yongtao Cui at UC

Riverside. MIM revealed many fascinating details, such as how the topological edge mode conforms to tiny cracks in the edges as can be seen in the bottom left image.

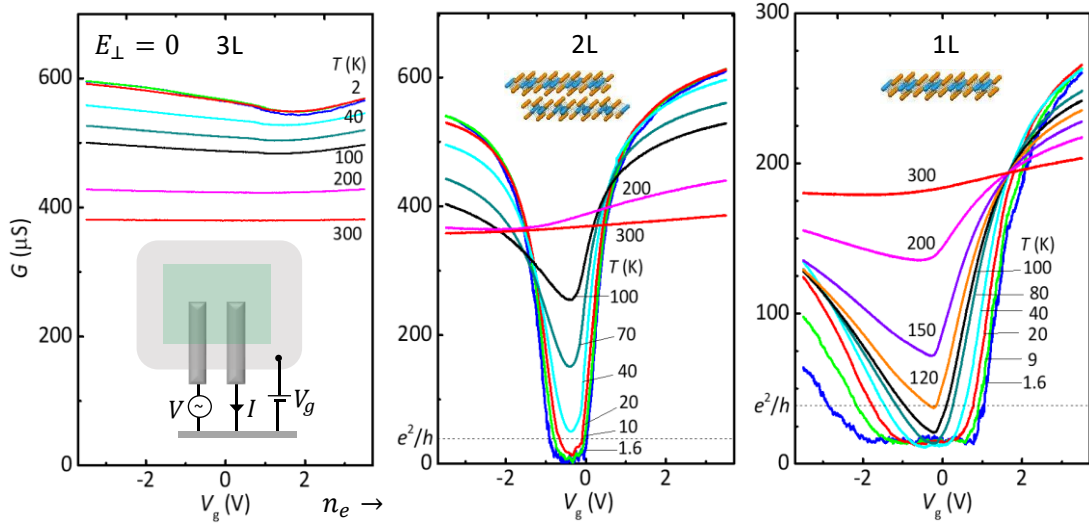


Figure 1. Gate and temperature dependence of the two-probe conductance for (left) trilayer, (center) bilayer, and (right) monolayer WTe_2 . The trilayer is metallic; the bilayer is insulating at $V_g = 0$ but metallic when n- or p-doped using the gates; and the monolayer has a plateau of conduction below ~ 100 K where the current only flows along the sample edges while the 2D bulk becomes insulating at low gate voltages.

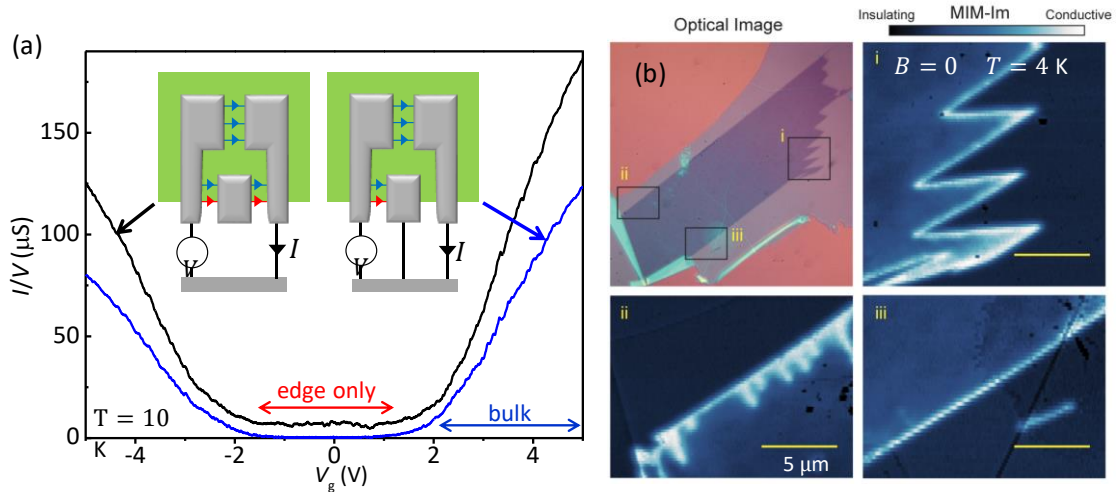


Figure 2. (a) Transport measurements of a “pincer” geometry device prove that the current on the plateau at low V_g flows along the edge; it is eliminated by grounding the intermediate contact. (b) Microwave impedance microscopy (MIM) images of a large monolayer WTe_2 flake protected by an even large hBN sheet (optical image, top left) showing that the edges are conducting (bright) while the 2D bulk is insulating (dark) as is the surrounding SiO_2 substrate.

Even more surprisingly, we found that the 2D bulk of the monolayer changes from insulating to a superconducting state under a positive gate voltage, as shown in Fig. 3a, at temperatures below about 1 K (Publication #1, in collaboration with Joshua Folk at the University of British Columbia). The transition is very broad, as expected since the normal state

areal conductivity is not much higher than e^2/h . The intermediate plateau is not understood. Suppression of the superconductivity by a perpendicular magnetic field occurs on a scale of 30 mT, giving a coherence length of ~ 100 nm. Suppression by an in-plane field occurs on a scale of 3 T, about twice the expected Pauli pair-breaking limit assuming a g -factor of 2. Figure 3b shows a phase diagram extracted from the measurements, where the x-axis is the doping density determined from the capacitance. It is particularly striking that the transition from 2DTI to 2D superconductor occurs at an electron doping level of only $\sim 5 \times 10^{12} \text{ cm}^{-2}$, an order of magnitude lower than in other doping-induced superconducting transitions in similar 2D materials.⁴

We further discovered that bilayer and trilayer WTe_2 exhibit a spontaneous out-of-plane electrical polarization, allowed by the known crystal symmetry (Fig. 3c). This polarization can be reversed by applying an electric field, that is, the material is ferroelectric (Publication #3).

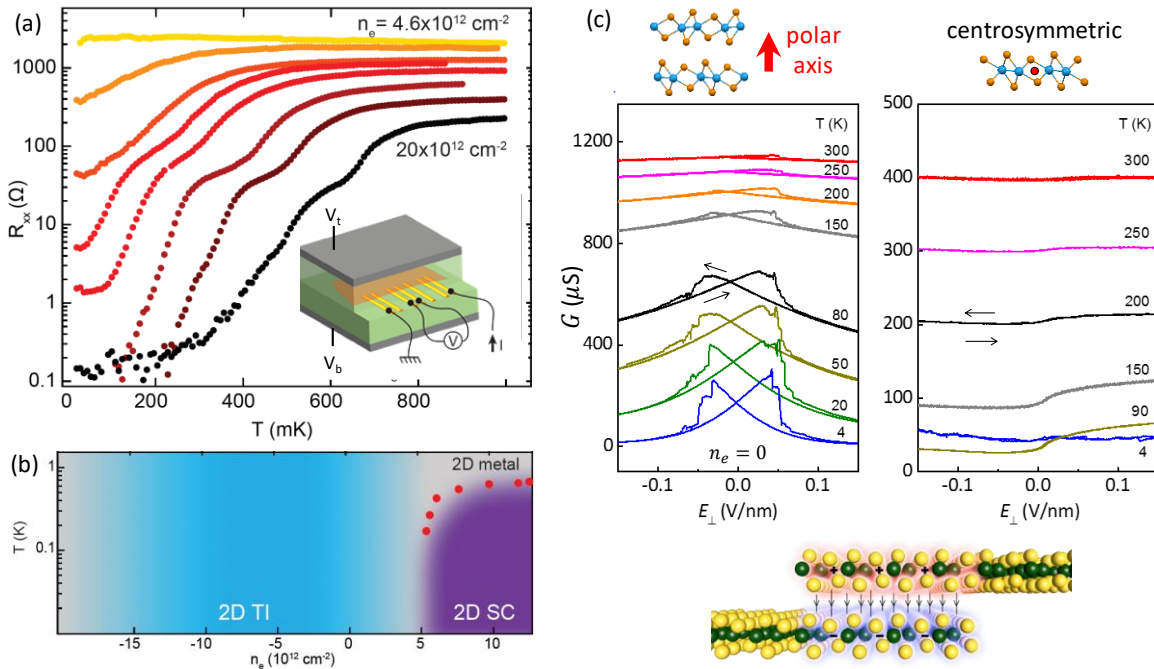


Figure 3. (a) Temperature dependence of four-terminal resistance of a monolayer WTe_2 device, measured as indicated in the inset, at a series of gate voltages. The electron doping density n_e , shown, is determined from the geometric capacitance. (b) Phase diagram. The insulator-superconductor boundary is taken to be the point where the the resistance is half that in the normal (high temperature) state. (c) Ferroelectric switching in bilayer and monolayer WTe_2 devices. The bilayer (left) has polar structure and its polarization can be flipped by applying a perpendicular electric field by putting opposite-sign voltages on the top and bottom gates. The monolayer (right) is centrosymmetric and cannot be flipped. We conclude that spontaneous polarization occurs when the monolayers are stacked, as indicated in the cartoon below.

In another thrust we have been further developing the capability to perform ARPES on 2D materials, in collaboration with Neil Wilson at the University of Warwick, UK and using the Spectromicroscopy meamline at Elettra in Trieste (Publication #8). Very recently, we have achieved the first in-situ electrostatic gating during photoemission spectroscopy. The results are

illustrated for the case of graphene in Fig. 4, demonstrating the accuracy and power of the approach. We are now adapting the technique to work with 2D semiconductors and semimetals.

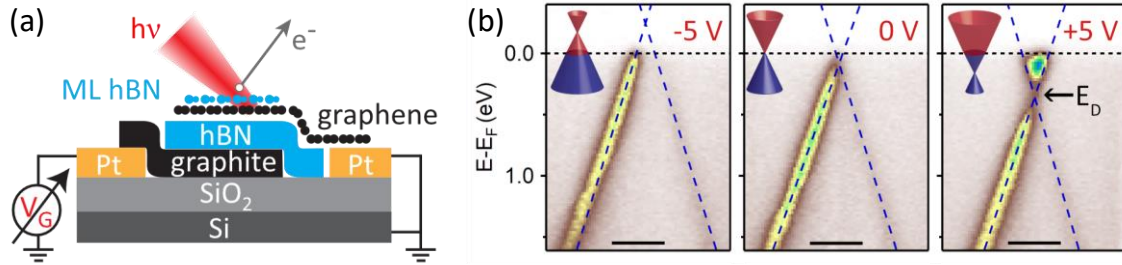


Figure 4. In-situ gating in μ -ARPES of graphene. (a) The sample geometry is similar to a standard operating graphene field-effect transistor. A gate voltage is applied to dope the graphene while performing photoemission (27 eV photons, 1 μ m beam spot.) (b) E-k momentum slices close to the graphene K-point, showing the expected conical (massless Dirac) dispersion (the dashed lines are fits). The chemical potential (E_F) can be swung by ~ 0.6 eV through the Dirac point), thanks to the excellent breakdown characteristic of hBN (thickness ~ 10 nm).

Future Plans

Given that WTe_2 is the first 2D semimetal to be studied experimentally (other than graphene, with its unique massless dispersion) it is likely that some of the properties of WTe_2 will be shared by other 2D semimetals, and may be quite generic, while others vary between materials. It is also likely that more surprises await in other members of this diverse group of materials. We therefore plan to take the combination of microscopy techniques and transport employed successfully to date and apply them to continuing to address the open questions in WTe_2 while widening the range of semimetallic layered materials under study. Targets of interest are $W_x/Mo_{1-x}Te_2$ (tunable gap 2DTI); Re-doped WTe_2 (n-doped); Cr-doped WTe_2 (magnetically doped 2DTI), $TaIrTe_4$ and $TaRhTe_4$ (Weyl metals and possible 2DTIs); $ZrTe_5$ (Dirac metal/strong topological insulator and possible 2D TI); $TiSe_2$ (semimetal/charge density wave/excitonic insulator); $PdSe_2$ (Dirac semimetal); $Nb_xW_{1-x}Se_2$ (interpolates between superconductor and semiconductor); $BiTeCl$ (giant Rashba self-doped topological insulator); $ZrSiS$ (Dirac nodal-line semimetal); and pure rhombohedral Sb (classic semimetal with spin-textured topological surface states, recently available in thin single-crystal platelets).

References

- 1 Qian, X., Liu, J., Fu, L. & Li, J. Quantum spin Hall effect in two-dimensional transition metal dichalcogenides. *Science* **346**, 1344-1347, doi:10.1126/science.1256815 (2014).
- 2 Hasan, M. Z. & Kane, C. L. *Colloquium*: Topological insulators. *Rev. Mod. Phys.* **82**, 3045 (2010).
- 3 Wu, S. *et al.* Observation of the quantum spin Hall effect up to 100 kelvin in a monolayer crystal. *Science* **359**, 76-79 (2018).
- 4 Fu, Y. *et al.* Gated tuned superconductivity and phonon softening in monolayer and bilayer MoS_2 . *npj Quantum Materials* **2**, 52, doi:10.1038/s41535-017-0056-1 (2017).

Publications supported by DoE BES ESPM award DE-SC0002197, past 2 years

1. "Gate-induced superconductivity in a monolayer topological insulator", Ebrahim Sajadi, Tauno Palomaki, Zaiyao Fei, Wenjin Zhao, Philip Bement, Christian Olsen, Silvia Luescher, Xiaodong Xu, Joshua A. Folk, and David H. Cobden, to appear in Science.
2. "Electrical Control of 2D Magnetism in Bilayer CrI₃", Bevin Huang, Genevieve Clark, Dahlia R. Klein, David MacNeill, Efren Navarro-Moratalla, Kyle L. Seyler, Nathan Wilson, Michael A. McGuire, David H. Cobden, Di Xiao, Wang Yao, Pablo Jarillo-Herrero, Xiaodong Xu, Nature Nanotechnology 13, 544 (2018).
3. "Ferroelectric switching of a two-dimensional metal", Zaiyao Fei, Wenjin Zhao, Tauno A. Palomaki, Bosong Sun, Moira K. Miller, Zhiying Zhao, Jiaqiang Yan, Xiaodong Xu, and David H. Cobden, Nature 560, 336–339 (2018).
4. "Giant Tunneling Magnetoresistance in Spin-Filter van der Waals Heterostructures", Tiancheng Song, Xinghan Cai, Matisse Wei-Yuan Tu, Xiaoou Zhang, Bevin Huang, Nathan P. Wilson, Kyle L. Seyler, Lin Zhu, Takashi Taniguchi, Kenji Watanabe, Michael A. McGuire, David H. Cobden, Di Xiao, Wang Yao, Xiaodong Xu, Science 360, 1214 (2018).
5. "Ligand-field helical luminescence in a 2D ferromagnetic insulator", Kyle Seyler, Ding Zhong, Dahlia Klein, Shiyuan Gao, Xiaoou Zhang, Bevin Huang, Efren Navarro-Moratalla, Li Yang, David Cobden, Michael McGuire, Wang Yao, Di Xiao, Pablo Jarillo-Herrero, Xiaodong Xu, Nature Physics 14, 277 (2017).
6. "Layer-dependent Ferromagnetism in a van der Waals Crystal down to the Monolayer Limit", Bevin Huang, Genevieve Clark, Efren Navarro-Moratalla, Dahlia R. Klein, Ran Cheng, Kyle L. Seyler, Ding Zhong, Emma Schmidgall, Michael A. McGuire, David H. Cobden, Wang Yao, Di Xiao, Pablo Jarillo-Herrero, Xiaodong Xu, Nature 546, 270 (2017).
7. "Edge conduction in monolayer WTe₂", Zaiyao Fei, Tauno Palomaki, Sanfeng Wu, Wenjin Zhao, Xinghan Cai, Bosong Sun, Paul Nguyen, Joseph Finney, Xiaodong Xu, and David H. Cobden, Nature Physics 13, 677 (2017).
8. "Band parameters and hybridization in 2D semiconductor heterostructures from photoemission spectroscopy", Neil R. Wilson, Paul V. Nguyen, Kyle Seyler, Pasqual Rivera, Alexander J. Marsden, Zachary P.L. Laker, Gabriel C. Constantinescu, Viktor Kandyba, Alexei Barinov, Nicholas D.M. Hine, Xiaodong Xu, and David H Cobden, Science Advances 3, e1601832 (2017).
9. "Many-body effects in nonlinear optical responses of 2D layered semiconductors", Grant Aivazian, Hongyi Yu, Sanfeng Wu, Jiaqiang Yan, David G. Mandrus, David Cobden, Wang Yao, Xiaodong Xu, 2D Materials 4, 025024 (2017).
10. "Visualization of one-dimensional diffusion and spontaneous segregation of hydrogen in single crystals of VO₂" by T. Serkan Kasirga, Jim Coy, Jae H. Park, and David H. Cobden, Nanotechnology 27, 354708 (2017).
11. "Photo-Nernst current in graphene", Helin Cao, Grant Aivazian, Jason Ross, Zaiyao Fei, David Cobden, and Xiaodong Xu, Nature Physics 12, 236 (2016).
12. "Ultrafast Nanoimaging of the Photoinduced Phase Transition Dynamics in VO₂", S.A. Donges, O. Khatib, B.T. O'Callahan, J.M. Atkin, J.H. Park, D.H. Cobden, and M.B. Raschke, Nano Letters 16, 5 3029-3035 (2016).

Novel Developments in Spectroscopy and *In Situ* Imaging of Photocatalytic Nanoparticles for Solar Fuel Generation

Principle Investigator: Peter A. Crozier

**School for Engineering of Matter, Transport and Energy, Arizona State University,
Tempe, AZ 85287-6106**

Email: crozier@asu.edu

Program Scope

We are investigating the structure and evolution of heterostructured semiconductor-based materials for H₂ generation via photocatalytic water splitting. Our catalysts are composite materials consisting of light harvesting semiconductors supporting catalytic nanoparticles that facilitate the transfer of excited electrons/holes for water reduction/oxidation. Characterizing light harvesting oxides and nitrides which may be functionalized with metal and metal oxide nanoparticles yielding model systems which are active under ultraviolet or visible light is the primary focus of this project. Advanced imaging and spectroscopy methods are developed and applied to these systems to elucidate structure-reactivity relations (EELS). *In situ* approaches for analysis under photoreaction conditions are also under development.

Recent Progress

Atomic Resolution Vibrational Spectroscopy: We have achieved atomic resolution vibrational spectroscopy by exploiting the impact interaction contributing to EELS. So far most vibrational EELS has employed the low spatial resolution dipole interaction to probe materials [1-3]. By identifying the peaks within the spectrum associated with impact scattering, we were able to perform atomic resolution. **Figure 1** shows the variation in the vibrational spectrum from Si as a small focused electron probe is moved around the unit cell recorded on a monochromated Nion scanning transmission electron microscope (STEM). Two peaks of varying intensity and energy are observed as the probe is translated across a Si atomic column. The high energy peak is dominated by optical phonons spanning a range of momentum transfers while the low energy peak corresponds to acoustic and optical excitations near the Brillouin zone boundary. This approach has also been demonstrated on ionic materials using SiO₂. The key strategy is separating the impact

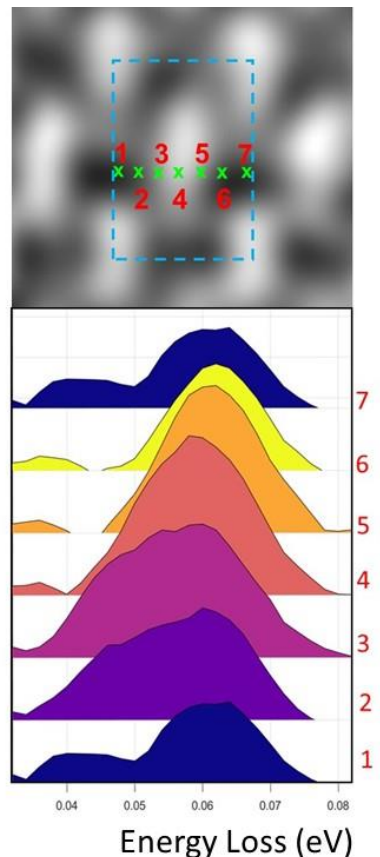


Figure 1: (Upper) Fourier filtered ADF image of the Si unit cell showing 6 points across a dumbbell column with probe moving in roughly 0.6 Å steps (step 7 is identical to step 1 because of the averaging). The dotted blue box shows the Si unit cell measuring 3.8 x 5.4 Å. (Lower) The vibrational spectrum recorded at each position.

signal from the dipole contribution to achieve high spatial resolution. An advantage of this approach is that atomic resolution is accomplished with conventional on-axis EELS geometry and should work on all STEM instruments equipped with suitable monochromators. Achieving atomic resolution vibrational EELS opens the door to atomic level probing of vibrational modes associated with nanoscale structural features and defects such as dislocations, grain boundaries, nanoparticles and surface defects.

Probing Hydrogen Heterogeneity in Carbon Nitrides with Vibrational EELS: In graphitic carbon

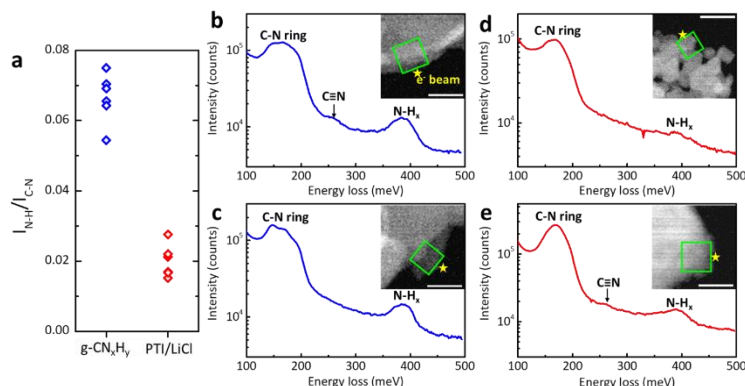


Figure 2: a) Comparison of the range in I_{N-H}/I_{C-N} values, extracted from individual aloof-beam vibrational EEL spectra from different regions, of $g-CN_xH_y$ and PTI/LiCl. b)-e) Direct comparison of aloof-beam vibrational EELS and corresponding HAADF images for $g-CN_xH_y$ (b)-c) and PTI/LiCl (c) - d)). Insets in b)-e) depict the corresponding low-dose HAADF images showing the aloof probe position marked by a yellow star and probed area represented by a green rectangle. All scale bars equal 50 nm.

nitrides, (photo)catalytic functionality is underpinned by the effect that residual hydrogen content, manifesting in amine ($N-H_x$) defects, has on its optoelectronic properties [4]. Therefore, a detailed understanding of the variation in the local structure of graphitic carbon nitrides is key for understanding structure-activity relationships. Here we apply vibrational EELS to locally detect variations in hydrogen content in two different layered carbon nitrides with nanometer resolution. By employing an aloof-beam configuration, radiation damage can be dramatically reduced yielding vibrational spectra from carbon nitrides to be assessed on 10's of nanometer length scales. We find that in disordered graphitic carbon nitrides, the relative amine content can vary locally up to 27%. cyano ($C\equiv N$) defects originating from uncondensed precursor are also revealed by probing small volumes, which cannot be detected by infrared absorption or Raman scattering spectroscopies. The utility of this technique is realized for heterogeneous soft materials, such as disordered graphitic carbon nitrides, in which methods to probe catalytically active sites remain elusive. **Figure 2** shows the results of probing variations in the amine content of two different carbon nitrides. In addition to confirming the large difference in amine content between the two materials there is a very large variation in the amine content between the two materials. More generally, local variation in hydrogen content in specimens of irregular morphology can be probed with aloof-beam EELS while also minimizing radiation damage and maintaining spatial resolutions of around 10's of nanometers.

Nanoscale Probing of Resonant Photonic Modes in Dielectric Nanoparticles: The excitation of resonant optical-frequency geometric modes in oxide nanoparticles is explored using

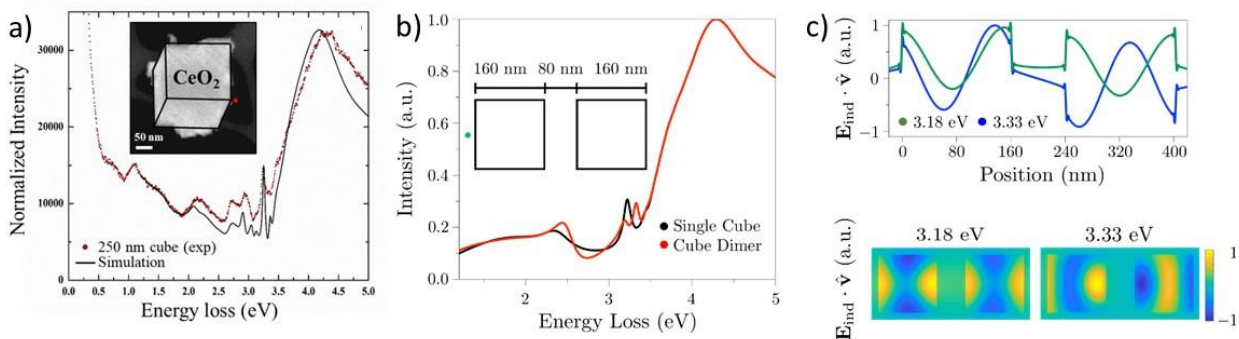


Figure 3: **a)** Experimental (red) and computed (black) aloof beam EEL spectra with the electron beam positioned 4 nm from the corner of a well-defined CeO₂ cube of 250 nm in size. The incident electron voltage is 60 kV. The insets are the ADF image with beam positions denoted by the red point. **b)** Calculated aloof EEL spectra of a 160 nm CeO₂ nanocube dimer (red) and monomer (black) showing the signature of cavity mode hybridization in the splitting of resonance peaks around 3.2 eV. **c)** The projected electric field profiles of the hybridized cavity modes observed in the spectrum in panel b). The lower and higher energy modes correspond to the in-phase and out-of-phase hybridized geometric resonances of the dimer.

monochromated EELS. These geometric or cavity modes are found to produce a progression of resonance peaks within the bandgap regions of the energy-loss spectra of CeO₂, TiO₂, and MgO nanoparticles as shown in Figure 1. The signal is easiest to observe for experiments performed in the aloof beam geometry. Complementary simulations of the electron probe combined with analytic Mie analysis were performed to interpret the complex spectral features and to understand their underlying physical origins. Interesting coupling effects are predicted to occur for adjacent particles resulting in significant changes in the photonic modes (see **Figure 3**). This work demonstrates the unique ability of fast electron spectroscopy to determine the photonic density of states in individual and complex assemblies of dielectric nanoparticles. It suggests new approaches to light manipulation in ways similar to plasmonics but with significantly smaller losses [5].

In Situ Probing of Structural Changes in TiO₂: To investigate changes in surface structure with photoreaction conditions we have installed a light source in our FEI Titan environmental TEM. Negative C_s imaging performed on an FEI Titan ETEM provides a powerful approach to determine the dynamic changes taking place due to the migration of oxygen vacancies. The image of **Figure 4** shows dumbbell pairs separated by about 2.36 Å corresponding to Ti-O columns with fainter O columns also visible. However, careful analysis of the image reveals the presence of cation displacements which are associated with oxygen vacancies in the structure. When the sample is exposed to H₂O and UV light, substantial structural changes take place as illustrated in the low-

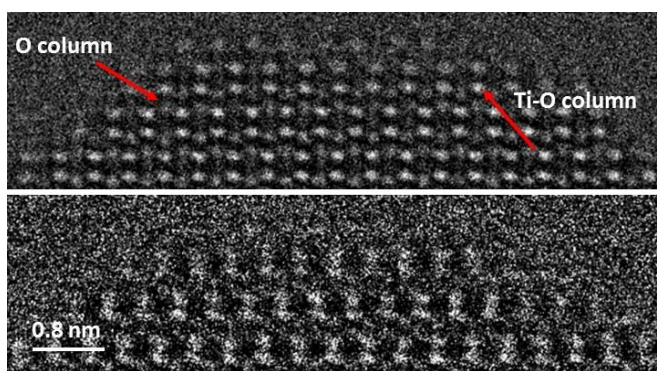


Figure 4: *In situ* negative C_s images of surface of anatase crystal before (*upper*) and after (*lower*) exposure to UV light and water vapor. The cation sublattice shows an increase in disorder and the Ti dumbbell spacing contracts by almost 0.5 Å. The contraction opens up potential path for water intercalation resulting in hydroxylation.

dose image of **Figure 4**. Under reaction conditions, the dumbbell spacing changes to around 1.9 Å and show random tilts. The changes are associated with the initial stages of hydroxylation.

Future Plans

Ultra-high Energy Resolution EELS: We will continue to push and develop vibrational, valence and photonic applications of high resolution EELS with special emphasis on the unique information that can be derive for catalytic systems. The photonic and valence loss techniques can be carried out on our Titan ETEM and will provide unique opportunities to investigate how these phenomena are influenced under reaction conditions. Atomic vibrational EELS will be employed to explore the vibrational modes at particle surfaces and defects. *In Situ Observations*: The *in situ* data acquired from the anatase particle is very high quality but requires intense processing and modeling to fully interpret the structural dynamics. We are performing molecular dynamics and image simulations to characterize the effect of oxygen vacancies on the structure. We then plan to fully interpret the structural changes induced during exposure to water and UV illumination. We have also performed high resolution low-dose imaging of the carbon nitride structure and are currently developing advanced processing methods to fully understand the structure disorder.

Acknowledgements

The financial support from U.S. Department of Energy, Office of Science, Office of Basic Energy Sciences (DE-SC0004954) and the use of the electron microscopes at John M. Cowley Center for High Resolution Microscopy at Arizona State University are gratefully acknowledged. I would like to acknowledge the contributions of my Ph.D. students especially Qianlang Liu, Diane Haiber and Kartik Venkatraman as well as postdoc Barnaby Levin. Also thanks to my ASU colleagues Peter Rez and Katia March. Thanks also to our collaborators on the photonic mode project, David Masiello and Steven Quillin at the University of Washington who performed the modelling of the photonic modes.

References

1. Crozier, P.A., *Vibrational and valence aloof beam EELS: A potential tool for nondestructive characterization of nanoparticle surfaces*. Ultramicroscopy, 2017. **180**: p. 104-114.
2. Lagos, M.J., et al., *Mapping vibrational surface and bulk modes in a single nanocube*. Nature, 2017. **543**(7646): p. 529-+.
3. Rez, P., et al., *Damage-free vibrational spectroscopy of biological materials in the electron microscope*. Nature Communications, 2016. **7**: p. 7.
4. Cao, S., et al., *Polymeric Photocatalysts Based on Graphitic Carbon Nitride*. Advanced Materials, 2015. **27**(13): p. 2150-2176.
5. Blaustein, G.S., et al., *Guiding optical modes in chains of dielectric particles*. Optics Express, 2007. **15**(25): p. 17380-17391.

Publications Supported by BES (2016-2018)

- 1) P. A., Crozier*, T. Aoki and Q. Liu (2016). "*Detection of water and its derivatives on individual nanoparticles using vibrational electron energy-loss spectroscopy*" *Ultramicroscopy*, 169: 30-36.
- 2) F. Tao and P. A. Crozier* (2016). "*Atomic-Scale Observations of Catalyst Structures under Reaction Conditions and during Catalysis.*" *Chemical Reviews*, 116(6): 3487-3539.
- 3) P.A. Crozier, (2017) "*Vibrational and valence aloof beam EELS: A potential tool for nondestructive characterization of nanoparticle surfaces*", *Ultramicroscopy* 180 104-114.
- 4) Q. Cheng, M.K. Benipal, Q. Liu, X. Wang, P.A. Crozier C. Chan, and R. Nemanich, (2017). "*Al₂O₃ and SiO₂ Atomic-Layer Deposition Layers on ZnO Photoanodes and Degradation Mechanisms*", *ACS Applied Materials and Interfaces* 9(19) 16138-16147.
- 5) Q. Liu, K. March, and P.A. Crozier* (2017). "*Nanoscale Probing of Bandgap States on Oxide Particles Using Electron Energy-Loss Spectroscopy*", *Ultramicroscopy* 178 2-11
- 6) D. Haiber and P.A. Crozier, (2018) "*Nanoscale Probing of Local Hydrogen Heterogeneity in Disordered Carbon Nitrides with Vibrational EELS*". *ACS Nano* 2018. DOI 10.1021/acsnano.8b00884.
- 7) Q. Liu, S C. Quillin, D. J. Masiello, P. A. Crozier, (2018) "*Probing Resonant Photonic Modes in Oxide Nanoparticles with Focused Electron Beams*", (submitted)
- 8) Liuxian Zhang, Qianlang Liu and Peter A. Crozier (2018) "*Light Enhanced Coarsening of Pt Co-Catalyst Nanoparticles on TiO₂ During Liquid-Phase Photocatalysis*", (submitted)
- 9) Kartik Venkatraman, Barnaby Levin , Katia March, Peter Rez, and Peter A. Crozier (2018) "*Vibrational Spectroscopy at Atomic Resolution*", (submitted)

Controlling Interfacial Spin Polarization due to Chemisorption

Dan Dougherty

Department of Physics and Organic and Carbon Electronics Lab, North Carolina State University

Research Scope

The project applies spin polarized scanning tunneling microscopy to the problem of interactions between organic semiconductors and substrates of interest for spintronic devices. The goal is to identify spin dependent interfacial interactions that can control spin injection.

Recent Progress

A Toy Model Approach to Interfacial Spin Polarization

To inject a spin polarized current from a metallic metal electrode into any of the novel non-metallic materials created in recent decades requires attention to the details of the injecting interfaces. This is because bulk conductivity mismatch must be alleviated by interfacial engineering to achieve efficient spin injection into non-metals [1]. In this work, we focus on a fruitfly materials class in organic semiconductor spintronics [2]: the metal quinolates. We discuss how different regimes of electronic coupling are realized in this materials class in the context of the famous Anderson-Newns-Grimley (ANG) model of chemisorption [3].

In previous work [4], where we measured the first evidence for magnetic interface states for metal-quinolate adsorbates that have dominated spintronic device research, detailed quantitative understanding of the nature of these states required first principles calculations. However, certain qualitative aspects such as the transition to bonding and antibonding states from molecular resonances as coupling increased can be understood within the framework of the Anderson-Newns-Grimley (ANG) model of chemisorption. This is a toy model that generalizes the Anderson impurity model to consider energy dependent hybridization expect when a molecular adsorbate couples to a continuum of metal substrate states.

In the final project year, we searched for experiments that would result in bonding and antibonding states that are more directly understandable within the ANG model paradigm. We hypothesized that the planar π -conjugated molecule called antradithiophene (ADT) might work for this purpose. The ADT molecule has two Sulphur atoms that could plausibly give rise to very strong surface interactions on a Cr surface (Sulphur is a common and difficult to remove impurity in Cr crystals). Importantly, unlike the magnetic Cr-quinolate from our previous work [4], ADT is a simple closed shell system that may not require detailed *ab initio* modeling to capture its interactions with the Cr surface.

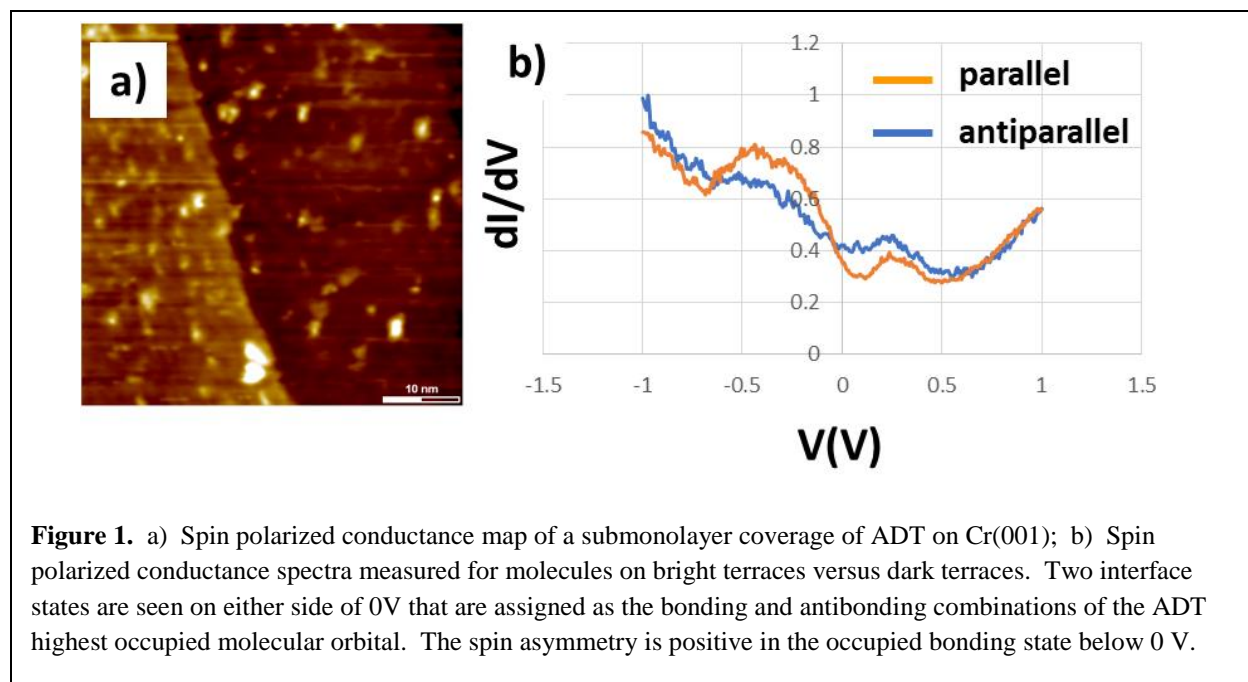
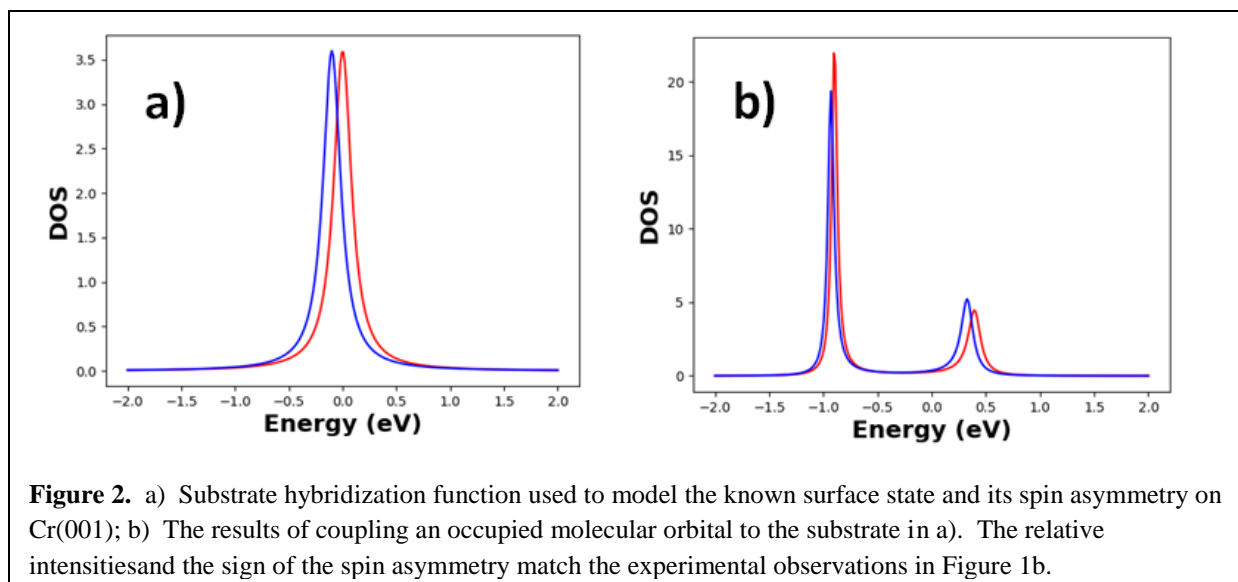


Figure 1a shows a spin polarized conductance map with protrusions corresponding to single ADT molecules. The bright terrace on the left has a local magnetization parallel to the SPSTM tip magnetization while the dark terrace on the right is antiparallel. Tunneling spectra measured above multiple molecular protrusions on each terrace in turn give rise to a clear spin asymmetry as shown in Figure 1b. This asymmetry is exactly opposite to found for Cr-quinolate in our earlier study.

Remarkably the observed spin-dependent electronic structure for ADT can be modelled within the ANG framework. For this work, we developed a specific realization of the ANG model for the Cr(001) surface. We assign a Lorentzian chemisorption function for each spin population that models the Cr(001) d-derived surface state as shown in Figure 2a. This chemisorption function results in straightforward numerical implementation of the ANG model that captures the two key features of our data. First we allow an occupied molecular orbital to interact with it, giving rise to two new interface states as shown in Figure 2b. In addition, the sign of the spin asymmetry in the occupied density of states is inherited from the original surface state on Cr(001). In other words it is positive. The alternative negative spin polarization was never observed in our adapted version of the ANG model. This is significant because our previous work showing negative spin asymmetry for a magnetic molecule clearly requires more than this simple model to capture. Nevertheless, we have shown that the ANG model provides a straightforward conceptual perspective on the problem of spin polarized interfaces due to chemisorption. The basic idea is that of a magnetic “surface molecule” that arises from the coupling of a nonmagnetic molecule to a magnetic surface.



Future Plans

This project is coming to a close on a one year no-cost extension to finalize analysis and publication of the last Spin Polarized STM observations of Anthrdithiophene on Cr(001).

References

- [1] G. Schmidt, *Journal of Physics D-Applied Physics* **38**, R107 (2005).
- [2] M. Cinchetti et al., *Nat. Materials* **16**, 507 (2017).
- [3] J.P. Muscat and D.M. Newns, *Prog. Surf. Sci.* **9**, 1 (1978).
- [4] Wang et al., *Phys. Rev. B* (2017).

Publications

- 1.) "Recovery of the Bulk-like Electronic Structure of Manganese Phthalocyanine Beyond the First Monolayer on Bi₂Te₃" *Surf. Sci.* 662, 87 (2017). (A.S. Hewitt, J. Boltersdorf, P.A. Maggard, and D.B. Dougherty)
- 2.) "Tuning Interfacial Spin Filters From Metallic to Resistive within a Single Organic Semiconductor Family" *Phys. Rev. B Rapid Communications* 95, 241410R (2017). (J. Wang, A. Deloach, W. Jiang, C.M. Papa, M. Myahkostapov, F.N. Castellano, F. Liu, and D.B. Dougherty)

Real-time Measurements of Complex Transition Metal Oxide Nanostructure Growth

Michael A. Filler

School of Chemical & Biomolecular Engineering, Georgia Institute of Technology

Frances M. Ross

Department of Materials Science and Engineering, Massachusetts Institute of Technology

Research Scope

Complex oxides and their heterostructures exhibit a range of exotic phenomena, including ferroelectricity, superconductivity, and catalytic activity, but new applications will require the formation of nanostructures with geometries and compositions that are difficult to achieve with, or entirely off-limits to, conventional growth methods. To this end, we are fundamentally interrogating the bottom-up crystal growth of complex oxide nanostructures and, in doing so, working to achieve precise control of their structure and properties. Real-time *in situ* transmission electron microscopy (TEM) and infrared (IR) spectroscopy experiments are coupled to understand the role of catalyst behavior, nanowire structure, and interface chemistry on nanostructure growth. We seek a complete picture of the process, not possible with either technique on its own, but essential to enable the growth of this class of materials. The main objectives are: (1) Develop new *in situ* TEM approaches to probe oxide nanowire growth; (2) understand the physicochemical phenomena underlying binary oxide nanowire growth; and (3) demonstrate and advance the VLS growth of ternary oxide nanowires and their heterostructures.

We are adapting a self-assembly technique – the vapor-liquid-solid (VLS) mechanism – to synthesize the oxide nanostructures. Constituent atoms supplied from gas phase precursors collect in metal seed droplets from which long thin crystals, or nanowires, nucleate and grow. The composition of the nanowire depends on the gas phase composition, so functional heterogeneity can be encoded along the nanowire's length by modulating the precursor flow. A remarkable degree of control has been demonstrated for semiconductor nanostructures grown with the VLS mechanism, but adapting this growth technique to complex oxides is complicated by the interplay between the droplet catalytic properties and the energetics of the multiple interfaces. We therefore carry out VLS growth of complex oxides with two unique *in situ* tools. Structure will be probed with *in situ* TEM while surface chemistry will be probed with *in situ* IR spectroscopy, both in real time as the nanowires grow. Directly measuring the response of nanowire and droplet structure and surface chemistry to changes in growth conditions can yield much-needed insights into the mechanisms that govern this self-assembly process.

Prior Progress

In situ Transmission Electron Microscopy. During growth experiments, *in situ* TEM allows us to observe directly the effects of changes in experimental conditions such as pressure and temperature. It enables characterization of a single structure without the limitations of

averaging: the evolution of an individual structure can be followed from nucleation to its final form, including short-lived intermediate stages. Using this experimental approach on semiconductor nanowires we have already examined growth kinetics, structure (of the nanowire, its sidewall and the catalyst), catalyst stability at the nanowire tip, growth front dynamics and interface formation, and phase transformations within the catalyst [1-12]. These *in situ* measurements provided information on the formation process of single-component nanowires as well as nanowires that contain interfaces and embedded nanocrystals. These observations have allowed the development of models explaining growth rates, the pathways of the atomic species through the catalyst to the growth interface, the nanowire surface structure, and the relationship between catalyst properties and the resulting morphology. The factors controlling interfacial abruptness and crystal phase control have also been addressed. A universal finding is that phase diagrams for the catalyst provide only limited guidance, given the small length scales and non-equilibrium nature of growth. By understanding these features of nanowire growth, the overall result is a better control of structures that potentially lead to new applications.

In situ Infrared Spectroscopy. *In situ* IR spectroscopy can probe the presence and atomic-level bonding of surface species on nanostructures during their synthesis. The acquisition of this chemical information is not possible with TEM, but is critical for understanding nanostructure synthesis. *In situ* IR spectroscopy has been used to demonstrate that surface adsorbates, including $-H$ and $-CH_3$, decorate Si and Ge nanowires and influence morphology [14], growth direction [15, 16], catalyst phase [17], and heterostructure formation [18]. The role of these species is multifaceted: they can control surface energy, precursor adsorption rate, and atomic diffusion on the nanowire surface. The coverage of hydrogen atoms provides a good example. It depends on precursor partial pressure and substrate temperature [14-16]; at large hydrogen coverages, Ge nanowires exhibit almost no taper since the hydrogen atoms prevent precursor chemisorption. Increasing taper is observed as hydrogen coverage decreases since precursor molecules can now access reactive dangling bonds.

Future Plans

The two techniques are complementary in addressing different

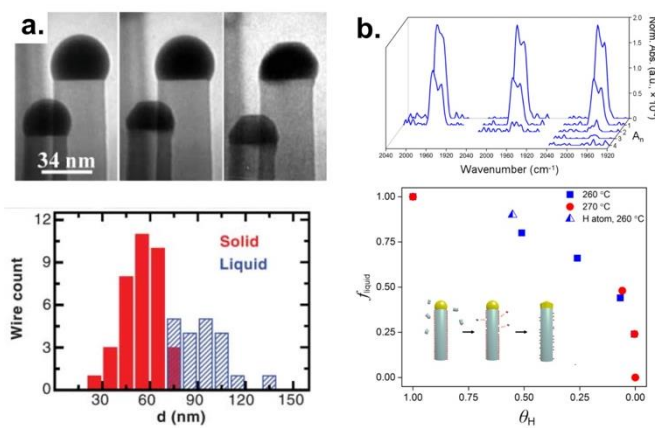


Figure 1. (a) Bright-field TEM image series showing the solidification of catalyst droplets of AuGe on two Ge nanowires when the pressure is reduced at constant temperature. The histogram was measured at a fixed time after reducing the pressure and shows that smaller droplets have solidified while larger ones require more time [8]. (b) Absorption spectra (A_n) of the $\nu(Ge-H)$ stretching region while annealing Ge nanowires in H_2 at 260 °C. H desorbs, lowering the hydrogen coverage (θ_H) and allowing Au to migrate to the nanowire sidewall. The fraction of AuGe catalyst droplets that remain liquid (f_{liquid}) can be correlated with (θ_H) [17].

aspects of nanostructure growth and will be applied to the study of complex oxides. Figure 1 shows an example of this for Ge nanowire growth. *In situ* TEM demonstrated that Ge nanowire growth below the eutectic temperature can occur with a liquid or solid catalyst, with the phase of the catalyst depending on the growth history [8], and that pressure influences catalyst migration and surface structure [19]. However, TEM could not probe the interfacial chemical processes underlying these effects. *In situ* IR spectroscopy revealed that hydrogen atoms can be covalently bonded to the nanowire sidewall, and changes in their coverage explain many of the *in situ* TEM observations. In particular, H atoms block the migration of Au atoms from the catalyst droplet [17]. Only when Au can access the sidewall, due to a decrease in H coverage, can Au identify a low barrier nucleation site and solidify. Since surface chemistry strongly depends on pressure (i.e., there is a dynamic equilibrium between precursor adsorption and adsorbate desorption), IR studies provide an explanation for many of the differences between nanowire growth at low and high pressure.

In terms of oxide nanostructure growth, we will begin by interrogating binary oxide nanowires as the current, limited understanding of their fundamental physicochemistry prevents the rational pursuit of other materials systems with more exotic properties. Insights from these studies will be applied to achieve nanostructures of complex oxides and those containing heterostructures. Modifications to the PIs' existing *in situ* TEM and IR techniques, including the capability to deposit relevant catalysts and deliver relevant precursors, will be required before oxide nanostructure growth can be observed. We will also expand the TEM's capabilities by increasing the pressure that can be attained at the sample without compromising the ability to form a clean surface for epitaxy.

References

1. Wen, C. Y.; Reuter, M. C.; Bruley, J.; Tersoff, J.; Kodambaka, S.; Stach, E. A.; Ross, F. M., Formation of Compositionally Abrupt Axial Heterojunctions in Silicon-Germanium Nanowires. *Science* **2009**, *326* (5957), 1247.
2. Jacobsson, D.; Panciera, F.; Tersoff, J.; Reuter, M. C.; Lehmann, S.; Hofmann, S.; Dick, K. A.; Ross, F. M., Interface Dynamics and Crystal Phase Switching in GaAs Nanowires. *Nature* **2016**, *531* (7594), 317.
3. Kallesoe, C.; Wen, C. Y.; Molhave, K.; Boggild, P.; Ross, F. M., Measurement of Local Si-Nanowire Growth Kinetics Using *in situ* Transmission Electron Microscopy of Heated Cantilevers. *Small* **2010**, *6* (18), 2058.
4. Panciera, F.; Norton, M. M.; Alam, S. B.; Hofmann, S.; Molhave, K.; Ross, F. M., Controlling Nanowire Growth through Electric Field-Induced Deformation of the Catalyst Droplet. *Nature Communications* **2016**, *7*.
5. Ross, F. M.; Tersoff, J.; Reuter, M. C., Sawtooth Faceting in Silicon Nanowires. *Physical Review Letters* **2005**, *95* (14).
6. Kodambaka, S.; Tersoff, J.; Reuter, M. C.; Ross, F. M., Diameter-Independent Kinetics in the Vapor-Liquid-Solid Growth of Si Nanowires. *Physical Review Letters* **2006**, *96* (9).
7. Hannon, J. B.; Kodambaka, S.; Ross, F. M.; Tromp, R. M., Fundamental Limits on the Growth of Si Nanowires. *Nature* **2006**, *440*, 69.

8. Kodambaka, S.; Tersoff, J.; Reuter, M. C.; Ross, F. M., Germanium Nanowire Growth Below the Eutectic Temperature. *Science* **2007**, *316* (5825), 729.
9. Kim, B. J.; Tersoff, J.; Kodambaka, S.; Reuter, M. C.; Stach, E. A.; Ross, F. M., Kinetics of Individual Nucleation Events Observed in Nanoscale Vapor-Liquid-Solid Growth. *Science* **2008**, *322* (5904), 1070.
10. Hillerich, K.; Dick, K. A.; Wen, C. Y.; Reuter, M. C.; Kodambaka, S.; Ross, F. M., Strategies to Control Morphology in Hybrid Group III-V/Group IV Heterostructure Nanowires. *Nano Letters* **2013**, *13* (3), 903.
11. Chou, Y. C.; Hillerich, K.; Tersoff, J.; Reuter, M. C.; Dick, K. A.; Ross, F. M., Atomic-Scale Variability and Control of III-V Nanowire Growth Kinetics. *Science* **2014**, *343* (6168), 281.
12. Panciera, F.; Chou, Y. C.; Reuter, M. C.; Zakharov, D.; Stach, E. A.; Hofmann, S.; Ross, F. M., Synthesis of Nanostructures in Nanowires Using Sequential Catalyst Reactions. *Nature Materials* **2015**, *14* (8), 820.
13. Ross, F. M., Controlling Nanowire Structures through Real Time Growth Studies. *Reports on Progress in Physics* **2010**, *73* (11), 114501.
14. Sivaram, S. V.; Shin, N. C.; Chou, L.-W.; Filler, M. A., Direct Observation of Transient Surface Species During Ge Nanowire Growth and Their Influence on Growth Stability. *Journal of the American Chemical Society* **2015**, *137*, 9861.
15. Shin, N.; Filler, M. A., Controlling Silicon Nanowire Growth Direction Via Surface Chemistry. *Nano Letters* **2012**, *12* (6), 2865.
16. Shin, N.; Chi, M.; Filler, M. A., Interplay between Surface Hydrogen and Defect Propagation in Si Nanowire Kinking Superstructures. *ACS Nano* **2014**, *8*, 3829.
17. Sivaram, S. V.; Hui, H. Y.; de la Mata, M.; Arbiol, J.; Filler, M. A., Surface Hydrogen Enables Sub-Eutectic Vapor-Liquid-Solid Semiconductor Nanowire Growth. *Nano Letters* **2016**, *16*, 6717.
18. Hui, H. Y.; de la Mata, M.; Arbiol, J.; Filler, M. A., Low-Temperature Growth of Axial Si/Ge Nanowire Heterostructures Enabled by Trisilane. *Chemistry of Materials* **2017**, *29*, 3397.
19. Gamalski, A. D.; Tersoff, J.; Kodambaka, S.; Zakharov, D. N.; Ross, F. M.; Stach, E. A., The Role of Surface Passivation in Controlling Ge Nanowire Faceting. *Nano Letters* **2015**, *15* (12), 8211.

Publications

N/A

Localized Spatiotemporal Behaviors of Coherent Structural Dynamics Revealed with Ultrafast Electron Microscopy

David J. Flannigan

Department of Chemical Engineering and Materials Science, University of Minnesota, Minneapolis, MN

Research Scope

The overall scope of the current project covers the following areas: (i) Elucidation of the localized spatiotemporal behaviors of coherent, photoexcited structural dynamics with various modalities of ultrafast electron microscopy (UEM; **Fig. 1**), and (ii) expansion of the accessible UEM experimental parameter space. Three specific research Topics within the scope of the project are being pursued: (1) Photoinduced Hypersonic Phonon Dynamics; (2) Phonon Nucleation, Evolution, and Decay; and (3) Expanding and Enhancing UEM Capabilities.

Topic 1. Photoinduced Hypersonic Phonon Dynamics. Ultrafast photoexcitation of semiconducting materials can lead to the generation of dense, transient charge-carrier plasmas. Such electron-hole plasmas display several intriguing fundamental behaviors reminiscent of structural acoustic modes; such as time-varying phase velocities, hypersonic phase fronts, and acoustic-type oscillatory behaviors. Here, femtosecond (fs) electron imaging with UEM is being used to study how these coherent electron-hole plasmas couple to the lattice and how the resulting energy deposition evolves in space and time. As described in the **Recent Progress** section, this discovery-based work has led to new insights into such behaviors.

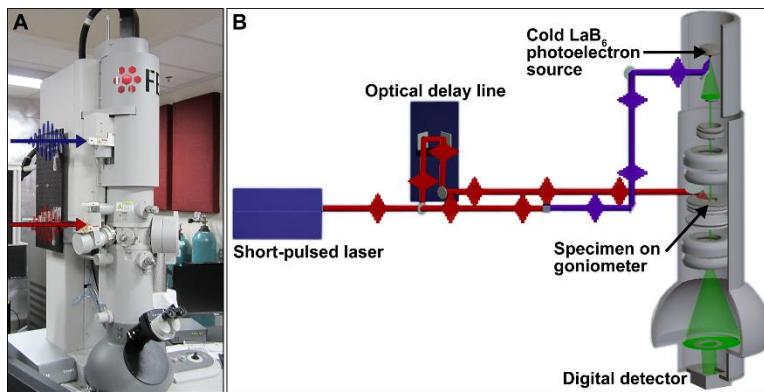


Fig. 1. Ultrafast electron microscopy (UEM). (A) Photograph of a 200-kV thermionic TEM modified for ultrafast operation. The pulsed-laser ports are indicated with red (pump) and blue (probe) arrows. (B) Schematic of the UEM stroboscopic pump/probe operation. Figure adapted from [3].

Topic 2. Phonon Nucleation, Evolution, and Decay. Photoexcitation of optically-absorbing materials leads to several discrete but inter-related energy-relaxation processes coupled through particle-particle scattering at high frequencies and wave mechanics at lower frequencies. Despite extensive study, a number of fundamental questions pertaining to the microscopic mechanisms associated with these relaxation processes have been challenging to address owing to the combined ultrafast and ultras small scales on which they operate. Accordingly, application of newly-emerging

experimental methods to otherwise well-studied systems is certain to reveal new physical insights and open new research avenues. Here, a combination of UEM imaging (BF, DF) and diffraction (PBED, CBED) modalities are being used to study the atomic- to micro-scale spatiotemporal evolution of coherent lattice excitation and relaxation.

Topic 3. Expanding and Enhancing UEM Capabilities. With the addition of pulsed-laser ports, the time resolution of conventional TEMs can be extended to the sub-picosecond scale.¹⁻³ Under certain conditions, the coherency and spatial resolution of these instruments is retained during pulsed-mode operation.⁴ However, many challenges – both fundamental and practical – remain, which pose challenges to the study of certain types of phenomena and impose limits to the resolvable dynamics. Here, a comprehensive approach comprised of both fundamental and applied systematic studies is being used to expand and enhance the UEM experimental parameter space.

Recent Progress

In the first year of the project, fs BF imaging with UEM has been used to directly image the spatiotemporal behaviors of highly-coherent propagating strain waves in single-crystal Ge (**Fig. 2**).⁵ Generally, such experiments are conducted using *in situ* fs photoexcitation, with 2.4-eV photon energies (though 1.2 eV has also been used) and fluences of ~ 1 mJ/cm². For freestanding wedges, such photoexcitation produces coherent contrast wave trains that arise from propagating strain waves. The waves are observable because they cause a slight local deviation of the crystal lattice relative to the fixed incident electron wave vector during in-plane propagation. Each (mostly) linear contrast band – which corresponds to a single wavefront – travels along a single in-plane direction and is readily discernible from others in the wavetrain. Accordingly, fs BF UEM imaging

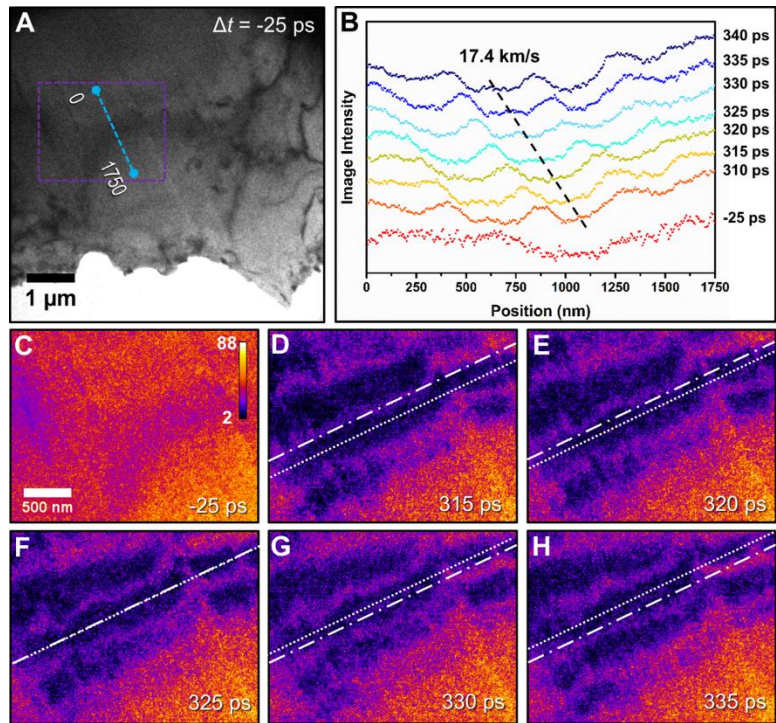


Fig. 2. Bright-field UEM imaging of directional, hypersonic strain waves. (A) Representative UEM image at $\Delta t = -25$ ps. The region of interest (purple) and position and length of line profiles (blue) are marked. (B) Contrast-profile line scans from the blue line in (A) at select Δt . The speed of one wavefront (17.4 nm/ps) is labeled. (C-H) Select UEM images showing the propagation of a single wavefront within the region of interest. The dot-dashed line marks a temporally static position, while the dotted line follows one wavefront. The color bar is scaled to the raw-image counts. Figure adapted from [5].

allows one to quantify the wavefront velocities and total wavetrain behaviors. Following this, it was found that all wavefronts propagate along a single in-plane direction and that the speeds were several times higher than the bulk speed of sound in Ge (~ 5 nm/ps).

Owing to the discrete nature of each wavefront in the UEM images – enabled by the high SNR and high spatiotemporal resolutions (here, nanometer-picosecond) with the instrument at Minnesota – *time-varying* velocity dispersion behaviors were determined (**Fig. 3**). To avoid experimenter bias when determining propagation direction, an approach employing Hough transforms was used to find the most-likely wavefront orientation within each UEM image in the time series. By selecting a region of interest, and collapsing pixel counts to one spatial dimension within this region, the time-varying behavior of each wavefront – as well as the entire wavetrain – can be visualized in a space-time contour plot. In **Figure 3(A)**, each dark, linear band represents the velocity behavior of a single wavefront with time. Plotting the data this way makes it readily apparent that while each wavefront travels with a constant velocity, the entire wavetrain experiences a relaxation to the bulk speed of sound within the first nanosecond following photoexcitation. That is, each wavefront that emerges is slower than the previous wavefront [**Fig. 3(B)**].

In addition to the time-varying velocity dispersion behavior, the space-time contour plot in **Figure 3** also reveals a significant delay in initial wavefront emergence following *in situ* fs photoexcitation. The temporal position of time zero ($\Delta t = 0$ ps) was determined using a plasma lensing method, with a precision of better than 100 fs ($n = 3$ measurements).⁶ Here, the first wavefront was observed to emerge ~ 100 ps after fs photoexcitation, and it was found to propagate with a measurable speed of 35 nm/ps. The hypothesis that stems from this observation is that strain-wave launch is highly-dependent upon the specific relaxation time of electron-phonon coupling, which in highly-excited Ge can be many tens of picoseconds owing to the hot-phonon bottleneck effect. This hypothesis is currently being tested.

In addition to the velocity behaviors of the strain waves summarized in **Figure 2** and **Figure 3**, the intrinsic nature (*e.g.*, symmetries and modes) of the coherent dynamics were also

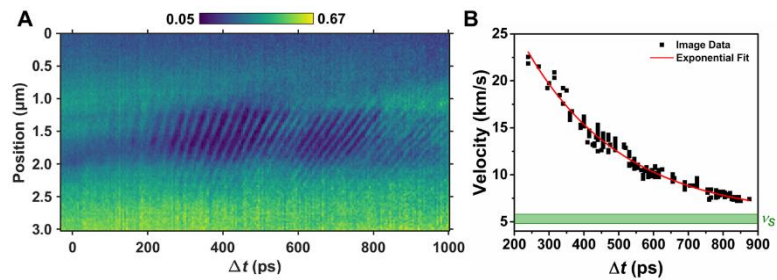


Fig. 3. Time-varying wavefront dynamics. **(A)** Space-time contour plot of individual wavefronts. For reference, the vacuum/crystal interface is located at larger position values. The color bar represents image intensity relative to vacuum. **(B)** Time-varying velocity dispersion, as determined from each individual wavefront. A single exponential fit is shown in red and is included to illustrate the basic dispersion behavior observed. The green band labeled v_s is the range of sound speeds in Ge. Figure adapted from [5].

explored. Owing to the measured velocities and the specimen geometry, the observed dynamics were compared to the theoretical behaviors expected for in-plane plate waves or Lamb-type modes (**Fig. 4**). A direct comparison with the symmetric and asymmetric modes of such waves, calculated from the crystal thickness and Ge elastic tensor values, shows that the observed phase-velocity dispersion behavior (in the frequency domain) matches the first-order symmetric mode [Fig. 4(A)]. This particular mode is essentially dispersionless at phase velocities above the bulk speed of sound [Fig. 4(B)]. The mechanisms are currently being studied.

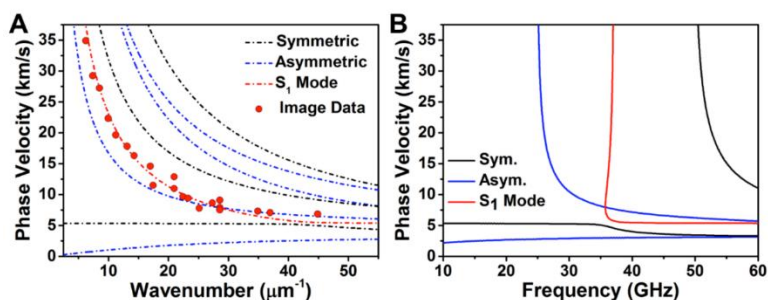


Fig. 4. Velocity dispersion of hypersonic strain waves. (A) Experimental phase velocity compared to calculated symmetric and asymmetric Lamb-type modes of varying order. (B) Calculated phase-velocity dispersion for representative modes. The first-order symmetric mode is shown in red. Figure adapted from [5].

This particular mode is essentially dispersionless at phase velocities above the bulk speed of sound [Fig. 4(B)]. The mechanisms are currently being studied.

Future Plans

The nature and the role of the crystal surface morphologies on acoustic-phonon guiding will be explored. This will be done through characterization of the physical and structural nature of the features, as well as on controlled orientation of the morphologies to determine the impact on wave propagation. In addition, the nature of the observed acoustic phonons will be explored, including precise determination of symmetry and coupling strengths to higher-frequency optical and acoustic modes. This, along with emergence times with respect to time zero, will be explored through fluence-dependent studies and excitation energy. Attention will be focused on developing robust UEM CBED methods for pinpointing and characterizing regions of phonon emergence, mainly through use of novel photocathode geometries.

References

1. Zewail, A. H. Four-Dimensional Electron Microscopy. *Science* **2010**, 328, 187-193.
2. Flannigan, D. J.; Zewail, A. H. 4D Electron Microscopy: Principles and Applications. *Acc. Chem. Res.* **2012**, 45, 1828-1839.
3. Plemmons, D. A.; Suri, P. K.; Flannigan, D. J. Probing Structural and Electronic Dynamics with Ultrafast Electron Microscopy. *Chem. Mater.* **2015**, 27, 3178-3192.
4. Barwick, B., *et al.* 4D Imaging of Transient Structures and Morphologies in Ultrafast Electron Microscopy. *Science* **2008**, 322, 1227-1231.
5. Cremons, D. R., *et al.* Picosecond Phase-Velocity Dispersion of Hypersonic Phonons Imaged with Ultrafast Electron Microscopy. *Phys. Rev. Mater.* **2017**, 1, 073801.
6. Plemmons, D. A.; Flannigan, D. J. Ultrafast Electron Microscopy: Instrument Response from the Single-Electron to High Bunch-Charge Regimes. *Chem. Phys. Lett.* **2017**, 683, 186-192.

Publications

1. Du, D. X.; Cremons, D. R.; Flannigan, D. J. Directed Hypersonic Strain Waves Imaged with Ultrafast Electron Microscopy. *Microsc. Microanal.* **2018**, *24* (Suppl. 1), 1912-1913. (*Student Scholar Award Winner; Best Poster Award Winner, Physical Division*)
2. Gnabasik, R. A.; Suri, P. K.; Flannigan, D. J. Imaging Coherent Acoustic Phonons in LaFeAsO with Ultrafast Electron Microscopy. *Microsc. Microanal.* **2018**, *24* (Suppl. 1), 1850-1851.
3. Flannigan, D. J.; Cremons, D. R.; Du, D. X.; McKenna, A. J.; Plemmons, D. A. Imaging Coherent Structural Dynamics with Ultrafast Electron Microscopy. *Microsc. Microanal.* **2018**, *24* (Suppl. 1), 1838-1839.
4. Flannigan, D. J.*; Lindenberg, A. M.* Atomic-Scale Imaging of Ultrafast Materials Dynamics. *MRS Bull.* **2018**, *43*, 485-490. (*Invited Introductory Article, Special Issue on Ultrafast Imaging of Materials Dynamics, Guest Editors*)
5. Cremons, D. R.; Du, D. X.; Flannigan, D. J. Picosecond Phase-Velocity Dispersion of Hypersonic Phonons Imaged with Ultrafast Electron Microscopy. *Phys. Rev. Mater.* **2017**, *1*, 073801.

Growth, characterization, and nanoscale transport of chiral magnetic materials

Gregory D. Fuchs, Cornell University Applied and Engineering Physics, Ithaca, NY

Research Scope

The overarching aim of this research is to investigate the interplay between charge, spin, heat, and light on the *dynamics* of nanoscale chiral, and topological spin textures. The prime example of a topological spin texture is a magnetic skyrmion, which is a “vortex-like” magnetic texture where the local magnetization vector can be topologically mapped to an outward facing vector on the surface of a sphere [1,2]. The topological nature of these magnetic textures makes them “particle-like” with extremely low critical current density for motion under spin-transfer torques [3,4]. These properties have formed the basis for proposals of ultra-low power information storage devices [5,6].

This project uses a wide range of experimental approaches: electrical, optical, thermal, and magnetic experimental probes to study chiral and topological magnetism, with a particular focus on the behavior of these materials in nanostructured environments. We have focused on chiral magnetic materials with broken inversion crystal symmetry, particularly the B20 monosilicides and monogermanides of transition magnetic elements, e.g. MnSi, FeCoSi, and FeGe [7]. The magnetism of these materials have chiral, noncollinear spin texture due to a competition between their exchange, anisotropy, and the Dzyaloshinskii-Moriya interaction (DMI) that arises from their broken inversion symmetry [8,9].

Recent Progress

We demonstrate control over lattice strain and DMI in thin films through stoichiometry, and thus tailor the helical pitch and skyrmion diameter. To do this we study solid solutions of $\text{Mn}_x\text{Fe}_{1-x}\text{Ge}$ as a function of the stoichiometric fraction of Mn, x , which can be continuously tuned between 0 and 1. We co-deposit the three components, Mn, Fe, and Ge, using molecular beam epitaxy (MBE), which enable use to precisely control deposition rates and to monitor the crystalline quality using an *in-situ* RHEED. This “during growth” feedback enables us to decrease the growth temperature down to 200 °C, which is critical to limiting the thermally induced. By reducing the growth temperature, we were able to reduce the strain in MBE grown films by a factor of four times as compared to sputtered films. Fig. 1 is a high-resolution scanning transmission electron micrograph of $\text{Mn}_{0.18}\text{Fe}_{0.82}\text{Ge}$ showing high-quality epitaxy and crystallinity.

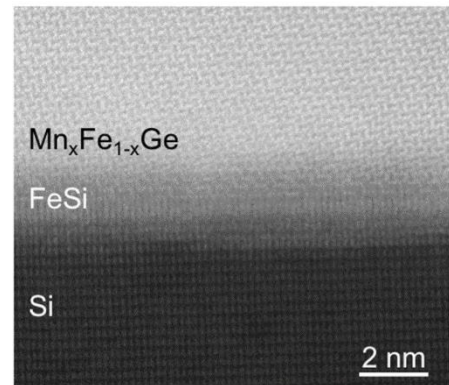


Figure 1. A high-resolution cross-sectional STEM image of thin-film $\text{Mn}_{0.18}\text{Fe}_{0.82}\text{Ge}$ along the $\langle 1\bar{1}0 \rangle$ zone axis that shows epitaxial growth on top of the FeSi seed layer.

To extract the helical periods and DMI as a function of x we perform magnetic characterization of the $\text{Mn}_x\text{Fe}_{1-x}\text{Ge}$ films. We first measure the magnetization as a function of magnetic field, from which we find the saturation magnetization M_s and the helical unwrapping field, H_d . We then apply a large magnetic field to saturate each film and measure the temperature-dependent magnetization, which follows Bloch- $T^{3/2}$ law due to thermal magnon excitations. From the Bloch- $T^{3/2}$ behavior, we extract the spinwave stiffness D_{sw} and find the symmetric and asymmetric exchange coefficients, A and D , respectively, in each film. The ratio of these two coefficient is proportional to the helical period L_D , which we plot in Fig. 2. There is a critical concentration, $x_c \sim 0.20$, where DMI vanishes and the helical period approaches infinity. As Mn fraction x increases further, the helical period starts to decrease again and it reaches 8 nm for the film with $x = 0.81$.

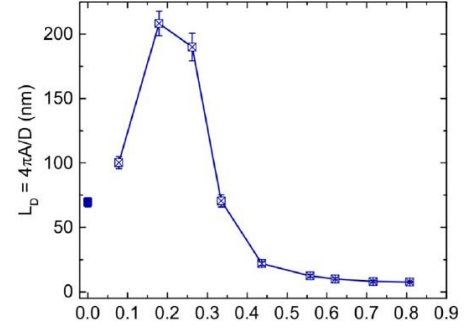


Figure 2. Mn-concentration dependent helical period in $\text{Mn}_x\text{Fe}_{1-x}\text{Ge}$ thin films. We for the first time show a sub-10 nm helical period in a thin film.

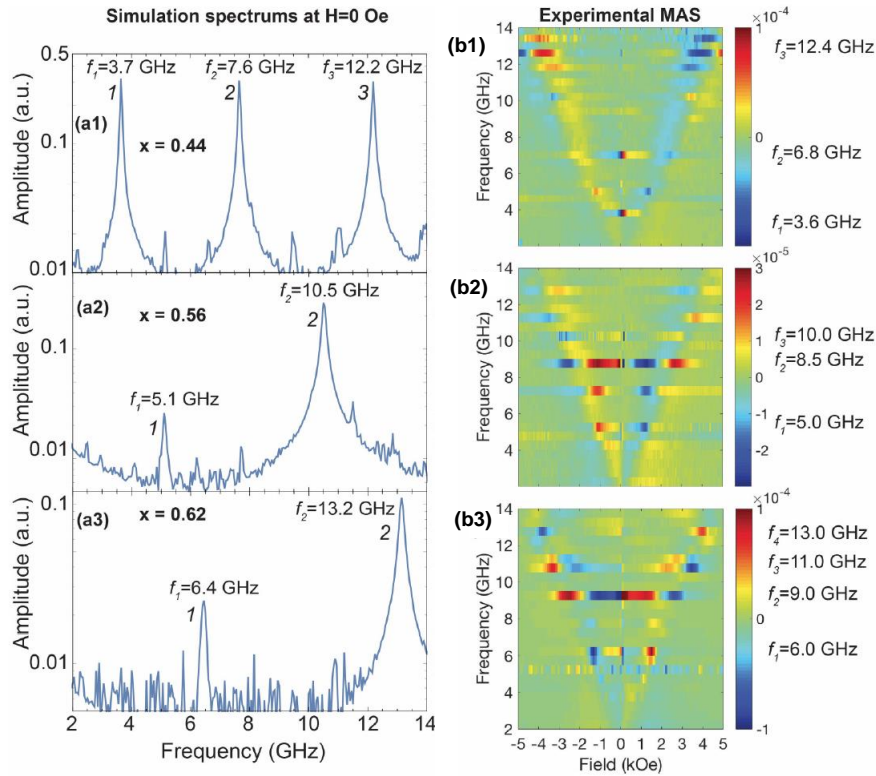


Figure 3. Results of micromagnetic simulations and experimental MAS of helical spin textures for $x=0.44$, $x=0.56$, and $x=0.62$ Mn. The simulation spectrums are calculated at 0 Oe field in (a) and we focus on resonance features near zero field in (b). There are more resonances at non-zero fields; however, we are unable to understand their profiles at the moment.

As verification of the helical textures and the quantitative values we extract from our measurements, we also performed microwave absorption spectroscopy (MAS). The parameters discussed above were used in micromagnetic calculations to extract the zero-field spin-wave spectrum. We compare the MAS data to the computational in Fig. 3. Here we focus on three films with $x = 0.44$, 0.56 , and 0.62 . Frequencies listed indicate quantitative agreement between the simulation and experimental data, which strongly supports

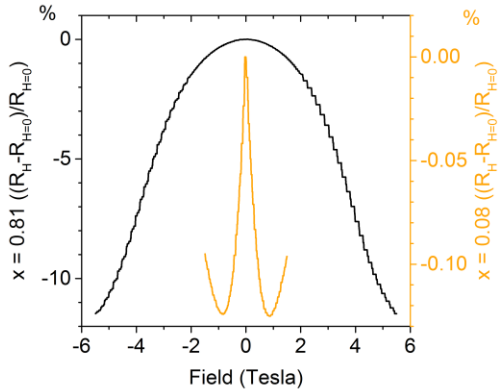


Figure 4. Anisotropic magnetoresistance of two $\text{Mn}_x\text{Fe}_{1-x}\text{Ge}$ films with $x=0.81$ (black) and $x=0.08$ (yellow).

our understanding that the zero-field state is a helix and that our extracted magnetic parameters (D , A , M_s) are accurate. This work [10] is the first demonstration of epitaxial, phase-pure growth of B20 $\text{Mn}_x\text{Fe}_{1-x}\text{Ge}$ thin films, which is exciting because these films represent a model-system to study basic physics and the device integration of sub-ten nm Bloch magnetic skyrmions. As such, thin film versions of DMI-controllable $\text{Mn}_x\text{Fe}_{1-x}\text{Ge}$ thin films could play a curial role in developing devices and prototype technology. This includes high-density, low power memory and logic technologies. Additionally, the nanoscale device

fabrication enabled by these thin-film materials will enable new access to transport nanoscale phenomena including understanding the connection between DMI and Berry phase with broken time-reversal and crystal-inversion symmetries.

To probe transport effects we fabricated Hall devices from the $\text{Mn}_x\text{Fe}_{1-x}\text{Ge}$ growth series. We measured the magnetoresistance, anomalous Hall effect, and the topological Hall effect. In Fig. 4 we plot the anisotropic magnetoresistance (AMR) for two films in the series that show a dramatic difference. For $x = 0.08$ Mn fraction, there is a 0.1% AMR, which is typical for ferromagnets (e.g. Co, Fe and their alloys); however, the film with $x = 0.81$ shows 13% AMR, which is surprisingly large and potentially significant for applications.

A central challenge in the field is to detect and manipulate single skyrmions in confined structures. Here we are working toward this goal in a current-perpendicular to film-plane spin-valve nanopillar geometry (Fig. 5). In these structures, geometric confinement of both the FeGe layer and the $\text{Ni}_{80}\text{Fe}_{20}$ (permalloy) layer facilitates formation of skyrmions and vortices, respectively. Such static spin texture allows us to explore mutual interactions between chiral and conventional magnetism in a nanostructure. We have recently succeeded in the film growth and nanofabrication of these structures. Figure 5 shows a schematic diagram of the finished device, and images taken in various stages of processing.

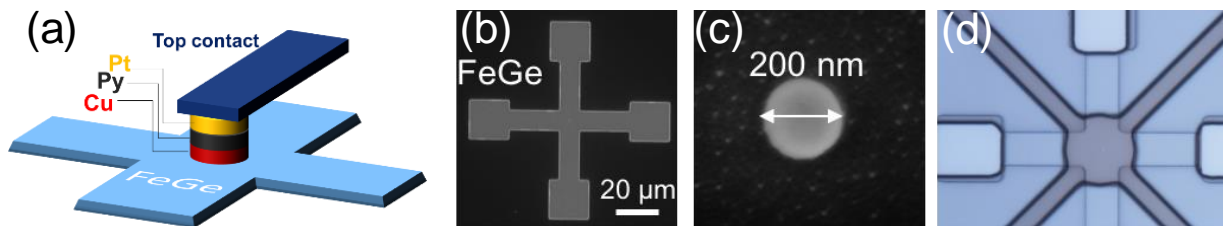


Figure 5. (a) Schematic of spinvalve nanopillar. $\text{Py}=\text{Ni}_{20}\text{Fe}_{80}$ (b) bottom FeGe layer on which we grow Cu/Py layers. (c) a 200-nm diameter disk after milling Cu/Py layers. (d) Optical micrograph before the final contact pad deposition. Some scattered light from the pillar can be seen.

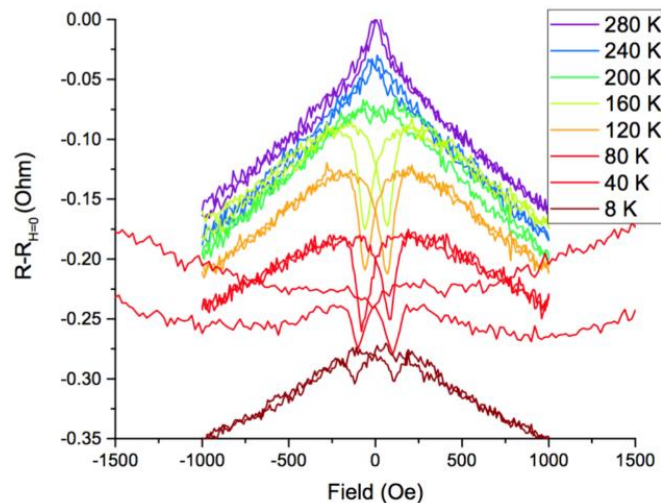


Figure 6. DC resistance as a function of magnetic field for a single 200 nm nanopillar fabricated from FeGe/Cu/permalloy films.

Figure 6 shows an initial transport study of a single, 200 nm diameter FeGe/Cu/Py nanopillar sample as a function of magnetic field and temperature. There are two effects that are immediately apparent. At high magnetic fields at temperatures above 40 K, there is a decreasing resistance with increasing in-plane field (in both directions.) By measuring the resistance of the FeGe channel only, we verified that this is the ordinary magnetoresistance response of FeGe. At lower magnetic fields, and at temperatures below 200 K, we see the emergence of a switching feature. Based

on the temperature in which it emerges, this feature is likely related to a chiral texture in FeGe.

Future Plans

We are still investigating the FeGe nanopillar resistance response and how it depends on geometry, and how it varies sample-to-sample. We are also modeling the geometry using micromagnetic calculations. We expect that by preparing the permalloy nanomagnet in a vortex state, we encourage the formation of a single skyrmion. In this way, we plan to trap a single skyrmion underneath the nanopillar, resonantly excite it, and electrically probe its creation and annihilation. Eventually, we hope to move the skyrmions in the FeGe channel as a step toward application-relevant control over single skyrmions.

References

- [1] S. Mühlbauer, B. Binz, F. Jonietz, C. Pfleiderer, A. Rosch, A. Neubauer, R. Georgii, and P. Böni, *Science* **323**, 915 (2009).
- [2] X. Z. Yu, Y. Onose, N. Kanazawa, J. H. Park, J. H. Han, Y. Matsui, N. Nagaosa, and Y. Tokura, *Nature* **465**, 901 (2010).
- [3] F. Jonietz, S. Mühlbauer, C. Pfleiderer, A. Neubauer, W. Münzer, A. Bauer, T. Adams, R. Georgii, P. Böni, R. A. Duine, K. Everschor, M. Garst, and A. Rosch, *Science* **330**, 1648 (2010).
- [4] X. Z. Yu, N. Kanazawa, W. Z. Zhang, T. Nagai, T. Hara, K. Kimoto, Y. Matsui, Y. Onose, and Y. Tokura, *Nat. Commun.* **3**, 988 (2012).
- [5] J. Iwasaki, M. Mochizuki, and N. Nagaosa, *Nat. Nanotechnol.* **8**, 742 (2013).
- [6] A. Fert, V. Cros, and J. Sampaio, *Nat. Nanotechnol.* **8**, 152 (2013).
- [7] N. Nagaosa and Y. Tokura, *Nat. Nanotechnol.* **8**, 899 (2013).
- [8] I. Dzyaloshinsky, *J. Phys. Chem. Solids* **4**, 241 (1958).
- [9] U. K. Rössler, A. N. Bogdanov, and C. Pfleiderer, *Nature* **442**, 797 (2006).
- [10] E. Turgut, H. Paik, K. Nguyen, D. A. Muller, D. G. Schlom, and G. D. Fuchs, *Phys. Rev. Mater.* **2**, 074404 (2018).

2-year Publication list

- Emrah Turgut, Albert Park, Kayla Nguyen, Austin Moehle, David A. Muller, Gregory D. Fuchs, “Chiral magnetic excitations in FeGe films.” *Phys. Rev. B* **95**, 134416 (2017).
- Emrah Turgut, Matthew J. Stolt, Song Jin, and Gregory D. Fuchs, “Topological spin dynamics in cubic FeGe near room temperature.” *J. Appl. Phys.* **122**, 183903 (2017).
- Emrah Turgut, Hanjong Paik, Kayla Nguyen, David A. Muller, Darrell G. Schlom, Gregory D. Fuchs, “Engineering Dzyaloshinskii-Moriya interaction in B20 thin film chiral magnets,” *Phys. Rev. Mater.* **2**, 074404 (2018).

Understanding Dynamic Processes in Hybrid Perovskite Semiconductors

PI: David S. Ginger, University of Washington Department of Chemistry, Box 351700

Research Scope

This project aims to develop and apply new combinations of scanning-probe-based hyperspectral chemical imaging with unique functional, *in situ*, *in operando*, and improved time-resolved measurements of local semiconductor materials properties. As part of this effort we seek to develop and adapt microscopy tools and analytical methods tailored to the challenges of extracting physical insight from complex multichannel nanoscale chemical imaging data, and, of maximizing the utility of such data when correlated with *in situ* functional imaging methods applied to halide perovskite semiconductors. We seek to understand the properties of reduced dimensionality hybrid perovskite phases, including 2D layered Ruddlesden-Popper phases, that have emerged as attractive materials for energy harvesting and conversion applications. We are applying new scanning-probe capabilities to explore microscopic structure-property relationships governing the electronic, interfacial, and mixed ionic/electronic transport properties of these materials to understand the origins of their seemingly improved stability, yet somewhat lower performance, compared to the prototype ABX_3 halide perovskite semiconductors. Specifically, we seek to (1) develop robust acquisition and data-science-based analysis protocols for utilizing hyperspectral photoinduced force microscopy (PIFM) data in ways suited to understanding soft halide perovskite semiconductors (2) understand how chemical and structural changes underpin functional properties in hybrid perovskites by combining nanoscale chemical imaging, functional imaging, and data informatics on lower dimensional and mixed-cation halide perovskite films; and (3) develop advanced new time-resolved electrostatic force microscopy methods to probe ion diffusion in 2D perovskite phases across multiple time and length scales, helping understand the origins of the stability and transport differences between these materials while broadly expanding the scope and utility of time-domain scanning-probe microscopy methods. The outcomes of the proposal will broadly advance state-of-the-art scanning probe microscopy tools used by many fields, as well as the basic science of an emerging class of materials with great promise in energy harvesting and energy efficiency applications.

Recent Progress

Over the past year, we have made several advances in our microscopy ability, and have also applied our scanning probe microscopy capabilities to better understand hybrid perovskites. These include using data-science-based AFM tools to map fast ion motion and perform hyperspectral imaging of 2D perovskites,¹ as well as the use of multimodal microscopy to understand slow ion motion, and measure activation energies and identify the role of electrochemistry upon defect formation in halide perovskites under bias.^{2,3}

Mapping Ion Motion in Mixed 2D Perovskites

We are studying light-induced ion motion in thin films comprising Ruddlesden-Popper phases of the layered 2D perovskite $(C_4H_9NH_3)_2PbI_4$ (BAPI). We have probed ionic and electronic carrier dynamics using two complementary data-intensive scanning probe methods, time-resolved G-mode scanning kelvin probe microscopy (G-SKPM)^{4,5} and fast-free time resolved electrostatic

force microscopy (FF-trEFM),^{6,7} as a function of position, time, and illumination. We have found that while the average surface photovoltage sign is dominated by the band bending at the buried perovskite-substrate interface, there are also time-dependent surface-mediated ionic effects occurring at the grain boundaries. As a result, these films exhibit substantial variations in the spatial and temporal response of the photovoltage (**Fig. 1**).

Under illumination, the photovoltages equilibrate over timescales of hundreds of microseconds, a timescale we associate with ionic motion. Surprisingly, we observe that the surface photovoltage of the 2D grain centers evolves more rapidly in time than that at the grain boundaries. We propose that this slower evolution at grain boundaries is due to ion migration at grain boundaries that occurs between PbI_4 planes,⁸ occurring as a result of photoinduced electric fields as proposed on conventional 3D hybrid perovskites⁹ and thereby changing the time-dependent band unbending at grain boundaries.

Our time-resolved electrostatic force microscopy data on this substrate show faster charging transients overall, consistent with a mix of electronic and ionic carrier dynamics.

These data provide new insight into the photoinduced mixed transport dynamics in 2D perovskites and are a useful basis for interpreting photovoltage dynamics on hybrid 2D/3D structures.

Photoinduced Force Microscopy

Correlating nanoscale chemical specificity with physical properties is a long-standing goal of functional scanning probe microscopy (SPM). We are exploring a data analytic approaches to combine multiple microscopy modes, using compositional information in infrared vibrational

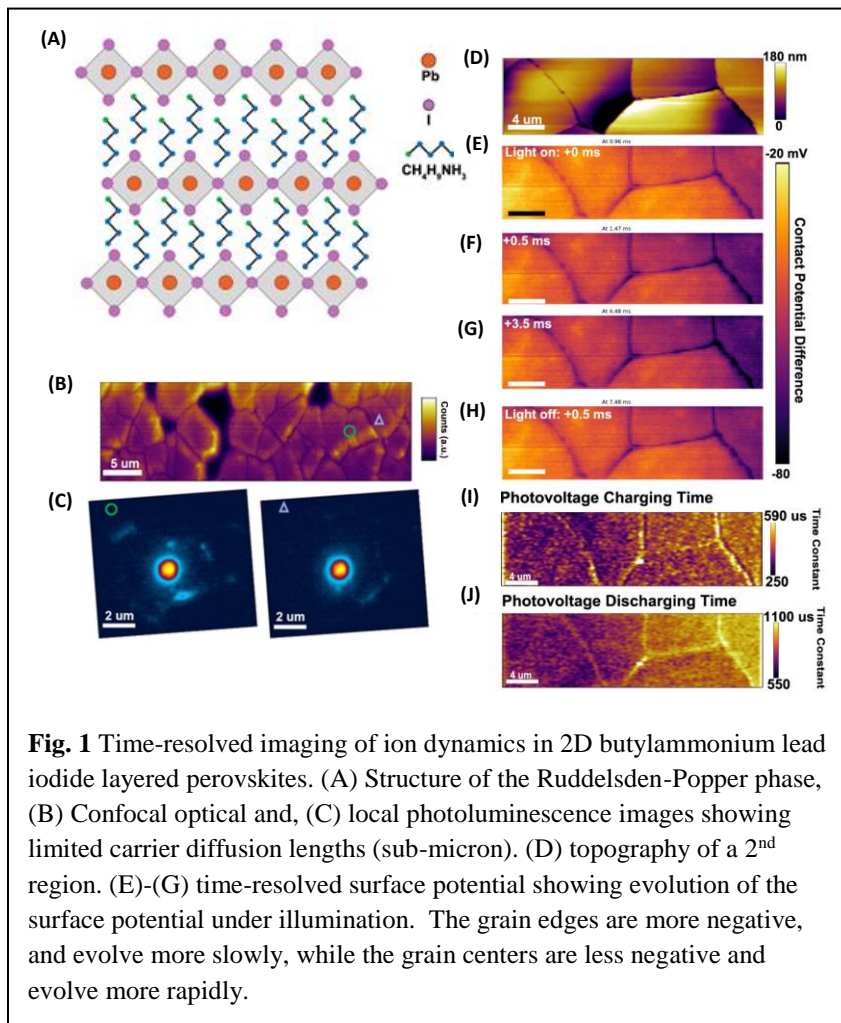
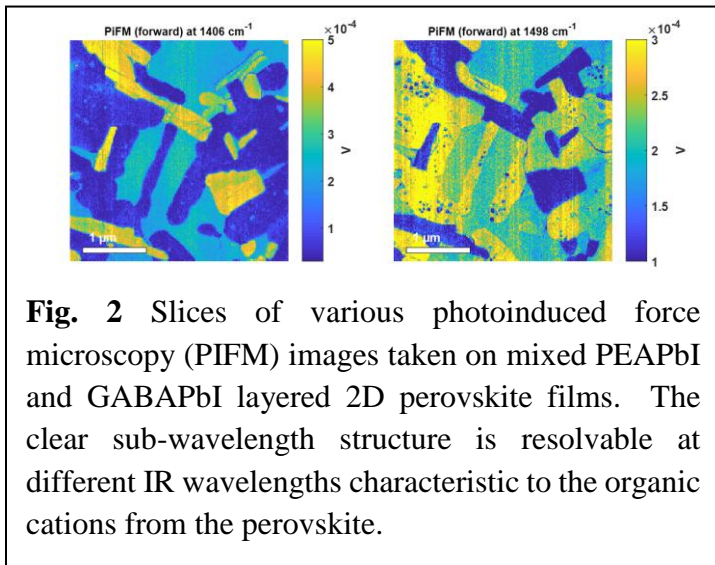


Fig. 1 Time-resolved imaging of ion dynamics in 2D butylammonium lead iodide layered perovskites. (A) Structure of the Ruddelsden-Popper phase, (B) Confocal optical and, (C) local photoluminescence images showing limited carrier diffusion lengths (sub-micron). (D) topography of a 2nd region. (E)-(G) time-resolved surface potential showing evolution of the surface potential under illumination. The grain edges are more negative, and evolve more slowly, while the grain centers are less negative and evolve more rapidly.

excitation maps acquired via photoinduced force microscopy (PiFM) with functional information from other microscopy modes. Briefly, PiFM generates spatial maps with chemical contrast by measuring the time-integrated photoinduced gradient force between a tip and sample due to the interaction between their polarizabilities at wavenumbers corresponding to vibrational modes of different chemical species.¹⁰ PiFM can also generate hyperspectral images containing a photoinduced force infrared spectrum at each pixel, enabling visualization of absorption maps at all wavelengths.

According to the theoretical description of PiFM, the PiFM signal response originates from the real part of the polarizability,¹⁰ though photothermal contributions can arise due to the imaginary part of the polarizability under certain imaging conditions.¹¹ In contrast, the absorption in FTIR spectra is proportional to the imaginary part of the linear susceptibility.¹² Thus, the signal in PiFM and FTIR spectra, at least in current understanding, probe different parts of a material's response to an electromagnetic field. Therefore, it is expected that there will be differences between local PiFM and macroscopic FTIR spectra, and it is therefore not generally possible to use FTIR libraries to determine the expected local PiFM spectra.



In the first year of the project, we are focusing on applying PIFM to model perovskite compounds, studying mixtures of the 2D perovskite phases phenylethylammonium lead iodide (PEAI), and gamma-ammoniumbutyrate lead iodide (GABA), **Fig. 2**. These materials generate clear IR spectral contrast, and we are comparing various methods for blind endmember reconstruction in order to decompose the film into its components.

Future Plans

Much of the work presented here is preliminary, with the current award period beginning July 15, 2018. Our future plans include:

(1) developing robust acquisition and data-science-based analysis protocols for utilizing hyperspectral photoinduced force microscopy (PIFM) data in ways suited to understanding soft halide perovskite semiconductors using the PEAPbI/GABAPbI mixed system, then moving to more applications oriented materials sets such as BAPI, and mixed 2D/3D phases.

(2) understanding how chemical and structural changes underpin functional properties in hybrid perovskites by combining nanoscale chemical imaging, functional imaging, and data informatics on lower dimensional and mixed-cation halide perovskite films by combining multimodal imaging;

(3) developing new time-resolved electrostatic force microscopy methods to probe ion diffusion in 2D perovskite phases across multiple time and length scales, helping understand the origins of the stability and transport differences between these materials while broadly expanding the scope and utility of time-domain scanning-probe microscopy methods.

References

- (1) Kong, J.; Giridharagopal, R.; Harrison, J. S.; Ginger, D. S.: Identifying Nanoscale Structure-Function Relationships Using Multimodal Atomic Force Microscopy, Dimensionality Reduction, and Regression Techniques. *J. Phys. Chem. Lett.* **2018**.
- (2) Birkhold, S. T.; Precht, J. T.; Giridharagopal, R.; Eperon, G. E.; Schmidt-Mende, L.; Ginger, D. S.: Direct Observation and Quantitative Analysis of Mobile Frenkel Defects in Metal Halide Perovskites Using Scanning Kelvin Probe Microscopy. *J. Phys. Chem. C* **2018**.
- (3) Birkhold, S. T.; Precht, J. T.; Liu, H.; Giridharagopal, R.; Eperon, G. E.; Schmidt-Mende, L.; Li, X.; Ginger, D. S.: Interplay of Mobile Ions and Injected Carriers Creates Recombination Centers in Metal Halide Perovskites under Bias. *ACS Energy Lett.* **2018**, 1279-1286.
- (4) Collins, L.; Ahmadi, M.; Wu, T.; Hu, B.; Kalinin, S. V.; Jesse, S.: Breaking the Time Barrier in Kelvin Probe Force Microscopy: Fast Free Force Reconstruction Using the G-Mode Platform. *ACS Nano* **2017**.
- (5) Collins, L.; Belianinov, A.; Somnath, S.; Balke, N.; Kalinin, S. V.; Jesse, S.: Full data acquisition in Kelvin Probe Force Microscopy: Mapping dynamic electric phenomena in real space. *Sci. Rep.* **2016**, 6, 30557.
- (6) Giridharagopal, R.; Rayermann, G. E.; Shao, G.; Moore, D. T.; Reid, O. G.; Tillack, A. F.; Masiello, D. J.; Ginger, D. S.: Submicrosecond time resolution atomic force microscopy for probing nanoscale dynamics. *Nano letters* **2012**, 12, 893-8.
- (7) Karatay, D. U.; Harrison, J. S.; Glaz, M. S.; Giridharagopal, R.; Ginger, D. S.: Fast time-resolved electrostatic force microscopy: Achieving sub-cycle time resolution. *Review of Scientific Instruments* **2016**, 87, 053702.
- (8) Tian, H.; Zhao, L.; Wang, X.; Yeh, Y.-W.; Yao, N.; Rand, B. P.; Ren, T.-L.: Extremely Low Operating Current Resistive Memory Based on Exfoliated 2D Perovskite Single Crystals for Neuromorphic Computing. *ACS Nano* **2017**, 11, 12247-12256.
- (9) deQuilettes, D. W.; Zhang, W.; Burlakov, V. M.; Graham, D. J.; Leijtens, T.; Osherov, A.; Bulović, V.; Snaith, H. J.; Ginger, D. S.; Stranks, S. D.: Photo-induced halide redistribution in organic-inorganic perovskite films. *Nat. Commun.* **2016**, 7, 11683.
- (10) Jahng, J.; Fishman, D. A.; Park, S.; Nowak, D. B.; Morrison, W. A.; Wickramasinghe, H. K.; Potma, E. O.: Linear and Nonlinear Optical Spectroscopy at the Nanoscale with Photoinduced Force Microscopy. *Accounts Chem. Res.* **2015**, 48, 2671-2679.
- (11) Jahng, J.; Park, S.; Morrison, W. A.; Kwon, H.; Nowak, D.; Potma, E. O.; Lee, E. S.: Nanoscale spectroscopic studies of two different physical origins of the tip-enhanced force: dipole and thermal. *arXiv [physics.optics]* **2017**.
- (12) Mukamel, S.: *Principles of Nonlinear Optical Spectroscopy*; Oxford University Press: New York, 2006.

Publications from 2017-2018

1. G. E. Eperon and D.S. Ginger. “B-Site Metal Cation Exchange in Halide Perovskites.” *ACS Energy Letters* **2**, 1190-1196 (2017). DOI: 10.1021/acseenergylett.7b00290.

Acknowledgment: “This Letter is based primarily on work supported by the DOE BES DE-SC0013957.”

2. M. T. Hörantner, T. Leijtens, M. E. Ziffer, G. E. Eperon, M. G. Christoforo, M. D. McGehee, H. J. Snaith. “The Potential of Multijunction Perovskite Solar Cells.” *ACS Energy Letters* **2**, 2506-2513 (2017). DOI: 10.1021/acseenergylett.7b00647.

Acknowledgment: “M.E.Z. acknowledges support from DOE BES DE-SC0013957.”

3. D. Moerman, G. E. Eperon, and D. S. Ginger. “Correlating Photoluminescence Heterogeneity with Local Electronic Properties in Methylammonium Lead Tribromide Perovskite Thin Films.” *Chemistry of Materials* **29**, 5484-5492 (2017). DOI: 10.1021/acs.chemmater.7b00235.

Acknowledgment: “This paper is based on research supported primarily by the Department of Energy BES DESC0013957.”

4. D. W. deQuilettes, S. Jariwala, S. Burke, M. E. Ziffer, J. T.-W. Wang, H. J. Snaith, D. S. Ginger. “Tracking Photoexcited Carriers in Hybrid Perovskite Semiconductors: Trap-Dominated Spatial Heterogeneity and Diffusion.” *ACS Nano*, **11**, 11488–11496 (2017). DOI: 10.1021/acsnano.7b06242

Acknowledgment: “D. deQuilettes and D. Ginger acknowledge DOE (DE-SC0013957) for supporting correlative microscopy work.”

5. S. M. Vorpahl, R. Giridharagopal, G. E. Eperon, I. M. Hermes, S. A. L. Weber, D. S. Ginger. “Orientation of ferroelectric domains and disappearance upon heating methylammonium lead triiodide perovskite from tetragonal to cubic phase.” *ACS Applied Energy Materials* **1**, 1534-153 (2018). DOI: 10.1021/acsaem.7b00330

Acknowledgment: “This Letter is based primarily on work supported by the DOE (DE-SC0013957).”

6. S. T. Birkhold, J. T. Pecht, H. Liu, R. Giridharagopal, G. E. Eperon, L. Schmidt-Mende, X. Li, D. S. Ginger. “Interplay of Mobile Ions and Injected Carriers Creates Recombination Centers in Metal Halide Perovskites under Bias.” *ACS Energy Letters*, **3**, 1279–1286 (2018). DOI: 10.1021/acseenergylett.8b00505

Acknowledgment: “This Letter is based primarily on work supported by the DOE (DE-SC0013957).”

7. W.-A. Quitsch, D. W. deQuilettes, O. Pfingsten, A. Schmitz, S. Ognjanovic, S. Jariwala, S. Koch, M. Winterer, D. S. Ginger, G. Bacher. “The Role of Excitation Energy in Photobrightening and Photodegradation of Halide Perovskite Thin Films” *Journal of Physical Chemistry Letters* **9**, 2062–2069 (2018). DOI: 10.1021/acs.jpcllett.8b00212

Acknowledgment: “D.S.G. acknowledges support for perovskite sample preparation by D.W.D from the DOE BES DE-SC0013957.”

8. S. T. Birkhold, J. T. Precht, R. Giridharagopal, G. E. Eperon, L. Schmidt-Mende, D. S. Ginger. “Direct Observation and Quantitative Analysis of Mobile Frenkel Defects in Metal Halide Perovskites using Scanning Kelvin Probe Microscopy.” *Journal of Physical Chemistry C*, 122, 12633-12639 (2018). DOI: 10.1021/acs.jpcc.8b03255

Acknowledgment: “This manuscript is based primarily on work supported by the DOE (DE-SC0013957).”

9. J. Kong, R. Giridharagopal, J. S. Harrison, D. S. Ginger. “Identifying Nanoscale Structure-Function Relationships Using Multimodal Atomic Force Microscopy, Dimensionality Reduction, and Regression Techniques.” *Journal of Physical Chemistry Letters* **9**, 3307–3314 (2018). DOI: 10.1021/acs.jpcllett.8b01003 In revision.

Acknowledgment: “This paper is primarily based on work supported by the Department of Energy BES under award number DESC0013957.”

10. R. Giridharagopal, J. T. Precht, S. Jariwala, L. Collins, S. Jesse, S. Kalinin, D. S. Ginger. “Time-Resolved Electrical Scanning Probe Microscopy of Layered Perovskites Reveals Spatial Variations in Photoinduced Ion Motion.” In preparation.

Acknowledgment: “We acknowledge support from DOE (DOE-SC0013957).”

Collaborative Research: Atomistic Studies of Individual Impurities and Impurity Complexes in III–V Semiconductors

Jay A. Gupta¹ and Michael E. Flatté²

¹Department of Physics, Ohio State University, Columbus OH 43210, USA

²Department of Physics and Astronomy, University of Iowa, Iowa City, IA 52242, USA

Research Scope

The miniaturization of electronic components such as transistors to nanoscale dimensions is nearing fundamental limits, motivating a rapidly emerging field of ‘solotronics’ in nanoscience [1]. Our joint experimental/theoretical program probes how reduced symmetries influence the properties, especially spin-dependent properties, of individual impurities and complexes in the III-V semiconductors, GaAs and InSb. Atomic-scale scanning tunneling microscopy (STM) and spectroscopy data are compared with atomistic wavefunction and density of state calculations using real-space Green's function methods and density functional theory (DFT) to:

1. Explore the dependence of impurity hybridization on proximity to surface and other defects.
2. Discover novel properties in impurity complexes, built with atomic precision.
3. Develop spin-polarized STM and theoretical methods to directly probe static and dynamic magnetic properties of dopants.

Recent Progress

Giant surface conductance tuning by an individual adatom on InSb(110). We have discovered a field-induced ionization feature that reveals how individual adatoms can be used to tune the tunneling conductance of an InSb(110) surface by two orders of magnitude over relatively large areas (Fig. 1) [2]. When the adatoms are in a positive charge state, adatom induced band bending leads to a high-conductance charge accumulation region that can extend for $\gg 100 \text{ nm}^2$ due to the very low binding energy of native donors in InSb. Under certain tunneling conditions, the adatom

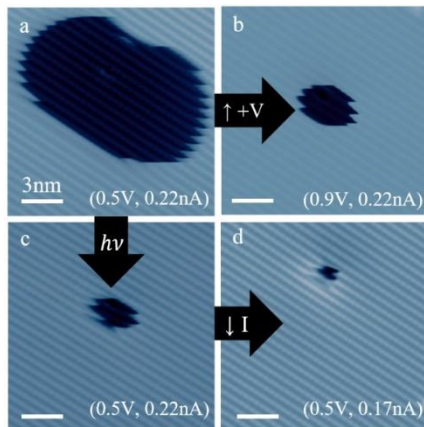


Figure 1. Surface conductance tuning by an individual adatom on InSb(110). (a) Adatom under positive bias conditions images as ‘crater’ with a change in apparent height of 1.5 \AA at the edge of the feature. (+0.5V, 0.22nA). The crater reflects an interplay of tip induced band bending and tip-induced ionization which can be tuned by changing bias voltage (b), adding optical illumination (c) and/or tunneling set current (d).

can be switched to a neutral state when the STM tip approaches, leading to a low-conductance region appearing as a 'crater' feature in topographic STM images. The crater size and depth can be tuned with bias voltage, set current, and optical illumination. We have developed a qualitative model to explain these phenomena, based on competing rates of tunneling into the adatom state from the tip, and drainage of the adatom electron to the bulk through a depletion region. These studies provide insight into how single atoms can be harnessed in future nanoscale opto/electronic devices, and how their metastable configurations can be tuned and manipulated to create atomistic systems far out of equilibrium. In particular, these adatoms provide a natural path to generate localized electronic states interacting with spin-dependent surroundings, including nuclear fields, exchange fields, and spin-orbit fields.

To provide guidance along this path we have developed a theoretical description of transport from a ferromagnetic tip through a localized state that interacts with spin-dependent surroundings [3]. We describe the coherent dynamics of electrical transport through a localized spin-dependent state, such as is associated with a defect spin, at the interface of a ferromagnet and a non-magnetic material during ferromagnetic resonance. As the ferromagnet's moment precesses, charge carriers are dynamically spin-filtered by the localized state, leading to a dynamic spin accumulation on the defect. We thus identify a new form of current-detected spin resonance that reveals the local magnetic environment of a carrier spin located at a defect, and thus potentially the defect's identity.

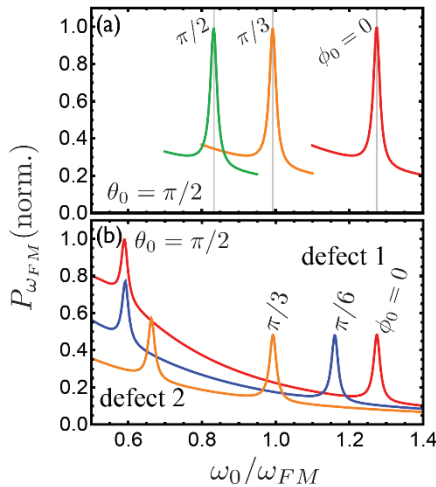


Figure 2. Plots showing the integrated current at ω_{FM} when the applied field, ω_0 , is swept. Resonances occur when $\omega_d = |\omega_{0+} \omega_l| = \omega_{FM}$. Here $\omega_l = (-0.3, 0.1, 0.2) \omega_{FM}$. (b) Two resonance features appear when two defects are probed. Each colored curve corresponds to an independent sweep of the magnetic field in the x-y plane at an angle ϕ_0 . For the two defects, $\omega_{l,1} = (-0.3, 0.1, 0.2) \omega_{FM}$ and $\omega_{l,2} = (0.4, 0.1, -0.1) \omega_{FM}$. Curves in (a) and (b) are normalized to the highest peak and labeled by the applied field's azimuthal angle ϕ_0 .

Tunable coupling of Mn-Mn dimers. Mn dimers were formed with varying spacing and orientation with respect to the surface unit cell, allowing us to confirm the transition between ferromagnetic and antiferromagnetic coupling first predicted by the co-PI (Fig.4). By developing a tip-approach method, we have discovered a richer spectrum of states in exchange-coupled Mn dimers than reported previously. For example, we found six states for the ferromagnetic dimer at nearest neighbor sites. These states exhibit bonding/anti-bonding character resembling earlier predictions by the co-PI, but with enhanced energy splittings due to the surface. STM atomic

manipulation was then used to position charged adatoms nearby the dimer to tune the exchange coupling. We find a systematic reduction in splitting with distance, revealing that Coulomb repulsion with the charged adatom influences the wavefunction overlap of the Mn-bound holes.

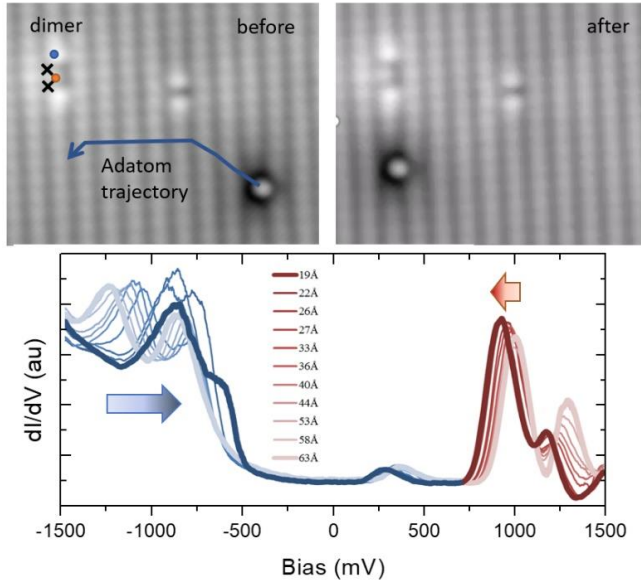


Figure 3. Tuning Mn-Mn ferromagnetic exchange in GaAs(110). (top) STM images of a Mn dimer and monomer before and after atomic manipulation of a charged Ga adatom. ‘x’ marks the Mn atomic positions, while blue/red circles indicate tip positions used to probe anti/bonding states respectively. (bottom) series of dI/dV spectra showing evolution of dimer states with proximity to Ga_{ad}^+ . Coulomb repulsion with the adatom influences the wavefunction overlap of the holes bound to the Mn.

We have theoretically explored the effect of a local exchange-coupled spin on the transport through a single magnetic dopant (Fig.4) [4]. To evaluate the I-V curves we calculated the spin dynamics using the stochastic Liouville equation in the presence of spin-dependent transport from the ferromagnetic tip and when a magnetic field is applied. We find new peaks in the current as a function of magnetic field when there is exchange interaction, due to a resonance between the singlet-triplet precession due to exchange coupling and the applied magnetic field's precession frequency. The exchange coupling can be detected spectroscopically, but only if the size is sufficiently large. This theoretical advance allows us to plan to accurately measure exchange interactions that are micro-eV in size due to their coherent effects on the coupled spin system.

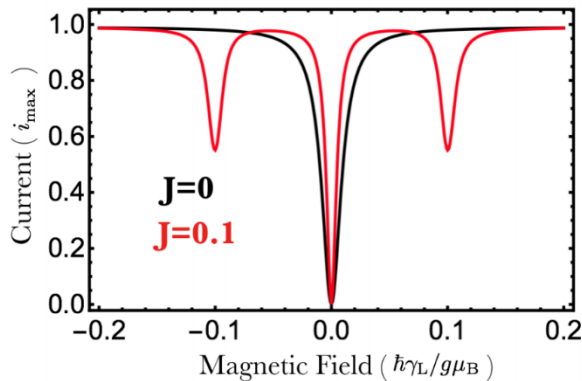


Figure 4. The total current through a spin-polarized tip that is transported through a localized spin state that is interacting via an exchange interaction with a neighbor. The strength of the interaction is shown: 0 for the black curve, and 0.1 in units of the hopping rate (thus $\sim \mu\text{eV}$) for the red curve. When the magnetic field is of the order of several hundred Gauss a second peak is shown in the current due to the beating of the exchange-induced precession with the spin precession from the magnetic field.

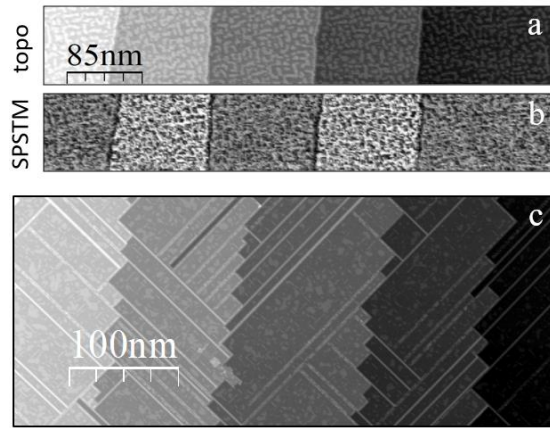


Figure 5. SPSTM imaging of Cr(001). (a) STM topograph of atomic terraces. (b) corresponding dI/dV map, showing alternating dark/bright contrast due to the SPSTM signal. (c) STM image of a different region of the sample, showing atomically-thin Cr nanowires originating from Cr step edges.

Spin polarized STM of Cr(001). To eliminate stray fields from ferromagnetic tips, we have developed etching recipes to shape bulk antiferromagnetic Cr tips for SPSTM studies. To characterize the spin properties of these tips, our initial efforts have focused on the Cr(001) surface. We developed a flash-annealing recipe to minimize the influence of surface adsorbates (e.g., C, O) that are known to produce reconstructions on Cr(001). While the topography channel is dominated by steps associated with the crystal (Fig.5a), the dI/dV channel reveals the alternating bright and dark contrast expected for SPSTM imaging of this antiferromagnetic surface (Fig.5b). Moreover, our flash annealing procedure produced regions of the Cr(001) surface where Cr migration from step edges produces novel nanowire structures with few-atom width and ~ 10nm in length (Fig.5c). These

regions also show periodic contrast that may reflect a rotation of the near-surface Cr spin density wave, suggesting that the near-surface antiferromagnetic ordering can be influenced by surface reconstructions.

Future Plans - We will focus on preparing heterodimers of Mn-X (with X=Fe, Co, Ni, Er) in GaAs(110) to study and theoretically calculate the magnetic states resulting from anisotropic exchange interactions. Tunneling spectroscopy will be compared with nonmagnetic PtIr tips and spin-sensitive Cr tips, along with theoretical calculations, to reveal differences due to ferro- and anti-ferromagnetic interactions in the dimers. We will also extend these methods to study magnetic dopants in InSb(110) to help clarify magnetic ordering in this narrow-gap III-V material.

References

1. Koenraad, P. M. and Flatté, M. E. “**Single Dopants in Semiconductors.**” *Nature materials* 10, no. 2 (2011): 91–100.
2. Mueller, S. M., Tjung, S. J., Repicky, J. J., Keast, A., Lang, E., Bergmann, F., Werner, K., Chowdhury, E., and Gupta, J. A. “**Tunable Control over InSb(110) Surface Conductance Utilizing Charged Defects**” (in preparation)
3. Harmon, N. J. and Flatté, M. E. “**Theory of Spin-Coherent Electrical Transport through a Defect Spin State in a Metal/Insulator/Ferromagnet Tunnel Junction Undergoing Ferromagnetic Resonance**” *Physical Review B* 98, no. 3 (2018): 035412.
4. McMillan, S. R., Harmon, N. J., and Flatte, M. E. (in preparation)

Publications

Harmon, N. J. and Flatté, M. E. “**Theory of Spin-Coherent Electrical Transport through a Defect Spin State in a Metal/Insulator/Ferromagnet Tunnel Junction Undergoing Ferromagnetic Resonance**” *Physical Review B* 98, no. 3 (2018): 035412.

Understanding and Control of Spin Currents at Magnetic Interfaces

P. Chris Hammel, Department of Physics, Ohio State University

Research Scope

The generation, control and detection of pure spin currents is a topic of intense study as a consequence of its fundamental richness and the range of technological opportunities it presents. Precessing magnetization emits spin currents (a process known as spin pumping); conversely, applied spin currents can reduce magnetization damping, even to the point that they drive magnetization precession and inversion. These phenomena have applications to high frequency signal generation and detection. Spin pumped currents flow from a region of excited magnetization into a neighboring quiescent material while an imposed spin current exerts an antidamping torque on a volume of dynamical magnetization. The study of these phenomena and the efficiency of the current transmission are highly sensitive to properties of the materials involved, to the spin wave spectrum of the dynamic region and the interface separating the two. Most studies involve spin currents transmitted across a material interface separating a ferromagnet (FM) and a normal material (NM), thus making the interfacial spin conductance sensitive to complex and often ill-characterized interface features. Our studies under recent DOE funding [1-9] have focused on two aspects of this problem i) discovering and understanding new materials and phenomena exhibiting favorable characteristics, and ii) developing new tools and approaches to studying this important problem. A particular focus of our work is the study of spin transport across magnetic-field defined interfaces thus avoiding material interfaces that can harbor defects and be difficult to characterize. We accomplish this by locally exciting magnetostatic modes in an extended, pristine FM, and measuring the spin currents out of these localized modes [10, 11], or by applying spin torque across the field-defined interface [3] (see below).

Recent Progress

Magneto-electronic devices operating on pure spin currents without accompanying charge current promise new functionalities and significant energy savings. We have explored promising new materials, improved understanding of currently heavily used materials and advanced the use of localized spin wave modes that enable local magnetization excitation either by imposed spin currents or by emission of spin currents by precessing magnetization into neighboring material.

Multi-Wave Vector Spin Wave Imaging of Magnetic Boundaries

Ferromagnetic resonance imaging by means of scanned, field-localized spin wave modes has demonstrated the ability to spectroscopically [11] image interfaces and to locally probe spin

dynamics and spin transport phenomena [10]. We find that employing low damping ferromagnets such as $\text{Y}_2\text{Fe}_5\text{O}_{12}$ (YIG) enable the confinement of several (so far, up to $n = 8$) spin wave modes. We see that the interaction of the various modes with the interface can be detected with spectroscopic precision, see Fig. 1. This has the important consequence that the higher modes have correspondingly larger wave vectors k , suggesting substantially improved spatial resolution $\Delta x \sim 1/k \sim r_{mode}/n$ where r_{mode} is the mode radius. The ability to simultaneously obtain coherent information from several scattered spin waves promises access to enhanced information regarding properties of interfaces in spintronic devices.

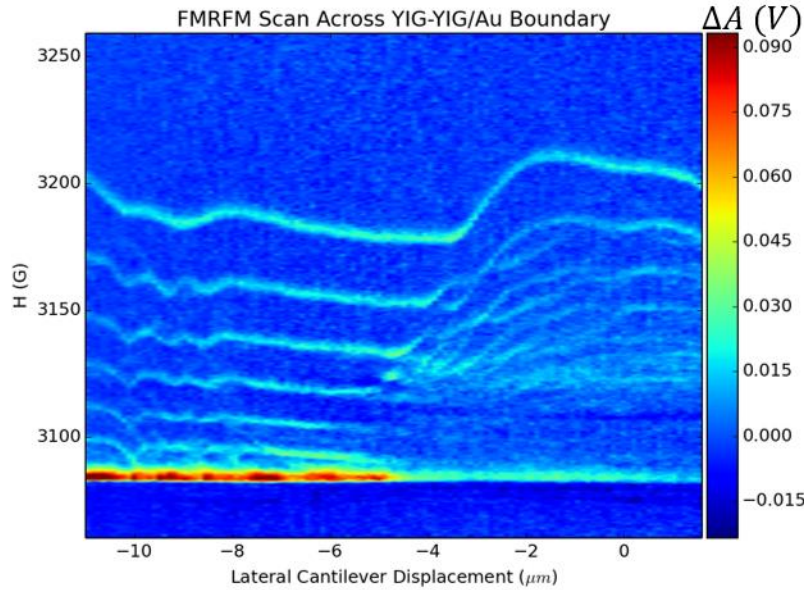


Figure 1. Evolution of scanned FMR modes with position as localized spin wave modes are scanned across an internal field interface arising from a 5 nm Au overlayer on YIG. The interface is located at $-2.5 \mu\text{m}$. Modes $n = 1$ (highest resonance field) through 6 are evident. Complex behavior is associated with the scattering of the various modes off the interface as they are scanned. The higher order modes have larger wavevectors potentially enabling higher spatial resolution.

Metallic Ferromagnetic Films with Magnetic Damping Under 1.4×10^{-3}

Low-damping magnetic materials are desirable for spin transport applications because of their low energy loss and high sensitivity. While the Gilbert damping constant can reach 10^{-4} to 10^{-5} in some insulating ferromagnets, metallic ferromagnets generally have larger damping due to magnon scattering by conduction electrons. However, low-damping metallic ferromagnets are desirable for charge-based spintronic devices. We find that metallic $\text{Co}_{25}\text{Fe}_{75}$ epitaxial films exhibit a damping constant less than 1.4×10^{-3} —comparable to values found for some high quality YIG films.

We measured $\text{Co}_{25}\text{Fe}_{75}$ epitaxial films grown using off-axis sputtering with the goal of further reducing the magnetic damping of this promising metallic FM towards an unprecedented level [5]. X-ray diffraction (XRD) and scanning transmission electron microscopy (STEM) verify that these films are single crystal with high crystalline quality. Variable frequency ferromagnetic resonance (FMR) measurements confirm that these films exhibit significantly reduced Gilbert damping—less than 1.4×10^{-3} —in contrast to polycrystalline films.

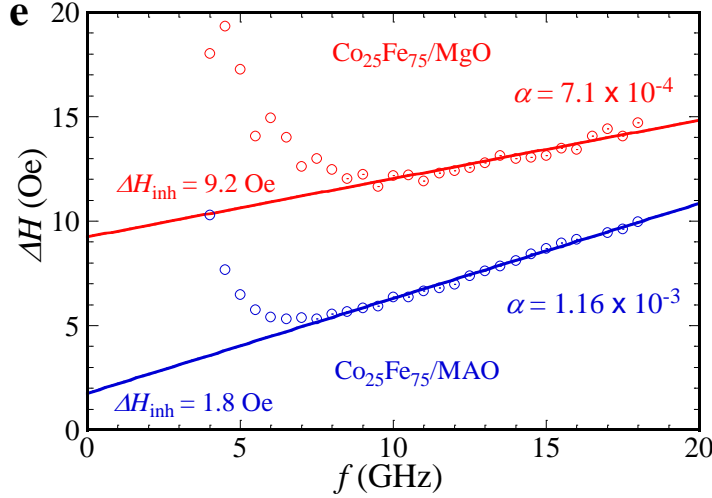


Figure 2. Frequency dependencies of the FMR linewidths for the $\text{Co}_{25}\text{Fe}_{75}$ films on MgO (red) and MAO (blue), where the behavior below 8 and 7 GHz, respectively, reflects incomplete saturation of the films leading to increases in the inhomogeneous broadening. The solid lines are linear fits to the frequency range above 8 (7) GHz for the film on MgO (MAO), from which the Gilbert damping and inhomogeneous broadening are extracted.

The measured Gilbert damping constant—less than 1×10^{-3} —is extremely low for metallic FMs and, remarkably, is comparable to those reported for YIG films. The lowest α (7.1×10^{-4}) for our epitaxial $\text{Co}_{25}\text{Fe}_{75}$ films is considerably lower than the values reported for polycrystalline $\text{Co}_{25}\text{Fe}_{75}$ films[12] (2.1×10^{-3}) and epitaxial Fe films (1.9×10^{-3}).[13] Our observation of extremely low magnetic damping in $\text{Co}_{25}\text{Fe}_{75}$ epitaxial thin films with excellent crystalline quality reveals the importance of crystalline quality in minimizing damping. This is the first direct measurement of a Gilbert damping constant in the 10^{-4} regime for metallic FM films. This record low damping for metallic ferromagnets offers new opportunities for charge-based applications such as spin-transfer-torque induced switching and magnetic oscillations.

Temperature Dependence of Magnetization Damping in YIG

We observe that even apparently high-quality YIG films, which possess small FMR linewidths at room temperature, can have linewidths that increase dramatically with decreasing temperature [6]. The 15 nm YIG film studied exhibited a linewidth that increased by a factor of 28 as the temperature was lowered from room temperature to 25 K. The linewidth of this thin YIG film also shows an increasingly nonlinear frequency dependence as the temperature is lowered. These strong temperature dependencies cannot be explained by two-magnon scattering from the YIG interfaces, the mechanism that dominates the linewidth at room-temperature. Instead, the increased linewidth at low temperature is due to magnetic damping associated with impurity mechanisms. Based on measurements of the temperature and frequency dependence of the expect, we point out that the increased low-temperature linewidth can be explained by slowly relaxing impurities, perhaps rare earth or Fe^{2+} impurities introduced during growth. High-purity starting materials and careful optimization of growth protocols to avoid non-stoichiometries should therefore be employed for making low-temperature thin-film YIG devices.

Engineering the Spectrum of Dipole Field-Localized Spin Wave Modes to Enable Spin-Torque Damping Control

We used tunable field-localized modes to define the magnon spectrum of a ferromagnetic element, thus enabling spin-Hall torque induced damping control [3]. We demonstrated that field localization generates a discrete spin wave mode spectrum observable as a series of well-resolved localized modes in the presence of imposed spin currents arising from the spin-Hall effect (SHE) in a permalloy/platinum (Py/Pt) microstrip. The linewidth of the modes was reduced through the applied spin currents. This damping control in micromagnetically engineered spectrum demonstrates that localized modes can be controlled as efficiently as the uniform mode, an important step toward continuously tunable SHE driven auto-oscillators.

Future Plans

Spatially resolved tools enabling study of spin dynamics at interfaces between dynamic magnetization and neighboring regions across which spin currents flow will guide optimization of materials and methods of creating interfaces optimized for the control and efficient transmission of itinerant spin waves. We will refine our spectroscopic and dynamical imaging of interfaces using scanned probe FMR imaging [10, 11]. In particular, high quality materials like YIG and CoFe provide low damping and narrow lines thus allowing confinement of multiple modes by the localized field. This will, in principle, enhance both the information content in scanned FMR mode spectroscopy and relaxometry and should enable improved spatial resolution. We will be further enhancing this imaging modality and applying it to a variety of internal field interfaces. We will further quantify the spatial characteristics of transmitted spin currents by means of spatially resolved imaging relative to engineered spin sinks and structures which alter the characteristics of transmitted spin waves.

References

10. R. Adur, C.H. Du, H.L. Wang, S.A. Manuilov, V.P. Bhallamudi, C. Zhang, D.V. Pelekhov, F.Y. Yang, and P.C. Hammel, *Damping of Confined Modes in a Ferromagnetic Thin Insulating Film: Angular Momentum Transfer across a Nanoscale Field-Defined Interface*. Physical Review Letters, **113**(17) (2014)
11. I. Lee, Y. Obukhov, G. Xiang, A. Hauser, F.Y. Yang, P. Banerjee, D.V. Pelekhov, and P.C. Hammel, *Nanoscale scanning probe ferromagnetic resonance imaging using localized modes*. Nature, **466**(7308): p. 845-848 (2010)
12. M.A.W. Schoen, D. Thonig, M.L. Schneider, T.J. Silva, H.T. Nembach, O. Eriksson, O. Karis, and J.M. Shaw, *Ultra-low magnetic damping of a metallic ferromagnet*. Nature Phys., **12**(9): p. 839 (2016)
13. C. Scheck, L. Cheng, I. Barsukov, Z. Frait, and W.E. Bailey, *Low relaxation rate in epitaxial vanadium-doped ultrathin iron films*. Phys. Rev. Lett., **98**(11): p. 117601 (2007)

Publications under DOE BES funding (9)

1. F.Y. Yang and P.C. Hammel, *FMR-driven spin pumping in $Y_2Fe_5O_{12}$ -based structures*. Journal of Physics D-Applied Physics, **51**(25) (2018)
2. W.T. Ruane, S.P. White, J.T. Brangham, K.Y. Meng, D.V. Pelekhov, F.Y. Yang, and P.C. Hammel, *Controlling and patterning the effective magnetization in $Y_2Fe_5O_{12}$ thin films using ion irradiation*. AIP Advances, **8**(5) (2018)
3. C. Zhang, Y. Pu, S.A. Manuilov, S.P. White, M.R. Page, E.C. Blomberg, D.V. Pelekhov, and P.C. Hammel, *Engineering the Spectrum of Dipole Field-Localized Spin-Wave Modes to Enable Spin-Torque Antidamping*. Physical Review Applied, **7**(5) (2017)
4. H.L. Wang, C.H. Du, P.C. Hammel, and F.Y. Yang, *Comparative determination of $Y_2Fe_5O_{12}/Pt$ interfacial spin mixing conductance by spin-Hall magnetoresistance and spin pumping*. Applied Physics Letters, **110**(6) (2017)
5. A.J. Lee, J.T. Brangham, Y. Cheng, S.P. White, W.T. Ruane, B.D. Esser, D.W. McComb, P.C. Hammel, and F.Y. Yang, *Metallic ferromagnetic films with magnetic damping under 1.4×10^{-3}* . Nature Communications, **8** (2017)
6. C.L. Jermain, S.V. Aradhya, N.D. Reynolds, R.A. Buhrman, J.T. Brangham, M.R. Page, P.C. Hammel, F.Y. Yang, and D.C. Ralph, *Increased low-temperature damping in yttrium iron garnet thin films*. Physical Review B, **95**(17) (2017)
7. Y.S. Ou, Y.H. Chia, N.J. Harmon, P. Odenthal, M. Sheffield, M. Chilcote, R.K. Kawakami, M.E. Flatte, and E. Johnston-Halperin, *Exchange-Driven Spin Relaxation in Ferromagnet-Oxide-Semiconductor Heterostructures*. Physical Review Letters, **116**(10) (2016)
8. J.C. Gallagher, A.S. Yang, J.T. Brangham, B.D. Esser, S.P. White, M.R. Page, K.Y. Meng, S.S. Yu, R. Adur, W. Ruane, S.R. Dunsiger, D.W. McComb, F.Y. Yang, and P.C. Hammel, *Exceptionally high magnetization of stoichiometric $Y_2Fe_5O_{12}$ epitaxial films grown on $Gd_3Ga_5O_{12}$* . Applied Physics Letters, **109**(7) (2016)
9. J.T. Brangham, K.Y. Meng, A.S. Yang, J.C. Gallagher, B.D. Esser, S.P. White, S.S. Yu, D.W. McComb, P.C. Hammel, and F.Y. Yang, *Thickness dependence of spin Hall angle of Au grown on $Y_2Fe_5O_{12}$ epitaxial films*. Physical Review B, **94**(5) (2016)

Probing Emergent Phenomena in Ferroelectric/MoS₂ Composite Structures

Xia Hong, Department of Physics and Astronomy, University of Nebraska-Lincoln

Research Scope

This research explores a range of novel electronic and optical phenomena emerged in the ferroelectric/van der Waals material composite structures, leveraging the synergy between the constituent materials coupled by the ferroelectric polarization and underlying symmetry. The current research projects include: 1) exploiting nanoscale domain patterning in a ferroelectric top-gate to engineer the contact work function in MoS₂, which can tune the device between a hetero-junction and a transistor state; 2) realizing steep slope switching in MoS₂ transistors through the polarization rotation in polycrystalline ferroelectric gates, and 3) developing effective optical techniques to probe the ferroelectric domain wall (DW) and its interaction with MoS₂. Our studies can enhance the fundamental understanding of the interfacial coupling mechanisms between ferroelectrics and MoS₂, as well as facilitating their functional design for novel nanoelectronic and optoelectronic applications.

Recent Progress

1. Ferroelectric-Controlled Contact Engineering in Monolayer MoS₂

The ferroelectric field effect, when combined with nanoscale domain patterning, is a powerful tool to induce local potential tuning in a neighboring two dimensional (2D) channel. By exploiting this technique to engineer the contact potential, we have achieved programmable transistor and hetero-junction states in monolayer (ML) MoS₂ [1]. As shown in Fig. 1(a) inset, we fabricated two-point MoS₂ field effect transistor (FET) devices top-gated by ferroelectric copolymer, poly(vinylidene fluoride-trifluoroethylene) [P(VDF-TrFE)], thin films. By applying a bias voltage to a scanning AFM tip exceeding the coercive voltage, we have imposed different domain configurations onto the ferroelectric polymer at the contact area. Poling the out-of-plane polarization in the P_{up} (P_{down}) state lowers (raises) the Fermi

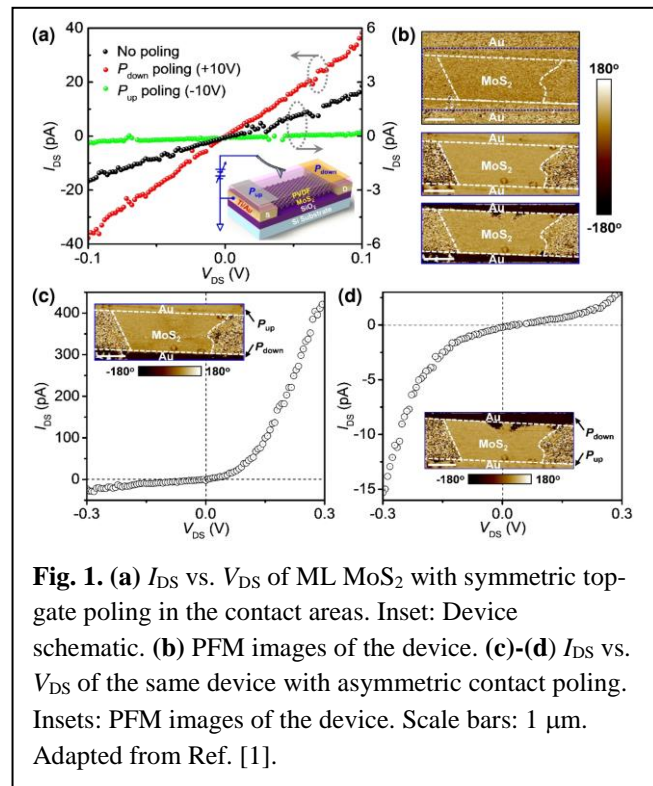


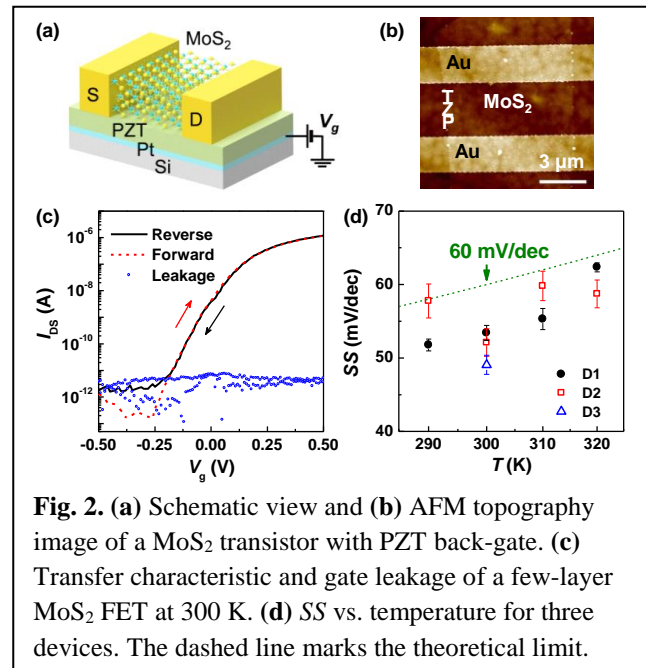
Fig. 1. (a) I_{DS} vs. V_{DS} of ML MoS₂ with symmetric top-gate poling in the contact areas. Inset: Device schematic. (b) PFM images of the device. (c)-(d) I_{DS} vs. V_{DS} of the same device with asymmetric contact poling. Insets: PFM images of the device. Scale bars: 1 μ m. Adapted from Ref. [1].

level of MoS₂, which in turn modulates the contact potential between MoS₂ and the metal contact (Ti/Au). Figure 1(a) shows the source-drain current-voltage (I_{DS} - V_{DS}) characteristics of the device with symmetric contact domains in the up-poled, P_{down} , and P_{up} states, with the corresponding piezoresponse force microscopy images shown in Fig. 1(b). We have achieved nonvolatile modulation of the channel current by a factor of more than 150 between the P_{down} and P_{up} states of contact doping, while the ferroelectric polymer above MoS₂ channel remains the same polarization. This result clearly highlights the critical role of contact electrodes in determining the electronic properties of MoS₂.

In all three symmetric contact domain configurations, we observed linear, ohmic I_{DS} - V_{DS} characteristics in the device. In sharp contrast, asymmetric contact doping can lead to programmable junction states in MoS₂. As shown in Fig. 1(c), when the polymer layer above the upper (lower) electrode is poled to the P_{down} (P_{up}) state, the device exhibits a rectified I_{DS} - V_{DS} relation with a forward to reverse current ratio exceeding 20 at ± 0.3 V. Fitting the diode-like I_{DS} - V_{DS} relationship to the thermionic emission model yields a room temperature Schottky barrier height ϕ_B^{eff} of about 530 meV, while the polarity of current rectification can be reversed by reversing the polarization at both contact areas [Fig. 1(d)]. This study points to a well-controlled, reconfigurable strategy to control the contact potential in layered 2D semiconductors, as well as modulating the conduction characteristic for multifunctional device applications.

2. Steep-Slope Switching in MoS₂ Transistors Mediated by Polarization Rotation

For conventional semiconductor transistors, the subthreshold swing (SS), defined as the gate voltage V_g required to change the channel current I_{DS} by a fact of 10, is determined by the Boltzmann statistics, which imposes a fundamental limit of 60 mV/dec at room temperature. As reducing the SS in FETs can lead to lower turn-on voltage and operation power, it is of high technological interest to develop steep-slope transistors. It has been proposed that by replacing the gate dielectric with a ferroelectric layer approaching ferroelectric instability, it is possible to achieve a positive internal feedback to the V_g -induced change in the channel potential [2], which in turn leads to steep-slope switching with the SS below the Boltzmann limit. While previous studies of steep-slope transistors focus on working with ultrathin ferroelectric gates approaching the finite size limit [3], an alternative proposal is to work with films close to the polarization rotational instability [4]. We



have explored the feasibility of the second scenario by exploiting polarization switching in a polycrystalline $\text{Pb}(\text{Zr},\text{Ti})\text{O}_3$ (PZT) back-gate [Fig. 2(a)]. We fabricated few-layer MoS_2 flake FETs on 300 nm polycrystalline PZT films [Fig. 2(b)]. The PZT films possess high dielectric constant of about 650 and exhibit nearly hysteresis-free dielectric response when the applied voltage is below ± 0.5 V. The high- κ nature of PZT leads to highly efficient modulation of the MoS_2 channel, with 10^7 current on-off ratio achieved within a small gate voltage V_g range of ± 0.25 V [Fig. 2(c)]. The transfer characteristics of the MoS_2 FETs show ultra-low SS of about 50 mV/dec at room temperature, transcending the theoretical limit imposed by the Boltzmann statistics [Fig. 2(d)]. Next, we will examine the effect of the MoS_2 channel thickness on the switching characteristics, explore the feasibility of working with a relaxor type ferroelectric-gate [5], and seek theoretical insights into the microscopic origin of the polarization-enabled steep-slope switching.

3. Probing Ferroelectric Domain Wall via Second Harmonic Generation

In the ferroelectric/ MoS_2 composite structure, the presence of a ferroelectric DW can imprint a homo/hetero-junction state in the MoS_2 channel underneath, which can be utilized to construct optoelectronic devices. Ferroelectric DW itself, as a prototypical topological defect, also exhibits interesting optical properties. For example, the distinct symmetry breaking between the Néel and Bloch types of DWs [Fig. 3(a)] can be detected by the second harmonic generation (SHG) signals [6]. As shown in Fig. 3(b), we have created a series of square domains on a ferroelectric $\text{Pb}(\text{Zr},\text{Ti})\text{O}_3$ (PZT) thin film. While the P_{up} and P_{down} domains do not show pronounced SHG response, high intensity SHG signals have been observed at the domain walls due to the breaking of in-plane inversion symmetry [Fig. 3(c)]. The SHG signal is always linearly polarized along the direction perpendicular to the DW [Fig. 3(d-e)], revealing Néel type characteristics. Next we will investigate the photo-response of a junction state in an interfacing ML MoS_2 , probing how the symmetry of the domain wall is coupled with the non-centrosymmetric 2D semiconducting channel.

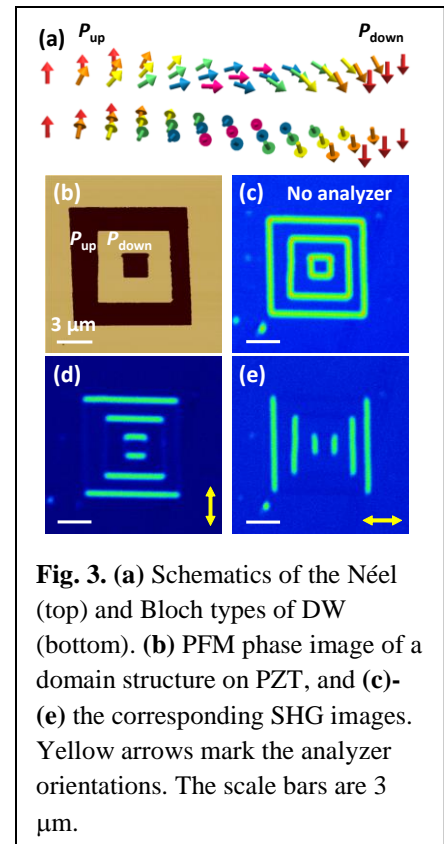


Fig. 3. (a) Schematics of the Néel (top) and Bloch types of DW (bottom). (b) PFM phase image of a domain structure on PZT, and (c)-(e) the corresponding SHG images. Yellow arrows mark the analyzer orientations. The scale bars are 3 μm .

Future Plans

Based on the current progress, we plan to carry out research in the following directions.

1) Use the MoS_2 homo-junction devices as a model system to gain fundamental understanding of the interactions between the ferroelectric and 2D layers, including various

mobility limiting mechanisms in the hybrid systems, and the effect of the 2D material on ferroelectric polarization asymmetry, domain instability and switching dynamics, etc.

2) Use the gained knowledge to create nano-constrictions in 2D transition metal dichalcogenides and graphene, and examine the emerging electronic and optical phenomena at the ferroelectric DW and 2D junction states.

3) Explore the size effect of the constituent layers on the switching characteristics of the ferroelectric-gated MoS₂ FETs. Compare the results with theoretical modeling to identify the possible contributions of the finite size effect, polarization rotation, depolarization field, and interfacial screening to the steep-slope switching behavior.

References

- [1] D. W. Li, Z. Y. Xiao, S. Mu, F. Wang, Y. Liu, J. F. Song, X. Huang, L. J. Jiang, J. Xiao, L. Liu, S. Ducharme, B. Cui, X. Hong, L. Jiang, J. F. Silvain, and Y. F. Lu, A Facile Space-Confined Solid-Phase Sulfurization Strategy for Growth of High-Quality Ultrathin Molybdenum Disulfide Single Crystals, *Nano Letters* **18**, 2021 (2018).
- [2] A. M. Bratkovsky, and A. P. Levanyuk, Depolarizing field and "real" hysteresis loops in nanometer-scale ferroelectric films, *Applied Physics Letters* **89**, 253108 (2006).
- [3] M. W. Si, C. J. Su, C. S. Jiang, N. J. Conrad, H. Zhou, K. D. Maize, G. Qiu, C. T. Wu, A. Shakouri, M. A. Alam, and P. D. Ye, Steep-slope hysteresis-free negative capacitance MoS₂ transistors, *Nature Nanotechnology* **13**, 24 (2018).
- [4] Y. B. Qi, and A. M. Rappe, Designing Ferroelectric Field-Effect Transistors Based on the Polarization-Rotation Effect for Low Operating Voltage and Fast Switching, *Physical Review Applied* **4** (2015).
- [5] R. M. Moghadam, Z. Y. Xiao, K. Ahmadi-Majlan, E. D. Grimley, M. Bowden, P. V. Ong, S. A. Chambers, J. M. Lebeau, X. Hong, P. V. Sushko, and J. H. Ngai, An Ultrathin Single Crystalline Relaxor Ferroelectric Integrated on a High Mobility Semiconductor, *Nano Letters* **17**, 6248 (2017).
- [6] S. Cherifi-Hertel, H. Bulou, R. Hertel, G. Taupier, K. D. Dorkenoo, C. Andreas, J. Guyonnet, I. Gaponenko, K. Gallo, and P. Paruch, Non-Ising and chiral ferroelectric domain walls revealed by nonlinear optical microscopy, *Nature Communications* **8**, 15768 (2017).

Publications

1. Dawei Li, Zhiyong Xiao, Sai Mu, Fei Wang, Ying Liu, Jingfeng Song, Xi Huang, Lijia Jiang, Jun Xiao, Lei Liu, Stephen Ducharme, Bai Cui, Xia Hong, Lan Jiang, Jean-Francois Silvain, Yongfeng Lu, “A Facile Space-Confined Solid-Phase Sulfurization Strategy for Growth of High-Quality Ultrathin Molybdenum Disulfide Single Crystals”, *Nano Letters* **18**, 2021 (2018).
2. Peter A. Dowben, Christian Binek, Kai Zhang, Lu Wang, Wai-Ning Mei, J. P. Bird, U. Singisetti, Xia Hong, Kang L. Wang, and Dmitri Nikonov, “Towards a Strong Spin-Orbit Coupling Magnetoelectric Transistor”, *IEEE Journal of Exploratory Solid-State Computational Devices and Circuits* **4**, 1-9 (2018).
3. Shi Cao, Zhiyong Xiao, Chun-Pui Kwan, Kai Zhang, Jonathan P. Bird, Lu Wang, W.N. Mei, Xia Hong, Peter A. Dowben, “Moving towards the Magnetoelectric Graphene Transistor”, *Applied Physics Letters* **111**, 182402 (2017).
4. Reza M Moghadam, Zhiyong Xiao, Kamyar Ahmadi-Majlan, Everett D Grimley, Mark Bowden, Phuong-Vu Ong, Scott A Chambers, James M Lebeau, Xia Hong, Peter V Sushko, Joseph H Ngai, “An Ultrathin Single Crystalline Relaxor Ferroelectric Integrated on a High Mobility Semiconductor”, *Nano Letters* **17**, 6248-6257 (2017).
5. Xuegang Chen, Xin Zhang, Mark A. Koten, Hanghui Chen, Zhiyong Xiao, Le Zhang, Jeffrey E. Shield, Peter A. Dowben and Xia Hong, “Interfacial Charge Engineering in Ferroelectric-Controlled Mott Transistors”, *Advanced Materials* **29**, 1701385 (2017).
6. D.W. Li,• Q.M. Zou,• H. Rabiee Golgir, K. Keramatnejad, X. Huang, J.F. Song, Z.Y. Xiao, X. Hong, L. Jiang, J.F. Silvain, and Y.F. Lu, “Controlled Defect Creation and Removal in Graphene and MoS₂ Monolayers”, *Nanoscale* **9**, 8997 (2017).
7. Dawei Li, Zhiyong Xiao, Hossein Rabiee Golgir, Li Jia Jiang, Vijay Raj Singh, Kamran Keramatnejad, Kevin E. Smith, Xia Hong, Lan Jiang, Jean-Francois Silvain, and Yongfeng Lu, “Large-Area 2D/3D MoS₂–MoO₂ Heterostructures with Thermally Stable Exciton and Intriguing Electrical Transport Behaviors”, *Advanced Electronic Materials* **3**, 1600335 (2017).
8. Zhiyong Xiao, Jingfeng Song, David K. Ferry, Stephen Ducharme, Xia Hong, “Ferroelectric Domain Patterning Controlled Schottky Junction State in Monolayer MoS₂”, *Physical Review Letters* **118**, 236801 (2017).

Superconductor/Ferromagnet Heterostructures

Maria Iavarone, Physics Department, Temple University, Philadelphia PA 19122

e-mail: iavarone@temple.edu

Research Scope

This program is aimed at understanding the fundamental features that underlie the behavior of mesoscopic superconductors and hybrid ferromagnet/superconductor heterostructures both in the regime of *magnetic coupling* and *proximity effect*.

In magnetically coupled structures the inhomogeneous stray field of the ferromagnet leads to an inhomogeneous superconducting state where superconductivity and vortices can be confined in channels determined by the underlying magnetic template and make these structures attractive model systems that offer the possibility to control the strength and the location of the superconducting nucleus by applying an external magnetic field.

In the proximity effect regime the ferromagnet and the superconductor are in contact and leakage of superconducting pairs is allowed into the ferromagnetic layer.

While traditionally considered competing phenomena, when artificially placed in contact, there is a wealth of physics at the interface between superconductors (S) and ferromagnets (F). Taking advantage of the competition between order parameters has led to advances in the emerging field of superconducting-spintronics [1]. By placing an inhomogeneous magnetic texture at the S–F interface, it is possible to generate the so-called long ranged triplet component or finite spin Cooper pair. Unlike the singlet Cooper pair, the LRTC is not dephased by the exchange field and can therefore penetrate over a longer distance into the adjacent F-layer. This opens the exciting possibility of performing spintronic logic operations on a dissipationless spin current [2].

Recent Progress

We have focused on different S/F heterostructures in the regime of proximity coupling. The theoretical understanding of the long ranged proximity effect inside the ferromagnet in a SF system assumes that singlet-triplet conversion happens because of a magnetic inhomogeneity in the vicinity of the S/F interface. This can be due either to domain walls [3], or a spin-active interface [4] or a multilayer magnetic structure with different magnetic orientations [5]. Spin-orbit coupling can also be a source of triplet superconducting condensate [6].

- **Co/Pb bilayers**

The magnetic structure of ultrathin films is largely dependent upon the interplay between surface, interface anisotropies and shape anisotropies. Whereas surface and interface anisotropies can cause an alignment of the magnetization perpendicular to the plane of the film, the shape anisotropy due to dipolar magnetic interactions tends to orient the magnetization in the plane of the film. With increasing thickness, dipolar interactions gain strength and hence may cause a transition from vertical to in-plane magnetization. However, in real systems, anisotropy of thin films is governed by many additional factors resulting from the film microstructure, size of grains and strain.

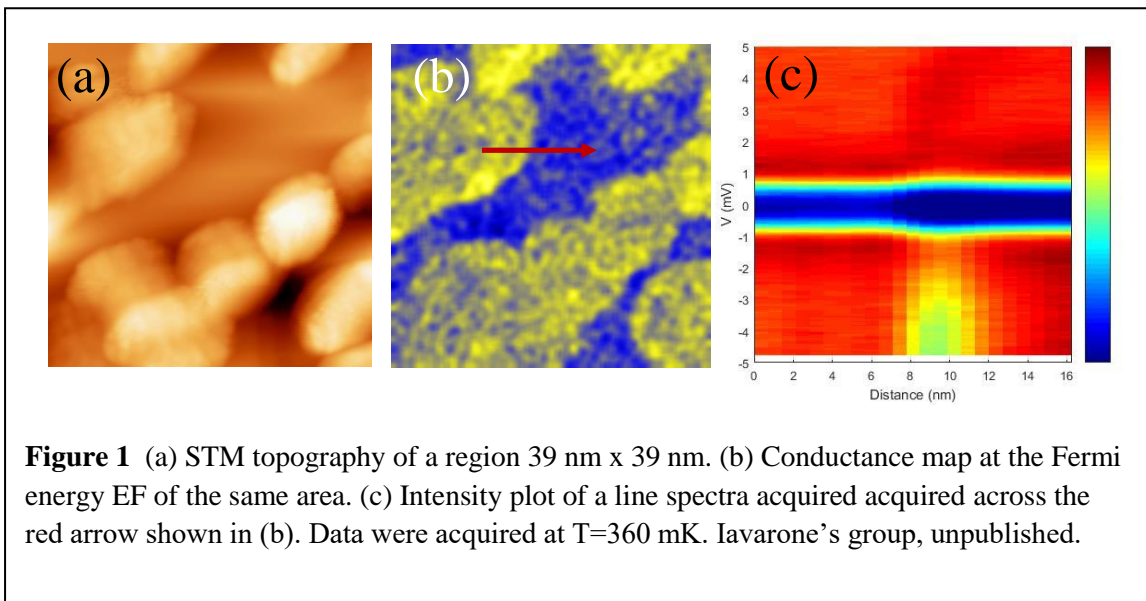
We have grown Co on ultrathin Pb films on HOPG cleaved substrates in a UHV chamber with a base pressure of low 10^{-11} Torr attached to the STM chamber. As prepared surfaces result in Co clusters that grow preferentially along the step edges of the underlying Pb film. This kind

of morphology allows to access the characteristic spectroscopic features as a function of distance from the SF interface.

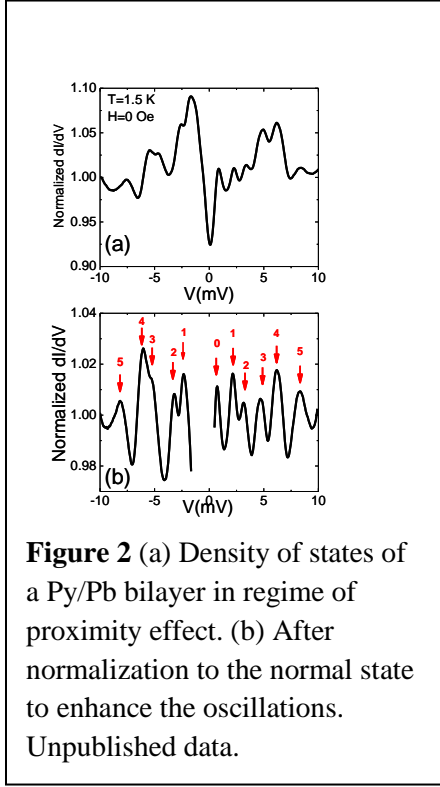
A suppression of T_c from 7 K (reference Pb film without Co islands) to 3.5 K (in the Pb/Co bilayer) suggests that the Co clusters have an out-of-plane magnetization consistent with previous results [4, 5]. This T_c suppression is indeed consistent with an exchange field in the ferromagnet $E_{ex} \gg 10 \Delta$ where Δ is the gap of the Pb without ferromagnet. We observe a quasiparticle density of states with strong suppression of the gap and high increase of the zero bias conductance. The spectra are consistent with the main singlet pairs channel as no zero bias peak or in-gap states were observed. Both triplet components (short range and long range) are indeed characterized spectroscopically by a zero-energy peak in the density of states. The tunneling spectrum change slightly at the border of Co clusters. The coherence peak shifts to slightly higher energy and the zero bias conductance becomes lower on the Pb side of the lateral Co/Pb junction. Since the distance between Co clusters is much less than the coherence length of Pb [7], the superconductivity is strongly affected also on the Pb side of the lateral junction (reverse proximity effect) and the spectrum of Pb is never recovered on the distance that are accessible in this experiment.

These results are summarized in Figure 1 where the conductance map at the Fermi energy E_F (b) acquired on a typical region of the sample shows that higher zero bias conductance is directly correlated with the presence of Co clusters in the topography (a). A line profile plotted in the intensity plot in (c) shows the evolution of the spectra across a lateral Co/Pb interface. The change in the tunneling spectra happens on a very short length scale of about 1 nm at the interface. However, the spectrum on the Pb side remains much broader than the tunneling spectrum acquired on the reference Pb spectrum. The density of states near the SF interface can be calculated from the Usadel equations [8] for the quasiclassical Green's functions in the diffusive limit. The calculated density of states on the superconductor side in the case of an ideal interface is dramatically affected even at distances larger than 2-3 ξ from the SF interface.

Following experiments should clarify indeed how superconductivity is affected if the size of the Co islands can be controlled to allow in-plane magnetization or even islands with magnetic domains could be obtained.



Py/Pb bilayers



We have prepared Py/Pb bilayers with different Py thicknesses.

We found a suppressed T_c corresponding to a correlation length in the ferromagnet side $\xi_f = \sqrt{\hbar D_f / E_{ex}} \approx 4 \text{ nm}$, where D_f is the diffusion constant in the ferromagnet and E_{ex} is the exchange field.

Furthermore, we find oscillations of the quasiparticle density of states that disappear at the critical temperature of the bilayer (Figure 2). These oscillations have been identified as McMillan Rowell resonances [9,10] and they scale consistently with the thickness of the ferromagnet.

The McMillan Rowell oscillations arise as a consequence of resonances in the non-superconducting side of the interface. In this case, the incident electron is Andreev reflected as a hole at the interface. However, unlike in the S (where the mixed character of quasiparticles allows for the interference between electron and hole-like ones), in a non-superconducting material an electron and a hole cannot interfere [9]. Therefore, for the interference to occur in the N, the Andreev-reflected hole must subsequently travel a distance d_f to the opposite interface and, after being normal reflected, propagate back to the S/N interface to undergo a

second Andreev reflection. This returns the hole to its original electron state. Here it will interfere with the first incident electron, which gives rise to conductance oscillations with peaks at bias:

$$V_n = V_0 + \frac{nhv_F}{4d_f} \text{ with } n=0,1,2,\dots \text{ Here } v_F \text{ is the Fermi velocity in the ferromagnet and } d_f \text{ is its}$$

thickness. Theoretical modeling suggests that these oscillations are due to proximity effect and very clean interfaces. In a diffusive system they are possible only if superconducting correlations extend through the ferromagnetic layer.

Future Plans

We will continue to explore the physics of mesoscopic and S/F structures with different magnetic and superconducting materials. In particular S/F systems with different singlet-triplet conversion mechanisms will be considered. We plan to study non-collinear magnetic system such as chiral magnets and thin films where broken inversion symmetry at the interface and the spin-orbit coupling of substrates lead to non-uniform magnetization.

References

- [1] J. Linder and J. W. A. Robinson, "Superconducting spintronics," *Nat. Phys.* **11**, 307–315 (2015).
- [2] M. Eschrig, "Spin-polarized supercurrents for spintronics," *Phys. Today* **64**, 43–49 (2011).
- [3] F. S. Bergeret, A. F. Volkov, and K. B. Efetov, *Phys. Rev. Lett.* **86**, 4096 (2001)
- [4] M. Eschrig and T. Löfwander, *Nat. Phys.* **4**, 138 (2008)
- [5] A. F. Volkov, F. S. Bergeret, and K. B. Efetov, *Phys. Rev. Lett.* **90**, 117006 (2003)

- [6] F. S. Bergeret, and I.V. Tokatly, *Phys. Rev. Lett* **110**, 117003 (2013)
- [7] M. Iavarone, S.A. Moore, J. Fedor, S.T. Ciocys, G. Karapetrov, J. Pearson, V. Novosad, S.D. Bader, *Nature Communications* **5**, 4766 (2014)
- [8] K.D. Usadel, *Phys. Rev. Lett.* **25**, 507 (1970)
- [9] J.M. Rowell, and W.L. McMillan, “Electron interference in a normal metal induced by superconducting contacts.” *Phys. Rev. Lett.* **16**, 453-456 (1966)
- [10] J.M. Rowell, “Tunneling observation of bound states in a normal metal-superconductor sandwich.” *Phys. Rev. Lett.* **30**, 167-170 (1973)

Publications (DOE sponsored 2016-2018)

- [1] “Observation of superconducting vortex clusters in S/F hybrids” Di Giorgio, C. F. Bobba, A. M. Cucolo, A. Scarfato, S.A. Moore, G. Karapetrov, D. D’Agostino, V. Novosad, V.Yefremenko & M. Iavarone *Sci. Rep.* **6**, 38557 (2016)
- [2]”Anisotropic Superconducting Gaps and Boson Mode in FeSe_{1-x}S_x single crystals”, C. Di Giorgio, A.V. Putilov, D.J. Trainer, O.S. Volkova, A.N. Vasiliev, D. Chareev, G. Karapetrov, J.F. Zasadzinski, M. Iavarone, *Journal of Superconductivity and Novel Magnetism* **30 (3)**, 763-768 (2017)
- [3] “Single crystal growth, transport and scanning tunneling microscopy and spectroscopy of FeSe_{1-x}S_x” Dmitriy Chareev, Yevgeniy Ovchenkov, Larisa Shvanskaya, Andrey Kovalskii, Mahmoud Abdel-Hafiez, Dan J. Trainer, Eric M. Lechner, Maria Iavarone, Olga Volkova and Alexander Vasiliev, *CrystEngComm* **20**, 2449 (2018)
- [4] “Superconducting Vortex-Antivortex Pairs: Nucleation and Confinement in Magnetically Coupled Superconductor-Ferromagnet Hybrids” C. Di Giorgio, D. D’Agostino, A.M. Cucolo, M. Iavarone, A. Scarfato, G. Karapetrov, S.A. Moore, M. Polichetti, D. Mancusi, S. Pace, V. Novosad, V. Yefremenko and F. Bobba Chapter in the book *Vortex Dynamics and Optical Vortices*, ISBN 978-953-51-2930-1, Edited by Hector Perez-de-Tejada (2017) DOI:10.5772/62608

Atomic Scale Imaging of Spin and Magnetism in Two-Dimensional Materials and Devices

Roland K. Kawakami and Jay A. Gupta

Department of Physics, The Ohio State University, Columbus OH 43210, USA

Research Scope

Our mission is to develop and utilize spin-polarized scanning tunneling microscopy (SPSTM) in conjunction with molecular beam epitaxy (MBE) and nanoscale device fabrication to explore new frontiers of spintronics and quantum science in two-dimensional (2D) van der Waals (vdW) materials. We are particularly motivated by understanding how the magnetic and spin-dependent properties at the atomic scale lead to interesting and potentially useful phenomena in spintronic devices at the macroscopic scale.

With the recent advent of ferromagnetism in monolayer vdW magnets [1,2], there has been great interest in developing new monolayer magnets and investigating the magnetic order down to the atomic scale. In the current program, we utilize MBE to synthesize novel monolayer magnetic materials and heterostructures, characterize the atomic scale structure by STM, and investigate the atomic scale magnetism by SPSTM. In addition, we will use atomic manipulation to systematically investigate magnetic interactions in 2D materials. To connect to device applications, we fabricate magnetic heterostructures and spin valve devices to investigate the interplay of the magnetic spin texture with electronic spin currents.

Recent Progress

Intrinsic 2D magnets synthesized by MBE. We have developed the MBE growth of monolayer MnSe₂, which is among the first monolayer magnets to exhibit ferromagnetism at room temperature [3] (concurrent with similar work on VSe₂ [4]). Together, these results on MnSe₂ and VSe₂ are the first monolayer ferromagnets at room temperature and these discoveries are gaining substantial interest within the magnetism and 2D materials communities. In our work, we report the observation of room temperature ferromagnetism in manganese selenide (MnSe_x) films grown by MBE. Magnetic and structural characterization provides strong evidence that in the monolayer limit, the ferromagnetism originates from a vdW manganese diselenide (MnSe₂) monolayer, while for thicker films it could originate from a combination of vdW MnSe₂ and/or interfacial magnetism of α -MnSe(111). Magnetization measurements of monolayer MnSe_x films on GaSe and SnSe₂ epilayers by superconducting quantum interference device (SQUID) magnetometry show ferromagnetic ordering with large saturation magnetization of ~ 4 Bohr magnetons per Mn, which is consistent with density functional theory calculations predicting ferromagnetism in monolayer 1T-MnSe₂ [5,6]. Growing MnSe_x films on GaSe up to high thickness (~ 40 nm) produces α -MnSe(111), and an enhanced magnetic moment ($\sim 2x$) compared to the monolayer MnSe_x samples. Detailed structural characterization by STM, scanning transmission electron microscopy (STEM), and reflection high energy electron diffraction

(RHEED) reveal an abrupt and clean interface between GaSe(0001) and α -MnSe(111). In particular, the structure measured by STEM is consistent with the presence of a MnSe₂ monolayer at the interface. The results are summarized in Figure 1.

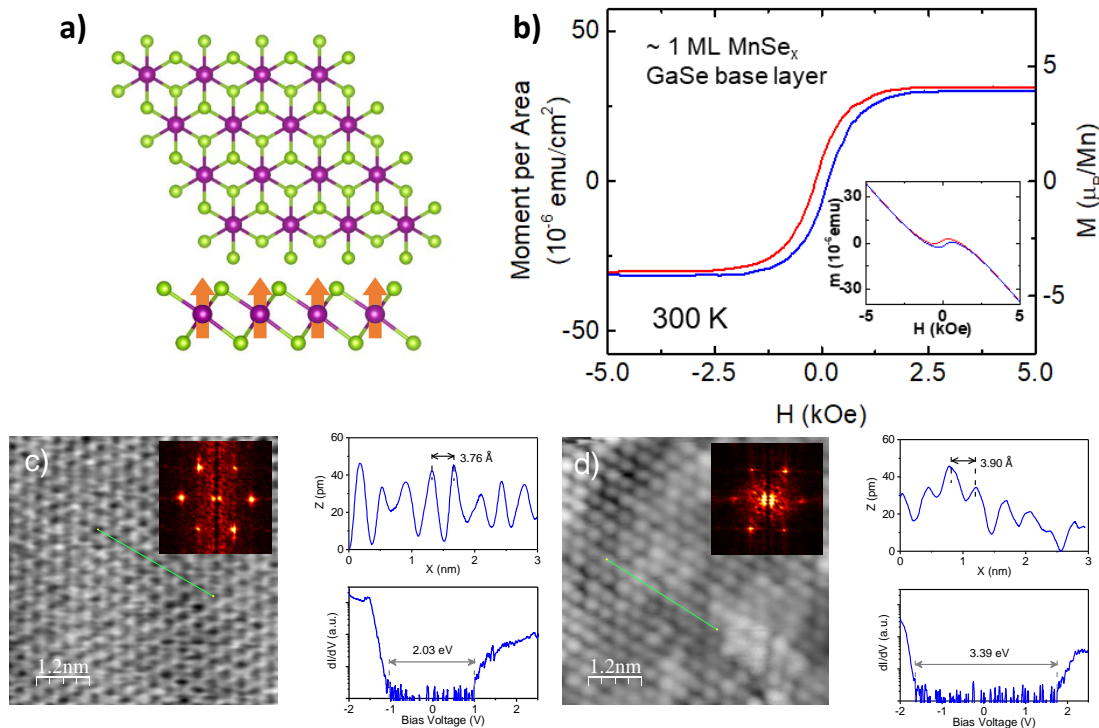


Figure 1. a) Schematic of the MnSe₂ lattice structure. b) Magnetic hysteresis loop of ~ 1ML MnSe_x on GaSe base layer showing ferromagnetic behavior. Inset: the unprocessed SQUID data prior to background subtraction. STM topography image and dI/dV spectroscopy of c) the GaSe substrate and d) ~3 layers of MnSe_x shows a quick structural transition of the deposited material into α -MnSe(111). These images show atomic resolution and the corresponding spectroscopy shows a band gap that is consistent with the literature for both GaSe and α -MnSe.

Beyond MnSe₂ on GaSe(0001) and SnSe₂(0001), we have progressed further to synthesize both MnSe₂ and VSe₂ on a variety of other substrates including highly-oriented pyrolytic graphite (HOPG), GaAs(111), and Bi₂Se₃(0001). SQUID measurements have verified room temperature ferromagnetism in these systems as well.

Developing extrinsic ferromagnetic ordering in graphene. We are interested in understanding the magnetic coupling between magnetic moments within non-magnetic 2D vdW materials such as graphene and transition metal dichalcogenides to generate extrinsic magnetic ordering. Graphene with hydrogen adatom doping is an interesting system for this study because the hydrogen generates localized magnetic moments within the graphene lattice [7,8]. In our current studies, we report a groundbreaking experimental observation of sublattice-resolved resonant

scattering in bilayer graphene (Fig. 2a). By performing simultaneous cryogenic atomic hydrogen doping and electron transport measurements on bilayer graphene nano-devices under ultrahigh vacuum (Fig. 2b), we detect two well-defined resonant scattering peaks in the gate-dependent resistance (Fig. 2c, 2d). Theoretical analysis shows they originate from hydrogen adatoms on the two inequivalent sublattices, α and β (Fig. 2a). These results allow us to monitor the atomic hydrogen adsorption on different sublattices of bilayer graphene without atomic-scale microscopy. Based on this new capability, we are able to realize hydrogen doping with adatoms primarily on a single sublattice via annealing, which is crucial for generating ferromagnetism [9]. We will next focus on STM imaging of such systems.

Optimizing Cr tips for spin-polarized imaging. Because the SPSTM signal varies as $\cos(\theta)$ between the tip and sample spin orientation, characterization of SPSTM tips on well-studied reference samples is essential. Our initial studies focused on the Cr(001) surface, which exhibits a 'topological' antiferromagnetism with an in-plane spin orientation that alternates between adjacent terraces in the surface. We have developed etching recipes for bulk Cr tips to achieve spin sensitive imaging while eliminating stray fields that may influence the measurement. The SPSTM signal is revealed by spatially mapping dI/dV simultaneously with a conventional topographic scan (Fig. 3a). While the topography channel is dominated by steps associated with the crystal, the dI/dV channel reveals the alternating bright and dark contrast expected for SPSTM imaging. As a further test, we repeated measurements with several distinct tip terminations, and found that the spin contrast varies as the atomic spin at the end of the tip changes orientation (Fig. 3c). Tunneling spectroscopy on adjacent terraces reveals the distinct spin-dependent density of states responsible for the SPSTM image contrast (Fig. 3b).

Future Plans

Our next steps will be toward atomic- and spin-resolved imaging of the 2D magnetic materials and spin valve devices. STM characterization has helped us refine the growth of the MnSe_2 and VSe_2 materials, and a sustained push for spin resolution is currently underway. Toward this end, we are developing 2D magnet growth on a variety of substrates to tailor the interfacial magnetic

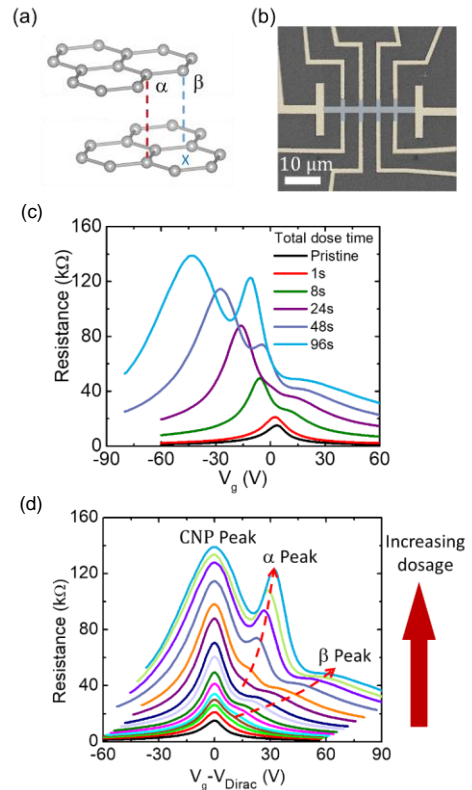


Figure 2. a) Schematic of bilayer graphene, depicting α and β sites. b) SEM picture of a typical device. c) Gate dependent resistance at 21 K of undoped (black color curve) bilayer graphene and after hydrogen exposure. d) The evolution of bilayer graphene resistance as a function of $V_g - V_{\text{Dirac}}$ with increasing hydrogen exposure.

properties. To image the resonant spin scattering in graphene, we have succeeded in fabricating graphene devices with atomically clean surface suitable for STM imaging. We have adopted a capacitive navigation method to position the STM tip onto the bilayer graphene channels, and have obtained atomic-resolution images of the graphene surface with concurrent device transport measurements. We will next image devices following *in situ* hydrogenation with spin-resolved tips to probe the resonant spin scattering channels observed in transport.

References

- [1] C. Gong *et al.*, *Nature* **546**, 265 (2017).
- [2] B. Huang *et al.*, *Nature* **546**, 270 (2017).
- [3] D. J. O'Hara *et al.*, *Nano Lett.* **18**, 3125 (2018).
- [4] M. Bonilla *et al.*, *Nat. Nanotechnol.* **13**, 289 (2018).
- [5] C. Ataca, H. Şahin, and S. Ciraci, *J. Phys. Chem. C* **116**, 8983 (2012).
- [6] M. Kan, S. Adhikari, and Q. Sun, *Phys. Chem. Chem. Phys.* **16**, 4990 (2014).
- [7] K. M. McCreary *et al.*, *Phys. Rev. Lett.* **109**, 186604 (2012).
- [8] H. González-Herrero *et al.*, *Science* **352**, 437 (2016).
- [9] M. Moaied, J. V. Alvarez, and J. J. Palacios, *Phys. Rev. B* **90**, 115441 (2014).

Publications

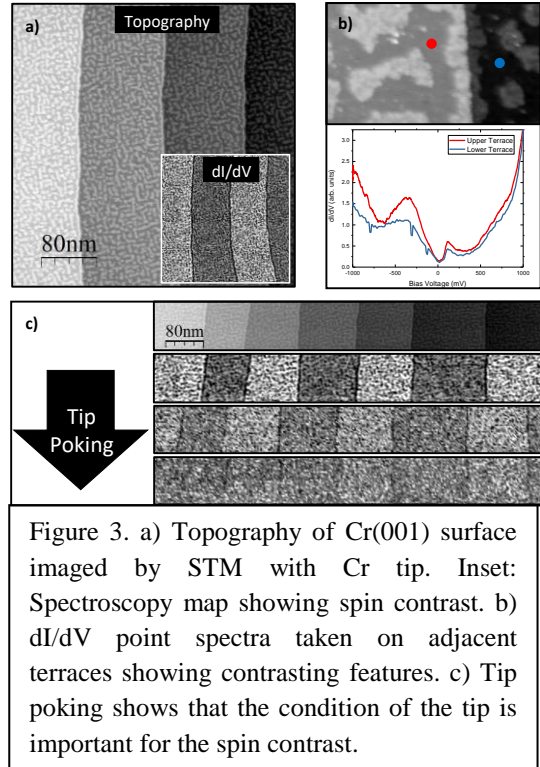
Dante J. O'Hara *et al.*, "Room Temperature Intrinsic Ferromagnetism in Epitaxial Manganese Selenide Films in the Monolayer Limit," *Nano Letters* **18**, 3125 (2018).

Tiancong Zhu and Roland K. Kawakami, "Modeling the Oblique Spin Precession in Lateral Spin Valves for Accurate Determination of Spin Lifetime Anisotropy: Effect of Finite Contact Resistance and Channel Length," *Phys. Rev. B* **97**, 144413 (2018).

Tiancong Zhu *et al.*, "Probing tunneling spin injection into graphene via bias dependence," *Phys. Rev. B* **98**, 054412 (2018).

Dante J. O'Hara *et al.*, "Importance of Paramagnetic Background Subtraction for Determining the Magnetic Moment in Epitaxially Grown Monolayer and Few-Layer van der Waals Magnets," *IEEE Magn. Lett.*, in press.

Jyoti Katoch *et al.*, "Transport Spectroscopy of Sublattice-Resolved Resonant Scattering in Hydrogen-Doped Bilayer Graphene", submitted.



Mesoscopic Conductivity Imaging of Novel Field-effect Transistors

PI: Keji Lai (kejilai@physics.utexas.edu)

Department of Physics, University of Texas at Austin, Austin, TX 78712

Program Scope

The goal of this DOE program is to explore the mesoscopic conductivity distribution in the field-effect transistor (FET) configuration, where charge carriers are electrostatically modulated in advanced materials. In particular, we utilize the microwave impedance microscope (MIM)¹, a novel technique capable of resolving nanoscale dielectric and conductivity information, to image the local conductance at the buried transistor interface. The research aims to address fundamental scientific problems, such as the emergence of carrier-induced electronic phase transitions in real space and the microscopic origin of the sub-threshold behavior in FETs. The results will ultimately facilitate the applications of novel quantum systems in energy science and technology.

Recent Progress

In the past two years, our team has focused on the sketch FET at the LaAlO₃/SrTiO₃ (LAO/STO) interface and the back-gated FET on two-dimensional heterostructures. For quantitative measurements of nanoscale permittivity and conductivity, we also developed tuning-fork (TF) based MIM, which successfully imaged the conductance evolution in a MoS₂/WSe₂ hetero-junction FET. Details of the experimental results are as follows.

Visualization of sketched FETs at the LAO/STO interface

The LAO/STO interface has been in the limelight of material research in the past decade². When 4 or more unit cells (uc) of LAO are epitaxially grown on a TiO₂-terminated STO substrate, a high-mobility quasi-two-dimensional electron gas (q2DEG) forms spontaneously on the STO side of the interface. At the critical LAO thickness of 3 uc, a metastable metal-insulator transition can be realized by a gate voltage applied either on the back of the STO substrate or on the top LAO surface using a conductive tip. In the latter case, the q2DEG can be reversibly written and erased underneath the tip with nanoscale lateral dimensions, enabling on-demand creation and control of conductive nanostructures at the interface³.

While the rich physics at the LAO/STO interface was studied by many scanning probes, one of the most important physical quantities in this system, the local 2D conductivity, had not been directly imaged before our work. With sub-surface imaging capability and a lateral resolution of 10-100 nm, the MIM is an ideal tool to visualize the local electrical properties at the buried LAO/STO interface. As illustrated in Fig. 1a, we can sketch the conductive regions, here several bands across two pre-patterned rectangular pads extended from a pair of electrodes, by applying a tip bias V_{tip} through the bias-tee [Jiang2017]. With no corresponding features in the topographic

image, the sketched pads and bands can be clearly observed in the MIM images (Fig. 1b). The sheet resistance estimated by comparing the MIM data with numerical analysis fits nicely to the measured conductance between the two electrodes, confirming the quantitative nature of MIM imaging. Finally, by recording the MIM signals during repeated line scans across two pads, we were able to visualize the insulator-to-metal transition as V_{tip} ramps from 0 to +5 V, as seen in Fig. 1c. The result suggests that the interfacial conductance is due to the field effect through charge writing at the sample surface. Our imaging work provide opportunities to study the emergent phenomena at various oxide interfaces.

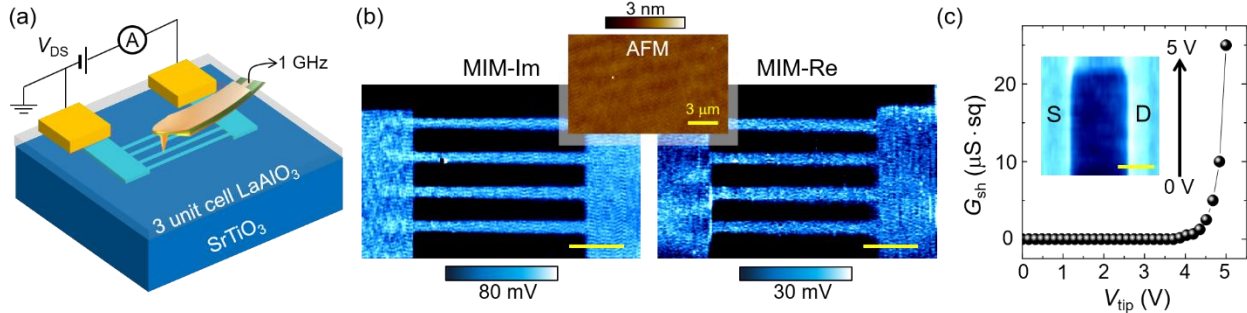


Figure 1. (a) Schematic of the sketched-FET experiment, where the two-terminal conductance is monitored by a source-drain bias across the Ti/Au electrodes. (b) AFM and MIM images of four bands across two pads, all written with $V_{\text{tip}} = +5$ V. (c) Sheet conductance G_{sh} as a function of V_{tip} . The conduction at the LAO/STO interface becomes evident above a threshold voltage of 4 V. The inset shows MIM signals as the tip repeatedly scans between two pads and V_{tip} ramps from 0 (bottom) to +5 V (top). All scale bars are 3 μm . [Jiang2017]

Development of tuning-fork-based MIM for quantitative imaging

In addition to the scientific research, tool development is also an important component of this DOE program. Conventional MIM experiments are based on contact-mode operation, during which the tip wearing is inevitable. Since the signal level is strongly affected by the condition of the tip apex, quantification of the contact-mode MIM is very difficult and an extensive calibration process is needed. In this regard, the recently developed tuning fork (TF) based MIM with etched metal tips provides an elegant solution to the problem⁴. Quartz TFs with small vibration amplitudes (<10 nm) are widely used as the feedback element to preserve the tip condition. More importantly, the distance modulation automatically provides the contrast between on and off the sample surface such that the demodulated signals carry absolute information at every point, which can be easily quantified to map out the local permittivity and conductivity.

In this work, we further develop the TF-MIM by using the driving amplitude modulation mode, which offers satisfactory stability on samples with rough surfaces [Wu2018]. As shown in Fig. 2a, a built-in phase locked loop and a PID controller are employed to keep the TF on resonance and to maintain a constant average tip-sample distance. An etched W tip with an apex of 100 nm, as seen in the SEM image, can be preserved over many scans on samples with large topographic features, such as contact electrodes. Quantitative measurements on bulk dielectrics are demonstrated in Fig. 2b. The setup is up and running for the study of FET devices.

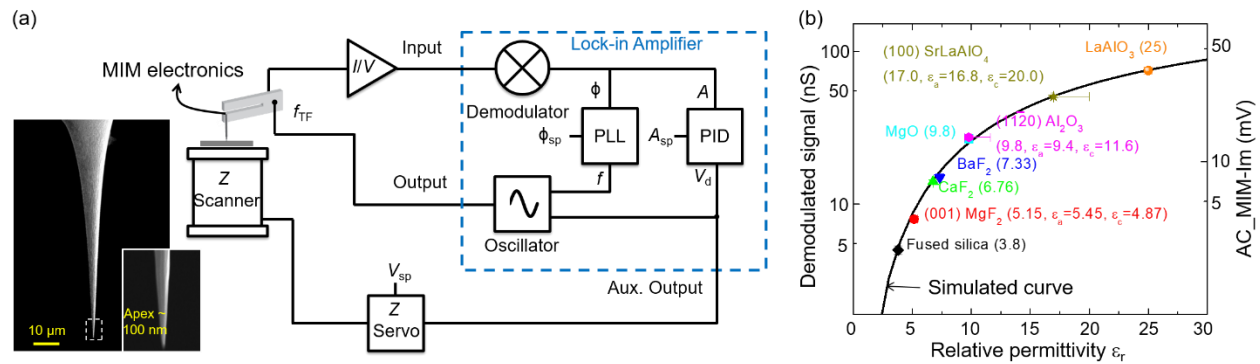


Figure 2. (a) Schematic of the TF-based MIM configured for the driving amplitude modulation mode. Details can be found in [Wu2018]. The SEM image to the left shows a typical etched W tip and a zoom-in view near the tip apex. (b) Demodulated tip-sample admittance and the corresponding AC_MIM signals as a function of the relative permittivity. The solid line is the simulated curve, which matches nicely to the measured signals [Wu2018].

Local conductivity in MoS₂/WSe₂ heterostructure FETs

Research on layered van der Waals (vdW) materials has evolved into a vibrant and dynamic field in the past decade. Among the numerous advantages in these systems, a unique feature here is the ease to form 2D heterojunctions⁵, where strong covalent bonds provide the in-plane stability and the weak vdW forces are sufficient to keep the stack together. Local probing is highly desirable for the understanding of charge transfer between disparate layers, which is responsible for the nontrivial electrical and optical properties in these vertical heterostructures.

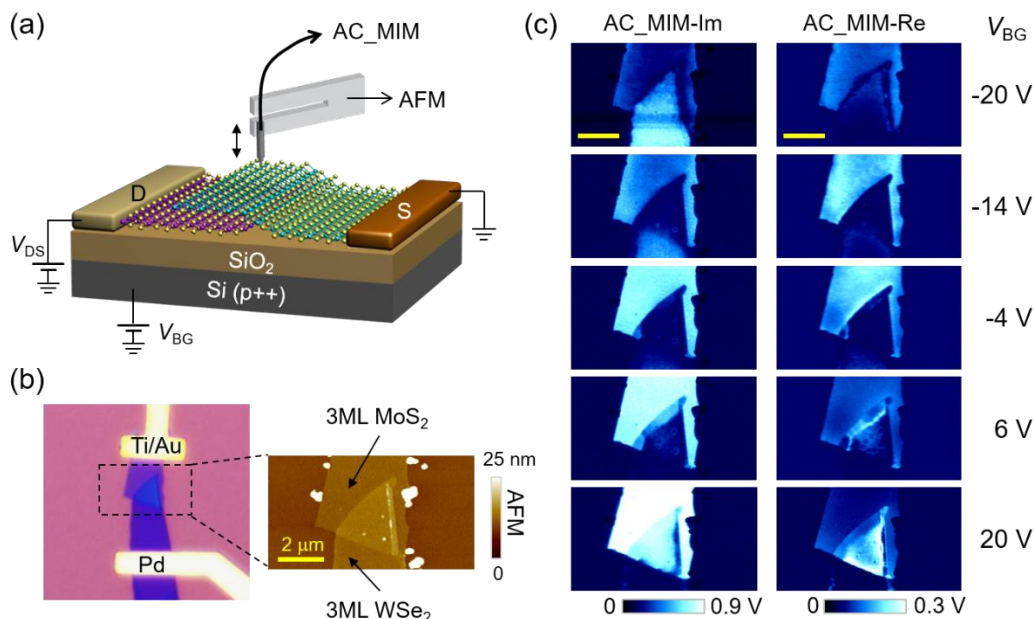


Figure 3. (a) Schematic of the MoS₂/WSe₂ heterostructure FET device and the TF-based MIM setup. (b) Optical (left) and a zoom-in AFM (right) images of the device. The 3-mono-layer (ML) MoS₂, WSe₂, and overlap regions are seen in the data. (c) AC_MIM images of the heterostructure sample at various back-gate voltages. All scale bars are 2 μm . [Manuscript in preparation]

Fig. 3 shows the preliminary MIM results on a MoS₂/WSe₂ heterostructure FET using the TF-based setup. Ohmic contacts were fabricated on the MoS₂ and WSe₂ flakes to change the Fermi level of the system. At high negative back-gate voltages (V_{BG}), both the p-type WSe₂ and overlap regions are conductive. Similarly, the n-type MoS₂ and overlap regions are conductive at high positive V_{BG} . For intermediate V_{BG} 's, however, the heterostructure exhibits insulating behaviors, presumably due to charge transfer between the two layers. A manuscript is currently under preparation to report this exciting result.

Future Plans

With the progress made in the past two years, we will be able to conclude this DOE program with substantial scientific discoveries on various FETs. Aside from completing the project on vdW heterostructure FET, we will continue to explore the LAO/STO interface with TF-based MIM at cryogenic temperatures. FETs with ferroelectric (Hf,Zr)O₂ as gate dielectrics will also be studied by the MIM.

Thanks to the continuing DOE support, we will start a new program in the fall, which expands the territory of our research to a much broader range of electronic phase transitions. With the successful demonstration of TF-based cryogenic MIM, we aim to investigate the local inhomogeneity in thin-film manganite and nickelate samples and compare the microscopic evolution of metal-insulator phase transitions induced by magnetic field and electric field. We expect to enter an exciting regime through the unique MIM measurements.

References

1. K. Lai, W. Kundhikanjana, M. A. Kelly and Z.-X. Shen, "Nanoscale microwave microscopy using shielded cantilever probes," *Appl. Nanoscience* **1**, 13 (2011).
2. J. A. Sulpizio, S. Ilani, P. Irvin, and J. Levy, "Nanoscale phenomena in oxide heterostructures," *Annu. Rev. Mater. Res.* **44**, 117 (2014).
3. C. Cen, S. Thiel, J. Mannhart, and J. Levy, "Oxide nanoelectronics on demand," *Science* **323**, 1026 (2009).
4. Y.-T. Cui, E. Y. Ma, and Z.-X. Shen, "Quartz tuning fork based microwave impedance microscopy," *Rev. Sci. Instrum.* **87**, 063711 (2016).
5. A.K. Geim and I.V. Grigorieva, "Van der Waals heterostructures," *Nature* **499**, 419 (2013).

Publications

1. [Jiang2017] Z. Jiang, X. Wu, H. Lee, J.-W. Lee, J. Li, G. Cheng, C.-B. Eom, J. Levy, and **K. Lai**, "Direct imaging of sketched conductive nanostructures at the LaAlO₃/SrTiO₃ interface", *Appl. Phys. Lett.* **111**, 233104 (2017).
2. [Wu2018] X. Wu, Z. Hao, D. Wu, L. Zheng, Z. Jiang, V. Ganesan, Y. Wang, and **K. Lai**, "Quantitative measurements of nanoscale permittivity and conductivity using tuning-fork-based microwave impedance microscopy", *Rev. Sci. Instrum.* **89**, 043704 (2018).

Interfacial superconductivity in epitaxial single layer FeSeTe on SrTiO₃(001)

PI: Lian Li

Department of Physics and Astronomy, West Virginia University, Morgantown, WV

Research Scope

Explore interfacial superconductivity in epitaxial single layer FeSeTe on SrTiO₃(001) through an integrated approach of molecular beam epitaxial growth, *in situ* characterization by scanning tunneling microscopy/spectroscopy (STM/S) and angle resolved photoemission spectroscopy (ARPES), corroborated with density functional theory (DFT) calculations.

Recent Progress

1. Engineering interfacial superconductivity in single layer FeSe/SrTiO₃

It's often said that "the interface is the device" [1]. Nowhere is this more evident than in single layer materials whose properties can be most meaningfully discussed only when their interfaces are clearly defined. The material system of focus here is the heterostructure of FeSe/SrTiO₃. Well known for its rich structural and electronic phases, SrTiO₃ (STO) has a 3.2 eV direct optical band gap. In contrast, FeSe is a layered superconductor that is stable down to the single layer limit, making it particularly amenable to proximity effects at interfaces, including charge transfer doping and electron-phonon scattering [2]. The integration of these two materials has led to T_C well above the bulk values of FeSe [3,4].

While most FeSe growth is carried out on TiO₂ terminated STO substrates, it's known that STO also exhibits a SrO termination [5], which has been much less investigated for the growth of FeSe. In this part of the research, we have prepared both TiO₂ and SrO terminated STO by controlling oxygen pressure during annealing in ultrahigh vacuum. STM imaging shows that the TiO₂ terminated regions exhibit a $(\sqrt{13} \times \sqrt{13})$ reconstruction [6], and the SrO regions a (3×1) structure. Single layer FeSe grown on this substrate also shows a mixed character: the (3×1) interfacial structure is preserved for the SrO terminated region, while only (1×1) is seen on the TiO₂ region. Most notably, the superconducting gap of the FeSe on the SrO region is reduced to 11 meV, compared to the 17 meV

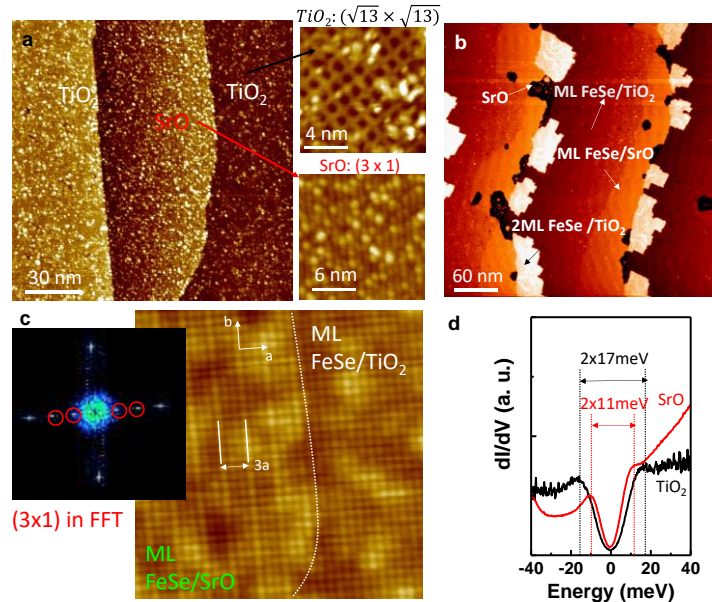


Fig. 1 Engineering interfacial superconductivity in FeSe/STO.

(a) STM images of STO with mixed TiO₂ and SrO termination ($V_s=1.0$ V, $I_t=0.1$ nA). (b)&(c) STM of FeSe grown on the mixed termination STO substrate ($V_s=1.2$ V, $I_t=0.1$ nA for (b); $V_s=80$ meV, $I_t=1.2$ nA for (c)). (d) dI/dV spectra showing the reduction of the pairing gap in SrO terminated regions.

the superconducting gap of the FeSe on the SrO region is reduced to 11 meV, compared to the 17 meV

on the TiO_2 termination, highlighting a strong dependence of the superconductivity on substrate termination.

Electronic structures calculations of FeSe on SrO-terminated STO were carried out by DFT. Of particular interest are the band structures of SrO-terminated STO with different surface reconstructions. The FeSe layer on the TiO_2 terminated STO(001) is electron-doped (**Fig. 2a**). On an ideal (1x1) SrO termination on the other hand, as shown in **Fig. 2b**, there is additional electron-doping to the FeSe, pushing the states at M further below the Fermi level, while the states at Γ are pushed slightly above the Fermi level, resulting in a hole pocket at the zone center, similar to that in bulk FeSe. However, the SrO-terminated STO surface is expected to reconstruct to structures such as the (3x1) shown in **Fig. 1a**, likely due to oxygen vacancy ordering that is common to oxides and STO in particular. The calculated relaxed structure has shifts in atomic positions for both the STO substrate and Se atoms near the oxygen vacancies (**Fig. 2c**). These changes cause the magnetic moments of the Fe sites to fluctuate by $\sim 0.1\text{-}0.2 \mu_B$.

The effect on the electronic bands is to push the states at M further below the Fermi level with an increased effective mass, and to partially occupy the second electron-like band (**Fig. 3d**). These changes are not, however, simply due to band filling, but rather strongly modify the dispersion of the bands away from M; in particular, the states at Γ are now significantly below the Fermi level and have rather flat dispersion. Thus, even though the overall dispersion of the bands around M is similar to that of the TiO_2 -terminated surface, the changes in magnetic properties, Fermi level, and states elsewhere in the zone likely will affect the superconducting properties, consistent with experimental observations (**Fig. 1d**).

2. Control high temperature interfacial superconductivity in single layer FeTeSe/STO

Bulk FeTe crystal at ambient conditions exhibits a distinct long-range bicollinear (BCL) antiferromagnetic (AFM) ordering. Alloying with Se suppresses the BCL order, leading to the emergence of superconductivity with a T_C of 10 K at a critical Se concentration of $x = 0.39$ [7]. Recent work has showed a much enhanced T_C of 50 K in epitaxial single layer $\text{FeTe}_{1-x}\text{Se}_x$ grown on STO substrates, with an even lower critical Se concentration of $x = 0.1$ [8]. In this part of the research, we explore the interplay between magnetism, spin-orbit coupling, and superconductivity in the $\text{FeTe}_{1-x}\text{Se}_x$ system.

$\text{FeTe}_{1-x}\text{Se}_x$ thin films have been grown by MBE on STO substrates, and characterized by *in situ* STM/S and ARPES. STS shows a superconducting gap of 15 meV for films with Se concentration >0.1 , consistent with earlier work [8]. **Figure 3** shows the evolution of the ARPES

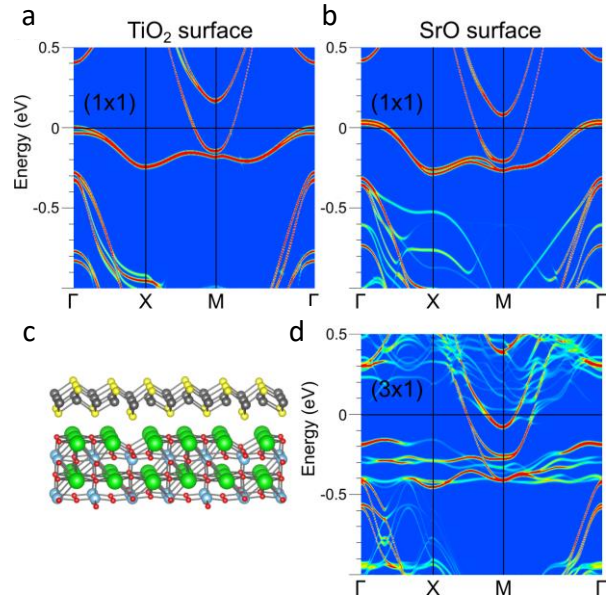


Fig. 2 Calculated bands of FeSe on different terminations of STO. k -projected bands (including SOC and assuming a checkerboard magnetic initial configuration) of monolayer FeSe on (a) (1x1) TiO_2 -, (b) (1x1) SrO-, and (c) (3x1) SrO-termination of STO(001). The structures were relaxed including vdW corrections; the relaxed (3x1) structure is given in (c).

intensity plot near Γ and M taken at 80 K for a series of single layer $\text{FeTe}_{1-x}\text{Se}_x/\text{STO}$ ($0 \leq x \leq 1$) thin films. For high Se concentrations ($x > 0.1$), both $\text{FeTe}_{1-x}\text{Se}_x$ and FeSe exhibit a hole pocket at M and electron pocket below the Fermi level at Γ , as expected [4]. The superconducting gap indeed opens at M when the temperature is decreased below 40K. In contrast, for low Se concentrations ($x < 0.1$), both the FeTe and $\text{FeTe}_{1-x}\text{Se}_x$ films have no features at M [9], and thus non-superconducting.

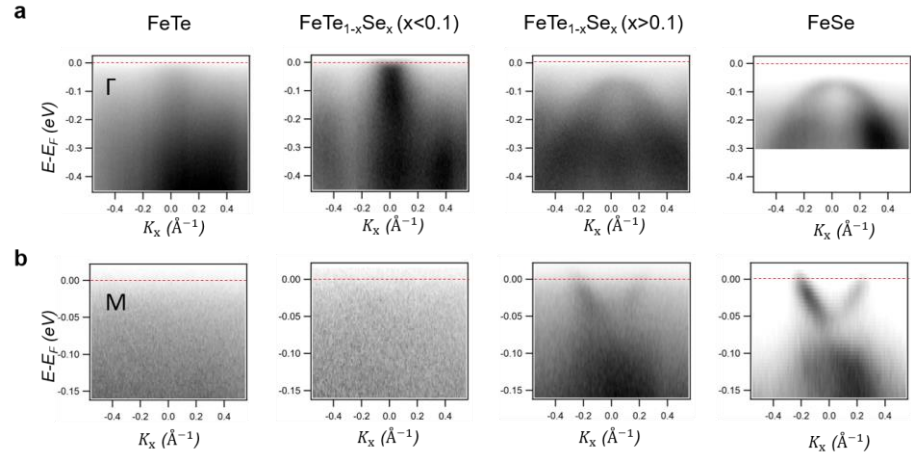


Figure 3 ARPES measurements of single layer $\text{FeTe}_{1-x}\text{Se}_x/\text{STO}$ with different Se concentrations. Evolution of the ARPES intensity plot near Γ (a) and M (b) for single layer FeTe, $\text{FeTe}_{1-x}\text{Se}_x$ ($x < 0.1$), $\text{FeTe}_{1-x}\text{Se}_x$ ($x > 0.1$), and FeSe taken at 80 K. The dashed red lines mark the Fermi level.

Our calculations (**Fig. 4**) indicate that this change in behavior is due to a magnetic phase change as a function of Se content. For monolayer $\text{FeTe}_{1-x}\text{Se}_x/\text{STO}$, the BCL phase is favored over the checkerboard (CB) phase, and the electronic bands (**Fig. 4b**) do not have any states in the vicinity of the Fermi level around M, where no superconductivity is observed for $x < 0.1$. This is in contrast to the case with higher Se concentration, where the paramagnetic phase is dominated by CB fluctuations, which gives rise to bands (**Fig. 4c**) similar to FeSe and hence conducive to superconductivity.

In addition, for the non-superconducting $\text{FeTe}_{1-x}\text{Se}_x$ films with $x < 0.1$, our STM imaging shows a (2×1) pattern. Calculations demonstrate that this (2×1) structure is a result of the combination of magnetic configuration and spin-orbit coupling, and not a structural reconstruction, as simulated STM image shows a (1×1) symmetry for the checkerboard ordering. For the BCL configuration, which is the ground state of FeTe, the simulation for $\text{FeTe}_{1-x}\text{Se}_x$ shows a (2×1) pattern, but a (1×1) if spin-orbit coupling is ignored. These results highlight the intricate interplay between magnetism

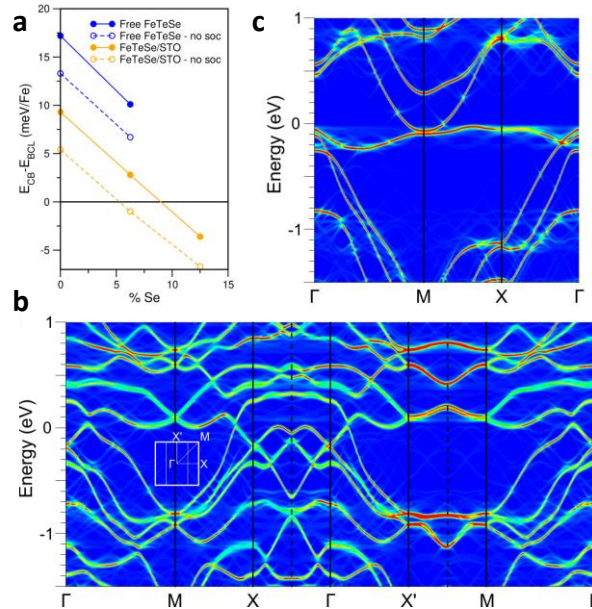


Fig. 4 Magnetism and band structure of FeTeSe/STO . (a) Calculated energy difference between the BCL and CB configuration as a function of Se content for free monolayer or supported on STO. k-projected bands for 6.25% Se in (b) BCL and (c) CB configurations. Note the lack of states around M near the Fermi level for in the BCL bands in (b).

and spin-orbit in these materials, and provide insights on the possible mechanisms giving rise to superconductivity.

Future Plans

The remarkable success of the integration of the STO substrate with the single layer FeTeSe system raises the obvious question whether there are even better perovskite oxide substrates that can enhance T_C to even higher temperatures. Addressing this question by tailoring the FeTeSe/substrate interactions to engineer desired functionalities will be the focus of our research. We also plan to probe impurity scattering in FeSe/STO with and without applied magnetic fields to gain further insight into the pairing symmetry.

References

1. Kroemer, H. Nobel Lecture: Quasielectric fields and band offsets: teaching electrons new tricks. *Reviews of Modern Physics* **2001**, 73 (3), 783-793.
2. Lee, D.-H. Routes to High-Temperature Superconductivity: A Lesson from FeSe/SrTiO₃. *Annual Review of Condensed Matter Physics* **9**, 261 (2018).
3. Wang, Q.-Y. et al. Interface-induced high-temperature superconductivity in single unit-cell FeSe films on SrTiO₃. *Chinese Physics Letters* **29**, 037402 (2012).
4. Tan, S. et al. Interface-induced superconductivity and strain-dependent spin density waves in FeSe/SrTiO₃ thin films. *Nature materials* **12**, 634 (2013).
5. Sánchez, F.; Ocal, C.; Fontcuberta, J., Tailored surfaces of perovskite oxide substrates for conducted growth of thin films. *Chemical Society Reviews* **43**, 2272 (2014).
6. Zou, K. et al. Role of double TiO₂ layers at the interface of FeSe/SrTiO₃ superconductors. *Physical Review B* **93**, 180506 (2016).
7. Liu, T. J. et al From $(\pi,0)$ magnetic order to superconductivity with (π,π) magnetic resonance in Fe_{1.02}Te_{1-x}Se_x. *Nature. Materials.* **9**, 716 (2010).
8. Li, F. et al. Interface-enhanced high-temperature superconductivity in single-unit-cell FeTe_{1-x}Se_x films on SrTiO₃. *Physical Review B* **91**, 220503 (2015).
9. Liu, Z. K. et al. Measurement of coherent polarons in the strongly coupled antiferromagnetically ordered iron-chalcogenide Fe_{1.02}Te using angle-resolved photoemission spectroscopy. *Physical review letters* **110**, 037003 (2013).

Publications resulting from work supported by the DOE grant over the previous two years

1. “Indirect interlayer bonding in graphene-topological insulator van der Waals heterostructure: giant spin-orbit splitting of the graphene Dirac states”, S. Rajput, Y. Y. Li, M. Weinert, and L. Li, *ACS Nano* **10**, 8450 (2016).
2. “Direct comparison of current-induced spin polarization in topological insulator Bi₂Se₃ Dirac states and InAs Rashba states”, C. H. Li, O. M. J. van ‘t Erve, S. Rajput, L. Li, and B. T. Jonker, *Nat. Commun.* **7**, 13518 (2016).
3. “Electrical detection of charge-to-spin and spin-to-charge conversion in a topological insulator Bi₂Te₃ using BN/Al₂O₃ hybrid tunnel barrier”, C. H. Li, O. M. J. van‘t Erve, C. Yan, L. Li & B. T. Jonker, *Sci. Rep.* **8**, 10265 (2018).
4. “Light induced non-volatile switching of superconductivity in single layer FeSe/SrTiO₃ heterostructures”, Ming Yang, Chenhui Yan, Yanjun Ma, Lian Li, and Cheng Cen, *Nat. Nanotechnol.* (submitted).
5. “Metallic graphene zigzag nanoribbons via selective edge oxidation”, Y. Y. Li, M. X. Chen, M. Weinert, and L. Li, *2D Mater.* (submitted).

STM studies of unconventional superconductors

Vidya Madhavan, University of Illinois, Urbana-Champaign

Research Scope

The goal of this project is to realize unconventional states such as topological superconductivity, proximity induced superconductivity and Majorana bound states (MBS) in bulk and thin films of topological materials and measure them using advanced STM spectroscopic techniques of Fourier transform scanning tunneling spectroscopy (FT-STs) and Landau level spectroscopy (LLS). Topological superconductivity has been postulated to exist in many different materials and geometries but so far there is no unambiguous experimental proof of the existence of this novel topological phase. The ability to directly measure the properties of Dirac surface states in both real- and momentum space makes scanning tunneling microscopy (STM) one of the most powerful tools for probing unconventional phases.

Recent Progress

Quasiparticle Interference and Strong Electron-Mode Coupling in the Quasi-One-Dimensional Bands of Sr_2RuO_4

The single-layered ruthenate Sr_2RuO_4 has attracted a great deal of interest as a spin-triplet superconductor with an order parameter that may potentially break time reversal invariance and host half-quantized vortices with Majorana zero modes. While the actual nature of the superconducting state is still a matter of controversy, it has long been believed that it condenses from a metallic state that is well described by a conventional Fermi liquid. In this work we use a combination of Fourier transform scanning tunneling spectroscopy (FT-STs) and momentum resolved electron energy loss spectroscopy (M-EELS) to probe interaction effects in the normal state of Sr_2RuO_4 . Our high-resolution FT-STs data show signatures of the β -band with a distinctly quasi-one-dimensional (1D) character. The band dispersion reveals surprisingly strong interaction effects that dramatically renormalize the Fermi velocity, suggesting that the normal state of Sr_2RuO_4 is that of a 'correlated metal' where correlations are strengthened by the quasi 1D nature of the bands. In addition, kinks at energies of approximately 10meV, 38meV and 70meV are observed. By comparison with M-EELS data we show that the two higher energy features arise from coupling with collective modes. The strong correlation effects and the kinks in the quasi 1D bands have important implications for the superconducting state.

Nanoscale measurements of the strain tensor and its effects on local electronic properties

We studied the influence of the orbital nature of bands on their strain response. Orbital degrees of freedom have strong effects on the fundamental properties of electrons in solids. In addition to influencing bandwidths, gaps, correlation strength, and dispersion, orbital effects have also been implicated in generating novel electronic and structural phases such as Jahn-Teller effect and colossal magneto resistance. Here we show for the first time how the orbital nature of bands can create non-trivial strain effects. We use scanning tunneling microscopy (STM) to study the influence of strain on the electronic structure of a hetero-epitaxial thin film of a topological crystalline insulator, SnTe. First, we demonstrate how the complete strain tensor can be directly measured on the local scale with nanometer precision using STM. This allows us to create two-dimensional maps of biaxial, uniaxial and sheer strain components which can then be correlated

with the local electronic structure using local Fourier-transform scanning tunneling spectroscopy. Applying these techniques to SnTe thin films, we find a surprising effect where uniaxial strain in one direction affects the band structure in the perpendicular direction. Theoretical calculations indicate that this arises from the effects of strain on hopping matrix elements, which depend on the orbital quantum number of the bands. Our results imply that a microscopic model capturing strain effects on band structure must include a consideration of the orbital nature of the bands.

Defect Role in the Carrier Tunable Topological Insulator $(\text{Bi}_{1-x}\text{Sb}_x)_2\text{Te}_3$ Thin Films

In this work, we used scanning tunneling microscopy and spectroscopy to study the electronic structure of epitaxially grown $(\text{Bi,Sb})_2\text{Te}_3$ thin films at nanoscale. We study Landau levels (LLs) to determine the effect of disorder on the quasiparticle lifetime as well as the position of the Dirac point with respect to the Fermi energy. A plot of the LL peak widths shows that despite the disorder, the quasiparticle lifetime is not significantly degraded. We further determine that the ideal Sb concentration to place the Fermi energy to within a few meV of the Dirac point is $x \sim 0.7$ but that post-annealing temperatures can have a significant effect on the crystallinity and Fermi level position. Specifically, high post-growth annealing temperature results in better crystallinity and surface roughness, but also produces a larger Te defect density which adds n-type carriers. Finally, in combination with quasiparticle interference imaging, the dispersion is revealed over a large energy range above the Fermi energy. Interestingly, the surface state dispersion for the $x \sim 0.7$ sample shows great similarity to pristine Bi_2Te_3 . This work provides microscopic information on the role of disorder and composition in determining carrier concentration, surface state dispersion, and quasiparticle lifetime in $(\text{Bi}_{1-x}\text{Sb}_x)_2\text{Te}_3$.

Searching for topological Fermi arcs via quasiparticle interference on a type-II Weyl semimetal MoTe_2

Weyl semimetals display a novel topological phase of matter where the Weyl nodes emerge in pairs of opposite chirality and can be seen as either a source or a sink of Berry curvature. The exotic effects in Weyl semimetals, such as surface Fermi arcs and the chiral anomaly, make them a new playground for exploring novel functionalities. Further exploiting their potential applications requires clear understanding of their topological electronic properties, such as Weyl points and Fermi arcs. In this work we carried out Fourier transform scanning tunneling spectroscopy (FT-STs) study on a type-II Weyl semimetal candidate MoTe_2 . By comparing our experimental data with first-principles calculations, we are able to identify the origins of the multiple scattering channels. Our calculations also show the existence of both trivial and topological arc like states above the Fermi energy. The FT-STs data show strong signals from intra-arc scatterings as well as from the scattering between the arc-like surface states and the projected bulk states. A detailed comparison between our experimental observations and calculated results reveals the trivial and non-trivial scattering channels are indistinguishable in this compound. Interestingly, we find that the broken inversion symmetry in this system changes the terminating states on the two inequivalent surfaces, which in turn changes the relative strength of the scattering channels observed in the FT-STs images on the two surfaces.

Superconductivity in Weyl systems

We have discovered superconductivity in a type-2 doped Weyl semimetal (MoTe_2) (Fig. 1) and carried out the first STM work on a superconducting type 2 Weyl system. The gap size Δ is 0.14meV with a T_c of 0.8K . The $2\Delta/k_B T_c \sim 4.4$ slightly larger than the 3.5 expected for weak coupling. We see clear isotropic vortices in the sample (Fig. 1). From our data the coherence length is about 60nm . We further find that doping shifts the Weyl points towards the Fermi energy. However, the higher energy states remain unperturbed. This system a potential candidate Weyl superconductor if we break time reversal symmetry.

Probing the superconducting order parameter in Sr_2RuO_4 by Bogoliubov quasiparticle interference

Sr_2RuO_4 is one of the only materials with evidence for unconventional triplet superconductivity. In this work we collaborated with the Davis group to measure the gap symmetry by measuring the Bogoliubov QPI patterns. Fig. 2 shows the first Bogoliubov QPI data $g(q,E)$ measured as the energy is varied from outside the gap ($400\mu\text{eV}$) to $0\mu\text{eV}$ (inside the gap) at $T \sim 100\text{mK}$. As the energy decreases, we observe a contour whose shape is consistent with the beta band change into something that looks like just alpha band. We find that the contour changes from what looks like a straight line to a concave contour which is consistent with gap minima along $(1,1)$.

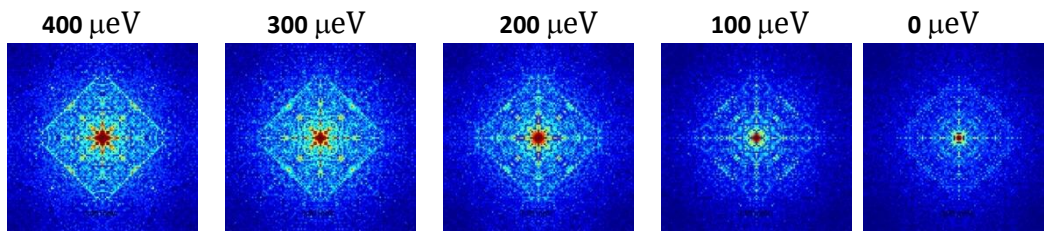


Fig. 2. 100mK Fourier transform Quasiparticle scattering data in the superconducting state of Sr_2RuO_4 . The evolution of the QPI pattern from outside the gap ($>300\mu\text{eV}$) to inside ($<300\mu\text{eV}$) is shown. This data was analyzed to obtain $|\Delta_{\text{SC}}(k)|$ for Sr_2RuO_4 .

Future Plans

We plan to develop back-gated STM to create and study phase transitions and emergent states realized by tuning the position of the Fermi energy. We plan to study interacting systems which host interesting phases such as Mott insulators, superconductors, and charge density wave systems. We will address questions such as: how does the ground state of the system change as

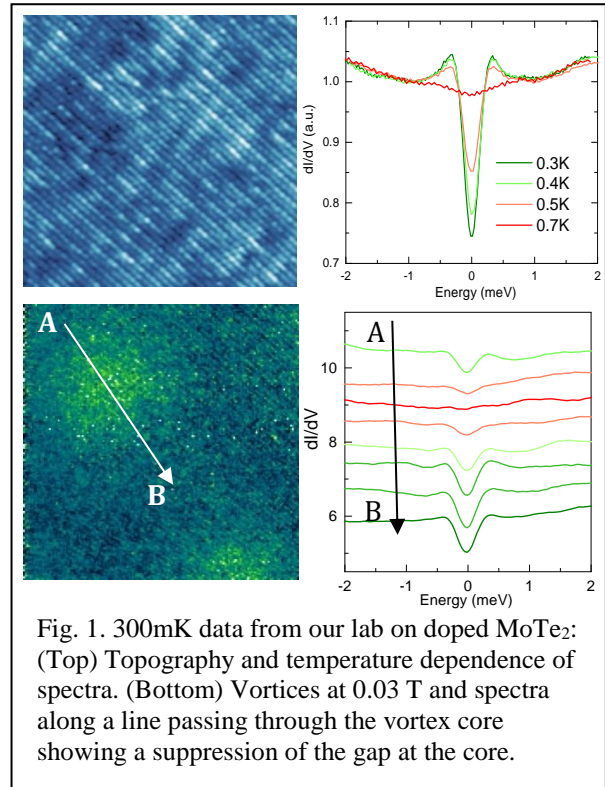


Fig. 1. 300mK data from our lab on doped MoTe_2 : (Top) Topography and temperature dependence of spectra. (Bottom) Vortices at 0.03 T and spectra along a line passing through the vortex core showing a suppression of the gap at the core.

the Fermi energy (E_F) is moved across the bands? This sensitivity of ground states to Fermi level position is not only determined by changes in the carrier concentration but also by many other factors such as the shape of the Fermi surface, the orbital nature of the bands etc., and is even more pronounced in materials with many competing phases. Establishing the methodology to perform back-gated STM on a large range of materials will give us a powerful control knob to position E_F into the most interesting regimes, which will allow us to explore and understand interactions effects. Gating will provide access to phase transitions at low temperatures, which will in turn allow us to leverage the powerful techniques of quasiparticle interference and Landau level spectroscopy with high-energy resolution to obtain critical information phase transitions in complex systems. To carry out the proposed projects, we will grow thin films of materials whose ground state properties are susceptible to being tuned by gating due to their complex band structure. This will allow us to explore the physical properties of these materials in the most interesting regimes. We will study the predicted dramatic effects as the E_F is moved into a high density of states region such as Van Hove singularity or the $n=0$ Landau level. Our proposed projects will allow us to answer questions such as: what are the new phases that emerge as correlations are strengthened when E_F is moved into a narrow band? Can we see signatures of Mott physics and unconventional superconductivity? How is superconductivity in these new Mott systems similar or different from the cuprates?

Publications

1. Searching for topological Fermi arcs via quasiparticle interference on a type-II Weyl semimetal MoTe_2 , Davide Iaia, Guoqing Chang, Tay-Rong Chang, Jin Hu, Zhiqiang Mao, Hsin Lin, Shichao Yan & Vidya Madhavan, *npj Quantum Materials* 3, 38 (2018)
2. Defect Role in the Carrier Tunable Topological Insulator $(\text{Bi}_{1-x}\text{Sb}_x)_2\text{Te}_3$ Thin Films, Kane L Scipioni, Zhenyu Wang, Yulia Maximenko, Ferhat Katmis, Charlie Steiner, and Vidya Madhavan, *Phys. Rev. B* 97, 125150 (2018)
3. Interplay of orbital effects and nanoscale strain in topological crystalline insulators, Daniel Walkup, Badih Assaf, Kane L Scipioni, R. Sankar, Fangcheng Chou, Guoqing Chang, Hsin Lin, Ilija Zeljkovic, V. Madhavan, *Nature Communications* 9, 1550 (2018)
4. Quasiparticle Interference and Strong Electron-Mode Coupling in the Quasi-One-Dimensional Bands of Sr_2RuO_4 , Zhenyu Wang, Daniel Walkup, Philip Derry, Thomas Scaffidi, Melinda Rak, Sean Vig, Anshul, Kogar, Ilija Zeljkovic, Ali Husain, Luiz H. Santos, Yuxuan Wang, Andrea Damascelli, Yoshiteru Maeno, Peter Abbamonte, Eduardo Fradkin, V. Madhavan, *Nature Physics* 13, 799–805 (2017)

Oxides Surfaces: Unexpected Flexoelectricity and New Phenomena

Laurence D. Marks

**Department of Materials Science and Engineering, Northwestern University
Evanston, IL 60208 USA**

Research Scope

The focus of this effort is: (1) fundamental studies of the atomic and electronic structure of oxides surfaces including new ways to characterize them, and (2) flexoelectric phenomena. Oxides are found in nearly every environment on earth, arising naturally and anthropogenically. This ubiquity has inspired a vast body of work on the structure and properties of oxides in their bulk and thin film forms. However, a comparable comprehensive understanding of oxides surfaces is still lacking. For example, most of the literature where oxides are used as substrates for growth tends to ignore the surface structure beyond an ad-hoc assumption of a simple bulk truncation despite the growing body of literature showing that oxides surfaces exhibit different structures and properties than their bulk counterparts. Over the past 20 years, the PIs group has solved more than 30 different surface reconstructions on bulk and nanoscale oxides surfaces and, via internal collaborations, studied the impact of oxides surfaces on properties such as catalysis.

Flexoelectricity, the electromechanical coupling between strain gradient and polarization, is comparably ubiquitous in oxides and their surfaces, i.e. this property exists in all oxides independent of symmetry¹. It has recently been the focus of much research because of predictions of large nanoscale flexoelectric responses. The PIs group, spurred by a serendipitous in-situ transmission electron microscopy (TEM) observation of flexoelectricity, has begun applying their experimental and theoretical expertise with oxides to this field with the goal of developing a mechanistic understanding of flexoelectricity to improve the efficacy of flexoelectric devices. There are also significant implications in diverse areas of electron microscopy ranging from simple charging to bending of samples in cryo-electron microscopy.

Recent Progress

Over the past two years, our approach of combining experiment with theory to study oxides surfaces and flexoelectricity has led to significant progress on both fronts.

Surface structure of complex oxides

SrTiO₃, the most well-studied perovskite, is a “242” material in which each element has even valence. Consequently, many SrTiO₃ main surfaces are inherently valence neutral. “332” perovskites such as LaAlO₃ and DyScO₃ are almost unexplored, despite their continued use as oxide MBE substrates. Moreover, these materials present additional complexities compared to the prototypical SrTiO₃ including rhombohedral distortions (LaAlO₃), and orthorhombic distortions and correlated 4f electrons (DyScO₃). This raises the question: how do these complexities impact surface structure and properties?

The (110) and (111) surfaces of LaAlO₃ were studied with a combination of TEM, scanning transmission electron microscopy (STEM), x-ray photoelectron spectroscopy (XPS), and density

functional theory (DFT)². Under dry annealing conditions, well-ordered and flat surfaces were prepared. The (110) surface was found to be single layered AlO_x with a (2×1) reconstruction. Unlike the previously solved (3×1) reconstruction on the (110) surface of LaAlO_3 , the (2×1) reconstruction is not hydrated. More work is required to understand the (111) surface, but we do know that it is Al rich.

In addition, the (110) surface of DyScO_3 was studied in detail. After annealing to yield a valence neutral surface, atomic force microscopy (AFM) imaging confirmed a flat surface with monatomic steps and angle-resolved XPS measurements indicated a Sc rich double-layer surface (Figure 1), similar to the well-established double-layer reconstructions on SrTiO_3 (001) [e.g.,³]. DFT calculations were used to determine that the lowest energy structure contained three rows of scandium oxide. This can be understood because the 1×1 (110) surface of DyScO_3 (a *Pbnm* orthorhombic perovskite) is similar to the 2×2 (001) surface of a cubic perovskite.

Via internal collaborations, this knowledge of the structure of DyScO_3 surfaces has been exploited in applications using hydrosol synthesized oxide nanoparticles⁴ as substrates for heterogeneous catalysis with Au or Pt nanoparticles on a family of LnScO_3 materials (Ln=La, Nd, Sm, Gd). All of these show an identical Sc-rich surface structure; further collaborative work is ongoing.

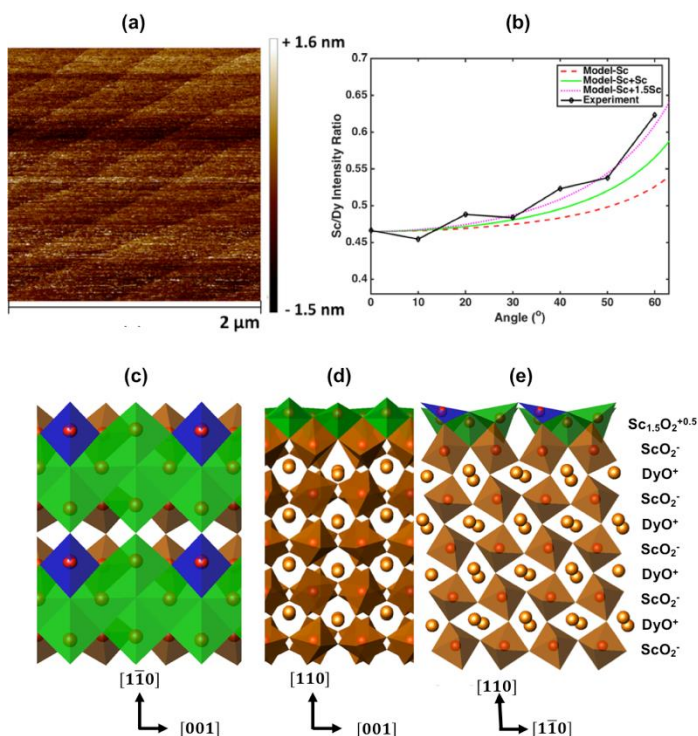


Figure 1. (a) AFM image of a [110] oriented DyScO_3 sample showing flat steps and terraces. (b) Angle resolved XPS experimental data and fit showing the composition of the Sc-rich surface. (c) – (e) DFT relaxed structure of DyScO_3 with 2.5 excess surface ScO_2 in a scandium-rich double layer from three different orientations. ScO_4 tetrahedra are in blue, $\text{ScO}_5[\]$ octahedra with an unoccupied oxygen site are in green and ScO_6 octahedra are in brown.

Electronic structure of lanthanide scandates

In order to understand the lanthanide scandates, it was necessary to explore how to properly treat correlated 4f states within a DFT framework to model electronic properties. To this end, a combination of experimental (XPS, UPS) and theoretical (DFT) approaches were used to study the electronic structure of GdScO_3 , TbScO_3 , and DyScO_3 . XPS spectra simulated from first-principles calculations (Figure 2) using a novel combination of on-site hybrid and GGA+U methods yielded good agreement with experimental spectra⁵. Contrary to previous works, which placed minority 4f states in the band gap or well below the valence band, the minority 4f states were found to be located close to, and in some cases at, the valence band maximum. This suggests that minority 4f electrons may play a larger role in lanthanide scandate properties than previously

thought. More work connecting this to charging and EELS is ongoing.

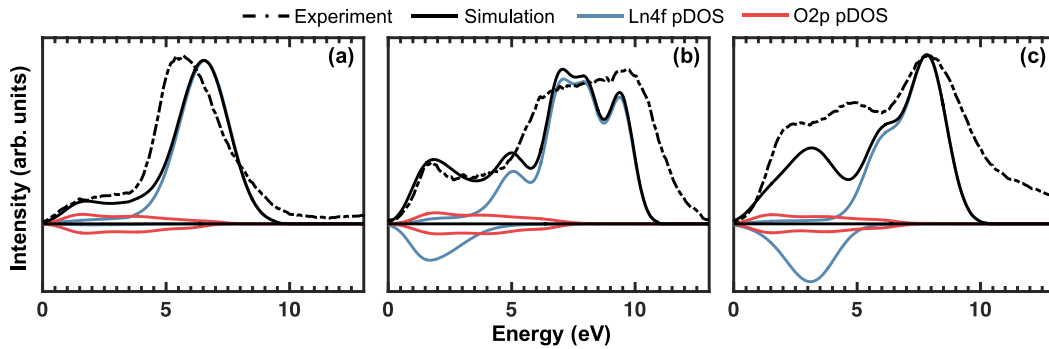


Figure 2. Comparison between experimental (dashed lines) and simulated XPS (solid lines, black) for (a) GdScO₃, (b) TbScO₃, and (c) DyScO₃. The upper and lower panels depict spin up and down pDOS, respectively. The simulations correspond to the sum of the O2p pDOS (solid lines, red), Sc3d pDOS (not shown), and Ln4f pDOS (solid lines, blue) which have been linearly scaled, normalized, and Gaussian broadened. Adapted from Ref 5.

Flexoelectric phenomena in complex oxides

Although there is a growing interest in the flexoelectric effect, since at the nanoscale it is predicted to be very large, there have been no direct observations of flexoelectric bending consistent with current theoretical work. We experimentally demonstrated extraordinarily large, two-dimensional reversible bending at the nanoscale in DyScO₃ (Figure 3) and fully established the origin of the bending as the flexoelectric effect by independently measuring the bulk flexoelectric coefficient⁶.

We showed that these measurements semi-quantitatively agree with in-situ observations and found that the magnitude of bending is limited by the achievable potential as set by the band gap. We thus directly demonstrated that flexoelectric scaling to the nanoscale is valid, and the flexoelectric effect can lead to strains which approach or exceed the nominal yield strength of typical, brittle ceramics.

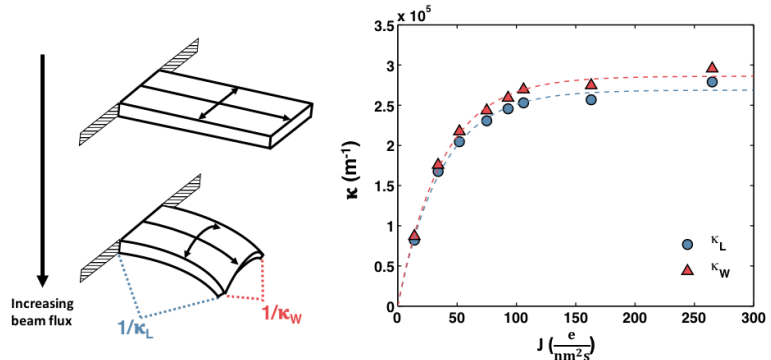


Figure 3. (a) Illustration of a sample bending in response to increasing beam flux. A bent sample exhibits curvature along its length (κ_L) and width (κ_W). (b) Experimental curvature (κ) along the length and width of a DyScO₃ feature is plotted as a function of incident electron beam flux (J). Adapted from Ref 6.

The majority of flexoelectric studies have focused on relatively simple single crystal materials (e.g. SrTiO₃) and ceramics. Twinned crystals such as LaAlO₃ bridge the gap between these two extremes. We found that the flexoelectric response can change by 37% by changing the orientation of a lamellar twin microstructure and by an order-of-magnitude by increasing the temperature to a regime in which twin domain walls are highly mobile (Figure 4). This is the first experimental demonstration of a strong coupling between twin domain microstructure and flexoelectricity.

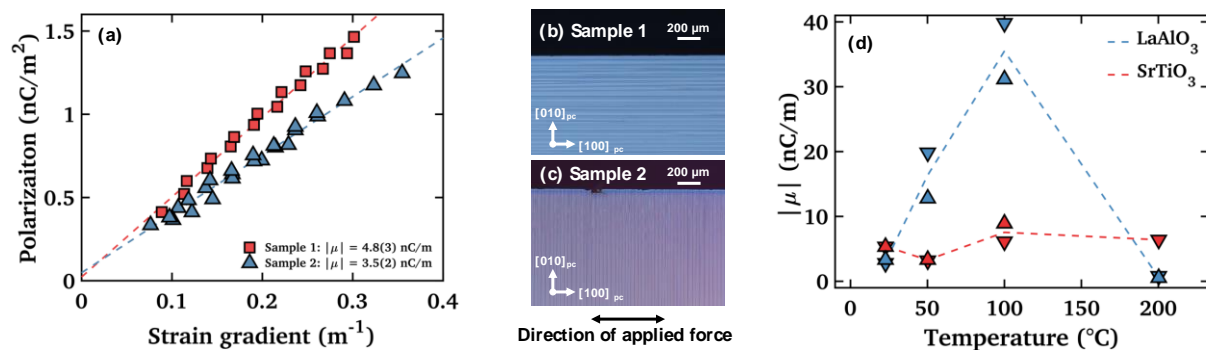


Figure 4. (a) The effective flexoelectric coefficient of $[100]_{pc}$ -oriented LaAlO_3 crystals varies by 37% for samples with lamellar twin microstructures with domain walls oriented (b) perpendicular and (c) parallel to the applied force. (d) Temperature dependent flexoelectric characterization results for $[100]_{pc}$ -oriented LaAlO_3 (blue) and $[100]$ -oriented SrTiO_3 (red) show the flexoelectric response in LaAlO_3 follows the temperature dependence of domain wall mobility, whereas SrTiO_3 exhibits a constant flexoelectric response over this temperature range. Dashed lines denote the average of the two measurements at each temperature.

Future Plans

Moving forward, there remain an abundance of open questions on oxides surfaces. For example, YAlO_3 and other $Pbnm$ perovskites will be studied to separate the complex interactions between octahedral rotations, correlated electrons, spin, and other degrees of freedom at oxides surfaces.

With regard to flexoelectricity, the field is still young and there is much work to be done. A few of the directions that we are currently pursuing are:

- (1) Unraveling the interplay between twins and flexoelectricity, with a particular emphasis on the role of twin domain wall polarity on flexoelectric response with collaborators at ORNL
- (2) Separating the role of octahedral rotations, correlated electrons, spin, and other degrees of freedom in the flexoelectric response of $Pbnm$ perovskites
- (3) Preliminary experimental results on a range of oxides indicate that exceeding the theoretical flexocoupling limit of 10 V seems to be the rule, not the exception. DFT studies are underway to shed light on the origins of this behavior.
- (4) Leveraging our expertise in oxides surfaces to experimentally investigate claims of surface control of flexoelectricity⁷

References

1. Zubko, P.; Catalan, G.; Tagantsev, A. K., Flexoelectric Effect in Solids. *Annual Review of Materials Research* **2013**, *43*, 387-421.
2. Koirala, P.; Steele, E.; Gulec, A.; Marks, L. D., Al rich (111) and (110) surfaces of LaAlO_3 . *Surface Science* **2018**, *677*, 99-104.
3. Erdman, N.; Poepelmeier, K. R.; Asta, M.; Warschkow, O.; Ellis, D. E.; Marks, L. D., The structure and chemistry of the TiO_2 -rich surface of SrTiO_3 (001). *Nature* **2002**, *419* (6902), 55-58.
4. Paull, R. J.; Mansley, Z. R.; Ly, T.; Marks, L. D.; Poepelmeier, K. R., Synthesis of Gadolinium Scandate from a Hydroxide Hydrogel. *Inorganic Chemistry* **2018**, *57* (7), 4104-4108.
5. Mizzi, C. A.; Koirala, P.; Marks, L. D., Electronic structure of lanthanide scandates. *Physical Review Materials* **2018**, *2*, 025001.
6. Koirala, P.; Mizzi, C. A.; Marks, L. D., Direct Observation of Large Flexoelectric Bending at the Nanoscale in Lanthanide Scandates. *Nano Letters* **2018**, *18*, 3850-3856.
7. Stengel, M., Surface control of flexoelectricity. *Physical Review B* **2014**, *90* (20), 5.

Publications

1. Koirala, P.; Steel, E.; Gulec, A.; Marks, L. D., Al rich (111) and (110) surfaces of LaAlO₃, *Surface Science* **677**, 99-104 (2018).
2. Mizzi, C. A.; Koirala, P.; Marks, L. D., Electronic structure of lanthanide scandates, *Physical Review Materials* **2**, 025001 (2018).
3. Koirala, P.; Mizzi, C. A.; Marks, L. D., Direct Observation of Large Flexoelectric Bending at the Nanoscale in Lanthanide Scandates, *Nano Letters* **18**, 3850-3856 (2018).
4. Koirala, P.; Mizzi, C. A.; Mansley, Z. R.; Marks, L. D., Sc-rich (110) surfaces of DyScO₃, GdScO₃, and TbScO₃, *in preparation*.
5. Mizzi, C. A.; Guo, B.; Marks, L. D., Flexoelectricity and twin domains in LaAlO₃, *in preparation*.
6. Koirala, P.; Gulec, A.; Mizzi, C. A.; Long, E.; Marks, L. D., Valence band electron energy loss spectroscopy of charged DyScO₃, *in preparation*.
7. Mansley, Z. R.; Paull, R. J.; Mizzi, C. A.; Poeppelmeier, K. R.; Marks, L. D., (110) surfaces of lanthanide scandate nanoparticles prepared by hydrosol synthesis, *in preparation*.

Advancing *In Situ* Analytical Electron Microscopy for Probing Dynamic Nano-Scale Solid State Electrochemistry

PI: Dr. Y. Shirley Meng University of California San Diego

Research Scope

The goal of this work is to develop characterization techniques to explore the dynamics of solid-solid interfaces in electrochemical systems. This includes developing *in situ* transmission electron microscopy (TEM) methodologies, nanobattery preparation techniques, and novel amorphous solid electrolytes for thin film and nanobattery applications. Advances include developed chemical and structural views of interfacial impedance at the LiCoO₂ (LCO)/lithium phosphorus oxynitride (LiPON) interface. Compliant behavior of LiPON is discovered through advanced nanoindentation, questioning commonly accepted metrics for prevention of lithium dendrite penetration. We have developed a novel amorphous lithium lanthanum titanate (a-LLTO) electrolyte, showing high ionic conductivity and low electron beam sensitivity. Focused ion beam (FIB) nanobattery preparation and *in situ* biasing methodologies were fully documented and disseminated in a video journal format, and robustness of nanobatteries was enhanced. These results have advanced one of the few existing *in situ* methods of characterizing solid-solid interfaces. Current efforts look to further preserve materials during preparation and analysis using cryogenic focused ion beam (cryo-FIB) and cryogenic transmission electron microscopy (cryo-TEM), driving a new frontier of characterization of the fundamentally important Li/solid-electrolyte interface.

Recent Progress

1. Elucidating root causes of interfacial impedance: Our previous work, first demonstrating the application of *in situ* scanning transmission electron microscopy/electron energy loss spectroscopy (STEM/EELS) of a FIB prepared solid state nanobattery, uncovered the nature of the interface between LCO and LiPON; this work highlighted the importance of *in situ* cycling, clearly demonstrating the presence of highly oxidized cobalt otherwise undetectable.¹ Following up on this critical result, LCO/LiPON/Li full cells were cycled at room temperature and at 80 °C to isolate the source of modified interfacial impedance. Interestingly, cells cycled at 80 °C showed steadily increasing charge transfer impedance via electrochemical

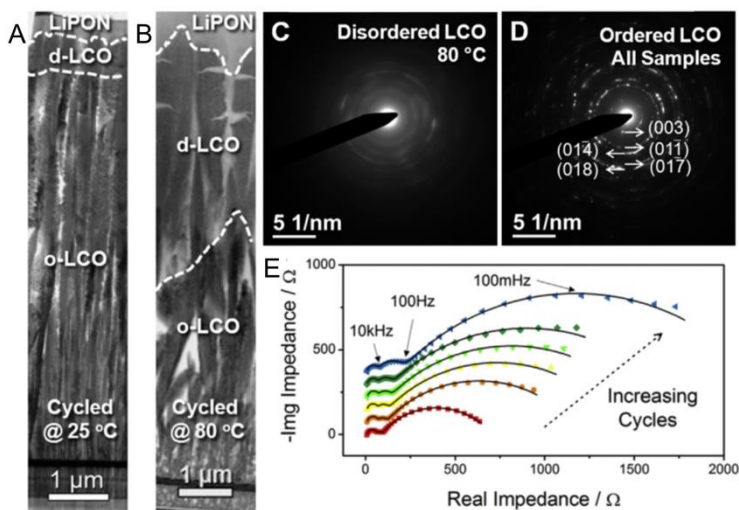


Figure 1. TEM bright field and diffraction patterns of the d-LCO interface cycled at (A) room temperature and (B,C) 80 °C, showing growth of the d-LCO when cycled at elevated temperatures, correlating with EIS measurements (E).

impedance spectroscopy (EIS). Application of TEM to the LCO/LiPON interface clearly showed the presence of a growing disordered interphase (d-LCO) with cycle number, also growing while held at a high state of charge. Interphase thickness was correlated to the increased charge transfer impedance measured via EIS (Figure 1).

Prior to *in situ* TEM testing of LNMO/LiPON/a-Si, the *in situ* FIB procedure was modified for general use across FIB dual beam systems. Preparation of thin film nanobatteries contains many nuances, and the community could benefit from explicit instruction during the procedure. These factors motivated the publishing of a video journal article, clearly describing the technique step-by-step; this should prove both informative and streamline future *in situ* exploration with the technique. A schematic summary is shown in Figure 2.

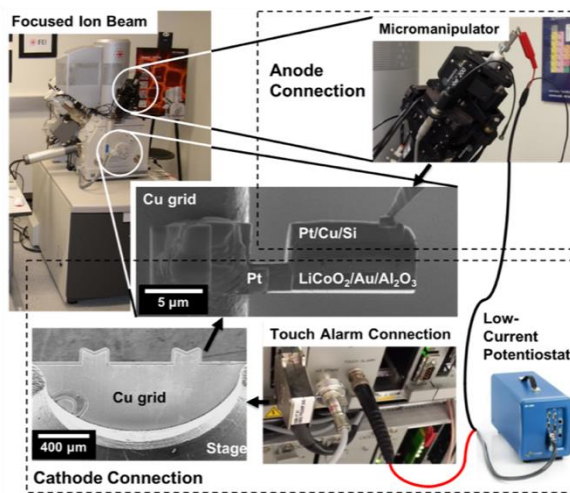


Figure 2. Schematic of electrical connections required for *in situ* FIB biasing.

2. Characterization and development of thin film solid electrolytes: Despite its low ionic conductivity, LiPON remains popular due to its remarkable stability against lithium metal anodes. To explore mechanical properties under environmental isolation, LiPON was mechanically probed using a novel form of nanoindentation, submerging the testing surface in mineral oil. Results of isolated nanoindentation showed reduced modulus results ranging from 200-400 MPa—in stark contrast to previous measurements of approximately 80 GPa.³ When samples were exposed to ambient air and measured, nanoindentation yielded results notably similar to those observed in the past. EDX, EELS, and XPS were performed to examine the surface chemistry showing the surface was dominated by the presence of lithium carbonate (Figure 3), emphasizing the importance of environmental isolation. These results suggest that mechanical rigidity is not as critical a factor as mentioned in past work.

LiPON, although the most popular thin film electrolyte, suffers from low ionic conductivity

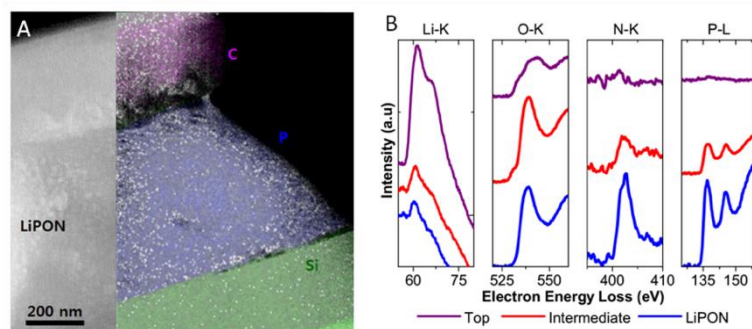


Figure 3. (A) TEM image with EDX elemental mapping, and (B) EELS Li K-edge, O-K-edge, N-K-edge, and P-L_{2,3} edge from different regions of reacted LiPON.

($\sim 10^{-6}$ S/cm) and is susceptible to electron beam damage in the TEM.⁴ Further, with many crystalline solid oxide electrolytes susceptible to lithium dendrite penetration at grain boundaries, mechanical homogeneity is looked to as one form of dendrite growth prevention. Amorphous lithium lanthanum titanate (a-LLTO) was explored

using pulsed laser deposition (PLD). The a-LLTO was characterized via STEM-EELS, showing the expected composition and structure, and temperature controlled EIS, showing conductivity on the order of 10^{-4} S/cm. Interestingly, the film cross-section appeared to be largely unaffected by the electron beam, showing no signs of mechanical or chemical degradation—such a material would be an ideal candidate for future exploration of electrode and interface dynamics via STEM/EELS, and will be further explored.

3. Thin film battery fabrication for new interface chemistries:

To explore solid-state interfaces beyond LCO/LiPON/a-Si, in house thin film capabilities were developed to enable synthesis of thin films of

spinel $\text{LiMn}_{1.5}\text{Ni}_{0.5}\text{O}_4$ (LNMO) via PLD, LiPON solid electrolyte, and amorphous silicon anode (a-Si), both by RF sputtering. These components were assembled to fabricate stable LNMO/LiPON/a-Si full cell thin film batteries; cyclability is shown in Figure 4A. Preliminary TEM results show no thermodynamic decomposition of the cathode at the LNMO/LiPON interface (Figure 4B,C), correlating with the high degree of cyclability of similar thin films with lithium anodes, as noted in literature.² *In situ* cycling of LNMO/LiPON/a-Si nanobatteries were demonstrated within the FIB, and *in situ* TEM efforts are currently underway. Further, nanobatteries with LNMO cathodes will serve as ideal lithium sources for dynamic anode studies. LNMO/LLTO showed a stable interface after cycling in half cells, and full cells were fabricated.

4. Technique development to enhance *in situ* characterization techniques:

Our recent demonstration of the stabilization of plated lithium metal⁵ in liquid electrolytes inspired application of cryo-FIB to lithium metal, showing remarkably improved stability. This not only preserves morphology of plated lithium in conventional cells, but has enabled preparation of all solid state batteries

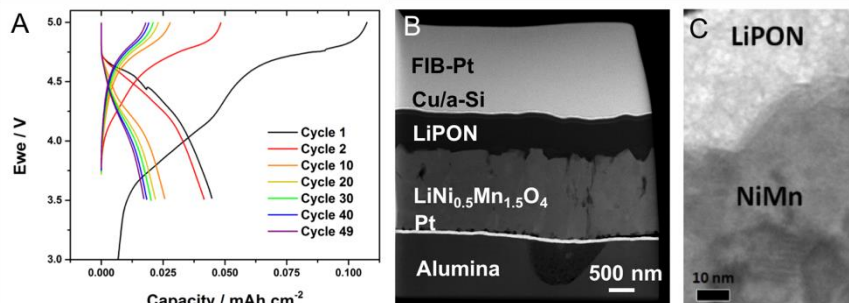


Figure 4. (A) Performance and (B,C) TEM characterization of a LNMO/LiPON/a-Si full cell thin film battery. (C) TEM of the interface showed a stable interface.

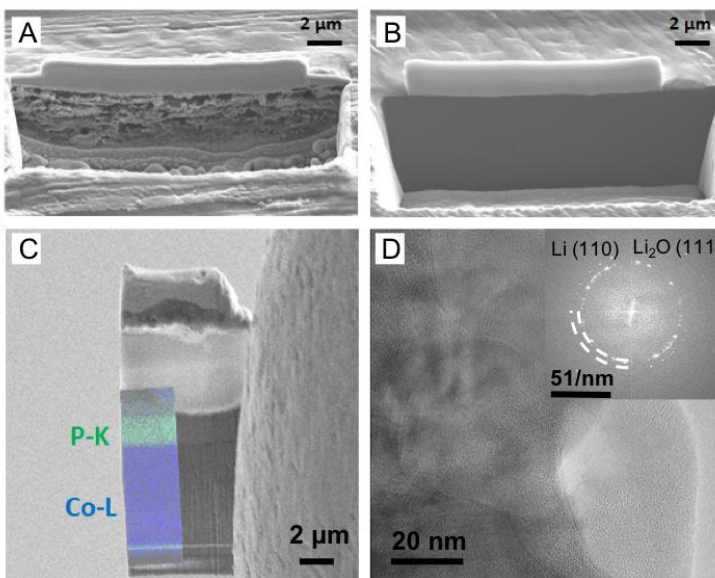


Figure 5. SEM images of cryo-FIB cross sections prepared at (A) room temperature and (B) using cryo-FIB. (C) TEM grid mounted cleaned lamella with EDS elemental mapping, and (D) cryo-TEM of Li-metal with diffraction from Li and Li_2O .

with lithium metal anodes for analysis with cryo-TEM (Figure 5). Figure 5A demonstrates notable degradation of alkali metals under standard room temperature FIB milling, which is mitigated at cryo temperatures. This is an essential step toward characterizing the lithium metal/solid state electrolyte interface.

Future Plans

Having developed robust *in situ* testing configurations, we look to increase the range of materials systems and interfaces, and further increase the range of observable compounds in TEM through incorporation of cryogenic techniques into our *in situ* methodologies. Amorphous LLTO will be applied to full cell geometries, to examine chemical stability and mechanical properties, and will be further explored within *in situ* TEM having demonstrated a high degree of beam resistance. A cryogenic biasing holder is currently in development, incorporating a Faraday cage to enable lower currents for *in situ* electrochemical measurements while preventing beam damage. Continuing development of thin film electrode and electrolyte materials follow, including amorphous lithium lanthanum zirconate and lithium-rich layered oxides, enabling new chemistries.

References

1. Z. Wang, D. Santhanagopalan, W. Zhang, F. Wang, H. L. Xin, K. He, J. Li, N. Dudney and Y. S. Meng, *Nano Lett.*, 2016, **16**, 3760–3767.
2. J. Li, C. Ma, M. Chi, C. Liang and N. J. Dudney, *Adv. Energy Mater.*, 2015, **5**, 2001–2004.
3. E. G. Herbert, W. E. Tenhaeff, N. J. Dudney and G. M. Pharr, *Thin Solid Films*, 2011, **520**, 413–418.
4. D. Santhanagopalan, D. Qian, T. McGilvray, Z. Wang, F. Wang, F. Camino, J. Graetz, N. Dudney and Y. S. Meng, *J. Phys. Chem. Lett.*, 2014, **5**, 298–303.
5. X. Wang, M. Zhang, J. Alvarado, S. Wang, M. Sina, B. Lu, J. Bouwer, W. Xu, J. Xiao, J. G. Zhang, J. Liu and Y. S. Meng, *Nano Lett.*, 2017, **17**, 7606–7612.

Publications

1. J.Z. Lee, Z. Wang, H.L. Xin, T.A. Wynn, and Y.S. Meng, “Amorphous Lithium Lanthanum Titanate for Solid-State Microbatteries”, *Journal of the Electrochemical Society* 164 (2017) A6268.
2. J.Z. Lee, T.A. Wynn, Y.S. Meng, and D. Santhanagopalan, “Focused Ion Beam Fabrication of LiPON-based Solid-state Lithium-ion Nanobatteries for In Situ Testing,” *Journal of Visual Experimentation*, (133), e56259, doi:10.3791/56259 (2018).
3. T.A. Wynn, J.Z. Lee, A. Banerjee, and Y.S. Meng, “In situ and operando probing of buried interfaces in solid-state electrochemical devices”, *Invited Prospective for MRS Bulletin* (2018 in press).
4. S.N. Raja, J.Z. Lee, T.A. Wynn, F.P. McGrogan, T. Swamy, Y.-M. Chiang, Y.S. Meng, and K.J. Van Vliet, “LiPON Solid Electrolyte Stiffens Upon Exposure to Ambient Humidity,” *Advanced Energy Materials* (submitted, under review).
5. J.Z. Lee, T.A. Wynn, J. Alvarado, and Y.S. Meng, “Cryogenic focused ion beam for characterization of alkaline metal anodes,” *ACS Energy Letters* (submitted, under review).

Capturing the Structure and Dynamics of Materials at 4D Atomic Resolution

Jianwei (John) Miao

Department of Physics & Astronomy and California NanoSystems Institute, University of California, Los Angeles, CA 90095-1547

Research Scope

Perfect crystals are rare in nature. Real materials often contain crystal defects such as grain boundaries, dislocations, stacking faults, interfaces, surface reconstructions and point defects. These crystal defects and their dynamics strongly affect material properties and functionality. A major challenge in materials characterization is to determine the 3D atomic positions of crystal defects and monitor their dynamics. To tackle this challenge, Miao and collaborators have developed atomic electron tomography (AET) to image the 3D crystal defects in materials at atomic resolution¹⁻⁴. More recently, we determined, for the first time, the 3D atomic arrangement of chemical order/disorder in an FePt nanoparticle with 22 pm precision⁵. The measured atomic positions and chemical species were used as direct input to quantum mechanical calculations to correlate crystal defects and chemical order/disorder with material properties at the single-atom level⁵. Moreover, using FePt nanoparticles as a model system, we advanced AET to study early stage nucleation at 4D atomic resolution⁶. We monitored the structure and dynamics of the same nuclei undergoing growth, fluctuation, dissolution, merging and/or division. We revealed that each nucleus has a core of maximum order parameter and an order parameter gradient points from the core to the boundary of the nucleus. We observed nucleation dynamics is regulated by the distribution of the order parameter and its gradient. These experimental results cannot be explained by classical nucleation theory (CNT) and to account for them we propose an order parameter gradient (OPG) model⁶. We show the OPG model is more general and thermodynamically more favorable than CNT. In addition to nanoparticles, we have also applied AET to determine the 3D coordinates of individual atoms in Re doped MoS₂ 2D materials with a precision of 16 pm. The experimentally measured 3D atomic coordinates were used as direct input to DFT calculations to correlate the crystal defects with the physical properties of 2D materials at the individual atom level. We anticipate that the series of experiments opens the door to study the structure and dynamics of materials at 4D atomic resolution.

Recent Progress

Deciphering chemical order/disorder and material properties at the single-atom level.

Correlating 3D arrangements of atoms and defects with material properties and functionality forms the core of several scientific disciplines. Using AET, we have determined the 3D coordinates of 6,569 iron and 16,627 platinum atoms in an FePt nanoparticle to correlate 3D atomic arrangements and chemical order/disorder with material properties⁵. We identified rich structural variety and chemical order/disorder including 3D atomic composition, grain boundaries, anti-phase boundaries, anti-site point defects and swap defects. We showed for the

first time that experimentally measured 3D atomic coordinates and chemical species with 22 pm precision can be used as direct input for first-principles calculations of material properties such as atomic magnetic moments and local magnetocrystalline anisotropy⁵.

Capturing nucleation at 4D atomic resolution.

Nucleation plays a critical role in many physical and biological phenomena ranging from crystallization, melting and evaporation to the formation of clouds and the initiation of neurodegenerative diseases⁷. However, nucleation is a challenging process to study especially in the early stage when several atoms/molecules start to form a new phase from its parent phase. Here, we trapped the same nuclei at different annealing times and applied AET to capture the structure and dynamics of the nuclei at 4D atomic resolution⁶

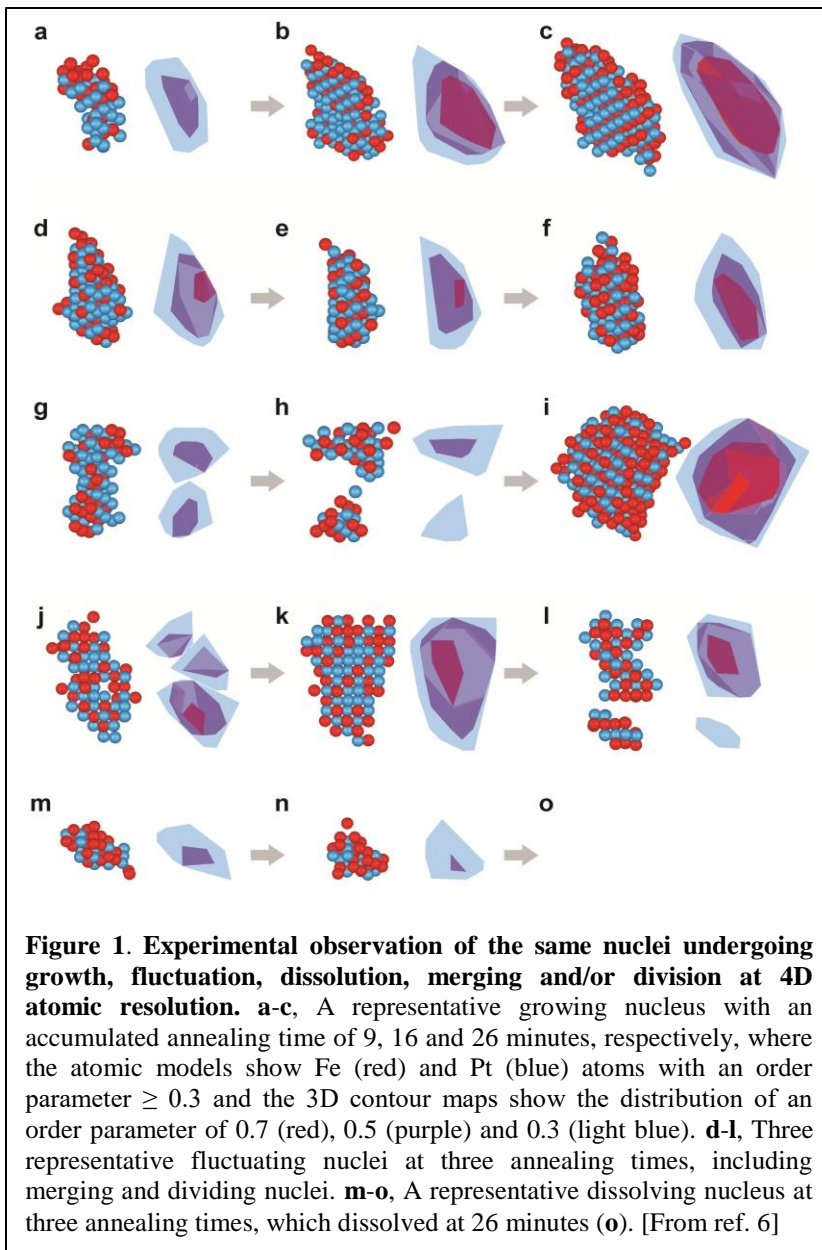


(Fig. 1). We revealed that early stage nuclei are irregularly shaped, each has a core of a maximum order parameter, and an order parameter gradient points from the core to the boundary of the nucleus. We captured the structure and dynamics of the same nuclei undergoing growth, fluctuation, dissolution, merging and/or division (Fig. 1), which are regulated by the distribution of the order parameter and its gradient. These experimental results differ from CNT and to explain them we proposed an OPG model⁶. We further corroborated this model using molecular dynamics simulations of heterogeneous and homogeneous nucleation in the liquid-solid phase transition of Pt. We anticipate that the order parameter gradient model is applicable to different kinds of nucleation processes.

Correlating 3D atomic defects and the physical properties of 2D materials. 2D materials exhibit a wide range of exotic physical properties, such as high and stable carrier mobility, topologically protected surface transport, excellent thermoelectric properties, and tunable electronic structure⁸. These exceptional physical properties enable new frontiers of device technologies, which could overcome fundamental limits in Si-based technology⁹. However, the exotic physical properties of these 2D materials strongly depend on their internal crystal defects such as vacancies, dopants, dislocations, grain boundaries and strain. We have applied AET to determine the 3D coordinates of individual atoms in Re-doped MoS₂ materials. Using a Nion microscope at ORNL operated at 60 keV, we acquired several tomographic tilt series and determined the coordinates of Re, Mo and S atoms in the materials with a 3D precision of 16 pm. We observed 3D vacancies, dopants and ripples in the 2D materials and mapped out the strain tensor. In collaboration with Prof. Narang's group at Harvard, the experimentally measured atomic coordinates were used as direct input to DFT calculations to correlate the 3D defects with physical properties such as the band structure and optical properties at the individual atom level.

Future Plans

Van der Waals heterostructures have been a very active research focus in materials science with the merit of great flexibility in tuning their electronic properties and abundant quantum effects due to low dimensionality and atomically assembled interfaces¹⁰. Novel devices based on van der Waals heterostructures such as tunneling transistors, resonant tunneling diodes, and light-emitting diodes-are also starting to emerge¹¹. Meanwhile, the exotic electronic/optical/mechanical properties of van der Waals heterostructures are extremely sensitive to atomic defects and displacements at the interface. Point defects in van der Waals heterostructures will localize excitons and strongly affect the optical properties, while dislocations on the other hand are expected to provide additional topologically protected modes, which can dominate over the surface transport in the case of disk-shaped geometry¹¹. Moreover, interlayer coupling in van der Waals heterostructures plays an important role in modulating their optical and electronic properties and has triggered abundant research interests¹¹. The capability to precisely determine the 3D coordinates and chemical species of individual atoms combined with *ab initio* calculations will reveal unprecedented details about the correlation between the atomic structure of van der Waals heterostructures and their strain tensor, photoluminescence, electronic conductivity and many other quantum properties. We will probe the 3D structure of van der Waals heterostructures at atomic level with AET. Using the 3D atomic structural information as a direct input, *ab initio* calculation can further reveal the structure-property relation regarding the interface structure and corresponding quantum optical/electronic properties. This success of this project may improve our basic understanding of van der Waals heterostructures and provide guidance of various related studies.

Ferroelectricity has found broad application ranging from actuators, non-volatile memory devices and field effect transistor to sensors and energy harvesting devices¹². In recent years, the research frontier of ferroelectricity has been the spatial downscaling of ferroelectric materials to the nano-architecture regime, aiming for a significant enhancement of device efficiency^{13,14}. However, since ferroelectric properties are strongly related to the size and dimensionality as well

as their polar nature, it is challenging to fully utilize them in nanoscale devices without a comprehensive understanding of the low-dimensional behavior of ferroelectrics. We will apply AET to determine the 3D atomic coordinates of $\text{Pb}(\text{Zr}_{0.5}\text{Ti}_{0.5})\text{O}_3$ (PZT) nanoparticles. Tomographic tilt series will be acquired using the TEAM microscopes at NCEM and the 3D reconstruction, atom tracing and data analysis will be performed at UCLA. The large Z contrast among the cations in PZT (Pb: 82, Zr: 40, Ti: 22) provides the best chance of successfully determining the atom species with AET. Ferroelectric polarizations will be obtained from relative displacements between cations within the perovskite unit cell. The cation displacement is expected to be about 30 pm for PZT¹⁵, which is within the capability of the AET method.

References

1. J. Miao, P. Ercius & S. J. L. Billinge. Atomic electron tomography: 3D structures without crystals. *Science* **353**, aaf2157 (2016).
2. M. C. Scott et al. Electron tomography at 2.4-ångström resolution. *Nature* **483**, 444–447 (2012).
3. C. C. Chen et al. Three-dimensional imaging of dislocations in a nanoparticle at atomic resolution. *Nature* **496**, 74–77 (2013).
4. R. Xu et al. Three-Dimensional Coordinates of Individual Atoms in Materials Revealed by Electron Tomography. *Nature Mater.* **14**, 1099–1103 (2015).
5. Y. Yang et al. Deciphering chemical order/disorder and material properties at the single-atom level. *Nature* **542**, 75–79 (2017).
6. J. Zhou et al. Capturing nucleation at 4D atomic resolution. arXiv:1807.10709 (2018).
7. K. F. Kelton & A. L. Greer. *Nucleation in Condensed Matter: Applications in Materials and Biology*. (Pergamon, 2010).
8. A. K. Geim & K. S. Novoselov. The rise of graphene. *Nature Mater.* **6**, 183–191 (2007).
9. S. Z. Butler et al. Progress, challenges, and opportunities in two-dimensional materials beyond graphene. *ACS Nano* **7**, 2898–2926 (2013).
10. A. K. Geim & I. V. Grigorieva. Van der Waals heterostructures. *Nature* **499**, 419–425 (2013).
11. K. S. Novoselov et al. 2D materials and van der Waals heterostructures. *Science* **353**, aac9439 (2016).
12. J. Varghese et al. Ferroelectric nanoparticles, wires and tubes: synthesis, characterisation and applications. *J. Mater. Chem. C* **1**, 2618–2638 (2013).
13. I. I. Naumov, L. Bellaiche & H. Fu. Unusual phase transitions in ferroelectric nanodisks and nanorods. *Nature* **432**, 737–740 (2004).
14. M. J. Polking et al. Ferroelectric order in individual nanometre-scale crystals. *Nature Mater.* **11**, 700–709 (2012).
15. C.-L. Jia et al. Atomic-scale study of electric dipoles near charged and uncharged domain walls in ferroelectric films. *Nature Mater.* **7**, 57–61 (2008).

Publications

1. Y. Yang, C.-C. Chen, M. C. Scott, C. Ophus, R. Xu, A. Pryor Jr, L. Wu, F. Sun, W. Theis, J. Zhou, M. Eisenbach, P. R. C. Kent, R. F. Sabirianov, H. Zeng, P. Ercius and J. Miao,

- “Deciphering chemical order/disorder and material properties at the single-atom level”, *Nature* **542**, 75-79 (2017).
2. J. Miao, P. Ercius and S. J. L. Billinge, “Atomic electron tomography: 3D structures without crystals”, *Science* **353**, aaf2157 (2016). (Review)
 3. Y. H. Lo, L. Zhao, M. Gallagher-Jones, A. Rana, J. Lodico, W. Xiao, B. C. Regan and J. Miao “In situ coherent diffractive imaging”, *Nat. Commun.* **9**, 1826 (2018).
 4. J. Zhou, M. Taylor, G. A. Melinte, A. J. Shahani, C. C. Dharmawardhana, H. Heinz, P. W. Voorhees, J. H. Perepezko, K. Bustillo, P. Ercius and J. Miao, “Quantitative characterization of high temperature oxidation using electron tomography and energy-dispersive X-ray spectroscopy”, *Sci. Rep.* **8**, 10239 (2018).
 5. A. Pryor, Jr., Y. Yang, A. Rana, M. Gallagher-Jones, J. Zhou, Y. H. Lo, G. Melinte, W. Chiu, J. A. Rodriguez and J. Miao “GENFIRE: A generalized Fourier iterative reconstruction algorithm for high-resolution 3D imaging”, *Sci. Rep.* **7**, 10409 (2017).
 6. A. Pryor Jr., C. Ophus and J. Miao, “A streaming multi-GPU implementation of image simulation algorithms for scanning transmission electron microscopy”, *Adv. Struct. Chem. Imag.* **3**, 15 (2017).
 7. M. Gallagher-Jones, C. S. Baraldi-Dias, A. Pryor, Jr., K. Bouchmella, L. Zhao, Y. H. Lo, M. B. Cardoso, D. Shapiro, J. Rodriguez and J. Miao, “Correlative cellular ptychography with functionalized nanoparticles at the Fe L-edge”, *Sci. Rep.* **7**, 4757 (2017).
 8. B. D.A. Levin, E. Padgett, C.-C. Chen, M. C. Scott, R. Xu, W. Theis, Y. Jiang, Y. Yang, C. Ophus, H. Zhang, D.-H. Ha, D. Wang, Y. Yu, H. D. Abruña, R. D. Robinson, P. Ercius, L. F. Kourkoutis, J. Miao, D. A. Muller and R. Hovden, “Nanomaterial datasets to advance tomography in scanning transmission electron microscopy”, *Sci. Data* **3**, 160041 (2016).
 9. B. Leshem, R. Xu, Y. Dallal, J. Miao, B. Nadler, D. Oron, N. Dudovich and O. Raz, “Direct single-shot phase retrieval from the diffraction pattern of separated objects”, *Nature Commun.* **7**, 10820 (2016).
 10. M. Gallagher-Jones, J. A. Rodriguez and J. Miao, “Frontier Methods in Coherent X-ray Diffraction for High-Resolution Structure Determination”, *Q. Rev. Biophys.* **49**, e20 (2016).
 11. J. Zhou, Y. Yang, Y. Yang, D. S. Kim, A. Yuan, X. Tian, C. Ophus, F. Sun, A. K. Schmid, M. Nathanson, H. Heinz, Q. An, H. Zeng, P. Ercius & Jianwei Miao. “Capturing nucleation at 4D atomic resolution”, arXiv:1807.10709 (2018).
 12. M. Nathanson, K. Kanhaiya, A. Pryor, Jr., J. Miao and H. Heinz, “Atomic Scale Structure and Deformation in Au-Pd Cubic Core-Shell Nanoparticles”, submitted.

Imaging of Topological Textures and Their Order Parameters enabled by a new generation of high-dynamic-range, momentum-resolved STEM detectors

David A. Muller¹, Craig J. Fennie¹, Darrell G. Schlom¹

¹Cornell University, Ithaca, NY 14853

Research Scope

Materials that couple electric and magnetic ordering create interesting possibilities for the next generation of data storage technologies. However, there are few of these multiferroic materials that exist at room temperature, and even fewer with strong, coupled polarization and magnetization. One promising avenue to develop these materials is through oxide molecular beam epitaxy, which can generate new combinations of properties through heterostructures and interface phases. Here, hexagonal rare earth ferrites and manganites offer a promising but relatively unexplored area for multiferroic materials design, and we have recently demonstrated magnetoelectric coupling up to 320 K in this system[1].

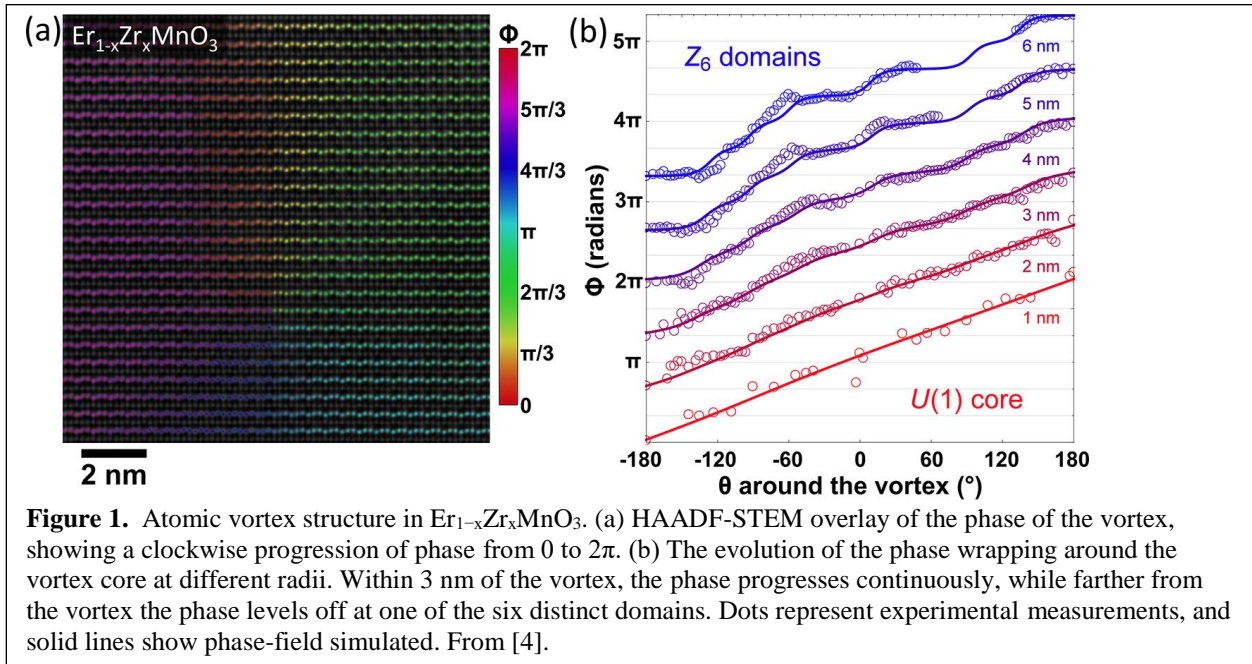
Diverse topological defects arise in these hexagonal systems, such as ferroelectric vortices, as well as neutral and charged domain walls. The topological defects are intriguing because their low symmetry enables unusual couplings between structural, charge, and spin degrees of freedom, holding great potential for novel types of functional 2D and 1D systems. Our goal here is to understand the presence, and nature of these defects, and especially how their behavior deviates from the bulk crystal case in the confined geometry of these layered films.

To do so, we have employed picometer-precision scanning transmission electron microscopy to image the inner structure of these topological defects, and developed a new approach for a 4-dimensional diffractive imaging to quantitatively image the physical properties of the complex magnetic and polarization textures - polarity, toroidal order and the local energy landscape – giving us multiple natural order parameters of the system. All of this is enabled by the high-speed (0.86 ms readout), high-dynamic-range ($10^6:1$) electron microscope pixel array detector (EMPAD) [2] developed at Cornell which acts as a universal detector and captures the full, and unsaturated convergent beam electron diffraction (CBED) pattern at every scan position. We have already used this detector elsewhere to demonstrate a world-record spatial resolution of better than 0.39 Å [3] at 80 keV, more than doubling the resolution of our microscope.

Here we will describe how these order parameters can be mapped with a higher precision than by traditional electron microscopy methods, in many cases simultaneously with structural and field information, and under conditions where direct imaging fails. This includes the tilts that occur to accommodate ferroelectric domains and the random orientations of nanoparticles. Our approach for measuring strains in such randomly oriented systems is more broadly applicable, including correlating catalytic activity with core-shell nanoparticle structures and other energy applications.

Recent Progress

Our approach to producing strongly-coupled room-temperature multiferroics was to grow epitaxial superlattices that combine the ferroelectric hexagonal LuFeO_3 with the ferrimagnetic LuFe_2O_4 using oxide molecular beam epitaxy [1]. While these lutetium ferrite superlattices demonstrated magnetoelectric coupling up to 320 K, for device applications we are also seeking



materials that have stronger magnetism well above room temperature. Here, we use a similar technique to combine h- LuFeO_3 with cubic spinel ferrites, such as CoFe_2O_4 which has a ferrimagnetic moment up to 860 K. domain walls host a variety of emergent behavior, such as conductivity and magnetism, due to their local symmetry breaking and electronic reconstruction.

Despite the considerable advances in analyzing the different topological defects in hexagonal manganites, the understanding of their key intrinsic properties is still rather limited and disconnected. In particular, a rapidly increasing number of structural variants are reported without clarifying their relation, leading to a zoo of seemingly unrelated topological textures. Here, we combine picometer-precise scanning-transmission-electron microscopy with Landau theory modeling to clarify the inner structure of topological defects in $\text{Er}_{1-x}\text{Zr}_x\text{MnO}_3$ [1]. By performing a comprehensive parametrization of the inner atomic defect structure, we demonstrate that one primary length scale drives the morphology of both vortices and domain walls. Our findings lead to a unifying general picture of this type of structural topological defects. We further derive novel fundamental and universal properties, such as unusual bound-charge distributions and electrostatics at the ferroelectric vortex cores with emergent $U(1)$ symmetry (Figure 1).

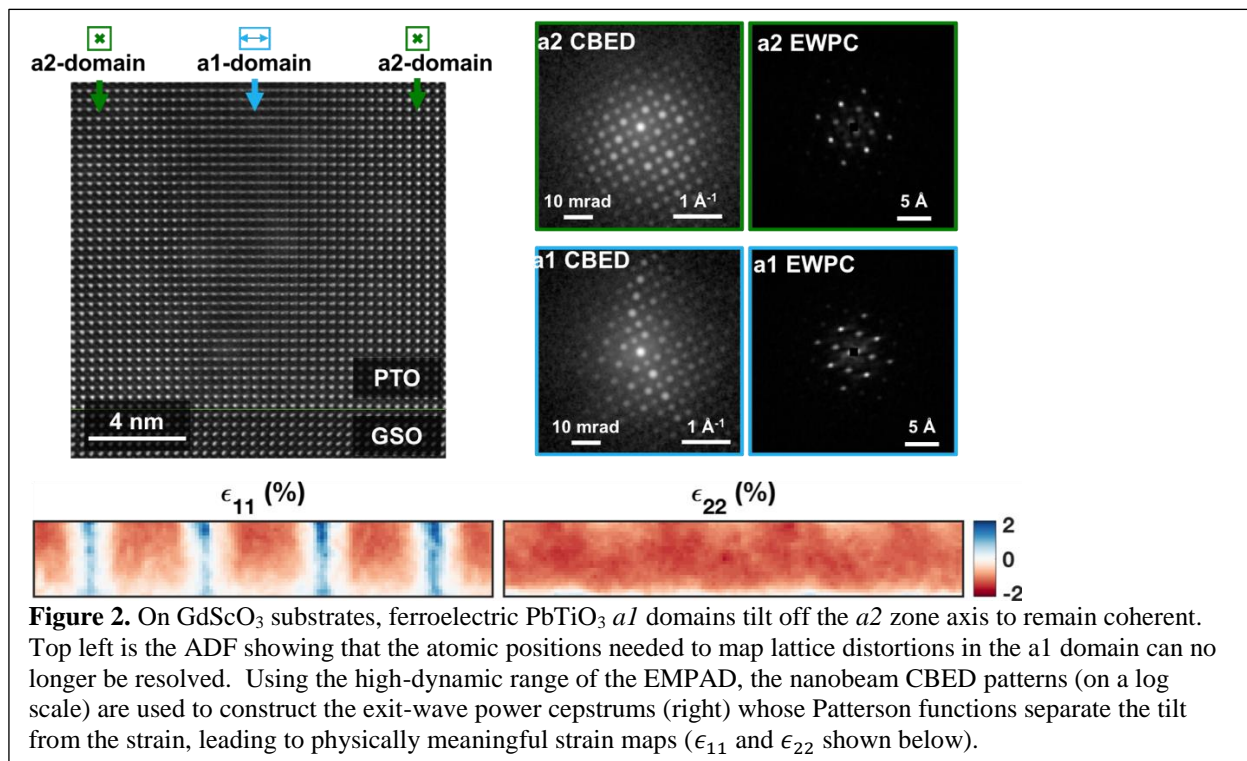
Next we show that charged ferroelectric domain walls in multiferroic $(\text{LuFeO}_3)_m/(\text{LuFe}_2\text{O}_4)$ superlattices are confined reproducibly due to charge compensation in the two layers. We explore how confinement affects the width of these domain walls and the ferroelectricity of the superlattice by mapping the order parameter with atomic resolution scanning transmission electron microscopy. We find the domain wall shrinks with the confinement width, indicating electrostatics play a role in determining domain wall width. As the walls are increasingly confined, ferroelectricity is suppressed, and we observe a coexistence of potential energy surfaces that explained expected by Landau theory.

To obtain information over larger length scale, convergent beam electron diffraction (CBED) a powerful tool for rapid, spatially resolved characterization of lattice structure over a wide range of length scales. However, to extract useful structural information from the large 4-dimensional datasets, especially for complex, 3D specimens, we must confront general

challenges with CBED intensity variations due to crystal mistilts and multiple scattering as well as challenges with precisely localizing diffracted disk centers. Applying physically motivated transformations can improve the interpretability of scanning diffraction data and reduce its sensitivity to unwanted artifacts. By computing the power cepstrum of the exit wave we separate the effects of mistilt from the underlying lattice information. The exit wave power cepstrum (EWPC) provides an effective basis for component analysis of specimens with large mosaic spreads and mistilts caused by crystal interfaces and defects (Figure 2).

The EWPC space is effective for quantitative measurement of lattice distortions. In the EWPC space, the signal can be viewed as a weighted Patterson function, with localized peaks corresponding to lattice spacings. By fitting these peaks, the lattice parameters, rotation, and strain can be extracted in maps at sub-nanometer spatial resolution with ~ 1 ms/pixel dwell time.

We analyze the strain and domain structure in epitaxial films of PbTiO_3 which is strained to different degrees by different scandate substrates. The PbTiO_3 accommodates the strain by altering its ferroelectric domain structure, where the long axis of the tetragonal unit cell orients either in the growth direction (c -domain) or in one of the in-plane directions (a_1 or a_2 domains). By fitting peaks in the EWPC, we can extract the lattice constant in the growth direction $[001]$, and in the film plane, as well as the lattice rotation and shear strain. These maps show the



Future Plans

As is well-known, materials properties are intimately connected to the symmetry they display (or not display), e.g., a material can't display an electrical polarization if inversion symmetry is present, nor could it display a magnetization if it has time-reversal symmetry. While the physics of such magnetoelectric effects in *electrical insulators* has been intensely studied and made clear the last twenty years, including the development of materials design strategies, much less is known about *magnetoelectric metals* (by which we mean, metals which lack both inversion and time-reversal symmetries). It is well-known that ferromagnetic metals display both interesting

transport and optical properties, the anomalous Hall and intrinsic Faraday effects respectively, due to breaking of time-reversal symmetry by magnetic order. Also, the lack of inversion symmetry in non-centrosymmetric metals (which we will refer to as polar, even though a polarization is absent in a metal) is known to lead the property of optical activity. Recently there has been a renewed interest in the transport properties of such polar materials for their topological properties, where various "gyrotropic" effects have been observed such as the spin-hall effect or have been predicted such as the gyrotropic magnetic effect and the dynamical (magneto)piezoelectric effects. However, what is missing in all of this recent activity is an understanding of how to take the known (somewhat abstract) theoretical predictions and turn them into a simple chemically and physically intuitive the "design rules" and synthesis strategies. Indeed, materials realizations of polar metals (no less magnetoelectric metals), that also have large spin-orbit coupling, are scarce.

We have identified materials systems which should be amenable to our materials-by-design loop approach, where properties can be designed *in-silico*, executed by MBE synthesis, and whose structure, symmetry and order parameters can be quantitatively mapped using our unique EMPAD detector technology.

References

1. J.A. Mundy, C.M. Brooks, M.E. Holtz, J.A. Moyer, H. Das, A.F. Rébola, J.T. Heron, J.D. Clarkson, S.M. Disseler, Z. Liu, A. Farhan, R. Held, R. Hovden, E. Padgett, Q. Mao, H. Paik, R. Misra, L.F. Kourkoutis, E. Arenholz, A. Scholl, J.A. Borchers, W.D. Ratcliff, R. Ramesh, C.J. Fennie, P. Schiffer, D.A. Muller, and D.G. Schlom, "Atomically Engineered Ferroic Layers Yield a Room-Temperature Magnetoelectric Multiferroic," *Nature* **537** (2016) 523–527.
2. Tate, M. W., P. Purohit, D. Chamberlain, K. X. Nguyen, R. Hovden, C. S. Chang, P. Deb, E. Turgut, J. T. Heron, D. G. Schlom, D. C. Ralph, G. D. Fuchs, K. S. Shanks, H. T. Philipp, D. A. Muller, and S. M. Gruner. "High Dynamic Range Pixel Array Detector for Scanning Transmission Electron Microscopy" *Microscopy and Microanalysis* **22**, (2016), 237–249.
3. Jiang, Y., Z. Chen, Y. Han, P. Deb, H. Gao, S. Xie, P. Purohit, M. W. Tate, J. Park, S. M. Gruner, V. Elser, and D. A. Muller. "Electron Ptychography of 2D Materials to Deep Sub-Ångström Resolution" *Nature* **559**, (2018), 343–349.
4. M.E. Holtz, K. Shapovalov, J.A. Mundy, C.S. Chang, Z. Yan, E. Bourret, D.A. Muller, D. Meier, and A. Cano, "Topological Defects in Hexagonal Manganites: Inner Structure and Emergent Electrostatics," *Nano Letters* **17** (2017) 5883–5890.
5. Elliot Padgett, Paul Cueva, Megan Holtz, Eric Langenberg, Dong Re, Héctor D. Abruñ, Darrell Schlom, and David A. Muller¹, "Grains and Strains from Cepstral Analysis of 4D-STEM Nano-Diffraction Datasets", *Microscopy and Microanalysis*, **24** (S1), 546-547 (2018). doi:10.1017/S1431927618003227

Publications

6. N.F. Quackenbush, H. Paik, M.J. Wahila, S. Sallis, M.E. Holtz, X. Huang, A. Ganose, B.J. Morgan, D.O. Scanlon, Y. Gu, F. Xue, L.Q. Chen, G.E. Sterbinsky, C. Schlueter, T.-L. Lee, J.C. Woicik, J.-H. Guo, J.D. Brock, D.A. Muller, D.A. Arena, D.G. Schlom, and L.F.J. Piper, “Stability of the M2 Phase of Vanadium Dioxide Induced by Coherent Epitaxial Strain,” *Physical Review B* **94** (2016) 085105.
7. L. Li, J. Britson, J.R. Jokisaari, Y. Zhang, C. Adamo, A. Melville, D.G. Schlom, L.Q. Chen, and X.Q. Pan, “Giant Resistive Switching via Control of Ferroelectric Charged Domain Walls,” *Advanced Materials* **28** (2016) 6574–6580.
8. J.A. Mundy, C.M. Brooks, M.E. Holtz, J.A. Moyer, H. Das, A.F. Rébola, J.T. Heron, J.D. Clarkson, S.M. Disseler, Z. Liu, A. Farhan, R. Held, R. Hovden, E. Padgett, Q. Mao, H. Paik, R. Misra, L.F. Kourkoutis, E. Arenholz, A. Scholl, J.A. Borchers, W.D. Ratcliff, R. Ramesh, C.J. Fennie, P. Schiffer, D.A. Muller, and D.G. Schlom, “Atomically Engineered Ferroic Layers Yield a Room-Temperature Magnetoelectric Multiferroic,” *Nature* **537** (2016) 523–527.
9. M.E. Holtz, J.A. Mundy, C.S. Chang, J.A. Moyer, C.M. Brooks, H. Das, A.F. Rebola, R. Hovden, E. Padgett, C.J. Fennie, P. Schiffer, D. Meier, D.G. Schlom, and D.A. Muller, “Imaging Local Polarization and Domain Boundaries with Picometer-Precision Scanning Transmission Electron Microscopy,” *Microscopy and Microanalysis* **22** (2016) 898–899.
10. W. Wang, J.A. Mundy, C.M. Brooks, J.A. Moyer, M.E. Holtz, D.A. Muller, D.G. Schlom, and W. Wu, “Visualizing Weak Ferromagnetic Domains in Multiferroic Hexagonal Ferrite Thin Film,” *Physical Review B* **95** (2017) 134443.
11. J.A. Mundy, J. Schaab, Y. Kumagai, A. Cano, M. Stengel, I.P. Krug, D.M. Gottlob, H. Doğanay, M.E. Holtz, R. Held, Z. Yan, E. Bourret, C.M. Schneider, D.G. Schlom, D.A. Muller, R. Ramesh, N.A. Spaldin, and D. Meier, “Functional Electronic Inversion Layers at Ferroelectric Domain Walls,” *Nature Materials* **16** (2017) 622–627.
12. N.F. Quackenbush, H. Paik, M.E. Holtz, M.J. Wahila, J.A. Moyer, S. Barthel, T.O. Wehling, D.A. Arena, J.C. Woicik, D.A. Muller, D.G. Schlom, and L.F.J. Piper, “Reducing Orbital Occupancy in VO₂ Suppresses Mott Physics while Peierls Distortions Persist,” *Physical Review B* **96** (2017) 081103.
13. L. Xie, L.Z. Li, C.A. Heikes, Y. Zhang, Z.J. Hong, P. Gao, C.T. Nelson, F. Xue, E. Kioupakis, L.Q. Chen, D.G. Schlom, P. Wang, and X.Q. Pan, “Giant Ferroelectric Polarization in Ultrathin Ferroelectrics via Boundary-Condition Engineering,” *Advanced Materials* **29** (2017) 1701475.
14. M.E. Holtz, K. Shapovalov, J.A. Mundy, C.S. Chang, Z. Yan, E. Bourret, D.A. Muller, D. Meier, and A. Cano, “Topological Defects in Hexagonal Manganites: Inner Structure and Emergent Electrostatics,” *Nano Letters* **17** (2017) 5883–5890.

15. Z. Chen, Z. Chen, Z.Q. Liu, M.E. Holtz, C.J. Li, X.R. Wang, W.M. Lü, M. Motapothula, L.S. Fan, J.A. Turcaud, L.R. Dedon, C. Frederick, R.J. Xu, R. Gao, A.T. N'Diaye, E. Arenholz, J.A. Mundy, T. Venkatesan, D.A. Muller, L.-W. Wang, J. Liu, and L.W. Martin, "Electron Accumulation and Emergent Magnetism in $\text{LaMnO}_3/\text{SrTiO}_3$ Heterostructures," *Physical Review Letters* **119** (2017) 156801.
16. J. Schaab, S. H. Skjærvø, S. Krohns, X. Dai, M. Holtz, A. Cano, M. Lilienblum, Z. Yan, E. Bourret, D. A. Muller, M. Fiebig, S. M. Selbach, and D. Meier, "Electrical half-wave rectification at ferroelectric domain walls", *Nature Nanotechnology*, (in press) <https://doi.org/10.1038/s41565-018-0253-5>
17. Elliot Padgett, Paul Cueva, Megan Holtz, Eric Langenberg, Dong Re, Héctor D. Abruñ, Darrell Schlom, and David A. Muller¹, "Grains and Strains from Cepstral Analysis of 4D-STEM Nano-Diffraction Datasets", *Microscopy and Microanalysis*, **24** (S1), 546-547 (2018). doi:10.1017/S1431927618003227

Magnetic imaging of spatially modulated superconductivity in focus ion beam defined microstructures

Katja C. Nowack, Laboratory of Atomic and Solid State Physics, Cornell University

Research Scope

The overarching goal of this project is to advance our understanding and control of electronic and magnetic phenomena emerging in topologically nontrivial materials. Our experimental approach consists of high sensitivity magnetic imaging combined with electronic transport.

To date, only a fraction of materials predicted to have a topologically non-trivial electronic structure have been experimentally explored in detail. In particular, ternary compounds such as the half-Heusler compounds are a diverse materials class to realize novel topological properties. The diversity of ternary compounds offers opportunities for optimizing topological insulator properties and realizing novel topological phases: many of the identified candidates contain rare earth elements combined with other heavy metals. Strongly correlated f-electrons in these elements give rise to intrinsic magnetism, superconductivity, and strongly correlated behavior which can coexist with a topologically non-trivial electronic structure. In particular, intrinsic magnetic order combined with a topologically non-trivial electronic structure may give rise to the quantum anomalous Hall effect¹ in a stoichiometric system without doping disorder.

A challenge is that many novel compounds are first available as bulk single crystals; limiting options for their characterization and device fabrication. While the growth of high quality thin films is possible, the development is often difficult and time consuming. Therefore, it is desirable to identify the most promising compounds through measurements on bulk single crystals. A major thrust of this project is to explore and characterize new materials predicted to realize topological phases of matter by using a combination of transport and magnetic scanning probes.

Recent Progress

Micromachining using a focused ion beam (FIB) is a versatile approach to fabricate highly oriented devices on the micron scale from bulk single crystals². This approach offers opportunities to study a variety of candidate topologically non-trivial materials that are not yet available as high quality thin films.

To demonstrate compatibility of magnetic imaging with FIB defined microstructures we have studied microstructures fabricated from the heavy fermion superconductor CeIrIn₅. Next to serving as a proof of principle that we plan to extend to topologically non-trivial materials, these studies have revealed a new opportunity for engineering strain fields: The combination of the FIB defined geometry and differential thermal contraction between CeIrIn₅ and the substrate results in a non-uniform strain field. At the same time, the superconducting transition temperature (T_c) of CeIrIn₅ depends on the strength and direction of strain. Uniaxial pressure

measurements have shown that the bulk T_c (400mK) increases (decreases) by 56mK/kbar (-66mK/kbar) for compression along the crystallographic a - (c -) direction. As a result, micrometer scale control over the strain field in the crystal leads to micrometer scale variation in T_c in a single crystal without chemical inhomogeneities. Magnetic imaging of different device geometries show that the spatial modulation of superconductivity can be predicted by finite element simulations of the strain field. This offers a route to engineer strain fields that are difficult to achieve in other ways.

The microstructures are prepared by first carving a lamella of typical dimensions $100\mu\text{m} \times 50\mu\text{m} \times 2\text{-}3\mu\text{m}$ from a bulk crystal. The lamella is joined to a sapphire substrate with predefined leads by a thin layer of epoxy. Contacts are made by sputtering gold through a shadow mask, which is patterned into the contact geometry through cutting trenches in another FIB step. Finally, the desired device shape is patterned. In Fig.1 and Fig.3 show images and simulations of two CeIrIn_5 devices. In both trenches define a square in the (a,c)-plane. In the first device the square is anchored by 4 constrictions in each corner (Fig. 1a). In second device, the constrictions connect to the center of each side of the square (Fig. 3a).

We use scanning superconducting quantum interference device (SQUID) microscopy to image the diamagnetic response of the devices. We apply a local magnetic field using a $\sim 6\mu\text{m}$ field coil integrated on the SQUID chip while monitoring the local magnetic susceptibility with a $\sim 1.5\mu\text{m}$ SQUID pickup loop. Superconducting regions of the sample exhibit a strong diamagnetic response, allowing us to distinguish them from metallic and insulating regions.

Susceptibility images as a function of temperature (Fig.1b-d) show that superconductivity develops on the edges aligned with the c -direction as the first device is cooled (Fig. 1d). These regions extend towards the center at lower temperature, eventually connecting in the middle of the device. From simulations of the strain field we compute a local T_c map using the known strain

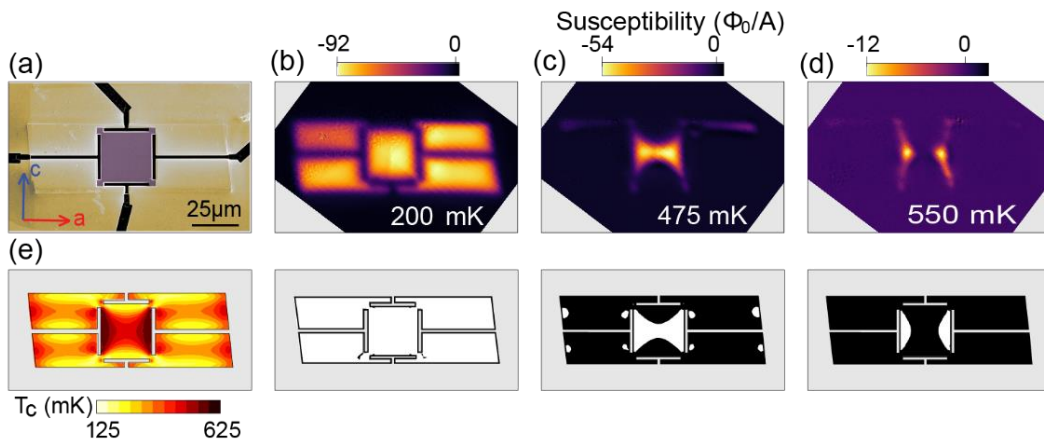


Fig. 1: (a) SEM-image. Au contacts are yellow. Center square is $25 \times 25 \times 3 \mu\text{m}^3$. Crystallographic axes as indicated. (b-d) Susceptibility images at three temperatures illustrate spatially modulated superconductivity. Lower panels show calculated superconducting patterns extracted from simulated T_c map in (e).

sensitivity of CeIrIn₅ (Fig. 1e). We find remarkable agreement between the simulation and the observed spatial modulation.

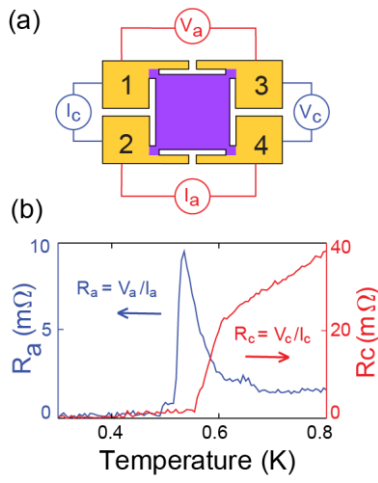


Fig. 2: (a) Schematic for transport measurement. (b) Transport of device shown in Fig. 1.

Strikingly, the observed patterns lead to three distinct regimes explaining unusual behavior in transport through the first device (Fig. 2): a) all contacts are separated by metallic regions, b) only the contact pairs along the *c*-direction are connected by superconducting regions, c) all contacts are connected by a single superconducting region. As a result, if current is sourced between contacts along *c* (1 and 2) a transition to zero voltage signaling superconductivity at a relatively high temperature is observed (Fig. 2, red trace). For currents sourced between contacts along *a* (2 and 4), (Fig. 2, blue trace) we observe a sharp upturn in voltage as *R_c* goes to zero. The elongated superconducting regions identified in Fig. 1d cause the current from contacts 2 to 4 to distribute evenly over the width of the device, causing a larger current to flow at the voltage probes (1 and 3). Eventually, a second transition to a zero-resistance state is observed when all terminals are connected by a single superconducting region.

Superconductivity emerges in a strikingly different spatial pattern in a second device (Fig. 3). As with the first device, simulations reproduce the observed in detail. The contrast between the two image series indicates that the spatial structure is determined by the interplay between the intrinsic strain sensitivity of the material and the strain field imposed by the FIB defined features.

This approach offers opportunities to generate superconducting circuitry in a homogeneous metallic device without physical interfaces in the future. More general, it presents a new approach to manipulating electronic order through strain on micron length scales in quantum materials.

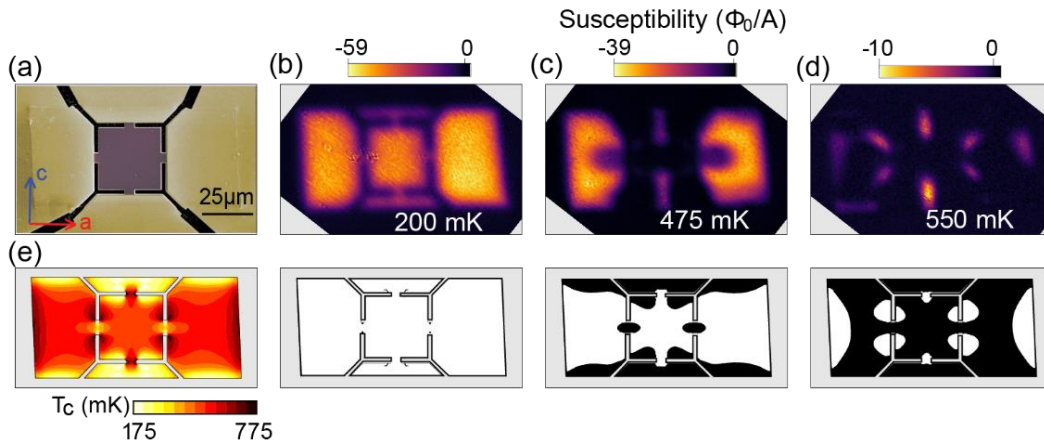


Fig. 3: (a) SEM-image. Au contacts are yellow. Center square is 30x30x3 μm³. Crystallographic axes as indicated. (b-d) Susceptibility images at three temperatures. Lower panels show calculated superconducting patterns extracted from simulated *T_c* map in (e).

Future Plans

Our recent progress on imaging FIB defined microstructures has opened up a number of interesting avenues to follow. An important tuning parameter for half-Heusler compounds is strain. In a range of compounds of interest strain is needed to induce a bulk energy gap^{3,4}. We plan to investigate applications of strain engineering in FIB defined microstructures of half-Heusler compounds that may have a topologically non-trivial electronic structure.

We further plan to study the quantum anomalous Hall (QAH) effect both in well-established magnetically doped insulators as well as candidate materials that feature intrinsic magnetism such as CoSn_2S_2 ⁵. We can operate our scanning probe microscope down to 10 mK at which the quantization of electronic transport in the QAH is fully visible. The overarching goal of our project remains to advance our understanding and control of phenomena in topologically nontrivial materials.

Acknowledgments

Work on the CeIrIn_5 microstructures is done in close collaboration with Philip Moll (Max Planck Institute for Chemical Physics of Solids in Dresden, Germany; EPFL, Switzerland).

References

1. Liu, C.-X., Zhang, S.-C. & Qi, X.-L. The Quantum Anomalous Hall Effect: Theory and Experiment. *Annu. Rev. Condens. Matter Phys.* **7**, 301–321 (2016).
2. Moll, P. J. W. Focused Ion Beam Microstructuring of Quantum Matter. *Annu. Rev. Condens. Matter Phys.* **9**, 147–162 (2018).
3. Chadov, S. *et al.* Tunable multifunctional topological insulators in ternary Heusler compounds. *Nat. Mater.* **9**, 541–545 (2010).
4. Lin, H. *et al.* Half-Heusler ternary compounds as new multifunctional experimental platforms for topological quantum phenomena. *Nat. Mater.* **9**, 546–549 (2010).
5. Liu, E. *et al.* Giant anomalous Hall effect in a ferromagnetic kagome-lattice semimetal. *Nat. Phys.* (2018). doi:10.1038/s41567-018-0234-5

Publications

“Spatially modulated heavy-fermion superconductivity in CeIrIn_5 ”, Maja D. Bachmann, G. M. Ferguson, Florian Theuss, Tobias Meng, Carsten Putzke, Toni Helm, You-Sheng Li, K.A. Modic, Michael Nicklas, Markus König, D. Low, Sayak Ghosh, Andrew P. Mackenzie, Frank Arnold, Elena Hassinger, Ross D. McDonald, Laurel E. Winter, Eric D. Bauer, Filip Ronning, B. J. Ramshaw, **Katja C. Nowack***, Philip J.W. Moll*, *These authors contributed equally to this work. (<https://arxiv.org/abs/1807.05079>).

Structure and Dynamics of Domains in Ferroelectric Nanostructures – In-situ TEM Studies

Xiaoqing Pan

Department of Materials Science and Engineering and Department of Physics and Astronomy, University of California, Irvine, CA 92697-257

Research Scope

Ferroelectric material is a prototypical example of functional oxides that has attracted considerable interest both in fundamental research and device engineering. The functionality of ferroelectric-based devices depends strongly on the structure and dynamics of ferroelectric domains. Advanced imaging techniques based on aberration-corrected transmission electron microscopy (TEM) have been a powerful method to study ferroelectric domain structures. The main goal of the proposed research is to explore the structure and dynamic behaviors of ferroelectric domains in thin films and nanostructures using aberration-corrected scanning transmission electron microscopy (STEM) and *in situ* TEM with a scanning tunneling microscopy (STM) holder, in combination with thin film growth and theoretical calculations. Nanoscale polarization states can be resolved unambiguously with sub-Angstrom resolution with aberration-corrected STEM; polarization switching dynamics under applied electric field can be followed by *in situ* TEM with high resolution in real time; and the TEM results can be quantitatively analyzed and directly compared with phase field simulations. We aim to understand the fundamental mechanisms of domain switching and domain wall motion under different electrical boundary conditions with controlled substrate constraints and to explore the interaction between ferroelectric polarization and crystal defects.

Recent Progress

Novel polarization states induced by nanoscale impurity defects

We have recently observed a strong interaction between ferroelectric polarization and charged impurity defects in ferroelectrics. We found that nanoscale planar charged defects in BiFeO₃ thin films can induce novel head-to-head mixed-phase polarization structures [1]. It was found that a strong build-in field pointing towards the defect exists, and this field can flip the polarization adjacent to the defect. This suggests that the impurity defects may be used as nano-building-blocks and provide a strong electrostatic driven force for stabilization of complex domain structures.

The planar defects observed above were accidentally introduced in the growth of thin films. Our recent studies show that by controlling the substrate temperature during film growth, an array of non-stoichiometric nanoregions can be deliberately introduced as charged defects into the host material, which leads to the stabilization of new polarization states such as novel hedgehog/antihedgehog nanodomains [2]. These nanodomains represent exotic patterns of polarization rotation that form mixed-phase structures and can be coupled with polarization vortices. As shown by three examples in Fig. 1a-c, the hedgehog/antihedgehog domains are ubiquitous around the defects in the BiFeO₃ thin films, and they can also induce polarization

vortices. In Fig. 1a, a tiny hedgehog polarization state with a diameter of 4 unit cells was observed within the nanoregion encircled by the defect. In both Fig. 1a,b, antihedgehog polarization states are stabilized at the shell regions surrounding the defects. On larger length scales outside of these defects, the overall continuous polarization rotation patterns lead to flux-closure vortex structures. In Fig. 1c, a pair of polarization semi-vortex and semi-antivortex structures form at the left and right side of this nearly linear defect as a result of the formation of a “head-to-head” polarization configuration above and below the defect.

It is clear that nanosized defects can be used to stabilize novel polarization structures at nanoscale, whereas the bulk domain patterns are not perturbed. In addition, we found that by introducing longer defects with the same type of non-stoichiometric structures, the typical 109° domain patterns in the $\text{BiFeO}_3/\text{TbScO}_3$ system can be transformed to 71° domains or a large monodomain, resulting in the formation of novel mixed-type domains containing “head-to-head” positively charged DWs located exactly at the defects (Fig. 2) [3]. This observation reveals a strong interaction between the defects and ferroelectric polarization. These defects are negatively charged, which cause strong built-in fields inducing the observed domain transformation and compensate the positive bound charge at the charged DWs.

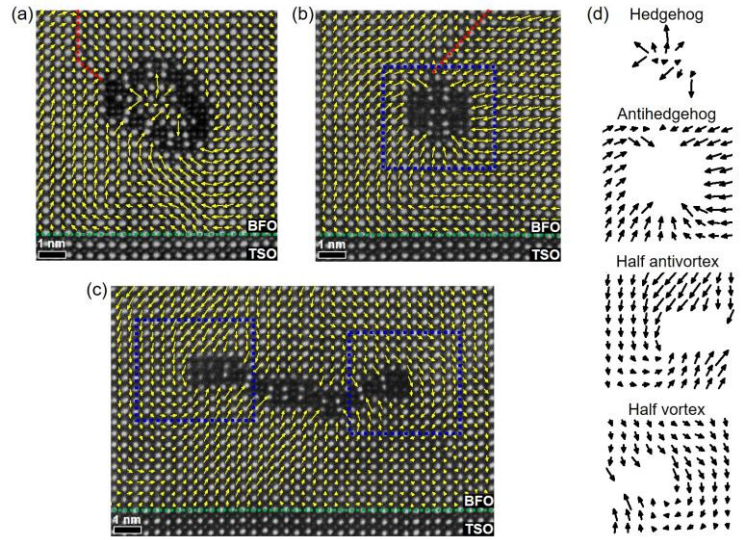


Fig. 1 | Polarization maps of nanodomains induced by three different defects in the BiFeO_3 thin film. (a-c) HAADF STEM images of three different defects above the $\text{BiFeO}_3(\text{BFO})/\text{TbScO}_3(\text{TSO})$ interface, where the polarization vectors ($-D_{FB}$, shown by yellow arrows) are overlaid on the BiFeO_3 lattice. The dashed red line marks the domain walls that penetrate to the top surface of the thin film. (d) Magnified map of the polarization vectors in the nanoregion enclosed by the loop defect in (a) and in the three different nanoregions highlighted by the blue rectangles in (b) and (c).

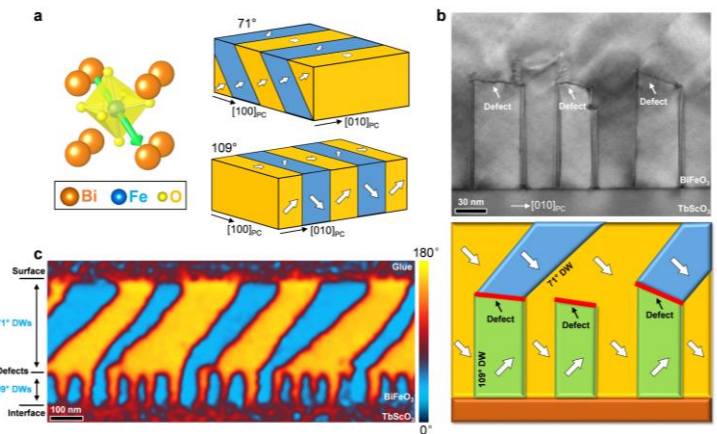


Fig. 2 | Domain structures in BiFeO_3 thin films. (a) Left, atomic model of BiFeO_3 pseudocubic structure (left), polarization is shown by the green arrow. Right, 71° and 109° domain patterns in BFO films. Polarizations are shown by white arrows. (b) Cross-sectional bright-field TEM image and corresponding schematic of polarization structures showing ordered 71° and 109° domains separated by an array of defects in a 400 nm BiFeO_3 film. (c) PFM phase image showing the same periodically ordered domain patterns in the same BiFeO_3 film.

Ferroelectric polarization induced ferromagnetic conduction at perovskite oxide interfaces

The above results show that charged defects strongly affect the configuration of polarization and thus result in the emergence of novel polarization states in ferroelectrics. On the other hand, the abrupt change of ferroelectric polarization at the ferroelectric/insulator interface could give rise to a polar discontinuity analogous to at (001) interface of $\text{LaAlO}_3/\text{SrTiO}_3$ (LAO/STO). Therefore, driven by polarization charge screening, an alternative route for creating 2-dimensional electron gas (2DEG) at the ferroelectric/insulator interfaces can be achieved.

Here, we report the discovery of spin-polarized 2DEGs at the interface between two well-known non-magnetic insulators: SrTiO_3 (STO) and ferroelectric $\text{PbZr}_{0.2}\text{Ti}_{0.8}\text{O}_3$ (PZT) by combination of *in-situ* transmission electron microscopy (TEM), electrical transport measurement, magneto-optical Kerr effect (MOKE), spin polarization detection, and first-principles calculations [4]. Using pulsed laser deposition (PLD), the STO/PZT heterostructures were grown on the (110) DyScO_3 (DSO) substrate, as schematically shown in the Fig. 3a. The crystalline quality and domain structure of the STO/PZT/SRO/DSO heterostructures were analyzed by TEM and atomic-resolution STEM (Fig. 3b and 3c). We found that the PZT layer is mono-domain (Fig. 3c) with its electric polarization pointing towards SRO. The polarization of PZT can be switched to upward by applying a negative bias on top of the STO layer, as depicted in Figs. 3d and e. It is important to note that almost the entire domain abruptly switches when the negative bias reaches -5 V (Fig. 3e), much different from the way of domain switching for an uncapped PZT layer for which the switching starts from a small area near the tip and gradually expands as the bias increases. The switched domain area as a function of the applied bias for these two structures were summarized in Fig. 3g. This uniform domain switching behavior is like what occurs in a planar ferroelectric capacitor and suggests a conducting STO/PZT interface, which

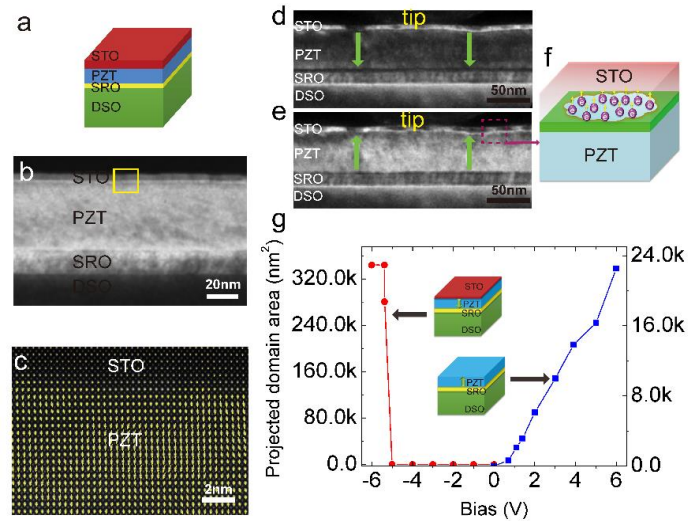


Fig. 3 | Structural characterization and *in-situ* domain switching in STO/PZT/SRO/DSO heterostructure. (a) Schematics of the STO/PZT/SRO/DSO heterostructures. (b) Low magnification TEM image of STO (5nm)/PZT (50 nm)/SRO(20nm)/DSO sample. The PZT layer is single-domain with SRO as the bottom electrode. Scale bar, 20nm. (c) HAADF STEM image shows a subarea on the STO/PZT interface marked in the rectangular box in b). Capacitor like domain switching in STO/PZT/SRO/DSO structure by *in-situ* TEM. (d) dark field TEM image shows a single-domain structure (downward polarization) at the initial state. (e) Capacitor-like domain switching occurs when a 0 \rightarrow -6 V DC voltage is applied by tungsten tip. (f) The sketch of SP-2DEG induced at the interface of STO/PZT. (g) The switched domain area as a function of bias extracted from the recorded movies for STO/PZT/SRO/DSO (red dot) and PZT/SRO/DSO (blue rectangular). The schematics of the corresponding structures are shown in the inset. The initial polarization directions of PZT layers are marked by arrows.

becomes a top electrode and thus a homogeneous electric field is generated across the PZT film when the bias is applied, as illustrated in the Fig. 3f.

Detailed studies by electrical transport and MOKE measurements show that the conducting STO/PZT interface is ferromagnetic with uniform magnetization and high conductivity. The spin polarization value is determined to be about 61% by Andreev reflection spectroscopy. Theoretical calculations revealed that the origin is the band bending in STO layers and the possibility of switching the magnetic states via electric bias. The present work demonstrates a prototypical case of designing interface physics from the interplay of multiple factors in ferroelectric-based heterostructures. It is foreseeable that these results and concepts are useful for the search and design of heterogeneous multiferroic materials and devices

Future Plans

In the next year we will continue exploring the static and dynamic properties of ferroelectric heterostructures to elucidate atomic structures and switching behavior of ferroelectrics, using atomic-resolution STEM and *in situ* TEM techniques in combination with thin film growth and theoretical simulations. We plan to continue the experiment on controlling the formation of local defects by performing a systematic examination of the growth parameters, such as temperature, flux ratio, or ozone pressure. By carefully adjusting one parameter at a time or a combination of different parameters, we may be able to stabilize defects with different chemistry such as Bi-rich or Fe-rich defects in BFO, or defects with different configuration, such as rod-like defects, small clusters of point defects, loop defects, stepped defects, and linear defects. This would allow us to further explore the interaction between the polarization and defects by using the polarization mapping techniques based on atomic-scale STEM imaging. Furthermore, we plan to further study the domain switching in ferroelectric films with the presence of different types of defects. The non-uniform built-in fields induced by circled or curved defects could lead to distinct switching dynamics. The interaction of the applied fields and the defect-induced built-in fields could also affect the domain stability and produce novel domain structures that may possess different functionalities.

References

- [1] L. Z. Li, Y. Zhang, L. Xie, J. R. Jokisaari, C. Beekman, J. C. Yang, Y. H. Chu, H. M. Christen, and X. Q. Pan, "Atomic-scale mechanisms of defect induced retention failure in ferroelectrics", *Nano Letters* **17**, 3556-3562 (2017).
- [2] L. Z. Li, X. X. Cheng, J. R. Jokisaari, P. Gao, J. Britson, C. Adamo, C. Heikes, D. G. Schlom, L. Q. Chen and X. Q. Pan. "Defect-Induced Hedgehog Polarization States in Multiferroics", *Physical Review Letters* **120**, 137602 (2018).
- [3] L. Z. Li, J. R. Jokisaari, Y. Zhang, X. X. Cheng, X. X. Yan, C. Heikes, Q. Y. Lin, C. Gadre, D. G. Schlom, L. Q. Chen and X. Q. Pan. "Control of domain structures in multiferroic thin films through defect engineering", *Advanced Materials* 1802737 (2018). DOI:10.1002/adma.201802737
- [4] Y. Zhang, L. Xie, J. Kim, A. Stern, H. Wang, K. Zhang, X. X. Yan, L. Z. Li, H. Liu, G. J. Zhao, H. Chi, C. Gadre, Q. Y. Lin, Y. C. Zhou, C. Uher, T. Y. Chen, Y. H. Chu, J. Xia, R. Q. Wu and X. Q. Pan. "Discovery of a magnetic conductive interface in $\text{PbZr}_{0.2}\text{Ti}_{0.8}\text{O}_3/\text{SrTiO}_3$ heterostructures", *Nature Communications* **9**, 685 (2018).

Publications

1. Y. Zhang, H. D. Lu, L. Xie, X. X. Yan, T. R. Paudel, J. W. Kim, X. X. Chen, H. Wang, C. Heikes, L. Z. Li, M. J. Xu, D. G. Schlom, L. Q. Chen, R. Q. Wu, E. Y. Tsybmal, A. Gruverman and X. Q. Pan. "Observing of anisotropic polarization-induced conductance at the ferroelectric/insulator interface". *Nature Nanotechnology* Accepted (2018).
2. L. Z. Li, J. R. Jokisaari, Y. Zhang, X. X. Cheng, X. X. Yan, C. Heikes, Q. Y. Lin, C. Gadre, D. G. Schlom, L. Q. Chen and X. Q. Pan. "Control of domain structures in multiferroic thin films through defect engineering", *Advanced Materials* 1802737 (2018), DOI:10.1002/adma.201802737
3. M. J. Xu, S. Dai, T. Blum, L. Z. Li and X. Q. Pan. "Double-tilt in situ TEM holder with ultra-high stability", *Ultramicroscopy* **192**, 1-6 (2018), DOI:10.1016/j.ultramic.2018.04.010
4. L. Z. Li, X. X. Cheng, J. R. Jokisaari, P. Gao, J. Britson, C. Adamo, C. Heikes, D. G. Schlom, L. Q. Chen and X. Q. Pan. "Defect-Induced Hedgehog Polarization States in Multiferroics", *Physical Review Letters* **120**, (2018), DOI:10.1103/PhysRevLett.120.137602
5. Y. Zhang, L. Xie, J. Kim, A. Stern, H. Wang, K. Zhang, X. X. Yan, L. Z. Li, H. Liu, G. J. Zhao, H. Chi, C. Gadre, Q. Y. Lin, Y. C. Zhou, C. Uher, T. Y. Chen, Y. H. Chu, J. Xia, R. Q. Wu and X. Q. Pan. "Discovery of a magnetic conductive interface in $\text{PbZr}_{0.2}\text{Ti}_{0.8}\text{O}_3/\text{SrTiO}_3$ heterostructures", *Nature Communications* **9**, 685 (2018), DOI:10.1038/s41467-018-02914-9
6. C. J. Cui, W. J. Hu, X. G. Yan, C. Addiego, W. P. Gao, Y. Wang, Z. Wang, L. Z. Li, Y. C. Cheng, P. Li, X. X. Zhang, H. N. Alshareef, T. Wu, W. G. Zhu, X. Q. Pan and L. J. Li. "Intercorrelated In-Plane and Out-of-Plane Ferroelectricity in Ultrathin Two-Dimensional Layered Semiconductor In_2Se_3 ", *Nano Letters* **18**, 1253-1258 (2018), DOI:10.1021/acs.nanolett.7b04852
7. Q. Zhang, L. Xie, G. Q. Liu, S. Prokhorenko, Y. Nahas, X. Q. Pan, L. Bellaiche, A. Gruverman and N. Valanoor. "Nanoscale Bubble Domains and Topological Transitions in Ultrathin Ferroelectric Films", *Advanced Materials* **29**, (2017), DOI:10.1002/adma.201702375
8. L. Xie, L. Z. Li, C. A. Heikes, Y. Zhnag, Z. J. Hong, P. Gao, C. T. Nelson, F. Xue, E. Kioupakis, L. Q. Chen, D. G. Schlom, P. Wang, and X. Q. Pan, "Giant Ferroelectric Polarization in Ultrathin Ferroelectrics via Boundary-Condition Engineering", *Advanced Materials*, 1701475 (2017); DOI: 10.1002/adma.201701475
9. L. Z. Li, Y. Zhang, L. Xie, J. R. Jokisaari, C. Beekman, J. C. Yang, Y. H. Chu, H. M. Christen, and X. Q. Pan, "Atomic-scale mechanisms of defect induced retention failure in ferroelectrics", *Nano Letters* **17**, 3556-3562 (2017), DOI: 10.1021/acs.nanolett.7b00696
10. F. Xue, L. Z. Li, J. Britson, Z. J. Hong, C. A. Heikes, C. Adamo, D. G. Schlom, X. Q. Pan and L. Q. Chen. "Switching the curl of polarization vectors by an irrotational electric field", *Physical Review B* **94**, 100103 (2016), DOI:10.1103/PhysRevB.94.100103.
11. Y. Heo, J. H. Lee, L. Xie, X. Q. Pan, C. H. Yang and J. Seidel. "Enhanced conductivity at orthorhombic-rhombohedral phase boundaries in BiFeO_3 thin films", *NPG Asia Materials* **8**, e297 (2016), DOI:10.1038/am.2016.120.
12. L.Z. Li, J. Britson, J. R. Jokisaari, Y. Zhang, C. Adamo, A. Melville, D.G. Schlom, L.Q. Chen, and X.Q. Pan, "Giant Resistive Switching via Control of Ferroelectric Charged Domain Walls", *Adv. Mater.* **28**, 6574–6580 (2016); DOI: 10.1002/adma.201600160.

Physics of complex materials systems through theory and microscopy/EELS

Sokrates T. Pantelides

Department of Physics and Astronomy, Vanderbilt University, Nashville, TN 37235

Research Scope

The main objective is to combine density functional theory (DFT) with Z-contrast imaging and electron-energy-loss spectroscopy (EELS), obtained with scanning transmission electron microscopes (STEMs), or imaging by scanning tunneling microscopy (STM) or other proximal probes to elucidate structure-property relations in complex materials structures and predict new functionalities. In the last several years we also developed codes that compute as-measured EELS by integrating DFT calculations of core or valence excitation spectra with simulations of the STEM electron beam's evolution in the sample and its collection at the detector. In the last two years we have collaborated and published jointly with STEM microscopists (Albina Borisevich, Matt Chisholm, Juan Carlos Idrobo, Andy Lupini) and proximal-probe practitioners (Petro Maksymovych, Nina Balke, Sergei Kalinin) at Oak Ridge National Laboratory, STEM microscopists in Tokyo (former student Junhao Lin, Kazu Suenaga), STEM and STM microscopists in Beijing (Wu Zhou and Hong-Jun Gao's group, respectively) and with Ward Plummer's group (Louisiana State University) with STEM-EELS by Yimei Zhu (Brookhaven). Here we describe a few recent case studies illustrating the diversity of our explorations.

Recent Progress

Intrinsic interfacial van der Waals monolayers and their effect on the high-temperature superconductor FeSe/SrTiO₃

H. Sims, D. N. Leonard, A. Y. Birenbaum, Z. Ge, T. Berlijn, L. Li, V. R. Cooper, M. F. Chisholm, and S. T. Pantelides, under review by *Physical Review Letters*.

It was recently demonstrated that monolayer FeSe on bulk SrTiO₃ is a superconductor with T_c between 60 and 100 K,¹ compared to 8 K in bulk FeSe² and only 3.7 K in bi-layer FeSe on graphene³, pointing to a major role by the FeSe/SrTiO₃ interface in the higher T_c . By combining STEM imaging and DFT calculations, we determined the atomic structure of an interfacial layer

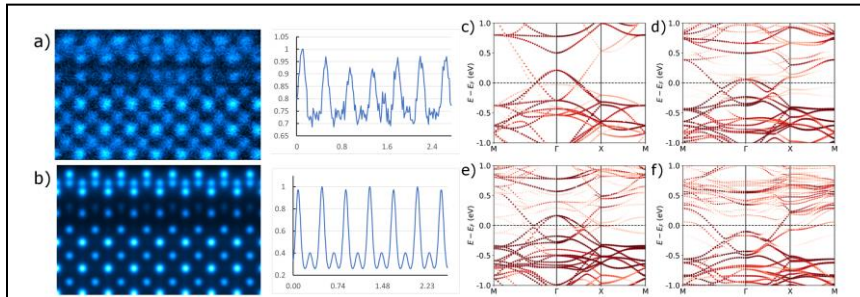


Fig. 1 (a-b) Comparison of (a) experimental and (b) simulated STEM images for the proposed structure of the STO/FeSe interface. (c-f) Fe d band structure for FeSe (c) as a free-standing monolayer, (d) in the presence of the $Ti_{1.5}O_2$ interfacial layer (at the distance suggested by the STEM images), (e) in the full FeSe/ $Ti_{1.5}O_2$ /SrTiO₃ heterostructure, again guided by the experimental interlayer distances, and (f) in the fully relaxed non-magnetic structure. Only in panel (d) is the hole pocket completely filled, although the interlayer does dope the FeSe layer to varying degrees in (d) and (e). Note that in our 2×2 supercell, the M point of the primitive cell is folded back to Γ .

(located between the typical TiO₂-terminated surface and the FeSe film – Fig. 1) and identified its role in the observed increase of T_c . This layer interlayer is best described as a (2×2) $Ti_{1.5}O_2$ layer (an additional Ti cation per 4 oxygens).

The distance between the interfacial layer and the substrate is about 30% greater than that between the SrO and TiO₂ layers in bulk STO. Indeed, we find that the interlayer is bonded by

Van der Waals interactions (it would float off if they are turned off). Nevertheless, the excess Ti in this layer dopes the FeSe monolayer, filling the Γ hole pocket, in good agreement with the ARPES data.⁴ We further found that this layer breaks the in-plane symmetry of the FeSe film, stabilizing an in-plane distortion similar to the nematic distortions seen in bulk FeSe. These distortions may increase T_c via enhanced electron-phonon coupling.⁵

Novel Pd₂Se₃ two-dimensional phase driven by interlayer fusion in layered PdSe₂

J. Lin, S. Zuluaga, P. Yu, Z. Liu, S. T. Pantelides, and K. Suenaga, *Phys. Rev. Lett.* **119**, 016101 (2017); S. Zuluaga, J. Lin, K. Suenaga, S. T. Pantelides, *2D Mater.* **5**, 3 (2018).

Two-dimensional (2D) materials are easily fabricated when their bulk form has a layered structure. The monolayer form is typically the same as a single layer of the bulk material. PdSe₂ seemed to be an exception as its monolayer form was theoretically shown to be stable, but its fabrication had not been reported. Junhao Lin, the PI's former graduate student, as a post-doc in Kazu Suenaga's STEM group in Tokyo, succeeded in exfoliating a monolayer, but STEM imaging showed that the monolayer does not have the expected PdSe₂ structure (Fig. 2A). By trial and error, jointly with Junhao, we found that the new monolayer phase has a stoichiometry of Pd₂Se₃ in a structure whose STEM simulation matches the experimental STEM image (Fig. 2B).

We investigate how the Pd₂Se₃ monolayer forms using DFT calculations. We found that the Pd₂Se₃ monolayer results from the fusion of two PdSe₂ layers by the emission of Se vacancies. The presence of Se vacancies causes the Pd backbones from two PdSe₂ layers to fuse into one, while the remaining Se atoms rearrange themselves. In Fig. 2C we show that, as the number of Se vacancies increases in a PdSe₂ bilayer, the distance between the two layers decreases and the energy barrier that has to be overcome for the fusion to occur. Inspection of the electron density reveals that chemical bonds form between the two layers that initially interact only via van der Waals forces. Figure 2D shows a schematic depiction of how the fusion takes place. The discovery that strong interlayer interactions can be induced by defects and lead to the formation of new 2D materials opens a new venue for the exploration of defect engineering and novel 2D structures.

In subsequent work, we investigated the formation of a junction between monolayer Pd₂Se₃ and bilayer PdSe₂. We found that empty interface states appear in the common energy gap. Thus, upon n-type doping of the base material, dopant electrons would naturally drop into the interface states, generating a conducting one-dimensional nanowire between two insulating 2D materials.

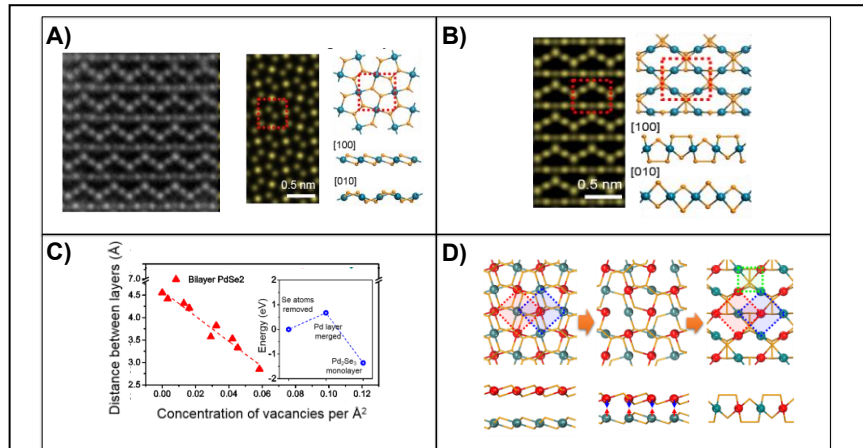


Fig. 2. (A) STEM image of the monolayer exfoliated from bulk PdSe₂ (left) and STEM simulation of the theoretical PdSe₂ monolayer (middle), shown schematically on the right. (B) Structure of the newly obtained monolayer phase Pd₂Se₃ and the simulated STEM image. (C) Distance between PdSe₂ layers as function of Se-vacancy concentration. The inset shows the energy profile and the energy barrier for the fusion of the two layers to form Pd₂Se₃. (D) Schematic diagrams of the merging and formation of the Pd₂Se₃ monolayer. Red and blue spheres represent Pd atoms in the top and lower layer. Se atoms are located at the junction of the orange connectors but are not shown.

Intrinsically-patterned two-dimensional materials for selective adsorption of molecules and nanoclusters

X. Lin, J. Lu, Y. Shao, Y.-Y. Zhang, X. Wu, J.-B. Pan, L. Gao, S.-Y. Zhu, K. Qian, Y. F. Zhang, D. L. Bao, L. Li, Y. Wang, Z. Liu, J.-T. Sun, T. Lei, C. Liu, J. Wang, K. Ibrahim, D. N. Leonard, W. Zhou, H. Guo, Y. Wang, S. Du, S. T. Pantelides, and H.-J. Gao, *Nature Mater.* **16**, 717 (2017).

To achieve desirable functionalization, 2D materials are often patterned using soft lithography and selectively decorated with molecules. In this paper, a collaboration with H.-J. Gao's group in Beijing, we announced the discovery of a new class of 2D materials that are *intrinsically patterned*, like a floor tiled with alternate black and white tiles, but on the nanoscale. The PI played a major role in the evolution of the entire project, not only in the theory component.

In a prior joint paper,⁶ we reported the fabrication of monolayer PtSe₂ in the 1T structure on a Pt substrate by direct “selenization”, analog of oxidation (Fig. 3a). In the new work, by annealing the PtSe₂ at higher temperatures, a triangular pattern of alternating 1T and 1H phases (Figs. 3b, 3c). The transformation occurs by the emission of Se atoms, as verified by the reversal to homogeneous PtSe₂ by cooling while providing Se atoms. Intrinsic patterning was also demonstrated in monolayer CuSe grown on a Cu substrate. The material exhibits periodic patterns of triangular nanopores in uniform size (Figs. 3d, 3e). Both STEM and STM images were employed to study the structures. DFT calculations established the atomic structures of the two intrinsically patterned 2D materials. Based on the theoretically proposed atomic models, simulated STM images are in excellent agreement with observed STM images. Using DFT calculations, we elucidated the mechanism of the formation of the intrinsically patterned 2D materials. We found that, for the patterned 1H/1T-PtSe₂ system, the thermally produced Se vacancies order to form triangular boundaries, which then stabilize the 1H phase. For the CuSe monolayer with periodic nanopores, we found that the removal of a central atom and three shells of atoms around it, totaling 13 atoms, lowers the energy and produces the observed nanopores at the observed periodicity. We also predicted that different molecules would adsorb preferentially on one or the other component of intrinsically patterned 2D materials. It was verified experimentally that Fe clusters preferentially adsorb in the periodic pores of CuSe while FePc molecules preferentially adsorb on the terraces of patterned CuSe. Thus, intrinsically patterned materials set the stage for dual functionalization on the nanoscale.

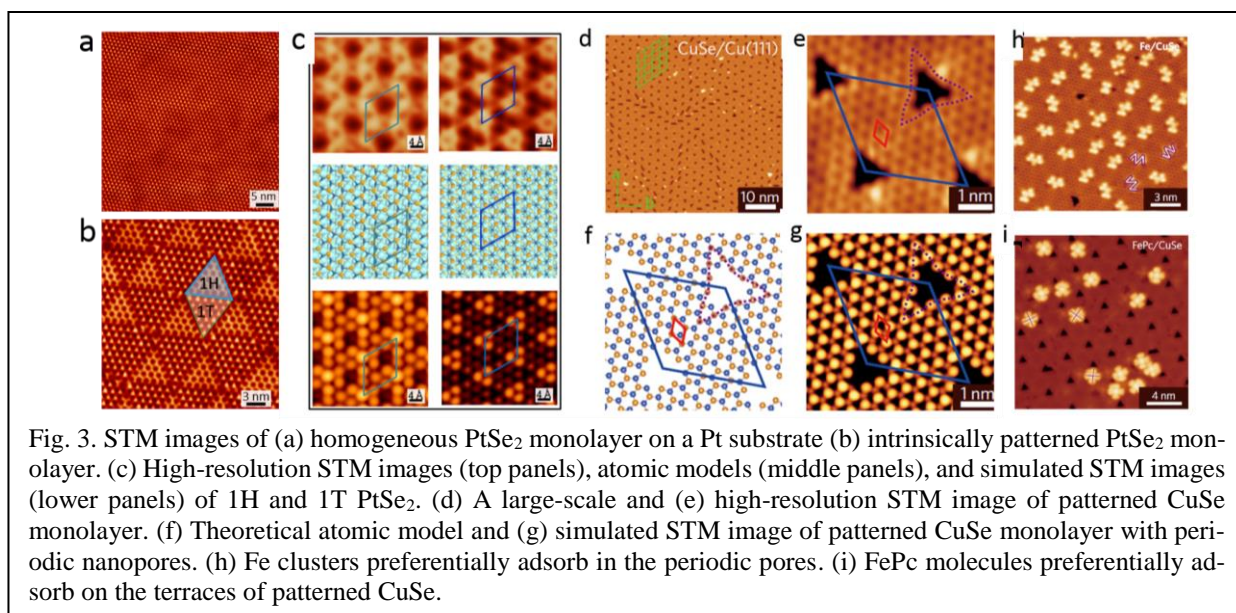


Fig. 3. STM images of (a) homogeneous PtSe₂ monolayer on a Pt substrate (b) intrinsically patterned PtSe₂ monolayer. (c) High-resolution STM images (top panels), atomic models (middle panels), and simulated STM images (lower panels) of 1H and 1T PtSe₂. (d) A large-scale and (e) high-resolution STM image of patterned CuSe monolayer. (f) Theoretical atomic model and (g) simulated STM image of patterned CuSe monolayer with periodic nanopores. (h) Fe clusters preferentially adsorb in the periodic pores. (i) FePc molecules preferentially adsorb on the terraces of patterned CuSe.

Structural “ δ doping” to control local magnetization in isovalent oxide heterostructures

E. J. Moon, Q. He, S. Ghosh, B. J. Kirby, S. T. Pantelides, A. Y. Borisevich, and S. J. May, *Physical Review Letters*, **119**, 197204 (2017).

δ -doping, in which atomically thin layers of dopants are inserted in a material are well known in semiconductors. In this work, in collaboration with Steve May of Drexel University and Albina Borisevich at ORNL, we demonstrated a purely structural “ δ -doping” in complex oxide heterostructures, namely insertion of an atomically thin manganite layer in an isovalent manganite host, modifying the local rotations of MnO_6 octahedra. Combined experiments and theory reveal how local magnetic exchange interactions are enhanced within the spatially confined regions of suppressed octahedral rotations.

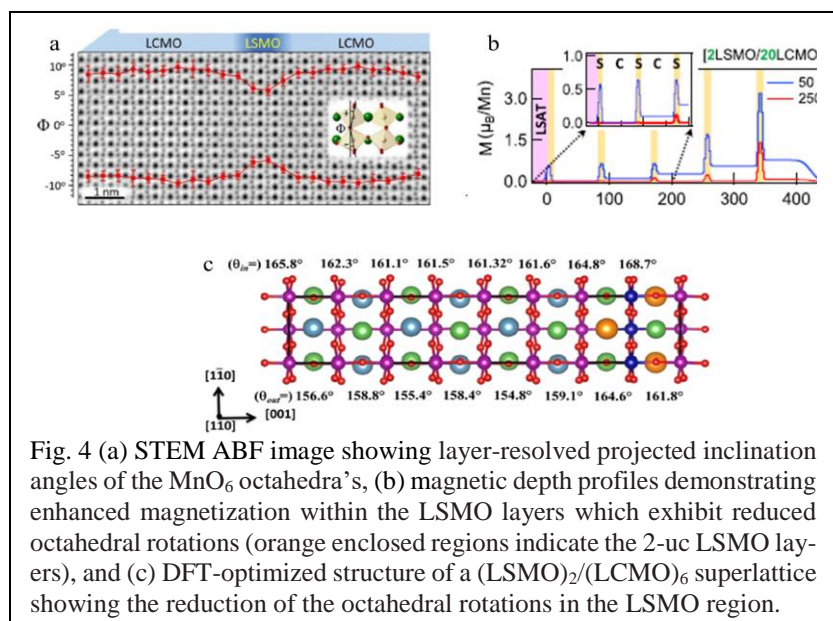


Fig. 4 (a) STEM ABF image showing layer-resolved projected inclination angles of the MnO_6 octahedra's, (b) magnetic depth profiles demonstrating enhanced magnetization within the LSMO layers which exhibit reduced octahedral rotations (orange enclosed regions indicate the 2-uc LSMO layers), and (c) DFT-optimized structure of a $(\text{LSMO})_2/(\text{LCMO})_6$ superlattice showing the reduction of the octahedral rotations in the LSMO region.

The experimental data demonstrate that insertion of two unit cells of $\text{La}_{0.5}\text{Sr}_{0.5}\text{MnO}_3$ (LSMO) into 20 unit cells of $\text{La}_{0.5}\text{Ca}_{0.5}\text{MnO}_3$ (LCMO) leads to a local reduction of octahedral rotations, while avoiding changes to the nominal Mn valence state due to the isovalent nature of the superlattices (Fig. 4a). The magnetization within the “doped” regions is enhanced (Fig. 4b). Parallel DFT calculations using superlattices (SL's) with relatively smaller periods, namely $[\text{LSMO}_2/\text{LCMO}]_6$, found that octahedral rotations in the LSMO region are suppressed and exhibit a tilt pattern ($a^-a^+c^+$) similar to the pattern in the LCMO region. The calculated average θ_{in} values are shown in Fig. 4c. We further found that the suppression of octahedral rotations has strong impact on magnetic properties i.e., in-plane and out-of-plane isotropic exchange interactions in the LSMO region are 1.8 and 1.5 times, respectively, higher than the LCMO region. These results validate a δ -doping approach, based purely on altering local structure, as a means to spatially confine or enhance local magnetic interactions in complex oxide heterostructures.

Future plans

Current projects include joint investigations of complex oxide interfaces with W. Plummer/Y. Zhu and with S. May/A. Borisevich, the origin of negative piezoelectric coefficient and other properties of CuInP_2S_6 with N. Balke's group, single-atom catalysis with W. Zhu, amorphous graphene with Junhao Lin and O. Barbaros's Singapore group, origami graphene, intercalation phenomena, and visualization of H transfer in molecules with H.-J. Gao's group, local electric fields in materials with J. C. Idrobo and M. Chi and more.

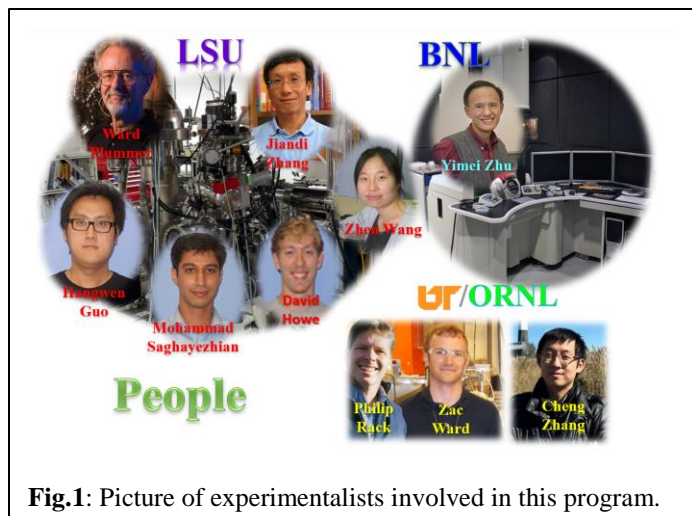
- [1] W. Qing-Yan, *et al.*, *Chin. Phys. Lett.* **29**, 037402 (2012).
- [2] F.-C. Hsu, *et al.*, *PNAS* **105**, 14262 (2008).
- [3] C.-L. Song, *et al.*, *Phys. Rev. B* **84**, 020503 (2011).
- [4] D. Liu, *et al.*, *Nat. Commun.* **3**, 931 (2012).
- [5] S. Coh, M L. Cohen, and S. G. Louie, *New J. Phys.* **17**, 073027 (2015).
- [6] Y. Wang, *et al.*, *Nano Lett.* **15**, 4013 (2015).

Emerging Functionality in Transition-Metal Compounds Driven by Spatial Confinement

Ward Plummer, Department of Physics and Astronomy, Louisiana State University

Research Scope: Interfaces between two different materials can display fascinating properties very different from either of the parent materials. The interface between two insulators, LaAlO_3 & SrTiO_3 , behaves like a 2D electron gas and as a superconductor [1-3]. The vacuum interface at the surface of a topological insulator hosts a topologically protected surface state [4]. The broken symmetry at an interface can drive reconstruction of the lattice, charge, or spin, which is the origin of the new functionality. The challenge is to understand and control such reconstruction to yield the desired functionality. Advances in atomically resolved electron microscopy and spectroscopy have allowed researchers to “see” the atomic structure, the chemical identity, and the bonding character of the atoms at an interface. The ability to “see” has empowered theoretical explanations and predictions of interface properties. We are entering an era where it is possible to close the loop of material fabrication, characterization, and modeling to design new properties of interfaces, heterostructures, and superlattices.

We have put together a team that can accomplish the goal of understanding and predicting new



properties of interfaces at the atomic level, shown in **Figure 1**. The group at LSU and UTK/ORNL will carry out growth, modification, and physical properties characterization. High-end electron microscopy and spectroscopy will be accomplished by our postdoctoral fellow (Zhen Wang), working in the group of Dr. Yimei Zhu at BNL. Theory will be done by several investigators around the world, but primarily in collaboration with the group of Professor Sokrates Pantelides at Vanderbilt University.

Recent Progress:

Designing Antiphase boundaries by atomic control of heterointerfaces [5]. Defects have been one of the central topics in condensed matter physics as they exist in all materials and have great impact on physical properties such as mechanical strength, superconductivity, topological protection, perovskite-based solar cells [6-8, 9]. In a perfect crystal, either bulk or thin films, the requirement of minimizing Gibbs free energy leads to increasing the entropy through disorder. This means that defects and their *random distribution* are unavoidable. This thermodynamic character makes it extremely complicated to predict the exact form (point, line, plane etc.) and location of the defects, let alone understanding their impacts on physical properties [10].

Understanding defect physics requires “seeing” (i.e. atomic-resolved electron microscopy and spectroscopy) defects to know their location and origin, followed by modeling.

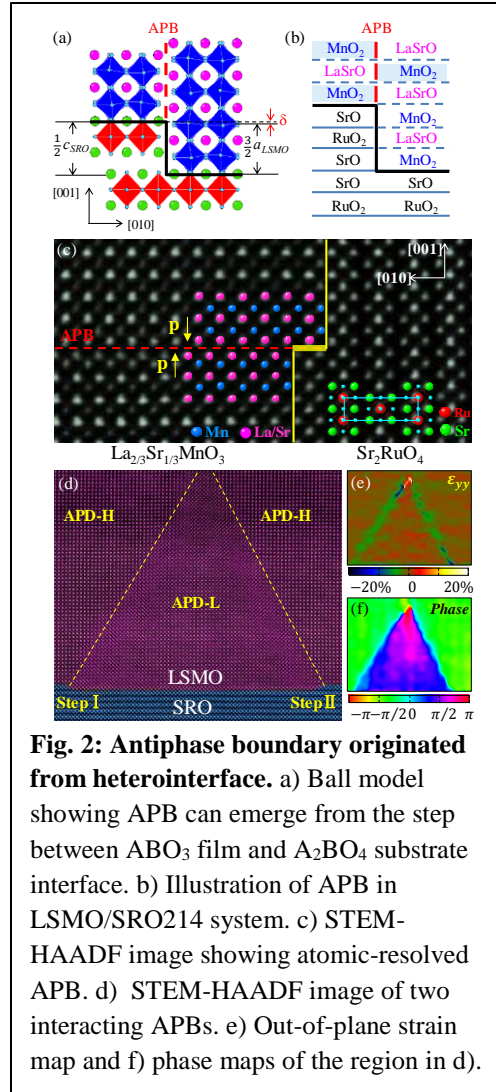


Fig. 2: Antiphase boundary originated from heterointerface. a) Ball model showing APB can emerge from the step between ABO₃ film and A₂BO₄ substrate interface. b) Illustration of APB in LSMO/SRO₂₁₄ system. c) STEM-HAADF image showing atomic-resolved APB. d) STEM-HAADF image of two interacting APBs. e) Out-of-plane strain map and f) phase maps of the region in d).

triangular antiphase domain.

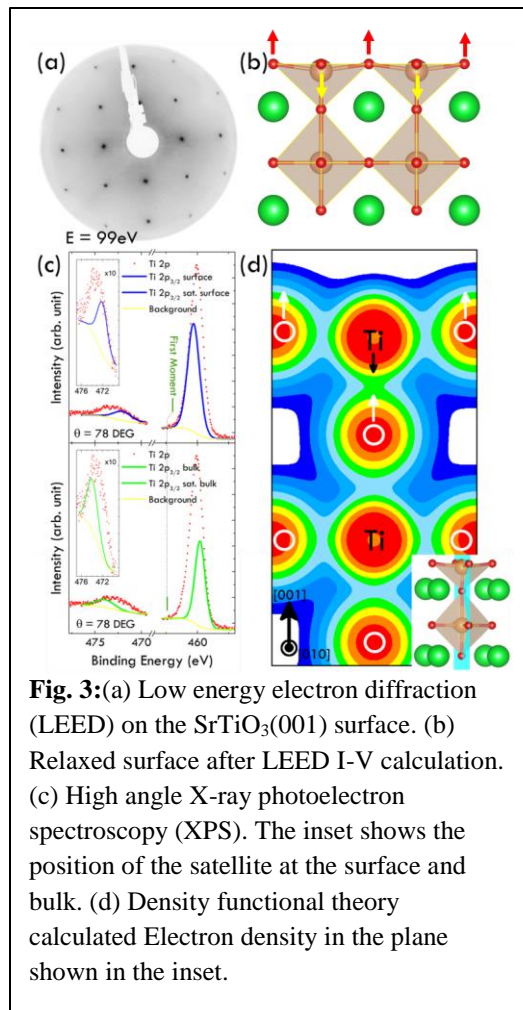
We have provided an exceptional interface phase to study a 2-dimensional defect: an Antiphase Boundary (APB) [5]. We have created well-defined APB by growing thin films on a single crystal of a layered oxide substrate (Sr₂RuO₄). **Figure 2a** shows a cross-sectional ball model of a 3D perovskite ABO₃ (La_{2/3}Sr_{1/3}MnO₃) structure grown on top of layered A₂BO₄ (Sr₂RuO₄) substrate. Due to the presence of a step in the substrate, the ABO₃ thin film exhibits a $\sim \frac{1}{2}$ unit cell shift from one substrate terrace to the next. As a consequence, an APB [11] nucleates at the substrate step edge and penetrates into ABO₃ thin film. **Fig. 2b** is a schematic of stacking sequence showing what the APB could look like for a single step in the substrate. **Fig. 2c** is our STEM-HAADF image of the APB boundary in the La_{2/3}Sr_{1/3}MnO₃ film, validating our schematic picture [5].

When there is only a single step in the Sr₂RuO₄ substrate the APB is perpendicular to the interface as shown in the HAADF image in Fig. 2c. But when two steps come close to each other the APBs interact and form a triangular antiphase domain as shown in Fig. 2(d). We have demonstrated theoretically that this occurs to minimize the surface energy [5] and morphology of the antiphase domains is mainly determined by the slight shift in LSMO₁₁₃ film (δ in Fig. 1(a)) and the step terrace width. **Fig. 2(e-f)** show out-of-plane strain and phase maps for the two interacting APBs, which are calculated by geometric phase analysis. It clearly shows the morphology of the

Rumpling and Enhanced Covalency at SrTiO₃(001) Surface [12].

The surface of STO has been extensively studied, both theoretically and experimentally [13,14] indicating that the surface atoms undergo rumpling normal to the surface. However, there are disagreements on the magnitude and the direction of atomic displacement [13,15,16]. The discrepancy between experimental data is most likely due to the absence of a well-defined and consistent sample preparation procedure [15]. The surface of SrTiO₃ (001) is considered to be weakly polar and in this work, we have investigated the validity of this notion. This surface,

shown in **Figure 3(b)**, exhibits a surface structural distortion, quantified here using low energy electron diffraction at room temperature (Fig. 3(a)). Structural analysis shows the presence of strong surface rumpling in the TiO_2 terminated surface (Fig. 3(b)) with the oxygen atoms moving outward and Ti atoms moving inward. Density functional calculations confirm the measured rumpling, and experimental data show the distortion is localized at the surface. Angle-dependent core-level X-ray photoemission spectroscopy (XPS) shows that the surface rumpling strongly impacts the electronic structure of the surface (Fig. 3(c)). The change in satellite structure (main-peak-satellite separation) of Ti 2p show that the surface undergoes electronic reconstruction. This observation is reinforced by density functional theory, which demonstrates that the valence state (derived from Bader charge analysis) of Ti at the surface is reduced, going from $2.23e$ (bulk) to $2.19e$ (surface) while O is enhanced, from $-1.27e$ (bulk) to $-1.21e$ (surface). Therefore, the Ti-O bonds are more covalent near the surface as shown in the charge density plot, Fig. 3(d). Our results show that surface rumpling is accompanied by a change in the bond hybridization of Ti-O at the surface. Changes in the XPS satellite structures at the surface (Fig. 3(c)) are consistent with this picture of the change in bonding, indicating that the (001) surface of SrTiO_3 is not polar and charge rearrangement is a consequence of surface rumpling. Our study shows that even in a wide bang gap insulator such as STO, the simple ionic picture fails to capture the underlying physics and nominal charge assignments do not represent the correct valence state of the elements.



Human resources: We have had an excellent group of researchers working with us on this project. Many of them have moved to new environments.

- Dr. Hangwen Guo was a research assistant professor at LSU and is now an assistant professor at Fudan University in Shanghai, China.
- Dr. Tony Wong graduated from UTK (PhD) and is now staff member at Jet Propulsion Laboratory.
- Dr. Meng Meng came from Sun Yat-Sen University, funded by national graduate exchange program in China, and is now a postdoc at the Institute of physics in Beijing.
- Dr. Lina Chen graduated from LSU and is now a research scientist at Nanjing University.
- Dr. Weimei Xie came to LSU from Nanjing university on a national graduate exchange program from China and now working in industry.
- Dr. Michael Stanford graduated from UTK and now is a post doc at Rice.

Future Plans:

a. Designing Interface-induced Magnetic Polar Metals: Our recent observations [17] demonstrate that ultrathin films can possess polar distortion when bracketed between ferroelectric materials. Moreover, in the case of $\text{BaTiO}_3/\text{LaSrMnO}_3/\text{BaTiO}_3$, LSMO not only possess polar structure in ultrathin regions, but experience a large modulation in magnetism due to changes in Mn-O-Mn bond angles associated with the polar structure. This example shows the possibility to utilize interface-induced polar structure as a *seed* to cultivate emergent properties in various oxide heterostructures.

Inspired by our recent results, we propose to design magnetic polar metals via heterointerfaces. As a prototype demonstration, we will start with $\text{BaTiO}_3/\text{SrRuO}_3/\text{BaTiO}_3$ sandwich structures. The choice of SrRuO_3 (SRO) is based on the fact that SRO is one of the best metals in perovskite oxide family, with strong ferromagnetism [18]. If Ru-O-Ru polar distortion can be induced via interfacial coupling with BTO, this system can possibly become a magnetic polar metal.

b. Ionic Liquid Electric Double Layering and Electrostatic Doping of $\text{FeSe}_{0.5}\text{Te}_{0.5}$. Low temperature dynamics of the electric double layer formation has largely been unstudied though the dynamics play an important role in many electrochemical and electrostatic doping effects in many interesting material systems. We will explore the charging dynamics of the electric double layer of the DEME-TFSI ionic liquid and subsequently elucidate chemical and electrostatic doping effects on the superconducting transition of $\text{FeSe}_{0.5}\text{Te}_{0.5}$.

c. Origin of magnetic phenomena in polar-nonpolar oxide heterostructure: Special attention has been paid to polar mismatch interfaces between thin film insulators, such as $\text{LaAlO}_3/\text{SrTiO}_3$ or $\text{LaMnO}_3/\text{SrTiO}_3$ while metal-insulator interface has remained almost unexamined. The presence of the metal alters the polar mismatch and as a result the microscopic interactions at the interface are different. Therefore, not only electronic reconstruction should appear at the interface, but also the interface layer can have different coupling to the rest of this thin film. This means the interface can be activated and play an independent role in the physical properties of the material. As a prototype we have grown $\text{La}_{2/3}\text{Sr}_{1/3}\text{MnO}_3/\text{SrTiO}_3$ a metal-insulator, polar-non-polar interface. **Figure 4** (a) and (b) show the electron microscopic images of high-quality thin film with well-ordered interface. Our initial magnetic measurements show that this thin film goes through spontaneous magnetic reversal and shows momentary

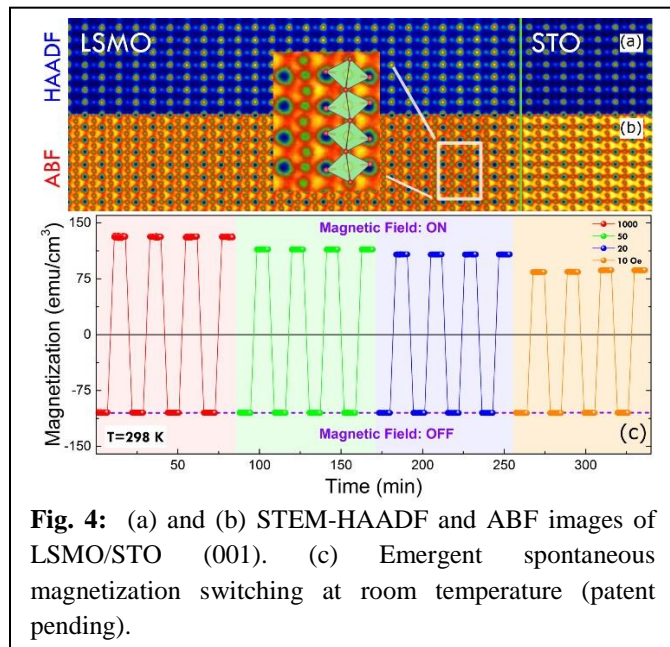


Fig. 4: (a) and (b) STEM-HAADF and ABF images of LSMO/STO (001). (c) Emergent spontaneous magnetization switching at room temperature (patent pending).

switching behavior at room temperature as seen in Fig. 4 (c). Technologically, this material offers great opportunities for device fabrications, but it raises fundamental questions about interface-driven magnetic interactions and polar-mismatched interfaces. Important questions to be addressed are how this interface responds to polar mismatch? Is it through charge transfer? What is the role of inevitable interface-intermixture? And how far away from the interface is influenced by the interface magnetism? We intend to use state-of-the-art electron microscopy and spectroscopy coupled with first principles calculation (Prof. S. Pantelides, Vanderbilt) to unravel the underlying physics behind these unexpected magnetic phenomena.

d. Advances in electron microscopy: Probing phase transitions and Dynamical behavior:

We will pursue two different projects aimed at expanding STEM/EELS capabilities that will impact our program and the general community. The first project, carried out at BNL, is to develop variable temperature atomically resolved imaging and spectroscopy to look at phase transitions at interfaces. The second project, to be carried out UTK, involves the use of a pulsed/continuous laser source to both photo-thermally heat and photo-excite the sample, where the heated and excited states can be probed with STEM/EELS. Both of these programs will be closely coupled with the nonlinear optical program described in the next section.

Our plan is to couple the cryo-STEM/EELS at BNL [19, 20] with temperature dependent nonlinear optical and transport measurement at LSU to characterize the structure, electronic and magnetic changes of films and interfaces as a function of temperature across a phase transition.

e. Nonlinear Optical Characterization of Interface Electronic and Magnetic Properties:

Nonlinear optics has been used for decades to characterize surface and interface properties [21-24]. When the materials being investigated are centrosymmetric, the nonlinear signal comes from the regions of broken symmetry at the interface [25]. In recent years, with developments in atomic resolved electron microscopy and spectroscopy, nonlinear optical studies have become extremely important as a tool to characterize and contrast the symmetry of the electrons and spin states at the interface with the structure determined with STEM [26]. We are constructing a UHV cryo-cooled sample for studies of surfaces. We will begin this project and the temperature dependent STEM studies looking at the coupled electronic/structural transition in IrTe₂ [27].

References

1. N. Reyren, S. Thiel, A. D. Caviglia, G. Fitting Kourkoutis, L. Hammert, C. Richter, C. W. Schneider, T. Kopp, A.-S. Ruetschi, D. Jaccard, M. Gabay, D. A. Muller, J.-M. Triscone, J. Mannhart, "Superconducting Interfaces Between Insulating Oxides," *Science* **317**, 1196 (2007).
2. A. Ohtomo, H. Y. Hwang, "A high-mobility electron gas at the LaAlO₃/SrTiO₃ heterointerface," *Nature* **427**, 423 (2004).
3. J. A. Bert, B. Kalisky, C. Bell, M. Kim, Y. Hikita, H. Y. Hwang, K. A. Moler, "A Direct imaging of the coexistence of ferromagnetism and superconductivity at the LaAlO₃/SrTiO₃ interface," *Nat. Phys.* **7**, 767 (2011).
4. M. Z. Hasan, C. L. Kane, "Colloquium: Topological Insulators," *Rev. Mod. Phys.* **82**, 3045 (2010).
5. Zhen Wang, Hangwen Guo, Shuai Shao, Mohammad Saghayezhian, Jun Li, Rosalba Fittipaldi, Antonio Vecchione, Prahald Siwakoti, Yimei Zhu, Jiandi Zhang, and E. W.

- Plummer, “Designing Antiphase Boundaries by Atomic Control of Heterointerfaces,” *Proceeding National Academy of Sciences*, doi/10.1073/pnas.1808812155 (2018).
6. S.V. Kalinin, N.A. Spaldin, “Functional Ion Defects in Transition Metal Oxides,” *Science* **341**, 858 (2013).
 7. G. Rajasekaran, P. Narayanan and A. Parashar, “Effect of Point and Line Defects on Mechanical and Thermal Properties of Graphene: A Review,” *Crit. Rev. Solid State Mater. Sci.* **41**, 47–71 (2016).
 8. J. M. Ball and A. Petrozza, “Defects in perovskite-halides and their effects in solar cells,” *Nat. Energy* **1**, 16149 (2016).
 9. G. Li, X. He, J. Zhang, R. Jin, A. S. Sefat, M. A. McGuire, D. G. Mandrus, B. C. Sales and E. W. Plummer, “Coupled structural and magnetic antiphase domain walls on BaFe₂As₂,” *Phys. Rev. B* **86**, 060512 (2012).
 10. R. J. D. Tilley, “Defects in Solids,” *John Wiley & Sons, Inc.*, Hoboken, New Jersey (2008).
 11. M. A. Zurbuchen, W. Tian, X. Q. Pan, D. Fong, S. K. Streiffer, M. E. Hawley, J. Lettieri, Y. Jia, G. Asayama, S. J. Fulk, D. J. Comstock, S. Knapp, A. H. Carim and D. G. Schlom, “Morphology, structure, and nucleation of out-of-phase boundaries (OPBs) in epitaxial films of layered oxides,” *J. Mater. Res.* **22**, 1439 (2007).
 12. M. Saghayezhian, S. M. Rezaei Sani, Jiandi Zhang, E. W. Plummer, “Rumpling and Enhanced Covalency at SrTiO₃(001) Surface,” *Journal of Physical Chemistry C*--accepted
 13. R. I. Eglitis, D. Vanderbilt, “First-Principles Calculations of Atomic and Electronic Structure of SrTiO₃ (001) and (011) Surfaces,” *Phys Rev B* **2008**, 77, 195408.
 14. R. I. Eglitis, “Ab Initio Calculations of SrTiO₃, BaTiO₃, PbTiO₃, CaTiO₃, SrZrO₃, PbZrO₃ and BaZrO₃ (001), (011) and (111) Surfaces as Well as F Centers, Polarons, KTN Solid Solutions and Nb Impurities Therein,” *Int. J. Mod. Phys. B* **2014**, 28, 1430009.
 15. N. Bickel, G. Schmidt, K. Heinz, K. Müller, “Ferroelectric Relaxation of the SrTiO₃ (100) Surface,” *Phys. Rev. Lett.* **1989**, 62 (17), 2009–2011.
 16. A. Ikeda, T. Nishimura, T. Morishita, Y. Kido, “Surface Relaxation and Rumpling of TiO₂-Terminated SrTiO₃(001) Determined by Medium Energy Ion Scattering,” *Surf. Sci.* **1999**, 433, 520–524.
 17. H. Guo, Z. Wang, S. Dong, S. Ghosh, M. Saghayezhian, L. Chen, Y. Weng, A. Herklotz, T. Z. Ward, R. Jin, S.T. Pantelides, Y. Zhu, J. Zhang and E. W. Plummer. “Interface-induced multiferroism by design in complex oxide superlattices,” *Proc. Natl. Acad. Sci.* **114**, E5062 (2017).
 18. G. Koster, L. Klein, W. Siemons, G. Rijnders, J. S. Dodge, C. –B. Eom, D. H. A. Blank and M. R. Beasley, “Structure, physical properties, and applications of SrRuO₃ thin films,” *Rev. Mod. Phys.* **84**, 253 (2012).
 19. M. Li, C.-Z. Chang, L. Wu, J. Tao, W. Zhao, M. H. W. Chan, J. S. Moodera, J. Li and Y. Zhu, “Experimental Verification of the Van Vleck Nature of Long-Range Ferromagnetic Order in the Vanadium-Doped Three Dimensional Topological Insulator Sb₂Te₃,” *Phys. Rev. Lett.* **114**, 146802 (2015).
 20. Q. Qiao, S. Zhou, J. Tao, J.-C. Zheng, L. Wu, S. T. Ciocys, M. Iavarone, D. J. Srolovitz, G. Karapetov and Y. Zhu, “Anisotropic charge density wave in layered 1T-TiSe₂,” *Phys. Rev. Mater.* **1**, 0504002 (2017).
 21. V. Mizrahi and J. E. Sipe, “Phenomenological treatment of surface second-harmonic generation,” *J. Opt. Soc. Am. B* **5**, 660 (1988).

22. T. F. Heinz, “Nonlinear Optics of Surfaces and Adsorbates”, *Ph.D. Thesis*, University of California, Berkeley, (1982).
23. A. Kirilyuk, “Nonlinear optics in application to magnetic surfaces and thin films”, *J. Phys. D. Appl. Phys.* **35**, R189 (2002).
24. T. Stehlin, M. Feller, P. Guyot-Sionnest and Y. R. Shen, “Optical second-harmonic generation as a surface probe for noncentrosymmetric media,” *Opt. Lett.* **13**, 389 (1988).
25. H. Y. Hwang, Y. Iwasa, M. Kawasaki, B. Keimer, N. Nagaosa, and Y. Tokura, “Emergent Phenomena at Oxide Interfaces,” *Nat. Mater.* **11**, 103 (2012).
26. K. T. Ko, H. H. Lee, D. H. Kim, J. J. Yang, S. W. Cheong, M. J. Eom, J. S. Kim, R. Gammag, K. S. Kim, H. S. Kim, T. H. Kim, H. W. Yeom, T. Y. Koo, H. D. Him and J. H. Park, “Charge-ordering cascade with spin-orbit Mott dimer states in metallic iridium ditelluride,” *Nat. Commun.* **6**, 7342 (2015).

Publications (2017-2018)

Papers acknowledging primarily supported:

1. Zhen Wang, Hangwen Guo, Shuai Shao, Mohammad Saghayezhian, Jun Li, Rosalba Fittipaldi, Antonio Vecchione, Prahalad Siwakoti, Yimei Zhu, Jiandi Zhang, and E. W. Plummer, “Designing Antiphase Boundaries by Atomic Control of Heterointerfaces,” *Proceedings National Academy of Sciences*, 1808812115 2018 [<https://doi.org/10.1073/pnas.1808812115>].
2. M. Saghayezhian, S. M. Rezaei Sani, Jiandi Zhang, E. W. Plummer, “Rumpling and Enhanced Covalency at SrTiO₃(001) Surface,” *Journal of Physical Chemistry C*—accepted
3. Michael G. Stanford, Philip D. Rack and Deep Jariwala, “Emerging Nanofabrication and Quantum Confinement Techniques for 2D Materials Beyond Graphene,” *NJP 2D Materials and Applications*, **2** 20(1-15) (2018). [10.1038/s41699-018-0065-3]
4. Cheng Zhang, Pushpa R. Pudasaini, Akinola D. Oyedele, Anton V. Ievlev, Amanda V. Haglund, Joo Hyon Noh, Anthony T. Wong, Kai Xiao, Thomas Z. Ward, David G. Mandrus, Olga S. Ovchinnikova, Philip D. Rack, “Ion Migration Studies in Exfoliated 2D Molybdenum Oxide via Ionic Liquid Gating for Neuromorphic Device Applications,” *ACS Applied Materials and Interfaces*, **10** 26 22623 (2018). [10.1021/acsami.8b05577]
5. Lin Li, Zhaoliang Liao, Zhenyu Diao, Rongying Jin, E. W. Plummer, Jiandong Guo, and Jiandi Zhang, “Reentrance of Insulating Phase of La_{2/3}Sr_{1/3}MnO₃(110) Thin Film at Low Temperature,” *Phys. Rev. Materials* **1**, 034405 (2017). [<https://doi.org/10.1103/PhysRevMaterials.1.034405>]
6. Hangwen Guo, Zhen Wang, Shuai Dong, Mohammad Saghayezhian, Lina Chen, Yakui Weng, Rongying Jin, Yimei Zhu, Jiandi Zhang and E. W. Plummer, “Interface-induced multiferroism by design in complex oxide superlattices”, *Proceeding National Academy of Sciences*, **114** (26), E5062 (2017). [<https://doi.org/10.1073/pnas.1706814114>]
7. Michael G. Stanford, Pushpa R. Pudasaini, Nicholas Cross, Kyle Mahady, Anna N. Hoffman, David G. Mandrus, Gerd Duscher, Matthew F. Chisholm, and Philip D. Rack, “Tungsten Diselenide Patterning and Nanoribbon Formation by Gas-Assisted Focused-Helium-Ion-Beam-Induced Etching” *Small Methods*, **1** 901 (2017) [10.1002/smt.201600060]

8. M. Saghayezhian, Zhen Wang, Hangwen Guo, Yimei Zhu, E.W. Plummer, and Jiandi Zhang “*Manipulating the polar mismatch at LaNiO₃/SrTiO₃(111) interface,*” *Phys. Rev. B* **95**, 165434 (2017). [Phys. Rev. B **95**, 165434 (2017)]
9. Zhaoliang Liao, Rongying Jin, E. W. Plummer, and Jiandi Zhang, “*Delicate Competing Electronic States in Ultrathin Manganite Films*”, *Phys. Rev. B* **95**, 085130 (2017). [https://doi.org/10.1103/PhysRevB.95.085130]
10. Michael G. Stanford, Brett B. Lewis, Kyle Mahady, Jason D. Fowlkes, and Philip D. Rack, “Advanced Nano-patterning, Characterization, and Material Synthesis with Gas Field Helium and Neon Ion Beams,” *Journal of Vacuum Science and Technology B*, **35** 030802 (2017) Review Article. [10.1116/1.4981016]
11. Michael G. Stanford, Pushpa R. Pudasaini, Elisabeth T. Gallmeier, Nicholas Cross, Liangbo Liang, Gerd Duscher, Masoud Mahjouri-Samani, Kai Wang, Kai Xiao, David B. Geohegan, Alex Belianinov, Bobby G. Sumpter, and Philip D. Rack, “High conduction hopping behavior induced in transition metal dichalcogenides by percolating defect networks: toward atomically thin circuits” *Advanced Functional Materials* **27** 1702829 (2017) [10.1002/adfm.201702829]
12. Pushpa Raj Pudasaini, Michael G. Stanford, Akinola Oyedele, Anthony T. Wong, Anna Hofmann, Kai Wong, Dayrl P. Briggs, David G. Mandrus, Thomas. Z. Ward, Philip D. Rack, “High performance top-gated multi-layer WSe₂ Field Effect Transistors” *Nanotechnology* **28** 475202 (2017). [10.1088/1361-6528/aa8081]

Papers with secondary acknowledgement:

13. J. Wang, X. Pan, C. Zhang, H.W. Guo, Zeev Vally Vardeny, "Light-controlled spintronic device based on hybrid organic-inorganic perovskites," *J. Photon. Energy* **8**(3), 032207 (2018).
14. Y.W. Cao, Z. Wang, S.Y. Park, Y. K. Yuan, X. R. Liu, S. M. Nikitin, H. Akamastu, M. Kareev, S. Middey, D. Meyers, P. Thompson, P. J. Ryan, P. Shafer, A. N'Diaye, E. Arenholz, V. Gopalan, Y. Zhu, K. M. Rabe, J. Chakhalian, “Artificial two-dimensional polar metal at room temperature,” *Nature Communications* **9**, 1547 (2018)
15. Fengmiao Li, Shanming Li, Zhenzhong Yang, Yan Liang, Qinghua Zhang, Fang Yang, Wentao Li, Xuetao Zhu, Lin Gu, Jiandi Zhang, E. W. Plummer, and Jiandong Guo, “ δ -Doping of Oxygen Vacancies in Epitaxial Oxide Films Dictated by Thermodynamics,” *AIP ADVANCES* **7**, 065001 (2017).
16. B.B. Lewis, R. Winkler, X. Sang, P.R. Pudasaini, M.G. Stanford, H. Plank, R.R. Unocic, J.D. Fowlkes, and P.D. Rack, “3D Nanoprinting Via Laser-Assisted Electron Beam Induced Deposition: Growth Kinetics Enhanced Purity and Electrical Resistivity” *Beilstein Journal of Nanotechnology*, **8** 801 (2017). [10.3762/bjnano.8.83]
17. Pushpa Raj Pudasaini, Akinola Oyedele, Michael G. Stanford, Nicholas Cross, Anthony T. Wong, A. N. Hoffman, Gerd Duscher, David G. Mandrus, Thomas. Z. Ward, Philip D. Rack, “High performance multilayer WSe₂ field effect transistors with carrier type control” *Nano Research* (online 2017 10.1007/s12274-017-1681-5). [10.1007/s12274-017-1681-5]
18. A.T. Wong, JH Noh, P.R. Pudasaini, B. Wolf, N. Balke, A. Herklotz, Y. Sharma, A.V. Haglund, S. Dai, D.Mandrus, P.D. Rack, T.Z. Ward, “Impact of Gate Geometry on Ionic Liquid Gated Ionotronic Systems” *APL Materials* **5** 042501 (2017). [10.1063/1.4974485]
19. A. Oyedele, S. Yang, L. Liangbo, A. A. Puzetky, K. Wang, J. Zhang, P. Yu, P.R. Pudasaini, A.W. Ghosh, Z. Liu, C. M. Rouleau, Bobby. G. Sumpter, M. F. Chisholm, W.

- Zhou, P. D. Rack, D. B. Geohegan, K. Xiao, “PdSe₂: Pentagonal 2D Layers with High Air Stability for Electronics” *Journal of the American Chemical Society* **139**14090 (2017). ***Image Selected for Journal Cover.*** [10.1021/jacs.7b04865]
20. Jennifer M. Black, Jeremy Come, Sheng Bi, Mengyang Zhu, Wei Zhao, Anthony T. Wong, Joo Hyon Noh, Pushpa Raj Pudasaini, Pengfei Zhang, M. Baris Okatan, Sheng Dai, Sergei V. Kalinin, Philip D. Rack, Thomas Z. Ward, Guang Feng, Nina Balke, *Role of Electrical Double Layer Structure in Ionic Liquid Gated Devices*, *ACS Applied Materials and Interfaces* **9** 40949 (2017). [10.1021/acsami.7b11044]

Nano-optical imaging, spectroscopy, and control of quantum materials

Markus B. Raschke, Department of Physics, and JILA, University of Colorado, Boulder

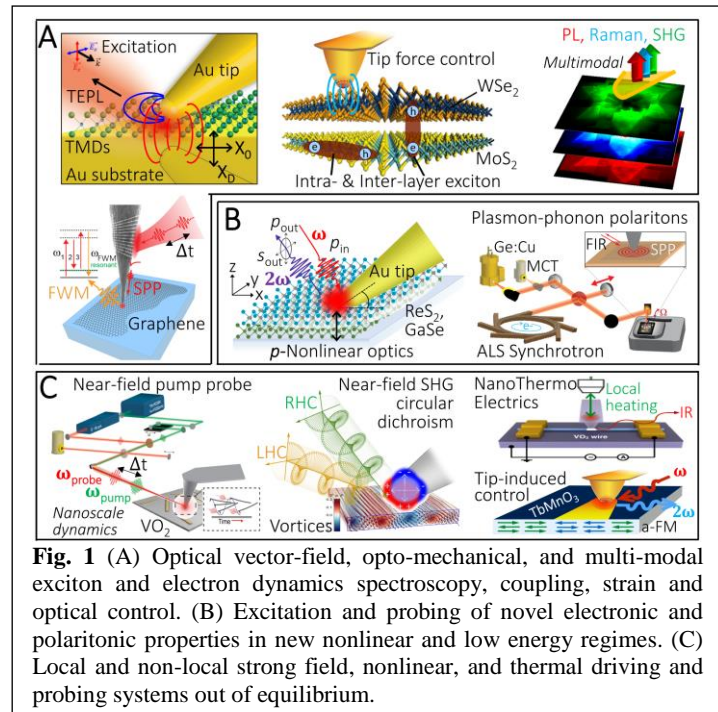
Research Scope: Optical tip-based scanning probe microscopy has emerged as a frontier in optical imaging proving *intrinsic few-nanometer spatial optical resolution* through near-field enhancement, localization, and coupling between the tip and sample. Unique to our method in this project is the extension towards a *multi-modal approach* combining a wider range of optical modalities as illustrated in Fig. 1, including nonlinear and ultrafast spectroscopy with as high as few-femtosecond temporal resolution. This allows *probing structure, coupling, and dynamics* of elementary excitations in different quantum materials on the nanoscale. Further, through selective optical antenna, vector-field, and tip-induced nano-opto-mechanical interactions we started to *control these quantum states* and with them the material response. In applications to 2D, polaritonic, and correlated materials we address the overarching question how intrinsic and extrinsic nano-scale phenomena in the form of microscopic defects, heterointerfaces, microscopic domain formation, of competing quantum phases, and other inhomogeneities influence the macroscopic material properties.

Recent Progress: In the past two years we have made advances in both application of optical nano-imaging for the study of outstanding phenomena in quantum materials as well as the

development and refinement of new nano-imaging modalities. We pursue method development, demonstration and application of optical nano-probe imaging in our lab, as well as in collaboration with EMSL/PNNL and ALS/LBL to disseminate the technique making it available as user facilities. In addition to the application to problems in complex materials our work ties into new fundamental questions of optical physics that enables, e.g., the combination with femtosecond spectroscopy to access ultrafast dynamics on the nano-scale, or taking advantage of the enhanced electromagnetic density of states of the thermal near-field or the coherence of mid-IR synchrotron radiation, for broadband spectroscopy within the only nanoscale sample volumes inherent with the increase in spatial resolution. Our work over the past 2 years encompasses:

2D materials: nanoscale imaging and control of exciton emission

In a series of systematic studies, we have used the optical antenna tip properties, in combination with nano-mechanical tip-sample force interaction, in new ways for nano-scale *excitation, imaging, and both optical and local strain control of excitonic properties in transition metal dichalcogenides (TMDs)*.



A) Exciton control in TMDs [1]. The physical properties of many classes of 2D materials are strongly influenced by nanoscale heterogeneities in the form of edges, twin boundaries, and nucleation sites. Using combined tip-enhanced Raman scattering (TERS, sensitive to lattice structure) and photoluminescence (TEPL, sensitive to the electronic degrees of freedom) nanospectroscopy and imaging, we resolve nanoscale correlations of exciton PL in WSe₂ with these crystal defects, notably the discovery that the atomic scale grain boundaries act as non-radiative recombination sites with length scale defined by the ~ 30 nm exciton diffusion length [1]. Through active atomic force tip interaction, we can image and control the crystal strain and locally tune the bandgap.

B) Turning dark excitons bright [2]. Excitons, Coulomb-bound electron-hole pairs, are elementary photo-excitations in semiconductors that can couple to light through radiative relaxation. In contrast, dark excitons show anti-parallel spin polarization with generally forbidden radiative emission. Here

we demonstrated a tip-enhanced nano-optical approach taking advantage of the orthogonal transition dipole orientation of bright and dark excitons, to *induce, switch, and modulate the dark exciton emission at room temperature* in WSe₂ with Purcell factor control through the tip-sample nano-cavity [2] as shown in Fig. 2. With previous approaches relying on cryogenic temperatures, this approach provides a new and facile way to harness excitonic properties in low-dimensional semiconductors for quantum optoelectronics and other applications. We will extend this tip-antenna polarization selectivity for the study of additional far-field selection rule forbidden transitions including interlayer excitons.

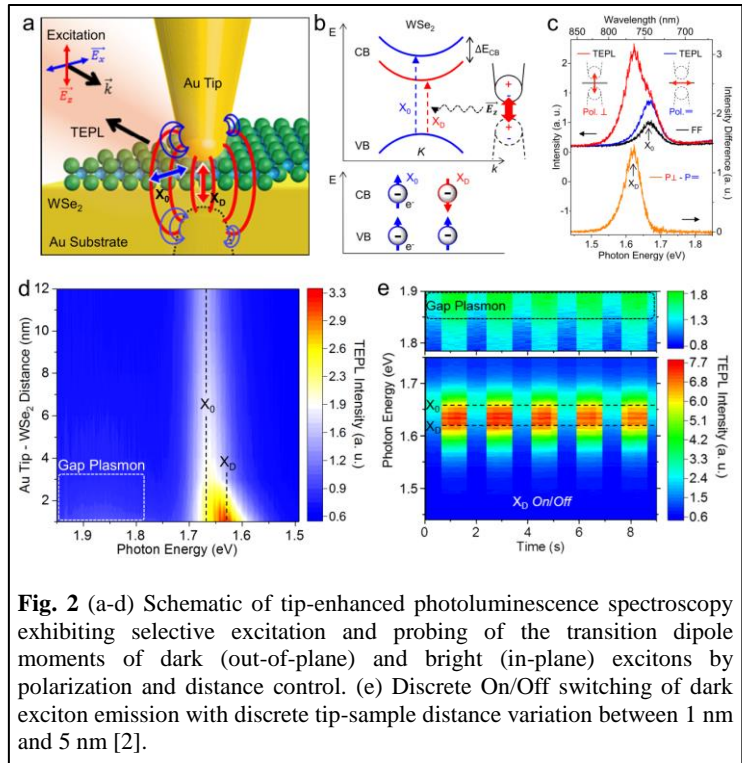


Fig. 2 (a-d) Schematic of tip-enhanced photoluminescence spectroscopy exhibiting selective excitation and probing of the transition dipole moments of dark (out-of-plane) and bright (in-plane) excitons by polarization and distance control. (e) Discrete On/Off switching of dark exciton emission with discrete tip-sample distance variation between 1 nm and 5 nm [2].

C) Optical crystallography of graphene grain boundaries [3]. We studied graphene to understand lattice and electronic structure at grain boundaries from correlated measurement of topography, near-field scattering, and multispectral tip-enhanced Raman spectroscopy (TERS) imaging with nanometer spatial resolution. We nano-imaged *twisting and orientation of grain boundaries* from differences in phonon scattering associated with modifications in electronic structure at the K-point in the Brillouin zone [3].

D) Vector-field optical response function imaging [4]. We present a novel tilted antenna-tip approach to control the optical vector-field by breaking the axial symmetry in tip-enhanced near-field microscopy. This gives rise to a localized plasmonic antenna effect with significantly

enhanced both in- and out-of-plane field components, allowing us to fully explore the symmetry selectivity in second-harmonic generation (SHG) for a *generalized approach to optical nano-crystallography and -imaging* demonstrated in monolayer MoS_2 and ferroelectric YMnO_3 [4] as shown in Fig. 3. This work provides the basis of the new work on nonlinear and ultrafast imaging of 2D materials and ferroic states including vortices.

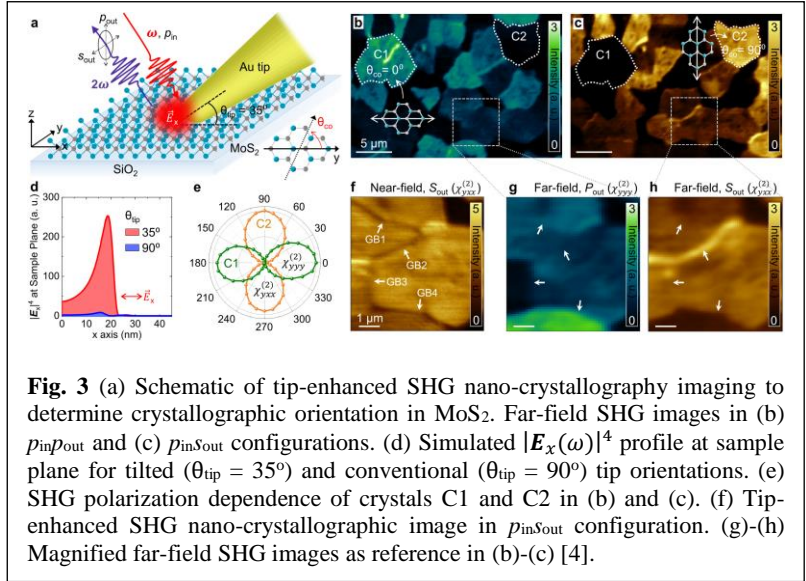


Fig. 3 (a) Schematic of tip-enhanced SHG nano-crystallography imaging to determine crystallographic orientation in MoS_2 . Far-field SHG images in (b) $p_{in}p_{out}$ and (c) $p_{in}s_{out}$ configurations. (d) Simulated $|E_x(\omega)|^4$ profile at sample plane for tilted ($\theta_{tip} = 35^\circ$) and conventional ($\theta_{tip} = 90^\circ$) tip orientations. (e) SHG polarization dependence of crystals C1 and C2 in (b) and (c). (f) Tip-enhanced SHG nano-crystallographic image in $p_{in}s_{out}$ configuration. (g)-(h) Magnified far-field SHG images as reference in (b)-(c) [4].

Nonlinear and multimodal nano-imaging of correlated and quantum materials

Heterogeneity in intrinsic defect induced doping [5]. In a multi-institutional collaboration, we presented the first multimodal *atomic-to-mesoscale resolution imaging of defects and heterogeneities* in topological insulator (TI) and thermoelectric materials of Bi_2Se_3 and Sb_2Te_3 [5]. In our contribution, using laser and IR *s*-SNOM, we imaged and spectroscopically probed heterogeneities in carrier concentration associated with defects during crystal growth [5].

Nonlinear nano-imaging of novel ferroic phases [6]. We extended the range of tip-enhanced nano-spectroscopy and nano-imaging studies to *nonlinear nano-crystallography and imaging*. In collaboration with R. Ramesh and L. W. Martin at UC Berkeley, we demonstrated nonlinear optical *second-harmonic-generation (SHG) nano-crystallography imaging* of $\text{PbTiO}_3/\text{SrTiO}_3$ superlattices to reveal nanoscale distribution of $a1/a2$ and vortex phases [6].

Mid- to far-infrared nano-imaging and -spectroscopy

Far-infrared *s*-SNOM [7]. Enabled by a new copper-doped germanium detector, we extended the spectral range of IR *s*-SNOM in *Synchrotron Infrared Nano-Spectroscopy (SINS)* to $31 \mu\text{m}$ (320 cm^{-1} , 9.7 THz), exceeding conventional limits by one octave into the far-infrared (FIR) regime [7]. We demonstrated its performance in an application to *gate-tuning coupled graphene plasmon-phonon polaritons* based on low energy phonon modes in the SiO_2 substrate. **Thermal infrared near-field spectroscopy (TINS) [8].** Following our earlier pioneering work on thermal infrared nano-spectroscopy (TINS) based on heated tips, we have completed an effort to transition to the use of regular AFM cantilever tips to control the *temperature up to 1800 K* by laser heating providing *localized ultra-broadband IR emission from the tip* [8]. This new and versatile probe for TINS will be used for the new work for simultaneous local excitation and probing quantum phase transitions.

Future Plans: In applications to 2D, polaritonic, and correlated materials we address the overarching question how intrinsic and extrinsic nano-scale phenomena in the form of microscopic defects, heterointerfaces, microscopic domain formation, of competing quantum phases, and other inhomogeneities influence the macroscopic material properties.

A) *2D layered materials and collective interfacial phenomena*: In semiconducting 2D materials, we will address questions on bright, dark, interlayer, and exciton polariton properties, from their coupling and control through lattice degrees of freedom to the exploration of condensate formation. In extension to the time domain in optical four-wave mixing and time resolved photocurrent, we will image the spatio-temporal few-femtosecond electronic coherence on the nanometer-femtosecond scale in graphene and TMDs (Fig. 4).

B) *Novel nonlinear optical and hybrid plasmon-polariton phenomena*: In vector-field nano-imaging with opto-mechanical control we explore novel nonlinear optical properties in materials of new symmetry properties (ReS₂, GaSe). We excite and image through tip- and gate-control plasmon-phonon polaritons in graphene coupled to phononic substrates in the far-infrared (FIR) regime.

C) *Correlated oxides and ferroics: domains and dynamics*: In ultrafast pump-probe nano-imaging with far-from-equilibrium excitation in combination with local thermal, strain, and photodoping control, we will probe the dynamics of the insulator-to-metal transition (IMT) in VO₂ and transient behavior in chalcogenide based thermoelectrics to distinguish static and dynamics heterogeneities in the coupled electron-lattice dynamics. We will apply a novel approach of vector-field nonlinear nano-imaging to probe coupled ferroelectric and antiferromagnetic order in multiferroics and skyrmions in ferroelectric superlattices.

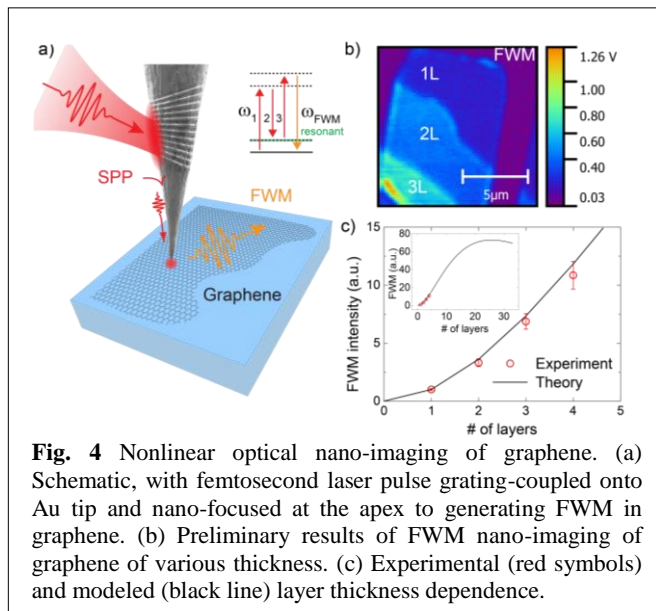


Fig. 4 Nonlinear optical nano-imaging of graphene. (a) Schematic, with femtosecond laser pulse grating-coupled onto Au tip and nano-focused at the apex to generating FWM in graphene. (b) Preliminary results of FWM nano-imaging of graphene of various thickness. (c) Experimental (red symbols) and modeled (black line) layer thickness dependence.

Publications (supported by BES, past 2 years)

- [1] K.-D. Park, O. Khatib, V. Kravtsov, G. Clark, X. Xu, and M. B. Raschke “Hybrid tip-enhanced nano-spectroscopy and nano-imaging of monolayer WSe₂ with local strain control” *Nano Letters*, **16**, 2621 (2016).
- [2] K.-D. Park, T. Jiang, G. Clark, X. Xu, and M. B. Raschke “Radiative control of dark excitons at room temperature by nano-optical antenna-tip Purcell effect” *Nature Nanotechnol.* **13**, 59 (2018).
- [3] K.-D. Park, M.B. Raschke, J.M. Atkin, Y.H. Lee, and M.S. Jeong “Probing bilayer grain boundaries in large area graphene with tip-enhanced Raman spectroscopy” *Advanced Materials* **29**, 1603601 (2017).
- [4] K.-D. Park and M. B. Raschke “Polarization control with plasmonic antenna-tips: A universal approach for optical nano-crystallography and vector-field imaging” *Nano Letters* **18**, 2912 (2018).
- [5] X. W. Lu, et al. “Nano-imaging of electronic heterogeneity in Bi₂Se₃ and Sb₂Te₃ nanocrystals” *Adv. Electron. Mater.* **4**, 1700377 (2018).
- [6] A. R. Damodaran et al. “Phase coexistence and electric-field control of toroidal order in oxide superlattices” *Nature Materials* **16**, 1003 (2017).
- [7] O. Khatib, H.A. Bechtel, M.C. Martin, M.B. Raschke, and G.L. Carr “Far-infrared synchrotron near-field nano-imaging and -spectroscopy”, *ACS Photonics* (in press, DOI: 10.1021/acsp Photonics.8b00565).
- [8] B.T. O’Callahan and M. B. Raschke “Laser heating of scanning probe tips for thermal near-field spectroscopy and imaging”, *APL Photonics* **2**, 021301 (2016).

Scanning Thermal Microscopy for Studying Nanoscale Thermal Radiation

Edgar Meyhofer, Department of Mechanical Engineering, University of Michigan, Ann Arbor, MI, 48109

Pramod Reddy, Department of Mechanical Engineering and Department of Materials Science and Engineering, University of Michigan, Ann Arbor, MI, 48109

Research Scope

The goal of this project is to develop novel scanning probe microscopy and calorimetric tools to investigate nanoscale heat transport and energy conversion. Specifically, we seek to study the flow of heat via electrons and phonons in atomic and molecular chains and the flow of heat via photons in nanoscale gaps (i.e. nanoscale thermal radiation). Further, we seek to understand how heat can be converted into electricity via photons in nanoscale gaps. Towards these goals we have already created novel probes and performed key experiments to obtain important new insights into nanoscale thermal transport and energy conversion that we describe below.

Recent Progress

Probing thermal transport in single atom junctions: The study of thermal conduction in nanoscale systems is critical to manage heat dissipation in nanoscale devices and to understand the potential of nanoscale systems for energy conversion (e.g. thermoelectric) and heat management (thermal-valves, -transistors etc.) technologies. Moreover, nanoscale systems hold the promise to reveal novel quantum effects related to energy transport, which are key to

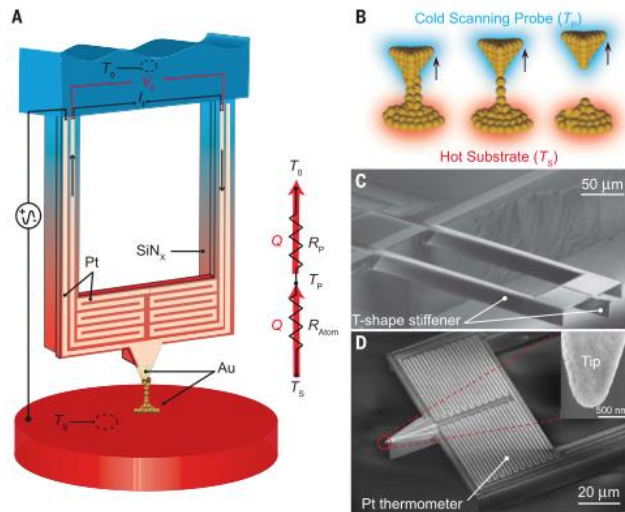


Figure 1: (a) Calorimetric scanning probe capable of resolving heat currents with pW resolution. (b) Schematic showing Au atomic junctions formed between a Au coated tip and substrate. (c, d) SEM images of scanning probes. Adapted from L. Cui *et al.*, *Science* (2017).

developing breakthrough energy conversion and information processing technologies. One of the central goals in the last two decades in nanoscale energy transport has been to extend thermal transport measurements all the way to the atomic scale and to elucidate the ultimate limits of energy and heat flow. However, while it has been possible to study charge transport and thermoelectric effects in single atom junctions, quantum thermal transport measurements involve formidable challenges that have turned out to be insurmountable. In our recent work (L. Cui *et al.*, *Science* (2017)) we achieved the first direct measurements of the thermal conductance of metallic atomic contacts at the single-atom limit and reported the first observation of quantized thermal transport at room temperature.

Specifically, to overcome the resolution limits

of thermal measurements *we developed novel custom-fabricated picowatt resolution scanning thermal probes* (Fig. 1) and show that the thermal conductance of gold single-atom junctions is quantized at room temperature. We also demonstrate that the Wiedemann-Franz law, a fundamental law in solid-state physics connecting the thermal and electrical conductance in metals, applies all the way down to single-atom contacts and irrespective of the metal. Moreover, we are able to quantitatively explain all our observations with state-of-the-art abinitio methods within the framework of the Landauer picture of quantum coherent thermal transport.

Peltier Cooling in Molecular Junctions: In the past few years much theoretical work has suggested that molecular junctions can achieve impressive thermoelectric properties highlighting the potential of molecular junctions for solid-state cooling. Yet, there was no experimental demonstration of cooling using molecular junctions. In our recent work (L. Cui *et al.*, *Nature Nanotechnology* (2018)) we achieved an important experimental breakthrough that enabled systematic probing of refrigeration in molecular junctions (Fig. 2) with picowatt resolution. Specifically, *we employed custom-fabricated calorimeters in conjunction with an ultra-high vacuum atomic force microscope* to create molecular junctions and study cooling in them with picowatt resolution. Further, we perform independent measurements of two key transport properties: the Seebeck coefficient and electrical conductance of the junctions and showed that the observed cooling and heat dissipation characteristics of the junctions are closely related to these transport properties. Finally, we showed that the cooling characteristics of molecular junctions can be dramatically changed by just varying a few atoms in the molecules. Our observations are also supported by state-of-the-art calculations that explain the observed cooling characteristics within the Landauer picture. These findings are expected to impact various

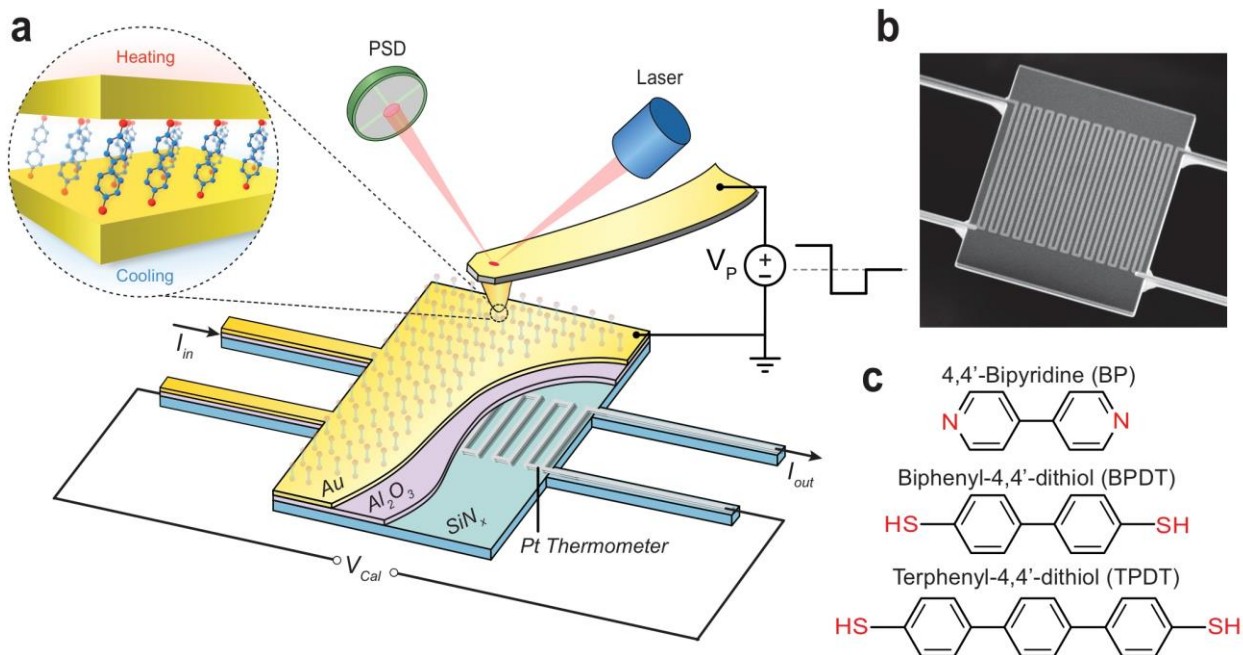


Figure 2: Probing cooling in molecular junctions. **a**, Schematic of the experimental platform where a Au-coated AFM tip is in gentle contact with a self-assembled monolayer of molecular junctions formed on a Au-coated calorimetric microdevice. The resistance of the Pt thermometer is continuously monitored by applying an electric current (I_{in}) into the resistor and measuring the voltage output (V_{cal}). **b**, SEM image of the custom-fabricated microdevice. Adapted from L. Cui *et al.*, *Nature Nanotechnology* (2018).

emerging fundamental fields and future applications, including nanoelectronics, quantum transport and the multi-disciplinary field of molecular thermoelectrics.

Nanogap Thermophotovoltaic Energy Conversion: Solid-state approaches for converting heat to electricity are extremely important for a broad range of diverse applications, including waste heat recovery in transportation (from cars to airplanes) and industry, decentralized power generation, micropower generation and electricity generation in extreme environments (e.g. deep space). Therefore, during the last two decades an enormous amount of research has focused on thermoelectric-based, solid-state energy conversion. An alternative approach for accomplishing solid-state energy conversion—thermophotovoltaics (TPV), which employs a hot emitter and a photovoltaic cell—has also been of significant research interest for several decades. Unfortunately, progress in employing TPV- based solid-state energy conversion has been virtually stalled by the limited power output, which arises due to the low density of electromagnetic modes that contribute to energy conversion in the far-field. This is, at first sight, rather perplexing, because numerous studies have suggested that the limitation of far-field TPV devices can be overcome by placing the hot emitter and the PV cell with nanoscale gap separation, which dramatically increases the electromagnetic density of states contributing to energy transfer. However, suitable nanogap TPV devices could never be demonstrated in the past

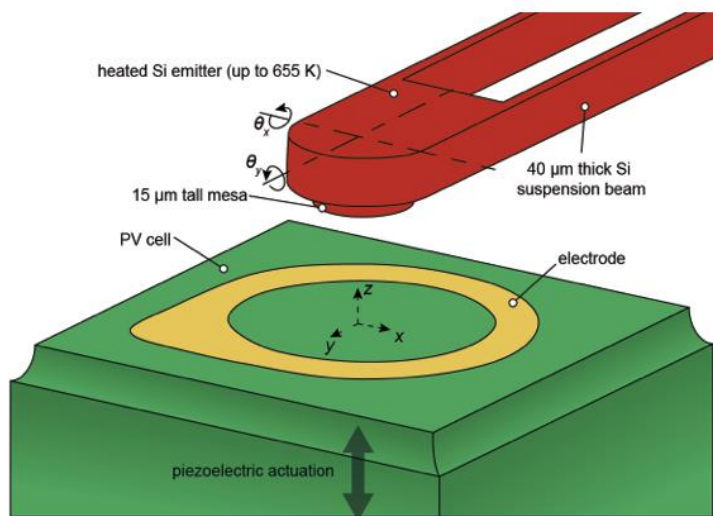


Figure 3: Probing nanogap thermophotovoltaic energy conversion. Schematic illustration of the of a microfabricated emitter (red) device placed in close proximity (nanogap) of a PV device. Both devices can be translated in the x - and y -dimensions. Angular control of the emitter allows for parallelizing the devices and a piezoelectric actuator is used to precisely control the vacuum gap size. Adapted from A. Fiorino *et al.*, Nature Nanotechnology (2018).

due to extraordinary experimental challenges in accomplishing the desired device geometries and measurements. In our recent work (A. Fiorino *et al.*, Nature Nanotechnology (2018)) we demonstrated an experimental breakthrough, which shows for the first time systematic studies of nanogap near-field thermophotovoltaic devices. Specifically, by employing microfabricated scanning probe based emitters (Fig. 3) and a novel nanopositioning platform, we varied the gap-size between hot emitters and PV cells all the way from 10 microns to 60 nm and showed that the power output of nanogap TPV devices can exceed those of far-field TPV devices by 40 times!

Probing Far-Field Thermal Radiation from Nanoscale Objects: All hot bodies emit energy in the form of electromagnetic waves. Understanding such thermal radiation is of great importance in engineering and science due to its impact on energy conversion (e.g. photovoltaics, thermo-photovoltaics), climate change (green house effects) and planetary atmosphere modeling, to name a few. The maximum heat flow rate between objects in the far-field, i.e. gap-sizes greater than the thermal wavelength ($\sim 10 \mu\text{m}$ at 300K), is given by the blackbody limit. However, it is well recognized this estimate

is only applicable to situations where the size of objects and separation between them are larger than the thermal wavelength. Surprisingly, no experiments have studied how radiative heat transfer rates are affected when the object dimensions are smaller than the thermal wavelength. We report a breakthrough (**D. Thompson *et al.*, Nature, 2018**) that shows for the first time that the blackbody limit can be exceeded in the far-field. In fact, we present detailed experimental evidence, using state-of-the-art, direct calorimetric measurements, which demonstrates that heat transfer rates between sub-wavelength structures can surpass the blackbody limit by 100 times! Further, via modern electromagnetic calculations, we provide a detailed, mechanistic analysis of the origin of these enhancements. These results are expected to open new research avenues in nanoscale thermal radiation.

Future Plans

We will continue to develop scanning probe metrology tools to perform highly sensitive measurements of energy transport at the nanoscale. We are confident that our instrumentation advances will yield important new insights into energy transport and energy conversion at the nanoscale.

Publications

1. D. Thompson, L. Zhu, R. Mittapally, S. Sadat, Z. Xing, P. McArdle, M. M. Qazilbash, P. Reddy and E. Meyhofer, “Hundred-fold enhancement in far-field radiative heat transfer over the blackbody limit” *Nature* (2018)
2. A. Fiorino, L. Zhu, D. Thompson, R. Mittapally, P. Reddy and E. Meyhofer, “Nanogap near-field thermophotovoltaics” *Nature Nanotechnology* (2018)
3. A. Fiorino, D. Thompson, L. Zhu, R. Mittapally, S-A. Biehs, O. Bezenenet, N. El-Bondry, S. Bansropun, P. Ben-Abdallah, E. Meyhofer and P. Reddy, “A thermal diode based on nanoscale thermal radiation”, *ACS Nano* (2018)
4. A. Fiorino, D. Thompson, L. Zhu, B. Song, P. Reddy and E. Meyhofer “Giant enhancement in radiative heat transfer in sub-30 nm gaps of plane parallel surfaces”, *Nano Letters* (2018)
5. L. Cui, R. Miao, K. Wang, D. Thompson, L. A. Zotti, J. C. Cuevas, E. Meyhofer and P. Reddy, “Peltier Cooling in Molecular Junctions”, *Nature Nanotechnology* (2018)
6. L. Cui, W. Jeong, S. Hur, M. Matt, J. C. Klockner, F. Pauly, P. Nielaba, J. C. Cuevas, E. Meyhofer and P. Reddy, “Quantized Thermal Transport in Single-Atom Junctions”, *Science* (2017)
7. L. Cui, W. Jeong, V. Fernandez, J. Fiest, J. C. Cuevas, E. Meyhofer, P. Reddy, “Study of Radiative Heat Transfer in Angstrom- and Nanometre-sized gaps ” *Nature Communications* (2017)

Symmetry-breaking mechanism and metastable states in charge-ordered systems probed using femtosecond electron diffraction and spectroscopy

Chong-Yu Ruan

Michigan State University, East Lansing, MI 48824. E-mail: ruan@pa.msu.edu

(i) Program Scope

This project seeks to understand the spontaneous and explicit symmetry-breaking mechanisms pertaining to charge-density wave (CDW) systems. The CDW is a primary electronic ordering phenomenon frequently identified in low-dimensional and strongly correlated electron materials. In these systems, the charge ordering, which may coexist or compete with other types of electronic ordering, such as spin and orbital ordering, and superconductivity, can conspire with the lattice distortion to drastically alter the properties of solids(1). Understanding when these states may co-exist or compete in order to predict the dependence of these states on control parameters such as doping, confinement, temperature, and stress state, is central for designing functionality(2). Furthermore, in the last few years, hidden states involving new types of charge ordering have been reported(3-6). Such states are formed primarily after a quench from a highly excited state, often prepared by applying strong laser excitation, high pressure, or under excessive strain field. The growing identification of these states has spurred interests in understanding the out-of-equilibrium control routes in preparing new types of materials(7). Our approach uses the controlled laser pulse as a tuning parameter to create the extreme environment where such hidden states may emerge, and examines their ensuing structural and electronic property evolution at far from equilibrium with ultrafast electron-based probes. With this method, our explicit goals are to: (I) Map the new nonequilibrium phase diagram based on the initial conditions, such as temperature and strain, and the external control parameter, namely the laser fluence or energy, for initiating the new states. Based on their transient responses at different timescales, these phase diagrams can be characterized as either thermally driven or interaction-driven; (II) Study the dynamical phase transitions and the associated self-organization to form long-range order near the critical laser fluences identified in the phase diagram. In particular, the correlated spatial and temporal fluctuations that may be described by the universal scaling law could be used to define new classes of phase transition under far-from-equilibrium conditions.

(ii) Recent Progress

To advance the project goals, we have developed new experimental capabilities in order to probe these nonequilibrium phase transitions. The most crucial step is to deliver a higher level of electron beam intensity, without sacrificing the time and energy resolutions. This has been accomplished, as detailed in reference (8) and (9). The key is to enable adaptive control of the electron phase space impacted by the space-charge effect associated with the intense ultrashort electron pulses. We accomplish this through employing one or more radio-frequency (RF) cavities as a new lens system for shaping the longitudinal optical

properties of the intense electron pulses. Together with other existing transverse magnetic lens system, full adjustment of the electron pulses' phase space can be delivered, leading to a higher level of performance. Fig. 1 demonstrates such a performance in ultrafast electron diffraction study of CDW. What's shown is the high momentum resolution (Fig. 1a) from the more coherent electron pulse (coherence length ≥ 30 nm) as well as the higher temporal resolution (≤ 100 fs, Fig. 1b, depending on the number of electrons employed), which are made possible by correcting the transverse and longitudinal chirps developed during the pulse evolution by the new lens systems. Furthermore, these improvements are accomplished while maintaining a reasonable beam dosage (~ 1 electron per square micron) – the diffraction is recorded with 10 second acquisition time (or 10,000 pulses), similar to more traditional approaches. In addition, our recent renovation in the ultrafast electron diffraction facility provides a more stable environment to allow RF-laser stabilization to the level of 20 fs (rms) over a long duration (> 48 hrs). This improved sensitivity and stability thus enables us to explore the full potential of our electron beam system to study the weaker and subtler features of phase transitions hidden from the view previously.

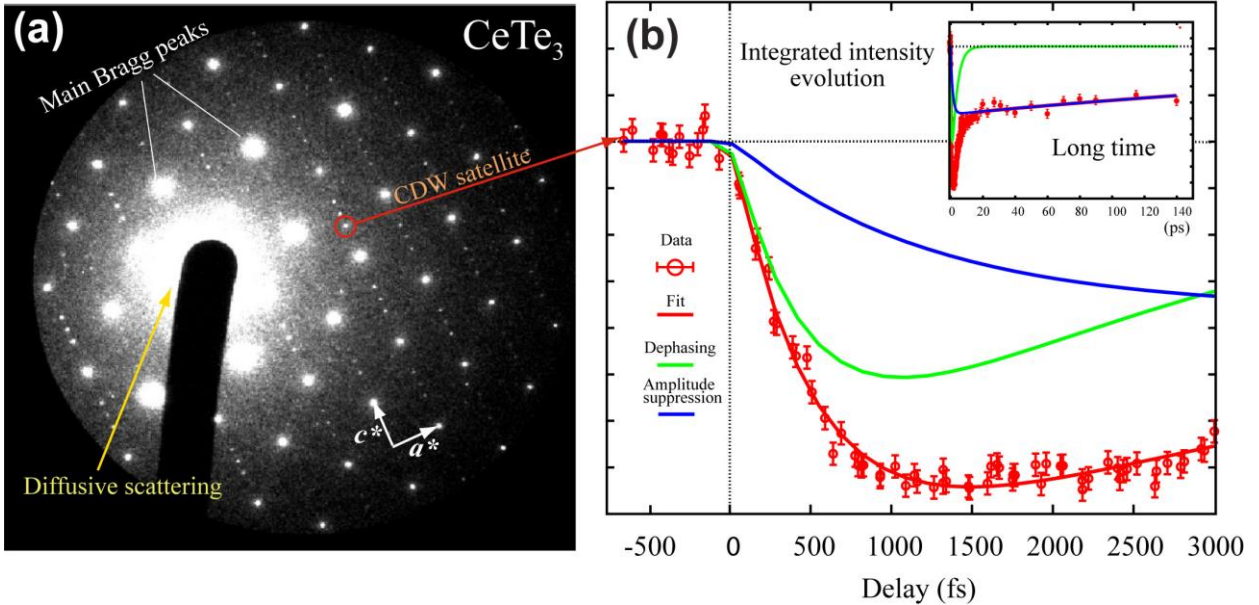


Fig. 1: Ultrafast electron diffraction of CeTe_3 thin flake by the high-brightness beam column. (a). Electron diffraction pattern obtained at the negative time. The major scattering features: the intense Bragg reflection from the square lattice, the diffusive scattering following the symmetry of Fermi surface, and the CDW satellite peaks for the stripe CDW phase are clearly visible. (b). Intensity evolution from a selected CDW satellite peak, indicating contrasting features of change that are dominant in the short time (green component) and in the long time (blue component), respectively.

We will report our new experimental results dedicated to the studies of photo-induced CDW phase transitions with the improved capabilities on the rare-earth telluride (RTe_3) and tantalum disulfide (TaS_2) systems. We will address the dynamical symmetry-breaking processes in the nonequilibrium phase transitions, which manifest in the changes of complex order parameters of the CDW. By exploiting the high momentum (Q) resolution, we can examine the dynamical correlation changes near the critical points. The Q -dependent

features also let us separate the amplitude and phase evolutions of the static and emerging orders that are either impacted or created by the photo-doping effects.

The findings from such studies reveal major differences in the nonequilibrium phase transition as compared to their counterparts at near equilibrium. The first is the ubiquitous observation of metastable states. Such states, which may be best characterized by the critical time, exist by resisting thermal equilibration process to run through its typical course as in a thermal transition (10). We are able to study the universal scaling feature of this state as a function of laser dose, establishing the nonthermal critical points(11). Furthermore, by exploiting the nonequilibrium transition, we can observe different types of symmetry breaking that would be prohibited in their thermal counterparts. For example, in the RTe₃ systems, we observe a route to the C₄ symmetry breaking (or the checkerboard phase), instead of the C₂ (or stripe phase) that is commonly observed at the steady-state transitions(12). In TaS₂, we exploit the photo-doping effects to create the Friedel oscillations in the charge-density wave collectives. Such effects break the time-invariant coupling between pre-existing triple-degenerate CDW branches through a noncollinear phase adjustment to form a new topological state.

(iii) Future Plans

We will pursue the leads on the establishment of non-thermal critical points to understand the nature of emerging orders, which would have been destroyed had the system maintained its thermal equilibrium. Such time ordering phenomena are closely linked to the dynamical fluctuations near the critical point, and their protection from rapid thermalization. The theoretical understanding of the prethermalization phenomenon has frequently associated it with the robustness in the pre-existing long-range phase correlations of the system. Nonetheless, currently there has not been clear understanding in such nature being a result of quantum protection or through entanglement of the nonlinearly coupled density waves in a classical sense. Furthermore, in the nonperturbatively driven transitions, the electron and lattice distributions are strongly at nonequilibrium. In such an environment, the new nesting conditions and different types of electron-lattice interplay could play an important part in the nonequilibrium CDW transformations. To complete this understanding, one would also like to know the electronic properties pertaining to the new states and understand how they would co-evolve along with the changing orders of the system. To this end, we will also pursue the ultrafast electron energy loss spectroscopy experiments on these systems. Providing both spectroscopic and spatial fingerprints of the hidden or transient meta-stable phases will be critical for their understanding.

(iv) References

1. E. Dagotto, Complexity in strongly correlated electronic systems. *Science* **309**, 257 (2005).

2. Z. Yang, C. Y. Ko, S. Ramanathan, in *Annual Review of Materials Research*, D. R. Clarke, P. Fratzl, Eds., Vol. 41, 337 (2011).
3. H. Ichikawa *et al.*, Transient photoinduced ‘hidden’ phase in a manganite. *Nat Mater* **10**, 101 (2011).
4. L. Stojchevska *et al.*, Ultrafast switching to a stable hidden quantum state in an electronic crystal. *Science* **344**, 177 (2014).
5. J. Zhang *et al.*, Cooperative photoinduced metastable phase control in strained manganite films. *Nature Materials* **15**, 956 (2016).
6. T.-R. T. Han *et al.*, Exploration of meta-stability and hidden phases in correlated electron crystals visualized by femtosecond optical doping and electron crystallography. *Science Advances* **1**, e1400173 (2015).
7. D. N. Basov, R. D. Averitt, D. Hsieh, Towards properties on demand in quantum materials. *Nature Materials* **16**, 1077 (2017).
8. F. Zhou, J. Williams, C.-Y. Ruan, Femtosecond electron spectroscopy in an electron microscope with high brightness beams. *Chemical Physics Letters* **683**, 488 (2017).
9. J. Williams *et al.*, Active control of bright electron beams with RF optics for femtosecond microscopy. *Structure Dynamics* **4**, 044035 (2017).
10. H. Markus, Dynamical quantum phase transitions: a review. *Reports on Progress in Physics* **81**, 054001 (2018).
11. L. Tim, G. Thomas, S. Jörg, Prethermalization and universal dynamics in near-integrable quantum systems. *Journal of Statistical Mechanics: Theory and Experiment* **2016**, 064009 (2016).
12. H. Yao, J. A. Robertson, E.-A. Kim, S. A. Kivelson, Theory of stripes in quasi-two-dimensional rare-earth tellurides. *Physical Review B* **74**, 245126 (2006).

(v) 2-Year Publications (DOE sponsored)

1. Z. Tao *et al.*, The nature of the photoinduced phase transition and metastable states in vanadium dioxide, *Scientific Reports* **6**, 38514 (2016).
2. F. Zhou, J. Williams, C.-Y. Ruan, Femtosecond electron spectroscopy in an electron microscope with high brightness beams. *Chemical Physics Letters* **683**, 488 (2017).
3. J. Williams *et al.*, Active control of bright electron beams with RF optics for femtosecond microscopy. *Structure Dynamics* **4**, 044035 (2017).
4. F. Zhou *et al.*, Imaging nonthermal critical dynamics of charge-density waves using femtosecond coherent electron pulss, submitted (2018).
5. J. William *et al.*, Observation of light-induced checkerboard charge orders in CeTe₃, submitted (2018).

Atomic-scale Surface Studies of Bulk Metallic Glasses

Udo Schwarz, Department of Mechanical Engineering and Materials Science, Yale University

Research Scope

Bulk metallic glasses (BMGs) are of both scientific and technological interest because the absence of periodic atomic arrangements provides them with unique physical, chemical, and mechanical properties. Their high strength, superior elasticity, and an ability to be easily formed into virtually unlimited shapes with feature sizes from centimeters to Angstroms by blow molding and thermoplastic forming makes them an attractive choice for more and more practical applications and products. Due to their complex internal structure, however, experiments that yield insight into their exact atomic arrangements have been scarce.

The main reason for the slow progress is the lack of experimental tools that enable access to atomic-scale structural and behavioral information for disordered materials combined with the difficulty to reproducibly produce samples with the exact same properties, the latter of which stems from the fact that metallic glasses are locked into metastable states that are highly preparation dependent. The aim of the research is to enable significant progress in our understanding of BMGs by introducing novel sample preparation schemes that results in well defined high-quality samples that are both ideally suited for inspection using an array of surface characterization methods and can be reproduced in other labs, which is thus far a challenge due to the above-mentioned preparation-dependent structural state BMG samples are featuring. The radically new step at the center of this project is that we are performing nanoimprinting by thermoplastic forming in ultrahigh vacuum with well ordered, in-situ cleaned oxide crystals as templates to produce atomically flat, uncontaminated surfaces that are yet fully amorphous. In parallel, the thermal history will be unambiguously defined by setting the sample's so-called fictive temperature, which will allow reliable recreation of the material's atomic-level sub-states. Alternately, atomically flat, uncontaminated surfaces will be produced for atomic-resolution inspection using a novel vacuum-based growth approach. Through a combination of innovative scanning probe studies complemented by more standard surface science experiments and mechanical property testing, we will then obtain unprecedented insight into the nature of the glassy state.

Recent Progress

Most of the work that has been accomplished since the project's start is still building up to the main goal of imaging the atomic structure of a metallic glass, as this ambitious goal requires that a lot of different puzzle pieces have to be lined up first. Towards this goal, we have

focused both on setting up two separate, unique pieces of equipment needed to carry out the final experiments planned as well as in parallel on a wide range of experiments designed to produce samples with well defined states and well characterized properties. With respect to the equipment setup, a centerpiece of the project is the installation of a novel in-situ sample press that will allow us to prepare clean, atomically flat surfaces of bulk metallic glasses directly in ultrahigh vacuum. The design, assembly, testing, and optimization of the press ended up being more time-consuming than originally anticipated and is only just nearing its full operational state. The second major equipment-related preparatory task is the setup of a custom in-house helium liquefier needed to allow us to run experiments continuously at helium temperatures. Like the press, it is a novel development. Pursued in collaboration with Cryomech, Inc., from Syracuse, NY, it includes the installation of a completely sealed, closed-cycle system. Evaporating helium is captured in storage tanks located away from the system in a back room and only re-liquefied by a liquefier that sits right on top of the cryostat after helium levels in the cryostat get low. In contrast to other solutions where the liquefier is constantly running and thereby inducing vibrations, this setup allows to operate with lower noise levels as the liquefier is off during measurement – a crucial feature when attempting to image the atomic structure of disordered materials. After months of iterative improvements, we have now achieved excellent mechanical vibration levels of around 2 pm peak-peak.

On the experimental side, our efforts were dedicated towards the characterization of the preparation-dependent evolution of materials properties and surface morphology using multiple approaches. Progress will be discussed in short using the following four figures for illustration purposes. All samples discussed were made from a $\text{Pt}_{57.5}\text{Cu}_{14.7}\text{Ni}_{5.3}\text{P}_{22.5}$ alloy, henceforth referred to as Pt-BMG or simply BMG.

First, we further improved and characterized the quality of the samples produced using our novel pressing approach that delivers the atomically flat surfaces crucial to the subsequent structural measurements. As illustrated in Fig. 1, we use a strontium titanate single crystal that has been prepared to show clean, atomically flat terraces (a) as a mold against which Pt-BMG is imprinted at 270 °C through thermoplastic forming. Panels (b) – (d) show three different replicas of the same area as in (a), but displayed after mirroring and inverting to ease comparisons (all images are $2\ \mu\text{m} \times 2\ \mu\text{m}$). As can be seen, all details of the atomic terraces are being reproduced, but with varying surface roughness due to the fact that loading rates of the press have been changed from 1 minute (b) to 2 and 3 minutes,

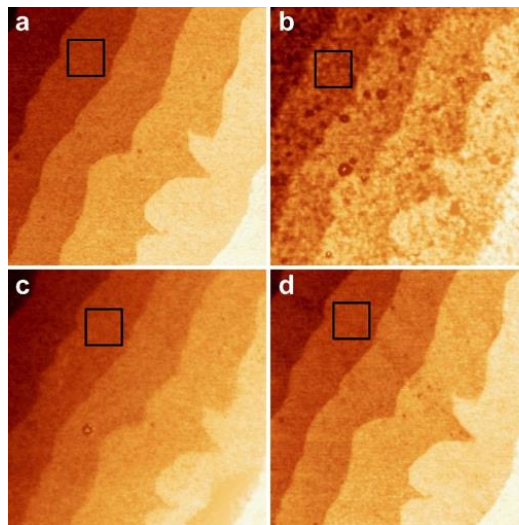


Figure 1: Reproducibility and flow property studies. RMS surface roughness inside the squares was 0.75 Å (SrTiO₃ mold, a), 1.38 Å (BMG replica 1, b), 1.06 Å (BMG 2, c), and 0.71 Å (BMG 3, d), indicating near-perfect replication of the mold (a) by the replica 3.

respectively (c and d). It can be clearly seen that the BMG's viscosity is too high for good replication at the fastest imprinting speed, while RMS roughness analysis (see caption) reveals near-perfect replication for the lowest loading rate in panel (d). From such kinds of experiments, information on the atomic-scale flow properties of BMGs can be extracted.

Next, we used imprinted samples optimized as shown in Fig. 1 for inspection in ultrahigh vacuum (UHV). Even though the samples have been prepared under ambient conditions as the in-situ press is not yet operational, we were already able to obtain high-resolution images that show surfaces with very fine detail. For example, Fig. 2a exposes cluster-like structures in the nm regime, which correspond to the anticipated dimensions of shear transformation zones in BMGs. Moreover, the corresponding phase image Fig. 2b shows phase fluctuations on the sub-nm scale, which are likely to be attributed to density fluctuations within the glass. Finally, the zoom-in of Fig. 2c reveals atomic-scale features.

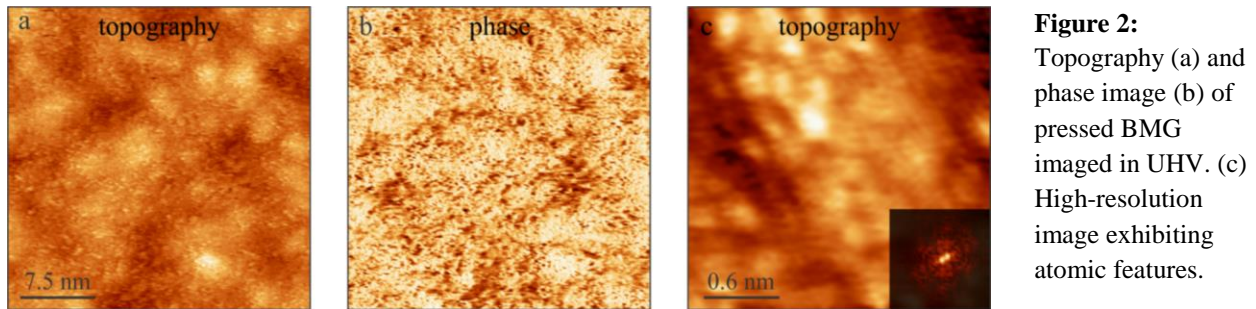


Figure 2: Topography (a) and phase image (b) of pressed BMG imaged in UHV. (c) High-resolution image exhibiting atomic features.

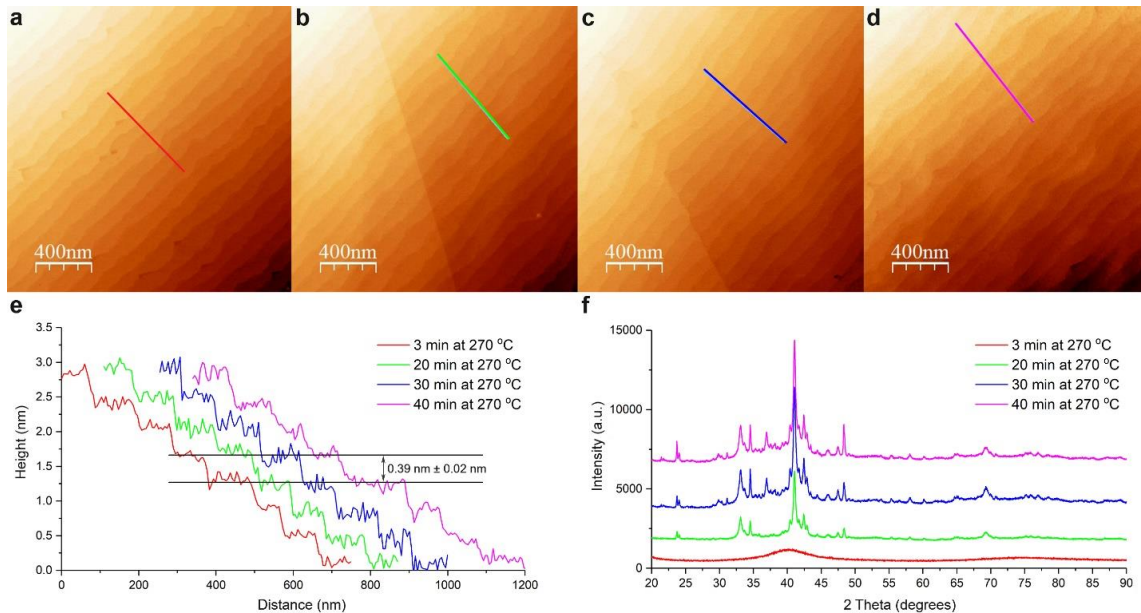
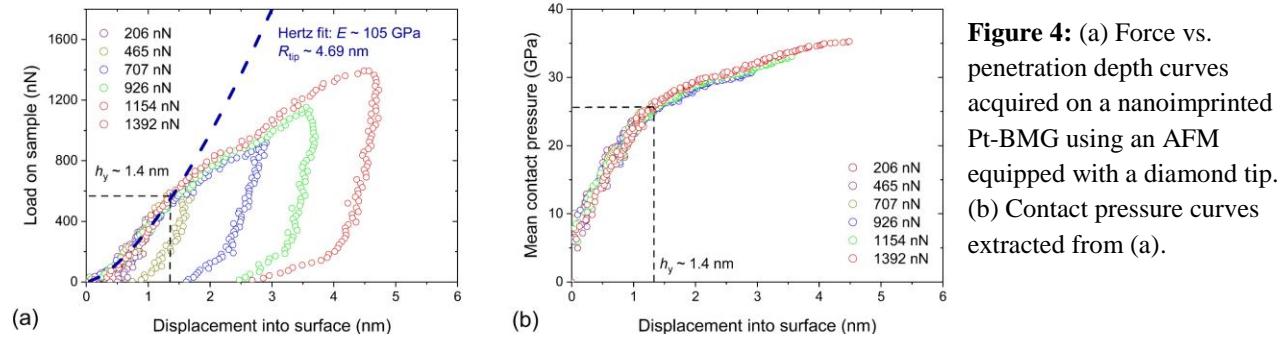


Figure 3: AFM images of BMG samples that have been kept at a processing temperature of 270 °C for a) 3 min.; b) 20 min.; c) 30 min.; and d) 40 min. during imprinting. (e) Line profiles indicating that despite the occurrence of partial or full crystallization, all samples still feature a terraced structure, with terraces separated by the 0.39 nm step height induced by the strontium titanate crystal mold. (f) X-ray diffraction (XRD) spectra indicating the phase of the materials. While the sample that has been held at 270 °C for 3 minutes is still completely amorphous as indicated by the red, featureless curve, the peaks in the other three spectra reveal an increasing degree of crystallization.

Expanding on the above studies, we conducted in-depth studies where the samples were kept after imprinting for extended amounts of times at their processing temperature of 270 °C (Fig. 3). Surprisingly, despite partial (Figs. 3b & 3c) or even full (Fig. 3d) crystallization occurring, all samples still expose clear terraces with steps height around 0.39 nm, and the roughness values are almost identical to that of the values of Fig. 1 (0.73 Å for b, 0.86 Å for c, and 0.80 Å for d). On a fundamental level, it is surprising that atomically flat, partially or fully crystallized Pt-BMG samples can still feature the step heights forced upon them by the imprinting into the SrTiO₃ mold surface while they were still amorphous. The underlying mechanisms for this behavior, as well as the details of the actual surface structure, are at this point unknown, but represent interesting targets for later investigations using the low-temperature high-resolution imaging.



Taking advantage of the availability of atomically smooth imprinted surfaces, we can now, for the first time, analyze localized sub-nm plastic flow to uncover information on size effects under loading and shear transformation zones, a subject that is still poorly understood. By AFM-based nanoindentation and applying a Hertz fit, we find for the tip of Fig. 4a a tip radius of $R_{tip} = 4.69$ nm and a displacement of $h_y = 1.4$ nm at which plastic deformation starts to occur. Using a sphero-conical model for further analysis, pressure-displacement curves as in Fig. 4b can be recovered that reveal very high yield strengths (≈ 25 GPa in Fig. 4b), which is at least $3\times$ higher than control measurements by conventional nanoindentation. This points towards a strong dependence on the dimensions of the stressed volume and can be contrasted to larger-scale models that explain the plastic deformation as originating from the formation of shear bands.

Future Plans

We will continue our experiments regarding the characterization of the structural development of the metallic glasses as a function of preparation history, in particular as a function of its pressing parameters (Fig. 1), fictive temperature (i.e., annealing history; not shown for brevity), and its progress towards crystallization (Fig. 3). Once the in-situ press is operational, the focus will be on producing such well-defined high-quality samples in-situ and image these with high resolution (Fig. 2) using advanced techniques such as repulsive-mode AFM imaging using CO-terminated tips. This will allow, for the first time, direct insight into the atomic structure of bulk metallic glasses.

Publications

1. Omur E. Dagdeviren and Udo D. Schwarz: *Optimizing qPlus sensor assemblies for simultaneous scanning tunneling and noncontact atomic force microscopy based on finite element method analysis*. Beilstein Journal of Nanotechnology **8**, 657-666 (2017).
2. Omur E. Dagdeviren, Chao Zhou, Eric I. Altman, and Udo D. Schwarz: *Quantifying Site-specific Chemical Interactions Accurately Using Cantilever-based Sensors: Strategies, Challenges, and Solutions*. Physical Review Applied **9**, 044040 (2017).
3. Jittisa Ketkaew, Wen Chen, Hui Wang, Amit Datye, Meng Fan, Gabriela Pereira, Udo D. Schwarz, Ze Liu, Rui Yamada, Wojciech Dmowski, Mark D. Shattuck, Corey S. O'Hern, Takeshi Egami, Eran Bouchbinder, and Jan Schroers: *Mechanical glass transition revealed by the fracture toughness of metallic glasses*. Nature Communications **9**, 3271 (2018).
4. Rui Li, Zheng Chen, Amit Datye, Georg H. Simon, Jittisa Ketkaew, Emily Kinser, Ze Liu, Chao Zhou, Omur E. Dagdeviren, Sungwoo Sohn, Jonathan P. Singer, Chinedum O. Osuji, Jan Schroers, and Udo D. Schwarz: *Atomic imprinting into metallic glasses*. Submitted.
5. Amit Datye, Jittisa Ketkaew, Jan Schroers, and Udo D. Schwarz: *Effect of the fictive temperature on the mechanical properties of $Zr_{44}Ti_{11}Cu_{10}Ni_{10}Be_{25}$ metallic glasses*. In preparation.
6. Jiaxin Yu, Amit Datye, Zheng Chen, Chao Zhou, Omur E. Dagdeviren, Jan Schroers, and Udo D. Schwarz: *Atomic-scale Homogeneous Plastic Flow of Bulk Metallic Glass*. In preparation.
7. Zheng Chen, Georg Hermann Simon, Yanhui Liu, Ze Liu, Rui Li, Chao Zhou, Yingbei Liu, Jonathan P. Singer, Chinedum O. Osuji, Jan Schroers, and Udo D. Schwarz: *Atomic-scale molding of amorphous metals by sputter deposition*. In preparation.

Electronic Properties of Organic Photovoltaic Systems under Mechanical Stress

Santiago D. Solares, Department of Mechanical and Aerospace Engineering, The George Washington University, Washington, DC 20052

Hanning Chen, Department of Chemistry, The George Washington University, Washington, DC 20052

Research Scope

The overarching goal of this project is to acquire new fundamental understanding into the evolution of the electronic structure, electrical transport and nanomechanical properties of single polymer chains and bulk organic photovoltaic (OPV) devices, which operate under practical working conditions, where uncontrollable static and dynamic stresses exist due to thermal or mechanical perturbations. This work is complementary to studies focusing on highly controlled laboratory conditions. Specifically, we seek (i) to explore the degradation of OPV device performance under the application of static and dynamic mechanical and thermal stresses, studied through scanning probe microscopies, explaining such phenomena in terms of the electron physics in bulk disordered systems, and (ii) to develop a simulation platform that combines virtual scanning probe microscopy with electronic structure and transport methods, with specific application to disordered polymeric systems, such as those found in OPV devices.

Recent Progress

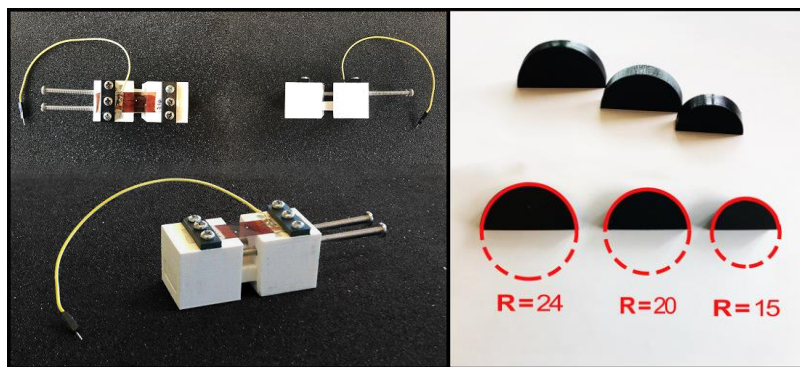


Figure 1. Stretching (left) and bending (right) stages used to impart mechanical stress to OPV devices under electronic and mechanical characterization with AFM.

A variety of atomic force microscopy (AFM) stages (Figure 1) have been fabricated in order to apply linear stretch and bending mechanical stresses to PCBM/PCDTBT OPV active layers, which have been prepared by established methods [1,2]. In some cases, a particular region of the surface was characterized using conductive AFM (C-AFM, electrical conductivity), contact-

resonance AFM (CR-AFM, mechanical properties) and Kelvin probe force microscopy (KPFM, electrical potential) before and after the application of stresses, in order to study local responses. In other cases, a set of areas was characterized and its response averaged, in order to study

macroscopic behaviors across a device. In all cases, changes in the response are expected due to molecular rearrangement, which in turn lead to different mechanical behaviors and electronic properties. In particular, focusing on the electronic properties of these disordered systems, it is expected that such molecular rearrangements should result in changes in the overlap of the wavefunctions of different molecules, which should in turn lead to changes in band structure (to be measured with scanning tunneling microscopy, STM), local conductivity and electrical potential. The experiments show that such changes do indeed take place, but the trends are not always as simplistic as one would expect from basic reasoning. Figure 2, for example, shows C-AFM measurements of two different samples consisting of ~ 90 -nm-thick PCBM/PCDTBT films on PEDOT:PSS/ITO, under the application of bending stress, one studied for a positive tip bias of $+5$ V, and one for negative bias of -5 V. Figure 2(a) shows that upon bending the sample (decreasing the radius of curvature of the bent surface), the conductivity of a particular location first increases, but then decreases (see electrical current histograms in Figure 2(b)). On the other hand, for the counterpart experiment with negative tip bias (Figure 2(c)), the trend is monotonic, with the current decreasing as the radius of curvature is decreased (i.e., as bending is increased). Similar experiments have been conducted for linear stretching (not shown), both below and above the failure limit of the ITO substrate.

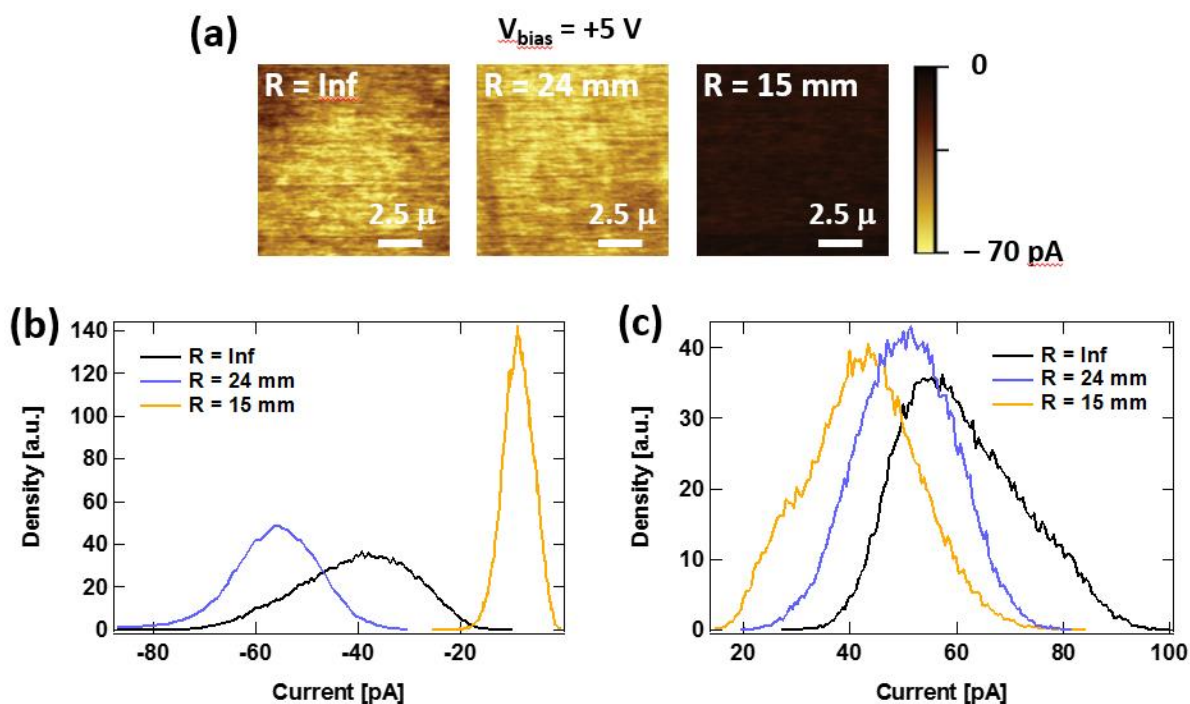


Figure 2. Electrical conductivity characterization of OPV active layers under bending stress using the stages shown in Figure 1. (a) Conductivity measurements under a positive bias of $+5$ V for different surface radii of curvature. (b) Histograms of measured current for the images in (a). (c) Histograms of measured current for an experiment similar to that of (a) but with a negative bias of -5 V.

In many cases where a single area was studied, the trends follow the expected monotonic behaviors, although not always. While the stress modes used so far are the simplest possible, one must realize that at the molecular level the changes are not as trivial as one would infer from macroscopic thinking. Furthermore, deformations such as bending of a film, impart different stresses on different locations of the film (different levels of tensile and/or compressive stress at different depths measured from the surface), depending on film thickness and properties, and substrate properties. There also exist experimental complications, such as changes in the scanning probe as it picks up polymeric material or residual solvent from the surface or deposits adsorbed molecules back onto it, or as its chemical nature changes. In other cases we have observed what appears to be molecular rearrangement of the surface simply due to scanning, without the application of any type of stress, and at times this is linked to the type of probe used, to the drying conditions used to prepare the sample or to the solvent used in the spin casting process. All these limitations place challenges in the ability to acquire statistically valid data.

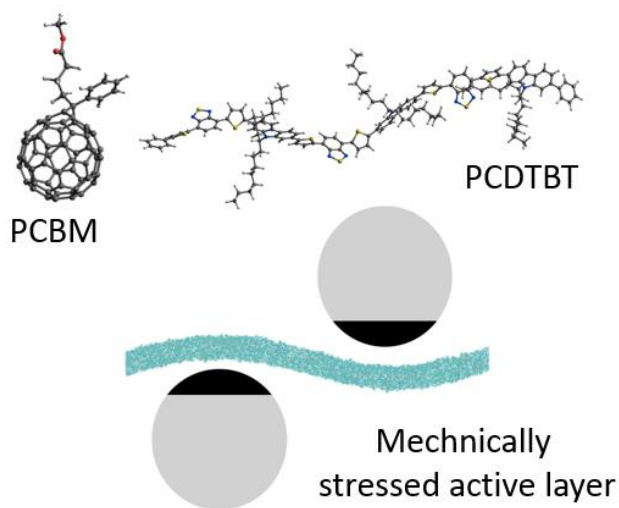


Figure 3. 1.2-million atomistic structures of the OPV active layer under mechanical stress, imparted in this case through “ghost” cylindrical structures.

In order to shed light into molecular mechanisms, large-scale atomistic simulations of our PCBM/PCDTBT systems are being conducted, which will be studied in terms of their mechanical behavior (molecular dynamics), electronic properties (density functional theory) and simulated experimental testing (simulated C-AFM and STM measurements using transport methods). So far, structures such as the film shown in Figure 3 have been constructed and subjected to extensive annealing and equilibration. After simulated annealing, the atomic configurations of the films have been fully relaxed to accommodate bending by adjusting the distribution of mechanical strain.

As a result, layered patterns have been formed through chemical bond stretching, valence angle distortion and disturbance of molecular ordering, in some cases leading to very small scale segregation. The models have then been subjected to stresses and subsequently relaxed under these configurations, prior to calculation of electronic structure and C-AFM and STM responses (this last step has not yet been completed).

Future Plans

On the experimental side, the second project period will focus on the completion of the experimental matrices for different levels of bending and uniaxial stresses for a large number of samples, in order to obtain statistically significant results. This will also include the study of different solvents for the spin casting sample preparation steps, specifically chlorobenzene and

dichlorobenzene, which have shown significantly different results. Once this step is completed, more complex cases will be analyzed, combining cyclic and static mechanical and thermal stresses. For the simulation component of the project, the polymer films will be transferred into a quantum chemistry simulation package for the study of their electronic properties. More specifically, electrical conductance, density of states and optical gaps will be calculated by the open-source CP2K package, which is numerically capable of handling million-atom systems using its massively parallel linear-scaling density functional theory (DFT) scheme on a DOE-supported Theta cluster managed by Argonne National Laboratory. Performing this exercise on films subjected to bending and stretching will reveal the gradual perturbation of their electronic properties, which will be referenced to specific molecular deformations, rearrangements and/or segregation within the films. Future studies include more complex types of stresses, following the experimental approach, as well as dynamic studies on polaron mobility in OPV polymer blends.

Future work on the methodology development component of the award includes efforts to implement intermittent-contact conductivity measurement schemes using AFM, whereby mechanical and electrical properties can be characterized simultaneously during an experiment, in addition to the development of large-scale simulation counterparts.

References

- [1] G. Li, R. Zhu, and Y. Yang, “Polymer solar cells,” *Nature Photonics*, vol. 6, no. 3, pp. 153–161, 2012.
- [2] S. Beaupré and M. Leclerc, “PCDTBT: en route for low cost plastic solar cells,” *Journal of Materials Chemistry A*, vol. 1, no. 37, p. 11097, 2013.

Publications

The above description of results and plans concerns OPV devices, but the project also includes a scanning probe microscopy methodology development component, which is not described in this document. The following publication describes advances in the understanding of time-resolved KPFM.

S. Sadewasser, N. Nicoara and S.D. Solares, “Artefacts in time-resolved Kelvin probe force microscopy,” *Beilstein J. Nanotech.* Vol. 9, pp. 1272-1281, 2018.

Probing Correlated Phenomena in Oxide Structures with Quantitative STEM

Susanne Stemmer, Materials Department, University of California, Santa Barbara

Research Scope

We combine advances in quantitative scanning transmission electron microscopy (STEM) and in oxide heterostructure engineering to establish the relationships between the atomic-scale structure and the electrical and magnetic properties of correlated oxides. The project makes use of advanced STEM-based diffraction and imaging techniques that allow for mapping of small lattice distortions and changes in the oxygen octahedral tilt patterns, with unit cell spatial resolution across interfaces and heterostructures. These are correlated with macroscopic properties that arise from strong electron correlations and coupling to the lattice, such as metal-insulator transitions and non-Fermi liquid behavior. The project also seeks to advance quantitative STEM for analysis of materials structure and defects by making use of variable angle imaging to improve contrast and interpretability, thereby contributing to the development of methods for atomic scale imaging of functional materials.

Recent Progress

Rare-earth titanates ($RTiO_3$, where R is a rare earth ion, but not Eu) are prototype Mott insulators with a d^1 electron configuration. Coulomb repulsion splits a half-filled $3d$ conduction band into upper and lower Hubbard bands, respectively. The Mott-Hubbard gap collapses upon hole doping (i.e. by replacing the R cation with Sr). It was furthermore known that the required doping concentration for this filling-controlled transition scales across the $RTiO_3$ series with the magnitude of the $GdFeO_3$ -type (orthorhombic) distortions (Fig. 1). For this reason, it was suggested in the literature that there was an underlying, first-order, *bandwidth-controlled* metal-insulator transition (MIT).

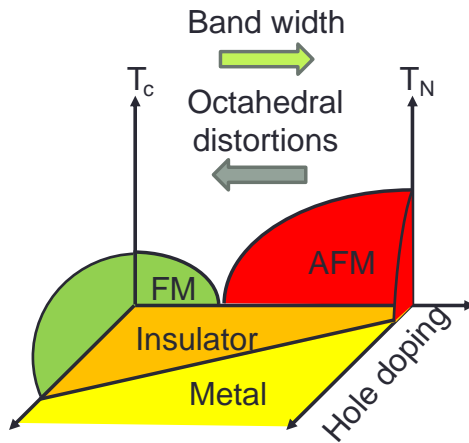


Figure 1: Prototype *filling-controlled* Mott metal-insulator transition in the perovskite rare earth titanates ($RTiO_3$, with R = rare earth ion, but not Eu). The degree of oxygen octahedral distortions in the orthorhombic crystal structure depends on R , systematically increasing from La to Y. Note that the required amount of hole doping for the transition depends on the degree of octahedral distortions, which led to suggestions of an underlying *bandwidth-controlled* transition. Our STEM results are not consistent with this picture. AFM – antiferromagnet, FM – ferromagnet.

In this project, obtained new insights into this prototype Mott MIT by correlating the atomic scale structure with the electrical properties across the filling-controlled MIT of SmTiO_3 . We used films that were grown by molecular beam epitaxy in our group and contained controlled amounts of hole doping (Sr dopants). We measured transport properties as a function of Sr concentrations and studied films both on the insulating and metallic sides of the MIT. We characterized the local lattice response, using STEM, which can resolve very small distortions, including those around individual point defects, as shown previously in this project¹. This allowed us to quantify the response of the lattice to hole (Sr) doping on both the insulating and metallic sides of the MIT and on length scales that range from extremely local (i.e., the distortion of atomic

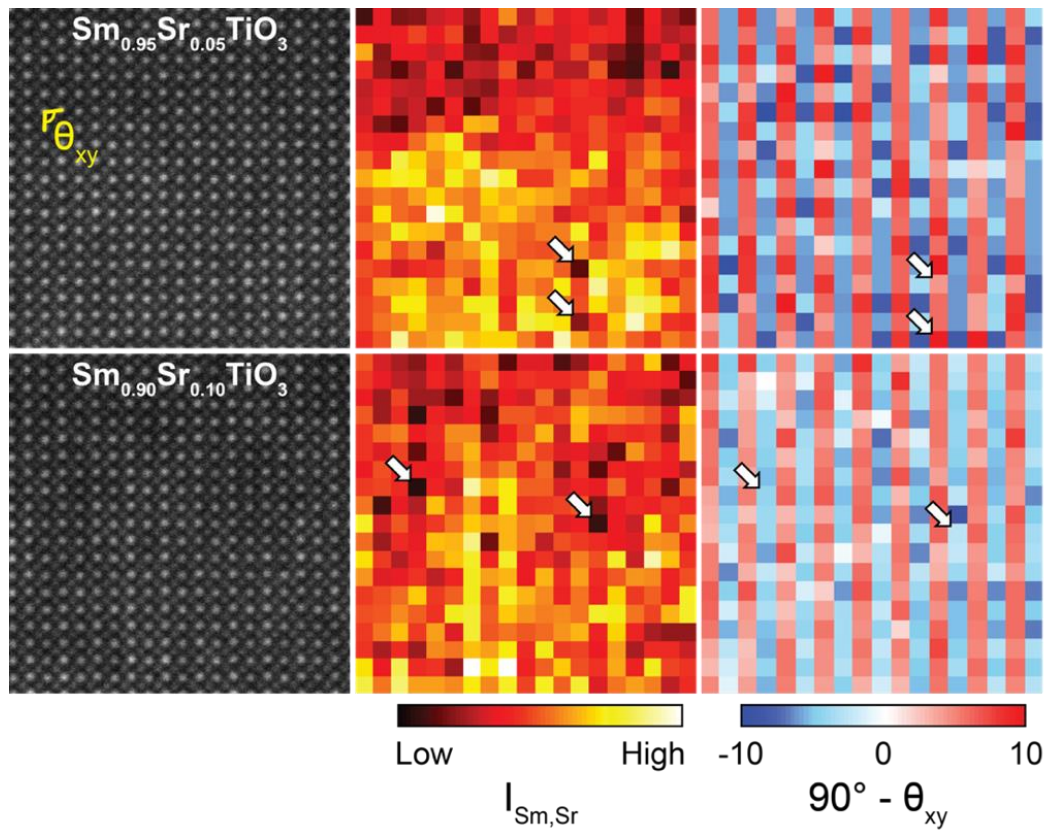


Figure 2: Probing the filling-controlled Mott metal-insulator transition in SmTiO_3 using quantitative HAADF-STEM. The bottom and top rows are from samples with two different Sr doping concentrations, on the insulating (top) and metallic (bottom) side of the metal-insulator transition, respectively. Shown are HAADF images (left), Sm(Sr) column intensity maps (middle), and deviation angle ($90^\circ - \theta_{xy}$) maps (right) of $\text{Sm}_{1-x}\text{Sr}_x\text{TiO}_3$ films with $x = 0.05$ (top row) and 0.1 (bottom row). The deviation angle is a measure of the oxygen octahedral tilt in the orthorhombically distorted perovskite structure. Low atomic column intensities marked by the white arrows in the $I_{\text{Sm,Sr}}$ maps and are associated with atomic columns containing Sr. A significant fraction of columns in each image do not contain Sr. While different degrees of distortions of the two films are visible (note the differences in color ranges), the deviation angles remain uniform, even for the columns that contain Sr (white arrows). The Sr dopants do not locally distort the lattice, within the picometer sensitivity of the method.

¹ H. Kim, J. Y. Zhang, S. Raghavan, and S. Stemmer, *Direct observation of Sr vacancies in SrTiO_3 by quantitative scanning transmission electron microscopy*, Phys. Rev. X **6**, 041063 (2016).

columns surrounding the dopant), shown in Fig. 2, to long-range (by analyzing images from different regions), as shown in Fig. 3. We found that this MIT is not strongly coupled to a specific lattice symmetry, unlike the rare earth nickelates, which we also studied in this project². For example, the orthorhombic distortions persist into the metallic regime. There is no abrupt symmetry change as the MIT boundary is traversed with doping.

The results provide strong evidence for a *continuous* phase transition with no phase separation. The results suggest an electron correlation-driven transition, to which the lattice responds. This is further corroborated by a surprisingly non-local response of the lattice to the presence of the Sr dopant atoms. Unlike other point defects that we studied previously, the Sr dopant atoms do not locally affect the neighboring atoms but instead produce a *global structure change*.

Other research in the present project period involved the characterization of novel oxide thin film systems and interfaces using advanced STEM techniques. For example, the analysis of

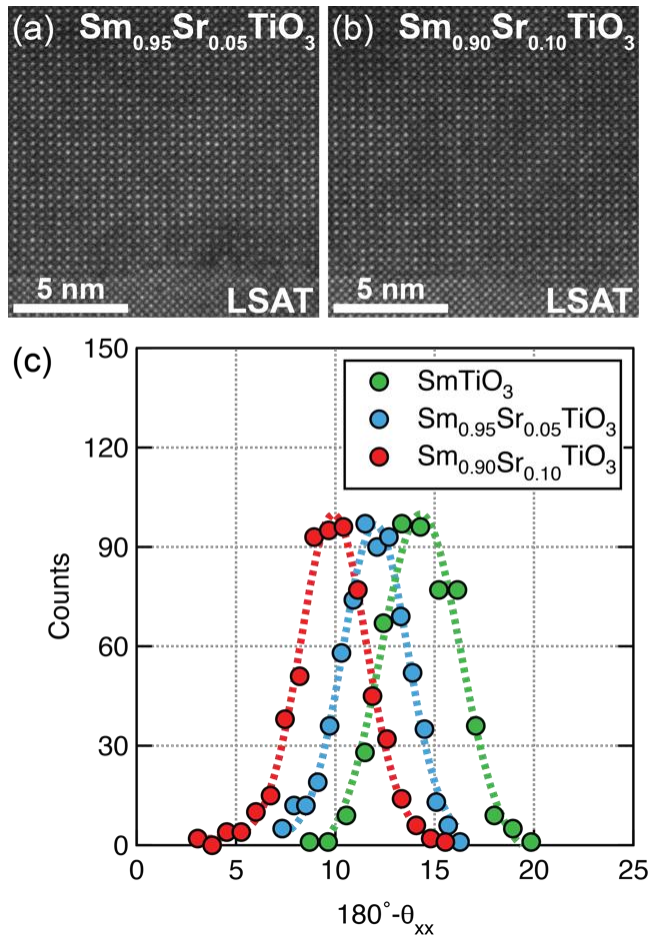


Figure 3: HAADF images of $\text{Sm}_{1-x}\text{Sr}_x\text{TiO}_3$ films with Sr concentrations of (a) 5 and (b) 10 %, corresponding to insulating and metallic films, respectively. (c) Distributions of measured deviation angles, $(180^\circ - \theta_{xx})$, of SmTiO_3 and $\text{Sm}_{1-x}\text{Sr}_x\text{TiO}_3$ films show the reduction in of orthorhombic-like unit cell distortions with increasing x . The vertical axis (counts) are the number of measured deviation angles in all analyzed images. The constant standard deviations, which were obtained across images recorded from several different regions of each sample, show that upon approaching the MIT, no phase separation into cubic (or less distorted) and orthorhombic regions occurs.

². Y. Zhang, H. Kim, E. Mikheev, A. J. Hauser, and S. Stemmer, *Key role of lattice symmetry in the metal-insulator transition of NdNiO_3 films*, *Sci. Rep.* **6**, 23652 (2016).

small tetragonal distortions at $\text{SmTiO}_3/\text{BaTiO}_3$ interfaces was key to understanding the metal-insulator transition and its competition with ferroelectricity in BaTiO_3 .

Future Plans

Our future plans include continuing to develop quantitative methods for 3D point defect imaging. We are particularly interested in understanding how the underlying microscopic structure determines whether a foreign atom or a vacancy acts as a dopant, which to date has only been achieved for very few point defects. We will also apply quantitative STEM techniques to understand other metal-insulator transitions.

Publications (2016-2018)

- S. Raghavan, T. Schumann, H. Kim, J. Y. Zhang, T. A. Cain, and S. Stemmer, *High-mobility BaSnO_3 grown by oxide molecular beam epitaxy*, APL Mater. 4, 016106 (2016).
- E. Mikheev, S. Raghavan, J. Y. Zhang, P. B. Marshall, A. P. Kajdos, L. Balents, S. Stemmer, *Carrier density independent scattering rate in SrTiO_3 -based electron liquids*, Sci. Rep. 6, 20865 (2016).
- J. Y. Zhang, H. Kim, E. Mikheev, A. J. Hauser, and S. Stemmer, *Key role of lattice symmetry in the metal-insulator transition of NdNiO_3 films*, Sci. Rep. 6, 23652 (2016).
- S. Raghavan, J. Y. Zhang, O. F. Shoron, and S. Stemmer, *Probing the metal-insulator transition in BaTiO_3 by electrostatic doping*, Phys. Rev. Lett. 117, 037602 (2016).
- H. Kim, J. Y. Zhang, S. Raghavan, and S. Stemmer, *Direct observation of Sr vacancies in SrTiO_3 by quantitative scanning transmission electron microscopy*, Phys. Rev. X 6, 041063 (2016).
- P. B. Marshall, H. Kim, K. Ahadi, and S. Stemmer, *Growth of strontium ruthenate films by hybrid molecular beam epitaxy*, APL Mater. 5, 096101 (2017).
- H. Kim, P. B. Marshall, K. Ahadi, T. E. Mates, E. Mikheev, and S. Stemmer, *Response of the lattice across the filling-controlled Mott metal-insulator transition of a rare earth titanate*, Phys. Rev. Lett. 119, 186803 (2017).
- K. Ahadi, H. Kim, and S. Stemmer, *Spontaneous Hall effects in the electron system at the $\text{SmTiO}_3/\text{EuTiO}_3$ interface*, APL Mater. 6, 056102 (2018).
- S. Stemmer, S. J. Allen, *Non-Fermi liquids in oxide heterostructures*, Rep. Progr. Phys. 81, 062502 (2018).

Atomically Thin Energy Materials: In-Situ Microscopy of Synthesis and Local Light-Matter Interactions

Peter Sutter, Dept. of Electrical & Computer Engineering, University of Nebraska-Lincoln, Lincoln, NE 68588 (psutter@unl.edu); Eli Sutter, Dept. of Mechanical & Materials Engineering, University of Nebraska-Lincoln, Lincoln, NE 68588 (esutter@unl.edu)

Research Scope

Atomically thin semiconductors offer extraordinary opportunities for the manipulation of charge carriers, many-body optical excitations, and non charge-based quantum numbers. Confinement and reduced dielectric screening in the 2D limit give rise to large characteristic energies so that many-body and quantum effects dominate even at room temperature. At scales above the diffraction limit, optical excitations in these materials have been investigated intensely. Much less understood are effects that arise locally in heterogeneous materials, either near naturally occurring defects, impurities, edges and grain boundaries, or as a result of intentional alloying and interface formation. Addressing such systems experimentally involves significant challenges: *Understanding atomistic growth mechanisms*, so that high-quality materials or systems with controlled interfaces or specific ‘imperfections’ can be realized; and *detecting local excitations* at scales that match the relevant (nanometer) length scales in heterogeneous materials. In this research program, we address these challenges by using novel platforms for quantitative *in-situ* microscopy of the growth of 2D materials and heterostructures, combined with local spectroscopic measurements of quasiparticles excited at the nanometer-scale using cathodoluminescence in scanning transmission electron microscopy (STEM-CL). Experiments are guided and analyzed *via* computations of the structure, chemistry, and excitation spectra. The primary focus of the program has been on two distinct classes of materials: (i) Transition metal dichalcogenides and heterostructures, for which optically excited quasiparticles at defects and their manipulation near interfaces are being investigated; and (ii) group IV chalcogenides, a largely unexplored family of 2D materials promising for energy conversion processes.

Recent Progress

Group IV monochalcogenides (SnX, GeX; X: S, Se) are anisotropic 2D/layered crystals representing compound analogues of black phosphorus/phosphorene. In bulk form, these materials have long been considered for energy conversion applications, e.g., thin film photovoltaics, and have shown other exceptional characteristics such as record thermoelectric performance. Recent theoretical calculations have predicted a number of intriguing properties for single-layer group IV monochalcogenides, including very large exciton binding energies, high carrier mobility, strain-tunable band offsets and charge separation in lateral heterostructures, selective valley polarization, and ferroelectricity/ferroelasticity up to above room temperature,

which in conjunction with bandgaps in the visible or near-infrared spectral range may enable the facile coupling between electromagnetic radiation and multiferroic order.

The controlled synthesis of few-layer and 2D group IV monochalcogenides, required to explore the unique properties of these materials, is a major challenge. On both dielectric and metal substrates, bottom-up growth typically produces slanted, randomly oriented, thick plates, likely due to a covalent interaction of nuclei edges with the support. Atomically smooth, inert van der Waals (vdW) substrates could promote the growth of well-ordered, basal-plane oriented layered crystals.

To test this hypothesis, we carried out extensive *in-situ* microscopy experiments focusing on SnS growth on carbon-based¹ and other vdW substrates. The results indeed confirm ordered growth with uniform crystal orientation on all vdW platforms, and provide insight into the fundamental nucleation and growth processes of 2D/layered crystals. In particular, the analysis of SnS growth on graphite shows an unusual imbalance between predominant adsorption on SnS nuclei and a vanishing sticking coefficient on the surrounding substrate (Fig. 1), which strongly favors vertical over lateral growth and prevents the synthesis of ultrathin (2D) crystals. We identified graphene/Ru(0001)² as a vdW substrate whose moiré structure promotes a higher surface reactivity. The resulting enhanced adsorption leads to growth of large, thin layered SnS single crystals that show a wealth of extraordinary properties, such as a facile generation and annihilation of dislocations, rapid lateral grain growth, as well as anisotropic lattice vibrations and optoelectronics. Recent work, finally, points to avenues for the controlled synthesis of group IV chalcogenides in the ultrathin (1-3 layer) limit, suitable for exploring predicted characteristics such as strongly bound excitons and multiferroic ordering in these materials. Our results have opened new avenues for studying the fundamental nucleation and growth mechanisms of layered and 2D materials as well as heterostructures via a quantitative analysis of *in-situ* microscopy data obtained during growth.

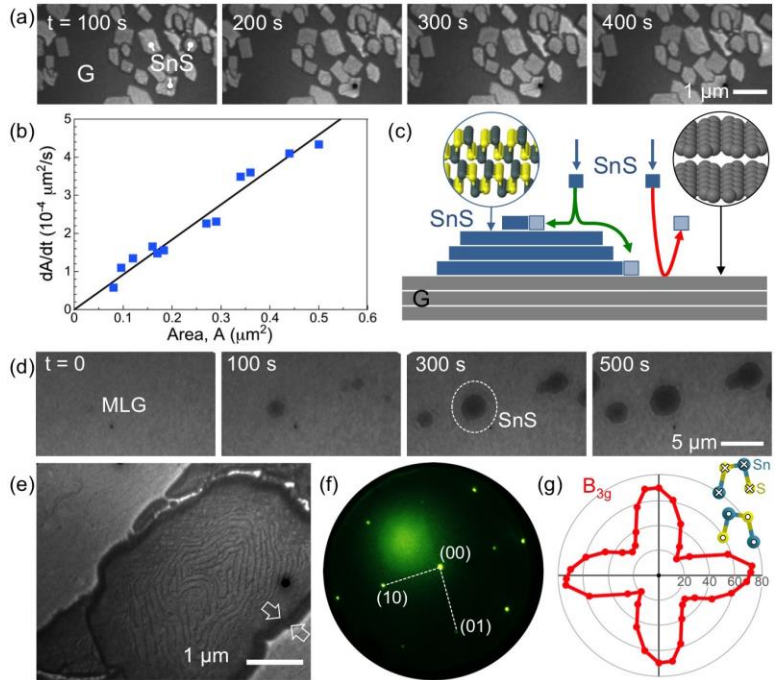


Figure 1: *In-situ* microscopy of SnS growth on vdW supports. (a) Time-lapse image series of SnS growth on graphite. (b) Analysis of the lateral growth rate (dA/dt) as a function of the projected flake area, A . (c) Schematic of the observed predominant adsorption of SnS on existing SnS nuclei and negligible sticking to the graphite substrate. (d) Time-lapse series showing growth of large few-layer SnS nuclei on graphene/Ru(0001). (e)-(f) Monocrystalline few-layer SnS. (g) Anisotropy of the B_{3g} phonon mode.

Light-matter interactions in group IV chalcogenide semiconductors have been investigated *via* nanospectroscopy based on STEM-CL (Fig. 2) that allows a direct correlation of the local optoelectronic properties with the atomic-scale structure and chemistry. Combining such measurements with *ab-initio* calculations, we identified luminescence signatures of key defects, notably sulfur vacancies, generated during the electron-beam driven transformation of SnS₂ into SnS.^{3,4} STEM-CL on high-quality mesoscale GeS prisms was used to demonstrate a novel nanooptical approach to probing confined (waveguide-) modes in layered crystals (Fig. 2).⁵ Interference of confined photonic modes due to internal reflection by highly specular prism facets causes a position dependent emission of narrow sub-bandedge luminescence peaks. The results demonstrate STEM-CL as a viable alternative to near-field optical methods for probing light-matter interactions far below the diffraction limit, and they demonstrate novel avenues toward tunable light emission in which the energy of emitted photons is selected geometrically via interference rather than by the conventional bandstructure engineering. Future work (see below) will address the challenges of probing nanometer-scale light-matter interactions, including strongly bound excitons and their manipulation by in-plane interfaces, in ultrathin crystals down to the monolayer limit.

Future Plans

Recent results by *in-situ* microscopy of synthesis processes and access to optoelectronic properties at the nanometer scale create exceptional opportunities for exploring novel phenomena in atomically thin energy materials. Understanding the fundamental growth processes, we can identify conditions for the growth of ultrathin group IV chalcogenide semiconductors and test theoretical predictions on their extraordinary properties, including strongly bound excitons and ferroelectricity/elasticity. We will also combine dissimilar materials (e.g., SnS, GeS) in monolayer heterostructures whose optoelectronic characteristics remain

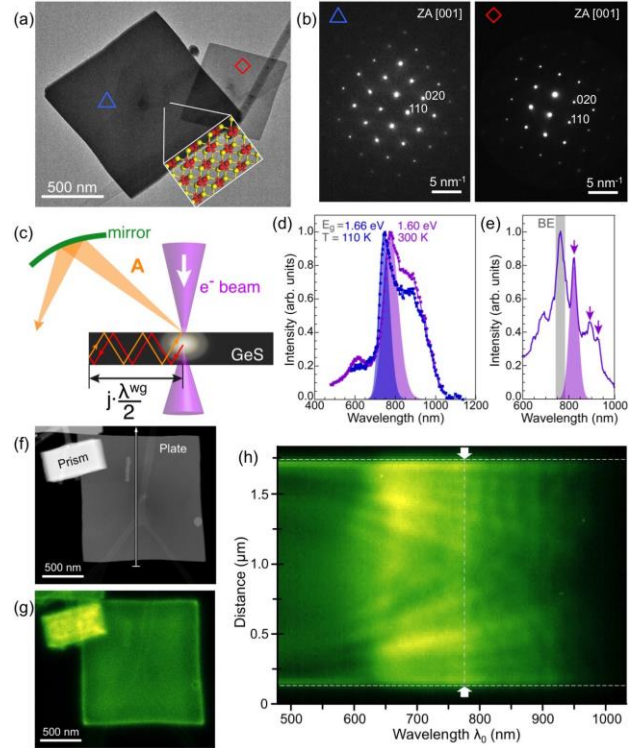


Figure 2: STEM-CL of traveling waveguide modes in layered crystals. (a)-(b) Electron microscopy and diffraction analysis of high-quality single crystalline GeS meso-prisms. (c) Principle of photonic waveguide mode excitation and detection in STEM-CL. (d) Integral CL spectra of GeS. (e) Narrow, intense sub-bandedge (BE) emission in mesoscopic GeS prisms. (f), (g) STEM image and panchromatic CL map of a GeS prism. (h) CL spectrum linescan along the line marked in (f), showing interference of confined waveguide modes in the GeS prism.

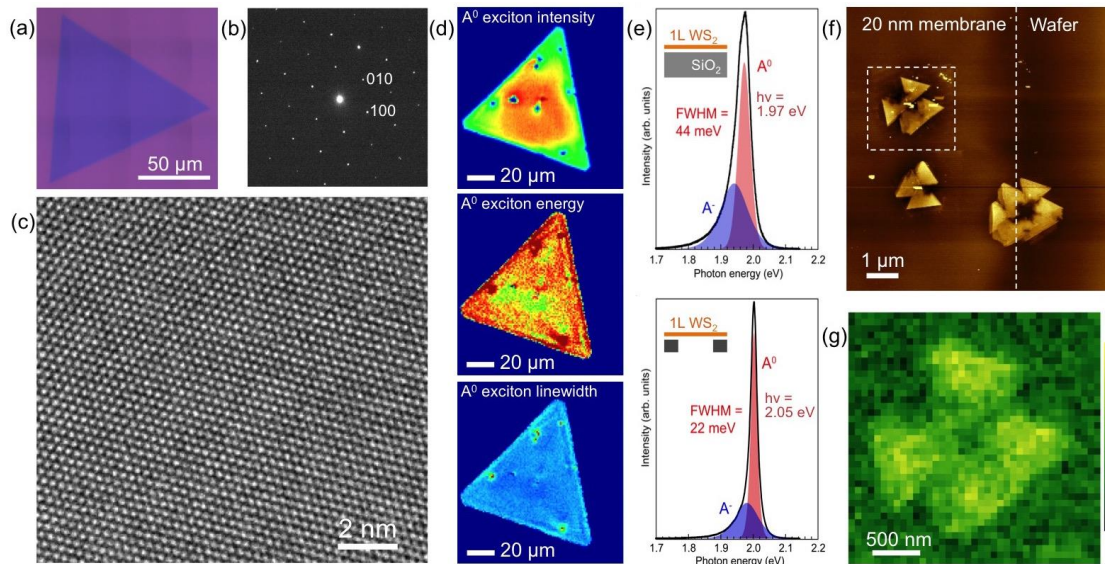


Figure 3: Growth, transfer, and light-matter interactions of TMDs. (a) Optical image, (a) electron diffraction pattern, and (c) HR-TEM image of a 2D WS₂ crystal. (d) Photoluminescence (PL) maps of 2D WS₂. (e) PL spectra of supported and suspended 1L WS₂. (f) AFM image, (g) Panchromatic STEM-CL of few-layer WS₂.

completely unexplored. Here, the capability of measuring local light emission by STEM-CL will allow us to probe interfacial phenomena with nanometer spatial and high spectral resolution. Transition metal dichalcogenides (TMDs), which received widespread attention due to their unique many-body physics, represent a second class of 2D materials for realizing the overarching goals of this program: A fundamental understanding of the ways in which defects, edges, and judiciously placed interfaces affect the interactions between light and many-body excitations, and its translation into robust materials platforms that harness imperfections for new functionality in energy conversion or computing. We established protocols for the synthesis and transfer of high-quality TMDs, as well as heterostructures (Fig. 4). STEM-CL spectroscopy correlated with the local structure and composition will be used to establish the effects of defects and to measure key characteristics of excitons in heterogeneous materials. Such experiments are challenging due to small cross-sections of electron-beam induced optical excitations. Heterostructures will be used to probe interface physics in 2D, e.g., the possibility of creating indirect excitons at lateral interfaces that may give rise to condensate many-body states or manipulation of neutral quasiparticles to direct energy and information flows at the nanoscale.

References

- [1] P. Sutter and E. Sutter, *ACS Appl. Nano Mater.* **1**, 3026 (2018).
- [2] P. Sutter, J.-I. Flege, and E. Sutter, *Nat. Mater.* **7**, 406 (2008).
- [3] P. Sutter, H.-P. Komsa, A.V. Krasheninnikov, Y. Huang, and E. Sutter, *Appl. Phys. Lett.* **111**, 262102 (2017).
- [4] E. Sutter, Y. Huang, H.-P. Komsa, M. Ghorbani-Asl, A.V. Krasheninnikov, and P. Sutter, *Nano Lett.* **16**, 4410 (2016).
- [5] P. Sutter, C. Argyropoulos, and E. Sutter, *Nano Lett.* **18**, 4576 (2018).

Publications

1. Y. Huang, J. Qiao, K. He, S. Bliznakov, E. Sutter, X. Chen, D. Luo, F. Meng, D. Su, J. Decker, W. Ji, R.S. Ruoff, and P. Sutter, *Interaction of Black Phosphorus with Oxygen and Water*, Chemistry of Materials **28**, 8330 (2016). [DOI: 10.1021/acs.chemmater.6b03592]
2. B. Maughan, P. Zahl, P. Sutter, and O.L.A. Monti, *Ensemble Control of Kondo Screening in Molecular Adsorbates*, Journal of Physical Chemistry Letters **8**, 1837 (2017). [DOI: 10.1021/acs.jpcllett.7b00278]
3. X. Zhao, J. Kotakoski, J.C. Meyer, E. Sutter, P. Sutter, A. Krasheninnikov, U. Kaiser, and W. Zhou, *Engineering and Modifying 2D Materials by Electron Beams*, Invited Review for a special issue of MRS Bulletin on Single Atom Fabrication with Beams and Probes, S. Kalinin, S. Pennycook, Eds., MRS Bulletin **42**, 667 (2017). [DOI: 10.1557/mrs.2017.184]
4. H. Qin, X. Chen, J. Li, P. Sutter, and G. Zhou, *Atomic-Step Induced Local Non-Equilibrium Effects on Surface Oxidation*, Journal of Physical Chemistry C **121**, 22846 (2017). [DOI: 10.1021/acs.jpcc.7b07321]
5. P. Sutter, H.-P. Komsa, A.V. Krasheninnikov, Y. Huang, and E. Sutter, *Defect Generation During Structural Transformations of Layered Tin Dichalcogenides*, Applied Physics Letters **111**, 262102 (2017). Highlighted in AIP Scilight, DOI: /10.1063/1.5020516. [DOI: 10.1063/1.5007060]
6. B. Maughan, P. Zahl, P. Sutter and O. L. A. Monti, *Configuration-Specific Electronic Structure of Strongly Interacting Interfaces: TiOPc on Cu(110)*, Physical Review B **96**, 235133 (2017). [DOI: 10.1103/PhysRevB.96.235133]
7. Y. Huang, E. Sutter, and P. Sutter, *Thick Layered Semiconductor Devices with Water Top-Gates: High On-Off Ratio Field-Effect Transistors and Aqueous Sensors*, ACS Applied Materials & Interfaces **10**, 23198 (2018). [DOI: 10.1021/acsami.8b05932]
8. P. Sutter and E. Sutter, *Growth Mechanisms of Anisotropic Layered Group IV Chalcogenides on van der Waals Substrates for Energy Conversion Applications*, ACS Applied Nano Materials **1**, 3026 (2018). Cover of ACS Applied Nano Materials. [DOI: 10.1021/acsanm.8b00660]
9. P. Sutter, C. Argyropoulos, and E. Sutter, *Germanium Sulfide Nano-Optics Probed by STEM-Cathodoluminescence Spectroscopy*, Nano Letters **18**, 4576 (2018). [DOI: 10.1021/acs.nanolett.8b01840]

Dielectrics under extreme electric fields: *In situ* studies on nanoscale mechanisms

Xiaoli Tan, Iowa State University, Materials Science and Engineering, Ames, IA

Geoff Brenneka, Colorado School of Mines, Metallurgical and Materials Engineering, Golden, CO

Research Scope

The prime target of the project is to identify the origins of premature dielectric breakdown in thin film oxides through directly imaging the breakdown events at various types of defects and interfaces and quantifying the effects of the defects on dielectric strength under pulsed electric fields ($<5 \mu\text{s}$) up to 1,000 MV/m. The limited understanding of the behavior and significance of atomic and nanoscale defects has made it difficult to improve the dielectric strength of materials which typically fail at 2~3 orders of magnitude below their intrinsic breakdown strength in electric devices [1,2]. Achieving higher energy efficiency is required in energy storage and distribution to meet the increasing demands on renewable energy, which requires next generation dielectrics to operate reliably in extreme environments [1,3]. It is toward these issues that this project is designed to focus on [4-7].

The project employs the electric biasing *in situ* TEM technique with the newly available Hysitron PI95 specimen holder which enables the application of super-critical but current-limited electric fields inside the TEM while observing the gradual process of early stage of dielectric breakdown at the nanometer scale with microsecond temporal resolution (**Fig. 1**). The probe tip, with a typical radius $<50 \text{ nm}$, is placed at pre-selected, interested areas to generate strong electric fields at the point of contact, hence circumventing the stochastic nature of dielectric breakdown and improving test efficiency. Model films to be examined include SiO_2 , TiO_2 , $\text{Pb}(\text{Zr},\text{Ti})\text{O}_3$, and PbZrO_3 . The *in situ* TEM experiments require thin film fabrication on non-planar substrates. Amorphous SiO_2 films are produced by thermal annealing of the Si-substrate in O_2 . Fabrication of other oxide films on non-planar substrates with best quality are expected to be challenging.

Recent Progress

Amorphous dielectric thin films, such as SiO_2 and HfO_2 , showed interestingly the formation of conductive crystalline phases under high electric fields as a result of oxygen removal. For example, Yao *et. al.* reported the resistive switch behavior of silicon oxide (SiO_x) through the voltage-driven formation and modification of silicon nanocrystals ($\sim 5\text{nm}$) embedded in the SiO_x matrix [7]. Recently, Li *et. al.* reported the gradual generation of oxygen vacancies in HfO_2 after applying high positive bias which eventually lead to the build-up of the conductive filaments [6]. These observations are relevant to our study on dielectric breakdown.

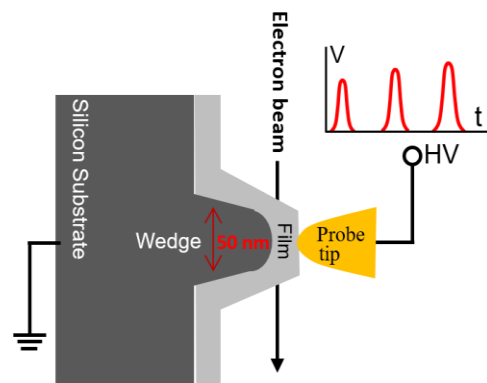


Fig. 1. Schematic illustration of the proposed *in situ* TEM experiments for dielectric breakdown study.

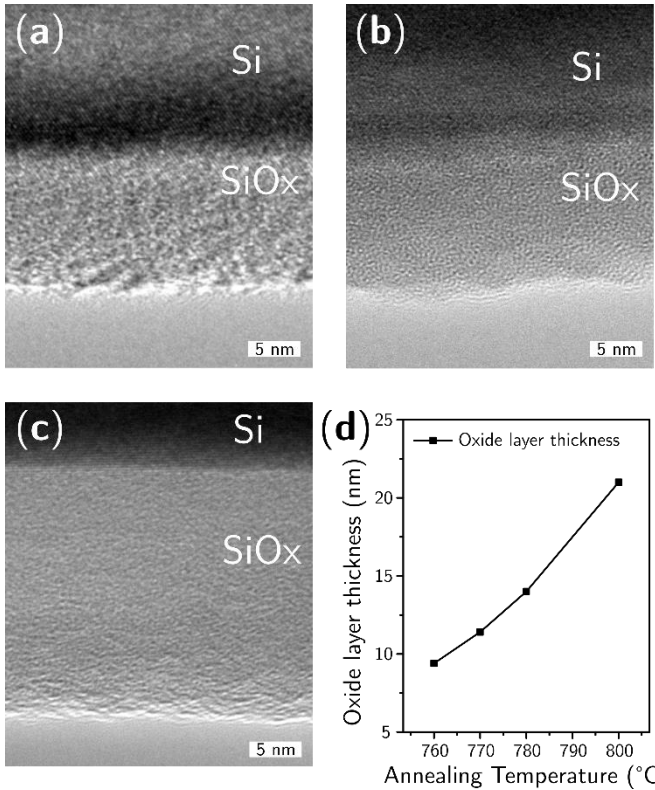


Fig. 2. Growth of the thermal SiO_x layer on the Si wedge substrate. **(a-c)**, TEM images of samples annealed in O₂ for 1 hr at (a) 760 °C, (b) 770 °C, and (c) 800 °C, respectively. **(d)** Diagram showing the oxide layer thickness as a function of annealing temperature.

In our work, we prepared SiO₂ dielectric films on non-planar Si-substrates via thermal annealing under O₂ atmosphere. The extruding narrow wedge with tip width <100 nm serves as the embedded bottom electrode to avoid flash-over breakdown (**Fig. 1**). Such a thin wedge geometry also enables multiple locations to choose from for the *in situ* TEM tests and makes the experiments efficient.

The dependence of the oxide layer thickness on the annealing temperature was studied first. TEM images of the grown SiO_x films on the Si wedge substrate are shown in **Fig. 2a-c**. The Si region shows visible lattice fringes which allows us to measure the oxide layer thickness directly from the images. Annealing in the range of 760-770°C results in the growth of an oxide film with a thickness of ~10 nm, while increasing the annealing temperature to 800°C produces a film of ~20 nm thick. The annealing period was kept for 1 hour with the same heating and cooling rates

of 1 °C/min throughout the experiments. The correlation between the thickness of the SiO_x films and the annealing temperature is shown in **Fig. 2d**. A simple estimate on the required voltage indicates that a film thickness of 20 nm is suitable for the observation of early stage dielectric breakdown without risking the damage to the PI95 holder.

The composition of the oxide layer was confirmed by using electron energy loss spectroscopy (EELS) and compared with that of the Si substrate. The volume plasmon peak shows a maximum at 16.6 eV for Si and 23.5 eV for SiO_x, respectively, indicating the oxide composition is close to SiO₂ [8].

The initial test of an *in situ* TEM experiment to observe the dielectric breakdown in the SiO_x films (20 nm thick) grown on Si substrate is shown in **Fig. 3**. A platinum-coated tungsten probe (tip radius ≈ 20 nm) was brought to gradually approach to the SiO_x film and aligned along the z-direction to the film. **Figure 3a** shows the size and shape of the probe tip as it approaches to the film using a step size of ~1 nm. As the tip was brought into the adjacent area of the film (about 1~2 nm distance), it was suddenly pulled into the film and hit the surface. As shown in **Fig. 3b**, the probe tip deformed and lost its sharpness. The possible reason for the uncontrolled

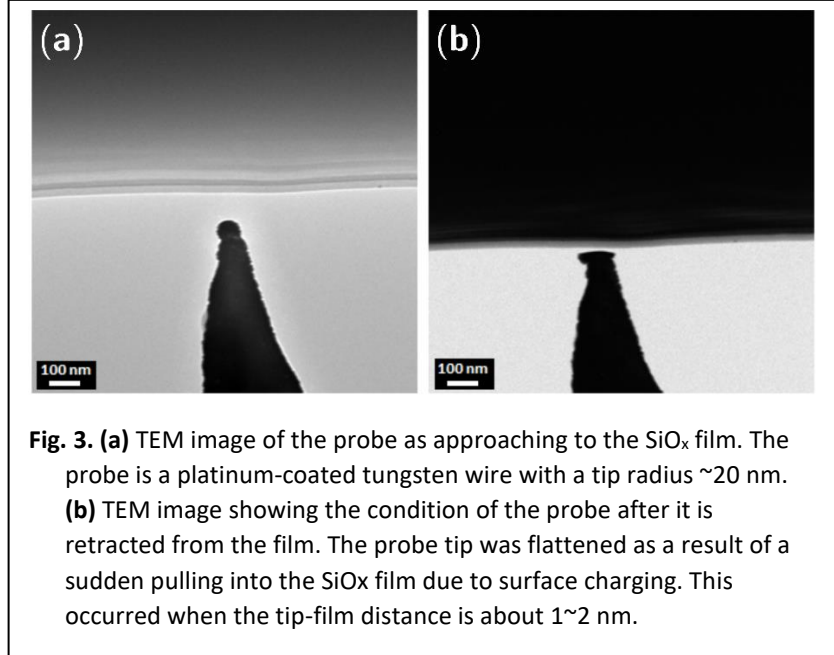
movement is the difference in the electrical potentials between the sample and the probe resulting in a strong electrostatic attraction. To overcome this problem, we are currently trying to (1) shorten the circuit between the sample and the probe during making contact; (2) use electron beam to charge the ungrounded probe tip; (c) apply an opposite voltage.

This project also plans to investigate dielectric breakdown in crystalline TiO_2 , $\text{Pb}(\text{Zr},\text{Ti})\text{O}_3$, and

PbZrO_3 films. Because studies on inferior, defect-riddled films would be of extremely limited applicability to other materials system, we have invested heavily in developing processes that lead to best-in-class films for *in situ* studies. The initial plan was to fabricate these films using the same solution-based process that has previously been demonstrated to be highly reliable and repeatable in the fabrication of complex $\text{Pb}(\text{Zr},\text{Ti})\text{O}_3$ films that exhibit significant variability by most other deposition techniques [9,10]. These techniques, however, were developed and optimized for depositing films on planar platinumized silicon ($\text{Si}/\text{SiO}_2/\text{TiO}_x/\text{Pt}$) substrates [11] that are not compatible with the current project. The special *in situ* TEM specimen holder requires that the non-planar substrate serves as a conductive back contact for application of an electric field through the film, eliminating the possibility of using the traditional $\text{Si}/\text{SiO}_2/\text{TiO}_x/\text{Pt}$ stack, and thus Pt as a non-reactive bottom electrode at all because of insufficient adhesion directly on Si. Because of aggressive reactions between Pb and Si when $\text{Pb}(\text{Zr},\text{Ti})\text{O}_3$ films are deposited directly on Si, a bottom electrode layer that is both sufficiently electrically conductive and non-reactive with the overlying film is required. Early efforts with sputtered TaN and Ti_3N_4 -based layers were abandoned because of quality control issues in the sputtered films and unacceptably high levels of interdiffusion with overlying $\text{Pb}(\text{Zr},\text{Ti})\text{O}_3$ films.

Efforts are now shifted to solution-deposition of LaNiO_3 as the bottom electrode, which have been significantly more effective. These films were found to have electronic conductivity values of $\sim 100 (\Omega\text{cm})^{-1}$, consistent with prior work and sufficiently conductive for the *in situ* TEM experiments.

Initial efforts to deposit $\text{Pb}(\text{Zr},\text{Ti})\text{O}_3$ films directly on this Si/LaNiO_3 stack have resulted in decidedly ferroelectric but not yet optimized $\text{Pb}(\text{Zr},\text{Ti})\text{O}_3$ films (**Fig. 4**). The remanent polarization has reached an impressive value of $>20 \mu\text{C}/\text{cm}^2$. In parallel with the development of the $\text{Si}/\text{LaNiO}_3/\text{Pb}(\text{Zr},\text{Ti})\text{O}_3$ procedures (all carried out using spin coating, as is most common



across the solution-derived thin film community), we have designed and built a dip coating setup around an Arduino-controlled stepper motor.

Future Plans

With the successful preparation of silicon oxide films with desired geometry, we will proceed to observe the early stage dielectric breakdown events in amorphous oxide thin films. We will take the suggested measures to address the issue of electrostatic attraction between the probe tip and film sample.

In the near future, we will be transferring the depositions to dip coating and optimizing the Si//LaNiO₃//Pb(Zr,Ti)O₃ fabrication process in order to reliably and repeatably fabricate samples that will enable the *in situ* study of dielectric breakdown in Pb(Zr,Ti)O₃ thin films. After that, we will use nearly-identical solution chemistry and thermal processing to fabricate TiO₂ and PbZrO₃ films for further study. With these high-quality oxide films, we will carry out *in situ* TEM electric biasing experiments to establish the nanoscale mechanisms of defect-initiated dielectric breakdown in solid crystalline films.

References

- [1] Basic Research Needs for Materials under Extreme Environments. U.S.-DOE BES workshop report, 2007. http://science.energy.gov/~media/bes/pdf/reports/files/muee_rpt.pdf
- [2] Y. Sun, C. Bealing, S. Boggs, R. Ramprasad, IEEE Electr. Insul. Mag. **29**, 8 (2013).
- [3] M.Z. Jacobson, M.A. Delucchi, G. Bazouin, Z.A. Bauer, C.C. Heavey, E. Fisher, S.B. Morris, D.J. Piekutowski, T.A. Vencill, T.W. Yeskoo, Energ. Environ. Sci. **8**, 2093(2015).
- [4] N. Raghavan, K.L. Pey, K. Shubhakar, Microelectr. Reliab. **54**, 847 (2014).
- [5] Z. Liao, M. Gall, K. B. Yeap, C. Sander, O. Aibel, U. Mühle, J. Gluch, S. Niese, Y. Standke, R. Rosenkranz, Adv. Eng. Mater. **16**, 486 (2014).
- [6] C. Li, B. Gao, Y. Yao, X. Guan, X. Shen, Y. Wang, P. Huang, L. Liu, X. Liu, J. Li, Adv. Mater. **29**, 1602976 (2017).
- [7] J. Yao, Z. Sun, L. Zhong, D. Natelson, J.M. Tour, Nano Lett. **10**, 4105 (2010).
- [8] F. Iacona, C. Bongiorno, C. Spinella, S. Boninelli, F. Priolo, J. Appl. Phys. **95**, 3723 (2004).
- [9] J. Sigman, G.L. Brennecka, P.G. Clem, and B.A. Tuttle, J. Am. Ceram. Soc. **91**, 1851 (2008).
- [10] G.L. Brennecka, J.F. Ihlefeld, J.P. Maria, B.A. Tuttle, and P.G. Clem, J. Am. Ceram. Soc. **93**, 3935 (2010).
- [11] C.T. Shelton, P.G. Kotula, G.L. Brennecka, P.G. Lam, K.E. Meyer, J.P. Maria, B.J. Gibbons, J.F. Ihlefeld, Adv. Funct. Mater. **22**, 2295 (2012).

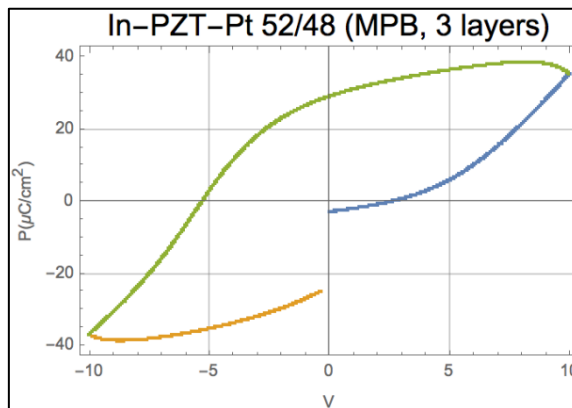


Fig. 4. The polarization vs applied voltage hysteresis loop of the Pb(Zr,Ti)O₃ film deposited on the LaNiO₃ bottom electrode.

Probing Majorana States in Topological-Superconductor Proximity Systems

Stuart Tessmer

Department of Physics, Michigan State University, East Lansing, MI 48824

Dale Van Harlingen

Department of Physics, University of Illinois at Urbana-Champaign, Urbana, IL 61801

Alex Levchenko

Department of Physics, University of Wisconsin, Madison, Madison, WI 53706

Research Scope

The primary goals of the projects involve the creation and detection of Majorana fermion (MF) states in topological-superconductor proximity systems. Working as a close collaboration between experiment and theory, we are advancing three interconnected projects: Probing Majorana States in Josephson-Junction Devices; Electronic and Magnetic Imaging of MF States; Development of Scanning Majorana Microscopy.

Recent Progress

Understanding the physics of the topological insulator (TI)/superconductor interface is key for all of the project goals. We have made significant progress elucidating the striking proximity effects at play [1]. Experimentally, Nb/ Bi₂Se₃ nanostructures were probed cryogenically with scanning tunneling microscopy. We observed spectroscopic features of the topologically-protected surface states of the Bi₂Se₃ leaking into the superconducting material. Theoretically, we studied the detailed hybridization mechanism of surface states in proximity junctions of Bi₂Se₃ and Nb. The experimental data was fitted to the predictions of a theoretical model of the set-up. We conclude that coupling between the topologically protected surface states and the Nb states results in an effective pairing mechanism for the surface states, leading to a modified model for a topological superconductor in these systems. Such a topological superconductor is a potential home for Majorana bound states.

Additional progress in theory includes exploring multi-terminal Josephson Junctions with and without topological components [2]. Even without a TI, the structure of Andreev bands could be topologically nontrivial. The physics is seen to be richer with topological materials included in the junctions. Moreover, the analysis shows that magnetic field can be an experimental knob to allow switching between different symmetry ensembles.

Future Plans

Development of Scanning Majorana Microscopy

MF bound states are predicted to be induced in two-dimensional *p*-wave superconductors at defects and vortices [3, 4], and the most obvious way detect them is to probe for the emergence of the zero-energy resonances. However, the main challenges of these measurements is to exclude the other false-positive contributions to the zero-bias peaks that are ubiquitous in condensed matter systems; for example, zero bias peaks can result

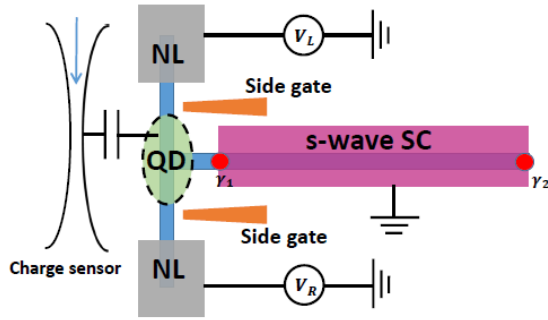


Figure 1. Schematics for the QD-Majorana mode coupling to measure the fluctuation statistics of transmitted charge.

from the Kondo effect [5, 6], disorder in the topological region and in the leads [7–13], as well as other resonant Andreev scattering phenomena [14, 15]. Levchenko has initiated a theoretical study of a mesoscopic device consisting of a quantum dot (QD) coupled to a Majorana bound state and two symmetric normal leads. Keldysh path-integral approach was used to compute the frequency dependence of the cumulants $C_n(w)$ of the current fluctuation flowing through the QD. The most remarkable property of cumulants is that they exhibit plateaus corresponding to the universal values $\{C_1(w), C_2(w), \dots, C_8(w)\} = \{1/2, 1/4, 0, -1/8, 0, 1/4, 0, -17/16\}$ in the frequency range $w < \min\{\Gamma, \kappa^2/\Gamma\}$,

where $\Gamma(\kappa)$ is tunnel coupling between the leads (Majorana mode) and the QD. The sequence of universality is governed by $C_n(0) = E_{n-1}(1)/2$ where $E_n(x)$ is the Euler polynomial. Interestingly this result is independent of the microscopic parameters such as the QD energy level and QD-MF coupling strength. The measurement of such cumulants has the potential to uniquely identify the presence of the Majorana modes, excluding false-positive signatures in the tunneling transport.

We are developing a new scanning probe microscope based on this theoretical insight. Fig. 2 shows a schematic of the instrument, consisting of a quantum dot and two electrical leads fabricated onto a glass tip. The counting statistics for electrons entering the dot can be

measured using the charge sensor circuit employed for Scanning Charge Accumulation imaging. If the QD is in tunneling contact with a MF state, interaction-induced corrections to the counting statistics result. Additional theoretical work will be performed to calculate the counting statistic for the specific geometry of the tip, for which the details of the electrical leads and

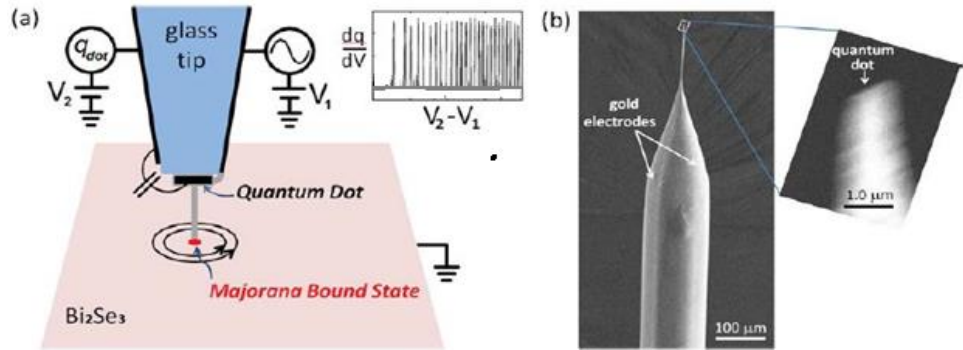


Figure 2. Scanning Majorana Microscope. (a) Schematic showing a quantum dot and two electrical leads fabricated onto a glass tip. The QD is asymmetric with respect to the leads, forming a tunnel junction with one (indicated in gray to the right of the QD) and a simple capacitor with the other (indicated left of the QD). We measure the counting statistics for electrons entering the dot using the same charge sensor constructed from high-electron mobility transistors. The inset schematically shows electrons entering the dot as a function of lead voltage, seen as peaks in the capacitance. If the QD is in tunneling contact with a MF state, interaction-induced corrections to the counting statistics result. Hence this method can uniquely identify the presence of the Majorana bound states. (b) Scanning electron microscopy image of microscope tip, fabricated in the Tessmer lab. Gold metal electrodes are evaporated on to each side, as indicated. The inset shows the apex at higher magnification; an aluminum quantum dot has been deposited on to it, separated from the electrodes by 2 nm of aluminum oxide to form the barriers.

junctions will be less ideal than those used for the initial calculations. In this way, our microscope can detect the signature of Majorana states that are beyond the reach of existing probes.

Scanning SQUID Microscopy Imaging

As a complement to imaging the electronic structure of superconductor-topological insulator devices via Scanning Tunneling Microscopy and Scanning Majorana Microscopy, we plan to image vortices in these systems using Scanning SQUID Microscopy (SSM). The Van Harlingen group helped to pioneer this powerful technique in which a SQUID detector or a pickup coil is scanned over the surface to detect the local magnetic field, offering unprecedented magnetic field sensitivity, and they have utilized it for imaging vortices and magnetic structures in superconducting materials and superconductor arrays. We will use SSM to detect the location of vortices in Josephson junctions with topological insulator barriers. As discussed above, these systems can support Majorana fermions that are bound to the vortices. By imaging the vortices, we can map out the location and develop schemes to create and manipulate them by applying magnetic fields, currents, phase differences, and/or voltages. In particular, we can explore schemes for exchanging vortices, a necessary step for braiding.

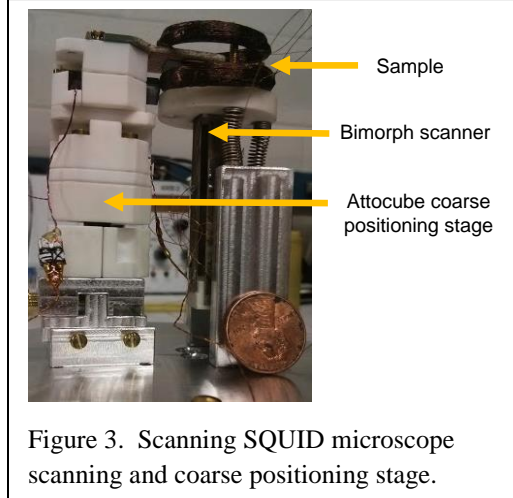


Figure 3. Scanning SQUID microscope scanning and coarse positioning stage.

For this project, we will incorporate the bimorph scanning stage which we have developed into a dry dilution refrigerator, enabling operation at ultralow temperatures in the range 1K to 10mK. Coarse positioning is done using a custom laser interferometer stage. A critical element will be achieving enhanced spatial resolution to 100nm using novel tip coil designs and the use of single Josephson junctions rather than SQUID loops for scanning. By adding local field coils, we can lasso and move vortices to perform Majorana fermion exchange operations.

We will use the SSM to image the entry and location of vortices in superconductor-topological devices as shown in Figure 4, the same devices that we will image electronically with STM and SCM probes:

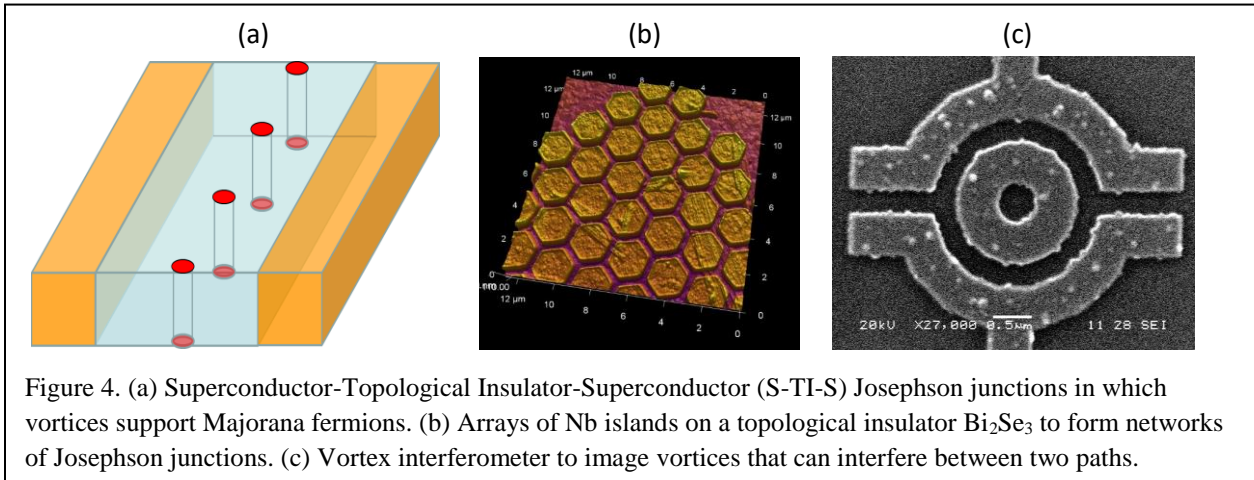


Figure 4. (a) Superconductor-Topological Insulator-Superconductor (S-TI-S) Josephson junctions in which vortices support Majorana fermions. (b) Arrays of Nb islands on a topological insulator Bi_2Se_3 to form networks of Josephson junctions. (c) Vortex interferometer to image vortices that can interfere between two paths.

References

- [1] Nicholas Sedlmayr, E. W. Goodwin, Michael Gottschalk, Ian M. Dayton, Can Zhang, Erik Huemiller, Reza Loloee, Thomas C. Chasapis, Maryam Salehi, NIKESH KOIRALA, Mercouri G. Kanatzidis, Seongshik Oh, D. J. Van Harlingen, Alex Levchenko, S. H. Tessmer, Dirac surface states in superconductors: a dual topological proximity effect, arXiv:1805.12330 [cond-mat.supr-con] (2018).
- [2] Hong-Yi Xie, Maxim G. Vavilov, and Alex Levchenko, Weyl nodes in Andreev spectra of multiterminal Josephson junctions: Chern numbers, conductances, and supercurrents, *Phys. Rev. B* **97**, 035443 (2018).
- [3] N. Read and D. Green, Paired states of fermions in two dimensions with breaking of parity and time-reversal symmetries and the fractional quantum Hall effect, *Phys. Rev. B* **61**, 10267 (2000).
- [4] A. Y. Kitaev, Unpaired Majorana fermions in quantum wires, *Physics-Uspekhi* **44**, 131(2001).
- [5] E. J. H. Lee, X. Jiang, R. Aguado, G. Katsaros, C. M. Lieber, and S. De Franceschi, Zero-Bias Anomaly in a Nanowire Quantum Dot Coupled to Superconductors, *Phys. Rev. Lett.* **109**, 186802 (2012).
- [6] J.-D. Pillet, P. Joyez, R. Zitko, and M. F. Goffman, Tunneling spectroscopy of a single quantum dot coupled to a superconductor: From Kondo ridge to Andreev bound states, *Phys. Rev. B* **88**, 045101 (2013).
- [7] J. Liu, A. C. Potter, K. T. Law, and P. A. Lee, Zero-Bias Peaks in the Tunneling Conductance of Spin-Orbit-Coupled Superconducting Wires with and without Majorana End-States, *Phys. Rev. Lett.* **109**, 267002 (2012).
- [8] P. Neven, D. Bagrets, and A. Altland, Quasiclassical theory of disordered multi-channel Majorana quantum wires, *New Journal of Physics* **15**, 055019 (2013).
- [9] A. M. Lobos, R. M. Lutchyn, and S. Das Sarma, Interplay of Disorder and Interaction in Majorana Quantum Wires, *Phys. Rev. Lett.* **109**, 146403 (2012).
- [10] J. D. Sau and S. Das Sarma, Density of states of disordered topological superconductor-semiconductor hybrid nanowires, *Phys. Rev. B* **88**, 064506 (2013).
- [11] H.-Y. Hui, J. D. Sau, and S. Das Sarma, Disorder-induced subgap states and Majorana zero-energy edge modes in two-dimensional topological insulator-superconductor hybrid structures, *Phys. Rev. B* **90**, 174206 (2014).
- [12] D. Bagrets and A. Altland, Class D Spectral Peak in Majorana Quantum Wires, *Phys. Rev. Lett.* **109**, 227005 (2012).
- [13] D. I. Pikulin, J. P. Dahlhaus, M. Wimmer, H. Schomerus, and C. W. J. Beenakker, A zero-voltage conductance peak from weak antilocalization in a Majorana nanowire, *New Journal of Physics* **14**, 125011 (2012).
- [14] Karsten Flensberg, Tunneling characteristics of a chain of Majorana bound states, *Phys. Rev. B* **82**, 180516(R) (2010).
- [15] Marco Gibertini, Fabio Taddei, Marco Polini, and Rosario Fazio, Local density of states in metal-topological superconductor hybrid systems, *Phys. Rev. B* **85**, 144525 (2012).

Publications

- (1) Nicholas Sedlmayr, E. W. Goodwin, Michael Gottschalk, Ian M. Dayton, Can Zhang, Erik Huemiller, Reza Loloee, Thomas C. Chasapis, Maryam Salehi, Nikesh Koirala, Mercouri G. Kanatzidis, Seongshik Oh, D. J. Van Harlingen, Alex Levchenko, S. H. Tessmer, Dirac surface states in superconductors: a dual topological proximity effect, arXiv:1805.12330 [cond-mat.supr-con] (2018).
- (2) Colin M. Whisler, Maxim G. Vavilov, and Alex Levchenko, Josephson currents in chaotic quantum dots, *Phys. Rev. B* **97**, 224515 (2018).
- (3) Hong-Yi Xie, Maxim G. Vavilov, and Alex Levchenko, Weyl nodes in Andreev spectra of multiterminal Josephson junctions: Chern numbers, conductances, and supercurrents, *Phys. Rev. B* **97**, 035443 (2018).

Imaging Point Defects with 4D STEM

Paul M. Voyles and Dane Morgan, Department of Materials Science and Engineering, University of Wisconsin-Madison

Research Scope

This project supports development of methods to characterize point defects in materials using scanning transmission electron microscopy (STEM). Quantitative, high precision STEM methods have been proven capable of imaging defects which increase the electron scattering from the sample, including high atomic number impurities, impurity interstitials, and self-interstitials.¹⁻⁴ Complexes of such defects also can be characterized. Such methods also can image point defects which decrease scattering, such as vacancies, but only under special circumstances where the changes in scattering and the change in the positions of the atoms surrounding the defect is particularly large.^{5,6}

This project exploits the recent development of very fast, pixelated detectors to enable 4D STEM, which, as shown schematically in Figure 1, is the acquisition of a complete convergent beam electron diffraction (CBED) pattern at every point in a 2D raster scan of the probe. 4D STEM has the potential to be very sensitive to local strain fields surrounding defects and small changes in electron scattering that generate phase contrast. We will (1) implement 4D STEM using a new, ultrafast pixelated electron detector being developed under separate support, (2) develop methods based on evolving techniques for phase imaging in 4D STEM and using machine learning to match experimental data to simulated libraries, and (3) apply these methods to characterizing point defects in a variety of materials, including perovskite oxides and halides. STEM experiments are intertwined throughout with density functional theory calculations of defect structures and thermodynamic models of equilibrium defect populations.

Recent Progress

We have implemented 4D STEM acquisition on our Titan STEM using a DE-16 direct electron camera and a custom-built scan generator. The DE-16 is a prototype for the ultrafast camera currently under development. It uses a back-thinned silicon active layer similar to the Gatan K2 /K3 STEMx system, but it offers

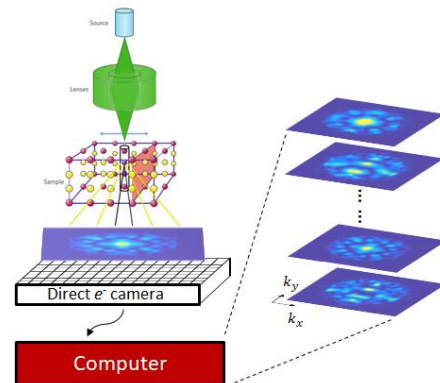


Figure 1: Schematic of 4D STEM acquisition. A fast direct electron camera captures a complete convergent beam electron diffraction pattern at every position in a raster scan of the probe across the sample.

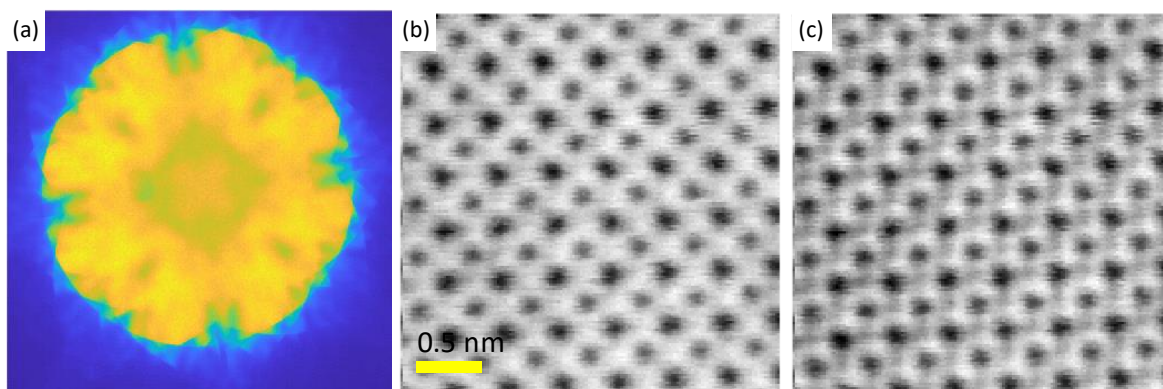


Figure 2: An example 4D STEM data set: (a) a CBED pattern from one probe position, (b) a reconstructed BF STEM image, (c) a reconstructed ABF STEM image.

greater flexibility in readout area, somewhat higher dynamic range, and a significantly higher peak frame rate, in excess of 5,000 frames per second (fps). The 4D STEM system has a dedicated pipeline to a small but dedicated high performance computing cluster for data storage and analysis. Figure 2 shows initial 4D STEM data acquired from a SrTiO_3 test sample.

In anticipation of 4D STEM experimental data, we have evaluated methods for denoising adapted to 4D STEM data sets and trained convolutional neural networks (CNNs) for matching experimental CBED patterns to simulated libraries of such patterns. Figure 3 shows denoising results on simulated data with varying level of Poisson noise added to it. Typical signal levels using the current speed camera are ~ 10 e^- /pixel, but the ultrafast camera will create data with peak signals of $1 e^-$ / pixel or less.

The algorithms we employed are based on iterative BM3D,⁷ iterative BM4D,⁸ and non-local principle component analysis (NLPCA),⁹ all adapted for Poisson noise and the 4D STEM data format. We have previously shown that NLPCA out-performs other approaches for denoising EDS spectrum images,¹⁰ but in this case, iterative BM4D offers the best performance, both qualitatively as shown in Figure 3, and quantitatively from the peak signal-to-noise ratio. We speculate that the combination of low redundancy inside each CBED and extremely high redundancy in the 4D STEM data set from a crystal make iterative BM4D the best approach.

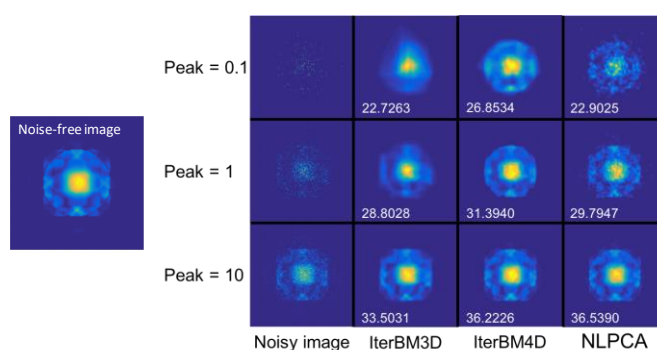


Figure 3: Denoising CBED patterns from 4D STEM. Poisson noise with the indicated peak signal value is added to a noise-free simulation, then removed using the indicated algorithms: iterative BM3D, iterative BM4D, and non-local PCA. In this test, iterative BM4D has the best qualitative performance.

As a first step into using CNNs, we have trained a network on a library of simulations to identify the local thickness of a SrTiO₃ sample from experimental data. This is very similar to the pioneering work of Xu and Lebeau,¹¹ except that where they used CBED patterns averaged over an entire unit cell, we have used CBED patterns averaged over single atomic columns in the crystal. Since our eventual goal is to characterize point defects, this increase in spatial resolution is essential. We have also adopted a simplified, single-network structure, although we use a more complicated base CNN, VGG-16.¹²

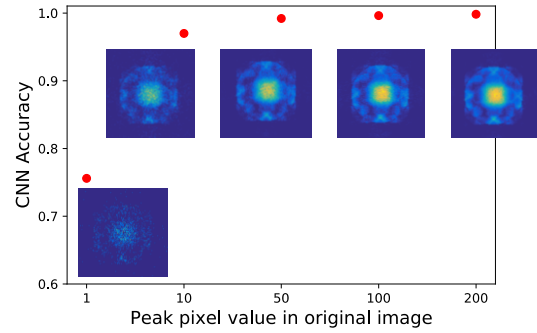


Figure 4: CNN cross validation test of determining the thickness of a SrTiO₃ sample from a atomic-column averaged CBED pattern. For peak signal in the image > 50 e⁻, the accuracy is >99%.

Figure 4 shows the results of a cross-validation test of a CNN trained on a multislice simulated library of CBED patterns. To augment the training data set, we varied the integration region position on the sample and the input peak signal value, as well as using more common image augmentation routines such as rescaling and rotation. The performance of the trained CNN is quite good, with the accuracy in identifying the correct thickness >99% when the peak signal value is >50 e⁻ / pixel. Although experimental data is likely to have lower peak signal values, we expect the denoising approaches above to improve the performance of the CNN at low signal levels.

Future Plans

A beta version of the ultrafast camera will be delivered within the next year. Planned design performance is summarized in Table 1. The sensor will have 1024 × 1024 physical pixels, but with subarea readout will run at up to 120,000 fps. It will have a high gain mode with a dynamic range of 8 e⁻/pixel and a low gain mode with 140 e⁻/pixel. A double sampling combined gain mode will offer the dynamic range of low gain but the noise performance of high gain, at the cost of a two-fold reduction in frame rate. The new camera will replace the DE-16 in the same custom 4D STEM system.

The new camera will enable 4D STEM imaging with less distortion and greater probe position oversampling; frame averaging of multiple 4D STEM acquisitions for distortion correction and improved signal to noise ratio; and great dynamic range through the combination of improve camera dynamic range and higher speed. The improved 4D STEM data quality will dramatically improve our efforts to identify point defects from 4D STEM data.

Table 1: Image readout size vs frame rate for the ultrafast camera.

Array size (square)	Readout speed (fps)
1024	2000
512	8000
256	32000
128	120,000

References

- ¹ P.M. Voyles, D.A. Muller, J.L. Grazul, P.H. Citrin, and H.-J.L. Gossmann, *Nature* **416**, 826 (2002).
- ² J. Hwang, J.Y. Zhang, A.J. D'Alfonso, L.J. Allen, and S. Stemmer, *Phys. Rev. Lett.* **111**, 266101 (2013).
- ³ S.H. Oh, K. van Benthem, S.I. Molina, A.Y. Borisevich, W. Luo, P. Werner, N.D. Zakharov, D. Kumar, S.T. Pantelides, and S.J. Pennycook, *Nano Lett.* **8**, 1016 (2008).
- ⁴ D. Alloyeau, B. Freitag, S. Dag, L.W. Wang, and C. Kisielowski, *Phys. Rev. B* **80**, 014114 (2009).
- ⁵ H. Kim, J.Y. Zhang, S. Raghavan, and S. Stemmer, *Phys. Rev. X* **6**, 041063 (2016).
- ⁶ H. Kim, Y. Meng, J. Kwon, J.-L. Rouvière, and J.M. Zuo, *IUCrJ* **5**, 67 (2018).
- ⁷ K. Dabov, A. Foi, V. Katkovnik, and K. Egiazarian, in *Image Process. Algorithms Syst. Neural Networks, Mach. Learn.*, edited by E.R. Dougherty, J.T. Astola, K.O. Egiazarian, N.M. Nasrabadi, and S.A. Rizvi (Proc. of SPIE-IS&T Electronic Imaging, SPIE Vol. 6064, 2006), p. 606414.
- ⁸ M. Maggioni, V. Katkovnik, K. Egiazarian, and A. Foi, *IEEE Trans. Image Process.* **22**, 119 (2013).
- ⁹ J. Salmon, Z. Harmany, C.-A. Deledalle, and R. Willett, (2012).
- ¹⁰ A.B. Yankovich, C. Zhang, A. Oh, T.J.A. Slater, F. Azough, R. Freer, S.J. Haigh, R. Willett, and P.M. Voyles, *Nanotechnology* **27**, 364001 (2016).
- ¹¹ W. Xu and J.M. LeBeau, *Ultramicroscopy* **188**, 59 (2018).
- ¹² K. Simonyan and A. Zisserman, in *ICLR* (2015).

Publications

1. “Homogeneous Core-shell Ti-Doped MnO₂ Nanowires for High-Rate and Long-Life Lithium Battery” K. Zhao, C. Sun, Y. Yu, Y. Dong, C. Zhang, C. Wang, P. M. Voyles, L. Mai, X. Wang (submitted)
2. “Metastable Intermediates in Amorphous Titanium Oxide: A Hidden Role Leading to Ultra-Stable Photoanode Protection” Yanhao Yu, Congli Sun, Xin Yin, Jun Li, Shiyao Cao, Chenyu Zhang, Paul M. Voyles, Xudong Wang *Nano Letter* (to be published).
3. “Ionic Layer Epitaxy of Nanometer-thick Palladium Nanosheets with Enhanced Electrocatalytic Properties” X. Yin, Q. Chen, P. Tian, P. Zhang, Z. Zhang, P. M. Voyles, X. Wang *Chemistry of Materials* **30**, 3308 (2018).
4. “H₂V₃O₈ Nanowire/Graphene Electrodes for Aqueous Rechargeable Zinc Ion Batteries with High Rate Capability and Large Capacity” Qiang Pang, Congli Sun, Yanhao Yu, Kangning Zhao, Ziyi Zhang, Paul M. Voyles, Gang Chen, Yingjin Wei, Xudong Wang, *Advanced Energy Materials* 1800144 (2018). DOI: 10.1002/aenm.201800144
5. “Informatics and Data Science in Materials Microscopy”, Paul M. Voyles, *Current Opinion in Solid State and Materials Science* **21**, 141 (2017).
6. “Counterintuitive reconstruction of the polar O-terminated ZnO surface with Zinc vacancies and Hydrogen” Ryan Jacobs, Bing Zheng, Brian Puchala, Paul M. Voyles, Andrew B. Yankovich, and Dane Morgan *J. Chem. Phys. Lett.* **7**, 4483 (2016).

Visualizing emergent phenomena in topological and quantum materials

Weida Wu

Department of Physics and Astronomy, Rutgers University, Piscataway, NJ, 08854

Research Scope

The objective of this project is to explore the emergent topological phenomena and to understand the unconventional properties of topological and correlated materials such as quantum anomalous Hall (QAH) systems and multiferroics. The giant magnetoelectric effect due to coupled ferroic orders in multiferroics is of both fundamental and technological interest, and is promising for energy-efficient multifunctional applications. The presence of domains and domain walls is a distinguishing feature of any ferroic order; their responses to external stimuli determine the macroscopic properties and the functionalities of ferroic materials, including magnetic topological insulators, where quantum Hall transition is coupled to magnetization reversal. To address the challenges and to directly visualize the cross-coupled phenomena and their responses to the applied electric and magnetic fields, the PI proposed and developed unique SPM techniques, e.g. magnetoelectric force microscopy (MeFM). The real space imaging of domains and domain walls shed new light on fundamental understanding of the nature of cross-coupling in multiferroic and topological materials.

Recent Progress

- **Instrumentation development**

- *Development of ultra-low temperature MFM with A-probe*

To investigate ultra-low temperature magnetic phenomena, the PI's group is investigating a new type self-sensing cantilever, called Akiyama probe (A-probe)¹. The power consumption of Quartz tuning fork sensor is of the order of nW, much less than that of piezo-resistive sensors (~mW), which opens up possibility of ultra-low temperature (mK) operation. To test the AFM/MFM performance A-probe, a dedicated SPM controller [Fig.1(a)] was acquired. The PI's graduate student Paul Sass had designed and constructed an AFM scanner head with both z- and xy-walkers shown in Figure 1(b)&(c). The AFM scanner head is based on the design of the PI's cryogenic MFM. This scanner head will be attached to the cool finger of He3 fridge for ULT-MFM. Supported by this grant, the PI already purchased a dedicated SPM controller shown in Fig. 1(a) for testing A-probe. Preliminary testing results are very promising. Fig. 1(d)&(e) show the topographic and magnetic images of the same location of a magnetic tape (Bruker) using an A-

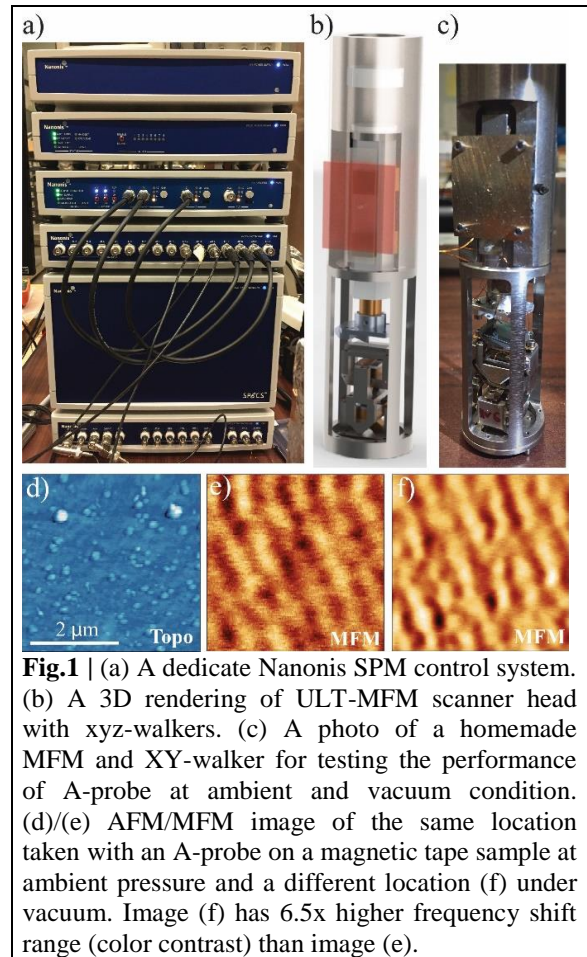


Fig.1 | (a) A dedicate Nanonis SPM control system. (b) A 3D rendering of ULT-MFM scanner head with xyz-walkers. (c) A photo of a homemade MFM and XY-walker for testing the performance of A-probe at ambient and vacuum condition. (d)/(e) AFM/MFM image of the same location taken with an A-probe on a magnetic tape sample at ambient pressure and a different location (f) under vacuum. Image (f) has 6.5x higher frequency shift range (color contrast) than image (e).

probe coated with magnetic coating in ambient condition. Fig. 1(f) shows the MFM image taken in high vacuum (10^{-6} mbar). These results demonstrate the feasibility of using A-probe for high sensitivity MFM measurements in air or vacuum.

➤ *Torque Differential Magnetometry with Qplus-Mode Quartz Tuning Fork*

The PI's group provides technical support to L. Li's group at U. Michigan Ann Arbor on the development of torque differential magnetometry with qplus-mode quartz tuning fork, which is comparable with conventional cantilever-based torque magnetometryⁱ.

• **Scientific accomplishments**

➤ *Magnetoelectric response in thin films and heterostructures*

In collaboration with D. Schlom (Cornell), the PI's group is investigating magnetic and ME properties of MBE thin films of hexagonal LuFeO_3 , a system related to hexagonal manganites. Recent theory predicts that LuFeO_3 might host strong ME coupling without applied magnetic field. The PI's group has obtained beautiful magnetic images of weak-ferromagnetic domains in LuFeO_3 thin films. Preliminary MFM results are in good agreement with transport measurements in literature⁴. A manuscript that summarizes these results is published in PRBⁱⁱ. In addition the PI collaborate with Y. Zhao's group at Tsinghua to investigate the electric field modulated magnetic anisotropy in $(\text{Co/Pt})_3/\text{PMN-PT}$ Heterostructureⁱⁱⁱ.

➤ *Magnetic imaging of ferromagnetic domains in quantum anomalous Hall systems*

Quantum anomalous Hall (QAH) systems are of great fundamental interest and potential application because of their dissipationless conduction without the need for an external magnetic field. The QAH effect has been realized in magnetically doped topological insulator thin films^{1,2}. However, full quantization requires extremely low temperature (<50 mK) in the earliest works. Thus, it is imperative to visualizing the magnetic texture to understand the magnetism.

The PI collaborated with Moodera's group at MIT on V doped BST thin films where robust QAHE effect was discovered⁶. A systematic MFM study of domain behavior in thin films of the magnetic topological insulator V doped Sb_2Te_3 revealed that in the virgin domain state, after zero-field cooling, an equal population of up and down domains occurs. The cooling field dependence of MFM images demonstrates that small cooling field (~5-10 Oe) is sufficient to significantly polarize the film despite the coercive field (H_C) for these films being on the order of a tesla at low temperature. By visualizing the magnetization reversal process around H_C of V-doped Sb_2Te_3 , a typical domain behavior of a ferromagnet, *i.e.* domain nucleation and domain wall propagation, was observed. This work is published in NPJ Quantum Materials^{iv}.

Recently, collaborators at Tsinghua University (K. He and Y. Wang) discovered enhanced QAHE temperature in Cr and V co-doped $(\text{Bi,Sb})_2\text{Te}_3$ thin films, suggesting improved ferromagnetism^v. In addition, the PI's group presents direct visualization of long-range ferromagnetic order in thin films of Cr and V co-doped $(\text{Bi,Sb})_2\text{Te}_3$ using VT-MFM with *in situ* transport. The magnetization reversal process reveals typical ferromagnetic domain behaviour—that is, domain nucleation and possibly domain wall propagation—in contrast to much weaker magnetic signals observed in the endmembers, possibly due to superparamagnetic behaviour³⁻⁵. The observed long-range ferromagnetic order resolves one of the major challenges in QAH systems, and paves the way towards high-temperature dissipationless conduction by exploring magnetic topological insulators. Furthermore, the ferromagnetism of co-doped thin films is

robust against a significant change in the bulk charge carrier density, although the exchange interaction is enhanced by hole-doping. This indicates a significant contribution from the Ruderman–Kittel–Kasuya–Yosida (RKKY) exchange coupling. This work is recently published in *Nature physics*^{vi}.

Furthermore, the PI collaborated with C. Chang, N. Sarmath, and M. Chan at Penn State on magnetic TI heterostructures for realizing the fascinating Axion insulators. The magnetic imaging of 2 separate magnetization reversals provide direct evidence of antiparallel magnetization state, a necessary condition of Axion insulator state. Combined with MFM results, the observation of zero Hall resistance state at mK unambiguously demonstrates the realization of Axion insulators. The manuscript summarizing these results was recently published in *Physical Reviews Letter*^{vii}.

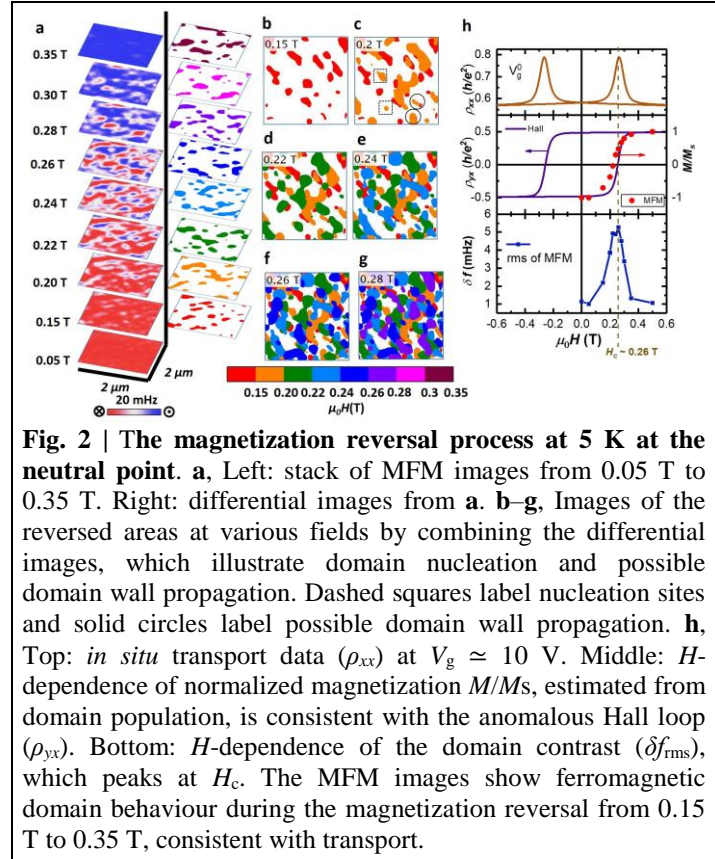


Fig. 2 | The magnetization reversal process at 5 K at the neutral point. **a**, Left: stack of MFM images from 0.05 T to 0.35 T. Right: differential images from **a**. **b–g**, Images of the reversed areas at various fields by combining the differential images, which illustrate domain nucleation and possible domain wall propagation. Dashed squares label nucleation sites and solid circles label possible domain wall propagation. **h**, Top: *in situ* transport data (ρ_{xx}) at $V_g \approx 10$ V. Middle: H -dependence of normalized magnetization M/M_s , estimated from domain population, is consistent with the anomalous Hall loop (ρ_{yx}). Bottom: H -dependence of the domain contrast (δf_{rms}), which peaks at H_c . The MFM images show ferromagnetic domain behaviour during the magnetization reversal from 0.15 T to 0.35 T, consistent with transport.

➤ *Magnetic imaging of ferromagnetic domains in 2D ferromagnets*

In collaboration with Prof. X. Xu at U. Washington, we investigate the domain state transition in itinerant ferromagnets Fe_3GeTe_2 using our MFM. The magnetic imaging provides direct evidence of domain state transition from stripe domains to single domain state as function of temperature and sample thickness. In addition, Prof. Xu’s group demonstrated the uniaxial ferromagnetism persists all the way to single monolayer with substantially high T_c (~ 100 K). The manuscript summarizing these work is recently accepted in *Nature Materials*^{viii}.

➤ *Imaging of nonlocal electromechanical power transduction in ferroelectric domains*

The PI’s group also contributed expertise in PFM and ferroelectrics to a beautiful work by K. Lai at UT Austin on interferometric imaging of nonlocal electromechanical power transduction in ferroelectric domains. The results are recently published (advanced online) in *PNAS*^{ix}.

Future Plans

MeFM studies of single phase multiferroics and heterostructures

The PI will continue to improve the sensitivity our unique MeFM technique for visualizing mesoscopic magnetoelectric coupling of domains or domain walls in either single-phase multiferroics (e.g. *hex-REMnO₃*, *hex-REFeO₃*) or heterostructural thin films where interfacial strain or exchange bias provide the cross-coupling.

Magnetic imaging of QAH systems and chiral edge states

The PI will investigate ferromagnetic domain behaviors in magnetic TIs, using VT-MFM with *in situ* high magnetic/electric field capabilities. The ultimate goal is to visualize one-way conduction of chiral edge states in these fascinating systems. Another direction is to investigate Axion insulators in magnetic TI heterostructure to explore the Axion physics.

Design and development of ULT-AFM based on A-probe

The PI's group will continue testing the AFM and MFM operation of A-probe in cryogenic environment. Because the design of new scanner head is compatible with the PI's cryogenic MFM probe, the new scanner head can be seamlessly integrated with the MFM probe for low temperature tests.

References

1. Chang, C. Z. *et al.* Thin films of magnetically doped topological insulator with carrier-independent long-range ferromagnetic order. *Adv Mater* **25**, 1065–1070 (2013).
2. Chang, C. Z. *et al.* High-precision realization of robust quantum anomalous Hall state in a hard ferromagnetic topological insulator. *Nat Mater* **14**, 473–477 (2015).
3. Grauer, S. *et al.* Coincidence of superparamagnetism and perfect quantization in the quantum anomalous Hall state. *Phys. Rev. B* **92**, 201304(R) (2015).
4. Lachman, E. O. *et al.* Visualization of superparamagnetic dynamics in magnetic topological insulators. *Sci. Adv.* **1**, 1500740 (2015).
5. Lachman, E. O. *et al.* Observation of superparamagnetism in coexistence with quantum anomalous Hall $C = \pm 1$ and $C = 0$ Chern states. *npj Quantum Mater.* **2**, 70 (2017).

Publications supported by BES

- ⁱ L. Chen, *et al.*, “Torque Differential Magnetometry with Qplus-Mode Quartz Tuning Fork”, *Phys. Rev. Applied*, **9**, 024005 (2018).
- ⁱⁱ W. Wang, *et al.*, “Visualizing weak ferromagnetic domains in multiferroic hexagonal ferrite thin film”, *Phys. Rev. B*, **95**, 134443 (2017).
- ⁱⁱⁱ Y. Sun, *et al.*, “Electric-Field Modulation of Interface Magnetic Anisotropy and Spin Reorientation Transition in (Co/Pt)₃/PMN–PT Heterostructure”, *ACS Applied Materials & Interfaces*, **9**, 10855 (2017).
- ^{iv} W. Wang, *et al.*, “Visualizing ferromagnetic domain behaviors of V-doped Sb₂Te₃ thin films”, *npj Quantum Materials*, **1**, 16023 (2016).
- ^v Y. Ou, *et al.*, “Enhancing the Quantum Anomalous Hall Effect by Magnetic Codoping in a Topological Insulator”, *Advanced Materials*, **30**, 1703062 (2017).
- ^{vi} W. Wang, *et al.*, “Direct evidence of ferromagnetism in a quantum anomalous Hall system”, *Nature Physics*, **14**, 791–795 (2018).
- ^{vii} D. Xiao, *et al.*, “The Realization of the Axion Insulator State in Quantum Anomalous Hall Sandwich Heterostructures”, *Phys. Rev. Lett.*, **120**, 056801 (2018).
- ^{viii} Z. Fei, *et al.*, “Two-Dimensional Itinerant Ising Ferromagnetism in Atomically thin Fe₃GeTe₂”, *Nature Materials*, **in press** (2018).
- ^{ix} L. Zheng, *et al.*, “Interferometric Imaging of Nonlocal Electromechanical Power Transduction in Ferroelectric Domains”, *PNAS*, **AOP**, (2018).

Transport and Imaging of Mesoscopic Phenomena in Novel Low-Dimensional Materials

Yacoby, Amir - Harvard University, yacoby@physics.harvard.edu
Jarillo-Herrero, Pablo – MIT, pjarillo@mit.edu

Project Scope

Layered materials offer a new playground for exploring novel physics in reduced dimensions. In particular, they allow exploring hybrid structures and the interface between different electronic phases. Our focus in this proposal is to use innovative methods to fabricate ultra-low disorder graphene and other novel 2D materials devices, in conjunction with ultra-sensitive scan probe, local tunneling, and capacitance methods, as well as low-temperature electronic transport techniques in order to explore new and spatially varying mesoscopic phenomena in graphene and TMD devices and heterostructures.

Recent Progress

In this talk we will focus on a particular hybrid structure that couples quantum Hall edges to superconductivity. This hybrid geometry is theoretically predicted to host non-Abelian excitations. Our work thus far has been to explore the interference of quantum Hall edge states and their coupling to a proximal superconductor through cross Andreev scattering.

Mach-Zehnder interferometry using spin- and valley-polarized quantum Hall edge states in graphene – Science Advances 3, 1700600 (2017).

Confined to a two-dimensional plane, electrons in a strong magnetic field travel along the edge in one-dimensional quantum Hall channels that are protected against backscattering. These channels can be used as solid-state analogues of monochromatic beams of light, providing a unique platform for studying electron interference. Electron interferometry is regarded as one of the most promising routes for studying fractional and non-Abelian statistics and quantum entanglement via two-particle interference. However, creating an edge-channel interferometer in which electron-electron interactions play an important role requires a clean system and long phase coherence lengths. Here we realize electronic Mach-Zehnder interferometers (Fig. 1A) with record visibilities of up to 98% using spin- and valley-polarized edge channels that co-propagate along a PN junction in graphene. We find that inter-channel scattering between same-spin edge channels along the physical graphene edge can be used to form beam splitters, while the absence of inter-channel scattering along gate-defined interfaces can be used to form isolated interferometer arms. Surprisingly, our interferometer is robust to dephasing effects at energies an order of magnitude larger than observed in pioneering experiments on GaAs/AlGaAs quantum wells. Our results shed light on the nature of edge-channel equilibration and open up new possibilities for studying exotic electron statistics and quantum phenomena.

To construct a MZI of spin- and valley-polarized edge channels, we use a hexagonal boron nitride (hBN) encapsulated monolayer of graphene (Fig. 1B). We tune into the quantum Hall regime using a perpendicular magnetic field B , and define two regions of different charge densities n_T and n_B using a bottom gate that affects both n_T and n_B and a top gate that affects only n_T (Fig. 1B). The number of edge channels in these regions is given by the filling factors $\nu_{T,B} = (h/eB)n_{T,B}$, where e is the electron charge and h is Planck's constant. The observation of integer quantum Hall steps in a measurement of the two-terminal conductance at $B = 4$ T in the regime where $\nu_T > 0$ and $\nu_B > 0$ confirms that the spin and valley-degeneracy is lifted. Next, we create a PN junction by tuning into the regime where $\nu_T < 0$ and $\nu_B > 0$ and

study which edge channels mediate charge transport across the junction. When we measure the conductance g as a function of $vT < 0$ and $vB > 0$ at $B = 4$ T, we observe four regions with distinct ranges of conductance values, as well as the first indications of conductance oscillations (Fig. 1C). In region I, the conductance of the junction is near zero, which we attribute to the situation depicted in the top panel

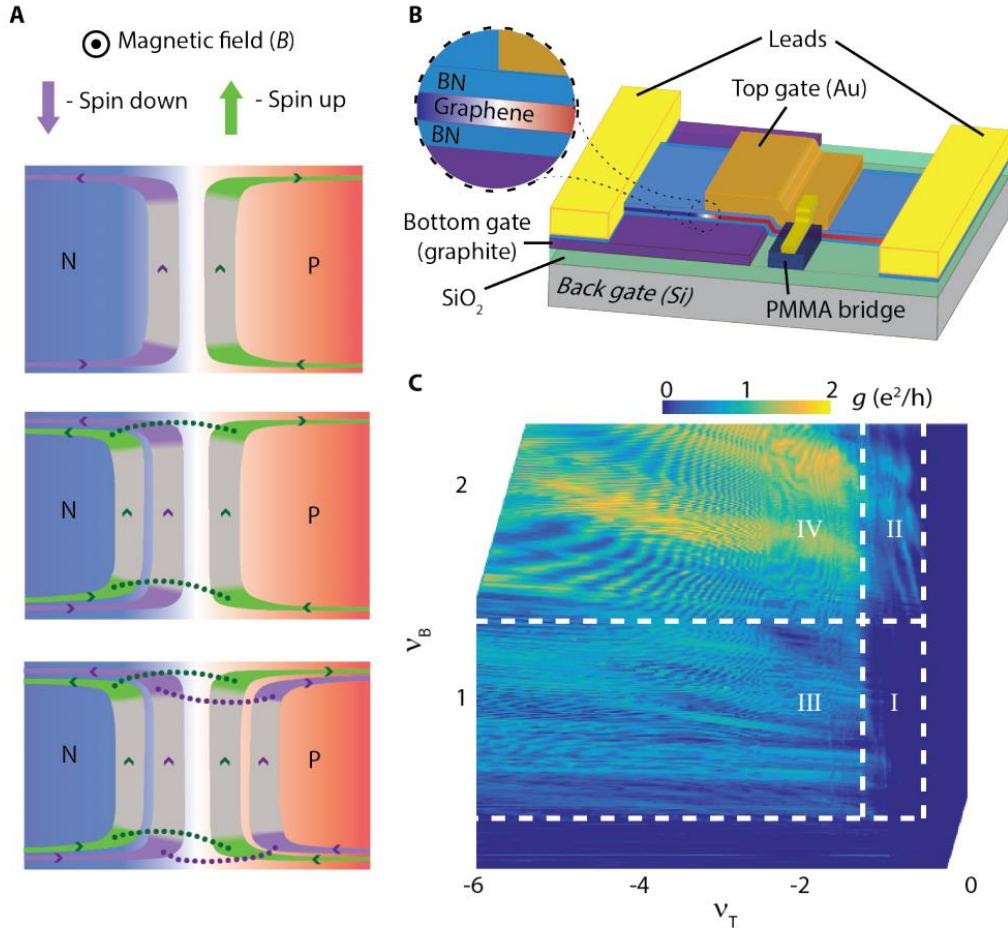


Figure 1. Mach Zender interferometer of QH edge states in graphene.

of Fig. 1A (where $vB = 1$ and $vT = -1$). Here, one N-type spin-down and one P-type spin-up edge channel co-propagate along the junction. As these channels have opposite spin, inter-channel scattering is suppressed. When we cross from region I into region II, we begin to observe transport across the junction. We attribute this to an additional spin-up edge channel having entered on the N-side (so that $vB = 2$ and $vT = -1$) and that electrons in this channel can scatter into the spin-up channel on the P-side (see middle panel in Fig. 1A). The observed conductance ranges approximately between 0 and e^2/h , consistent with one pair of edge channels mediating transport across the junction. Similarly, in region III we obtain the situation in which $vB = 1$ and $vT = -2$, and we attribute the observed conductance to scattering between the two spin-down edge channels. Strikingly, in region III the conductance does not change notably as we keep adding edge channels on the P-side (going to $vB = 1$ and $vT < -2$). We conclude that these additional channels do not contribute to the trans-junction conductance, presumably because they belong to a higher LL which makes them spatially too distant from the PN interface. Crossing into region IV ($vB \geq 2$ and $vT \leq -2$), we observe that the average conductance increases and ranges between 0 and $2e^2/h$. We attribute

this to two pairs of same-spin edge channels mediating transport across the junction. Again, we see no sign of edge channels belonging to higher LLs entering the system and contributing to the trans-junction conductance. We conclude that the edge channels belonging to the zLL mediate the transjunction conductance, well isolated from edge channels belonging to higher LLs.

Inducing Superconducting Correlation in Quantum Hall Edge States – Nature Physics 13, 693 (2017).

The quantum Hall (QH) effect supports a set of chiral edge states at the boundary of a 2-dimensional electron gas (2DEG) system. A superconductor (SC) contacting these states can induce correlations of the quasi-particles in the dissipationless 1D chiral QH edge states. If the superconducting electrode is narrower than the superconducting coherence length, the incoming electron is correlated to the outgoing hole along the chiral edge state by the Andreev process across the SC electrode. In order to realize this crossed Andreev conversion (CAC), it is necessary to fabricate highly transparent and nanometer-scale superconducting junctions to the QH system. Here we report the observation of CAC in a graphene QH system contacted with a nanostructured NbN superconducting electrode. The chemical potential of the edge states across the SC electrode exhibits a sign reversal, providing direct evidence of CAC. This hybrid SC/QH system is a novel route to create isolated non-Abelian anyonic zero modes, in resonance with the chiral QH edge.

The microscopic picture of charge flow across the SC/QH system can be described by extending the Andreev process between a SC and a normal conductor. Figure 2a depicts local Andreev reflection at zero magnetic field. An electron with energy (eV), which is smaller than the superconducting gap (Δ), can enter the grounded SC electrode to form a Cooper pair, while retro-reflecting a hole back to the source of the electron. In the presence of a magnetic field, however, the chiral nature of the QH edge state forces the converted hole to keep flowing with the same chirality as the incoming electron. Note that the hole has the same chirality as the electron, because the sign of its charge and mass are both opposite to those of the electron. There can be two different regimes in this Andreev process, depending on the width of the SC electrode (W) compared to the superconducting coherence length (ξ_s). When $W \gg \xi_s$, the electron and hole will propagate along the edge of the SC electrode forming an Andreev edge state (AES) (Fig. 2b). In a quasi-classical picture, the AES is an alternating skipping orbit of electrons and holes. Unless the probability of each Andreev reflection (PAR) is very close to zero or unity, the AES quickly becomes an equal mixture of electrons and holes after a few bounces. The resulting mixed AES along the ground SC (i.e. at zero chemical potential) carries the averaged chemical potential equal to zero. However, when $W \ll \xi_s$ the converted hole can tunnel through the SC electrode and continue to flow on the other side of the QH edge state, a process termed as crossed Andreev conversion (CAC) (Fig. 2c). Note that in the CAC process, the converted hole in the downstream carries negative (electron) chemical potential. Therefore, unlike the case of the AES, the spatial separation of electrons and holes in CAC facilitates their independent detection by measuring the chemical potential of upstream and downstream edge states with respect to the ground SC electrode, which we demonstrate in this paper. Interestingly, in the asymptotic limit of $W \ll \xi_s$ and a long finger-like SC electrode whose length $L \gg \hbar v_F/\Delta$, the CAC picture corresponds to creating two non-Abelian anyons in resonance with the QH edge state. Here, \hbar is a Planck constant and v_F is the Fermi velocity of QH edge states. The counter propagating QH edge modes along the both sides of the finger electrode are coupled by the SC, creating two zero modes: one in resonance with the QH edge and the other at the end of the SC finger (inset of Fig. 2c). In order to measure the chemical potential of QH edge states across the SC electrode, we fabricate a multiterminal graphene device with a SC drain electrode as shown in Fig. 2d. To obtain a high-quality graphene channel, we encapsulated

mechanically exfoliated graphene samples with two h-BN crystals using a dry-transfer technique. NbN was chosen for the SC drain contact, since its high upper critical field ($B_{c2} \sim 25$ T) and high critical temperature ($T_c = 12$ K) enable us to experimentally access a wide range of magnetic fields where superconductivity and the QH effect in graphene coexist.

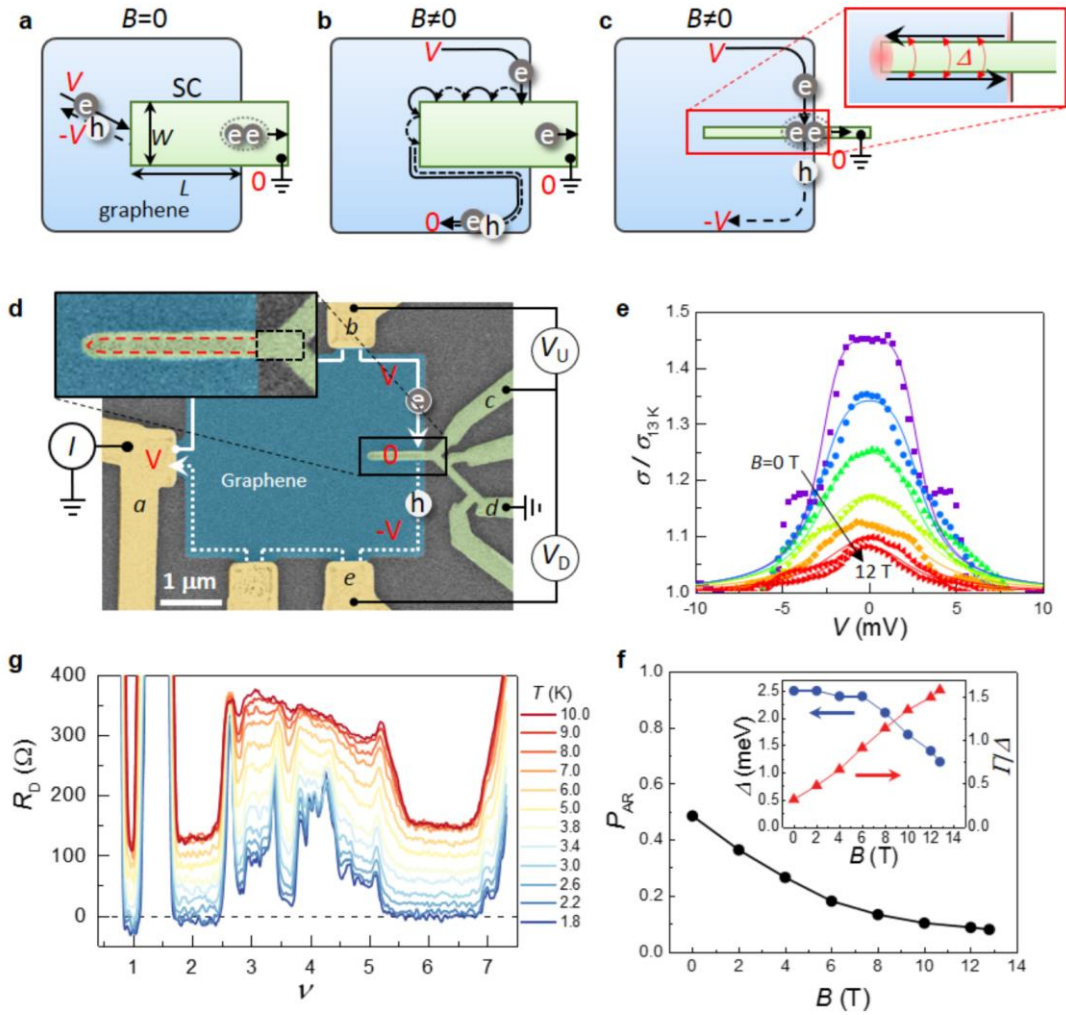


Figure 2. Cross Andreev scatter in Quantum Hall edges.

Future Plans - Our research effort for the next years will focus on the following topics:

1. Induced superconductivity and Andreev tunneling spectroscopy in graphene.
2. Imaging Josephson current in proximitized graphene and other TMD.
3. Interplay between superconductivity and quantum Hall physics.
4. Transport and imaging of graphene in inhomogeneous electric and magnetic fields.
5. Compressibility in TMD and graphene using capacitance and gateable scanning SET's
6. Imaging graphene edge magnetism using scanning diamond NV centers.

Publications from DOE supported research – past 2 years (also used as references)

1. Mach-Zehnder interferometry using spin- and valley-polarized quantum Hall edge states in graphene, D. S. Wei, T. van der Sar, J. D. Sanchez-Yamagishi, K. Watanabe, T. Taniguchi, , P. Jarillo-Herrero, B. I. Halperin, A. Yacoby, *Science Advances* **3**, 1700600 (2017).
2. Inducing superconducting correlation in quantum Hall edge states, Gil-Ho Lee, Ko-Fan Huang, Dmitri K. Efetov, Di S. Wei, Sean Hart, Takashi Taniguchi, Kenji Watanabe, Amir Yacoby & Philip Kim, *Nature Physics* **13**, 693 (2017).
3. Spatially resolved edge currents and guided-wave electronic states in graphene M. T. Allen, O. Shtanko, I. C. Fulga, A. Akhmerov, K. Watanabi, T. Taniguchi, P. Jarillo-Herrero, L. S. Levitov, and A. Yacoby. *Nature Physics* **12**, 128 (2016).
4. Observation of Electron Coherence and Fabry-Perot Standing Waves at a Graphene Edge – M. T. Allen, O. Shtanko, I. C. Fulga, J. I.-J. Wang, D. Nurgaliev1 , K. Watanabe, T. Taniguchi, A. R. Akhmerov, P. Jarillo-Herrero, L. S. Levitov, and A. Yacoby, *Nano Letters* **17**, 7380 (2017).
5. Tunnelling spectroscopy of Andreev states in graphene. Landry Bretheau, Joel I-Jan Wang, Riccardo Pisoni, Kenji Watanabe, Takashi Taniguchi, Pablo Jarillo-Herrero. *Nature Physics*, **13**, 756 (2017).
6. Enhanced Superconductivity and Suppression of Charge-density Wave Order in 2H-TaS₂ in the Two-dimensional Limit. Yafang Yang, Shiang Fang, Valla Fatemi, Jonathan Ruhman, Efrén Navarro-Moratalla, Kenji Watanabe, Takashi Taniguchi, Efthimios Kaxiras, Pablo Jarillo-Herrero. *Phys. Rev. B* **98**, 035203 (2018).
7. Tunneling spectroscopy of graphene nanodevices coupled to large gap superconductors. Joel I-Jan Wang, Landry Bretheau, Daniel Rodan-Legrain, Riccardo Pisoni, Kenji Watanabe, Takashi Taniguchi, and Pablo Jarillo-Herrero. *Phys. Rev. B* (in press, 2018).

Probing Correlated Superconductors and Their Phase Transitions on the Nanometer Scale

Ali Yazdani
Department of Physics
Princeton University, Princeton, NJ 08544

Research scope:

Our experimental program provides an atomic scale perspective of unconventional superconductivity — how it evolves from an unconventional conducting state and how it competes with other forms of order in correlated electronic systems. Such phenomena are at the heart of some of the most debated issues in condensed matter physics, and understanding these phenomena is an intellectual driver for many of the DOE-BES projects for the development of novel materials, including the search for higher temperature superconductivity. Our aim is to provide a microscopic view of these exotic materials and their phase transitions into the superconducting state using some of the most sophisticated scanning tunneling microscopy (STM) and spectroscopy techniques.

Our research efforts have built on our previous advances in the study of heavy fermion systems to examine such systems in new ways — not only to understand the connections between unconventional superconductivity and other exotic electronic orders — but to also examine the role of materials' dimensionality in both the normal and superconducting properties. The layered heavy fermion compound CeCoIn_5 offers an electronically rich system for such studies. Moving beyond unconventional superconductivity emerging from strong electronic interactions, we also propose to examine the emergence of exotic superconductivity in the presence of ferromagnetism in proximity-type heterostructures as well as in materials with strong spin-orbit interactions. Our work in this area is motivated by recent theoretical proposals and experimental efforts that topological superconductivity can be engineered into hybrid materials by proximity-inducing pairing on their spin-textured bands. This is an effort in which the combination of magnetism, spin-orbit material and superconductivity is used to create topological superconductivity that will host a Majorana zero mode. Finally, the proposed program is focused on developing novel new imaging techniques for characterization of correlated electronic states. For example, we have established Josephson tunneling spectroscopy at the atomic scale under this program during the first year. More recently, we have developed imaging techniques to probe quantum Hall states by directly visualizing Landau orbits and have applied these techniques to visualize novel broken symmetry states that involve valley degrees of freedom.

Highlights of breakthroughs under the DOE grant in last two years:

- Visualizing heavy fermion confinement and Pauli-limited superconductivity in layered CeCoIn_5 (Nature Communications 2018).
- Direct visualization of Landau orbits with the STM (Science 2016).
- Detection of a nematic quantum Hall phases (Science 2016).
- Detection of ferroelectric quantum Hall phase (Nature Physics 2018).

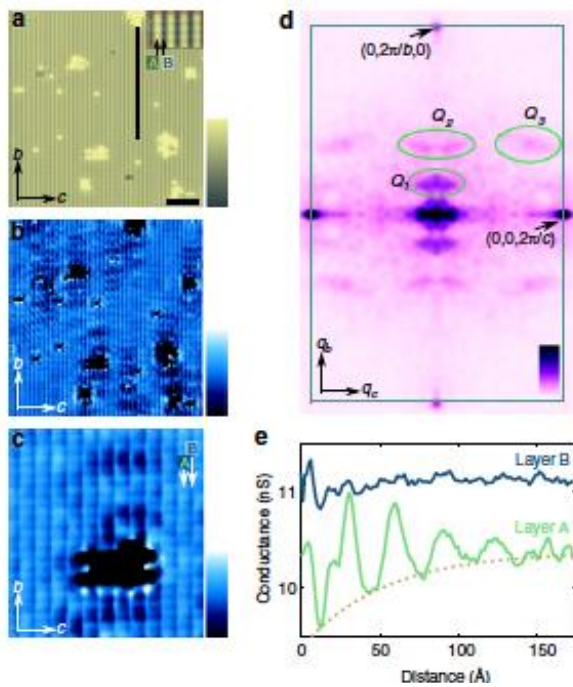


Figure 1. STM studies on heavy fermion CeCoIn₅. (a) Topographic image of surface S where the conductance map was acquired. Inset shows an enlarged topographic image with the position of layers A and B indicated. Horizontal scale bar: 50 Å, vertical scale bar: 5 Å. (b) Conductance map showing quasiparticle standing waves around the atomic islands. Scale bar indicates the conductance from 9 nS to 12 nS. (c), Enlarged conductance map, which demonstrates the strongly one-dimensional scattering of the quasiparticles. Arrows indicate the position of two layers: layers A and B. Horizontal scale bar: 20 Å, vertical scale bar: conductance from 5 nS to 7 nS. (d), Fourier transform of the conductance maps shown in b. Green rectangle shows the border of the unit cell in reciprocal space. Scale bar indicates the magnitude of the power spectral density. (e) The modulation of the local density of states (LDOS) along a line parallel to *b* axis (shown as white line on panel a) on top of layer B (blue).

Recent Progress:

Visualizing heavy quasiparticle confinement and Pauli-limited superconductivity

We had an important breakthrough that allowed us to probe the electronic states of the heavy fermion superconductor in CeCoIn₅ by performing STM measurements on the (100) surface of this compound (Figure 1). Previously, we had been able to probe the development of heavy quasiparticles in this compound as well as the emergence of d-wave superconductivity by performing STM measurements along the *c*-axis of the compound. These experiments probed the in-plane properties of this expected two-dimensional material. In a manuscript that was published in Nature Communications (2018), we reported on the study of heavy quasiparticle confinement and direct visualization of Pauli-limited superconductivity in CeCoIn₅. By examining this layered heavy fermion in a cross section, we were able to make atomic scale measurements of the electronic properties of this compound that revealed remarkable changes of its electronic structure from layer to layer. Combining these experiments with quasiparticle interference spectroscopy, we were able to further show that when the heavy fermions emerge in this compound, they are strongly confined within specific layers. This highly anisotropic normal state property appears to strongly influence the development of superconductivity, which is reflecting this anisotropy, although it is averaging over length scale of superconducting coherence. Visualizing magnetic vortices in this orientation we characterized the anisotropy of the superconducting coherence length, the measurements of which matches the strong difference between in-plane and out-of-plane upper critical field of this compound (Figure 2). Most remarkably, in this study we found evidence for magnetic vortices in a magnetic field range slightly higher than the thermodynamically measured upper critical field. It appears that local superconductivity survives above the bulk upper critical field, a behavior that is also believed to occur in other strongly correlated superconductors. Finally, we have been able to show that the suppression of superconductivity in this system near this first

order Pauli-limited transition, occurs in a spatially inhomogeneous manner, with normal and superconducting regions coexisting (Figure 2e). These experiments were published in Nature Communications in 2018.

Visualizing Landau orbits with the STM—from nematic to ferroelectric quantum Hall phases

The quantum Hall effect is the first example of a topological electronic phase discovered in materials. While there have been decades of research in the study of this phenomenon, imaging the Landau orbit wavefunction in the quantum Hall phase was not considered possible. An important breakthrough with our DOE program has been to show that it is possible to image individual Landau wavefunction for quantum Hall states formed for the two-dimensional electron gas on the surface of Bi at high magnetic fields (Figure 3). This imaging breakthrough has opened up a number of very important possibilities, from study of interaction-induced nematic and ferroelectric two-dimensional quantum Hall phases, to one-dimensional states that can emerge at the boundary of these systems.

In correlated systems, such as high- T_c superconductors, there has been a long-standing interest in the possibility that interaction between electrons can result in phases that break the underlying crystalline symmetry. Although there has been some evidence for such phases in high- T_c superconductors, in these systems we do not have accurate knowledge of electronic wavefunctions or actual measurements of the interaction strength between the electrons. Therefore, it has been difficult to be confident that the observed symmetry breaking is indeed due to such interactions. The quantum Hall states formed for two-dimensional surface states of Bi provide an ideal setting to investigate this phenomena by combining STM imaging and spectroscopy. The STM imaging is used to see whether the underlying state breaks the symmetry of the surface while STM spectroscopy is used to determine if the effect is driven by interactions, as such interactions would open up a gap in the spectra at the Fermi level. The combination of these two techniques was used to determine and confirm that interaction can favor

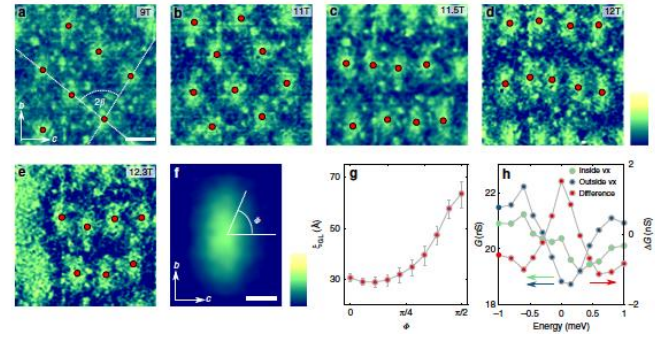
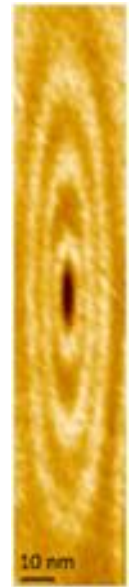


Figure 2. Anisotropic vortices and vortex lattice transition in 115. (a-e) Conductance maps (G_{sub}) obtained on a $500 \text{ \AA} \times 500 \text{ \AA}$ area with magnetic fields applied parallel to the a axis, which show elongated vortices on the (100) surface. The vertical scale bar corresponds to the normalized subtracted conductance map $G_{\text{sub,norm}} = G_{\text{sub}} / |\overline{G_{\text{sub}}}|$, where $\overline{G_{\text{sub}}}$ is the mean of the subtracted conductance value over the entire field of view. The scale bar has a range from -2 to 2, while the horizontal scale bar corresponds to 100 \AA . (f) Averaged vortex shape obtained by overlaying 90 measured vortices at different fields. Horizontal scale bar corresponds to 30 \AA , while vertical color bar indicates $G_{\text{sub,norm}}$ from -1 to 1. (g) Extracted effective coherence length as a function of angle ϕ . Spatially averaged density of states in the vortex core (green), far from the vortex (blue) and their difference (red), which show the existence of the bound states inside the vortex shows a broad peak around $0.2 < H < 0.4$.

Figure 3. Visualizing Landau orbits. Spatially resolved conductance map at the center of the LL peak shows suppression near an individual atomic defect in the shape of the LL wavefunction. The data corresponds to the LL orbit for the elliptical shape of the anisotropic Bi's hole pockets. The wavefunction has lower symmetry than the threefold symmetry of the surface, as the system is a nematic quantum Hall phase.



electrons occupying a combination of valley states that have lower symmetry than the crystalline structure of the surface. These experiments were published in Science in 2016.

Following these experiments, subsequent studies of Landau orbits with higher spatial resolution revealed additional interference features in the STM conductance maps, when different types of nematic phases were formed by tuning the magnetic field. These features provided the impetus to examine all the different forms of valley-polarized nematic phases that can form in our system. A key finding was that under the right occupation of the valleys tuned by the magnetic field, it is possible to have a single valley occupied, in which both rotation and inversion symmetry of electronic states are broken. This observation is consistent with the theoretical prediction that interaction in a highly anisotropic valley system can drive the electrons into a single valley and produce a quantum Hall ferroelectric state. These experiments have just been published in Nature Physics.

Future plans:

Our plans moving forward will focus on the following key ideas:

1. One of the key goals of the program is to realize unconventional topological superconducting phases. As such we have been working on the platform that combines magnetism, spin-orbit coupling, and superconductivity. We have had recent success in introducing proximity effect in ultra-thin films of Bi. The edge of Bi bilayer islands have quantum spin Hall-like topological edge states, in which superconductivity is supposed to be p-wave. We are carrying on a series of experiments to investigate this possibility.
2. We are examining the boundary modes that form at the domain wall between different quantum Hall nematic phases. We have found evidence of these edge modes to spontaneously emerge on the surface of Bi using STM conductance maps. In collaboration with Prof. Siddharth Parameswaran (University of Oxford, UK), we have determined that these edge modes are a new form of 1d Luttinger liquids, which valley flavor can strongly constrain electron-electron interactions. We are in the process of writing a combined experiment-theory paper to explore this exciting new arena for interacting electrons in a 1D system that is accessible for direct spatially resolved experiments with the STM.

Publications supported by the DOE-BES (2016-2018):

In addition to publications directly related to DOE-BES projects, the DOE funding that supports the instrumentation in our lab has assisted other projects. The publications from these projects benefiting from DOE support are also included in the list below (marked as partially supported by DOE).

1. M. T. Randeria, B. E. Feldman, F. Wu, H. Ding, A. Gyenis, H. Ji, R. J. Cava, A. H. MacDonald, and A. Yazdani, "Ferroelectric quantum Hall phase revealed by visualizing Landau level wavefunction interference," Nature Physics **14.15** (2018).
2. J. Li, S. Jeon, Y. Xie, A. Yazdani, and B. A. Bernevig, "Majorana spin in magnetic atomic chain systems," Physical Review B **9**, 125119 (2018). Partially Support by DOE

3. A. Gyenis, B. E. Feldman, M. T. Randeria, G. A. Peterson, E. D. Bauer, P. Aynajian, and A. Yazdani, “Visualizing heavy fermion confinement and Pauli-limited superconductivity in layered CeCoIn₅,” *Nature Communications* **9**, 549 (2018).
4. S. Jeon, Y. Xie, J. Li, Z. Wang, B. A. Bernevig, and A. Yazdani, “Distinguishing a Majorana zero mode using spin resolved measurements,” *Science* **358**, 772 (2017). Partially Support by DOE
5. B. E. Feldman, M. T. Randeria, J. Li, S. Jeon, Y. Xie, Z. Wang, I. K. Drozdov, B. A. Bernevig, and A. Yazdani, “High-resolution studies of the Majorana atomic chain platform,” *Nature Physics* **13**, 286 (2016). Partially Support by DOE
6. B. E. Feldman, M. T. Randeria, A. Gyenis, F. Wu, H. Ji, R. J. Cava, A. H. MacDonald, and A. Yazdani, “Observation of a nematic quantum Hall liquid on the surface of bismuth,” *Science* **354**, 6310 (2016).
7. A. Gyenis, E. H. da Silva Neto, R. Sutarto, E. Schierle, F. He, E. Weschke, M. Kawai, R. E. Baumbach, J. D. Thompson, E. D. Bauer, Z. Fisk, A. Damascelli, A. Yazdani, and Pegor Aynajian, “Quasiparticle interference of heavy fermions in resonant x-ray scattering,” *Science Advances* **2**, 10 (2016).
8. A. Gyenis, H. Inoue, S. Jeon, B. B. Zhou, B. E. Feldman, Z. Wang, J. Li, S. Jiang, Q. D. Gibson, S. K. Kushwaha, J. W. Krizan, N. Ni, R. J. Cava, B. A. Andrei Bernevig, and A. Yazdani, “Imaging electronic states on topological semimetals using scanning tunneling microscopy,” *New Journal of Physics* **18**, 105003 (2016). Partially Support by DOE
9. H. Inoue, A. Gyenis, Z. Wang, J. Li, S. W. Oh, S. Jiang, N. Ni, B. A. Bernevig and A. Yazdani, “Quasiparticle interference of the Fermi arcs and surface-bulk connectivity of Weyl semimetals,” *Science* **351**, 1184 (2016). Partially Support by DOE
10. M. T. Randeria, B. E. Feldman, I. K. Drozdov, and A. Yazdani, “Scanning Josephson spectroscopy on the atomic scale,” *Physical Review B Rapid Communication* **93**, 161115R (2016). Selected as an Editor’s choice.
11. A. Yazdani, E. H. da Silva Neto, and P. Aynajian, “Spectroscopic imaging of strongly correlated electronic states,” *Annual Review of Condensed Matter Physics* **7**, 11 (2016).

Dislocation avalanche mechanism in high entropy alloys

Jian-Min Zuo

Dept. of Materials Science and Engineering and Materials Research Laboratory,
University of Illinois, Urbana-Champaign, IL 61801

Program Scope

The proposed work is to develop Scanning CBED (SCBED) for the study of multi-element crystals, including multiple principal elements alloys or high entropy alloys and relaxor-ferroelectric crystals.

SCBED works like scanning transmission electron microscopy (STEM) but records the whole CBED at each probe position. Since CBED is a highly sensitive electron diffraction technique, SCBED combines the full benefits of CBED and STEM. Specifically, the SCBED based approach enables a quantitative determination of local atomic and electronic structures. The proposed work is thus to take advantage of SCBED for the study of complex multi-element crystals. The results from SCBED are expected to complement the methods of electron energy loss spectroscopy (EELS) near edge fine structure for probing local bonds, and X-ray and neutron scattering using the total scattering approach for probing local structure.

Under the DOE BES support, we have developed SCBED to determine the structure of high entropy alloys, and we have coupled the work with in-situ compression study of dislocation dynamics to uncover the fundamental mechanisms of crystal slip.

Recent Progress

Background: Recent research efforts have focused on intermittency in crystal plasticity. For example, acoustic emissions from stressed ice revealed discrete dislocation avalanches, whose magnitudes follow a power-law distribution [1, 2]. Mechanical testing on microcrystals detected sudden strain bursts, which also follow the power-law scaling between the number of bursts and their magnitudes [3-6]. Together, these experiments convincingly demonstrated criticality among relatively large and rapid dislocation events.

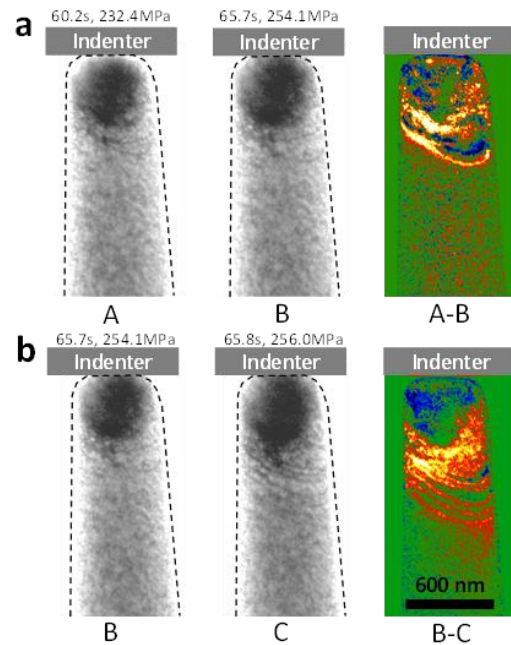


Fig. 1 The formation of dislocation pileup in front of a dislocation band in a high entropy alloy. a) the bowing out of the mobile part of a dislocation under an applied stress. b) the Frank-Read dislocation source operated and generated a dislocation pileup that also resulted with a sudden movement of the dislocation band, as evidenced in the difference image. The dislocation pileup and dislocation band interaction plays a critical role dislocation avalanche.

On the other hand, the fundamental operating units in crystal plasticity are individual dislocations. There is a long history of transmission electron microscopy (TEM) studies of dislocations and their interaction mechanisms[7-9], which have also revealed complex dislocation patterns in deformed crystals, including dislocation cells[10] and persistent slip bands[11]. However, how intermittent dislocation activities stem from complex dislocation patterns, how these activities impact the dislocation pattern formation, and how this trend leads to crystal slip, are all unresolved critical questions[4, 12, 13].

Results: Through direct electron imaging and precise measurements, we followed individual avalanche events and determined their properties in the slowly compressed nanopillars of a high entropy alloy (HEA), $\text{Al}_x\text{CoCrFeNi}$ ($x = 0.1$). Surprisingly, our results show that dislocations accumulate and are stored in the HEA nanopillars in a manner opposite to mobile dislocation starvation seen sometimes in fcc metal nanopillars[5, 14, 15]. Dislocation storage leads to the formation of dislocation bands that propagate intermittently along the compression direction through dislocation slips. We find dislocation pileups in front of the dislocation bands, which perform the important role of controlling dislocation avalanches, similar to a floodgate. The avalanches give rise to displacements from few to 10^2 nm with the power-law distribution similar to earthquakes[3, 16]. The study identifies the dislocation interaction mechanism for sudden large crystal slips, and provides guidance for the design of new multi-component alloys.

Impact: The avalanche mechanism that we identified for HEAs is based on interactions between the dislocation pileup and the dislocation band, and between the pileup and dislocation pinning centers. Unlike the slip of individual dislocations, which can be approximated as elastic strings of constant stiffness, the stiffness of a pileup is dependent on the long-range interactions between dislocations[17]. Our statistical analysis shows the slip avalanche's dependence on the stress level, which indicates that the applied stress is a critical tuning parameter.

Future Plans

Further study is planned the nanoscale dislocation dynamics that we have observed in the high entropy alloys and how the dislocation dynamics related to the structure of high entropy alloys. We are specifically interested in the so-called severe lattice distortion effect and would like to determine the nature of lattice distortions in these fascinating alloys.

References

- [1] J. Weiss, F. Lahaie, J.R. Grasso, Statistical analysis of dislocation dynamics during viscoplastic deformation from acoustic emission, *Journal of Geophysical Research: Solid Earth*, 105 (2000) 433-442.
- [2] M.C. Miguel, A. Vespignani, S. Zapperi, J. Weiss, J.R. Grasso, Intermittent dislocation flow in viscoplastic deformation, *Nature*, 410 (2001) 667-671.
- [3] D.M. Dimiduk, C. Woodward, R. LeSar, M.D. Uchic, Scale-Free Intermittent Flow in Crystal Plasticity, *Science*, 312 (2006) 1188-1190.

- [4] M. Zaiser, J. Schwerdtfeger, A.S. Schneider, C.P. Frick, B.G. Clark, P.A. Gruber, E. Arzt, Strain bursts in plastically deforming molybdenum micro- and nanopillars, *Philosophical Magazine*, 88 (2008) 3861-3874.
- [5] S. Brinckmann, J.-Y. Kim, J.R. Greer, Fundamental Differences in Mechanical Behavior between Two Types of Crystals at the Nanoscale, *Physical Review Letters*, 100 (2008) 155502.
- [6] N. Friedman, A.T. Jennings, G. Tsekenis, J.-Y. Kim, M. Tao, J.T. Uhl, J.R. Greer, K.A. Dahmen, Statistics of dislocation slip avalanches in nanosized single crystals show tuned critical behavior predicted by a simple mean field model, *Physical Review Letters*, 109 (2012) 095507.
- [7] P. Hirsch, A. Howie, R.B. Nicolson, D.W. Pashley, M.J. Whelan, *Electron Microscopy of Thin Crystals*, Robert E. Krieger Publishing Company, Malaba, Florida, 1977.
- [8] J.C.H. Spence, Chapter 77 Experimental studies of dislocation core defects, *Dislocations in Solids*, 13 (2007) 419-452.
- [9] U. Messerschmidt, *Dislocation dynamics during plastic deformation*, Springer, 2010.
- [10] L.P. Kubin, Dislocation patterning, in: H. Mughrabi (Ed.) *Treatise in Materials Science and Technology*, VCH, D-Weinberg, 1993, pp. 138.
- [11] Z.S. Basinski, S.J. Basinski, Fundamental aspects of low amplitude cyclic deformation in face-centred cubic crystals, *Progress in Materials Science*, 36 (1992) 89-148.
- [12] L.M. Brown, Constant intermittent flow of dislocations: central problems in plasticity, *Materials Science and Technology*, 28 (2012) 1209-1232.
- [13] F.F. Csikor, C. Motz, D. Weygand, M. Zaiser, S. Zapperi, Dislocation avalanches, strain bursts, and the problem of plastic forming at the micrometer scale, *Science*, 318 (2007) 251-254.
- [14] Z.W. Shan, R.K. Mishra, S.A.S. Asif, O.L. Warren, A.M. Minor, Mechanical annealing and source-limited deformation in submicrometre-diameter Ni crystals, *Nature Materials*, 7 (2008) 115-119.
- [15] J.R. Greer, W.D. Nix, Nanoscale gold pillars strengthened through dislocation starvation, *Physical Review B*, 73 (2006) 245410.
- [16] J.T. Uhl, S. Pathak, D. Schorlemmer, X. Liu, R. Swindeman, B.A.W. Brinkman, M. LeBlanc, G. Tsekenis, N. Friedman, R. Behringer, D. Denisov, P. Schall, X.J. Gu, W.J. Wright, T. Hufnagel, A. Jennings, J.R. Greer, P.K. Liaw, T. Becker, G. Dresen, K.A. Dahmen, Universal Quake Statistics: From Compressed Nanocrystals to Earthquakes, *Scientific Reports*, 5 (2015) 16493.
- [17] P. Moretti, M.C. Miguel, M. Zaiser, S. Zapperi, Depinning transition of dislocation assemblies: Pileups and low-angle grain boundaries, *Physical Review B*, 69 (2004) 214103.

DOE Sponsored Publications in refereed journals (2016-2018):

1. Y. F. Meng and J. M. Zuo, "Three-dimensional nanostructure determination from a large diffraction data set recorded using scanning electron nanodiffraction", *IUCrJ* 3, 300 (2016).

2. Yifei Meng and Jian-Min Zuo, "Improvements in electron diffraction pattern automatic indexing algorithms", *Eur. Phys. J. Appl. Phys.* 80 (1), 10701 (2017).
3. Yu-Tsun Shao and Jian-Min Zuo, "Nanoscale symmetry fluctuations in ferroelectric barium titanate, BaTiO₃", *Acta Crystallographica Section B* 73 (4), 708 (2017).
4. Y. T. Shao and J. M. Zuo, "Lattice-Rotation Vortex at the Charged Monoclinic Domain Boundary in a Relaxor Ferroelectric Crystal", *Physical Review Letters* 118 (15), 157601 (2017).
5. W. P. Gao, J. B. Wu, A. Yoon, P. Lu, L. Qi, J. G. Wen, D. J. Miller, J. C. Mabon, W. L. Wilson, H. Yang, and J. M. Zuo, "Dynamics of Transformation from Platinum Icosahedral Nanoparticles to Larger FCC Crystal at Millisecond Time Resolution", *Scientific Reports* 7 (2017).
6. Erfan Mohammadi, Chuankai Zhao, Yifei Meng, Ge Qu, Fengjiao Zhang, Xikang Zhao, Jianguo Mei, Jian-Min Zuo, Diwakar Shukla, and Ying Diao, "Dynamic-template-directed multiscale assembly for large-area coating of highly-aligned conjugated polymer thin films", *Nature Communications* 8, 16070 (2017).
7. W. Guo, Y. F. Meng, X. Zhang, V. Bedekar, H. B. Bei, S. Hyde, Q. Y. Guo, G. B. Thompson, R. Shivpuri, J. M. Zuo, and J. D. Poplawsky, "Extremely hard amorphous-crystalline hybrid steel surface produced by deformation induced cementite amorphization", *Acta Materialia* 152, 107 (2018).
8. Yang Hu, Li Shu, Qun Yang, Wei Guo, Peter K. Liaw, Karin A Dahmen, Jian-Min Zuo "Dislocation Avalanche Mechanisms in Slowly Compressed High Entropy Alloy Nanopillars", *Communications Physics*, Accepted

AUTHOR INDEX

Bakaul, Saidur	44
Balke, Nina.....	3
Balsara, Nitash	11, 35
Batson, P. E.	71
Borisevich, Albina.....	3
Brennecka, Geoff	232
Camden, Jon P.....	76
Chan, Emory	55
Chandrasekhar, Venkat	81
Chen, Hanning	219
Chen, Long-Qing	86
Chisholm, M. F.	31, 40
Cobden, David H.....	93
Crozier, Peter A.....	98
Davis, J.C. Séamus.....	15
Dougherty, Dan	103
Downing, Kenneth	11, 35
Ercius, Peter	55
Fennie, Craig J.	174
Filler, Michael A.	106
Flannigan, David J.	110
Flatté, Michael E.	126
Fu, Xuewen	60
Fuchs, Gregory D.....	115
Fujita, Kazuhiro.....	15
Garlow, Joe	27
Ginger, David S.....	120
Goldhaber-Gordon, David.....	23
Gupta, Jay A.....	126, 144
Hammel, P. Chris	130
Han, Myung-Geun.....	27
Hong, Xia	135
Iavarone, Maria	140
Jarillo-Herrero, Pablo.....	249
Kalinin, S. V.....	31, 40
Kastner, Marc	23
Kawakami, Roland K.	144
Konstantinova, Tatiana	60
Lagos, M. J.....	71
Lai, Keji.....	148
Levchenko, Alex	236
Li, Jun.....	50
Li, Junjie.....	50, 60
Li, Lian	152
Lupini, A. R.	31, 40
Madhavan, Vidya	156
Maksymovych, Petro	3
Manoharan, Hari C.....	23
Marks, Laurence D.....	160
Masiello, David J.	76
Meng, Y. Shirley	165
Meyhofer, Edgar	206
Miao, Jianwei (John).....	169
Minor, Andrew	11, 35
Morgan, Dane.....	241
Muller, David A.	174
Nelson, C. T.	31, 40
Nowack, Katja C.	180
Orenstein, Joseph	23
Oxley, M. P.	31, 40
Pan, Xiaoqing.....	184
Pantelides, Sokrates T.	189
Petford-Long, Amanda K.....	44
Phatak, Charudatta	44
Plummer, Ward	193
Prendergast, David	11, 35
Raschke, Markus B.	202
Reddy, Pramod.....	206
Ross, Frances M.....	106
Ruan, Chong-Yu	210
Schlom, Darrell G.	174
Schwarz, Udo	214
Solares, Santiago D.	219
Stemmer, Susanne.....	223
Sutter, Eli	227
Sutter, Peter	227
Tan, Xiaoli.....	232
Tao, Jing.....	50, 60
Tessmer, Stuart.....	236
Van Harlingen, Dale.....	236
Vasudevan, Rama.....	3
Voyles, Paul M.....	241
Wang, Lin-Wang.....	55
Wu, Lijun	60
Wu, Weida.....	245
Yacoby, Amir	249
Yazdani, Ali	254
Zhang, Shoucheng.....	23
Zheng, Haimei.....	55
Zhu, Yimei	27, 60
Zuckermann, Ronald.....	11, 35
Zuo, Jian-Min	259

PARTICIPANT LIST

Name	Organization	Email Address
Arslan, Ilke	Argonne National Laboratory	arslan@anl.gov
Bakaul, Saidur	Argonne National Laboratory	sbakaul@anl.gov
Balsara, Nitash	Lawrence Berkeley National Laboratory	nbalsara@lbl.gov
Batson, Philip	Rutgers University	batson@physics.rutgers.edu
Camden, Jon	University of Notre Dame	jon.camden@nd.edu
Chandrasekhar, Venkat	Northwestern University	v-chandrasekhar@northwestern.edu
Chen, Long-Qing	The Pennsylvania State University	lqc3@psu.edu
Cobden, David	University of Washington	cobden@uw.edu
Crozier, Peter	Arizona State University	crozier@asu.edu
Davis, J.C. Séamus	Cornell Univ./Brookhaven National Lab	jcseamusdavis@gmail.com
Dougherty, Daniel	North Carolina State University	dbdoughe@ncsu.edu
Filler, Michael	Georgia Institute of Technology	mfiller@gatech.edu
Flannigan, David	University of Minnesota	flan0076@umn.edu
Flatté, Michael	University of Iowa	michael_flatte@mailaps.org
Fuchs, Gregory	Cornell University	gdf9@cornell.edu
Ginger, David	University of Washington	dginger@uw.edu
Goldhaber-Gordon, David	Stanford University	goldhaber-gordon@stanford.edu
Gupta, Jay	The Ohio State University	gupta.208@osu.edu
Hammel, P. Chris	The Ohio State University	hammel.7@osu.edu
Han, Myung-Geun	Brookhaven National Laboratory	mghan@bnl.gov
Hong, Xia	University of Nebraska, Lincoln	xia.hong@unl.edu
Iavarone, Maria	Temple University	iavarone@temple.edu
Jesse, Stephen	Oak Ridge National Laboratory	sjesse@ornl.gov
Kalinin, Sergei	Oak Ridge National Laboratory	sergei2@ornl.gov
Kasevich, Mark	Stanford University	kasevich@stanford.edu
Kawakami, Roland	The Ohio State University	kawakami.15@osu.edu
Lai, Keji	University of Texas, Austin	kejilai@physics.utexas.edu
Lee, Honyung	Oak Ridge National Laboratory	hnlee@ornl.gov
Levchenko, Alex	University of Wisconsin, Madison	levchenko@physics.wisc.edu
Li, Lian	West Virginia University	lian.li@mail.wvu.edu
Lupini, Andrew	Oak Ridge National Laboratory	9az@ornl.gov
Madhavan, Vidya	University of Illinois, Urbana-Champaign	vm1@illinois.edu
Masiello, David	University of Washington	masiello@uw.edu
Meng, Ying Shirley	University of California, San Diego	shirleymeng@ucsd.edu
Miao, Jianwei	University of California, Los Angeles	miao@physics.ucla.edu
Minor, Andrew	University of California, Berkeley, Lawrence Berkeley National Laboratory	aminor@lbl.gov
Muller, David	Cornell University	dm24@cornell.edu
Nelson, Christopher	Oak Ridge National Laboratory	nelsonct@ornl.gov
Nowack, Katja	Cornell University	kcn34@cornell.edu
Oxley, Mark	Oak Ridge National Laboratory	oxleyp@ornl.gov
Pan, Xiaoqing	University of California, Irvine	xiaoqing.pan@uci.edu
Pantelides, Sokrates	Vanderbilt University	Pantelides@vanderbilt.edu

Petford-Long, Amanda	Argonne National Laboratory	petford.long@anl.gov
Plummer, Ward	Louisiana State University	wplummer@phys.lsu.edu
Raschke, Markus	University of Colorado	markus.raschke@colorado.edu
Reddy, Pramod	University of Michigan	pramodr@umich.edu
Ross, Frances	Massachusetts Institute of Technology	fmross@mit.edu
Ruan, Chong-Yu	Michigan State University	ruan@pa.msu.edu
Schwarz, Udo	Yale University	udo.schwarz@yale.edu
Solares, Santiago	George Washington University	ssolares@gwu.edu
Stemmer, Susanne	University of California, Santa Barbara	stemmer@mrl.ucsb.edu
Sutter, Eli	University of Nebraska, Lincoln	esutter@unl.edu
Sutter, Peter	University of Nebraska, Lincoln	psutter@unl.edu
Tan, Xiaoli	Iowa State University	xtan@iastate.edu
Tao, Jing	Brookhaven National Laboratory	jtao@bnl.gov
Tessmer, Stuart	Michigan State University	tessmer@pa.msu.edu
Van Harlingen, Dale	University of Illinois, Urbana-Champaign	dvh@illinois.edu
Voyles, Paul	University of Wisconsin, Madison	paul.voyles@wisc.edu
Wisinger, Nina	Oak Ridge National Laboratory	balken@ornl.gov
Wu, Lijun	Brookhaven National Laboratory	ljwu@bnl.gov
Wu, Weida	Rutgers University	wdwu@physics.rutgers.edu
Yacoby, Amir	Harvard University	yacoby@g.harvard.edu
Yazdani, Ali	Princeton University	yazdani@princeton.edu
Zheng, Haimei	Lawrence Berkeley National Laboratory	hmzheng@lbl.gov
Zhu, Jane	U.S. Department of Energy	jane.zhu@science.doe.gov
Zhu, Yimei	Brookhaven National Laboratory	zhu@bnl.gov
Zuo, Jianmin	University of Illinois	jianzuo@illinois.edu